



SFERA-III

Solar Facilities for the European Research Area

Mid-term report on the doctoral colloquia/schools, including booklet of abstracts/lectures.

Deliverable D1.1

Estimated delivery date: 30.06.2021

Actual delivery date: 26.07.2021

Lead beneficiary: CNRS

Person responsible: DOLLET Alain

Deliverable type: R DEM DEC OTHER ETHICS ORDP

Dissemination level: PU CO EU-RES EU-CON EU-SEC



AUTHORS

| Author | Institution | E-mail |
|--------------|-------------|-----------------------------|
| Alain DOLLET | CNRS | alain.dollet@promes.cnrs.fr |
| | | |
| | | |
| | | |

DOCUMENT HISTORY

| Version | Date | Change |
|---------|------------|---|
| 1.0 | 30.06.2021 | Original |
| 2.0 | 26.07.2021 | Corrections according to reviewer's recommendations (21.7.2021) |
| | | |
| | | |

VALIDATION

| Reviewers | Validation date |
|-----------------|-----------------|
| Ricardo Sanchez | |
| | |
| | |

DISTRIBUTION LIST

| Date | Recipients |
|------------|------------|
| DD.MM.YYYY | |

Disclaimer

The content of this publication reflects only the author's view and not necessary those of the European Commission. Furthermore, the Commission is not responsible for any use that may be made of the information this publication contains.

Executive Summary

This Document summarizes the mid-term progress of Task 1.1 (Organisation of the Doctoral Colloquia) and Task 1.2 (Organisation of the Winter/Summer Schools) of the SFERA-III project.

The objectives of these joint tasks are first briefly reminded. The first DC and School which were organized in CNRS premises (Odeillo, France) in September 2019 are reviewed and the main outcomes of these coupled events are highlighted. A synthesis of the evaluation performed by the participants is annexed, as well as the program of the coupled events, the book of abstracts of the talks presented at the DC by the PhD students and the courses (slides) presented at the Summer School by the speakers.

The 2nd DC and Schools which should have been held in 2020 in Spain have been postponed because of the COVID-19 pandemic. Thanks to the 12-month extension of the project, they will be organized before late 2021. They will be reviewed in the final deliverable (D1.2) together with the 3rd and 4th events to be held in 2022 and 2023 respectively. Only the provisional program of the 2nd Summer School has been provided in the present document.



Table of Contents

| | |
|---|----|
| Executive Summary | 3 |
| Table of Contents | 4 |
| 1. Objectives (reminder) | 5 |
| 1.1. Objective of task 1.1 | 5 |
| 1.2. Objective of task 1.2 | 6 |
| 2. Results | 7 |
| 2.1. First Doctoral Colloquium (task 1.1) | 7 |
| 2.2. First Summer School (task 1.2) | 9 |
| 2.3. Second School & Colloquium | 11 |
| List of abbreviations | 13 |
| Annexes | 14 |
| Annex 1. Results of the satisfaction surveys | 15 |
| Annex 2. Program of the 1st Doctoral Colloquium and Summer School | 18 |
| Annex 3. Booklet of abstracts (Doctoral Colloquium) | 27 |
| Annex 4. Presentations at the 1 st Summer School | 62 |

1. Objectives (reminder)

Task 1 (Organisation of the Doctoral colloquia) and Task 2 (Organisation of the Winter/Summer schools) are important components of the "Capacity building and training activities", together with task 1.3 (Onsite training for industries). They aim at strengthening the collaboration between the SFERA laboratories, fostering the use of their research infrastructures, training early-stage researchers in the CST field, enhancing the transfer of knowledge and sharing the latest developments with the CST community...

The schools and doctoral colloquia should be organised preferably in a different place each time in order to attract and involve a maximum number of partners from different countries and allow the participants to visit at least one infrastructure of the hosting country. The Doctoral Colloquia and the Schools should coincide in order to save travelling resources. There are no entrance fees neither for the Colloquia nor for the Schools but the attendees must bear the costs of both the travel and lunches. The PhD students are traditionally involved in the organisation of the Colloquium, especially those from the host institution who provide support to the other PhD students (information for venue, train or buses timetables, hotel booking...) as well as for the organisation of social and networking activities.

1.1. Objective of task 1.1

4 Doctoral Colloquia (DC) have been planned (target 1DC/year) in order to allow the PhD students preparing their thesis in the laboratories involved in the project to meet each other, to present the outcomes of their research in the CST field and to see what others are doing in the same topic. These meetings should contribute to improve the services of the laboratories and to strengthen the collaboration between them in order to further develop joint research activities. The participation of both the directors of the laboratories and the managers of the facilities where these PhD theses are conducted is encouraged. The planned duration of a DC is two and half days (15-20h) and it is always organized together with the winter/summer schools (task 1.2). The DC should be preferably hosted by CNRS, CIEMAT, DLR and ETH (i.e. the members of the Alliance of European Laboratories for Research and Technology on Solar Concentrating Systems: SolLAB), but a second institution could also be closely

involved in the organization with the host. The activities undertaken in this task consist in preparing the on-site logistics and organizing the agenda of the meetings (including networking activities between PhD students), facilitating the travel information and the accommodation to the participants, editing a booklet of the abstracts that will be made available on the project website (while making available the full presentations onto the restricted area of the website).

1.2. Objective of task 1.2

4 Summer (or winter/fall/spring) Schools, whose duration is also typically 2.5 days (15-20h) have also been planned. The main goal is to bringing researchers from both academia and industry, especially early stage researchers, to promote the use of the SFERA research infrastructure and provide them with valuable knowledge and methodological tools for further advancing their researches in the CST field. The topic of the school (which must be approved by the Steering Committee) changes each year. The activities undertaken in this task consist in developing the scientific programme, providing the on-site logistics, organizing the agenda of the meetings, facilitating the travel information and the accommodation to the participants, publishing the presentations on the project website and performing an evaluation of the school with the participants to improve future schools.

2. Results

2.1. First Doctoral Colloquium (task 1.1)

The 1st Doctoral Colloquium was held in Odeillo (CNRS premises, France) from September 11th to 13th 2019. A pre-announcement of this event was sent to the project partners early March 2019 and disseminated by the participants inside their own institutions; it was also published on the project website as well as on the institutional websites of the partners.

The provisional program of the Colloquium was available early July and registrations were opened at the same time. 26 abstracts were received by early August and the final version of the full program was completed at that time. The full program of the Colloquium and the book of abstracts have been uploaded on the public part of the SFERA-III project website (<https://sfera3.sollab.eu/2019/10/31/content-1st-summer-school-and-doctorial-colloquium/>). These documents are also annexed hereafter (Annex 2 and Annex 3).

23 oral presentations were given by PhD students and 40 scientists (PhD students and supervisors) from 6 countries among SFERA-III laboratories attended the Colloquium. The meeting was organized in 4 sessions co-chaired by the Sollab Alliance members (CNRS, CIEMAT, DLR and ETH-Z):

- Energy storage & solar fuels
- Solar receivers
- Solar field
- Hybrid and advanced solar processes.

A technical visit of the CNRS solar facilities was also organized (September 11th) prior to the above scientific sessions. The main social activity (tree trail) was unfortunately cancelled due to bad weather conditions (wind and snow).

4 PhD students from the host laboratory strongly contributed to the organisation, especially for setting up networking and social activities, for providing the guests with information and on-site support and for facilitating the contacts between all the PhD

students. Each attendee was provided with some material for the Colloquium upon on-site registration : hard copy of the final full program, badge, list of attendees, brochure of the SFERA-III project and brochure of the host laboratory, notebook + pen, and ecocup.



Figure 1. **Picture of the participants to the 1st DC held in CNRS premises**
(Odeillo, France)

The participants were asked to fill a (anonymous) satisfaction survey after the completion of the Colloquium. 33 participants (over 40) filled the questionnaire. They had to rate 13 different criteria related to the scientific content of the Colloquium and to the local organisation as well, using simple scoring rules (good, medium, bad). They were also invited to write comments and recommendations at their convenience. The feedback was generally very good, the general opinion on the DC received an average score of 1.97/2. The strongest point was the quality of the program (2.0/2.0), the weakest point was related to the quality of the coffee breaks (0.91/2). A synthesis of the answers received has been included in Annex 1.

2.2. First Summer School (task 1.2)

The 1st Summer School was held in Odeillo (CNRS premises, France) from September 9th to 11th 2019. The topic was “Thermal energy storage systems, solar fields and new cycles for future CSP plants”. The program supervised by CNRS and University of EVORA was prepared with the other SFERA laboratories involved in the task.

The pre-announcement of this event was sent early March to the project partners (together with the announcement of the DC) who disseminated it into their own professional networks and published it on their institutional websites at the same time. The event was also pre-announced on the SFERA-III project website early April. The final program was available only early July due to several late cancellations of speakers who had to be replaced; it was published on the project website and the information was disseminated by all partners through their own networks. On-line registrations were also open at that time. 66 registrations were received by late July 2019 (16 countries, 9 outside from SFERA-III). No selection was required since the maximum capacity of the meeting room was not reached. Finally, 60 people from 10 countries (including India, Lybia, Poland and UK) attended the School. 13 lectures were given by recognized experts from 5 countries and a technical visit of the CNRS solar facilities was organized September 11th after completion of the speeches (just before the start of the DC).

As for the DC, a hard copy of the final full program was given to the participants upon registration with additional material (badge, list of attendees, brochure of the SFERA-III project, brochure of the host laboratory, notebook + pen, and ecocup). The full program is available on the public part of the project website as well as the presentations of the speakers <https://sfera3.sollab.eu/2019/10/31/content-1st-summer-school-and-doctorial-colloquium>. The program and the presentations are also annexed to this document.



Figure 2. **Snapshot of the classroom during the 1st Summer School in CNRS premises (Odeillo, France)**

As for the DC, the participants were invited to fill a (anonymous) satisfaction survey after the completion of the School. 38 participants (over 60) filled this survey (see Annex 1 for more details). They also had to rate 13 different criteria related to the scientific content of the School and to its organization using simple scoring rules (good, medium, bad). They were also invited to write comments and recommendations at their convenience. The feedback was generally very good although the score obtained was a little bit lower than the score of the DC. The general opinion received an average score of 1.76/2 (against 1.92/2 for the DC). The weakest point was again related to the quality of the coffee breaks. Details can be found in annex 1.

2.3. Second School & Colloquium

On closing the 1st events on September 13th 2019, and after discussion between the SolLab laboratories/WP1 participants, it has been proposed to organize the 2nd Summer School and Doctoral Colloquium of SFERA-III in Almeria (Spain) in June 2020. The Doctoral Colloquium (restricted to SFERA-III members) was scheduled June 15-17th (including technical visit/networking activities on June 17th afternoon) while the Summer School (open to a large audience) was supposed to be held from June 17th to 19th (including technical visit on June 17th afternoon). The topic proposed was “Solar process heat for Industrial applications and Desalination”.

The pre-announcement of these coupled events was sent to the project partners early January 2020 and published on the SFERA-III website at the same time. The partners also published this information on their own websites and forward it using their own professional contact lists. The full program and the opening of the registrations should have started late March; however, the COVID-19 pandemic led us to cancel both events and postpone them sine die. It has been decided (only late June) to organize the 2nd events physically in Spain during this Autumn, the exact date will be fixed and announced early July.

The provisional program supervised by CIEMAT already prepared in March 2020 is provided below. The results of the 2nd meetings will be included in the next (final) deliverable of task 1.1 and 1.2 (D1.2).

SFERA-III Summer School-2020

Solar Process Heat Applications and Water Desalination

Day 1: “Solar Heat for Industrial Processes (SHIP)”

| Time | Lecture | Speaker |
|---------------|--|-----------------------------|
| 09:00 – 09:15 | Opening of Summer School 2020 | t.b.c. |
| 09:15-10:00 | Market potential for SHIP applications | Theda Zoschke |
| 10:00-10:45 | SHIP applications at medium temperatures | Dirk Krueger |
| 10:45-11:15 | Coffee break | |
| 11:15-11:45 | Solar steam generation for SHIP applications | Eduardo Zarza |
| 11:45 – 12:15 | SHIP applications at high temperatures | Alfonso Vidal |
| 12:15-13:00 | Thermal storage for SHIP applications | Esther Rojas |
| 13:00-14:30 | Lunch break | |
| 14:30 – 15:00 | R+D lines for Medium temperature SHIP applications | Mario Biencinto |
| 15:00 – 15:30 | Innovative collector designs for medium Temperature SHIP applications | Tiago Osorio/ Pedro Orta |
| 15:30-16:00 | Operation & maintenance of SHIP systems | t.b.n. |
| 16:00-16:30 | Coffee break | |
| 16:30-17:00 | The new Task 64/IV of SHC and SolarPACES | Eduardo Zarza |
| 17:00-17:30 | Towards an European R+D strategy for SHIP applications | Julián Blanco |
| 17:30 | End of the first day | |

Day 2: “Solar Heat for Industrial Processes (SHIP)”

| Time | Lecture | Speaker |
|--|--|---------------------|
| 09:00-10:00 | Influence of the system design on the pay-back time and solar fraction of SHIP applications | Miguel Frasset |
| <u>Solar Thermal Desalination</u> | | |
| 10:00 – 10:40 | Fundamentals of water desalination | Diego C. Alarcón |
| 10:40-11:10 | Coffee break | |
| 11:10-11:50 | Overview of thermal desalination processes | Diego C. Alarcón |
| 11:50 – 12:30 | Solar thermal cogeneration plants | Patricia Palenzuela |
| 12:30 – 13:00 | Advanced control of solar process heat applications | Lidia Roca |
| 13:00-13:15 | Closing of Summer School 2020 | Eduardo Zarza |
| 13:15 – 14:30 | Lunch break | |

Figure 3. **Provisional program of the 2nd Summer School** (as prepared in March 2020)



List of abbreviations

| | |
|--------|--|
| CST | Concentrating Solar Thermal |
| DC | Doctoral Colloquium |
| EU | European Union |
| RI | Research Infrastructure |
| SolLab | Alliance of European Laboratories for Research and Technology on Solar Concentrating Systems |



Annexes

Annex 1. Results of the satisfaction surveys

38 out of 60 (resp. 33 out of 40) participants filled the satisfaction survey which was distributed at the end of the School (resp. at the end of the Colloquium). They had to use simple scoring rules (good, medium, bad) to evaluate the 13 indicators proposed and they were free to add comments and recommendations in a dedicated insert. The general (overall) appreciation was excellent for the DC which received an average score of 1.92/2. The mean score of the School was also very good (1.76/2) although a bit lower than the one obtained for the DC. As illustrated in fig.4 below, none considered that either of the events was bad.

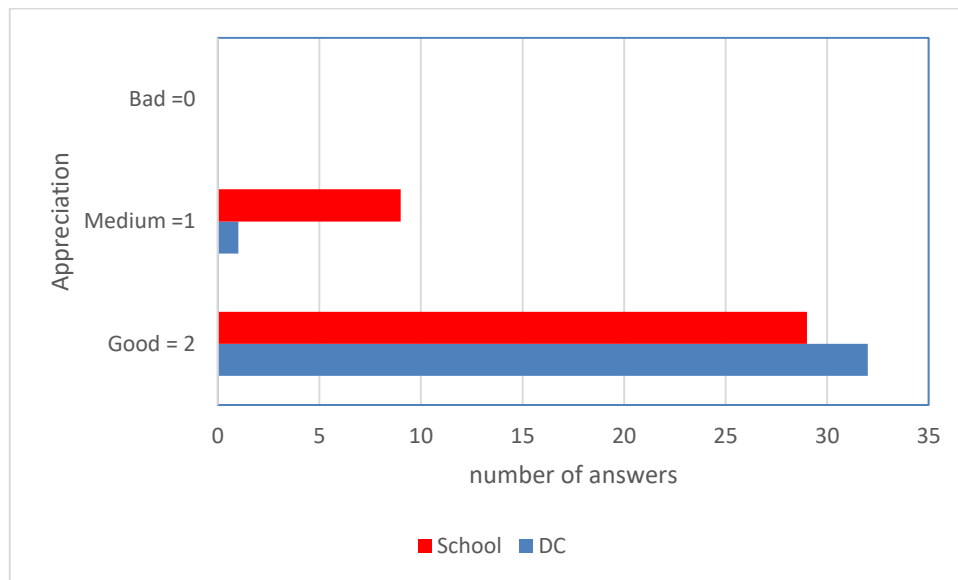


Figure 4. **Assessment of the 1st Summer School and DC: overall appreciation**

Going further into details, the analysis of the questionnaires filled for the DC (fig. 5) revealed that only 1 out of 13 indicators obtained a low score. Everyone found that the program was very good (but we should keep in mind it was built a posteriori from the abstracts received). Most people were very satisfied by the presentations and discussions and by the technical visit of the Solar furnaces (Odeillo) and the Themis Solar Plant (Targassonne, 5 km from the meeting place). Although the support provided was good for a large majority of the participants, a few of them experienced

some problems with the internet connexion. A few other mentioned they would have preferred receiving the information for travel and accomodation earlier (it was sent only in July with the final program).

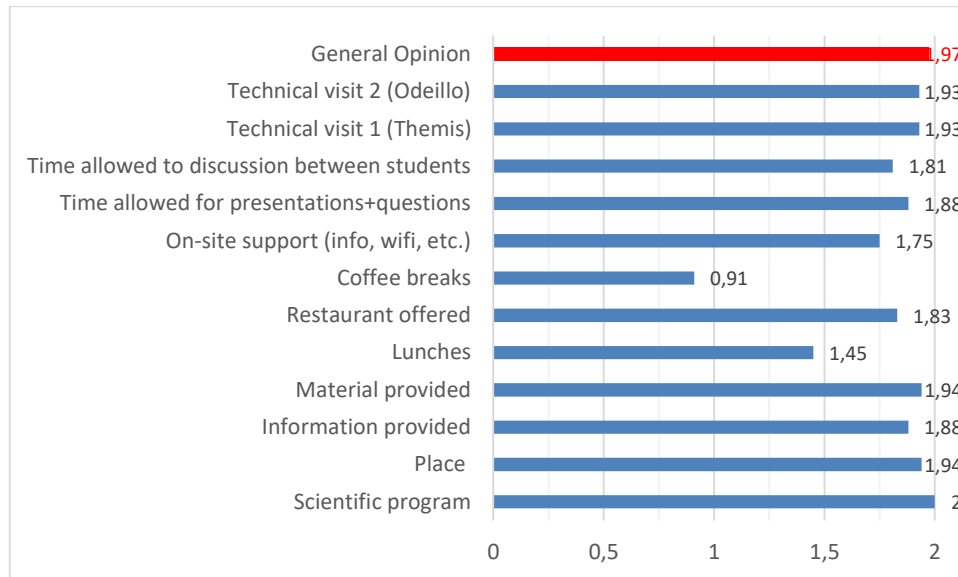


Figure 5. **Assessment of the 1st Doctoral colloquium (score out of 2)**

The mean scores obtained at the questionnaires filled for the School (fig. 6) revealed similar trends. Most people were satisfied but the scores are usually slightly lower than those obtained by the DC. Not surprisingly, the coffee breaks were often scored as medium or even sometimes bad (mean score : 0.97/2.0), clearly, this was the weakest point of both events. With very few exceptions, the attendees enjoyed the scientific program and the technical visits, even if a few of them mentioned that they did not like one or several particular presentations, but on the whole, the scores obtained by the speakers for day 1 and day 2 remained good.

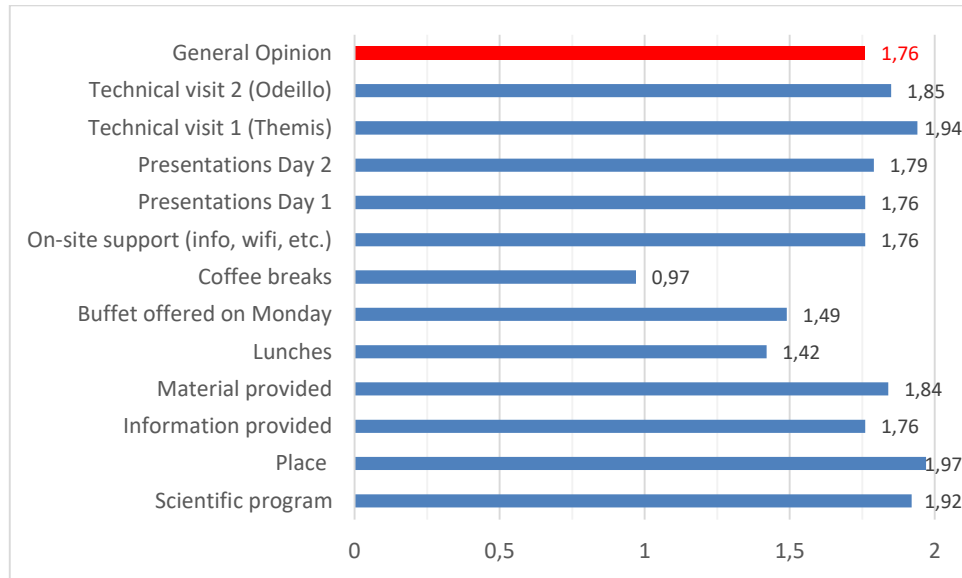


Figure 6. **Assessment of the 1st Summer School (score out of 2)**



Annex 2. Program of the 1st Doctoral Colloquium and Summer School



Depuis 80 ans, nos connaissances
bâtissent de nouveaux mondes



SFERA-III

1st Summer School & Doctoral Colloquium

September, 9th- 13th, 2019

CNRS- PROMES, Odeillo, France



FULL PROGRAM



THIS PROJECT HAS RECEIVED FUNDING FROM THE EUROPEAN UNION'S HORIZON 2020
RESEARCH AND INNOVATION PROGRAMME UNDER GRANT AGREEMENT NO 823802

Summer School

“Thermal energy storage systems, solar fields and new cycles for future CSP plants”

Chairs

Alain Ferrière, CNRS-PROMES
Diogo Canavarro, University of Evora

Program

Day 1 : Monday, September 9th, 2019

- | | |
|----------|---|
| 8:15 am | Registrations |
| 9:30 am | Welcome address by Alain Dollet (CNRS) Introduction of the School, by Alain Ferrière (CNRS) & Diogo Canavarro (Univ. Evora) |
| 9:45 am | Introductory talk, by Alain Ferrière (CNRS) “The CSP technologies: market status and opportunities for R&D” |
| 10:30 am | Coffee break |
| 11:00 am | Thermal Energy Storage - Class 1, by Eduardo Zarza (CIEMAT) “TES for solar thermal power plants: introduction, commercial systems, integration issues and latent heat” |
| 12:00 pm | Thermal Energy Storage - Class 2, by Anna Chiara Tizzoni/Salvatore Sau (ENEA) “Novel molten salts for TES application in CSP plants” |
| 12:30 pm | Lunch at CNRS restaurant |
| 2:30 pm | Thermal Energy Storage - Case study, by Shahab Rohani (Fraunhofer ISE) “Lessons learned from a lab-scale thermochemical storage” |
| 3:30 pm | Coffee break |
| 4:00 pm | Thermal Energy Storage - Class 3, by Sylvie Rougé (CEA) “Thermochemical TES: challenges and issues” |
| 4:45 pm | Thermal Energy Storage - Class 4, by Pierre Garcia (CEA) “TES performance assessment” |
| 5:30 pm | Group picture |
| 6:00 pm | End of 1st day session |
| 7:00 pm | Get together buffet (offered by CNRS) in PROMES' premises |

Day 2 : Tuesday, September 10th, 2019

- 9:00 am Introductory lecture, by Manuel Romero (IMDEA Energy)
“Next generation of CSP plants: technology developments and market opportunities”
- 10:00 am Coffee break
- 10:30 am Collectors - Class 1, by Diogo Canavarro (Univ Evora)
“New concepts of line focus and point focus collectors”
- 11:00 am Collectors - Class 2, by Jose González-Aguilar (IMDEA Energy)
“New concepts of heliostats for solar tower systems”
- 11:30 am Collectors - Case study, by Shahab Rohani (Fraunhofer ISE)
“A design tool for heliostat field layout”
- 12:30 pm Lunch at CNRS restaurant
- 2:00 pm Cycles - Introductory lecture, by Eduardo Zarza (CIEMAT)
“Thermodynamic cycles for CSP plants: state-of-the-art and challenges”
- 3:30 pm Cycles - Class 1, by Manuel Romero (IMDEA Energy)
“sCO₂ cycles for CSP plants: challenges and issues”
- 4:00 pm Coffee break
- 4:30 pm Cycles - Class 2, by Daniel Benitez (DLR)
“Hybrid CSP-PV plants: examples of configurations and simulation using Greenius”
- 5:30 pm: End of 2nd day session

Day 3 : Wednesday, September 11th, 2019

- 8:45 am Transfer to Themis solar tower platform in Targasonne (group 1)
Transfer to CNRS solar facilities in Odeillo (group 2)
- 9:00 am Visit of Themis platform (group 1)/Visit of CNRS solar facilities (group2)
- 10:30 am Coffee break and transfer to Odeillo/Targasonne
- 11:00 am Visit of Themis platform (group 2)/Visit of CNRS solar facilities (group1)
- 12:30 pm Lunch at CNRS restaurant
- 2:00 pm End of the Summer School

Note: The visits are organized for both events (Summer School and Doctoral Colloquium)

Doctoral Colloquium

(SFERA members only)

Session Chairs

Alain Dollet, CNRS
Sixto Malato, CIEMAT
Robert Pitz-Paal, DLR
Aldo Steinfeld, ETH-Z

Program

Day 1 : Wednesday, September 11th, 2019

- 8:45 am Transfer to Themis solar tower platform in Targasonne (group 1)
Transfer to CNRS-PROMES solar facilities in Odeillo (group 2)
- 9:00 am Visit of Themis platform (group 1)/Visit of CNRS solar facilities (group2)
- 10:30 am Coffee break and transfer to Odeillo/Targasonne
- 11:00 am Visit of Themis platform (group 2)/Visit of CNRS solar facilities (group1)
- 12:30 pm Lunch at CNRS restaurant
- 13:45 pm Registrations
- 2:00 pm Departure for social activity: «Tree trail «(Parc Aventure, Font-Romeu L'hermitage).
(Registered persons only).
- 6:00 pm Free time (hotel or city of Font-Romeu)
- 7:00 pm Departure for Llivia province
- 7:30 pm Get together dinner at Cal Rita Porta in Llivia (offered by CNRS)
- 9:30 pm Return to hotels in Font-Romeu

Day 2 : Thursday, September 12th, 2019

Session 1: Energy storage & Solar fuels

Chair: Aldo Steinfeld, ETH Zurich

- 9:00 am «The importance of Energy Storage (ES) in Isolated Islands. Cyprus Case Study»
George Partasides, Constantinos Taliotis, Manuel Blanco, The Cyprus Institute
- 9:25 am «Modelling & Experimental Validation of a Thermochemical Energy Storage Reactor»
Michael Wild, Aldo Steinfeld, ETH Zürich
- 9:50 am «Influence of mass flow rate on thermocline storage performance»
Ségolène Vannerem, Quentin Falcoz, Pierre Neveu, CNRS/University of Perpignan
- 10:15 am «Thermal-energy storage system integration with focus on advanced adiabatic compressed air energy storage plants»
Philipp Roos, Andreas Haselbacher, Aldo Steinfeld, ETH Zürich
- 10:40 am Coffee break
- 11:00 am «High-temperature thermochemical heat storage: development of materials and lab-scale packed-bed prototype»
Marco Gigantino, Aldo Steinfeld, ETH Zurich
- 11:25 am «The solar refinery: techno-economic potential of producing carbon-based fuels with concentrated solar power»
Andreas Rosenstiel, Martin Roeb, Nathalie Monnerie, Stefan Brendelberger, Christian Sattler, DLR -Institute of Solar Research
- 11:50 am «Performance Optimization of the CeO₂-CH₄-CO₂ Redox Cycle for Solar Fuel Production»
Mario Zuber, Simon Ackermann, Philipp Furler, Aldo Steinfeld, ETH Zürich
- 12:15 pm «Solar-thermal oxygen pumping»
Mathias Pein, Christos Agrafiotis, Martin Roeb, Christian Sattler, DLR
- 12:40 pm Lunch at CNRS restaurant

Session 2: Solar receivers

Chair: Sixto Malato, CIEMAT

- 2:00 pm «Numerical Simulation of 3D-Shaped Volumetric Absorbers»
Robin Tim Broeske, DLR
- 2:25 pm «Process Assistance System for a molten salt receiver based on dynamic simulation models and artificial neural networks»
Christian Schwager, Peter Schwarzböz, Aachen University of Applied Sciences and DLR
- 2:50 pm «High-temperature solar volumetric air receiver: lab-scale testing and computational modeling»
Vikas R. Patil, Aldo Steinfeld, ETH Zurich
- 3:15 pm «Test setup for the experimental evaluation of the convective heat transfer for nitrate salt in tubular solar receivers»
Cathy Frantz, Reiner Buck, DLR
- 3:40 pm Coffee break

- 4:00 pm «Measurement of high solar irradiance on receivers in solar tower plants»
M. Casanova, J. Ballestrín, R. Monterreal, J. Fernández, E. Setien, J. Rodríguez, CIEMAT
- 4:25 pm «Numerical Modelling of Particle Motion in Centrifugal Receiver»
Serdar Hicdurmaz, Lars Amsbeck and Bernhard Hoffschmidt, DLR

Session 3a: Solar field

Chair: Robert Pitz-Paal, DLR

- 4:50 pm «Deep Learning Algorithms for Heliostat Field Calibration»
Max Pargmann and Daniel Maldonado, DLR
- 5:15 pm «Dynamic Wind Loads on Heliostats: Experimental Investigation and Development of Acceptance Tests Based on Artificial Excitation»
Kristina Blume, Marc Röger, Robert Pitz-Paal, DLR
- 5:40 pm «Dynamic aimpoint management for performance enhancement in solar tower power plants»
Laurin Oberkirsch, DLR
- 6:05 pm «Experimental and numerical evaluation of drift errors in a solar power tower facility with tilt-roll tracking-based heliostats»
Alejandro Martínez Hernández, Iván Bravo Gonzalo, Manuel Romero and José Gonzalez-Aguilar, IMDEA Energy
- 6:30 pm End of 2nd day sessions

Day 3 : Friday, September 13th, 2019

Session 3b: Materials and durability

Chair: Robert Pitz-Paal, DLR

- 9:00 am «Elaboration, performance and durability analysis of selective coatings for CSP»
D. Ngoue, A. Diop, A. Carling-Plaza, A. Grosjean, V. Pares, A. Soum-Glaude, S. Quozola, E. Hernandez, L. Thomas, CNRS and University of Perpignan
- 9:25 am «An effective simulation route for the ternary phase diagram: $\text{NaNO}_3\text{-KNO}_3\text{-NaNO}_2$ »
Tiziano Delise, University of Rome Tor Vergata and ENEA
- 9:50 am «Aging and durability studies of solar selective absorber coatings in air at high temperature»
A. Carling-Plaza, M. Bichotte, A. Soum-Glaude, M.A. Keilany, L. Dubost and L. Thomas, CNRS/University of Perpignan and HEF-IREIS
- 10:15 am «Lifetime prediction of solar mirrors used in concentrating solar thermal energy»
Francisco Buendía-Martínez, Aránzazu Fernández-García, Florian Sutter, Johannes Wette and Loreto Valenzuela, CIEMAT and DLR
- 10:40 am Coffee break

Session 4: Hybrid and advanced solar processes

Chair: Alain Dollet, CNRS

- 11:00 am «Electrochemical wastewater treatments enhanced by combination with solar energy»
I. Salmerón, G. Rivas, I. Oller, S. Malato, CIEMAT
- 11:25 am «Evaluation of a new solar photo-reactor for solar water disinfection»
A. Martínez-García, I. Oller, P. Fernández-Ibáñez, M.I. Polo-López, CIEMAT and University of Ulster (UK)
- 11:50 am «Application of Advanced Integrated Technologies (Membrane and Photo-Oxidation Processes) for the Removal of CECs contained in Urban Wastewater»
Dennis Deemter, Isabel Oller, Sixto Malato, Ana M. Amat. CIEMAT and Universitat Politècnica de València
- 12:15 pm Group picture
- 12:30 pm Buffet at CNRS restaurant with PROMES staff
- 2:00 pm «PV/CSP hybrid system»
Dounia Ziyati, Alexis Vossier, Alain Dollet, CNRS
- 2:25 pm «Investigation of electrostatic precipitation to avoid particles deposition on a solar reactor window»
Juan P. Rincon-Duarte, Stefania Tescari, Thomas Fend, Martin Roeb, Christian Sattler, DLR
- 2:50 pm Concluding remarks
Alain Dollet, CNRS
- 3:00 pm **End of the Doctoral Colloquium**

Transportation

A special bus will transport participants between Font-Romeu city centre and the meeting places
Departure times from Font-Romeu (front of the «Casino», 46 Avenue Emmanuel Brousse) :
Monday: 8:00 am, Tuesday: 8:30 am, Wednesday: 8:30 am and 7:00 pm, Thursday: 8:30 am,
Friday: 8:30 am



Meeting address

PROMES/CNRS laboratory, 7 rue du Four solaire, 66120 Odeillo

Organizing committee

PROMES CNRS

Alain Dollet
Alain Ferrière
Romie Lopez
Alex Carling-Plaza (PhD student)
Charlène Pellegrini (PhD student)
Segolène Vannerem (PhD student)
Donia Ziyati (PhD student)



Depuis 80 ans, nos connaissances
bâtissent de nouveaux mondes

University of Evora

Diogo Canavarro



Solar Facilities for the European Research Area



THIS PROJECT HAS RECEIVED FUNDING FROM THE EUROPEAN UNION'S HORIZON 2020
RESEARCH AND INNOVATION PROGRAMME UNDER GRANT AGREEMENT NO 823802



Annex 3. Booklet of abstracts (Doctoral Colloquium)



Depuis 80 ans, nos connaissances
bâtissent de nouveaux mondes



Solar Facilities for the European Research Area



Doctoral Colloquium

Book of abstracts



THIS PROJECT HAS RECEIVED FUNDING FROM THE EUROPEAN UNION'S HORIZON 2020
RESEARCH AND INNOVATION PROGRAMME UNDER GRANT AGREEMENT NO 823802

Session 1

Energy storage & Solar fuels

Chair: Aldo Steinfeld, ETH Zurich





SFERA-III - 1st Doctoral Colloquium

Odeillo, France.

September 11th - 13th, 2019

The importance of Energy Storage (ES) in Isolated Islands

Cyprus Case Study

George Partasides^{1,a}, Constantinos Taliotis^{1,b}, Manuel Blanco^{1,c}

1. The Cyprus Institute

a PhD Candidate and Energy Officer A', at Ministry of Energy of Cyprus

b. PhD Post-Doctoral Fellow

c. ERA Chair, Solar Thermal Technologies, Vice-Chair, SolarPACES TCP, IEA

Abstract

This thesis focuses on assessing storage technologies (thermal, chemical, electrical, mechanical and gravitational) using modelling tools and evaluates the importance of Energy Storage on isolated Islands (Cyprus case Study). The thesis assesses *services* that storage can provide versus other alternatives via linear optimization methods. The work will focus in identifying a framework methodology to prioritize policy measures, that can benefit end consumers with the greatest benefits for the society, government and investors perspective. Various barriers for small islands will also be identifies and provide insights for stakeholders to plan the implementation roadmap for Storage Technologies by accelerating the energy transformation in Cyprus towards 2050.

The forward-looking analysis of new disruptive Storage technologies will also be analyzed and identify the possible impact that they will have in the Energy Storage Roadmap for the Island. Advance smart management methods will be also considered; i.e. machine learning and artificial intelligence¹ in combination with the advance weather forecasting tools that are also under development. Through the assessment, a more detailed representation of Large-Scale Storage, Distributed Storage and Small-Scale storage will be analyzed and compared with alternative options such as level of interconnector, demand side management and Grid to Vehicle options (through smart charging) respectively. The role of community storage, active consumers and the importance of the digitalaization techniques will also be identified and discussed. Various new innovative concepts, methodological approaches and revised framework will be introduced, in order to serve in the best efficient and optimum way the energy consumption at various levels using renewable energy technologies and achieve the overall target of net-zero emissions levels in 2050.

During the Colloquium the preliminary results of this study will be presented.

¹ The recent developments and advances from 'deep learning' algorithms, a system where machines learn on their own from spotting patterns and anomalies in large data sets, will revolutionize both the demand and supply side of the energy economy.



SFERA-III - 1st Doctoral Colloquium

Odeillo, France.

September 11th - 13th, 2019

Modelling and Experimental Validation of a Thermochemical Energy Storage Reactor

Michael Wild, Aldo Steinfeld

Professorship of Renewable Energy Carriers, ETH Zürich, Switzerland

A thermochemical reactor design is presented for high-temperature thermal energy storage via endothermic/exothermic reversible gas-solid reactions. It consists of an array of modular tubes, each containing a packed bed of solid reactants/products and a concentric inner porous tube for inlet/outlet of gaseous reactants/products. By adjusting the pressure inside the reactor, the reaction equilibrium and thus indirectly the reaction rate can be controlled. Coupling a thermochemical storage to a packed-bed sensible heat storage alleviates the problem of thermocline degradation.

A numerical heat and mass transfer simulation model is developed for controlling the reactor operation, e.g. the outflow temperature of the heat transfer fluid, and for optimizing its design. A lab-scale reactor prototype is fabricated and tested using the CaO-CaCO₃ carbonation-calcination reaction. The test material is stabilized using an Mg-based inert matrix to achieve cycle-over-cycle performance and characterized experimentally.

After code verification, model validation is accomplished by comparing theoretically calculated and experimentally measured temperature distributions and reactions extents.



SFERA-III - 1st Doctoral Colloquium

Odeillo, France.

September 11th - 13th, 2019

Influence of mass flow rate on thermocline storage performance

Ségolène Vannerem¹, Quentin Falcoz^{1,2}, Pierre Neveu²

¹ PROMES-CNRS UPR-8521 Laboratory, 7 rue du Four Solaire, 66120 Font-Romeu-Odeillo-Via, France

² Université de Perpignan Via Domitia, 52 av. P. Alduy, 66860 Perpignan Cedex, France

Concentrated solar power plants enable us to use the heat from the sun to produce electricity. However, the solar resource being intermittent and uncontrollable, the energy supply doesn't always match the demand and the discrepancies make the power grid very difficult to manage, with fluctuant electricity cost. To handle those issues, thermal energy can be stored during sunny periods and used later, when it is most needed. Thermal energy storage systems are thus essential to the successful integration of concentrated solar power in electricity production.

One of those systems consists in a single tank that is used for storing a heat transfer fluid (HTF) that has been heated up by the sun. Initially, the tank is full of cold HTF, which is pumped from the bottom of the tank during the charge phase to go in the solar field. The hot HTF is then injected back at the top of the tank, storing its thermal energy. During discharge, the HTF flow direction is reversed: hot fluid is pumped from the top of the tank to be used in a power block. The cold HTF is then put back at the bottom of the tank and the cycle can start again.

The key point of this kind of storage is that hot and cold fluids are present simultaneously in the same tank during the charge and discharge phases. The objective is to obtain a plug flow within the tank, so that the fluid that is being injected doesn't mix with the one initially present. The region where hot and cold fluids meet and that presents a temperature gradient is called the thermocline region and should be minimised.

It can be seen that the inlet flow distribution plays a key role in establishing a plug flow within the tank, and thus in obtaining good thermal stratification between hot and cold regions. In particular, the influence of the mass flow rate on storage performance is studied both numerically and experimentally. The fluid velocity impacts the thickness of the thermocline through opposing physical phenomena, and it appears that there is an optimal mass flow rate that maximises the charging efficiency. Moreover, the value of this optimum depends on operating conditions such as the temperature difference between hot and cold fluids and the average working temperature.

Thanks: this work was supported by the "investissement d'avenir" program organised by the Agence Nationale pour la Recherche under the contracts ANR-10-LABX-22-01 (SOLSTICE), ANR-10-EQPX-49-SOCRATE and ANR-17-CE06-0013 (OPTICLINE).



SFERA-III - 1st Doctoral Colloquium

Odeillo, France.

September 11th - 13th, 2019

Thermal-energy storage system integration with focus on advanced adiabatic compressed air energy storage plants

Philipp Roos¹, Andreas Haselbacher^{1,2}, Aldo Steinfeld¹

¹*Professorship of Renewable Energy Carriers, ETH, Switzerland*

²*Energy Science Center, ETH, Switzerland*

Grid electricity generated by intermittent renewable sources such as solar and wind energy can be stored via advanced adiabatic compressed air energy storage (AA-CAES) systems which convert electrical energy into mechanical and thermal energies. High-temperature thermal energy storage (TES) thus becomes a key element of AA-CAE plants. In contrast to current diabatic CAES plants, combustion of fossil fuels is not required to convert back to electrical energy. Previous experimental and theoretical studies showed that thermocline-based TES systems using a packed bed of rocks operate reliably and with high exergy efficiencies during steady cycling. Theoretically, the round-trip efficiency of an AA-CAES plant can reach 75%.

Energy-storage technologies operating in an electricity grid do not necessarily see steady cycling and therefore also need to be designed to operate efficiently under part load and irregular cycling. Grid simulations of a 100 MW / 500 MWh AA-CAES plant showed that the plant operates under multiple, uneven charge/discharge phases and varying loads. The present work investigates how the TES system can be designed to cope with the varying loads and how it can improve the overall plant performance.



SFERA-III - 1st Doctoral Colloquium

Odeillo, France.

September 11th - 13th, 2019

High-temperature thermochemical heat storage: development of materials and lab-scale packed-bed prototype

Marco Gigantino¹, Aldo Steinfeld¹

¹ *Department of Mechanical and Process Engineering, ETH Zurich, 8092 Zurich, Switzerland*

Heat delivered by concentrated solar systems can be stored for dispatchable use in the form of sensible heat, latent heat or chemical energy. The highest possible energy storage density can be theoretically achieved by the latter approach, the so-called thermochemical energy storage (TCS). Reversible gas-solid reactions of metal oxides are suitable to store/release heat at temperatures higher than the ones of commercially available thermal energy storage (TES) systems based on molten salts (~600°C). Of special interest are the carbonate system SrO/SrCO₃ and the redox system Cu₂O/CuO, which do not involve hazardous gases and store/release heat at around 1000°C, so that they can be safely integrated into more efficient heat engines, high-temperature chemical processes (e.g. cement manufacturing, mineral and metallurgical extraction, solid waste gasification), and advanced solar fuel synthesis. Due to thermal sintering, the energy storage capacity of these materials decreases during multiple temperature-swing cycles and prolonged exposure at high temperatures, but its detrimental effect can be hindered by engineering the materials properties. A systematic study on the use of different preparation methods (i.e. dry-mixing, wet-mixing, co-precipitation and sol-gel), as well as synthesis precursors and operating temperatures, has been carried out for SrO mixed with the sintering-resistant MgO in different concentrations. All the varied parameters affected the physical properties of the resulting materials and, in turn, their cycling performance. A formulation of MgO-stabilized SrO prepared by wet-mixing method featured a stable value of energy density of 810 kJ/kg over 100 consecutive carbonation/calcination cycles performed in a thermogravimetric analyzer by varying CO₂ partial pressure at 1000°C. Similarly, a particular composition of CuO mixed with the high-temperature-resistant Yr₂O₃-stabilized ZrO₂ (YSZ) featured a stable energy density of 560 kJ/kg over of 100 consecutive reduction/oxidation cycles between 950 and 1050 °C in air. Under similar conditions, the same material was also tested over 20 consecutive reduction/oxidation cycles in the form a packed-bed (50 mm Ø x 40 mm) of round-shaped granules. The latter were produced with an in-house developed granulation method.



Solar Facilities for the European Research Area

SFERA-III - 1st Doctoral Colloquium

Odeillo, France.

September 11th - 13th, 2019

The solar refinery: techno-economic potential of producing carbon-based fuels with concentrated solar power

Andreas Rosenstiel, Martin Roeb, Nathalie Monnerie, Stefan Brendelberger, Christian Sattler

German Aerospace Center (DLR) - Institute of Solar Research

CO₂ emissions in the transportation sector have to decrease significantly and as soon as possible in order to reach the target of the Paris agreement. One challenge is that some sectors strongly depend on the high energy density of carbon-based fuels. Especially in the aviation sector it seems that there are no alternatives to kerosene in the near future.

A possible solution to this problem is to produce carbon-based fuels with concentrated solar power, using as resources only water and CO₂. If the CO₂ is captured from air, the produced solar fuels are almost CO₂ neutral [1]. Using this technology in big scale would also give the possibility to import efficiently chemically stored renewable energy from countries with abundant solar irradiation.

In this work, different process configurations are evaluated in order to identify the most promising approach. Therefore, overall process concepts are developed, from the provision of the resources to the final product. Based on a process simulation, a techno-economic study will be performed for each concept. The basic concept is to use a thermochemical two-step redox cycle to split water and CO₂ and to produce thereby solar syngas, a mixture of hydrogen and carbon monoxide. For comparison, the solar syngas production via high-temperature electrolysis (HTE) powered by a hybrid power station, which combines CSP and PV electricity generation, is investigated. For the final fuel production from solar syngas there are two main possibilities which will be compared to each other: using a Fischer-Tropsch reactor or producing first the intermediate methanol and then the final product, e.g. gasoline (MtG). The demonstrated reactor efficiencies in thermochemical redox cycles are still relatively low and in the range of 5 % [2]. One part of the work is to investigate the potential of improving the overall efficiency through heat recuperation in the solar part. For example by using a thermal storage between the oxidation and the reduction step of the thermochemical cycle [3]. Furthermore, heat integration concepts shall be developed. A promising approach is, for example, to increase the overall efficiency and economic viability by using excess heat for the co-production of electricity [4]. As a final result, having identified the most auspicious technological approach, it will be possible to determine the framework under which these solar fuels can be introduced to the market.

References:

- [1] Falter, C. et al., Environmental science & technology (2015) 50(1), 470-477.
- [2] Marxer, D., et al., Energy & Environmental Science (2017), 10(5), 1142-1149.
- [3] Brendelberger, S. et al., Journal of Solar Energy Engineering (2019), 141(2), 021008.
- [4] Budama, V. et al, International Journal of Hydrogen 43 (2018).



SFERA-III - 1st Doctoral Colloquium

Odeillo, France.

September 11th - 13th, 2019

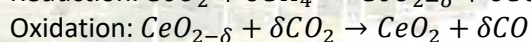
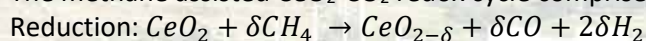
Performance Optimization of the CeO₂-CH₄-CO₂ Redox Cycle for Solar Fuel Production

Mario Zuber¹, Simon Ackermann², Philipp Furler², Aldo Steinfeld¹

¹ *Professorship of Renewable Energy Carriers, ETH Zürich, Switzerland*

² *Synhelion SA, Switzerland*

The methane assisted CeO₂-CO₂ redox cycle comprises two steps:



This cycle has been experimentally assessed to understand the effect of the CeO₂ morphology on the redox performance. A collection of specific surface areas (SSA) (0.04-4.85 m²/g) are tested over a range of temperatures. Morphologies include: laminate, pellet, felt, and reticulated porous ceramics (RPCs) with varying pore formers (5, 150 μm), pore former volume contents (PFC) (30, 50%), and sintering temperatures (1100, 1600°C).

Thermogravimetric relaxation experiments were carried out to provide a controlled environment for investigation of the reaction rates. Temperatures ranged from 900-1100°C with uniform gas composition (5% educt diluted in argon, 200 mL/min, L standard liters). The ceria reduction rates increased from 0.00024 to 0.28 min⁻¹ with increasing SSA and temperature. The oxidation rates increased from 0.050 to 0.182 min⁻¹ with higher SSA and lower temperature.

A tubular packed-bed reactor (d_i=1.9 cm, l≈30 cm) was used to investigate performance indicators such as conversions, selectivities, overall rates, and mechanical stability. Flow rates (1.1 L/min) and educt concentrations (5% diluted in argon) were kept constant. Samples with varying surface areas (1.61-230 m²) and mass loadings (22.62-92.76 g) were tested at various temperatures (900-1150°C). Experiments revealed an increase of the conversions (X_{CH₄}=0.091-0.98, X_{CO₂}=0.18-0.78) and redox rates (0.0030-0.043 min⁻¹ for reduction, 0.00090-0.0136 min⁻¹ for oxidation) with high SSAs (0.040-2.51 m²/g). Final multi-cycle testing at 990°C was conducted with the Standard RPC (150 μm-30% PFC, sintered at 1600°C) vs. the 5 μm-30% PFC RPC (sintered at 1100°C). The new morphology outperforms the standard with higher conversions (X_{CH₄}=0.16 vs. 0.83, X_{CO₂}=0.79 vs. 0.91) and selectivities (S_{CO}=0.75 vs. 0.91, S_{H₂}=0.65 vs. 0.85) due to its high SSA (2.51 m²/g) and mass loading (92.76 g).



SFERA-III - 1st Doctoral Colloquium

Odeillo, France.

September 11th - 13th, 2019

Solar-thermal oxygen pumping

Mathias Pein, Christos Agrafiotis, Martin Roeb, Christian Sattler

Deutsches Zentrum für Luft- und Raumfahrt e.V. (DLR)

Thermochemical H_2O and CO_2 splitting is a promising approach to convert and store solar energy. Further processing of the produced H_2 and CO , for instance via Fischer-Tropsch synthesis, enables a path to renewable carbon based fuels. Besides capable energy storage units for off-sun operation, efficient cycling of the active redox material (e.g. CeO_2) and high solar-to-fuel efficiencies are mandatory for economic CSP-plants. For high splitting ratios, low oxygen partial pressures during reduction are desirable. We report an approach to overcome the present energy penalties of high vacuum pumping or intensive inert-gas sweeping, using perovskite based oxides as a thermochemical oxygen pump. Our experimental campaign showed that Ca-Mn-based perovskites, used as oxygen pumping materials, can effectively increase the reduction extent of the state-of-the-art splitting material ceria (CeO_2). Utilizing the redox potential of the examined perovskite compositions in a temperature swing setup, oxygen can be removed from the reduction chamber of the ceria. Hereby the reduction extent of the ceria and hence the water-splitting capability of the reactor is increased. The oxygen pump material requires operational temperatures below $1000\text{ }^\circ\text{C}$, which allows implementing this application down-stream of the main reactor in a concentrated solar power (CSP) plant. Additionally, showing significant heat effects in the desired temperature range, oxygen pumping units may as well function as thermochemical energy storage in a plant. Our work includes a study of the thermal redox behavior using thermogravimetric analysis (TGA) and differential scanning calorimetry (DSC), exhibiting phase transitions between $800\text{-}1000\text{ }^\circ\text{C}$. We offer a derived model to predict and interpret phase transitions in the investigated perovskite compositions. The observed phase transitions are linked to endo- and exothermal heat effects, as well as substantial oxygen uptake and release. In future applications this correlation may be exploited to increase performance oxygen pumping and/or thermochemical storage units in the desired temperature range.

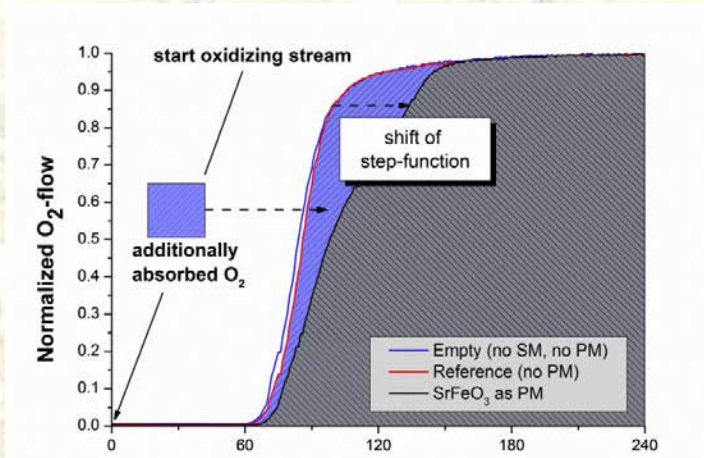
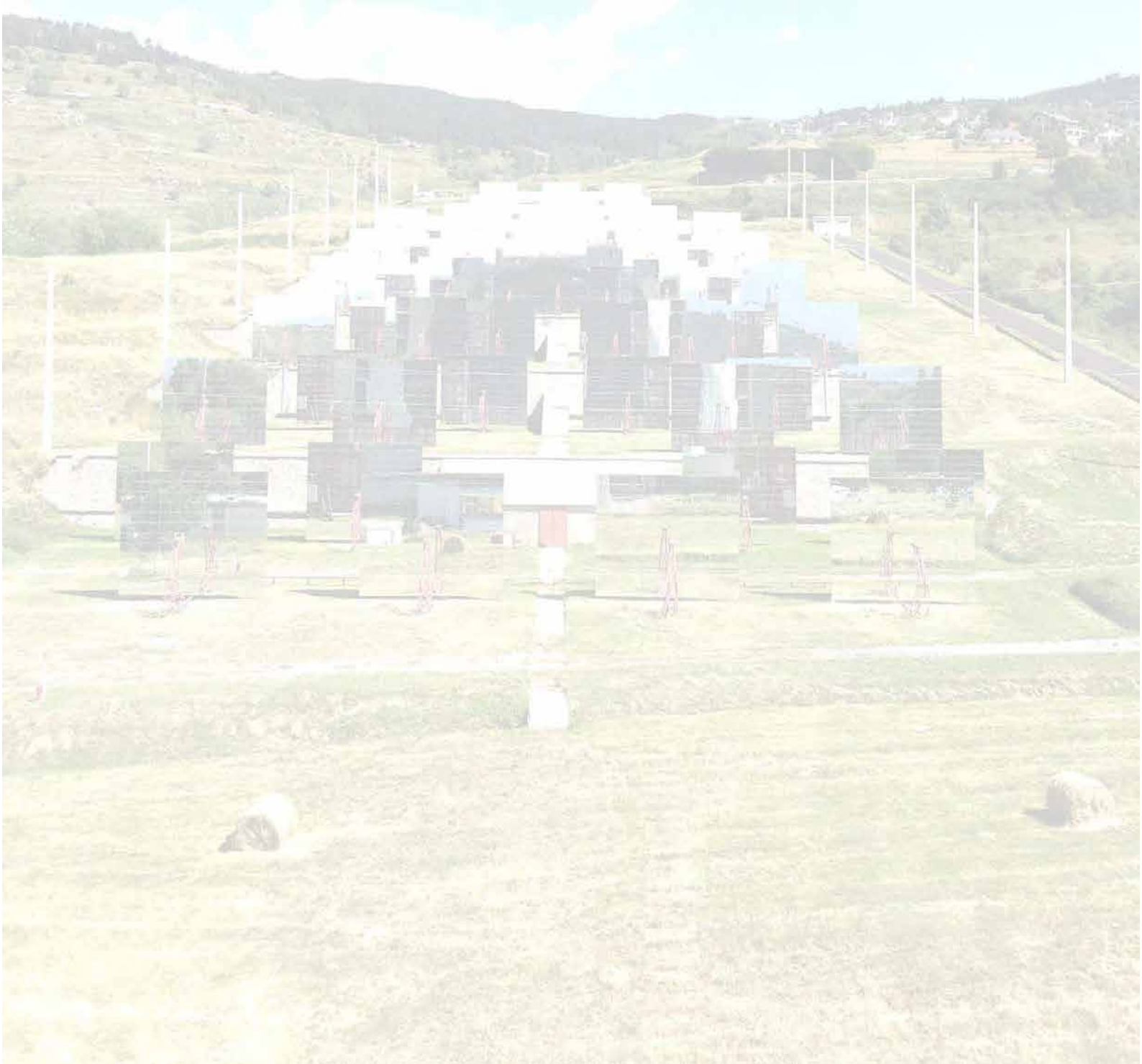


Figure 1: Graphical showing of the shift in the oxygen step function, illustrating the additional oxygen absorbed by the pumping material.

Session 2

Solar receivers

Chair: Sixto Malato, CIEMAT





SFERA-III - 1st Doctoral Colloquium

Odeillo, France.

September 11th - 13th, 2019

Numerical Simulation of 3D-Shaped Volumetric Absorbers

Broske, Robin Tim

German Aerospace Center (DLR), Institute of Solar Research

Recently developed new manufacturing methods, such as 3D printing, offer great potential to improve the open volumetric receiver technology for solar thermal power plants. The open volumetric receiver at the solar tower Jülich consists of ceramic honeycomb absorber structures manufactured by extrusion. Ceramic extrusion significantly limits possible shapes and sizes of the absorber flow channels. 3D printing and other additive and advanced manufacturing technologies allow a much greater degree of freedom, setting the task to design new absorber structures which take advantage of these new technologies and exploit the potential of the volumetric absorber principle. Therefore, a new concept is proposed for the numerical optimization of volumetric absorbers. This concept combines raytracing with 3D and 1D fluid simulations. The optimizations will be conducted with a 1D CFD model, a volume-averaged approach which does not resolve the absorber geometry, but instead makes use of effective parameters. Utilizing raytracing and 3D fluid simulations, numerical correlations are developed that link the effective parameters to the actual absorber geometry. This allows the optimization process to directly optimize the absorber geometry while taking advantage of the low computational effort required by the 1D model. This presentation focuses on the numerical correlations for the effective parameters. For the absorber employed at the solar tower Jülich and for a new design, numerical correlations have been developed for the optical, thermal and hydraulic effective parameters required by the 1D approach. The new design consists of a stair-shaped entrance region, rectangular channels in the middle section, and shifted-rectangular channels at the end. For each section, separate correlations were calculated, thus allowing each section to be optimized individually. The presented results are the first step towards realizing the proposed optimization concept. However, the numerical effort necessary for the calculation of the correlation needs to be further investigated with respect to the effort of the optimization itself.



SFERA-III - 1st Doctoral Colloquium

Odeillo, France.

September 11th - 13th, 2019

Process Assistance System for a molten salt receiver based on dynamic simulation models and artificial neural networks

Christian Schwager¹, Peter Schwarzbözl²

¹ *Solar-Institut Jülich of FH Aachen University of Applied Sciences, Germany,*

² *Institute of Solar Research, German Aerospace Center, Prof. Rehm-Strasse 1, 52428 Jülich, Germany*

A Molten salt central receiver (MSCR) is a mature and commercially proven technology for flexible solar power generation. Still, operating such a receiver system under real solar conditions serves some challenges. The need for draining the receiver during operation – especially when related to cloudy conditions – demands appropriate decision making by the operator and is crucial for the safety and yield of the plant.

For a better understanding of the system behavior during transitions between operation modes, a detailed process model of the receiver system including a dynamic two-phase (2P) fluid model for salt and air has been developed. The implemented process control system covers all operation modes as well as possible transitions including preheating, flooding and draining procedures. Since this model is coupled to a raytracing tool, it allows to simulate cloud passage scenarios considering partial shading of the heliostat field. Time dependent DNI-maps are either generated with a synthetic cloud passage algorithm or taken from measurement data such as cloud cameras and shading cameras.

The dynamic simulations revealed that the shape of passing clouds as well as the direction and velocity of their movement has significant impact on the short-term behavior of the receiver system and the net yield. Moreover, the development of a process assistance system based on the dynamic simulation model and results is in progress. It is supposed to predict trends of relevant state variable during the operation and provide suggestions for optimal decision making in regard to timing start-up procedures and temporary receiver drainage. A novel concept for applying an artificial neural network as replacement of a complex physical model has been devolved and will be open for discussion during the doctoral colloquium.



SFERA-III - 1st Doctoral Colloquium

Odeillo, France.

September 11th - 13th, 2019

High-temperature solar volumetric air receiver: lab-scale testing and computational modeling

Vikas R. Patil, Aldo Steinfeld

Department of Mechanical and Process Engineering, ETH Zurich, 8092 Zurich, Switzerland

We report on the results of lab-scale testing of a solar volumetric air receiver that could serve as a clean source of high-temperature heat for industrial applications that proceed at temperatures above 1000 °C. Examples of applications include the production of fuels from H₂O and CO₂ by redox cycles, processing of minerals by calcination and carbothermic reductions, and conversion of waste carbonaceous feedstock by gasification, reforming and pyrolysis. These highly endothermic processes proceed at high temperatures and discharge vast amounts of greenhouse gases derived from the combustion of fossil fuels. Emissions can be eliminated by supplying process heat via a heat transfer fluid (air) heated by concentrated solar energy. The solar receiver considered in this work consists of a cavity, lined with a reticulated porous ceramic (RPC) structure that is directly exposed to concentrated solar radiation entering the cavity through an open (windowless) aperture. A pump downstream of the receiver suctions ambient air into the cavity through the same open aperture. Air heats up as it flows across the hot RPC cavity and exits the receiver from the rear end. Two different RPC materials were tested: ceria (~7 ppi) and silicon-infiltrated silicon carbide (SiSiC, ~10 ppi). The receiver was tested at the High-Flux Solar Simulator of ETH Zurich, with four solar power input levels between 2.5-5.0 kW and for a range of air mass flow rates between 2-10 kg/h. Air outlet temperatures between 500°C to 1150°C were achieved under approximate steady-state conditions, with receiver thermal efficiencies – defined as the enthalpy change of the air flow divided by the solar radiative power input – up to 0.58. High air outlet temperatures (>1000°C) are achievable with reasonable thermal receiver efficiencies (>0.50) at high solar input powers (>4.0 kW). The experimental results will also serve to validate a computational heat transfer and fluid flow model, which is being developed to optimize receiver performance and scale-up.



SFERA-III - 1st Doctoral Colloquium

Odeillo, France.

September 11th - 13th, 2019

Test setup for the experimental evaluation of the convective heat transfer for nitrate salt in tubular solar receivers

Cathy Frantz, Reiner Buck

German Aerospace Center (DLR), Pfaffenwaldring 38-40, 70569 Stuttgart, Germany

Solar thermal power plants (CSP) can play an important role in the future international energy supply because of their ability to integrate cost-effective thermal storage and thereby decouple the energy generation from the fluctuating solar resource. Most recent project development news suggest that central receiver systems using Solar Salt (60wt% NaNO₃, 40wt% KNO₃) as a heat transfer fluid will turn to an industry standard in the near future. Central receiver systems consist of several thousand dual-axes tracking reflectors (heliostats), which concentrate sunlight on a tower-mounted heat exchanger (receiver) located at the center of the heliostat field. Inside the receiver, the solar salt flows through receiver tubes and is heated by the solar radiation. Thermomechanical analysis is fundamental in sizing of the receiver surface during plant design and in establishment of operational heat flux limits for heliostat field control. This requires an accurate estimate of the convective heat transfer coefficient on the medium side of the tube, typically done by using correlations for heat transfer in turbulent flow. However process flow conditions in molten salt receiver heat transfer tubes exceed the experimentally explored range of Reynolds number by a large margin. A.K. Das et al. found that in the region of interest for practical receiver design ($Re > 50'000$; $q_{flux} > 1000 \text{ kW/m}^2$), the correlations did overestimate the experimentally determined heat transfer data by up to a factor of three. It is the goal of the ongoing project to experimentally determine the heat transfer for the turbulent flow of molten salt at varying flux densities and to deduce correlations able to accurately model the convective behavior. For this purpose a test setup has been developed for the molten salt test area at the TESIS:com plant in Cologne. The measurement approach and design of the test setup will be presented and discussed with regards to the expected uncertainties.



SFERA-III - 1st Doctoral Colloquium

Odeillo, France.

September 11th - 13th, 2019

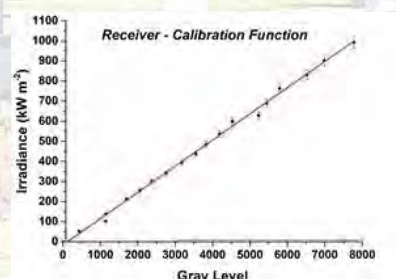
Measurement of high solar irradiance on receivers in solar tower plants

M. Casanova, J. Ballestrín, R. Monterreal, J. Fernández, E. Setien, J. Rodríguez

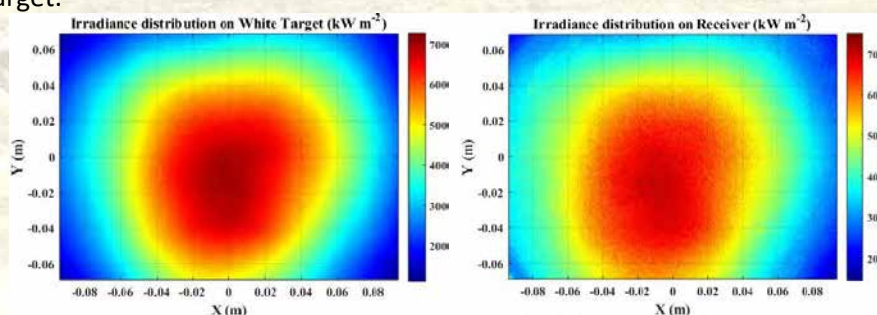
CIEMAT-Plataforma Solar de Almería

The solar tower power plants demand the measure of high solar irradiance on the receiver. Its measure would facilitate the operation of the plant and would contribute to a greater receiver security. These plants do not have a flux measurement system in their receiver as it is not considered in their design. The estimation of the incident irradiance is only calculated by simulations.

Traditional flux measurement methods, used during the evaluation of small solar receiver prototypes, turn to moving parts that can not extrapolate to large receivers of commercial solar tower plants due to upscaling problems. This work presents a simple method that allows characterizing a large target and quantifying its degree of homogeneity and diffusivity. With favourable information about receiver diffusivity, a procedure to measure directly high solar irradiance on the surface of the receivers of solar tower plants, without using moving parts, is presented. This measurement system would consist of a digital camera and a radiometer. A test to compare this system with the reference system (white lambertian target) has been done. The calibration of the measurement system is performed with the radiometer, as shown in the next figure:



With the calibration done with the radiometer, some images are taken with the digital camera. The calibration function is applied to these images to obtain a flux map. Finally, the flux map obtained with the measurement system is compared to the flux map obtained with the white lambertian target.





SFERA-III - 1st Doctoral Colloquium

Odeillo, France.

September 11th - 13th, 2019

Numerical Modelling of Particle Motion in Centrifugal Receiver

Serdar Hicdurmaz¹, Lars Amsbeck¹ and Bernhard Hoffschmidt²

¹*German Aerospace Center (DLR), Stuttgart*

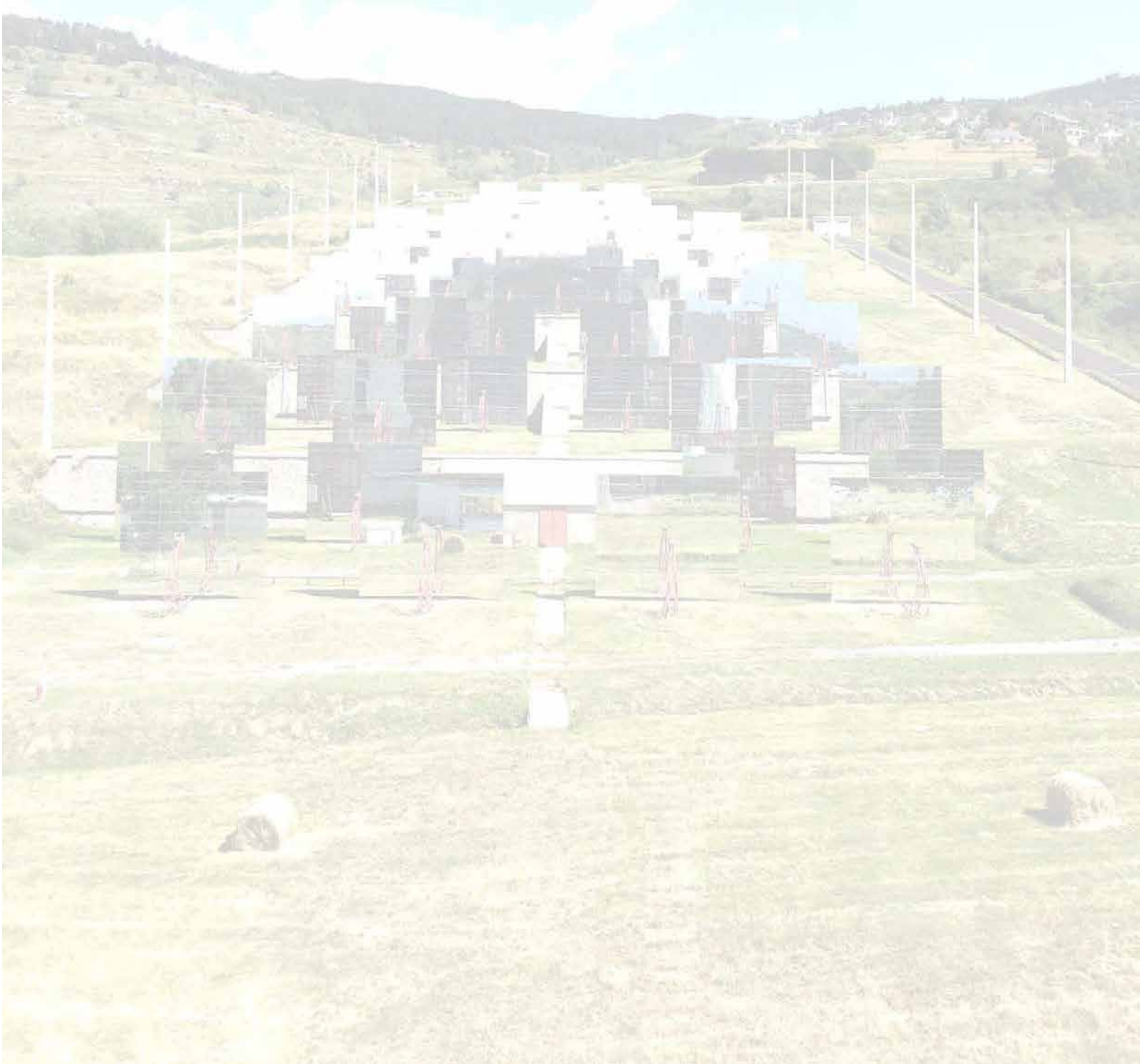
²*German Aerospace Center (DLR), Cologne*

Particle based solar receivers have some advantages as higher maximum receiver temperature and more efficient heat storage, over molten salt based systems. Centrifugal Receiver[®] designed by DLR is a promising technology in terms of scalability and receiver efficiency. In this type of solar receiver, the ceramic particles with various diameters (0.3 – 1 mm), which are accelerated centrifugally and gravitationally, are moving in an inclined rotating drum, and exposed to solar radiation. Particle residence time and eventually particle outlet temperature are controlled by adjusting the rotational speed and particle mass flow rate, which provides more operational flexibility compared to current designs. In this PhD study, four main tasks are planned. Firstly, the particle flow is numerically simulated by means of commercial (Rocky[®]) and/or open source (LIGGGHTS) Discrete Element Method (DEM) tools in order to form a basis for thermal model and experiments. This particle dynamics simulation is validated by experiments for many different operational parameters like rotational speed and mass flow rate. Secondly, a continuum model in Eulerian basis developed by exploiting DEM results is developed. In accordance with this purpose, moving particle bulk thermal conductivity model at near wall region will be developed. Thirdly, thermal model of complete receiver including insulations, convective, conductive and radiative losses are to be modelled. Finally, the results obtained in first three tasks will be used in scaling up of the numerically modeled receiver to larger receivers.

Session 3a

Solar field

Chair: Robert Pitz-Paal, DLR





SFERA-III - 1st Doctoral Colloquium

Odeillo, France.

September 11th - 13th, 2019

Deep Learning Algorithms for Heliostat Field Calibration

Max Pargmann¹ and Daniel Maldonado²

¹ *Phd-Student, Institute of Solar Research, German Aerospace Center (DLR), Linder Hoehe, 51147 Cologne (Germany)*

² *Dr.-Ing.-Researcher, Institute of Solar Research, German Aerospace Center (DLR), Linder Hoehe, 51147 Cologne (Germany), +4922036013981, Daniel.MaldonadoQuinto@dlr.de*

A precise and reliable alignment of the two axis heliostat tracking is of great importance for an efficient operation of solar power towers. In order to minimize the tracking error of heliostats, especially in large plants, it is essential to re-calibrate the heliostat control unit. Conventional calibration methods with regression can meet the requirements of frequent and regular use, but they cannot adequately account for the many factors that cause misalignment. We present an improved regression method based on deep learning algorithms which is independent of the number of influencing factors and demonstrate that it is possible to reduce tracking errors, compared to common algorithms. On the one hand we have created an image generative neural networks (NN), which can generate the target image during callibration exclusively from the sun position. On the other hand, we want to use these images to increase the accuracy of a second NN, which is used to control the heliostats smartly.

We use three different NN types. First, we use conditional Generative Adversarial Networks (cGANs). These are two competing NN where one (the generator) takes the sun position as inputs and generates target-images of it. The training is performed with images we took from our demonstration plant in Jülich. The second NN (the Discriminator) tries to distinguish the real images from the generated. The third has all inputs of the previous, but tries to predict the perfect Heliostat position, given by the measured Axes positions.

Since we generated the training data artificially, we focused on reducing the alignment error with as little training data as possible. In real power plants, depending on the size of heliostat field, only a few hundred data points per heliostat can be recorded within a year. We were able with less than 1000 images to compensate the error down to the machine accuracy.



SFERA-III - 1st Doctoral Colloquium

Odeillo, France.

September 11th - 13th, 2019

Dynamic Wind Loads on Heliostats: Experimental Investigation and Development of Acceptance Tests Based on Artificial Excitation

Kristina Blume¹, Marc Röger², Robert Pitz-Paal³

¹German Aerospace Center (DLR), Institute of Solar Research, Karl-Heinz-Beckurts-Str. 13, 52428 Juelich

²German Aerospace Center (DLR), Institute of Solar Research, Plataforma Solar de Almería, 04200 Tabernas, Spain

³German Aerospace Center (DLR), Institute of Solar Research, Linder Höhe, 51147 Cologne, Germany

Kristina.Blume@dlr.de

Wind loads, occurring as static and dynamic loads, are of major importance for heliostats in a number of ways. Static loads can cause damage to heliostats due to overstressing during strong wind conditions while dynamic loads may cause fatigue failure. Such aspects regarding mostly survivability and lifetime have been investigated extensively in the past for example in wind tunnel tests [1]-[2]. Regarding dynamic loads, not only fatigue failure is a concern but especially the tracking accuracy as well as the optical performance can be significantly affected. Investigations on those concerns have yet been mostly limited to numerical [3]-[4] or wind tunnel [5] investigations, both in the need of using heliostat models which can represent neither a realistic dynamic behavior nor realistic wind conditions entirely. To address both problems, experimental investigations on real-scale heliostats under real wind conditions were performed at the DLR site in Juelich and give insights into a heliostat's dynamic behavior. One focus of the presented work is to firstly understand the response of a heliostat to dynamic wind loads, for example which eigenmodes get excited and how the heliostat oscillates under certain wind conditions. Such experimental investigations come at the cost of test execution time. Proper wind conditions are rare and parameters such as mean wind speed and wind direction are not adjustable. For this reason, a second part of the presented work focuses on the development of methods to artificially excite heliostats in a similar fashion to wind. Once an artificial excitation method is developed, the aim is to implement acceptance tests in order to compare the performance of different heliostat types under wind loads.

- [1] Peterka, J. et al. *Mean and peak wind loads on heliostats*, Journal of Solar Energy Engineering, 111(2), pp. 158-164, 1989
- [2] Pfahl, A. *Wind loads on heliostats and photovoltaic trackers*, Dissertation, Technische Universiteit Eindhoven, 2018
- [3] Vásquez-Arango, J. F. *Dynamic Wind Loads on Heliostats*, Dissertation, Rheinisch-Westfälische Technische Hochschule Aachen, 2016
- [4] Zang, C. et al. *Numerical simulation of wind loads and wind induced dynamic response of heliostats*, Proc. of the 19th SolarPACES Int. Conference, Las Vegas, USA, Sept. 17-20 2013
- [5] Huss, S. et al. *Evaluating effects of wind loads in heliostat design*, Proc. of the 17th SolarPACES Int. Conference, Granada, Spain, Sept. 20-23 2011



SFERA-III - 1st Doctoral Colloquium

Odeillo, France.

September 11th - 13th, 2019

Dynamic aimpoint management for performance enhancement in solar tower power plants

Laurin Oberkirsch

DLR, Institute for Solar Research, Cologne

The main objective of aimpoint management systems is the safe operation of solar tower power plants at higher efficiencies than with conventional, conservative control techniques. In order to achieve this aim, aimpoint optimization is indispensable, even though it suffers from highly fluctuating environmental conditions such as cloud courses. Nowadays, solar tower power plants can be equipped with measurement systems. These systems nowcast the cloud course on the one hand and determine the temperature of the receiver as well as the irradiation onto the receiver's surface on the other. An aimpoint management system is able to process these measurement data and selects based on a decision tree the operation mode. The applied aimpoint optimization is based on the raytracing software "STRAL" and uses a hybrid optimization technique that couples an ant colony optimization algorithm with a local search algorithm. Moreover, a grouping strategy is employed to reduce significantly the solution space for the optimizer. The grouping is performed by the k-means clustering method based on the heliostats' radial and circumferential position. In order to reduce the optimization time further the irradiation onto the receiver's surface is precalculated for each heliostat group and for each aimpoint during the off-time of the plant for multiple sun positions. This outlined aimpoint optimization contains several tunable parameters such as optimization duration or number of groups. Depending on the cloud nowcast, the aimpoint management system assigns values to these parameters. The processing of nowcast data and the enhanced convergence rates from the optimizer convert the previously static aimpoint optimization into a dynamic one. Consequently, the implementation of an aimpoint management system in a real plant is feasible despite the fluctuating environmental conditions, so that the plant's performance is enhanced.



SFERA-III - 1st Doctoral Colloquium

Odeillo, France.

September 11th - 13th, 2019

Experimental and numerical evaluation of drift errors in a solar power tower facility with tilt-roll tracking-based heliostats

Alejandro Martínez Hernández, Iván Bravo Gonzalo, Manuel Romero and José Gonzalez-Aguilar

IMDEA Energy Institute, Ramón de la Sagra 3, 28935 Móstoles, Spain

Solar power tower facilities make use of sun-tracking mirrors, called heliostats, to focus solar radiation in a specified aiming point on a target. In this context, a relevant problem to be tackled is the deviation of the focused solar beam with respect to the aiming point along the time of the day, known as drift. In this work, we experimentally and numerically evaluate the drift errors in a solar tower facility with tilt-roll tracking-based heliostats. For this investigation, the solar power tower facility located at IMDEA Energy in Móstoles (Spain) is used as a test case. By acquiring flux maps at different times of the day and representing their maximum irradiance point as a function of the time, the drift is evaluated experimentally. We observed that the experimental drift can be divided in two components, vertical and horizontal, with a constant velocity of the maximum irradiance point of -7.4 cm/h and 2.2 cm/h, respectively. In order to investigate the source of the drift observed in the experiment, detailed Monte Carlo ray-tracing simulations including possible misalignments in the heliostat tracking system were performed. We found out that by considering rotations of the heliostats pedestal, the experimental drift is very well reproduced by the simulations. In particular, for a rotation of the pedestal of 17 mrad towards the east, the velocities of the maximum irradiance point in the simulations are -7.6 cm/h and 1.1 cm/h for the vertical and horizontal drift components, respectively.

Session 3b

Materials and durability

Chair: Robert Pitz-Paal, DLR





SFERA-III - 1st Doctoral Colloquium

Odeillo, France.

September 11th - 13th, 2019

Elaboration, performance and durability analysis of selective coatings for CSP

D. Ngoue^{1,2}, A. Diop², A. Carling-Plaza¹, A. Grosjean^{1,2}, V. Pares^{1,2}, A. Soum-Glaude¹, S. Quioizola^{1,2}, E. Hernandez^{1,2}, L. Thomas^{1,2}

¹ PROMES-CNRS laboratory, Odeillo/Perpignan

² University of Perpignan Via Domitia (UPVD)

Energy consumption is increasing every day while the usual resources (fossil fuels: oil, coal, and gas) are declining. To overcome this energy resource problem, technologies using renewable energies are in full development. Among them, concentrated solar power plants (CSP) allow producing heat and electricity from solar energy. Their expected contribution to the energy mix in 2050 is estimated between 8% and 12% (830 GW deployed) by different sources (SolarPACES, ESTELA, Greenpeace). In CSP plant technologies, the solar field is a major part of the total investment cost (40%) and the first cause of energy losses: only 50% of the incident solar energy is converted into heat (first conversion step). To improve the global efficiency of CSP, it is necessary to improve the efficiency of the receivers by coating the key optical elements: mirrors, glass windows and absorbers. In the case of absorbers, coatings lead to selective thermo-optical surfaces with a high absorptivity in the solar spectrum (0.28-2.5 μ m) and a low emissivity in the infrared spectrum that limits radiative thermal losses. Due to the solar intermittence and needed high working temperatures (> 400°C), it is necessary to develop coatings with a high thermal resistance in air. To achieve this goal, our work is focused on the elaboration and optimization of metal/dielectric selective coatings by plasma technologies. These metal/dielectric coatings are W/SiCH multilayers, synthesized by microwave-assisted PACVD of TMS (Tetramethylsilane) for SiCH layers, and magnetron sputtering of Tungsten targets for W layers. Correlations between the nature of the plasma and the monolayers physicochemical composition, both depending on the deposition process parameters, were investigated to better control the materials properties. Indeed, process parameters influence the chemical and thermo-optical characteristics of the coatings and give rise to a wide range of optical properties ($n(\lambda)$, $k(\lambda)$) for the monolayers [$1.7 < n < 2.7$ (SiC:H), $3.2 < n < 3.7$ (W)]. The corresponding W/SiCH multilayers present interesting optical properties with a solar absorptance up to 80% and IR emissivity down to 15% at 550°C, allowing for high solar thermal efficiencies. They were deposited on high temperature metals (steels, Inconel) and did not exhibit any surface or thermo-optical degradations after annealing for few tens of hours at 500°C under oxidant atmosphere. In order to improve efficiencies, thermo-optical simulations were performed. They suggest that composites with W metallic particles directly embedded in a SiCH matrix lead to even higher efficiencies than the W/SiCH corresponding multilayers.



SFERA-III - 1st Doctoral Colloquium

Odeillo, France.

September 11th - 13th, 2019

An effective simulation route for the ternary phase diagram: $\text{NaNO}_3\text{-KNO}_3\text{-NaNO}_2$

Tiziano Delise^{1,2}

¹ *Department of Chemical Science and Technologies, University of Rome Tor Vergata, Via della Ricerca Scientifica 1, 00133 Rome, Italy*

² *ENEA- Italian National agency for new technologies, energy and sustainable economic development, DTE-STSN-ITES Technical unit for renewable energy sources, Casaccia Center Rome*

The liquidus temperatures of nitrate/nitrite based mixtures are a crucial key parameter to take into account for the development of feasible Heat Transfer Fluids (HTF) and Heat Storage Materials (HSM). The scientific literature is poor about this topic, despite the high variety of molten salt mixtures proposed for practical use. The experimental determination of phase diagrams for ternary or multicomponent systems can be expected to be very time demanding and costly.

For this reason, the computing simulation looks as a preferable way. At this aim, a thermodynamic model for equilibrium phase transitions was developed and validated, in particular, a semi-empirical regular solution model was adapted to obtain nitrate/nitrite ternary phase diagram and a Matlab code was utilized to implement the algorithm.

The ternary $\text{NaNO}_3/\text{KNO}_3/\text{NaNO}_2$ was considered for the modeling, and the three binary sub-system were employed to determine the fitting parameters.

The result of the simulation were validated with experimental data obtained by DSC. The calculated isothermal curves were in very good accordance with the experimental values.

This modeling campaign allowed to detect several innovative good candidates as HTF or TES, especially considering the possibility to reduce the more costly component (KNO_3) maintaining at the same time a low liquidus temperature.



SFERA-III - 1st Doctoral Colloquium

Odeillo, France.

September 11th - 13th, 2019

Aging and durability studies of solar selective absorber coatings in air at high temperature

A. Carling-Plaza¹, M. Bichotte², A. Soum-Glaude¹, M.A. Keilany¹, L. Dubost² and L. Thomas³

¹ PROMES-CNRS, Font-Romeu Odeillo, France

² HEF-IREIS, Saint-Etienne, France

³ PROMES-CNRS, Tecnosud / Université Perpignan Via Domitia, Perpignan, France

Corresponding author: Alex.Carling-Plaza@promes.cnrs.fr, +33 788 981 161

In CSP applications, the optical efficiency of solar receiver is pivotal. A selective behavior, combining high solar absorptance to increase the amount of absorbed solar energy, and low infrared emittance to limit radiative thermal losses, is sought for, especially for receiver temperatures below 650°C. In the latter case, these properties can be achieved by functionalizing the surface of the metallic receivers with solar selective absorber coatings (SSACs). The SSACs must however withstand extreme conditions of use during several tens of years of operation: concentrated solar irradiation, high temperatures, cyclic and quick thermal loads, contact with oxygen and water vapor, etc. This implies many thermally-induced and thermomechanical aging phenomena, such as oxidation and corrosion, diffusion, cracking, fatigue, creep, etc. These phenomena can be detrimental to the optical properties and efficiency of the materials, and must be studied to provide more efficient and durable solutions.

As an example, a TiAlN tandem absorber SSAC on Inconel is tested, showing one of the most promising coating solutions for CSP receivers operating at medium-high temperature (500°C), in terms of their durability. A programmable electrical tubular furnace (Fig. 1) working in static ambient air was used to apply long-term cumulative aging, both at a temperature representative of real conditions of use, i.e. 500°C, for up to 1000 h, and at higher temperatures up to 800°C (accelerated aging). Spectral reflectance was systematically measured as-deposited and after each aging step of typically 24 hours and the chemical composition was regularly measured by EDS to follow the oxidation behavior. The samples show long-term thermal stability of their optical properties at 500°C in air (Fig. 2) and low oxidation indicating the formation of a stable oxide layer acting as barrier for further oxidation. Such high durability has seldom been demonstrated for a high temperature SSAC in air, rendering it very promising for CSP applications.

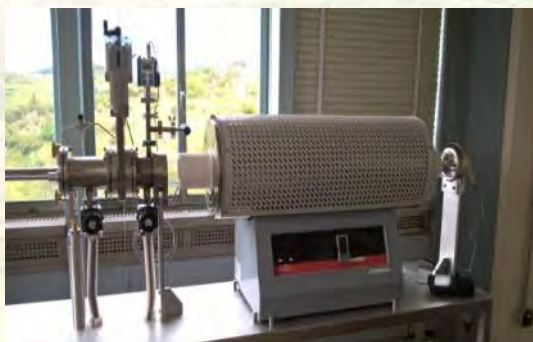


Figure 1 - ALTHAIA facility (Aging Long-term Tests in Humid Air or Inert Atmosphere)

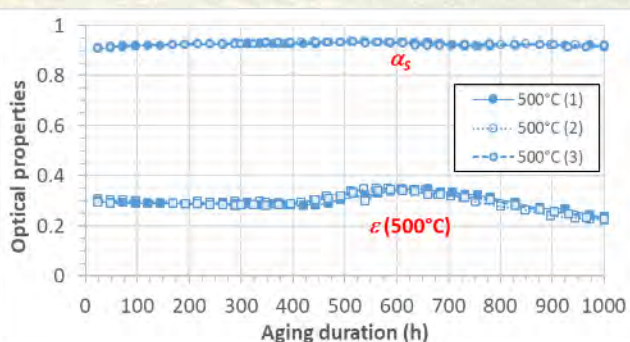


Figure 2 - Performance evolution of TiAlN tandem selective coating vs. aging duration at 500°C in air



SFERA-III - 1st Doctoral Colloquium

Odeillo, France.

September 11th - 13th, 2019

Lifetime prediction of solar mirrors used in concentrating solar thermal energy

Francisco Buendía-Martínez¹, Aránzazu Fernández-García¹, Florian Sutter², Johannes Wette² and Loreto Valenzuela¹

¹CIEMAT-Plataforma Solar de Almería, Senes Road, km. 4.5, P.O. Box 22, E04200 Tabernas, Spain.

²German Aerospace Center (DLR), Plataforma Solar de Almería, Senes Road, km. 4.5, P.O. Box 44, E04200 Tabernas, Spain

CIEMAT-PSA

Lifetime prediction of solar mirrors used for concentrating solar thermal (CST) energy is a relevant topic to improve this kind of renewable energy technology. Usually, materials employed in CST should maintain their initial behavior over 25 years for making profitable the construction, operation and maintenance of a CST plant. Hence, it is necessary to estimate the durability of the different components before being installed. In this work, primary and secondary solar reflectors are analyzed to obtain suitable correlations that predict their useful life.

Primary reflectors are the first elements where solar radiation impacts in a concentrating solar collector and is reflected to reach the receiver. The installation of adequate primary mirrors is vital for a proper operation of a plant. Newly developed and commercial mirrors were tested in several accelerated aging chambers and exposed in 11 representative sites worldwide. Samples were collected every year to know the main degradation mechanisms. Three main degradation mechanisms were identified: solarization and erosion of the glass and corrosion of the silver layer. Different climatic chambers were used to simulate those effects in the laboratory. It was observed that reflectors with a smaller number of paint layers are much more affected by corrosion. In addition, it was demonstrated that the use of high-iron glass is neither appropriate for commercial nor research purposes because of absorption losses and the effect of solarization, which may lead to erroneous conclusions about the degradation rates of the silver layer.

Regarding the secondary mirrors, they are employed to minimize spillage losses of the receiver by focusing part of the scattered radiation of the primary mirrors in some concentrating solar technologies. Batches of samples manufactured by an experienced solar institution were studied. In this case the testing conditions were focused on the high temperatures achieved by the secondary mirrors under real operating conditions. A test in a solar furnace was carried out to reach high flux and temperature on the reflector material (see Figure 1). Moreover, additional aging chamber experiments were performed under accelerated aging conditions to simulate the start-up and shut-down of the plant, the normal operation and the night conditions.



Figure 1. Secondary mirror thermal test in a solar furnace (CIEMAT-PSA).

Session 4

Hybrid and advanced solar processes

Chair: Alain Dollet, CNRS





SFERA-III - 1st Doctoral Colloquium

Odeillo, France.

September 11th - 13th, 2019

Electrochemical wastewater treatments enhanced by combination with solar energy

I. Salmerón ^{a,b}, G. Rivas ^{a,b}, I. Oller ^{a,b}, S. Malato ^{a,b}

^a *Plataforma Solar de Almería-CIEMAT, Carretera de Senés Km 4, 04200 (Tabernas, Almería), Spain*

^b *CIESOL, Joint Centre of the University of Almería-CIEMAT, 04120 Almería, Spain*

Contaminants of emerging concern (CECs) are compounds which their presence in water entails a great risk to the ecosystems and human health. They are commonly personal care products, pesticides, pharmaceuticals, etc. at very low concentrations ($\mu\text{g L}^{-1}$ - ng L^{-1} range) which escape from conventional municipal wastewater treatment plants (MWWTP) based on a biological treatment due their biorecalcitrant character.

In this context, Electrochemical Advanced Oxidation Processes (EAOPs) are an interesting alternative for the removal of these contaminants due to their ability to generate radicals and oxidant species such as $\cdot\text{OH}$ ($E^0 = 2.8 \text{ V}$), HClO ($E^0 = 1.49 \text{ V}$); and ClO^- ($E^0 = 0.89 \text{ V}$) from ions present in water. These processes might be improved by using a carbon-based electrode as cathode responsible of the electrogeneration of H_2O_2 , thus being only necessary the addition of iron to promote Fenton reactions. Additionally, the combination of EAOPs with solar energy allows not only the regeneration of iron (II) from electro-Fenton process but also it promotes the formation of Cl^* ($E^0 = 2.4 \text{ V}$) from electrogenerated ClO^- and so increasing significantly the oxidative power of the treatment.

This study addresses a comparison of electrochemical processes (Fig. 1), assisted or not by solar energy, in a real effluent of a secondary treatment from a MWWTP (Almería, Spain) previously pre-concentrated by nanofiltration (NF) membranes. Permeate of NF produces a clean effluent and microcontaminants contained in the NF retentate can be removed by EAOPs, easier to operate in a highly saline effluent as NF retentate. Selected target compounds were pentachlorophenol, terbutryn, chlorfenvinphos and diclofenac in a concentration of $100 \mu\text{g L}^{-1}$ each.

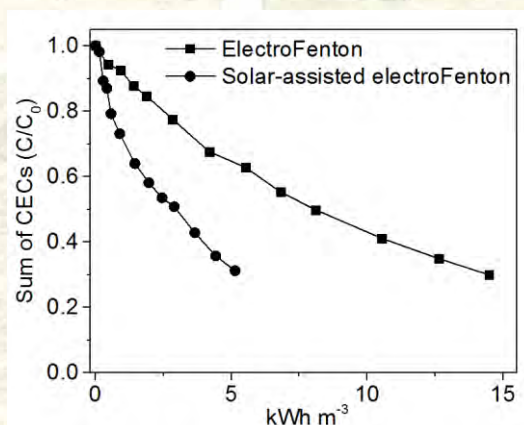


Figure 1. Degradation profile of the sum of CECs by electroFenton and solar-assisted ElectroFenton processes



Solar Facilities for the European Research Area

SFERA-III - 1st Doctoral Colloquium

Odeillo, France.

September 11th - 13th, 2019

EVALUATION OF A NEW SOLAR PHOTO-REACTOR FOR SOLAR WATER DISINFECTION

A. Martínez-García^a, I. Oller^a, P. Fernández-Ibáñez^b, M.I. Polo-López^a

^aPlataforma Solar de Almería-CIEMAT, Carretera Senés Km 4, Tabernas (Almería), Spain.

^bNanotechnology and Integrated BioEngineering Centre, School of Engineering, University of Ulster, Newtownabbey, Northern Ireland, United Kingdom.

Nowadays, access to fresh water is becoming one of the main concerns all around the world with a higher impact in developing countries where the lack of sanitation ends in diseases outbreaks associated to contaminated water consumption. To prevent and reduce the impact on human health, the improvement of safe drinking water is required. The commonly recommended water treatment procedures at household level are chlorination, filtration and boiling. However, another feasible treatment that can be use in these low-income countries is solar water disinfection (SODIS). Typically, it consists on the exposition of 1-2L PET (polyethylene terephthalate) bottles filled with dirty water to solar radiation under sunny conditions for 6 h, after this the water quality is improved and it is safer to drink it for the next 24 hours after treatment (McGuigan et al., 2012). The SODIS method procedure has some major drawbacks, including the reduced volume of water treated per batch and the long time required for effective treatment. In this line, a number of studies on developing new engineered designs of low-cost solar reactors to increase the water output have been reported last years (McGuigan et al., 2012). Some of them use the Compound Parabolic Collector (CPC) solar mirrors to increase the solar UV input. They have been demonstrated to be a promising option, although still being expensive for low income areas (Ubomba-Jaswa, et al., 2009).

In this research, a new design of solar photo-reactor with tilted-flat U-shaped reflectors has been conceptualized to reduce complexity and the manufacturing and installation costs. A V-trough solar pilot plant has been built to assess the solar disinfection performance of the new reflector against the commonly used CPC. In addition to the comparison of the two designs, some key factors for solar disinfection, i.e. dissolved oxygen, water circulation, and water temperature, have been evaluated. The inactivation of *Escherichia coli* K-12 (CECT 4624), *Enterococcus faecalis* (CECT 5143), *Salmonella sub enteritidis* (CECT 4155) and *Pseudomonas aeruginosa* (CECT 110) spiked on demineralised water (DW) with 0.9% of NaCl and on Synthetic Rain Water (SRW) with an initial concentration of 10⁶ CFU/mL have been assessed. Results showed similar inactivation profiles in both CPC and V-trough solar reactors, though no improvement on the disinfection efficiency was detected when testing the influence of the aforementioned key factors. Therefore, this work shows that the easiest and lowest cost option for disinfecting large amount of water is the new V-trough mirror working on a static mode operation.

References

- McGuigan, K.G., Conroy, R.M., Mosler, H.J., du Preez, M., Ubomba-Jaswa, E., Fernández-Ibáñez, P., J Hazard Materials, 29–46 (2012) 235.
- Ubomba-Jaswa, E., Navtoft, C., Polo-Lopez, M.I., Fernández-Ibáñez, P., McGuigan, K.G., Photochemical & Photobiological Sciences, 8 (5) (2009), 587.



SFERA-III - 1st Doctoral Colloquium

Odeillo, France.

September 11th - 13th, 2019

Application of Advanced Integrated Technologies (Membrane and Photo-Oxidation Processes) for the Removal of CECs contained in Urban Wastewater

Dennis Deemter^{1*}, Isabel Oller¹, Sixto Malato¹, Ana M. Amat².

*(1) Plataforma Solar de Almería-CIEMAT, Carretera de Senés Km 4, Tabernas (Almería), Spain; (2) Grupo Procesos de Oxidación Avanzada, Campus de Alcoy, Universitat Politècnica de València. Spain; *ddeemter@psa.es*

The availability of clean water is decreasing due to climate variation, droughts, rising population and pollution. Therefore, new methods must be found to recycle used water and prevent contaminants to pass conventional wastewater treatment techniques. Contaminants of Emerging Concern (CECs) are substances increasingly found in urban wastewater in ranges up to $\mu\text{g/L}$ and originate from usage and disposal of many modern products. Their main sources are traceable to the use of pesticides, pharmaceuticals and other organic compounds. New perspectives in the solution of this problem can be found in the combination of Nano filtration (NF) by membranes and Advanced Oxidation Processes (AOPs). The latter are processes whereby highly reactive hydroxyl radicals are generated to eliminate the CECs. Photo-Fenton is an AOP based on the catalytic cycle of iron ($\text{Fe}^{2+}/\text{Fe}^{3+}$), promoted by hydrogen peroxide and UV-vis light, producing hydroxyl radicals. Its main advantage is that it uses simple chemicals and irradiation coming from the Sun, with already available technology.

In this project the AOPs will be combined with NF systems in a unique innovative hybrid tool. The key objectives of this work are the development and operation (batch and later continuous mode) of NF membrane systems based on a commercial polyamide material and to develop high-flux ceramic membranes within the MSCA-AQUALITY project. These new membranes must show high rejection for CECs, high water permeability, high resistance to fouling and high stability for cleaning and disinfection treatments.

An evaluation of the effect of salinity and operational parameters has been performed. Contaminants were selected based on their common presence and/or persistence in urban wastewater effluents at a working concentration of $100 \mu\text{g/L}$. Naming: Caffeine, Imidacloprid, Thiacloprid, Carbamazepine and Diclofenac. The used matrices are well water (Tabernas, Spain) and urban wastewater treatment plant effluents that were spiked with these compounds. The next step in this work will be the application of the solar photo-Fenton to the filtration effluents. All having variable concentration factors and CEC concentrations at conventional photo-Fenton optimal pH (pH 3) and at natural pH using Fe-EDDS complexes.

Acknowledgements. The authors wish to thank the European Union for funding under the Marie Skłodowska-Curie Actions (MSCA) – Innovative Training Networks (Call: H2020-MSCA-ITN-2017). Project Nr. 765860 (<https://www.aquality-etn.eu/>) and furthermore Mr. D. Deemter wishes to thank CIEMAT-PSA (<https://www.psa.es>) for their cooperation.



Solar Facilities for the European Research Area

SFERA-III - 1st Doctoral Colloquium

Odeillo, France.

September 11th - 13th, 2019

PV/CSP hybrid system

Dounia Ziyati, Alexis Vossier, Alain Dollet

Processes, Materials and Solar Energy (PROMES)-CNRS, Odeillo, France

How can we meet the energy needs of the population while protecting our planet? Are we going to be able one day to rely on clean and green energy sources to provide our electricity? Two of many more questions that keep coming out during the last years. Due to, the climate change issues and the drastic rise in CO₂ emissions, scientists and researchers are more than before determined to develop and study new and/or existents technologies that can use free and renewable energies.

One of the most abundant sources of energy on earth is solar energy. Free to get, but hard to convert into useful energy with high efficiencies. Therefore, hybrid systems, combining concentrated photovoltaic (CPV) with concentrated solar power (CSP) systems may offer an interesting approach, thanks to the important amount of benefits this system may represent comparing to CPV-alone or CSP-alone technologies. Offering a better quality production of electricity combined with a low cost, which are the main problems of the stand-alone CPV and CSP technologies.

Developing a compact CPV/CSP hybrid system implies that both technologies will have to operate under similar temperatures up to 400°C. A temperature range that is well known and experimentally tested for the CSP systems, while until today it remains quite unknown for PV.

Before going forward, we should be able to develop adequate models describing the behavior of solar cells operating under very high temperatures and concentrations, and then conduct experimental tests to confront theory to experiments. After conducting a detailed state of the art we observed that the gap between existent models tend to become more important when we move toward high temperatures for that our work has been concentrated on identifying the adequate model.



SFERA-III - 1st Doctoral Colloquium

Odeillo, France.

September 11th - 13th, 2019

Investigation of electrostatic precipitation to avoid particles deposition on a solar reactor window

Juan P. Rincon-Duarte, Stefania Tescari, Thomas Fend, Martin Roeb, Christian Sattler

German Aerospace Center (DLR), Institute of Solar Research, Linder Hoehe, 51147 Cologne, Germany

Solar production of Calcium Oxide (CaO) is a promising way to reduce the CO₂ emissions from the cement industry. To carry out this thermochemical process, closed solar reactors with continuous processing are needed. Indirect heated solar reactors to carry out this process have been designed and tested at lab-scale. However, the main drawback of these designs is the low reactor efficiency, because of the formation of a solid material layer in the inner reactor wall that works as a thermal resistance of contact. Therefore a higher energy input and higher temperatures at absorbing surfaces are needed to reach the reaction temperature inside the reactor.

On the other hand, in designs where the material is directly heated, a window is needed to allow the access of solar radiation into the reactor. After some time of operation, this window tends to be damaged due to the overheating of solid material deposited on it [1]. For this reason, one of the major challenges here is to prevent the migration of particles to the reactor window.

The most well-known method to protect the window of solar reactors is implementing a gas curtain or a gas vortex flow, as shown in the solar reactor of Koepf et al. [2]. Nevertheless, results of a 100 % protected window have not been reported yet, and the low reactor efficiency of these approaches due to the high amount of inert gas used is still a topic of discussion.

The focus of the present work is the investigation of using electrostatic precipitation, to solve the task of keeping the window free of particles and fines in a solar rotary kiln for the solar production of CaO. An Electrostatic Precipitator (ESP) works using the corona discharge effect. Here, an electrical field between two electrodes ionizes the gas molecules which charge the solid particles in the gas. The charged particles can be collected on the surface of the collecting electrode. ESPs have been operated in high concentrated CO₂ atmospheres, as well as in other gas media at temperatures over 900 °C, showing separation efficiencies higher than 90 %. The electrical resistivity of CaO at temperature values of 950 °C is in the range where an ESP can be operated (10⁴-10¹¹ Ω-cm) [3]. However, the construction of an ESP to separate CaO from a 100 % CO₂ atmosphere at temperature values over 900 °C and the possibility of its later implementation in a solar reactor has to be demonstrated.

References:

[1] T. Litterst, *Investigation of window damage by hot particles in solar heated circulating fluidized beds*, Deutsche Forschungsanstalt für Luft- und Raumfahrt (DLR), 1993

[2] E. Koepf, W. Villasmil, A. Meier, *Demonstration of a 100-kWth High-Temperature Solar Thermochemical Reactor Pilot Plant for ZnO Dissociation*, AIP Conference Proceedings 1734, 2016.

[3] N. A. Surplice, *The electrical conductivity of calcium and strontium oxides*, Brit. J. Appl. Phys, 1966.



THIS PROJECT HAS RECEIVED FUNDING FROM THE EUROPEAN UNION'S HORIZON 2020 RESEARCH AND INNOVATION PROGRAMME UNDER GRANT AGREEMENT NO 823802



Solar Facilities for the European Research Area



Annex 4. Presentations at the 1st Summer School

SFERA-III

Solar Facilities for the European Research Area

1st Summer School “Thermal energy storage systems, solar fields and new cycles for future CSP plants”
WPI Capacity building and training activities
Odeillo, France, September 9th-11th 2019



“The CSP technologies: market status and
opportunities for R&D”
Alain FERRIERE, CNRS-PROMES

NETWORKING



THIS PROJECT HAS RECEIVED FUNDING FROM THE EUROPEAN UNION'S HORIZON 2020 RESEARCH AND INNOVATION PROGRAMME UNDER GRANT AGREEMENT NO **823802**

“The CSP technologies: market status and opportunities for R&D”

LABORATOIRE
PROCÉDÉS, MATÉRIAUX
et ENERGIE SOLAIRE

UPR 8521 du CNRS,
conventionnée avec
l'université de Perpignan

PROCESSES, MATERIALS
and SOLAR ENERGY
LABORATORY



Alain
FERRIERE

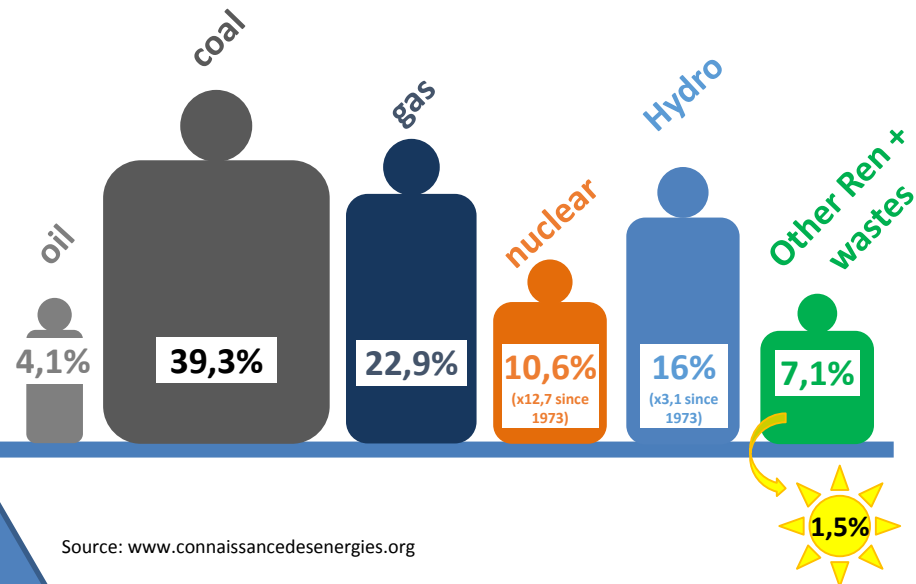


Resources for Electricity Generation

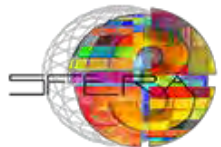
Worldwide electricity generation



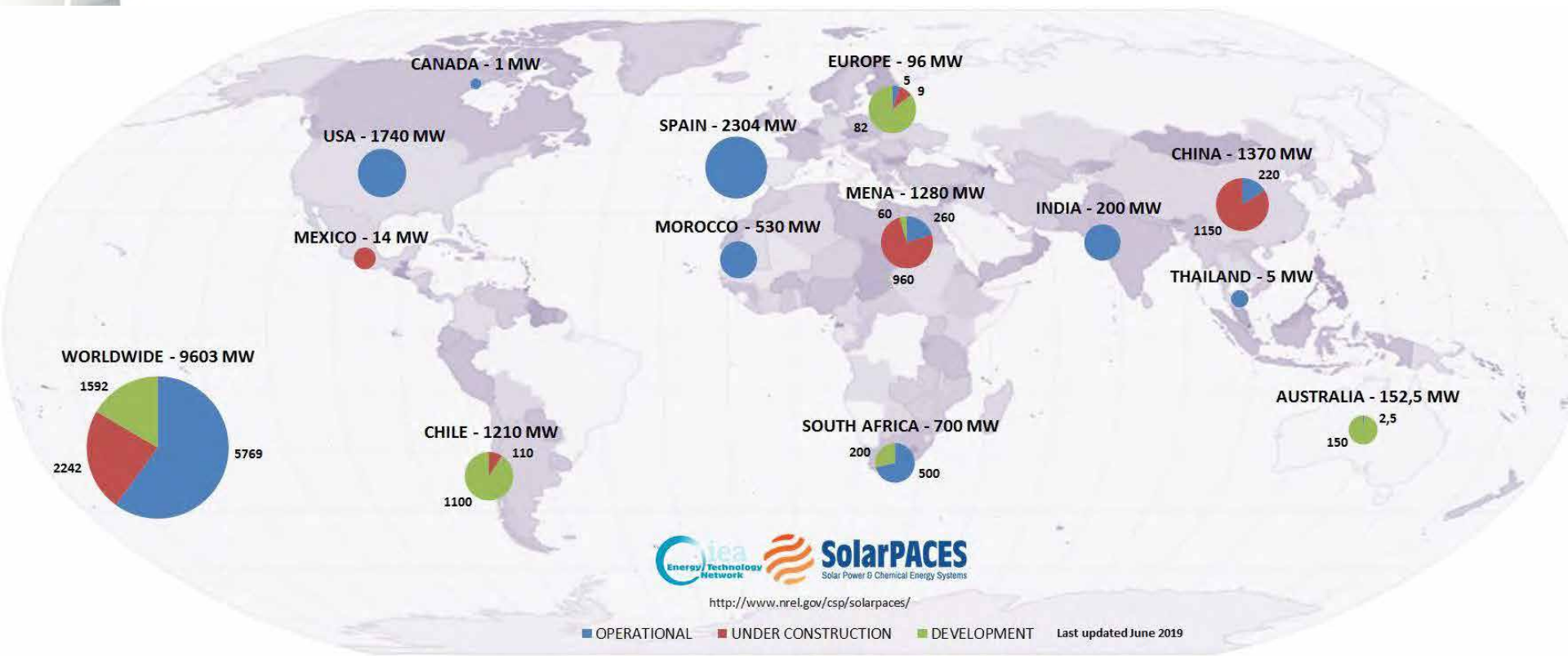
66,3%
Share of fossil energy into worldwide electricity mix



Source: www.connaissancedesenergies.org

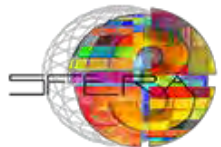
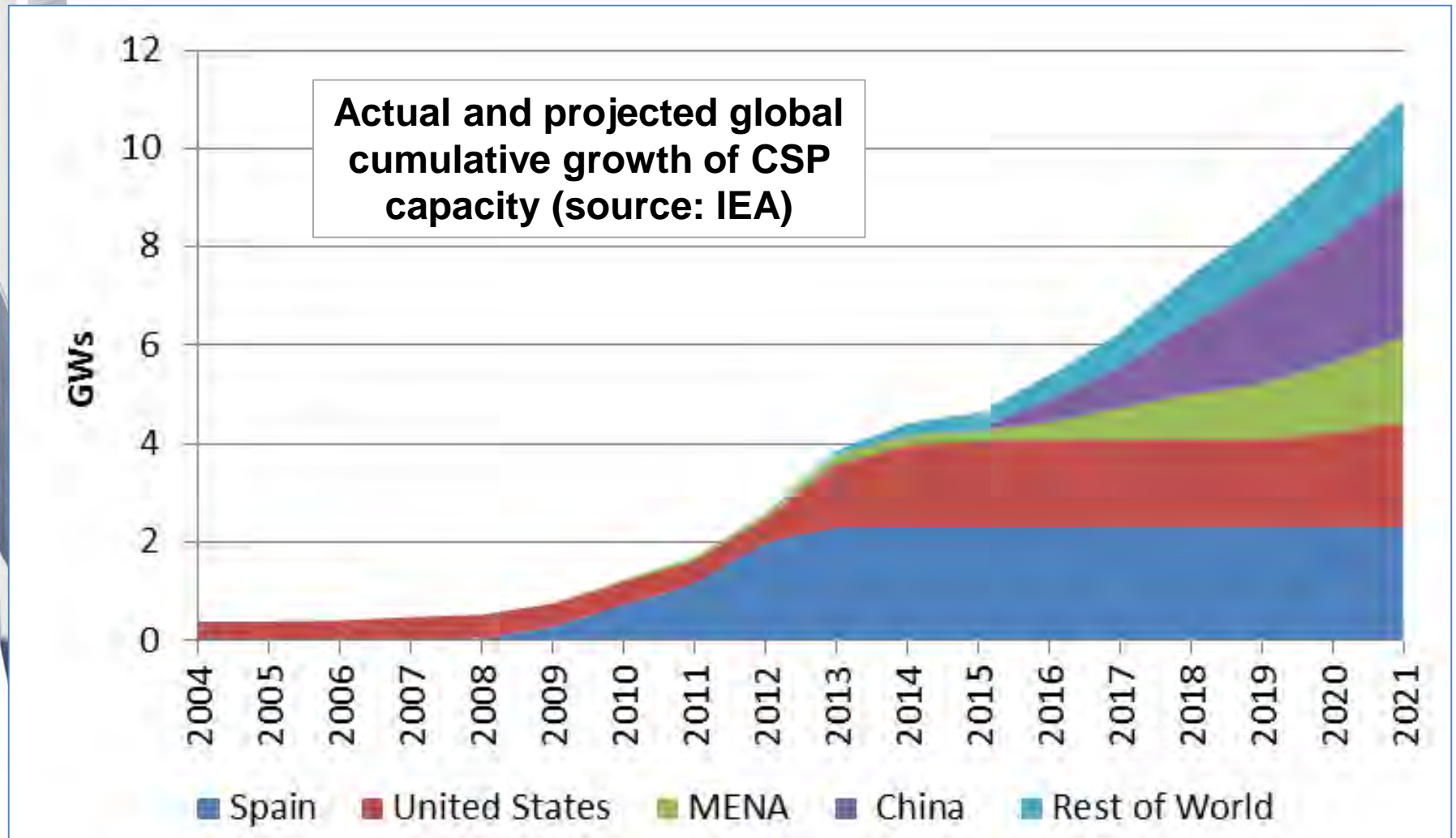


Worldwide CSP Market



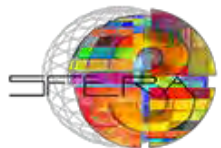
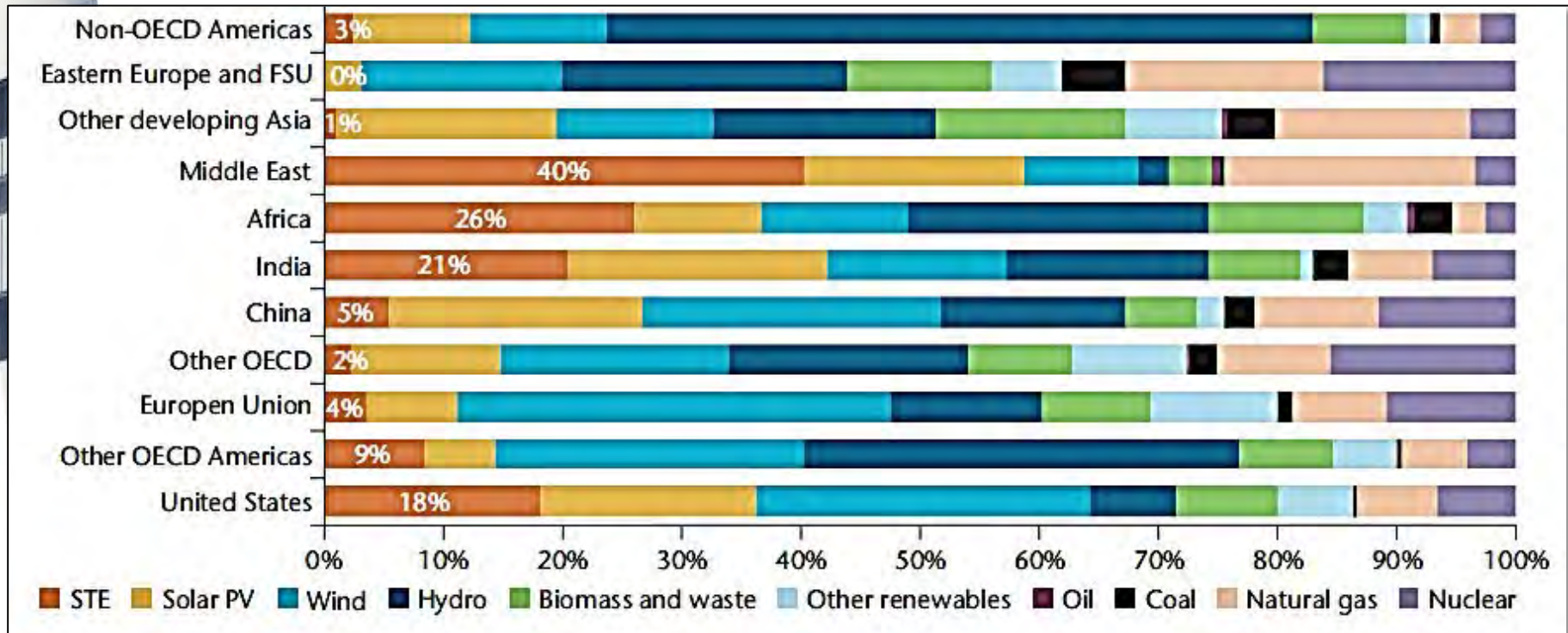
Total capacity in operation (2019): 5769 MW
In construction: 2242 MW

Near-term deployment of CSP



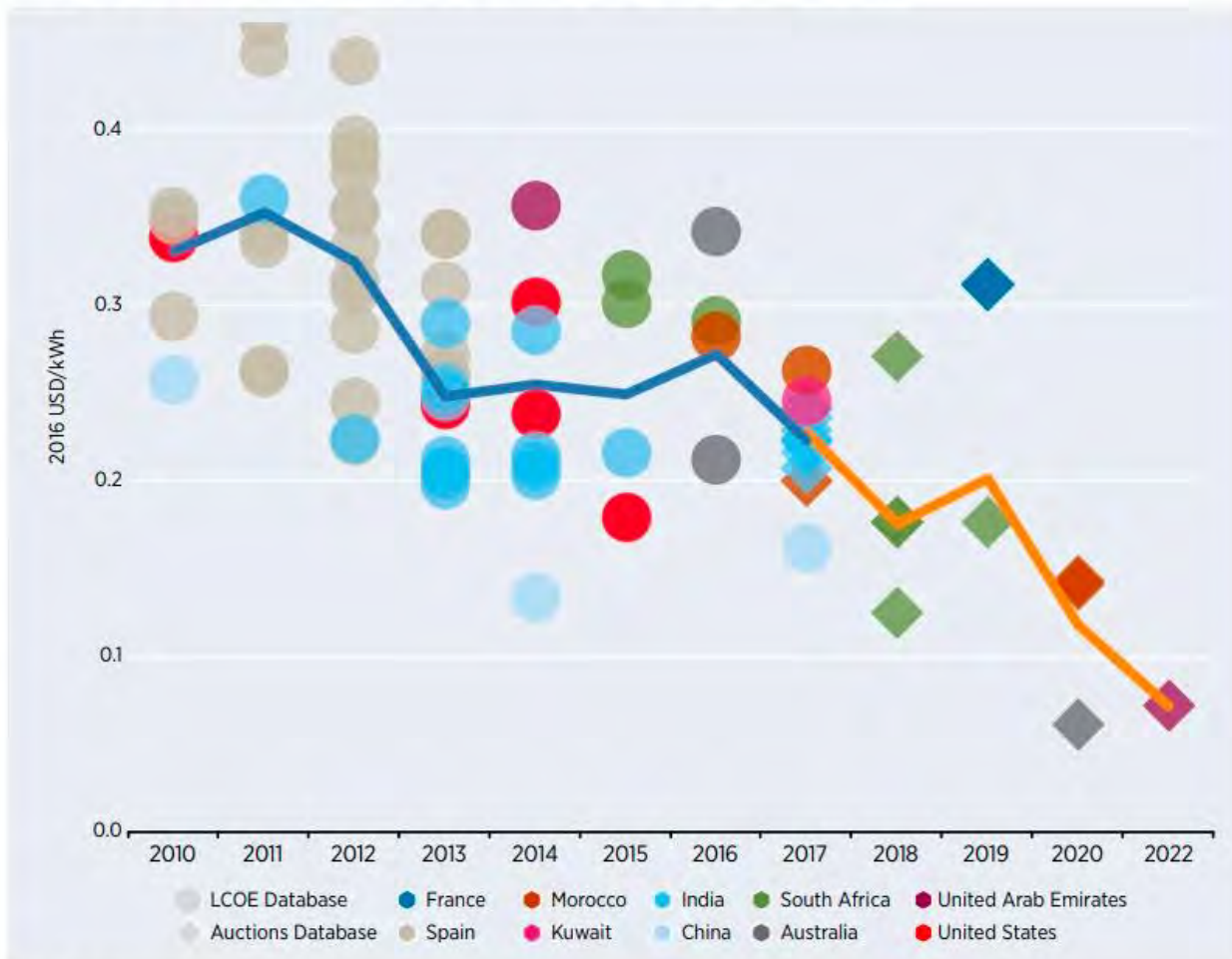
IEA 2050 Roadmap

According to the forecasts of the International Energy Agency (IEA), CSP could account for up to **11% of the electricity generated worldwide** and up to **4% of the electricity generated in Europe** by 2050.



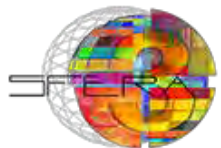
LCOE for CSP

Figure 4.10 Levelised cost of electricity and auction price trends for CSP, 2010-2022

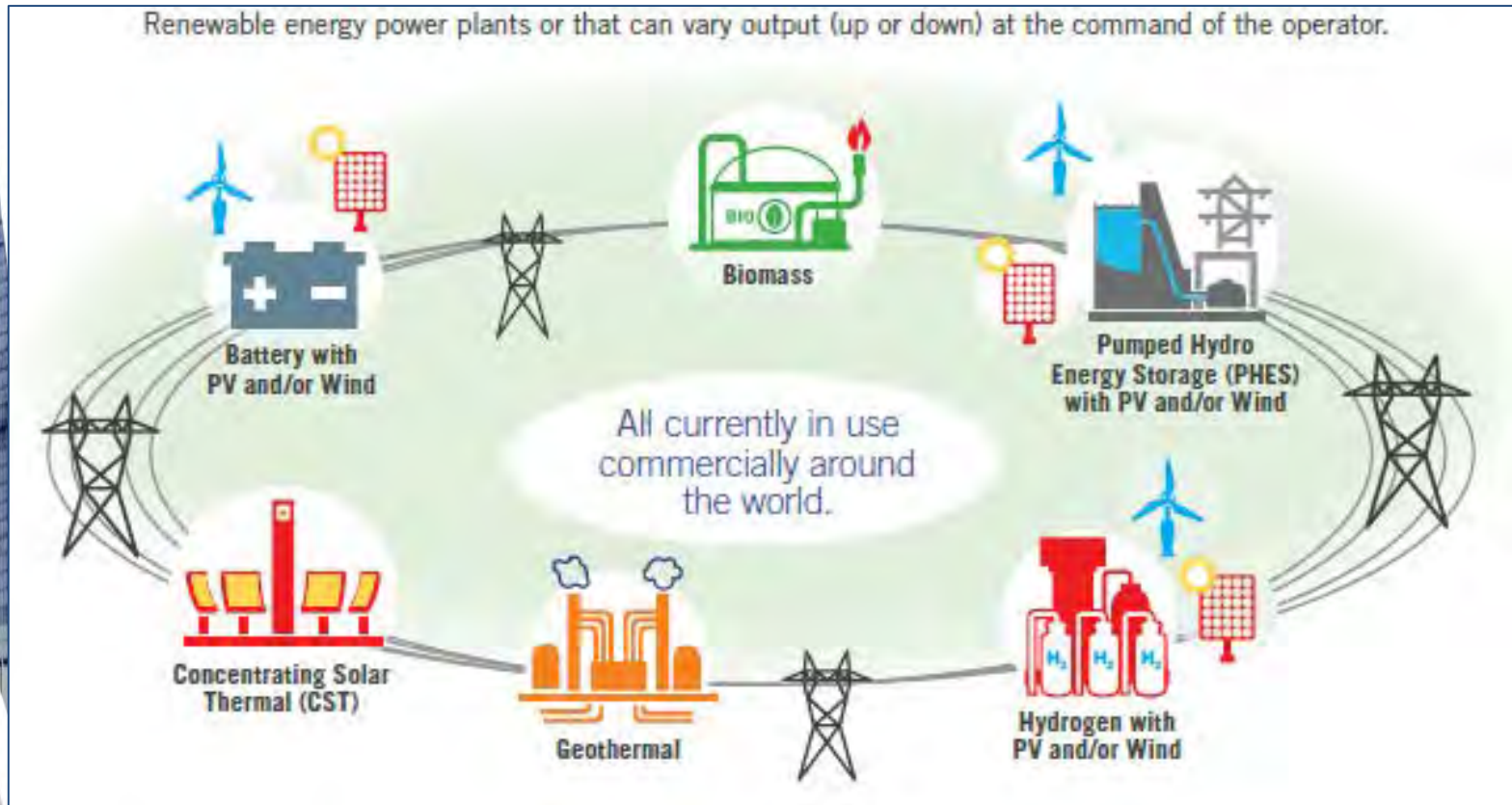


Note: Each bubble represents a renewable energy project. The center of the bubble is the winning bid price in that year.

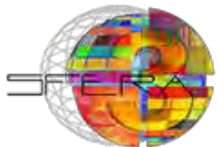
Source: IRENA Renewable Cost Database and Auctions Database.



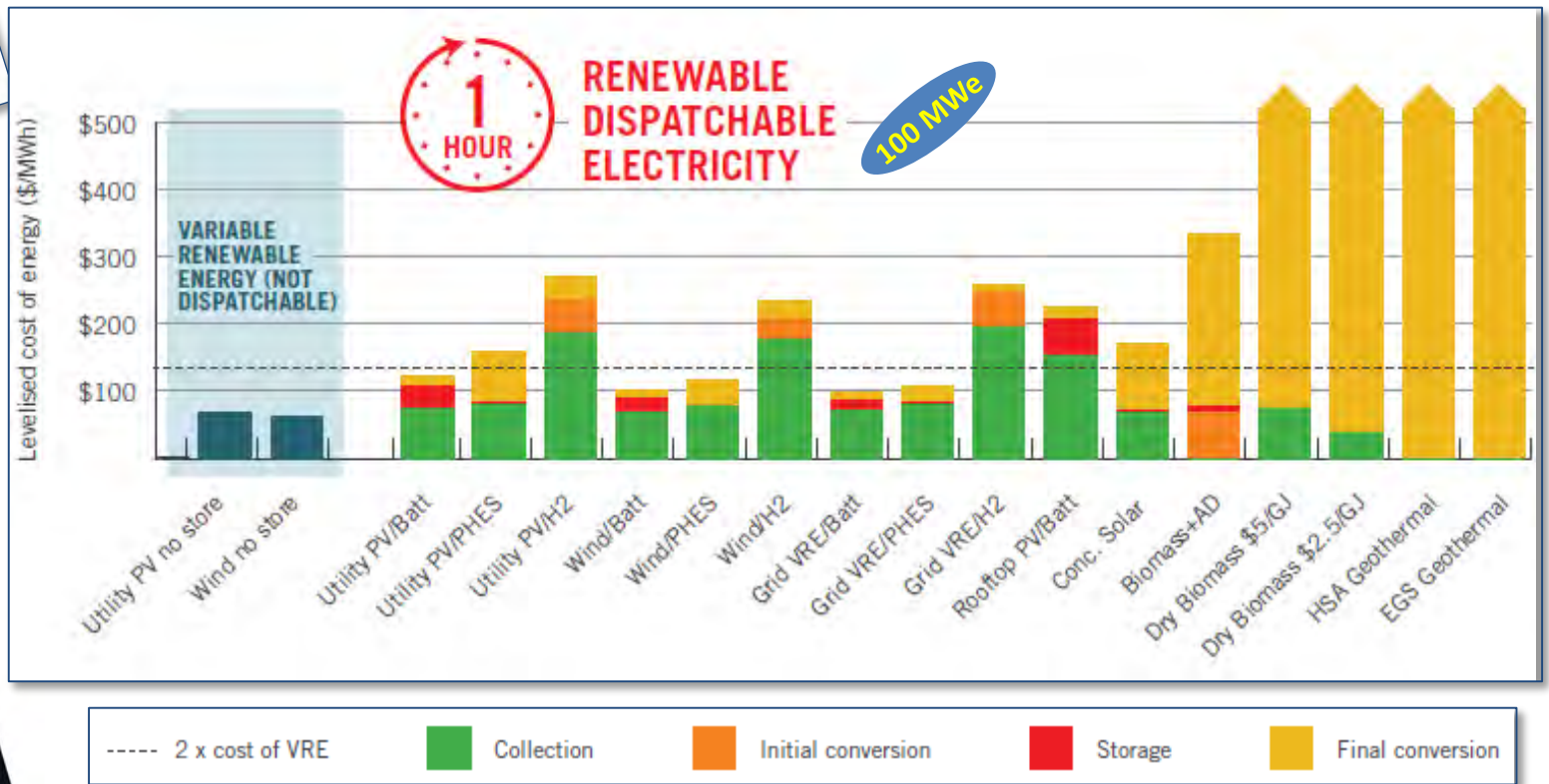
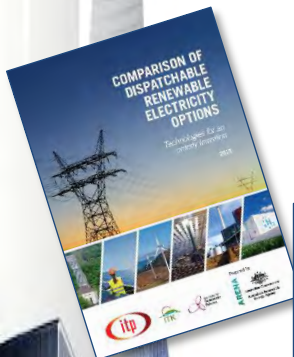
Dispatchable Renewable Electricity



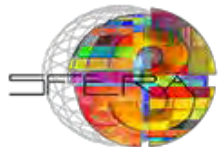
Source: Comparison of Dispatchable Renewable Electricity Options, ARENA-ITP, 2018



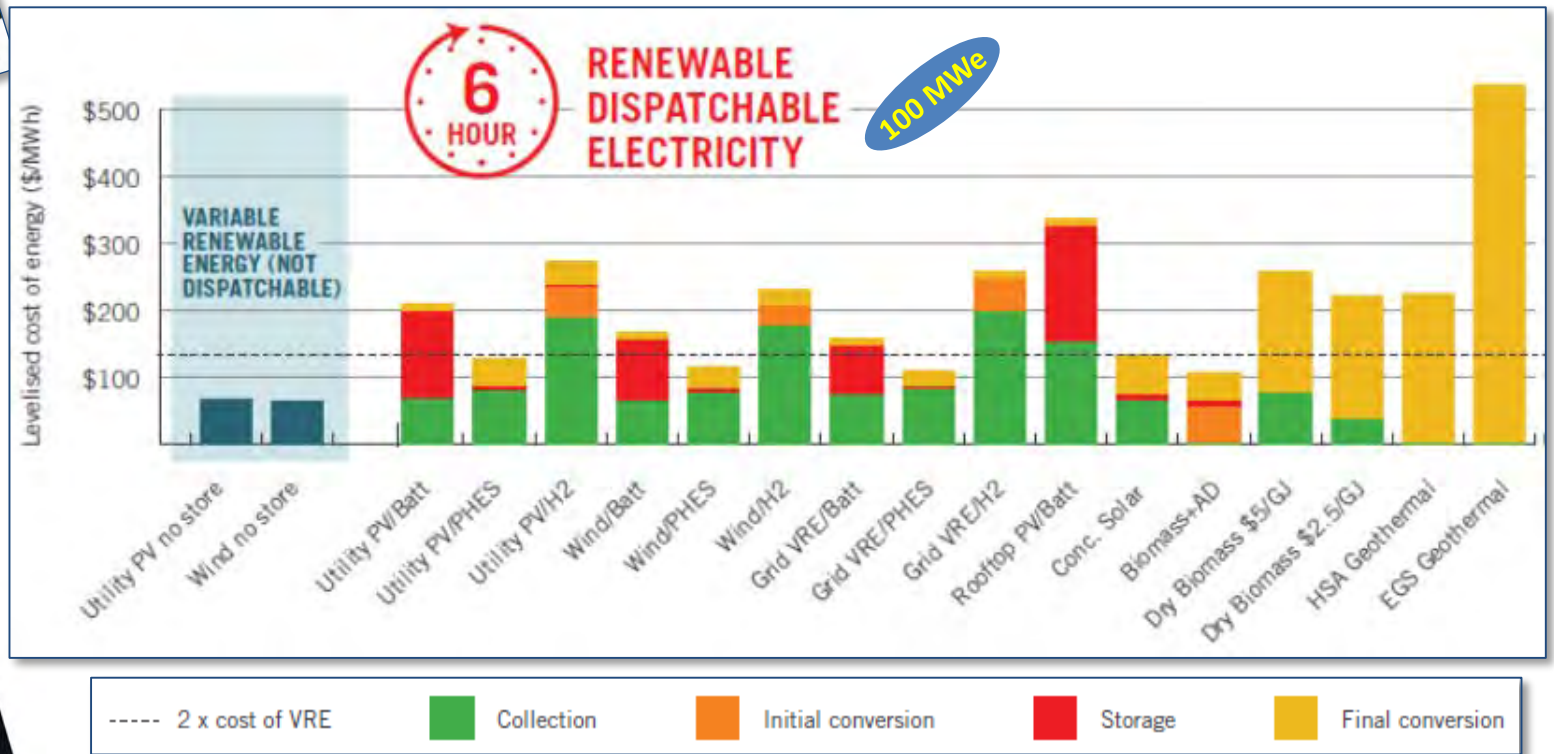
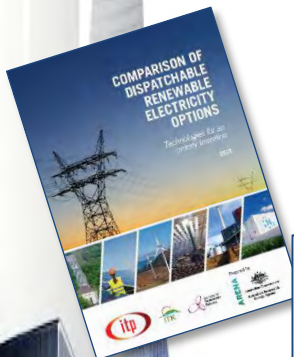
Dispatchable Renewable Electricity



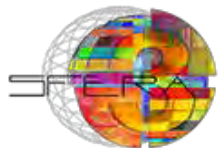
Source: ARENA-ITP, 2018



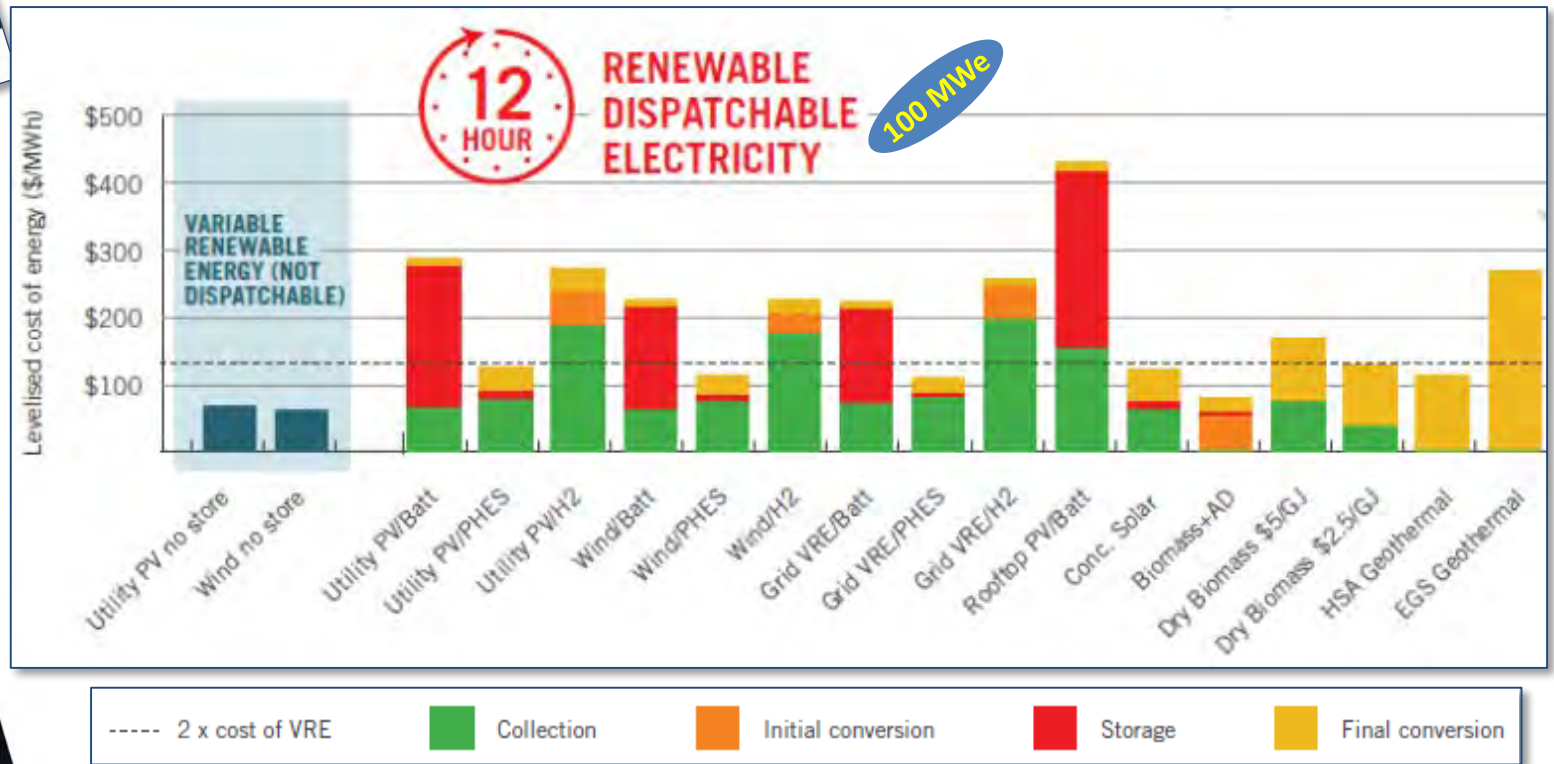
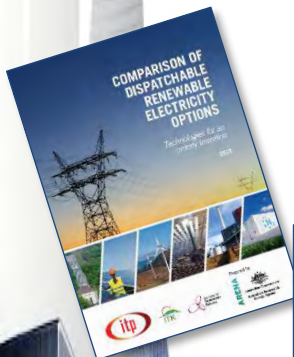
Dispatchable Renewable Electricity



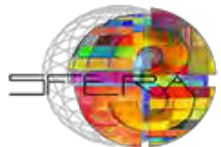
Source: ARENA-ITP, 2018



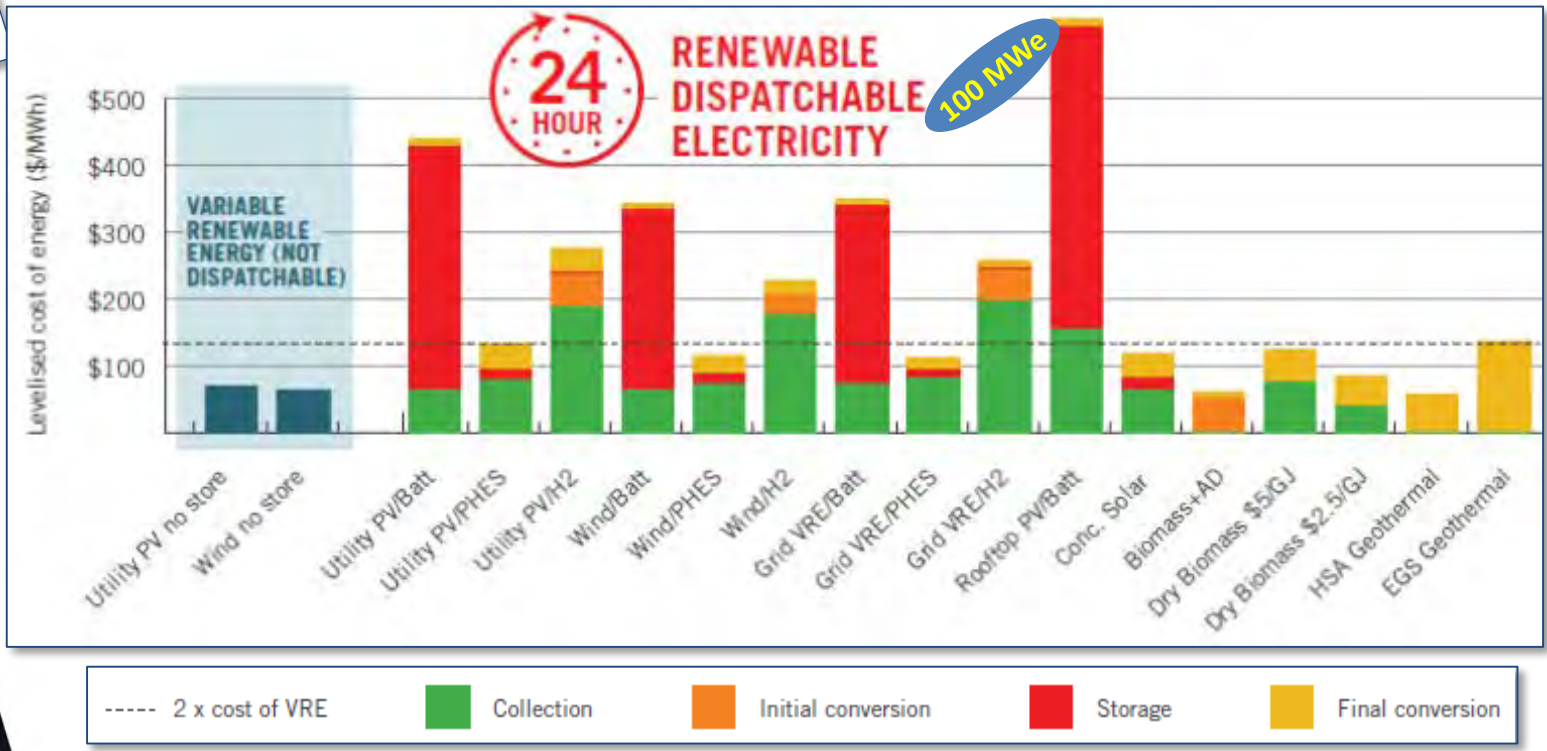
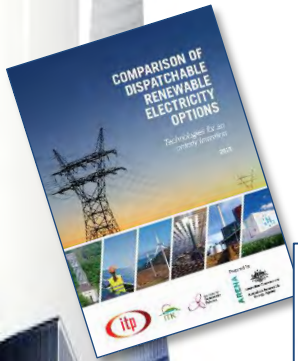
Dispatchable Renewable Electricity



Source: ARENA-ITP, 2018



Dispatchable Renewable Electricity



Source: ARENA-ITP, 2018



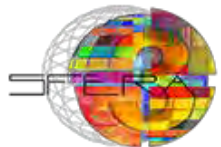
Dispatchable Renewable Electricity



Concentrating Solar Power

- CSP competitive >6hrs storage
- **high LCOE** for **short** durations of storage (<3 hrs) reflects the relatively **high installed cost** of **power** related components
- **lower LCOEs** for **longer** durations (>6hrs) reflect the **low cost per stored energy** of the **molten salt** system
- **Minimum LCOE** in the range **15 - 20 hrs** of storage
- CSP with **less storage** may be preferred to target generation in **peak** periods
- CSP with **molten salt** storage has been applied commercially since 2006
 - ✓ **growth rate** of deployment **~40%/year**
 - ✓ high potential for **cost reduction**

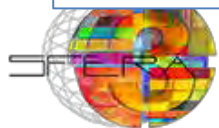
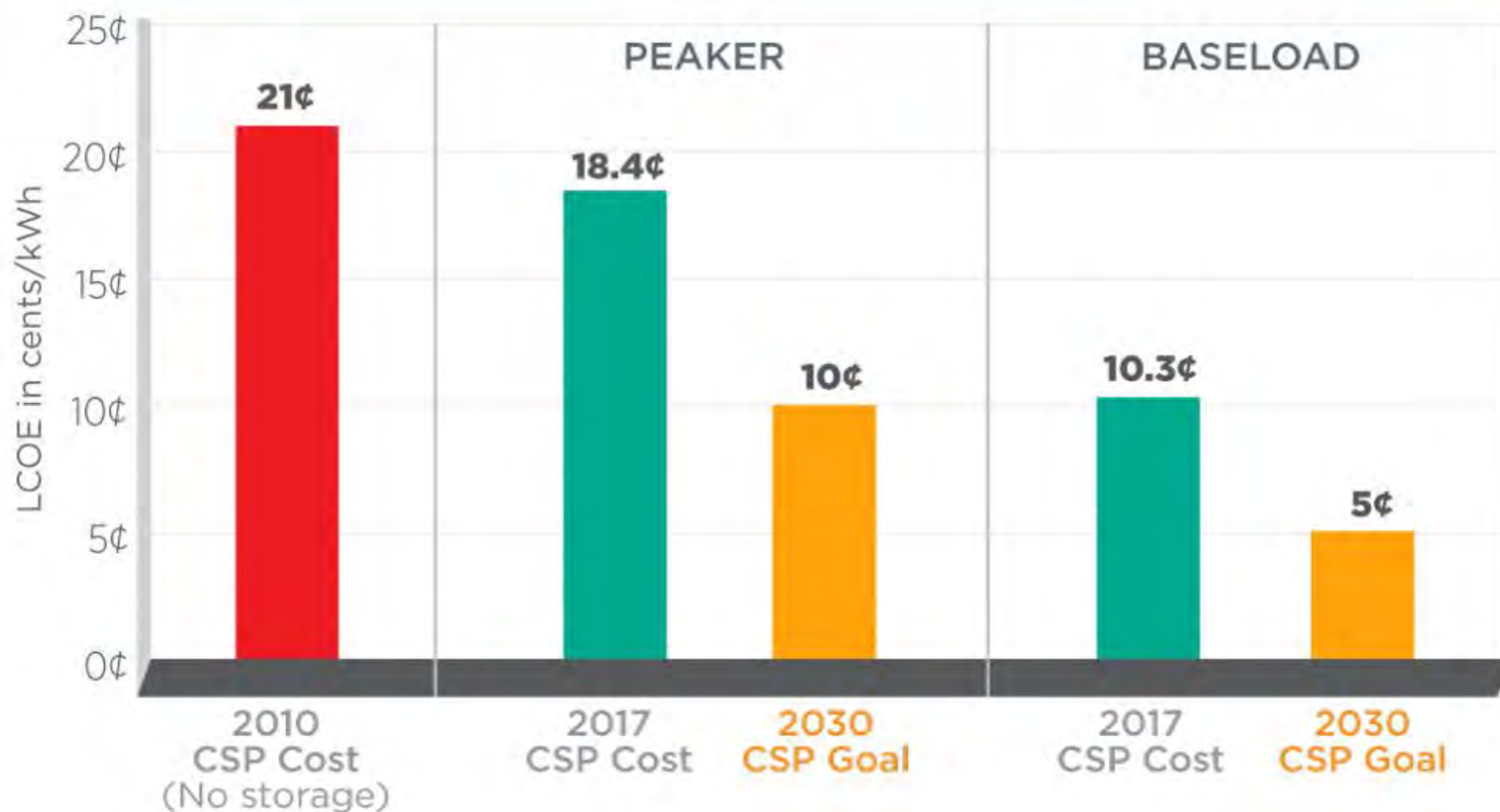
Source: ARENA-ITP, 2018



Cost perspective

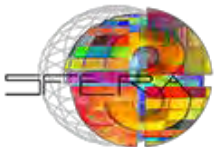
SunShot CSP Progress and Goals

The office's 2030 cost targets for CSP peaker (<6 hours of storage) and baseload (>12 hours of storage) plants will help the solar industry stay on pace.



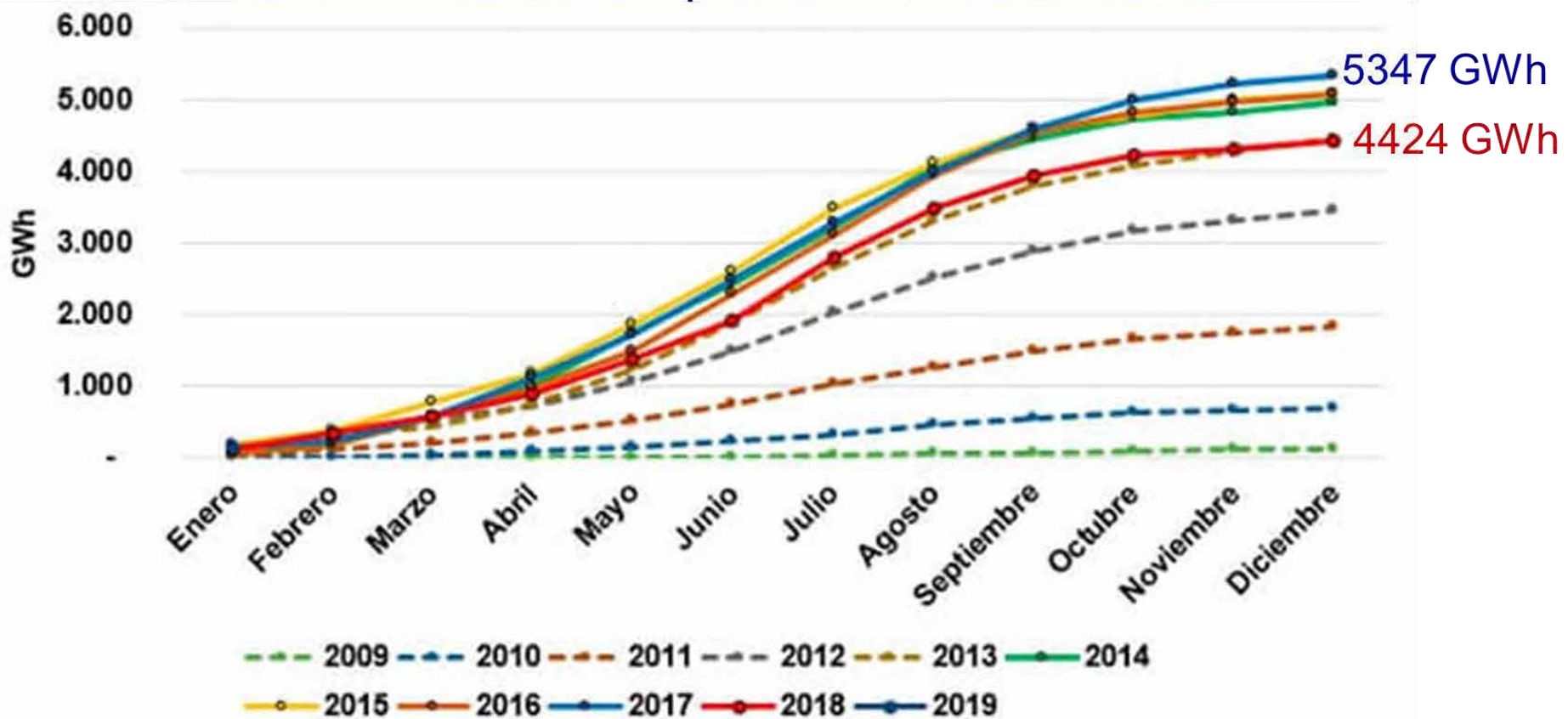
Trends

- **CSP roadmaps** released in several countries with high solar resource
- **Projects development** supported by public incentives (Feed-in tariffs)
- **Implementation plans in USA and in EU** to support market penetration by US and EU industries
- Market present in USA, competition with PV
- Limited market in EU, need for firm Ren power

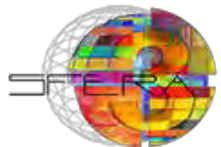


CSP performs very well in Spain

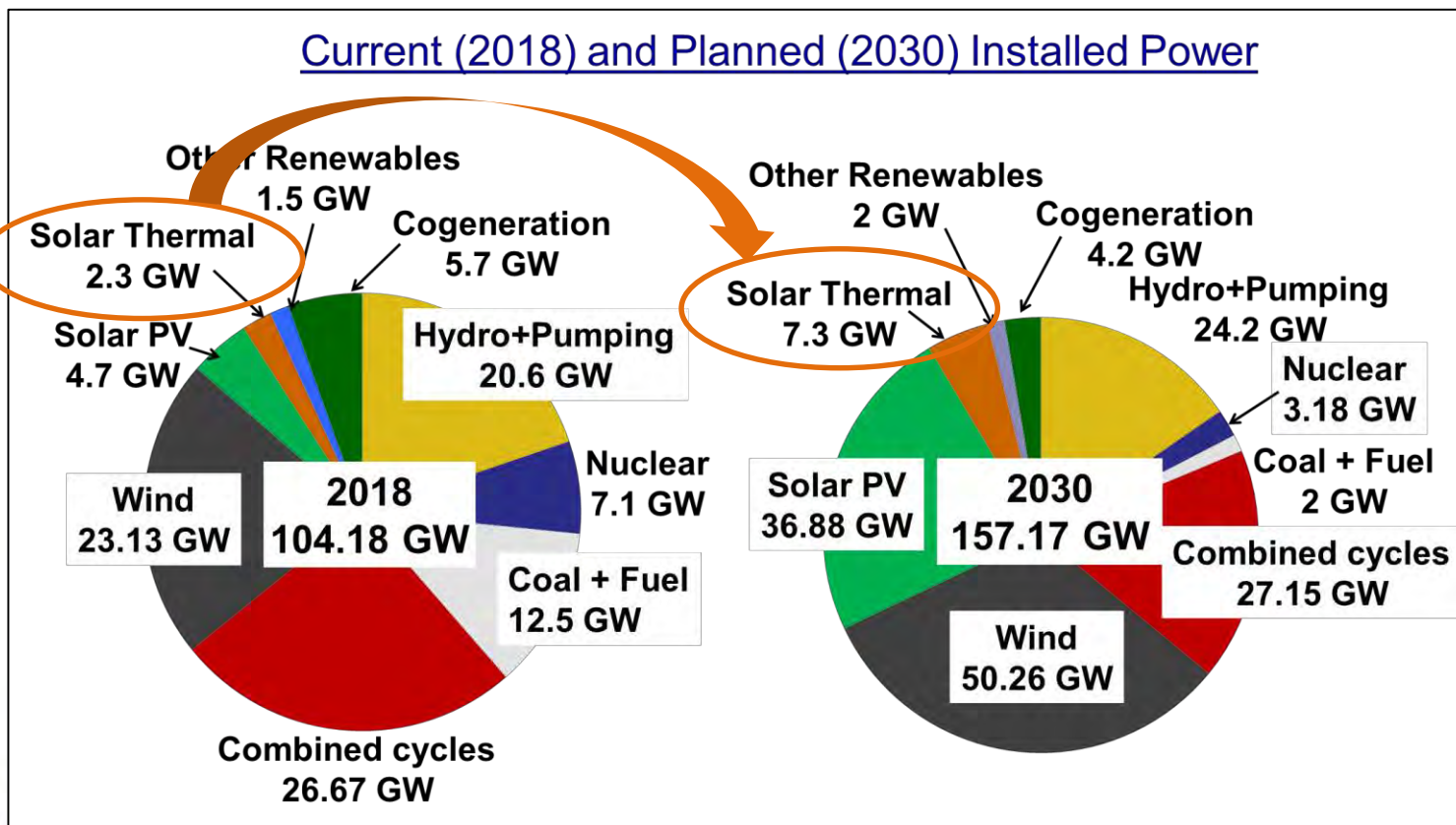
Accumulated STE production 2009-2019



Source: E. Zarza, SolarPACES ExCO #96, 2019



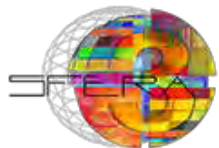
Expected growth in Spain



Integrated National Plan for Energy and Climate (PNIEC) 2021-2030 (02/2019)

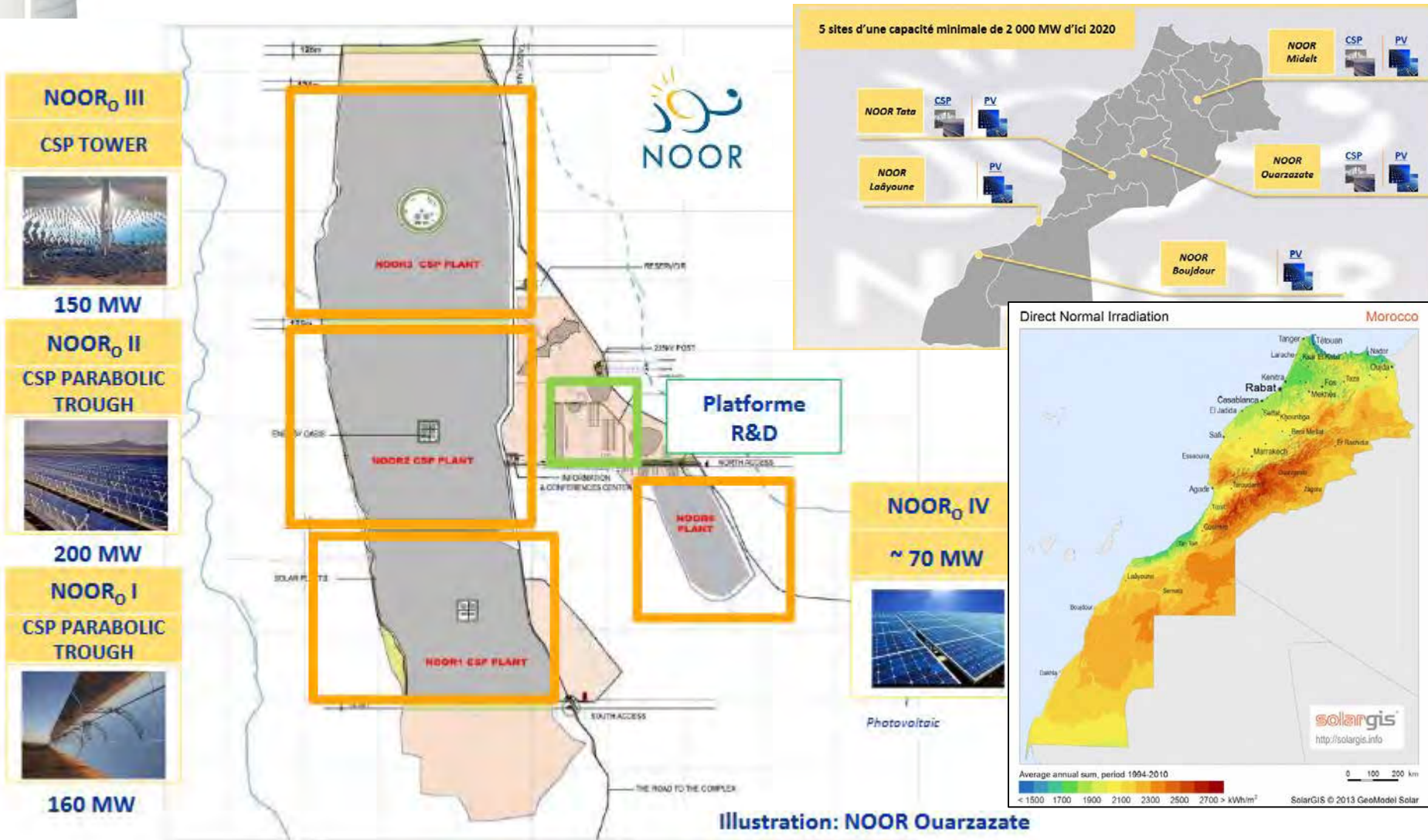
- ✓ 74% of electricity will be produced with renewable energies
- ✓ 42% of overall energy consumption will be supplied by renewable energy
- ✓ A total investment of 236.124 M€ will be required between 2021 and 2030 (80% private and 20% public) to achieve the proposed objectives
- ✓ 363.000 new jobs will be created

Source: E. Zarza, SolarPACES ExCO #96, 2019



CSP in Morocco

2000 MW solar in 2020 (14% of total capacity), REn = 42% of energy mix



Morocco's 800 MW CSP-PV Noor Midelt

NOOR MIDELT HYBRID SOLAR PLANT

MOROCCO 

Consortium of **EDF Renewables**, **Masdar** and **Green of Africa** named as successful bidder for Morocco's landmark Noor Midelt Phase 1 hybrid solar project



The world's first advanced hybridisation of **concentrated solar power (CSP)** and **photovoltaic (PV) technologies**

The plant will be located 20km north of the town of **Midelt** in central **Morocco**



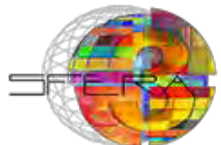
800 MW
Total capacity

Tariff at peak hours set at a record-low **0.68** Moroccan dirhams per kilowatt-hour

Auction price record: USD 7 cents/kWh

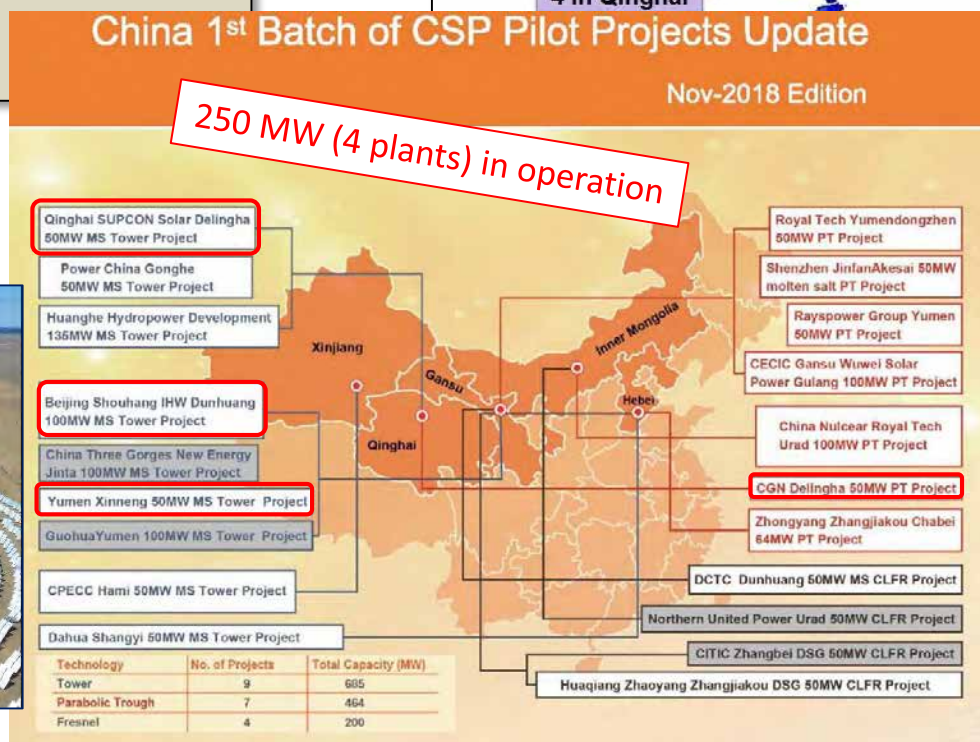
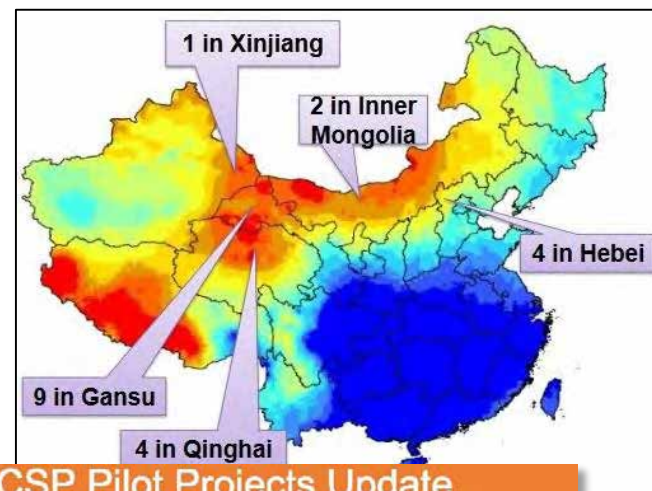


Courtesy of MASEN



CSP in China

- 5 GW total CSP in 2020
- 2016-2019: 1,35 GW, 20 projects, all with thermal storage (min 4h, max 10h)
 - 7 molten salt towers (50-100 MW)
 - 2 DSG towers (50 MW, 135 MW)
 - 5 oil PT (50-100 MW)
 - 2 molten salt PT(50 MW, 64 MW)
 - 4 Linear Fresnel (50 MW)
- **Tariff: 0,15 €/kWh**



Sustainable Energy Technologies SET Plan

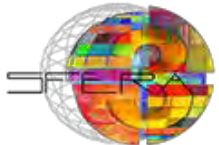


Initiative for Global Leadership
in Concentrated Solar Power

Implementation Plan

(11/2017)

- By means of **thermal energy storage**, CSP can make a significant contribution to the transformation of the European energy system by providing an important share of **dispatchable renewable electricity**.
- By providing **flexibility for grid services**, CSP can facilitate the **integration of variable output renewables** such as photovoltaic (PV) or wind energy, thereby contributing to the **reliability of the transmission grid**.



Sustainable Energy Technologies SET Plan

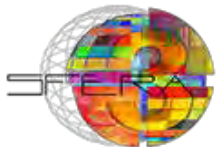


Initiative for Global Leadership
in Concentrated Solar Power

Implementation Plan

(11/2017)

- There is a clear **market failure in Europe** to bring new CSP technologies to the market
- **CSP innovation** needs to be reactivated
- **Reduce costs**
 - ✓ technology improvements
 - ✓ volumes deployed
 - ✓ risk-financing to support innovation projects
- **First-of-a-kind demonstration** projects
- Subsequent **market deployment**
 - ✓ ability to supply dispatchable electricity generated by CSP plants from Southern Europe to Central/Northern Europe
 - ✓ facilitating CSP access to **new markets**



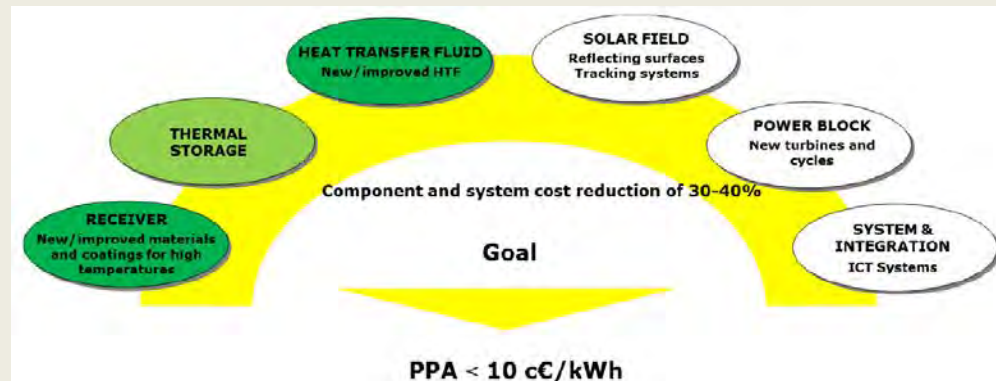
Sustainable Energy Technologies SET Plan

Strategic Targets on CSP

Short term target

Cost reduction: PPA price < **10 c€/kWh** for a radiation of 2050 kWh/m²/year (conditions in Southern Europe)

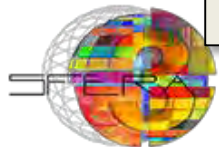
→ 40% cost reduction by 2020 (from 2013)



Longer term target

Develop the **next generation of CSP technology: new cycles** (sCO₂ & Supercritical Steam)

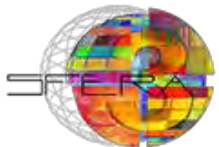
- first demonstrator by 2020
- achieve additional **cost reductions**
- open **new business opportunities**



Sustainable Energy Technologies SET Plan

R&I Activities to reach the targets

1. Improved central receiver molten salt technology
2. Parabolic trough with silicon oil
3. Next generation of central receiver power plants
4. Advanced linear concentrator Fresnel technology with direct molten salt circulation as heat transfer fluid and for high temperature thermal energy storage
5. Parabolic trough with molten salt
6. Solar tower power plant to commercially scale-up and optimize the core components of the open volumetric air receiver technology
7. Multi-tower central receiver beam down system
8. Thermal energy storage
9. Development of supercritical steam turbines optimized for CSP applications
10. Development of advanced concepts for improved flexibility in CSP applications
11. Development and field test of CSP hybrid air Brayton turbine combined cycle sCO₂ systems
12. Pressurized air cycles for high efficiency solar thermal power plants



Sustainable Energy Technologies SET Plan

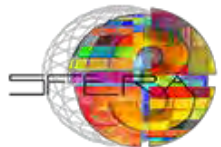
1. **More efficient components:**
HTF, receivers, reflecting surfaces
2. **Storage** systems
3. **Hybridization** of CSP plants
4. Reliability of CSP plants
5. Weather forecasting
6. Water consumption

1. **Cooperation** mechanisms
2. European **standards**

Innovative &
Market Uptake
Program

Industrial
Research &
Demonstration
Program

Advanced
Research
Program



EU Work Program

Secure Clean and Efficient Energy: active calls

Reduce the cost and increase performance and reliability of CSP plants

Deadline: 11 December 2019

The proposals will demonstrate innovations that **reduce the cost and/or increase the performance and/or the reliability of CSP plants**, in relation to any of the plant subsystems.

Proposals are expected to bring the solutions to **TRL 6-8**

Efficient combination of Concentrated Solar Power and desalination (with particular focus on the Gulf Cooperation Council region)

Deadline: 01 September 2020

Support will be given to demonstrate efficient solutions that **couple the thermal cycle of a CSP plant to a water desalination system**.

The proposals are expected to bring technologies to **TRL 6**.

International cooperation is encouraged, in particular with Bahrain, Kuwait, Oman, Qatar, Saudi Arabia, and the United Arab Emirates.

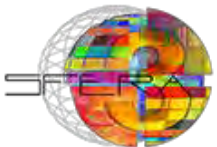
Solar Energy in Industrial Processes

Deadline: 27 August 2019

The potential of applying **solar energy for industrial purposes** is still largely untapped. Using solar energy to provide the heat or cooling necessary to industrial processes that need high reliability and high quality **heat and cooling and continuous operation** requires innovative advances in solar energy technology. Also, industrial processes might need to be adapted to the use of the solar resource. Industrial actors expect solutions with limited installation, maintenance and operation requirements and which are **easy to operate**. This challenge is also in line with the roadmap of the SPIRE cPPP.

Support will be given to solutions that cover by means of solar thermal energy the highest possible share of the heating and/or cooling demand of one or more industrial processes. In the case of heating, the **process temperature** shall be **higher than 150°C**.

Proposals are expected to bring the technologies to **TRL 4-5**



EU Work Program

Secure Clean and Efficient Energy: active calls

Integrated solutions for flexible operation of fossil fuel power plants through power-to-X-to-power and/or energy storage

Deadline: 27 August 2019

With a **growing share** of energy produced from **renewable resources**, **fossil fuel power plants** will have to increasingly shift their role from providing base-load power to providing fluctuating back-up power (i.e. **ramping up and down**) in order to **control and stabilize the grid**. Severe ramping up and down can be limited through load-levelling i.e. **storing power during periods of light loading** on the system and **delivering it** during periods of **high demand**.

Validation and pilot demonstration of the integration of **energy storage and/or use of excess energy** (including via power-to-X-to-power) in fossil fuel power plants.

Proposals are expected to bring technologies to **TRL 6-7**

Converting Sunlight to storable chemical energy

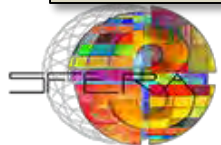
Deadline: 27 August 2019

To replace fossil energy with sustainable alternatives that provide the same flexibility and convenience of use, we need to **store sustainable energy on a large scale and for a long time** in new kind of energy storage compounds.

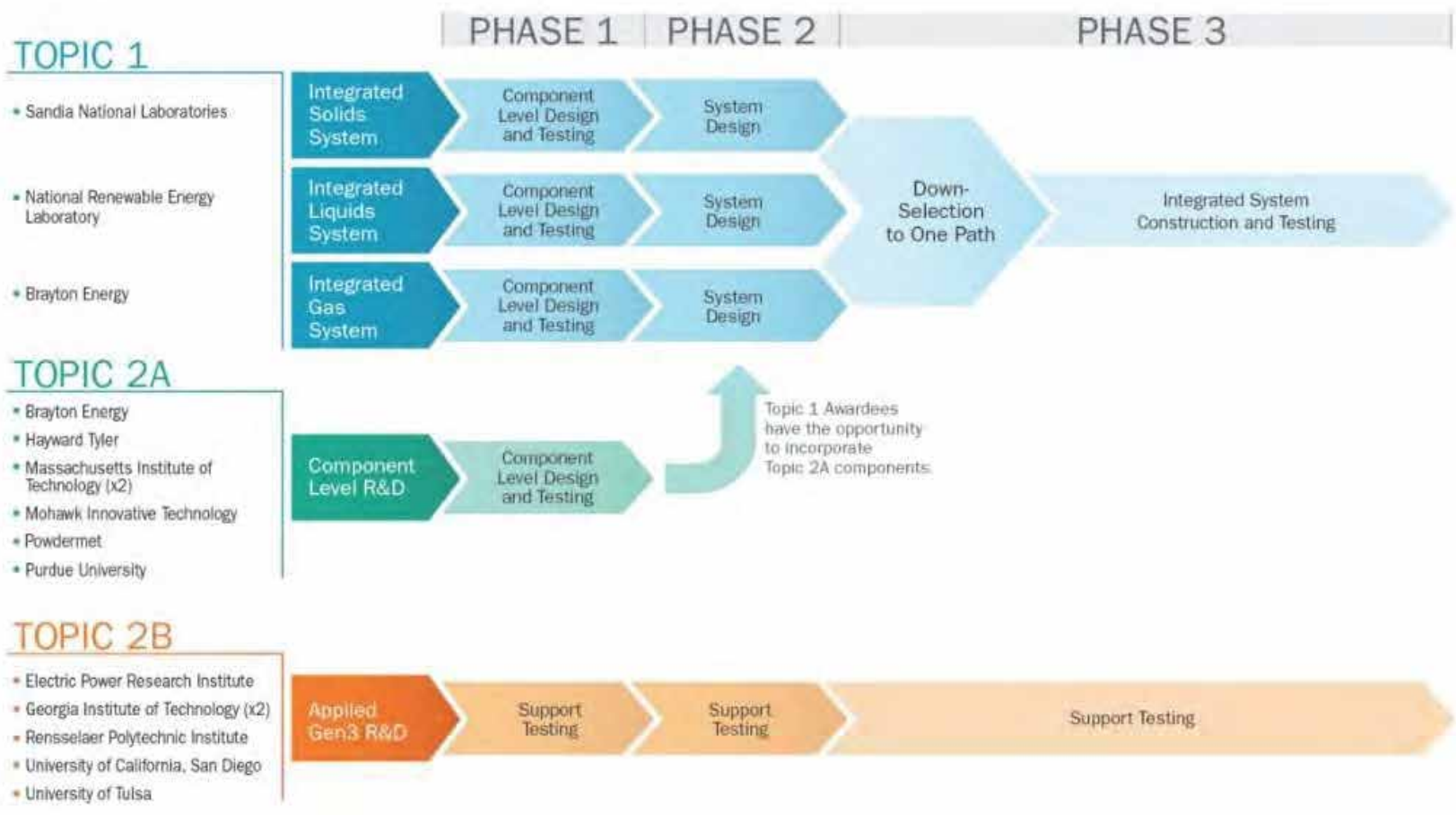
Proposals are expected to address renewable energy technologies that will answer the challenge described in the "Converting Sunlight Innovation Challenge" of Mission Innovation, bringing them up to **TRL 4 or 5**. At least one of the following technology-specific challenges has to be addressed:

- Improved light-harvesting and efficient charge separation in photocatalytic systems;
- Photoelectrochemical cells – PECs and catalyst development;
- **Thermochemical pathways to energy rich chemicals (using concentrated solar light)**
- Design and engineering of devices, systems or prototypes integrating together the different processes, with day and night control and applicability for the production of chemical energy rich carriers.

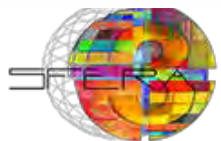
The area of **electrolysers** efficiently utilizing a renewable electricity input, such as provided by photovoltaics, wind turbines or other sustainable means, is **not covered** by this challenge.



R&D: Programme Gen3 US DOE



Main research centers in CSP



An aerial photograph of a large-scale solar farm. The image shows a dense grid of solar panels, with several rows of panels missing, revealing the underlying metal support structure and concrete foundations. The panels are arranged in a regular, repeating pattern across the landscape. The text "Thank you" is superimposed in the center of the image in a white, italicized font with a black outline.

Thank you

alain.ferriere@promes.cnrs.fr

SFERA-III

Solar Facilities for the European Research Area

1st Summer School “Thermal energy storage systems, solar fields and new cycles for future CSP plants”
WPI Capacity building and training activities
Odeillo, France, September 9th-11th 2019



“TES for solar thermal power plants : Introduction,
Commercial systems, Integration issues & Latent heat”
Eduardo Zarza, Esther Rojas, CIEMAT-PSA (Spain)

NETWORKING



THIS PROJECT HAS RECEIVED FUNDING FROM THE EUROPEAN UNION'S HORIZON 2020 RESEARCH AND INNOVATION PROGRAMME UNDER GRANT AGREEMENT NO **823802**



SFERA-III
1st Summer School
September, 9th- 10th, 2019
CNRS- PROMES, Odeillo, France

TES for solar thermal power plants

Introduction, Commercial systems,
Integration issues and Latent heat

Presented by Eduardo Zarza (eduardo.zarza@psa.es)
Esther Rojas (esther.rojas@ciemat.es)



Contents

- Introduction
- Commercial systems → Sensible heat storage
- Latent heat storage → Integration Issues

Contents

- Introduction
- Commercial systems → Sensible heat storage
- Latent heat storage → Integration Issues

Electricity generation from thermal power

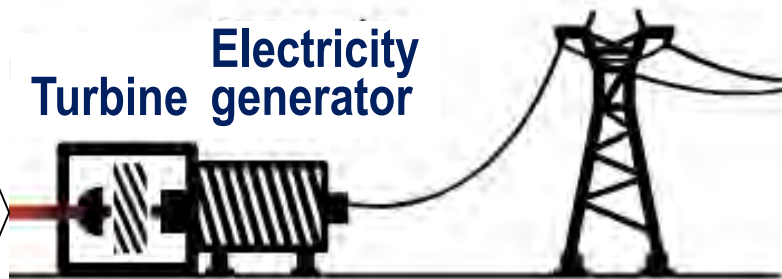
- **Fossil (gas&coal)**
- **Nuclear**
- **Renewables**
 - ◆ biomas
 - ◆ solar-thermal
 - ◆ geothermal

Thermal Storage

Thermal Energy
(steam, gas, T,P)

Turbine generator

Electric network



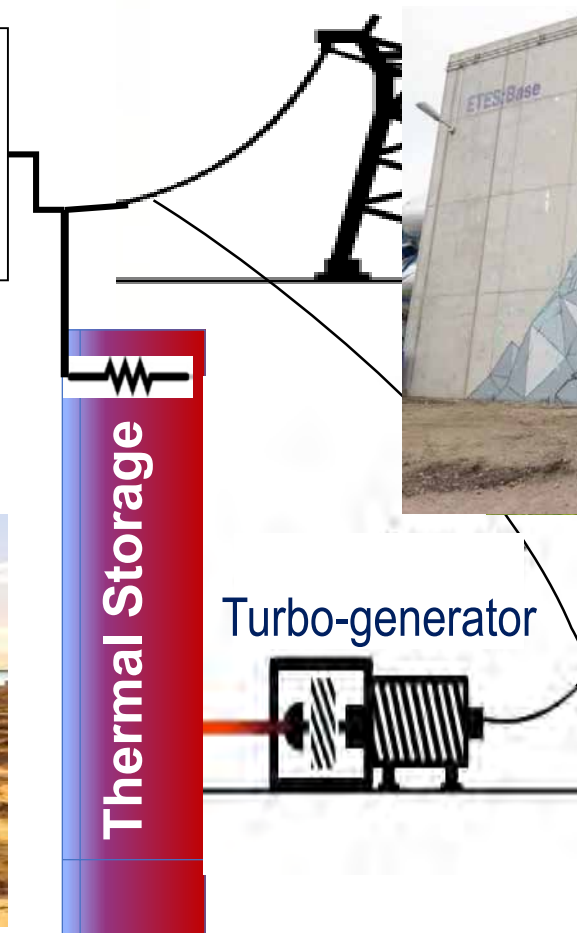
Storing “low-cost electricity”

➤ Renewables

- ◆ PV
- ◆ Wind

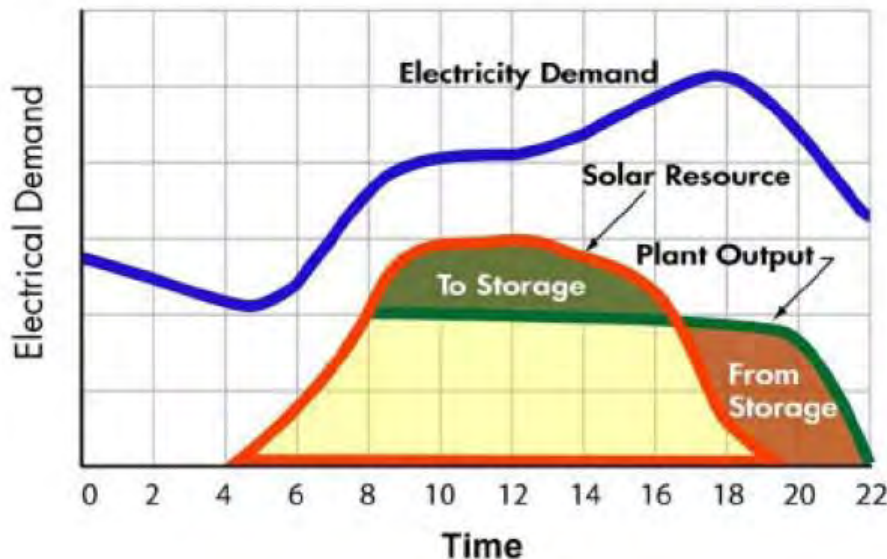


Electric network



Having thermal storage for STE means...

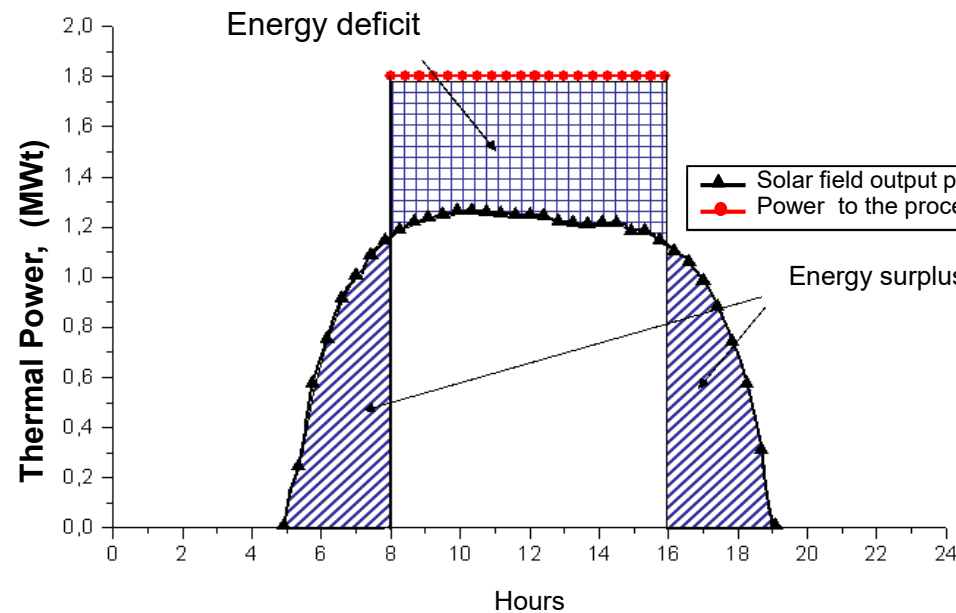
- Power generation becomes independent of solar resource
 - Overcome transients (clouds occurrence)
 - Extend operation time (during the night)



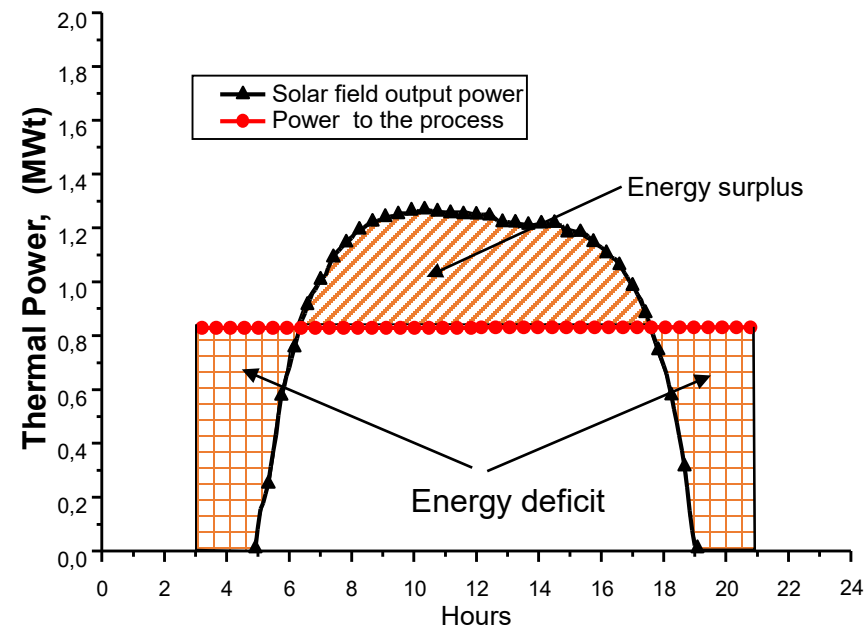
DISPATCHABLE
ENERGY/POWER

Having thermal storage for STE means...

- Power generation becomes independent of solar resource
 - Overcome transients (clouds occurrence)
 - Extend operation time (during the night)
 - Provide constant power



Case a)

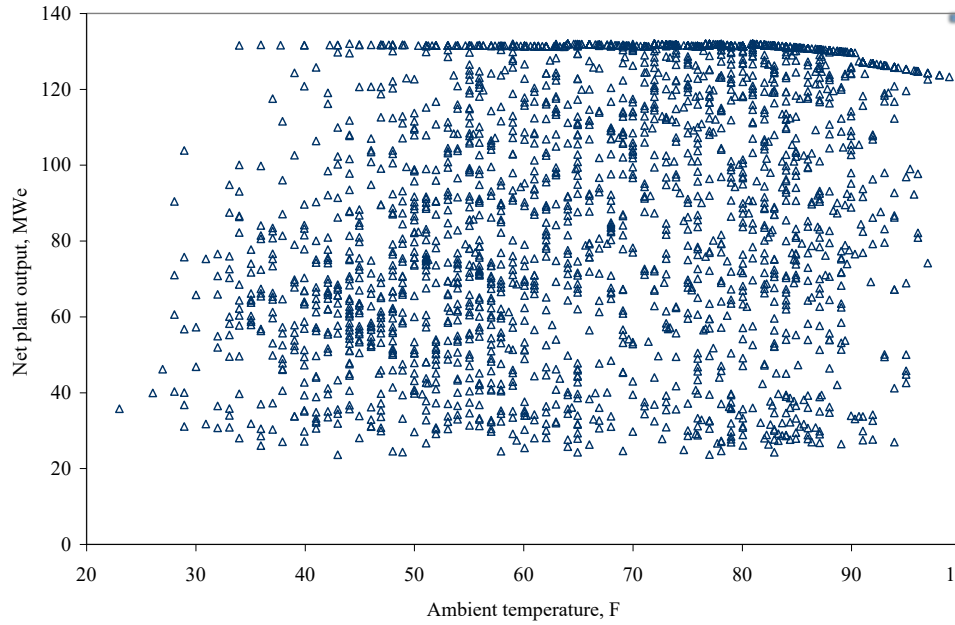


Case b)

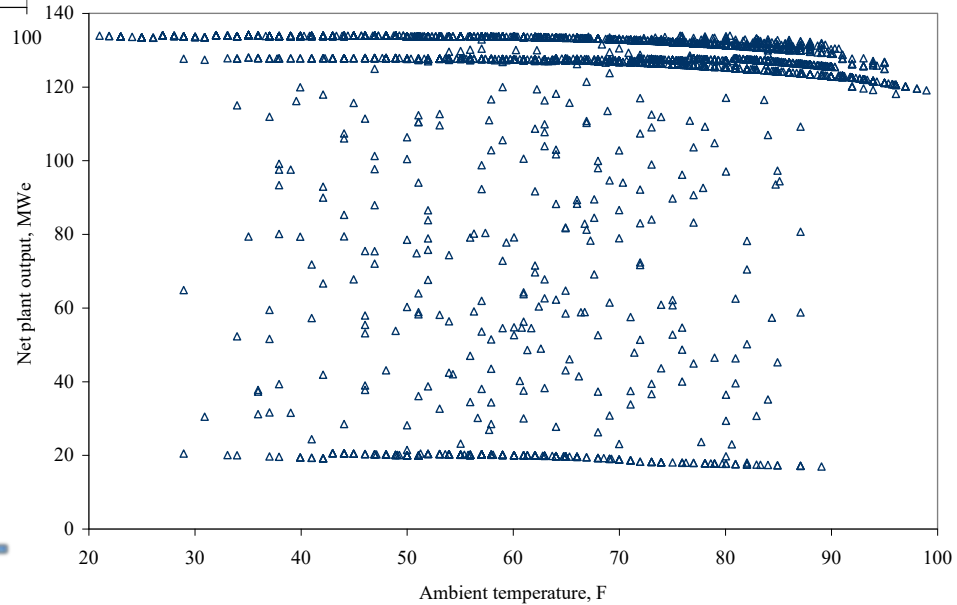
Having thermal storage for STE means...

- Power generation becomes independent of solar resource
 - Overcome transients (clouds occurrence)
 - Extend operation time (during the night)
 - Provide constant power
 - Favors electrical production under nominal conditions
 - Increases the annual performance of the power block

Simulation of a 125 MWe STE plant without storage



**And with 9
hours of
storage**

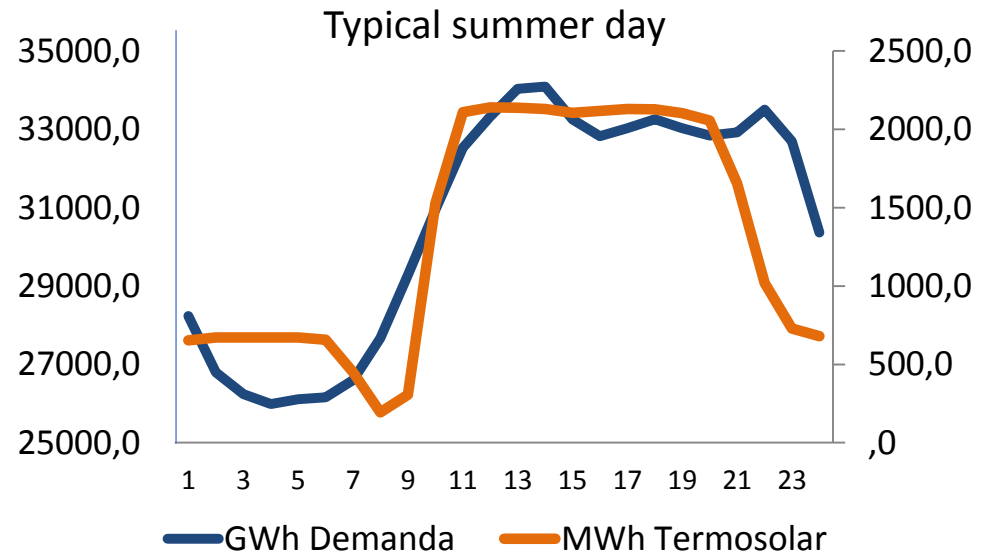


Having thermal storage for STE means...

- Power generation becomes independent of solar resource
 - Overcome transients (clouds occurrence)
 - Extend operation time (during the night)
 - Provide constant power
 - Favors electrical production under nominal conditions
 - Increases the annual performance of the power block
 - Promoting other renewables to be integrated in the energy mix

'Dispatchable' implies that power production is well-foreseen and managed

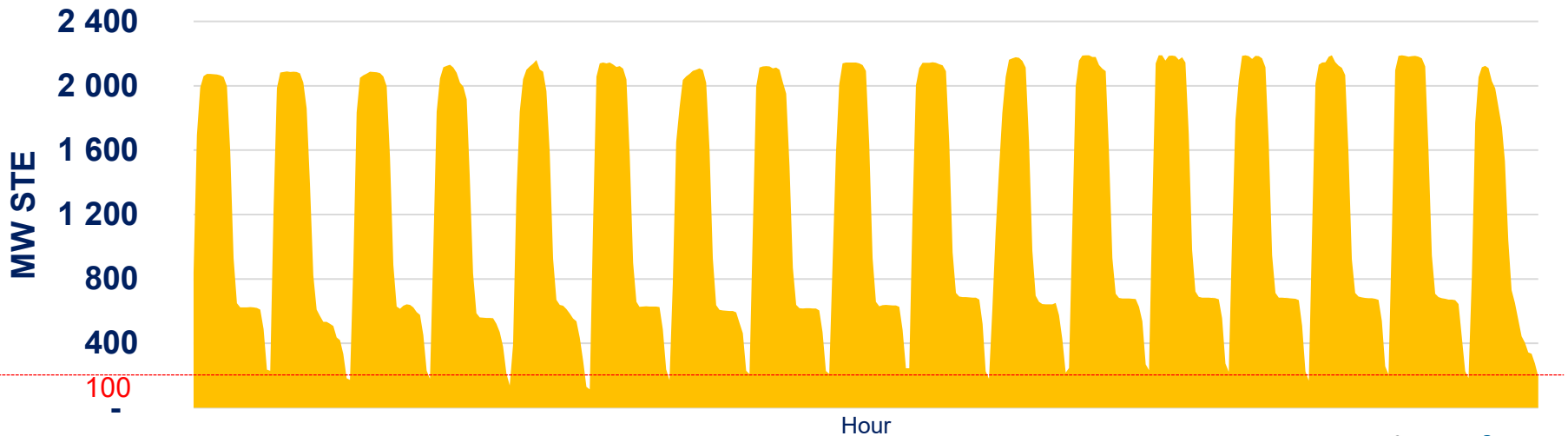
- Spanish case:
 - Around 2.3 GWe of STE installed
 - 40% STE plants have a 1GWh_t TES
- ✓ Profiles of power provided by STE is similar to demand profile (see figure, left scale for GWh demand and right scale for STE power generation)



Example of continuous STE power generation in Spain

With large thermal energy storage systems STE plants can provide base load

Continuous power generation over 100MWe during 405h = 17 days



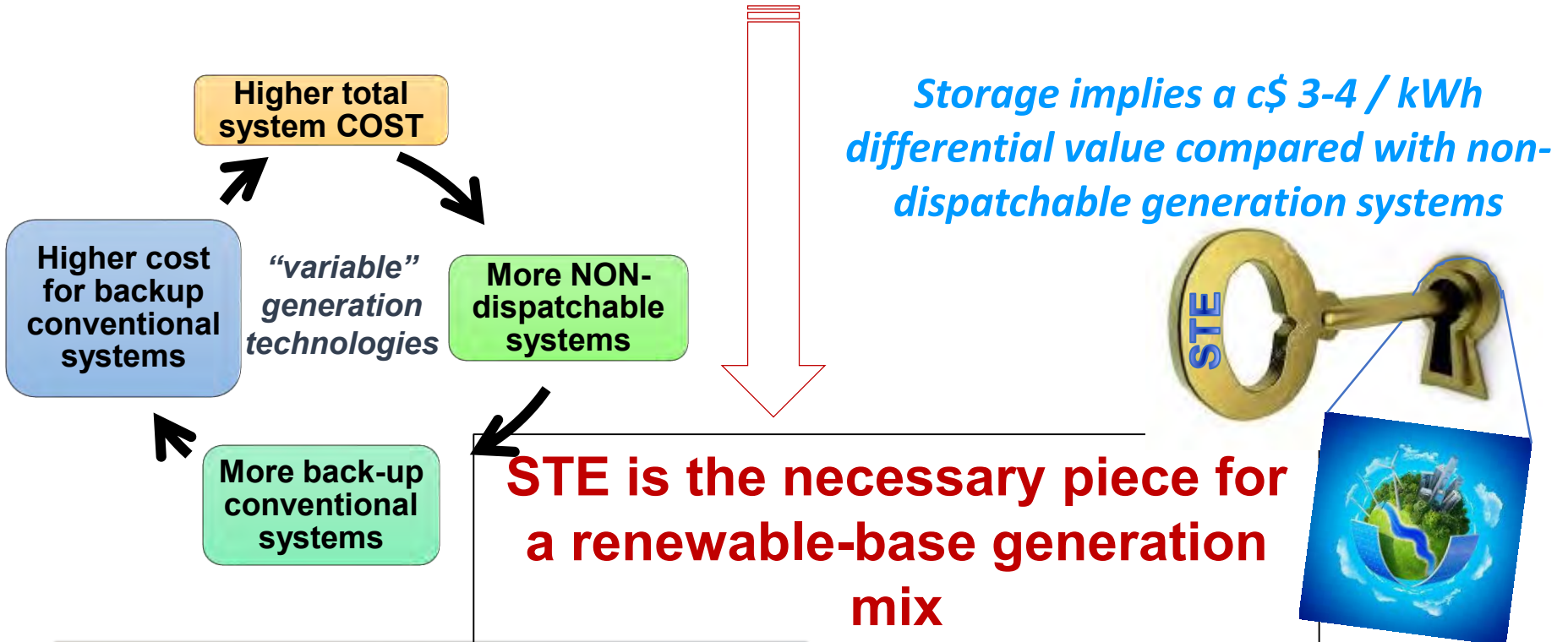
July 2018 data

STE's treasure



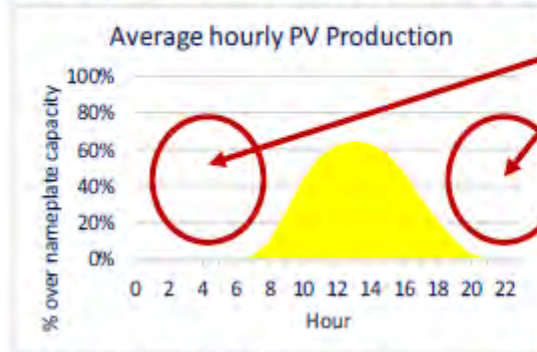
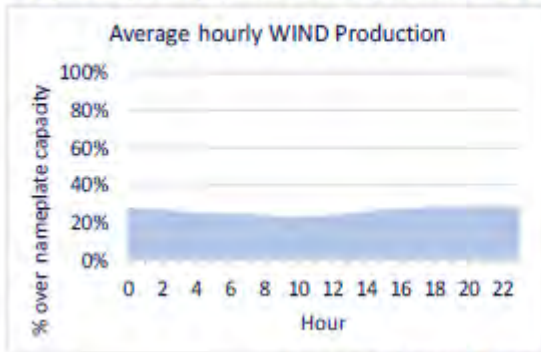
Commercial Thermal Storage Systems with large capacity mean:

- For the owner: electricity sold when the pool price is higher (more profit)
- For System operator : **Dispatchability**, Grid stability



Complementarity of STE with PV and Wind

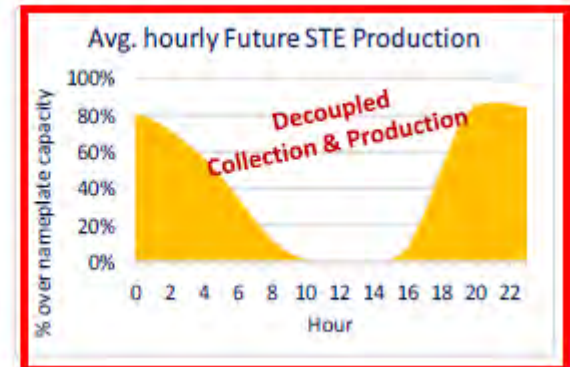
Typical yearly generation profiles of the most deployed renewable technologies



Which technology could fill up these gaps?

Average hourly production on a long historical series

What is the missing piece?



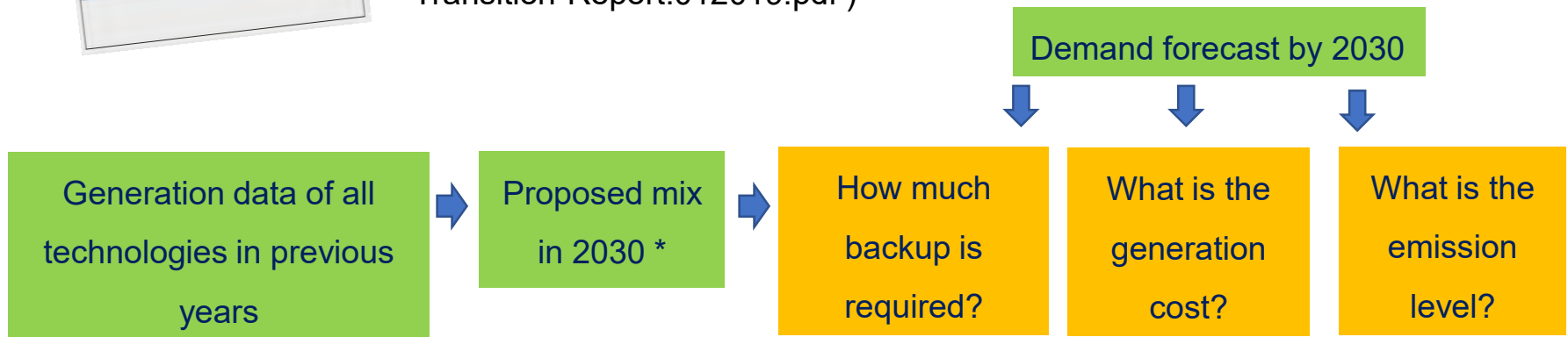
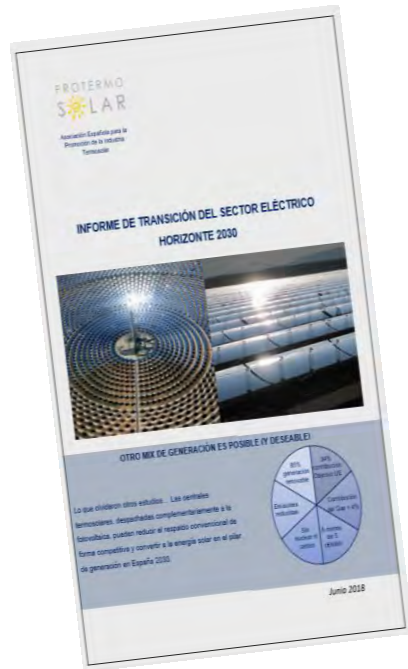
PROTERMOSOLAR Electrical Sector Transition Report

Study based on real hourly data of demand and power generation with different RES

www.protermosolar.com

(English presentation at

<https://www.protermosolar.com/wp-content/uploads/2019/02/Protermosolar-Transition-Report.012019.pdf>)



Impacts of having TES of large capacity

1. Impacts on the Power network

- ✓ Promoting an energy mix with RES, not only STE but also others like wind and PV
- ✓ Possibility to use dumping electricity from wind and PV
- ✓ Permanent back-up capacity at low cost

Benefits of using large TES systems for back-up



50 STE plants, each of 100MWe and with 12hour TES, could provide a strategic back-up of 30GWh_e without additional investment.

The cost of pumping power stations for the same capacity would be of **7.500 Mio €**



Impacts of having TES of large capacity



Impacts on the Power network

- ✓ Promoting an energy mix with RES, not only STE but also others like wind and PV
- ✓ Possibility to use dumping electricity from wind and PV
- ✓ High back-up capacity at low cost



Impacts on Plant management

- ✓ Dispatchable power production to meet the peak demand

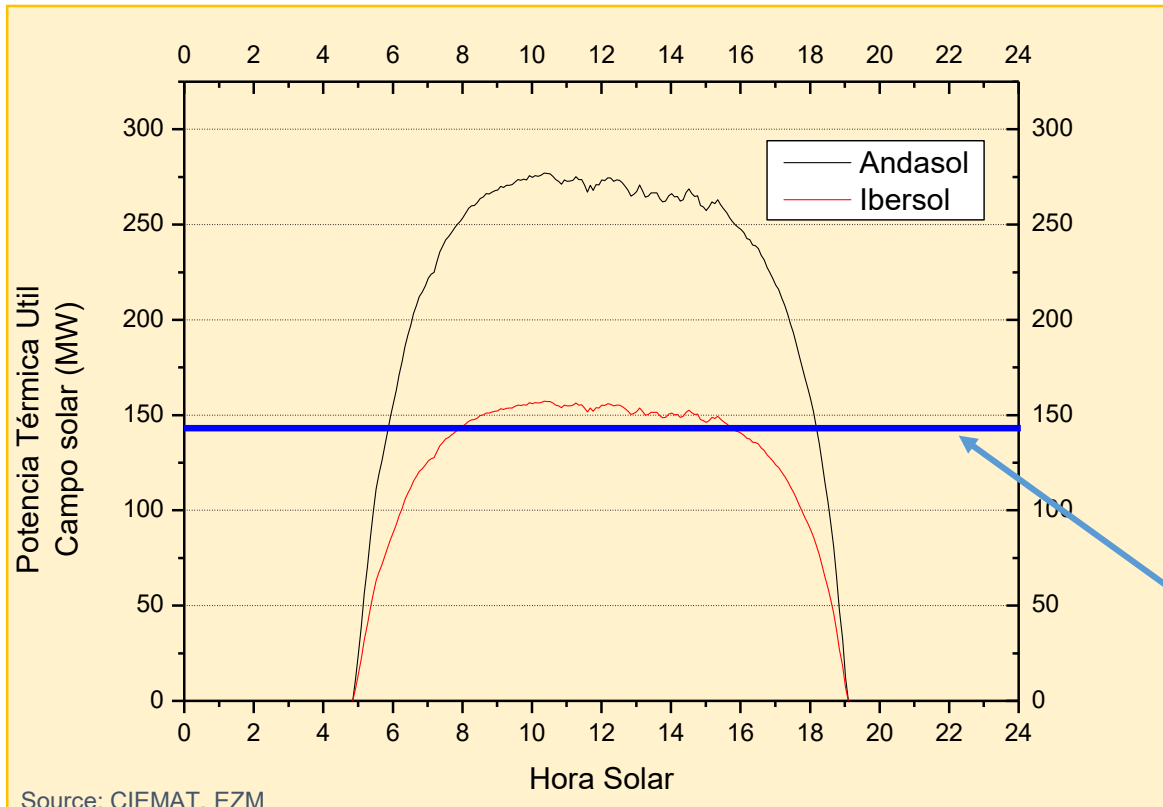


Impact on the STE plant

- ✓ Adding a new subsystem
- ✓ Bigger solar field

Impacts of having TES of large capacity

The size of the solar field depends not only on the nominal electric power of the plant but also on the existence or not of a thermal energy storage (TES) system and on its capacity.



Source: CIEMAT, EZM

With thermal storage (Andasol)

- 50 MWe nominal power
- 510000 m² of PTCs
- Thermal storage 1000 MWh**

Without thermal storage (Ibersol)

- 50 MWe nominal power
- 288000 m² of PTCs
- NO thermal energy storage**

Thermal power required by the power block (50 MWe)



Contents

- Introduction
- Commercial systems → Sensible heat storage
- Latent heat storage → Integration Issues

Commercial TES Systems: Two-tank systems



- Most widely used in commercial STE plants
- Solar salt as storage media

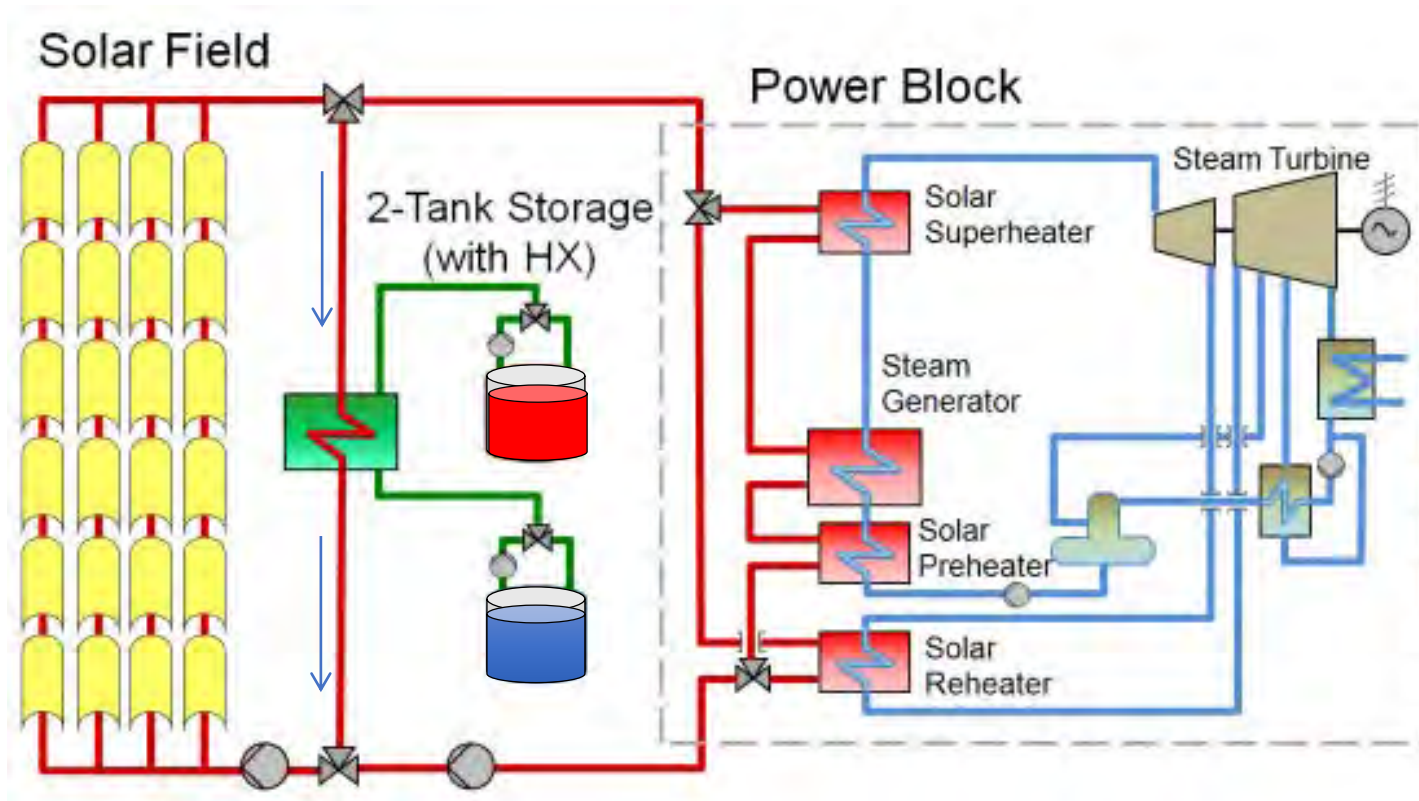
SOLAR SALT: Non-eutectic mixture of nitrate salts:
w-60%NaNO₃+w-40%KNO₃

Why Solar Salt?

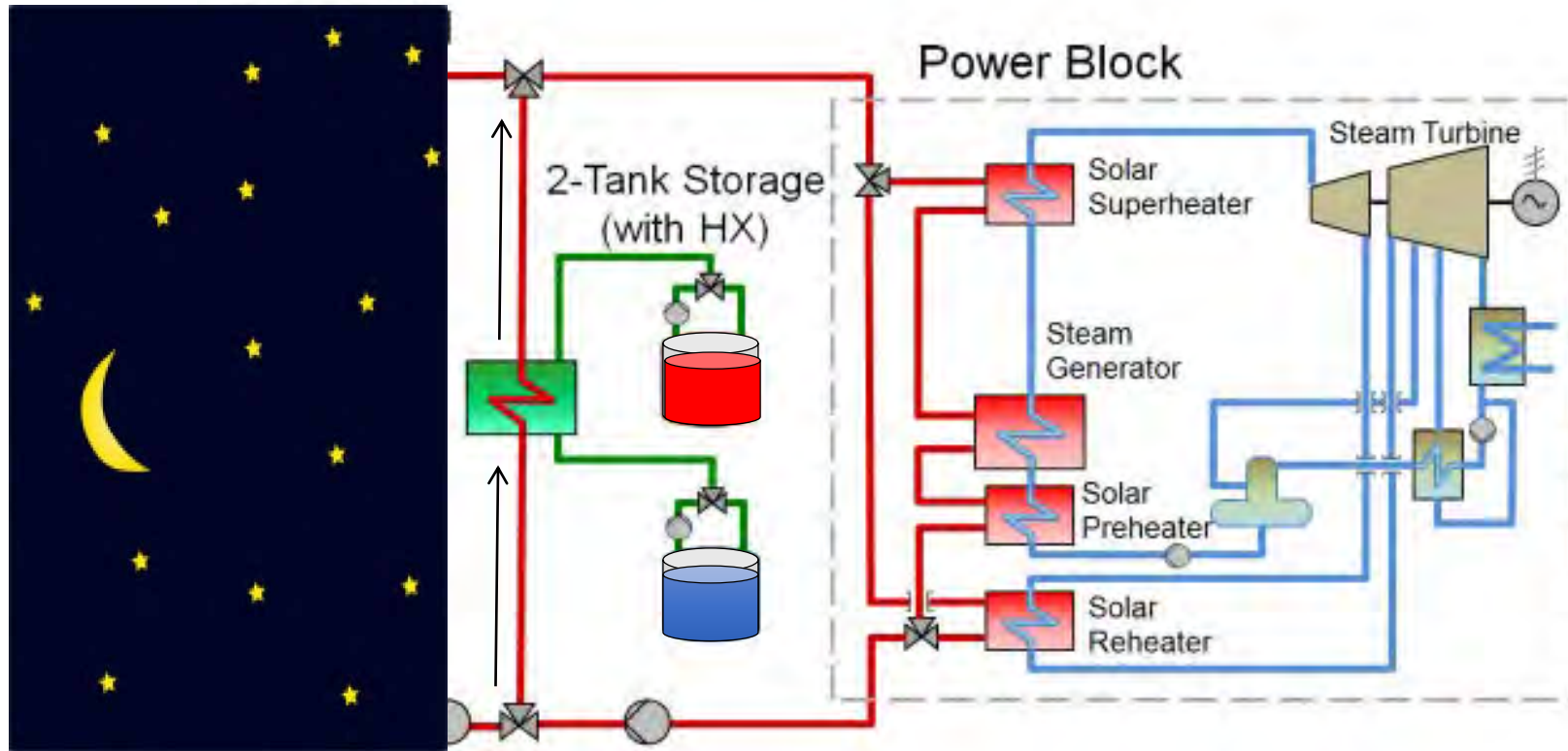
- ☺ Maximum working temperature ~575°C
- ☺ High thermal capacity (~2800 kJ/m³ °C)
- ☺ Low vapour pressure
- ☺ Non explosive or hazardous material
- ☺ Previous experiences in Solar Two (USA, 105 MWh), CESA-1 (Spain, 12MWh), Themis (France, 40MWh), CRTF (NM,USA, 7MWh)
- ☹ At 240 °C they solidify
- ☹ Corrosion issues specially at high temperatures



Two tank storage system. Charging



Two tank storage system. Discharging



Examples of commercial parabolic trough plants with TES

Extresol 1, 2 and 3



Spanish case :

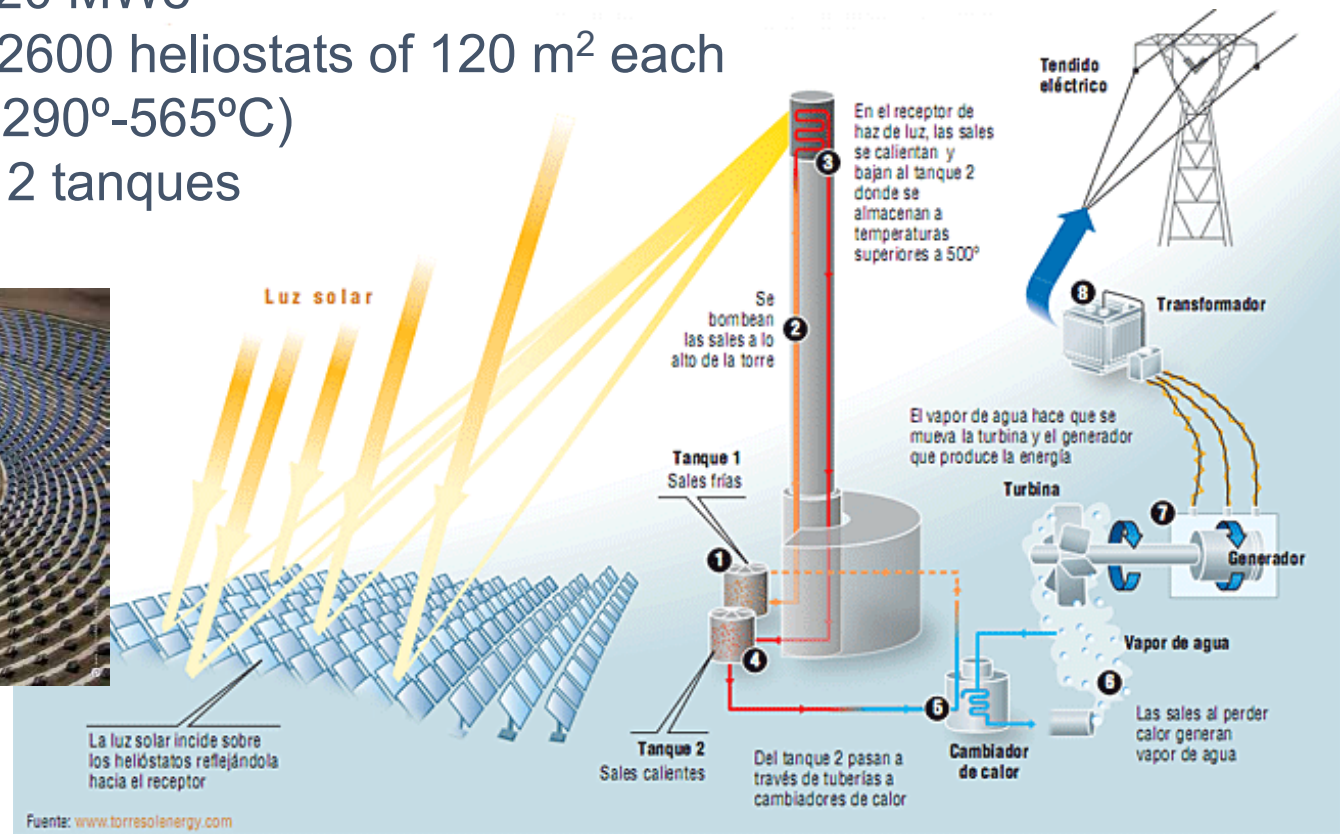
- 50 MWe
- Oil as HTF => 293°C (cold tank) & 393°C (hot tank)
- 7.5 h of storage in two-tank solar salt storage system:
 - 2 tanks of $\text{Ø} \sim 36 \text{ m} \times \text{H} \sim 14 \text{ m}$
 - ~ 28000 Tons of salts

Andasol Complex



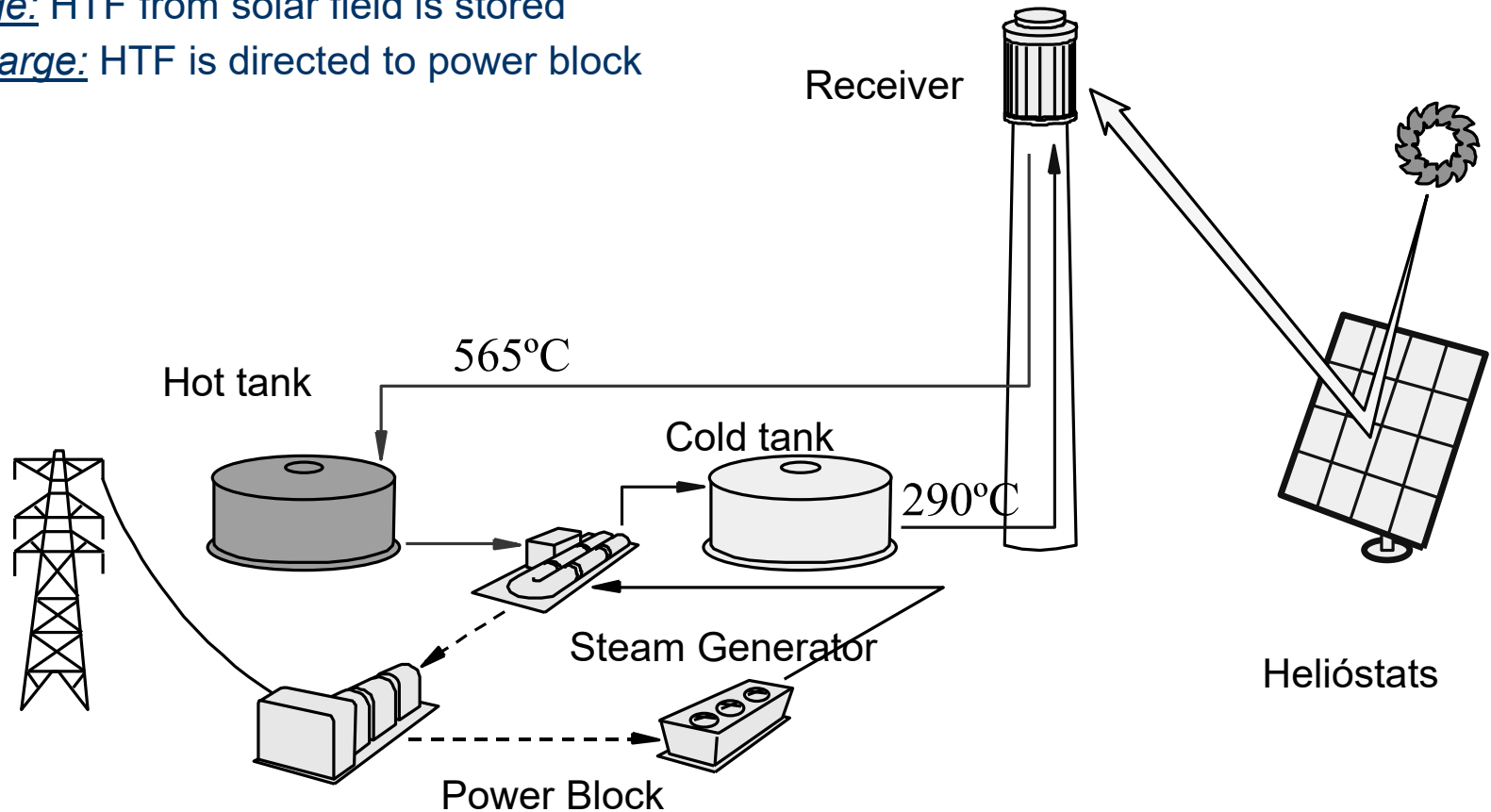
GemaSolar: 1st commercial tower plant with storage

- ◆ Located at Fuentes de Andalucía (Sevilla)
- ◆ Owned by Torresol Energy
- ◆ Nominal power: 20 MWe
- ◆ 140m tower & : 2600 heliostats of 120 m² each
- ◆ HTF: solar salt (290°-565°C)
- ◆ 15 h of storage, 2 tanques



Sensible heat storage: principles

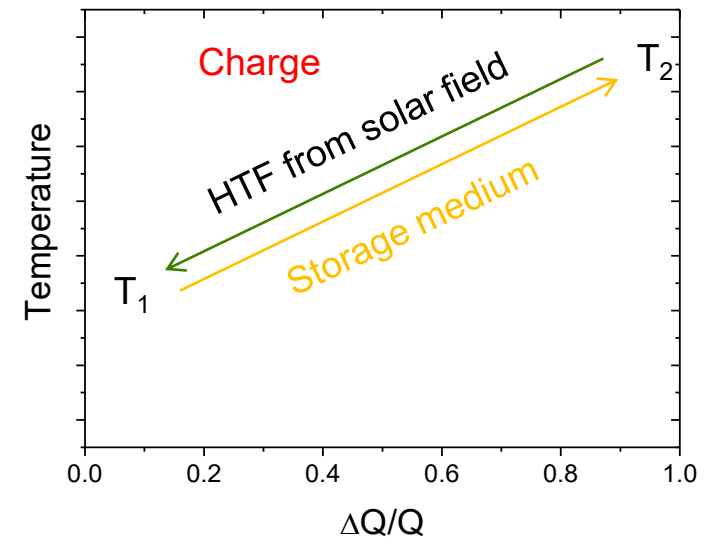
- There is a temperature change in the storage medium
- **Direct storage:**
 - Charge: HTF from solar field is stored
 - Discharge: HTF is directed to power block



Sensible heat storage: principles

- There is a temperature change in the storage medium
- **Direct storage:**
 - Charge: HTF from solar field is stored
 - Discharge: HTF is directed to power block
- **Indirect storage:**
 - Charge: HTF from solar field transfers energy to storage medium

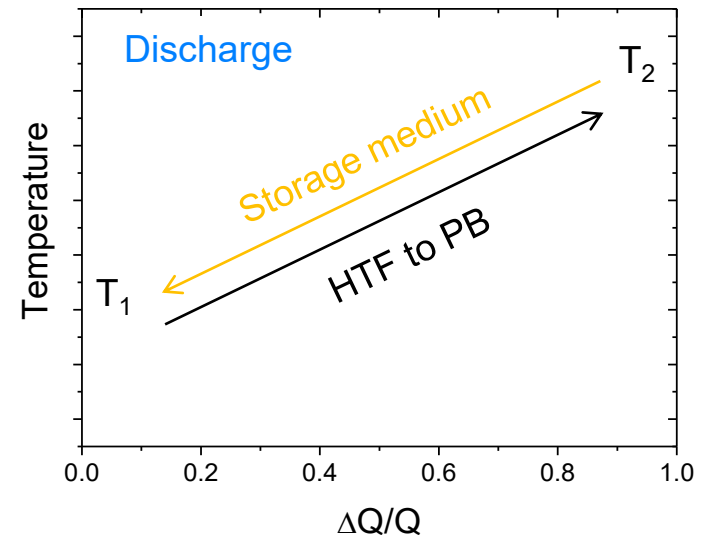
Indirect storage (HTF \neq storage medium)



Sensible heat storage: principles

- There is a temperature change in the storage medium
- **Direct storage:**
 - Charge: HTF from solar field is stored
 - Discharge: HTF is directed to power block
- **Indirect storage:**
 - Charge: HTF from solar field transfers energy to storage medium
 - Discharge: Storage medium transfers energy to HTF going to power block

Indirect storage (HTF≠storage medium)



Sensible heat storage: principles

➤ There is a temperature change in the storage medium

➤ **Direct storage:**

- Charge: HTF from solar field is stored
- Discharge: HTF is directed to power block

➤ **Storage capacity** (kWh) depends on temperature interval in the storage medium:

$$\Delta Q = m \cdot C_p \cdot (T_2 - T_1) \Leftrightarrow (>0 \text{ in charge; } <0 \text{ in discharge}) \Leftrightarrow T_2 - T_1$$

➤ For **liquid storage media**:

- Heat transfer mechanism is convection
- Discharge power may be kept constant

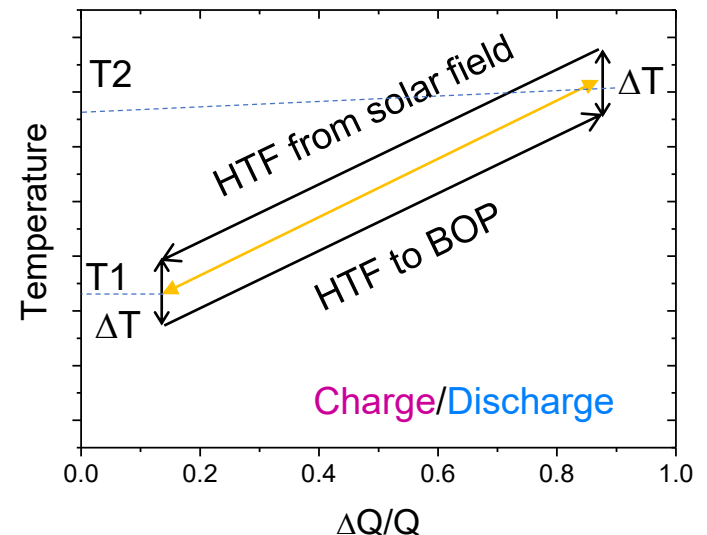
➤ For **solid storage media**:

- Heat transfer mechanism is conduction
- Discharge power might not be constant

➤ **Indirect storage:**

- Charge: HTF from solar field transfers energy to storage medium
- Discharge: Storage medium transfers energy to HTF going to power block
- There is a temperature gap in HTF between charge and discharge (ΔT)

Indirect storage (HTF \neq storage medium)



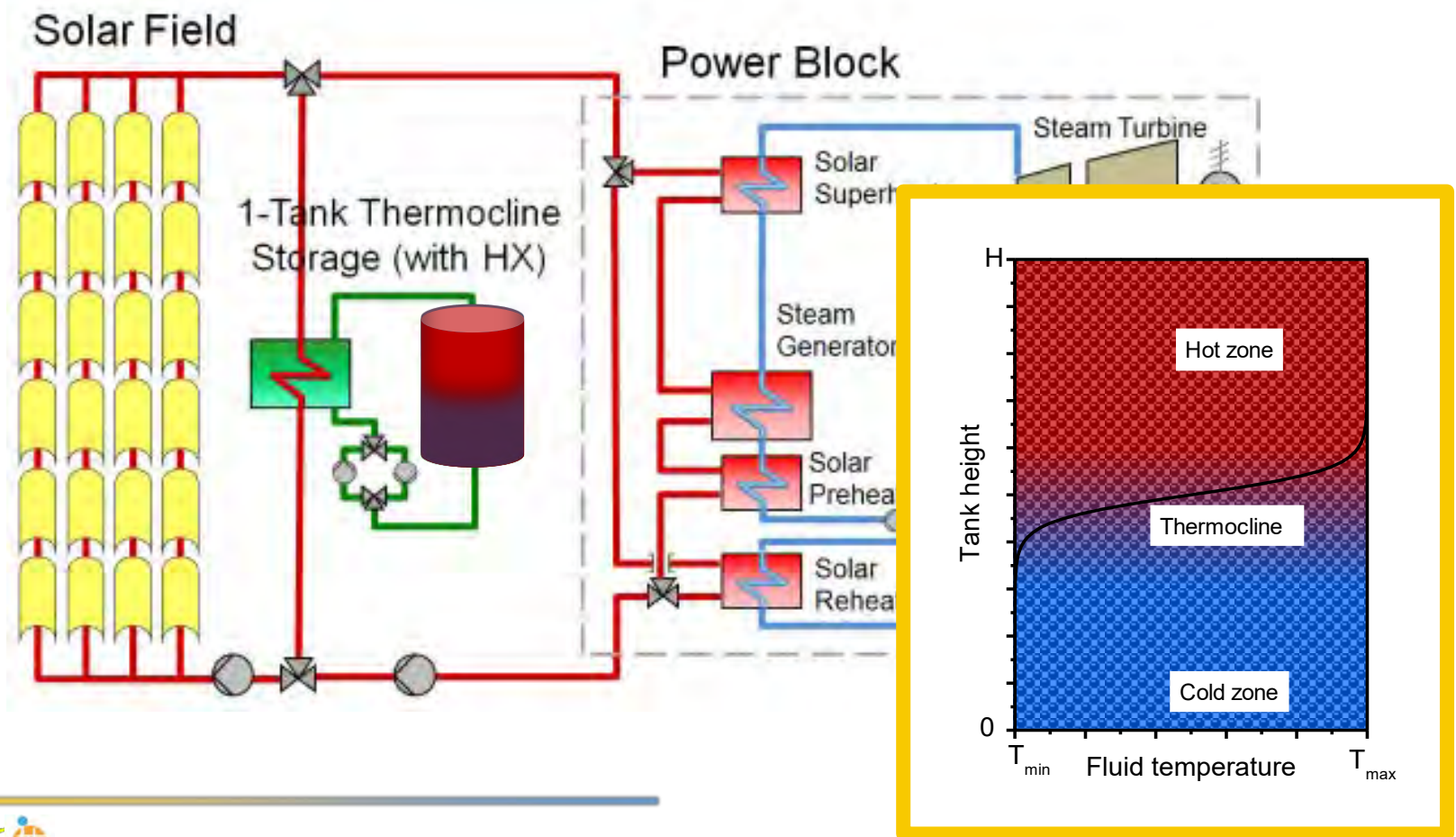
Sensible heat storage: storage medium requirements

- **High volumetric thermal capacity, ρC_p**
 - Solar salt (60%NaNO₃+40%KNO₃): ~2800 kJ/m³ °C
 - Synthetic oil: ~ 1900 kJ/m³ °C
 - water: ~ 4200 kJ/m³ °C
 - concrete: ~2500 kJ/m³ °C
 - rocks: ~2700 kJ/m³K
 - Vitriified industrial wastes (Cofalit y Plasmalit): ~3000 kJ/m³K
- **Low vapor pressure for liquid media** → avoiding pressurized tanks
 - Water has to be under pressure: 30bar/230°C; 100bar/311°C (*)
 - Therminol VP1 has a vapor pressure of 11bar at 395°C
- **Stable** in the temperature range of operation, (T_1, T_2)
- **Non explosive or hazardous materials**
- **Low price materials**

Molten salts fulfil these requirements

Configurations of sensible heat storage:

Single tank system. Thermocline

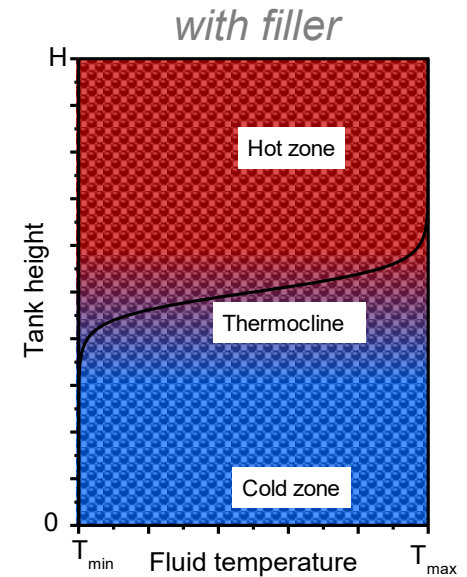
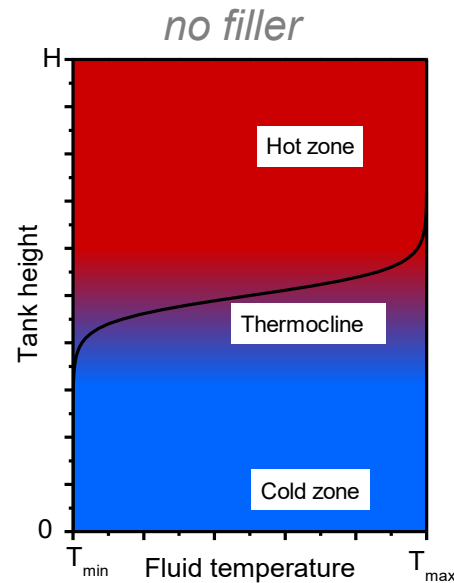


Thermocline tank: benefits and drawbacks



ADVANTAGES:

- Just one tank \Rightarrow expected cost reduction up to 33%
- Having a solid filler \Rightarrow cost reduced down to 75%



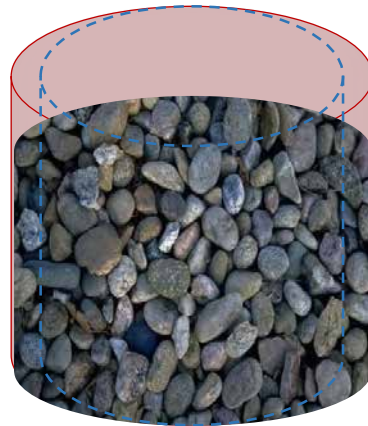
CHALLENGES

- Thermocline region degradation
- Having a solid filler \Rightarrow Compatibility of media (HTF and filler)
- Having a solid filler \Rightarrow Thermal ratcheting

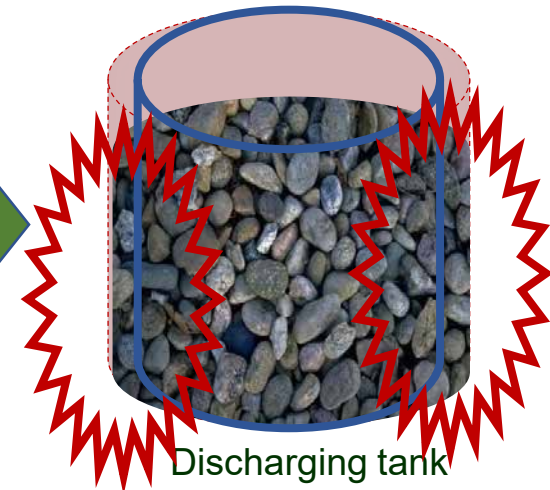
Thermal ratcheting



Discharged tank
cold wall tank and filler



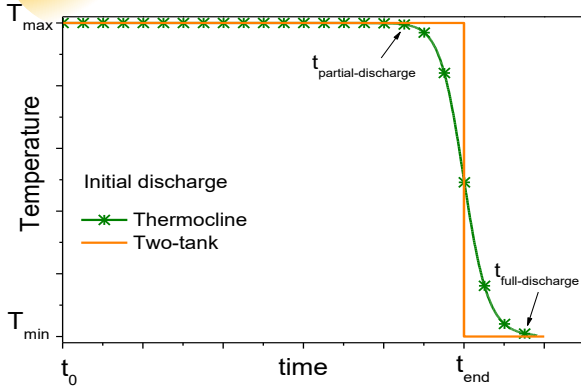
Charging tank
thermal walls expansion



Discharging tank
thermal walls contraction

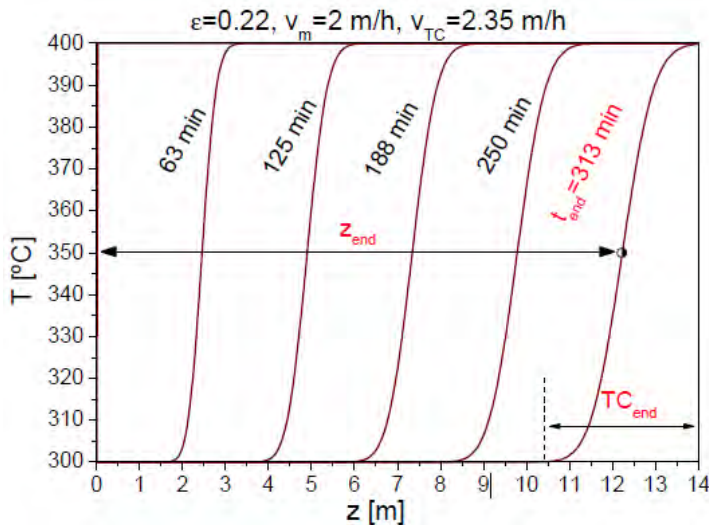
potential unfordable
mechanical stresses!!!:
for the walls and/or the filler

Thermocline region behavior

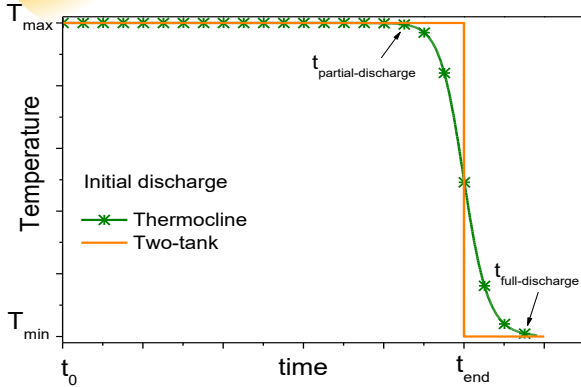


- **Not all the energy is useful for power generation:**
For a similar capacity thermocline tank need a bigger tank size than each tank in a two-tank configuration

- **Thermocline region increases its size along the time**



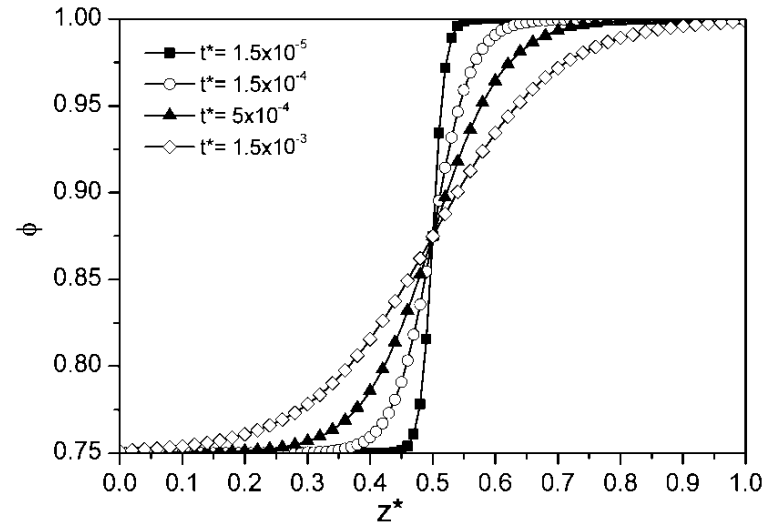
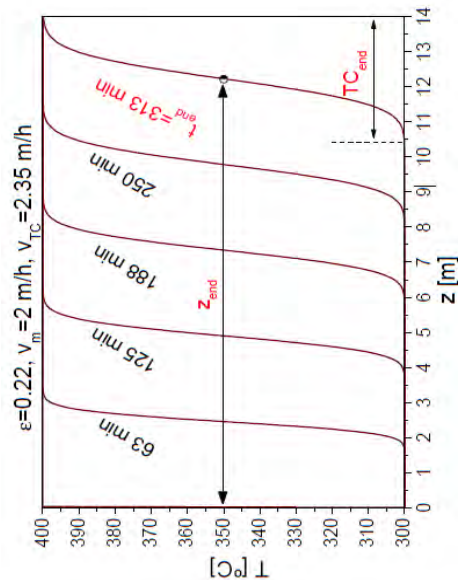
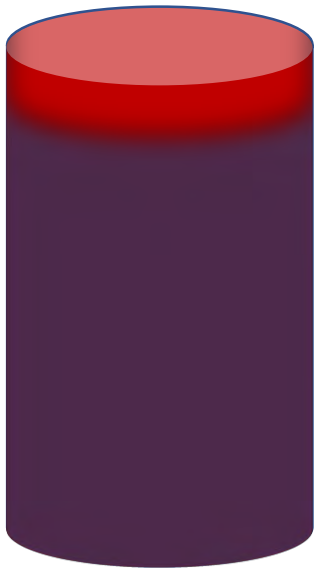
Thermocline region behavior



Not all the energy is useful for power generation:

For a similar capacity thermocline tank need a bigger tank size than each tank in a two-tank configuration

➤ Thermocline region increases its size along the time



during charging/discharging processes

and during stand-by situations

Thermocline tank requires...



Extracting (remove) completely the thermocline region out of the tank

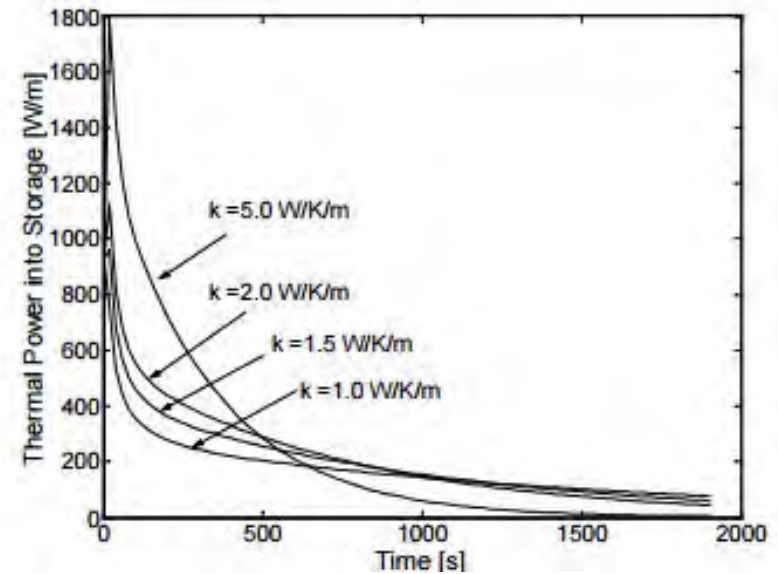
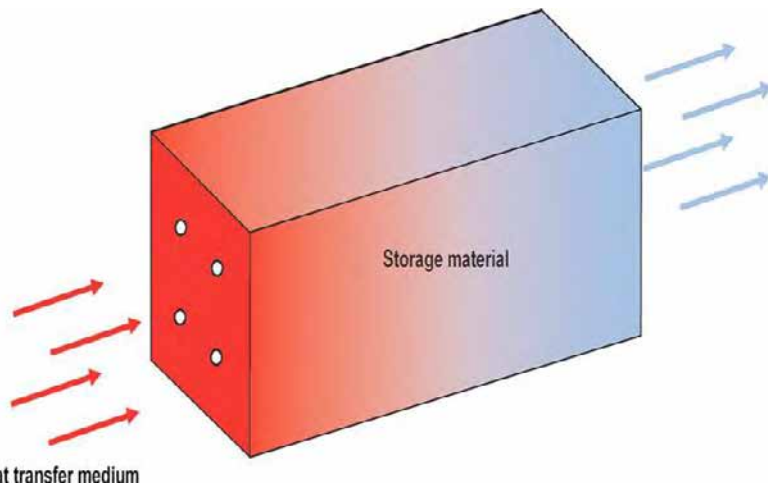


What to do with this energy?

- Solar field preheating during start-up
- Steam turbine preheating before starting operation
-

Sensible heat in solids (I)

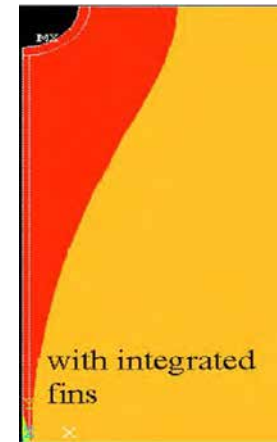
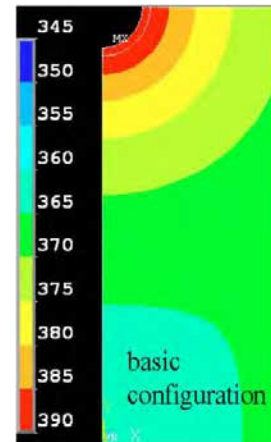
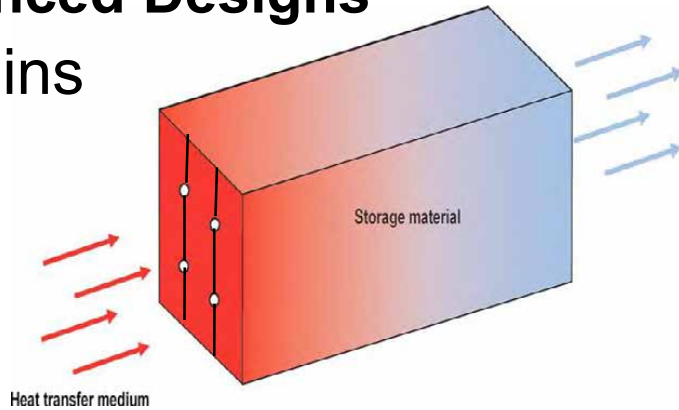
- **Special Concrete** ($\sim 2500 \text{ kJ/m}^3\text{K}$), ceramic, industrial wastes (Cofalit, Plasmalit)
- Mechanical strength is critical
- **Conduction** is the main heat transfer mechanism ($k_{\text{tipica}} \leq 1.5 \text{ W/mK}$)



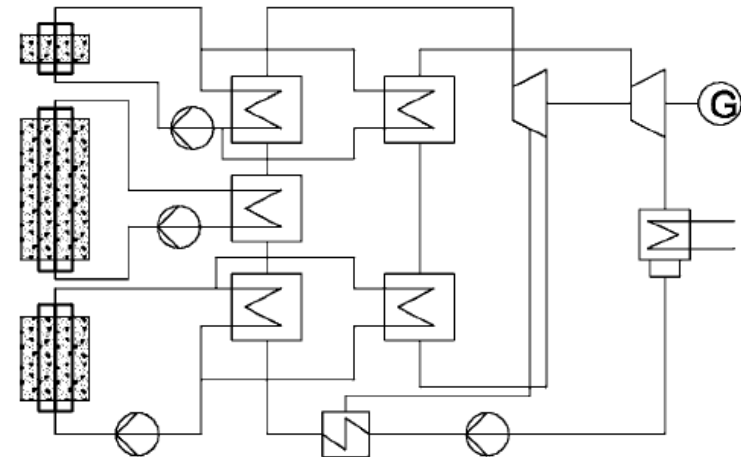
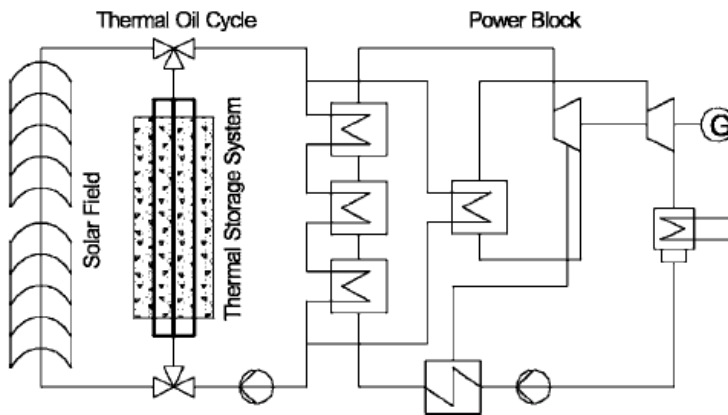
Sensible heat in solids (II)

- Enhanced Designs

 - Fins



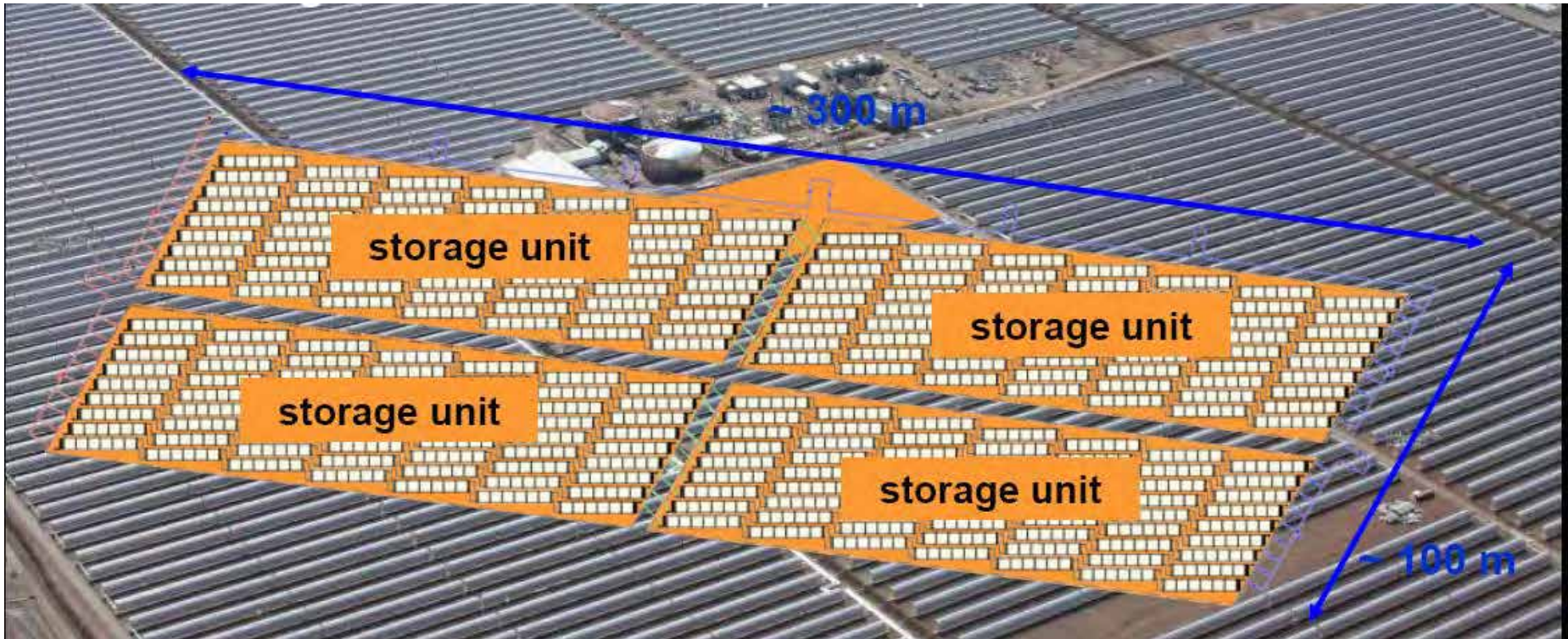
- Modular systems (smaller ΔT : $\Delta T = \Delta T_1 + \Delta T_2 + \Delta T_3$)



D. Laing et al., 2008, J. Solar Energy Engineering, V 130.

Size comparison of concrete and 2-tanks with molten salts for 1GWht of capacity

The plot of land required is 5 times smaller for molten salt system



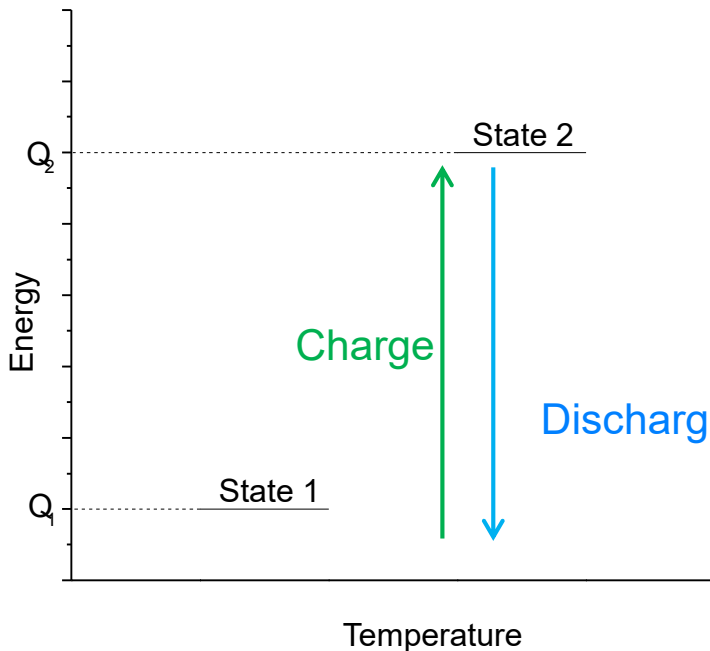
Laing, 2008

Contents

- Introduction
- Commercial systems → Sensible heat storage
- Latent heat storage → Integration Issues

Latent heat storage. Fundamentals

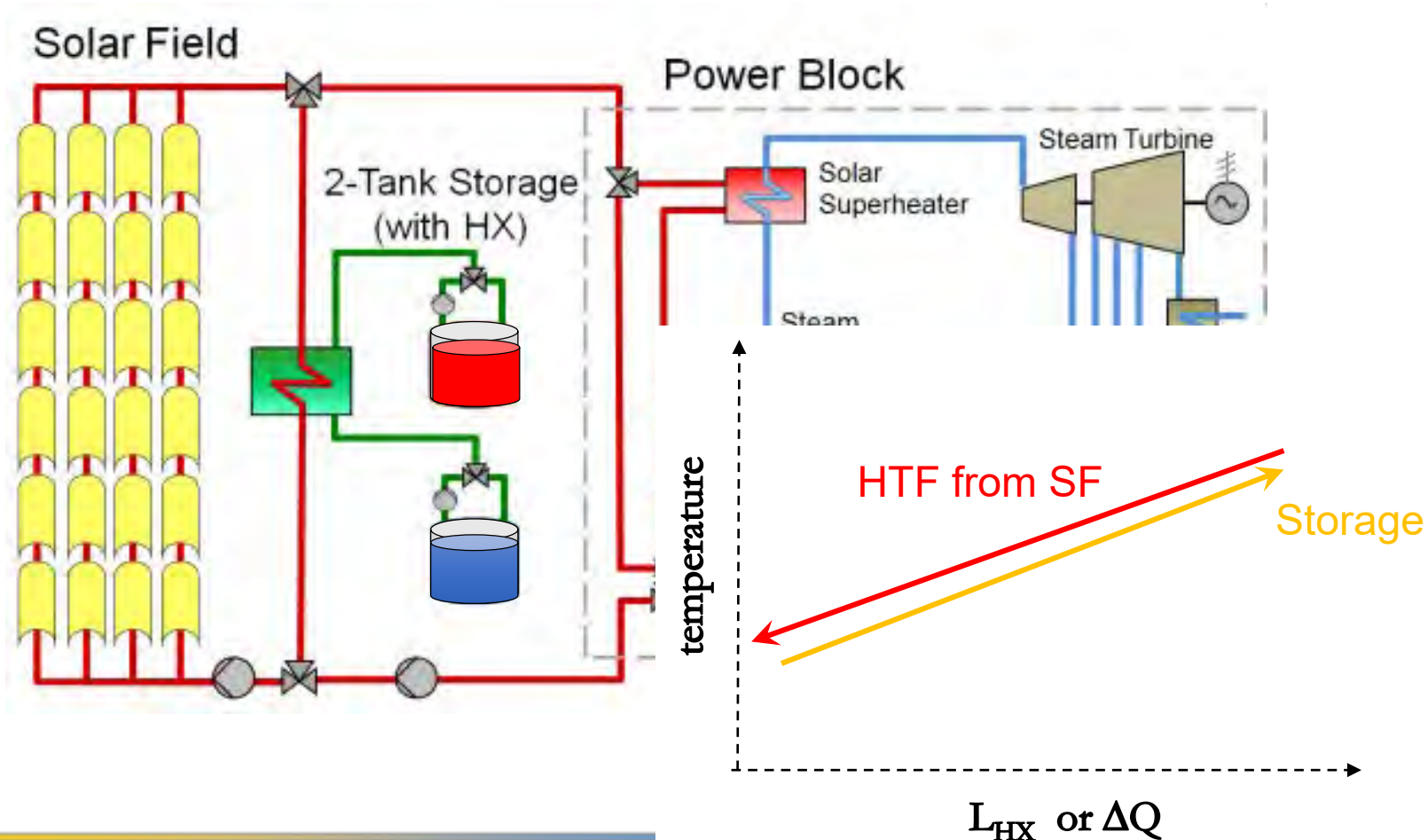
- The storage medium **undergoes a phase change** \Rightarrow Phase change material (PCM)



- Charge process: $Q_{TES} = Q_2 - Q_1 = m_{PCM} \cdot \Delta H_{phase} > 0$
- Discharge process: $Q_{TES} = Q_1 - Q_2 = m_{PCM} \cdot \Delta H_{phase} < 0$
- Storage capacity, Q_{TES} , depends on Latent enthalpy, ΔH_{phase}
- PCM is chosen taking into consideration its phase change temperature, T_{phase}
- T_{phase} is imposed by the system delivering the energy to be stored

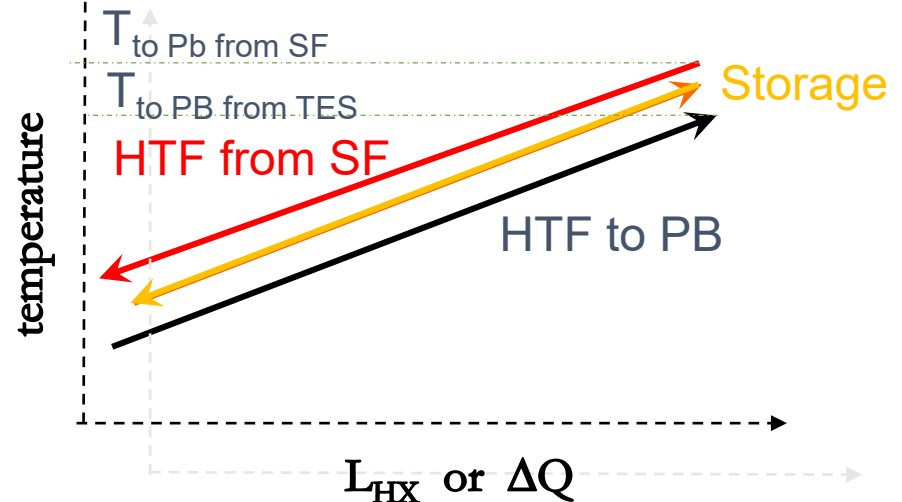
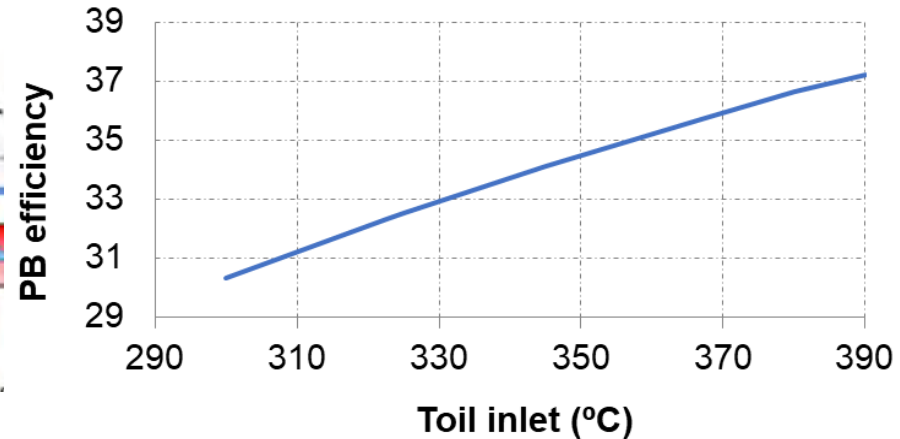
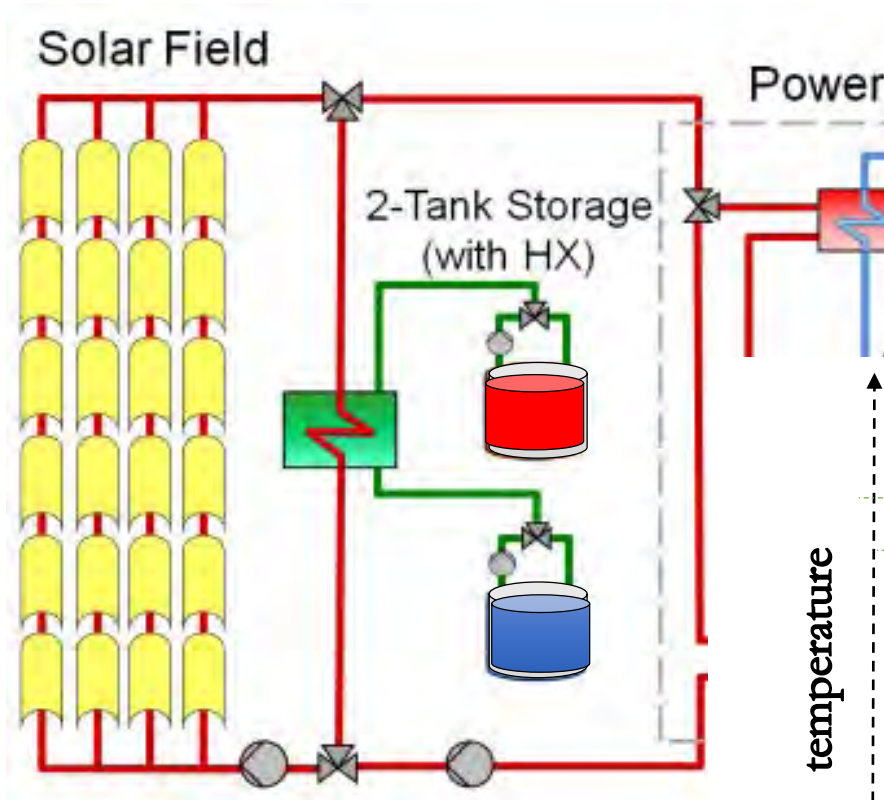
Is an Andasol type STE plant appropriate for a latent storage system?

Charge

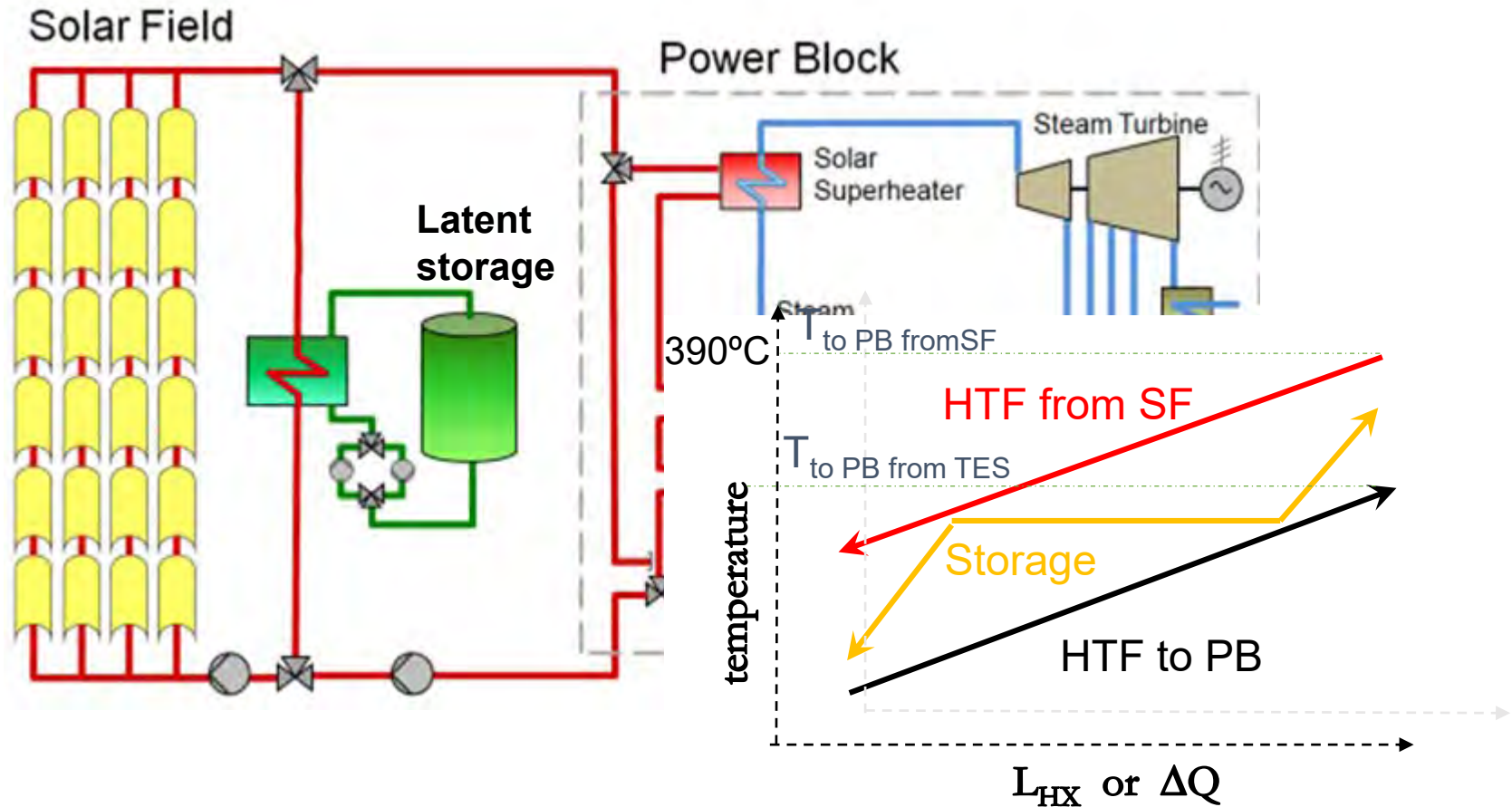


Is an Andasol type STE plant appropriate for a latent storage system? (II)

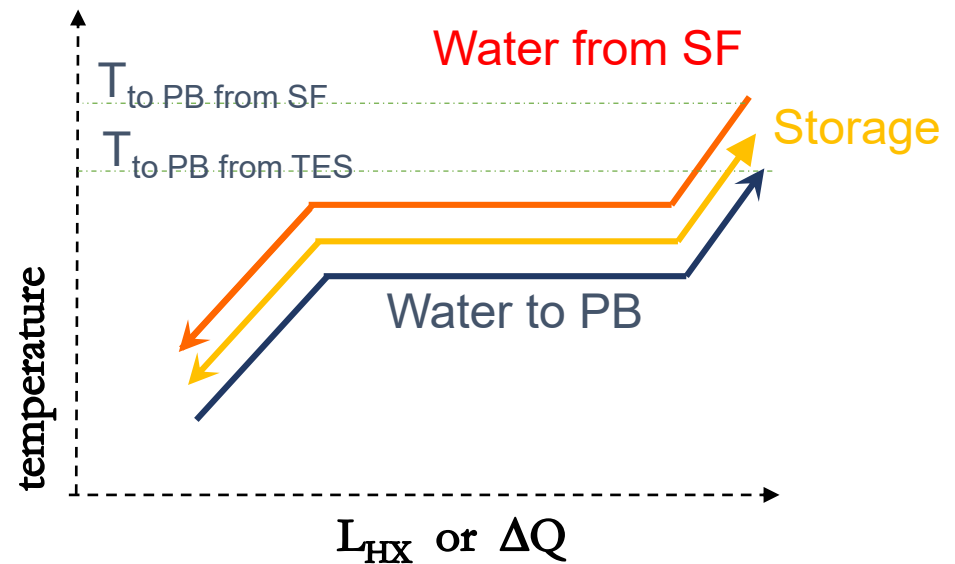
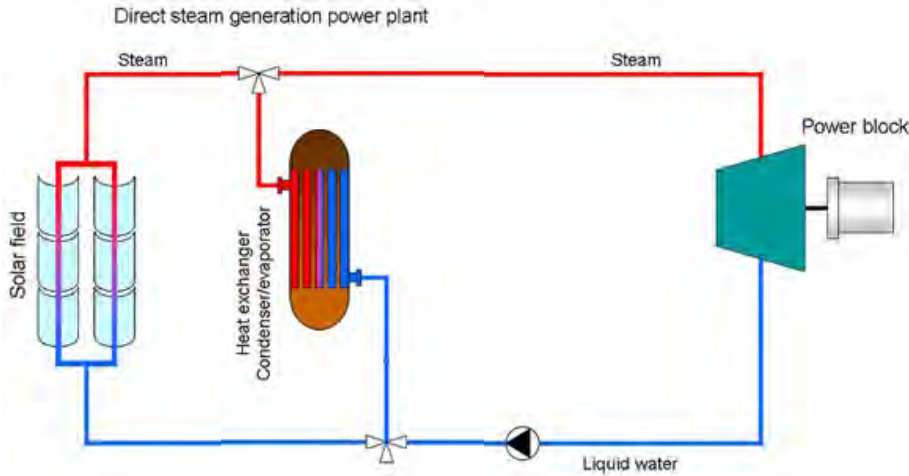
Discharge



Is a Andasol type STE plant appropriate for a latent storage system? (III)

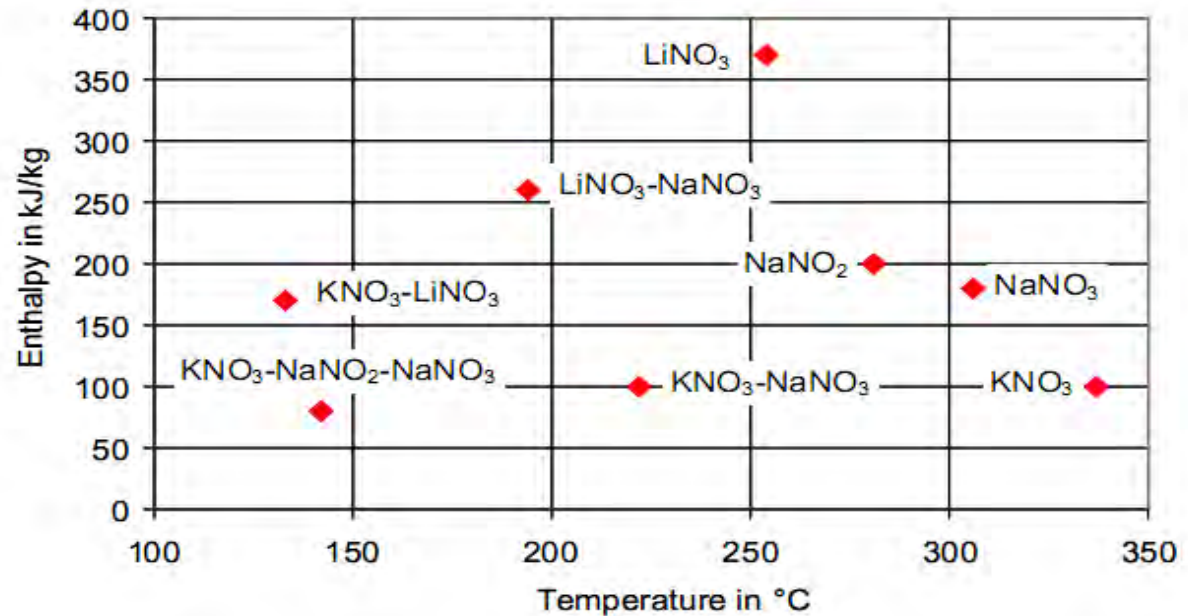


Direct Steam Generation STE Plant



T_{phase} suitable for DSG STE plants

- for parabolic troughs, T_{phase} should be of about 310°C (~100bar)
- For towers, T_{phase} should be in the range 310-350°C (~100-155bar)



Commercial STE plants with DSG

Tower



<http://www.abengoasolar.com/>

Tower: PS10 and PS20

- Sanlúcar la Mayor (Sevilla)
- Abengoa Solar
- 10/20 MWe
- HTF: water liquid/vapor (240°C)
- Storage: 1 h ⇒ RUTHS ACCUMULATOR

Fresnel: Puerto Errado 1 & 2

- Calasparra (Murcia)
- Novatec Solar España S.L.
- 1.4/30 MWe
- HTF: water liquid/vapor (140-270°C)
- Storage: 0,5 h ⇒ RUTHS ACCUMULATOR

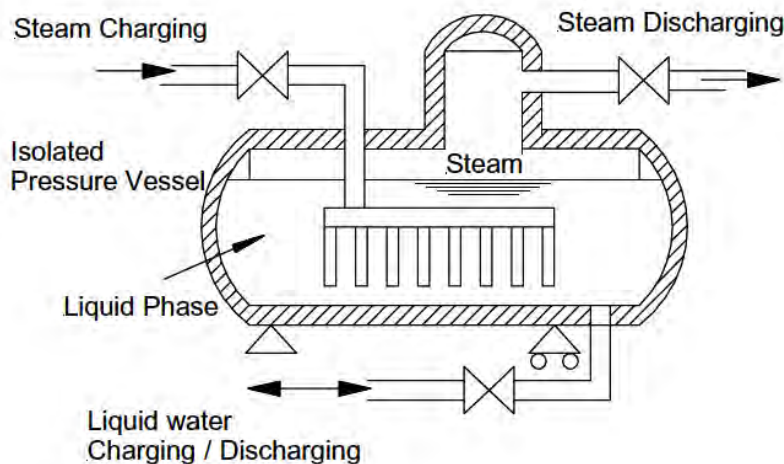
Fresnel



<http://www.novatecsolar.com>

Thermal storage with steam accumulators

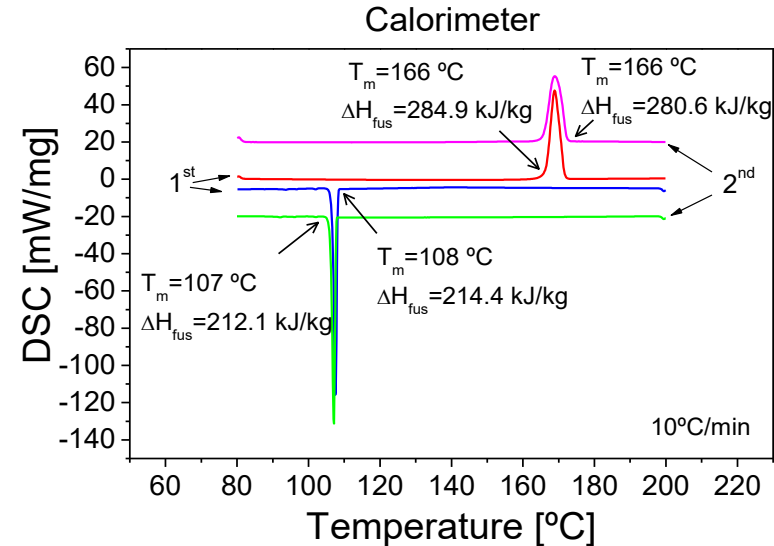
- Water as storage medium
- Use **sensible** heat storage in pressurized saturated liquid water
 - \Rightarrow Take advantage of the high volumetric heat capacity of water: $4200 \text{ kJ/m}^3\text{K}$
- Sliding pressure systems: **Ruths** accumulators (American patent 1929)
- **Charge:** Superheated or saturated steam is stored as saturated water \Rightarrow pressure, temperature and water mass increases in the vessel
- **Discharge:** Saturated steam is produced by lowering the pressure inside the storage vessel



- ☺ Facilitate the operation of DSG plants under solar radiation transients
- ☹ Turbine has to work at lower pressure conditions (“sliding pressure”)
- ☹ They are not a long term storage option

Features of a good Phase Change Material (PCM)

- Adequate phase change temperature:
 T_{phase}
- No degradation in the working temperature range
- Stability under cycling
- Reversible process: low supercooling
- High phase change enthalpy: $\Delta H_{\text{PhaseChange}}$
- solid/liquid & liquid-solid phase changes:
 - Conduction is the main heat transfer mechanism
=> **High thermal conductivity**



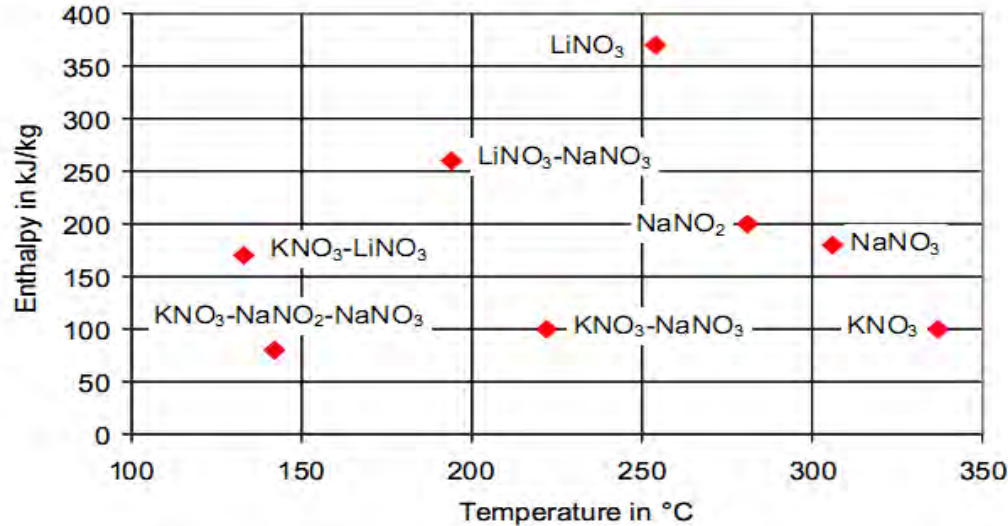
Heating peak: 166°C
Cooling Peak: 107 °C
60°C supercooling!!!



D-Mannitol

Possible Phase Change Materials (PCM)

• INORGANIC salts



Thermal conductivity

<1W/mK

High thermal resistance

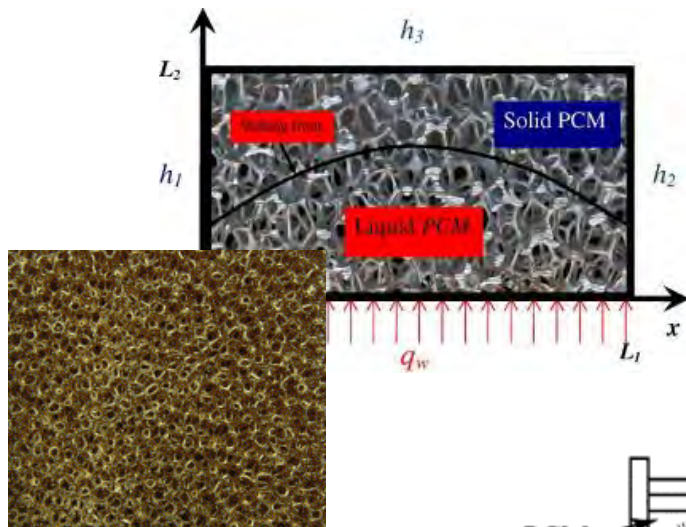
Since inorganic salt can't be in direct contact with steam, they must be separated by walls, which must withstand the high pressure of the steam.

Solidification of the PCM in contact with these walls creates a thermal barrier for heat conduction (a great problem) because convection is avoided.

Reducing thermal resistance (I)

- Packing the PCM in a matrix with high k

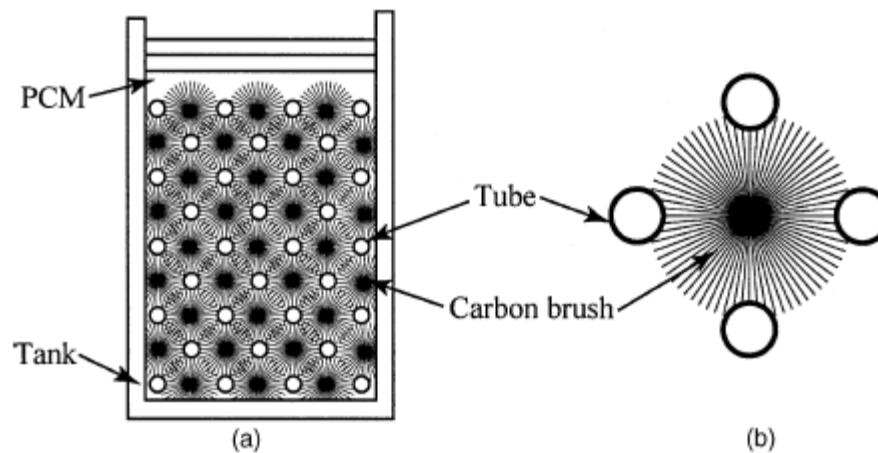
Metal foams



Composites:
Graphite+salt



Carbon fibers



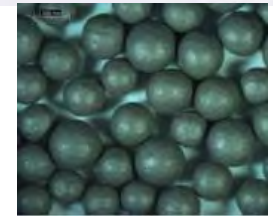
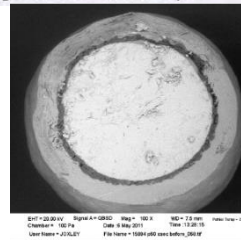
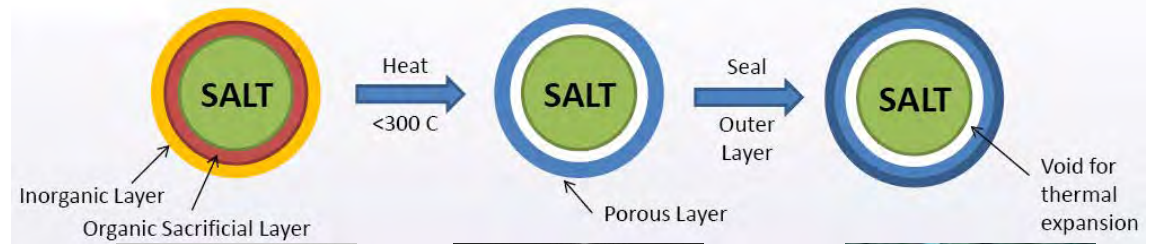
Reducing thermal resistance (II)

• Macroencapsulation

Metallic shells



Clay & Metal Shell & Sacrificial material



Porous PCM pellets & coating



Additional Problems:

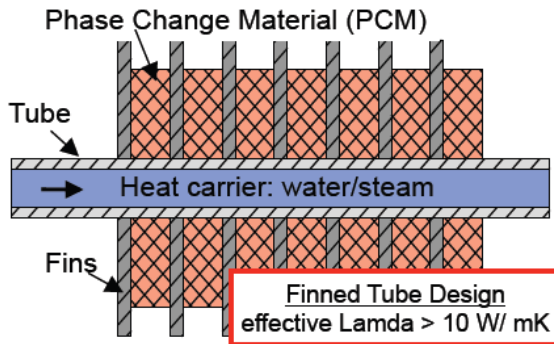
- $\Delta V/V$ high
- corrosion

♦ (*) Courtesy of Terrafore

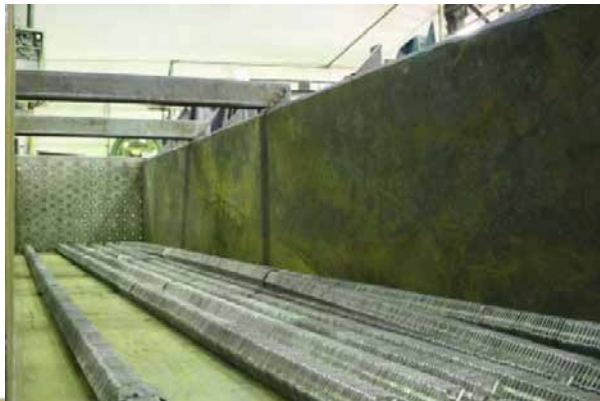
Reducing thermal resistance (III)

Extended Surfaces

Graphite foils (horizontal pipes)



Aluminium fins (vertical pipes)



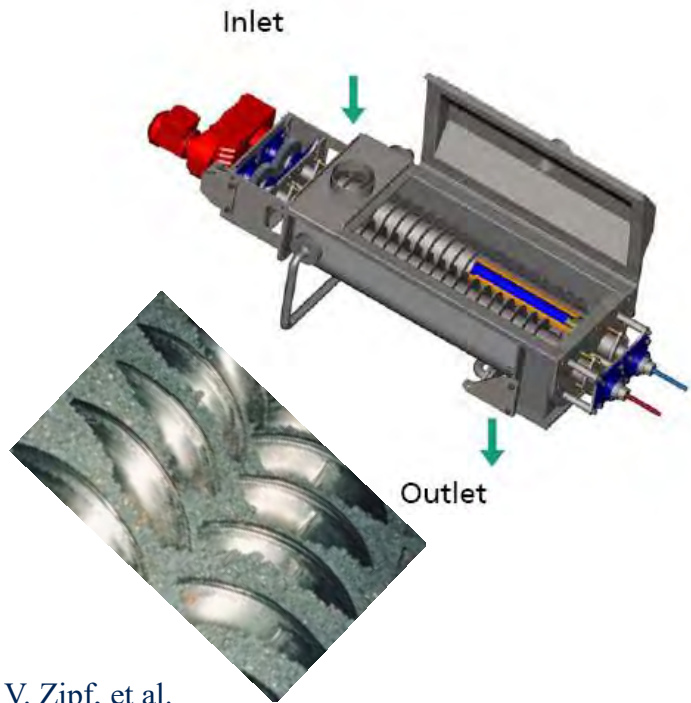
Extruded longitudinal fins

680 kWh

Latent heat storage: moving PCM

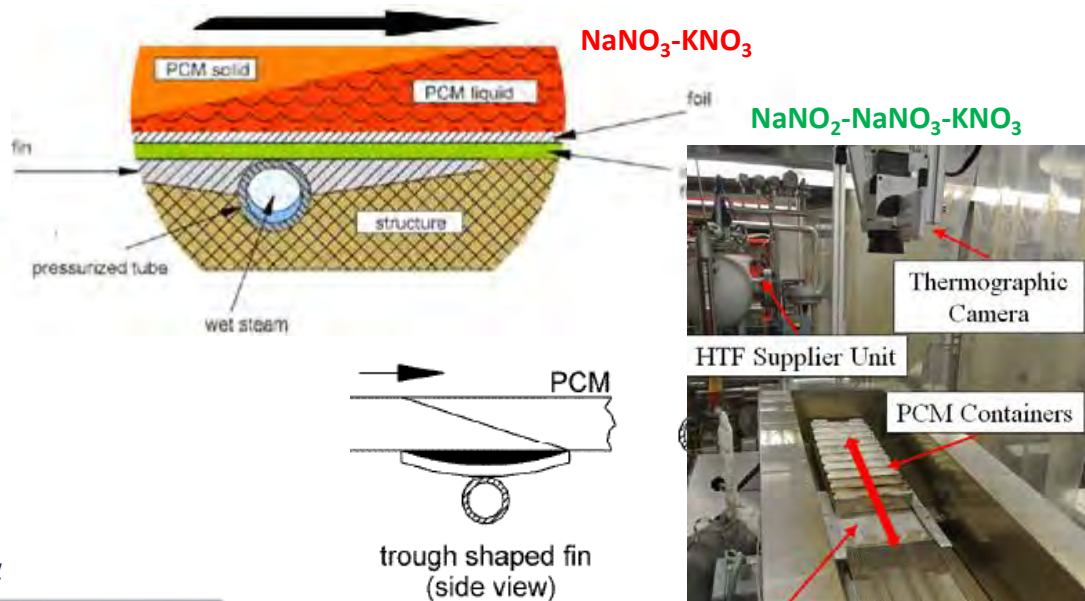
decoupling heat transfer area and storage place

- Innolat Project : Fraunhofer ISE
 - Screw heat exchanger
 - Both heat and material transport
 - Self-cleaning



- **PCMflux concept: DLR**

- Thin liquid layer connects PCM and HTF piping
- eutectic mixture $\text{NaNO}_2\text{-NaNO}_3$ & Tin as candidates for thin liquid layer
- Self-cleaning

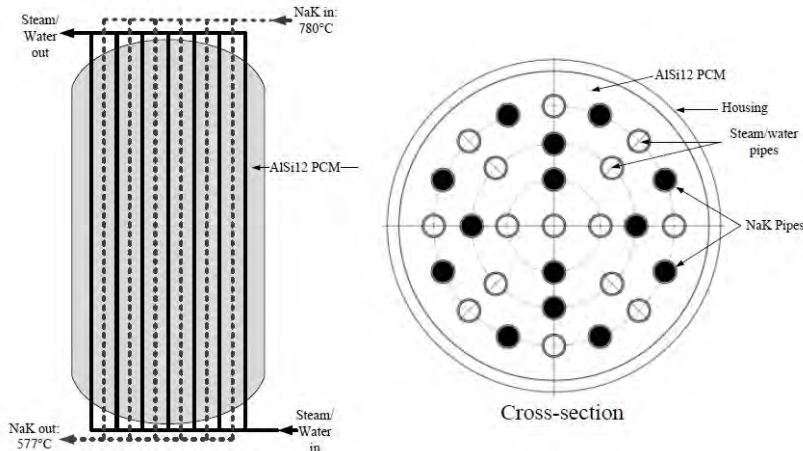


V. Zipf, et al.
 Applied Energy DOI: 10.1016/j.apenergy.2012.11.044

Possible Phase Change Materials (PCM)

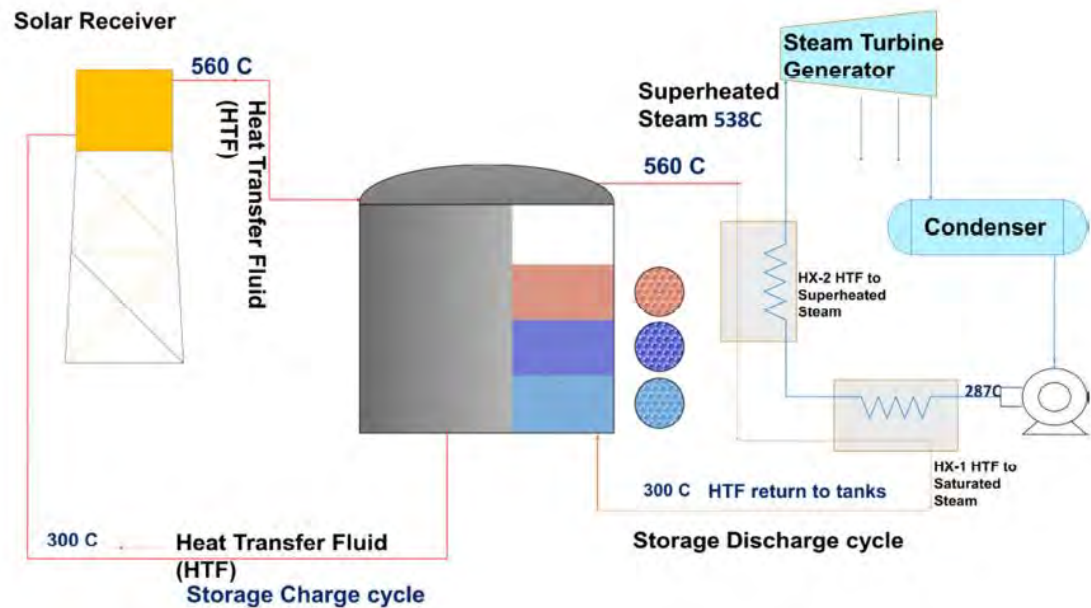
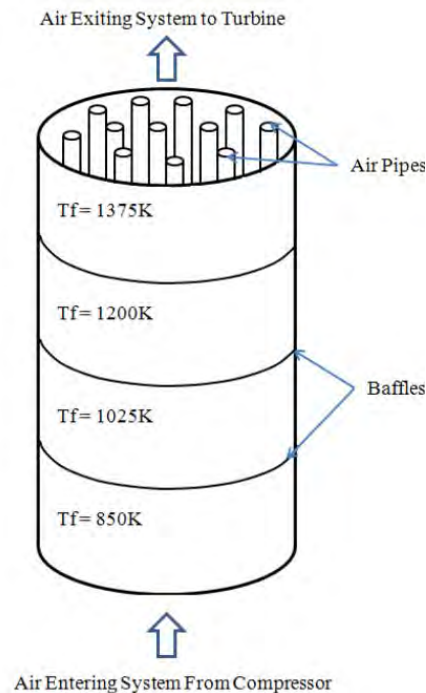
METALLIC alloys:

- Mg (49%)-Zn(51%): $T_m=340^{\circ}\text{C}$; 138 - 180 kJ/kg
- Al(60%) – Mg(34%) – Zn (6%): $T_m=450^{\circ}\text{C}$, non stable?
- Mg (22%)-Zn(45%)-Cu(32%): $T_m=305^{\circ}\text{C}$; 157kJ/kg (Tecnalia)



Further applications of latent storage

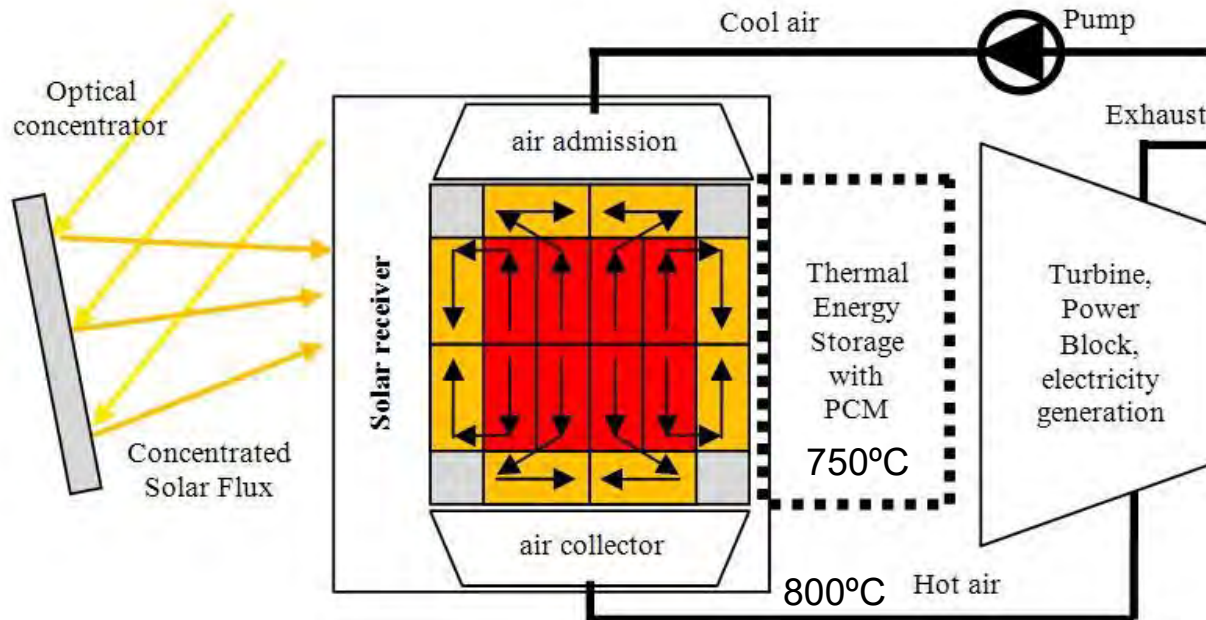
Substitution of a sensible TES by a cascade latent TES



Further applications of latent storage (II)

Receivers protection

PCM: Li_2CO_3 + Copper for enhancing thermal conductivity



...final comments..

- STE provides dispatchable power thanks to large capacity storages available today commercially (two-tank configuration with molten solar salt as storage medium)
- There is a lot of room for reducing the cost of this type of systems (sensible TES): thermoclines –with/without fillers-, solids, etc.
- There is still a lot of work to do to provide complete TES solutions to STE plant with Direct Steam Generation (DSG)
- **Follow a holistic approach when studying TES**



SFERA-III
1st Summer School
September, 9th- 10th, 2019
CNRS- PROMES, Odeillo, France

TES for solar thermal power plants

Questions ?

Presented by Eduardo Zarza (eduardo.zarza@psa.es)
Esther Rojas (esther.rojas@ciemat.es)



SFERA-III

Solar Facilities for the European Research Area

1st Summer School “Thermal energy storage systems, solar fields and new cycles for future CSP plants”

WP1 Capacity building and training activities

Odeillo, France, September 9th-11th 2019



Solar Facilities for the European Research Area

“Novel molten salts for TES applications in CSP plants”

Anna Chiara Tizzoni – ENEA – Rome- Italy

NETWORKING



THIS PROJECT HAS RECEIVED FUNDING FROM THE EUROPEAN UNION'S HORIZON 2020 RESEARCH AND INNOVATION PROGRAMME UNDER GRANT AGREEMENT NO **823802**



Solar Facilities for the European Research Area

Contents:

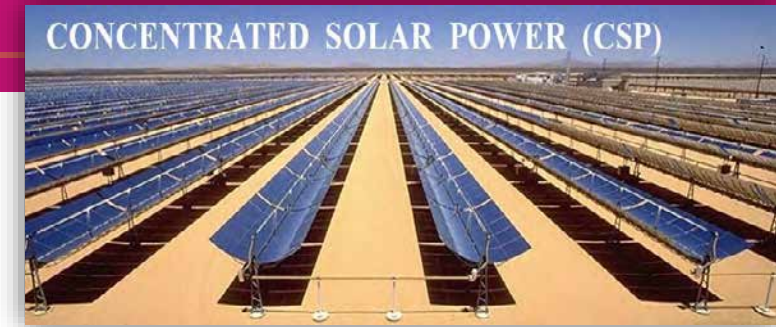
- ❖ Thermal Energy Storage in general
- ❖ Novel molten salts mixtures: selection criteria
 - ❖ Working temperatures
 - ❖ Thermophysical characterization
 - ❖ Environmental safety and risk for human health
 - ❖ Material cost
 - ❖ Construction materials compatibility and corrosion resistance of alloys
- ❖ Results & future perspectives



Concentrated Solar Power (CSP) is one of the most promising technologies:

- for **carbon free energy production**
- to **store** large amounts of heat that can be reused in many useful ways.

A proper storage systems is a crucial point for the economic dispatchability of CSP technology.



Molten salts are increasingly becoming the most used heat transport fluids (HTF) and heat storage materials (HSM) in these types of installations.

A binary mixture of $\text{NaNO}_3\text{-KNO}_3$, indicated as “solar salt” is currently the most employed molten nitrate, used as reference material.

High $T_{\text{solidification}}$ → an external heating system is necessary during the startup such as the tracing of pipelines, and the electrical heaters are expected to provide for the minimum storage temperature tank.

CSP Technology



Heat Transfer Fluids
(HTF)

Heat Storage
Materials (HSM)



Useful to investigate **other mixtures** with low melting points, which can be employed both as HTF or HSM.

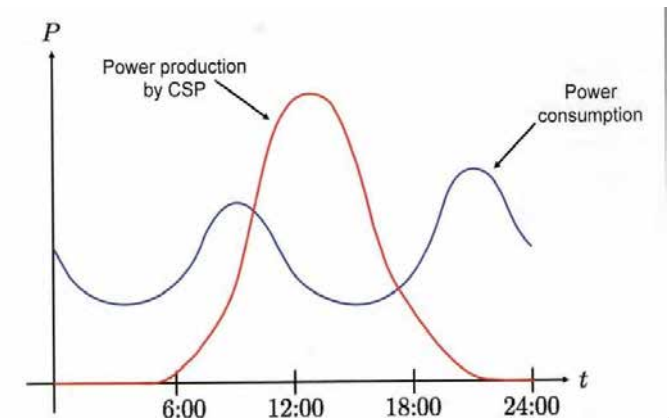
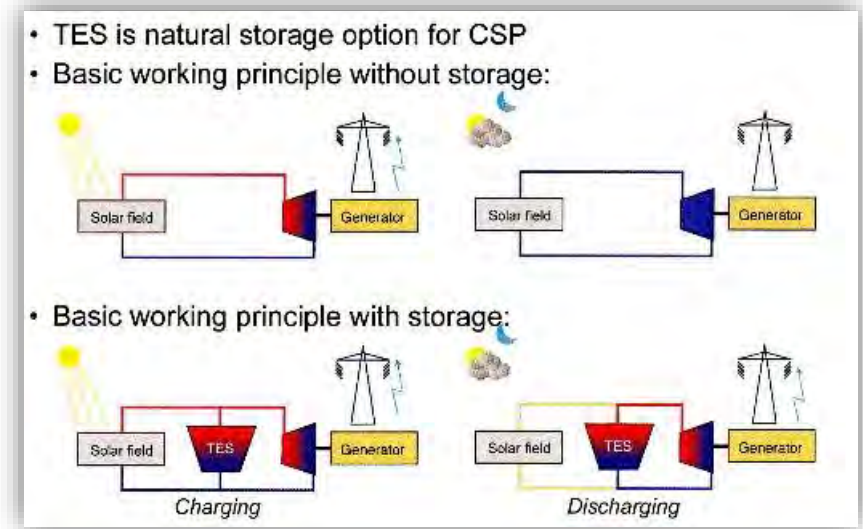
- Predictive modelling methods for the design of new inorganic low melting fluids.
- Exact characterization of their thermal, chemical and physical properties

Topic of this lesson: define a proper selection criteria and summarize the state of the art about the main molten salt HTFs HSMs for real life CSP applications at **medium temperatures (100-600 °C)**.

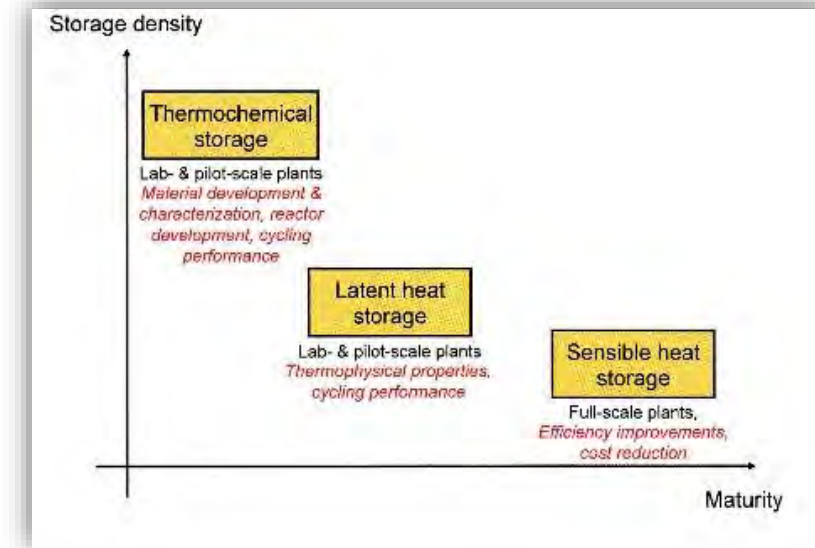
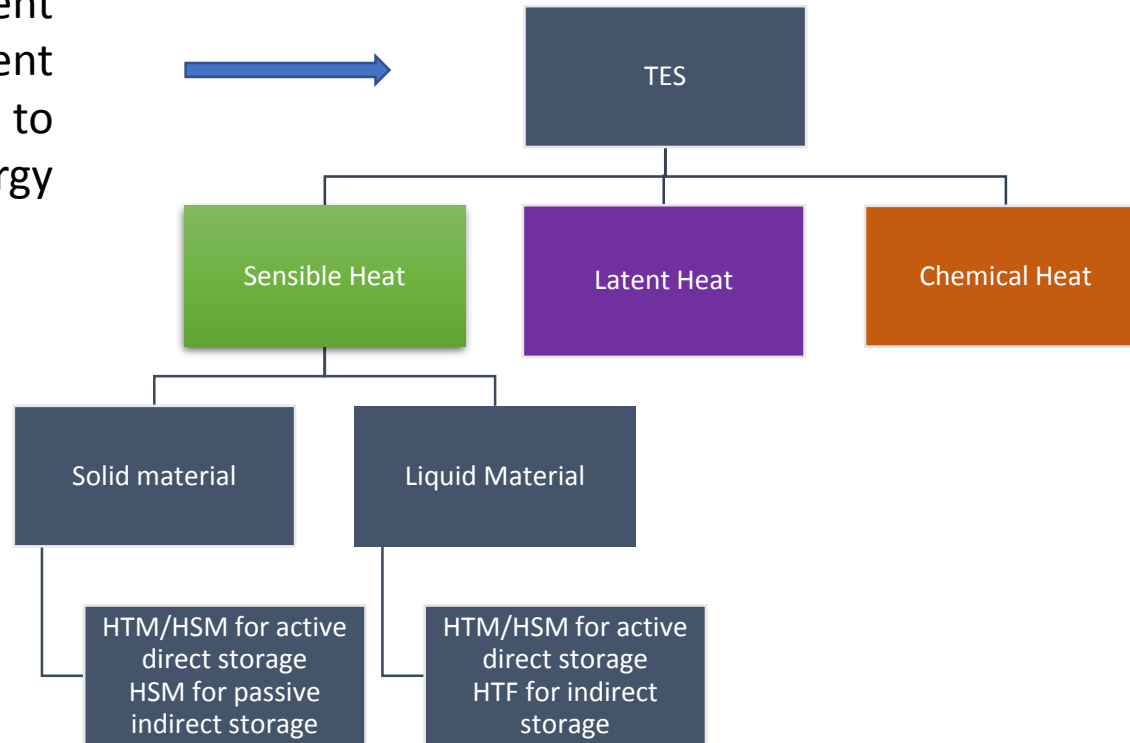
All kinds of **TES** can be classified in four categories:

- **Active/Passive systems**
- **Direct/Indirect systems**

- ✓ In an **active** system the HSM directly transfers the thermal heat to a working fluid in a power block.
- ✓ In a **passive** system another fluid it is employed for transferring the thermal energy from the HSM to the power block.
- ✓ In **direct** storage systems, the HTF and HSM are the same, while, in an **indirect** configuration, the two fluids are different, and the heat is transferred between them by an intermediate heat exchanger (HX).



According to the different types of heats, different materials can be used to obtain thermal energy storages.



The choice of feasible thermal fluids (TES) is a crucial point for the dispatchability and economic effectiveness of CSP technology!

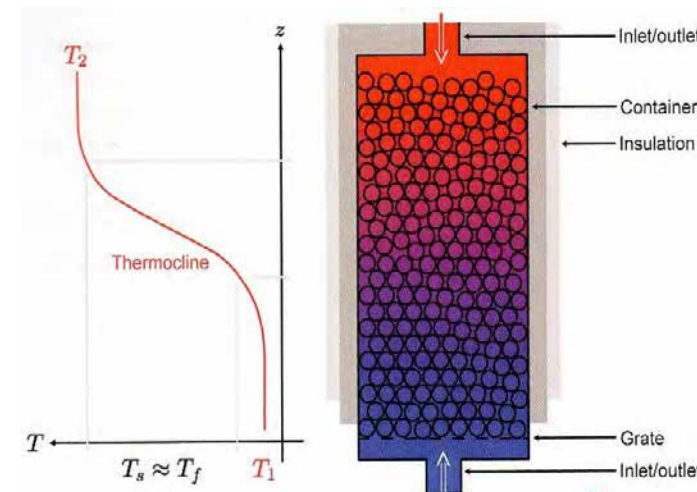
Liquid materials

- ✓ Diathermic oils as HTF, that are composed by a mixture of organic compounds, mostly diphenyl and diphenyl oxides.
- ✓ Nitrate alkaline mixtures are generally used as HTMs.



Solid materials

- ✓ An intermediate HTF is necessary in order to ensure the contact with the HX.
- ✓ It must maintain a thermocline stratification.
- ✓ Can be less costly (per weigh and volume) than molten nitrates.



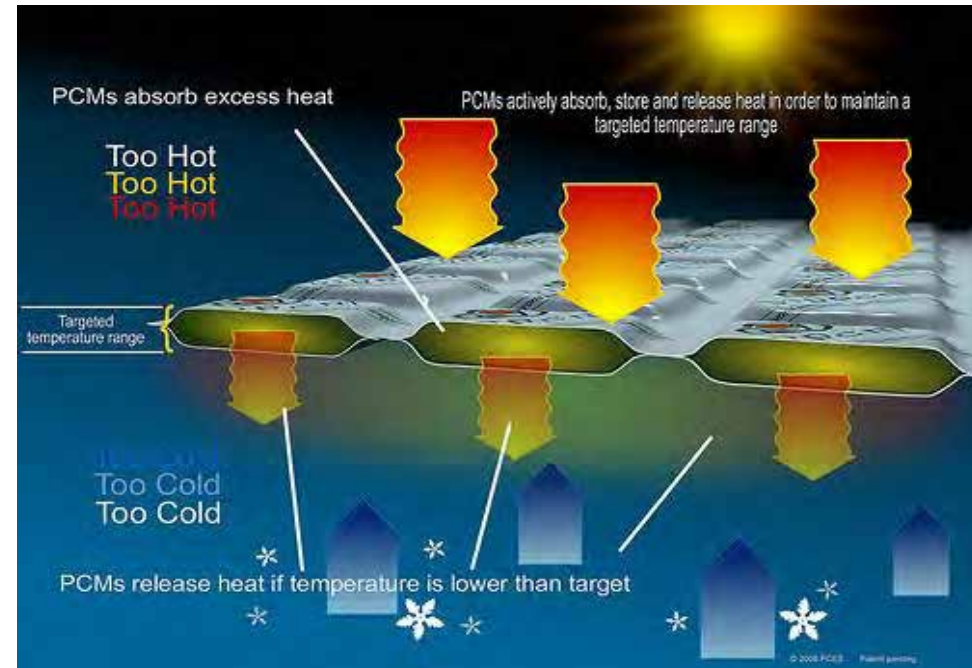
Phase change materials (PCMs)

- ✓ energy storage density is high per volume
- ✓ possibility to discharge it at constant temperature
- ✓ problems of designing a proper heat exchanger, given the change in volume during phase transition.

• Store thermal energy in phase change of material

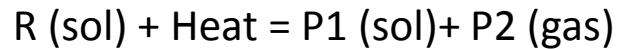


• Heat can be delivered at (nearly) constant temperature



Possibility to accumulate the solar heat in the energy of a single reversible reaction

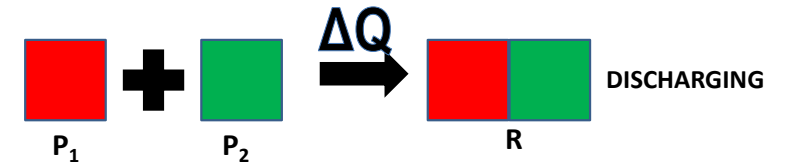
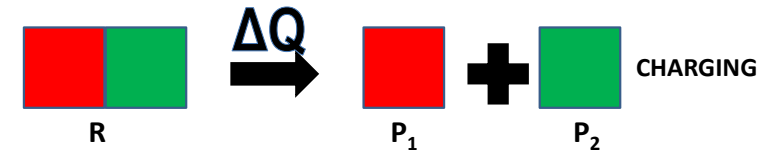
The most common systems use a solid-gas reaction:



✓ By this method can be possible to carry out seasonal heat storage.

| Reaction type | Example of Reaction | T _{charging} (°C) | T _{discharging} (°C) | ΔH _{reaz} (Kj/mol reagent) | Energy density (Gj/m ³) |
|---------------|-----------------------------------|----------------------------|-------------------------------|-------------------------------------|-------------------------------------|
| Hydroxides | $Ca(OH)_2 = CaO + H_2O$ | 550 | 450 | 104.4 | 1.6 |
| Carbonates | $CaCO_3 = CaO + CO_2$ | 850-950 | 550-700 | 178 | 2.5 |
| | $MgCO_3 = MgO + CO_2$ | 510-750 | na | 125 | 2.0 |
| | $CaCO_3/CaO/Ca_{12}Al_{14}O_{33}$ | 850-950 | 750 | 178 | not available |
| Oxides | $2BaO_2 = 2 BaO + O_2$ | 650-850 | 450-580 | 77 | 1.2 |
| | $2Co_3O_4 = 6CoO + O_2$ | 915-920 | 835-850 | 354.6 | 1.1 |
| | $6Mn_2O_3 = 4Mn_3O_4 + O_2$ | 920-1000 | 500-650 | 202.8 | 1.2 |

The whole process can be divided into three parts:

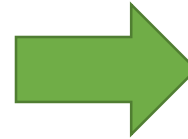


$$Q = m \Delta H_{react}$$

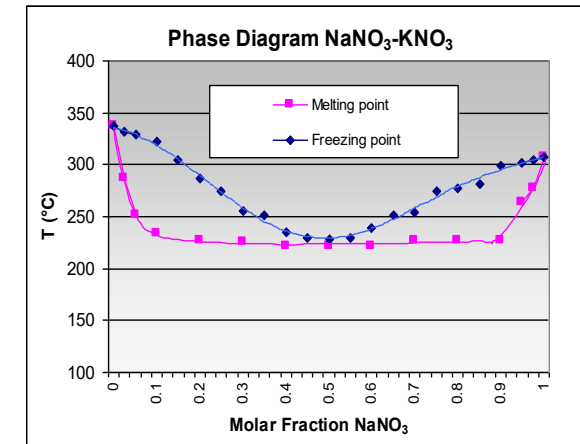
- **Molten salts mixtures** are known to exhibit satisfactory thermal and physical features, both for heat exchange and storage, in the temperature range concerned, together with low corrosion properties and a relatively low cost .

Advantages of molten salts (nitrates/nitrites) :

- *safe*
- *non-toxic*
- *available at low cost*
- *stable at relatively high temperatures*



“**Solar Salt**” (NaNO₃-KNO₃ 60-40 % w/w corresponding to 64/36 mol/mol) is currently the most employed material both as HTF and HSM.



| | |
|-------------------------------|--------------------------|
| T liq(°C) | 238 |
| Cp(J/ K g) | 1.6 (238-600 °C) |
| Viscosity (cP) | 4.5-1.6(238-600 °C) |
| Density (gr/ml) | 1.95 – 1.70 (238-600 °C) |
| Thermal conductivity(W / K m) | 0.50 – 0.55 (320-550 °C) |

DIATHERMIC OIL

- ✓ low freezing point (-18÷12 °C), which avoids the HTF solidification in the plant receiver tube and pipelines;
- ✓ No necessity for a heating system to maintain the plant lines at a temperature higher than the one in the external ambient.

Advantages

SOLAR SALT

- ✓ quite inexpensive
- ✓ not flammable
- ✓ high thermal stability point (≈ 600 °C)
- ✓ low viscosity
- ✓ high heat capacity
- ✓ Rankine electric power generating block is slightly affected by a decrease of the lower operative point of the thermal fluids below 270 °C , the “solar salt” formulation can be considered the only realistic choice.

Disadvantages

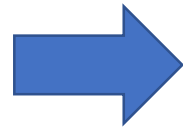
- ❑ expensive, toxic for humans and environment;
- ❑ relatively low thermal stability, they can be employed up to about 250 °C at atmospheric pressure, and under pressure from nitrogen or inert gases up to around 440 °C.
- ❑ Above this temperature they undergo an irreversible degradation and are also very flammable materials.

- ❑ Compatibility with materials up to 600°C (but expensive 347H-321H stainless steels are to be used at least above about 500°C)
- ❑ **relatively high freezing point (238 °C)**

Considerable attention must be paid to avoid salt freezing in the CSP plant, which can seriously affect the power plant's operating conditions, by plugging valves and pipes, and reducing heat transfer surface.

The **key factors** to be considered are:

- ✓ heat transport
- ✓ storage efficiency
- ✓ cost effectiveness
- ✓ environmental friendliness



The following characteristics are to be evaluated:

- 1) **Working temperatures** (freezing temperature, upper thermal stability point, and range of operating temperature)
- 2) **Thermophysical properties** (density, viscosity, heat capacity, and thermal conductivity)
- 3) **Environmental safety and risk for human health**
- 4) **Material cost**
- 5) **Construction materials compatibility and corrosion resistance of alloys**

Considerations

- Molten salts (MS), which in general consist of $\text{NO}_3^-/\text{NO}_2^-$ mixtures are mostly considered, avoiding rare and costly ones.
- Given temperature ranges, only $\text{NO}_3^-/\text{NO}_2^-$ containing Na/K/Li/Ca can be taken into account.
- Carbonates, chlorides or other salts are little soluble in molten nitrates, so their addition results not interesting.
- NaNO_2 cannot be coupled with $\text{Ca(NO}_3)_2$ because of metathetical reaction ($\text{Ca(NO}_2)_2$ which leads to $\text{Ca(NO}_3)_2$).
- Mixtures must be stable in air to avoid inert storage systems.

1) Working temperatures
 (freezing temperature, upper thermal stability point and range of operating temperature)

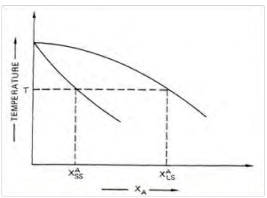
Semi-predictive modelling based on the "Theory of regular solutions"

Multi-components Phase diagrams: individuation of a low melting zone

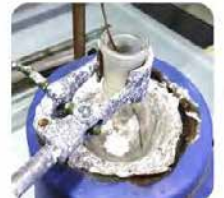
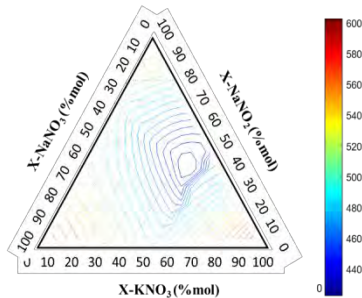
Novel promising mixtures to be characterized

Experimental results validation:

- DSC
- Rheometer
- XRD/Neutron Scattering
- Thermal stability tests



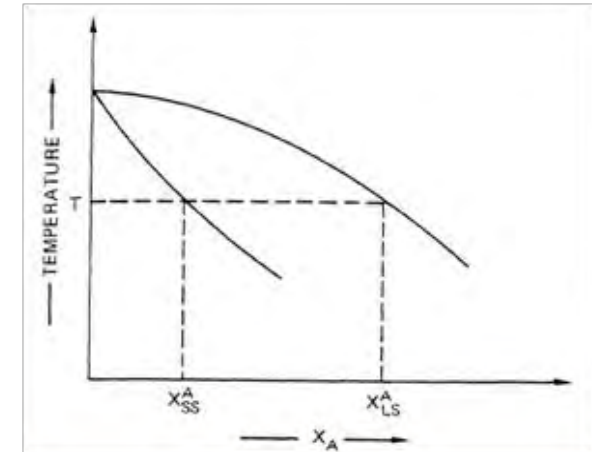
| | |
|--------------------------|--|
| $A_S \rightarrow A_L$ | $\Delta H_A - T\Delta S_A$ |
| $A_L \rightarrow A_{LS}$ | $\overline{\Delta H_{mLx}^{A_L}} - T\overline{\Delta S_{mLx}^{A_L}}$ |
| $A_S \rightarrow A_{SS}$ | $\overline{\Delta H_{mLx}^{A_S}} - T\overline{\Delta S_{mLx}^{A_S}}$ |
| $A_{SS} = A_{LS}$ | $\Delta G \equiv 0$ |



In order to simulate the phase diagrams of the binary mixtures **A and B**

when the **free energy** of one of the components is set equal to zero, the liquid and solid solution of that component are in **thermodynamic equilibrium** and the **overall free energy of the reaction must be zero**.

On an isothermal value of the phase diagram it is possible to calculate ΔH_{mix} and ΔS_{mix} (both for the solid and liquid phase)



| | |
|--------------------------|--|
| $A_S \rightarrow A_L$ | $\Delta H_A - T\Delta S_A$ |
| $A_L \rightarrow A_{LS}$ | $\overline{\Delta H}_{mix}^{A_L} - T\overline{\Delta S}_{mix}^{A_L}$ |
| $A_S \rightarrow A_{SS}$ | $\overline{\Delta H}_{mix}^{A_S} - T\overline{\Delta S}_{mix}^{A_S}$ |
| $A_{SS} = A_{LS}$ | $\Delta G \equiv 0$ |

The free energy of the overall reaction for **component A** may be expressed as:

$$\Delta G \equiv 0 = (\Delta H_A - T\Delta S_A) + (\overline{\Delta H}_{mix}^{A_L} - T\overline{\Delta S}_{mix}^{A_L}) - (\overline{\Delta H}_{mix}^{A_S} - T\overline{\Delta S}_{mix}^{A_S})$$

Kirchoff law

$$\Delta H_A = \Delta H_A^0 - \int_T^{T_{MP}} (C_{PL} - C_{PS}) dT$$

$$\Delta S_A = \Delta S_A^0 - \int_T^{T_{MP}} \frac{(C_{PL} - C_{PS})}{T} dT$$

Gibbs-Duhem equation

$$\left(\overline{\Delta H}_{mix}^{A_L} = \Delta H_{mix} - X_{BL} \frac{d\Delta H_{mix}}{dX_{BL}} \right)_L \quad \left(\overline{\Delta S}_{mix}^{A_L} = -R \ln X_{AL} \right)_L$$

$$\left(\overline{\Delta H}_{mix}^{A_S} = \Delta H_{mix} - X_{BS} \frac{d\Delta H_{mix}}{dX_{BS}} \right)_S \quad \left(\overline{\Delta S}_{mix}^{A_S} = -R \ln X_{AS} \right)_S$$

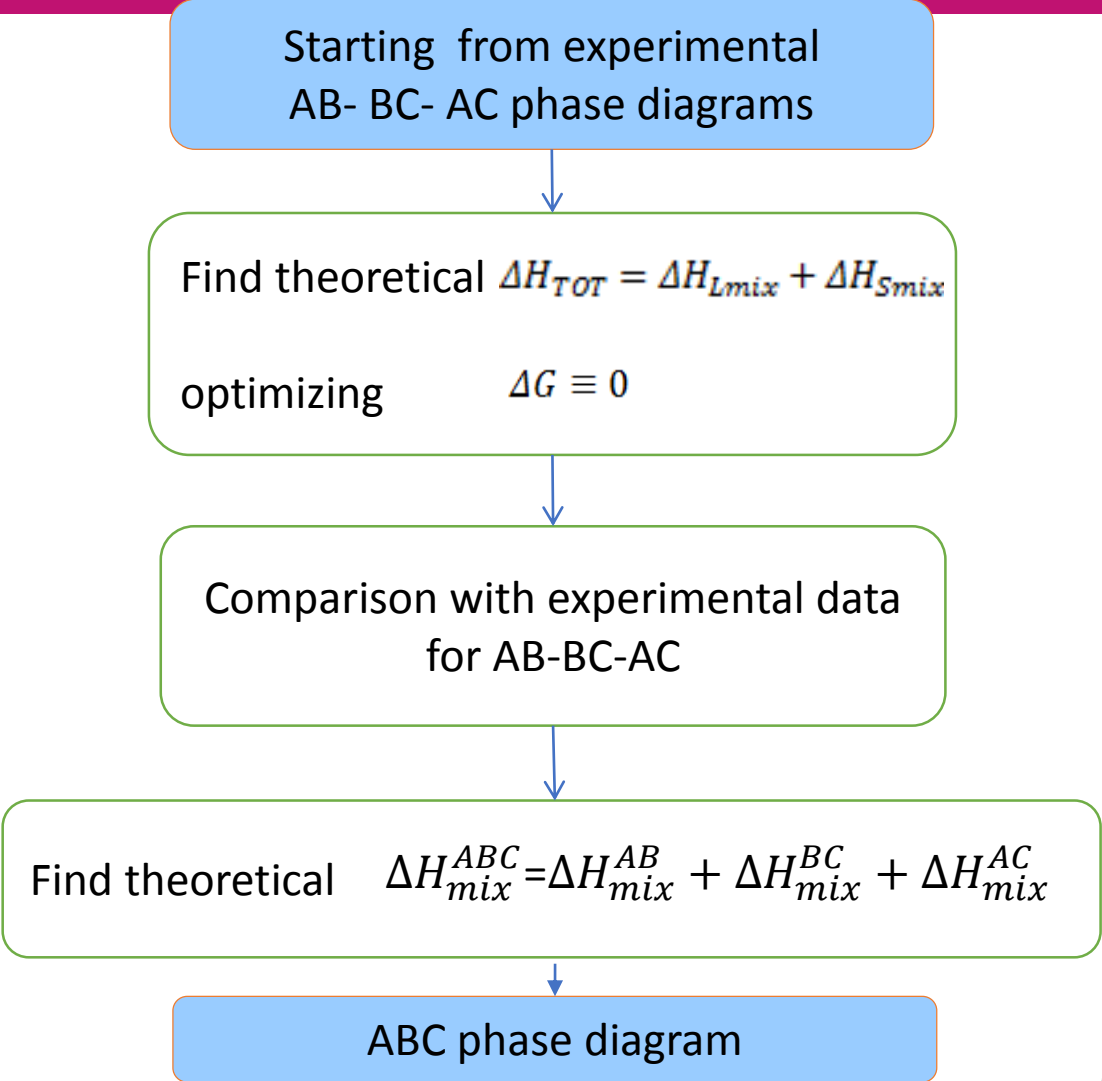
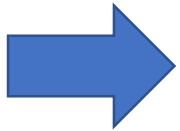


$$\Delta H_{Lmix} = X_{AL} X_{BL} (a_L + b_L X_{AL} + c_L X_{AL} X_{BL}),$$

$$\Delta H_{Smix} = X_{AS} X_{BS} (a_S + b_S X_{AS} + c_S X_{AS} X_{BS})$$

Assuming that all the non-ideality is from enthalpy and entropy follows an ideal mixing rule

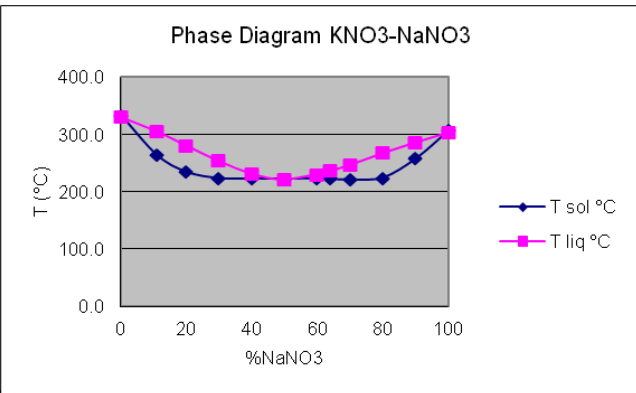
Only experimental data that show a good precision and accuracy are the **phase diagrams.**



DSC



Applying a controlled temperature ramp on a Al pan 100 ul, filled with salt allowing the salt to melt and then to solidify it is possible to detect “onsets” of solidification and melting (T_{liq} and T_{sol})



Rheometer

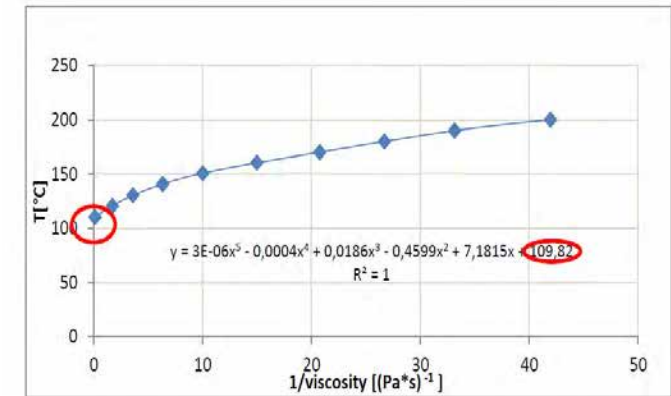
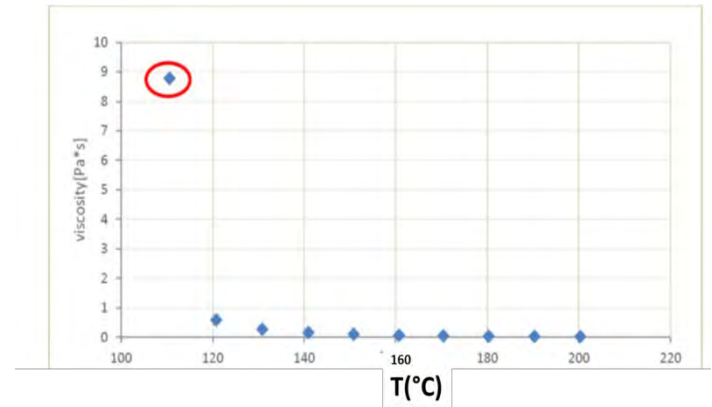


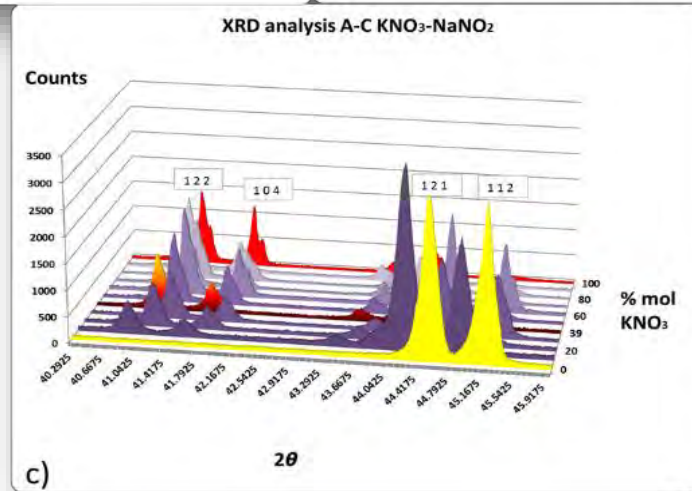
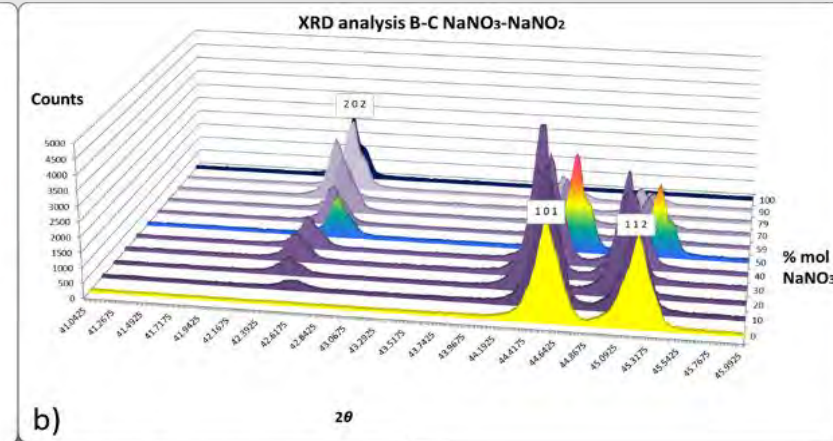
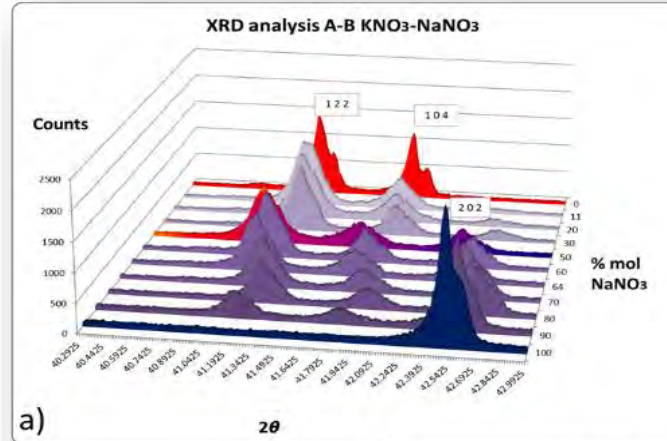
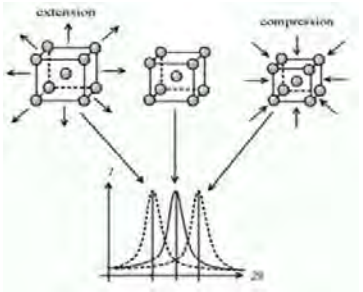
The dynamic viscosity of a Newtonian fluid (such as a molten nitrate) is directly dependent on the materials temperature.

$$\log_{10} \mu = A + BT - T0$$

It is not possible to detect phase transition points (liquidus and solidus) of Na/K/Ca//NO₃ mixtures when the calcium nitrate molar percentage exceeds 20%, because of a slow transition rate and low transition enthalpy.

NaNO₃/KNO₃/Ca(NO₃)₂ 21-54-25 (% mol)





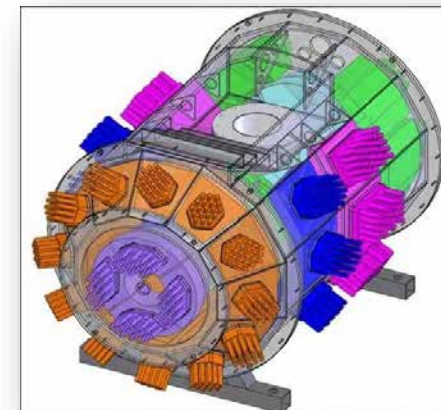
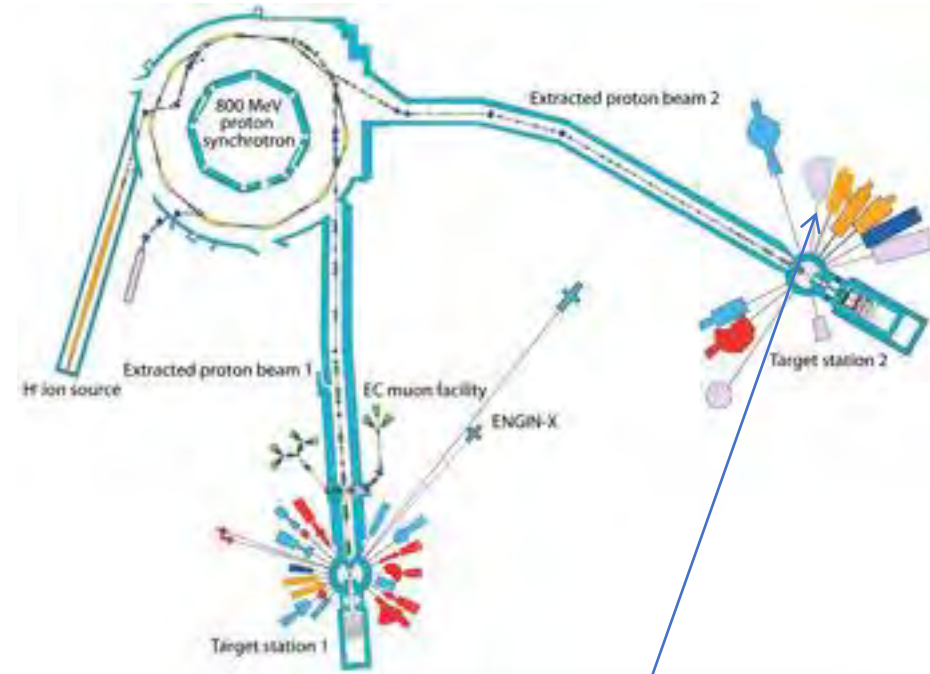
A modification of the distance between the crystallographic planes is related, considering that λ is constant, to a change in the 2θ values.

Not a formation of new phases but, by varying concentrations, **the crystal lattice undergoes a deformation that is maximum in correspondence of the composition of the eutectic point.**

- An exploratory XRD study of the binary mixtures, **AB**, **BC**, **AC**, has been carried out, with the aim to improve the understanding of the phase diagrams.
- Given the unavailability of a heating system for the cell of the XRD apparatus used, only **room temperature** data were collected.

Neutron Scattering

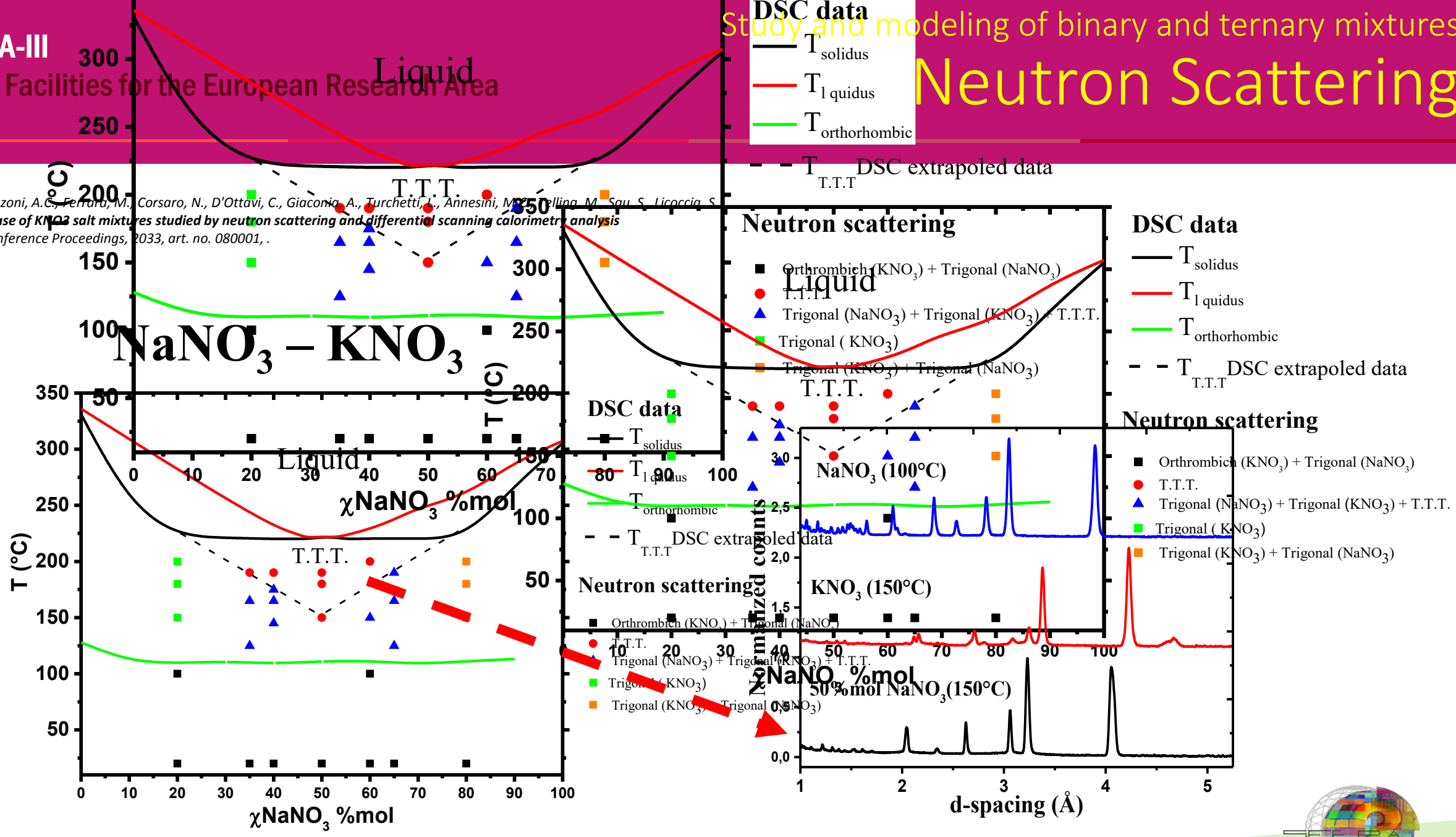
- Neutron diffraction experiments determine the atomic structure of a material.
- The technique is similar to X-ray diffraction but the different type of radiation gives complementary information.
- A sample to be examined is placed in a beam of neutrons and the intensity pattern around the sample gives information of the structure of the material



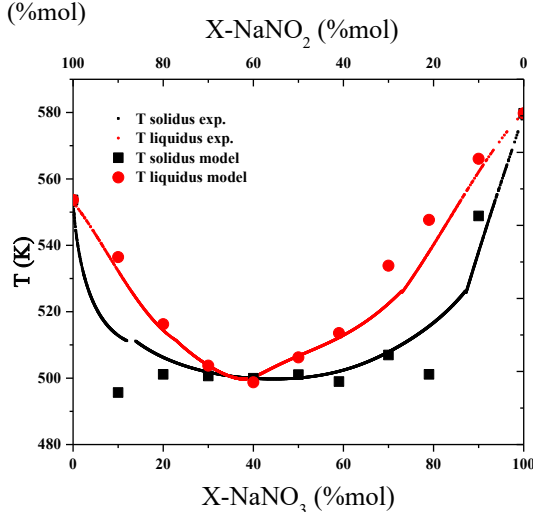
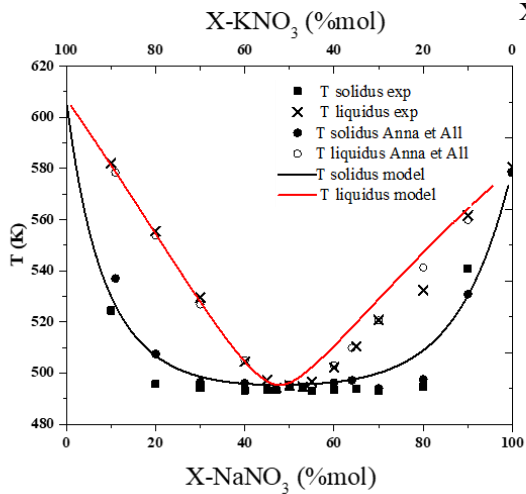
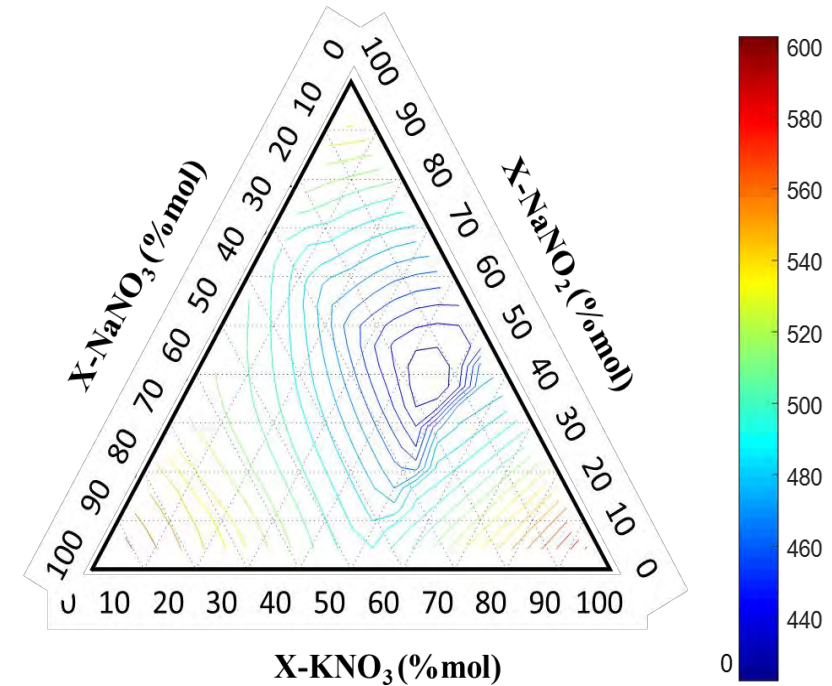
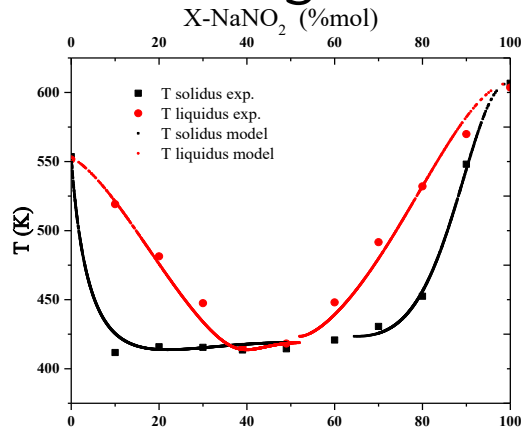
**Polaris
Instrument-
Rutherford
Labs (UK)**



*Delise, T., Tizzoni, A.C., Ferrara, M., Corsaro, N., D'Ottavi, C., Giaconio, A., Turchetti, L., Annesini, M., Bellina, M., Sai, S., Liccig, S.
 New solid phase of KNO_3 salt mixtures studied by neutron scattering and differential scanning calorimetry analysis
 (2018) AIP Conference Proceedings, 2033, art. no. 080001, .



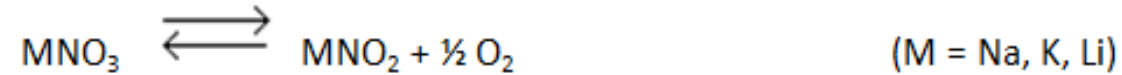
$\text{KNO}_3\text{-NaNO}_3\text{-NaNO}_2$: Ternary phase diagrams example



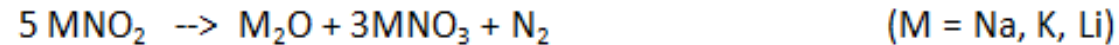
Thermal stability mechanism

The molten nitrates degradation mechanism consists of two steps:

- ✓ Firstly nitrites and oxygen are produced:

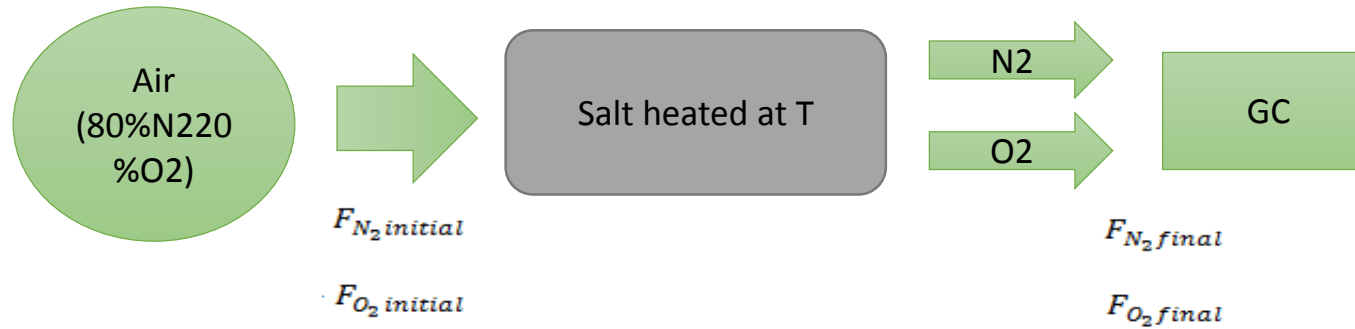


This reaction is reversible. In turn, nitrites can lead to a second reaction:



- ✓ This process is not expected to be easily reversible, so alkaline oxides can:
 - ❖ accumulate and **increase the melting point** of the mixture
 - ❖ react **producing alkaline hydroxides (very corrosive) and carbonates**
 - ❖ **precipitate** leading to problems with valves and pipeline occlusions due to limited solubility

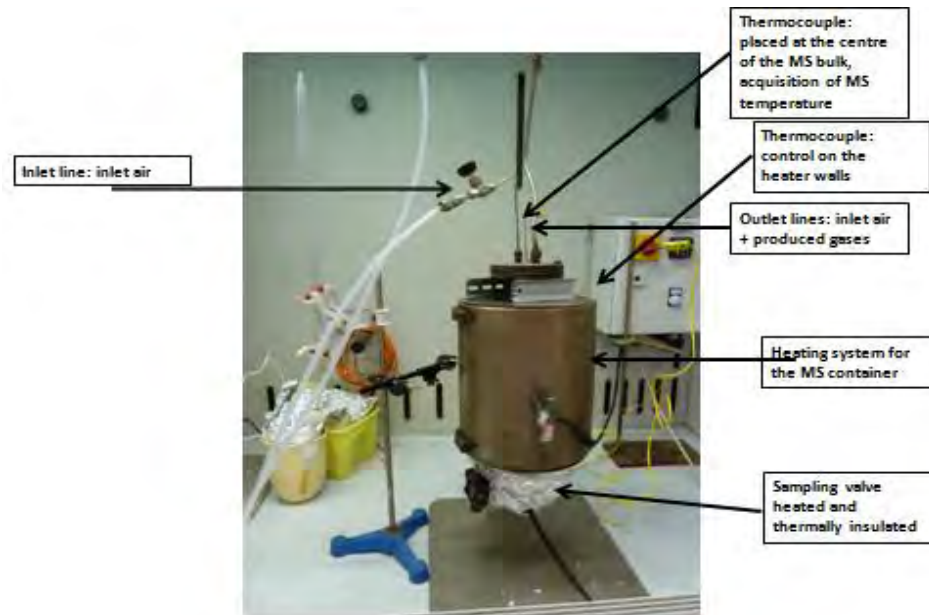
Discriminating point to determine the **upper** stability temperature for MS employment as HTF or HSM.

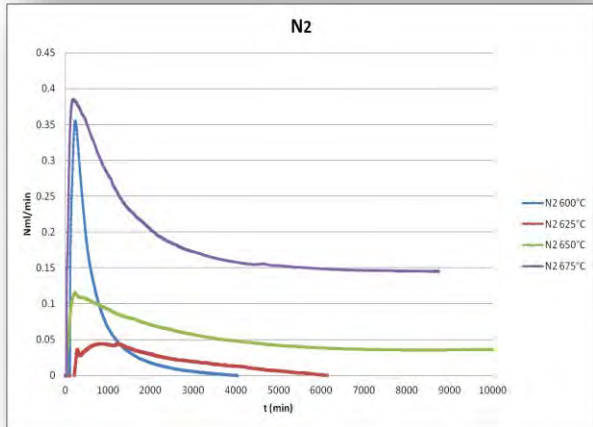
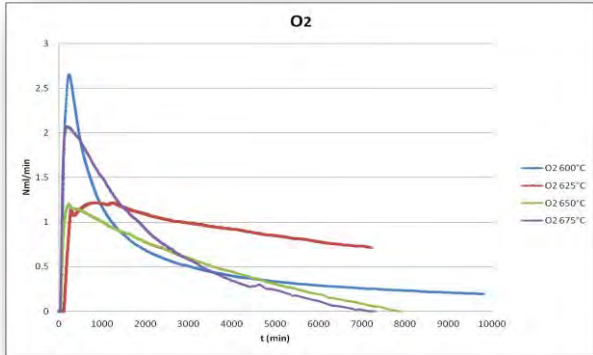


✓ Salt mixture is placed inside a stainless steel (304 SS) autoclave. The mixture is heated at various T.

✓ A continuous flow of air is necessary in order to carry out experiments under 1 bar of air.

✓ Evolved gases are analyzed by using gas chromatography, measuring O₂ and N₂ volume percentages.





During the experimental period (7 days tests for each temperature), the bulk was measured by a thermocouple immersed in the center of the melt.

After each isothermal test few grams of molten salt is sampled to investigate the presence of:

- ❖ NO_2^- (by Ion Chromatography)
- ❖ **Oxides** (by automatic acid/base titration)

Thermal stability
upper limit:
about 600°C

| 7 Day Tests | 600 °C | 625 °C | 650 °C | 675 °C |
|---|--------|--------|--------|--------|
| wt% NO_2^- (measured) | 2.98 | 3.35 | 9.00 | 9.99 |
| wt% NO_2^- (est. from O_2 production) | 2.94 | 6.76 | 9.14 | 11.82 |
| wt% OH^- | 0.0003 | 0.0004 | 0.0010 | 0.0023 |
| Onset T _{sol} [°C] | 207.90 | 204.14 | 180.50 | 176.67 |
| Onset T _{liq} [°C] | 225.31 | 226.12 | 204.32 | 199.11 |

| Properties | Interest for HTF | Interest for HSM |
|--------------------------|---|--|
| phase diagrams | Determination of the lowest T _{liq} | Determination of the lowest T _{liq} |
| specific heat | Capacity of solar heat transfer to the storage system | Capacity of heat storage |
| viscosity | Determination of the necessary pumps hydraulic head | It depends on the storage system. In "Archimede" configuration HTF and HSM are the same fluid. |
| density | Related to heat capacity; capability of heat storage per volume | Related to heat capacity; capability of heat storage per volume |
| heat conductivity | Necessary parameter to determine the heat exchange surfaces | Necessary parameter to determine the heat exchange surfaces |
| thermal stability | Maximum operative T | Maximum operative T |
| XRD diffraction | Integration to investigate solid nitrates structures: prediction for phase diagrams | Integration to investigate solid nitrates structures: prediction for phase diagrams |

DSC

Rheometer

Archimedian based test

C-Therm TCi thermal conductivity analyzer.

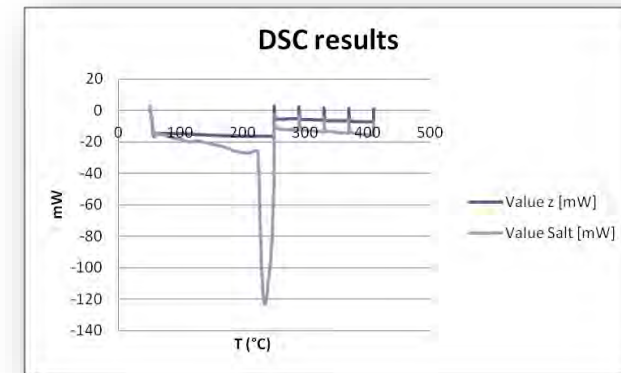
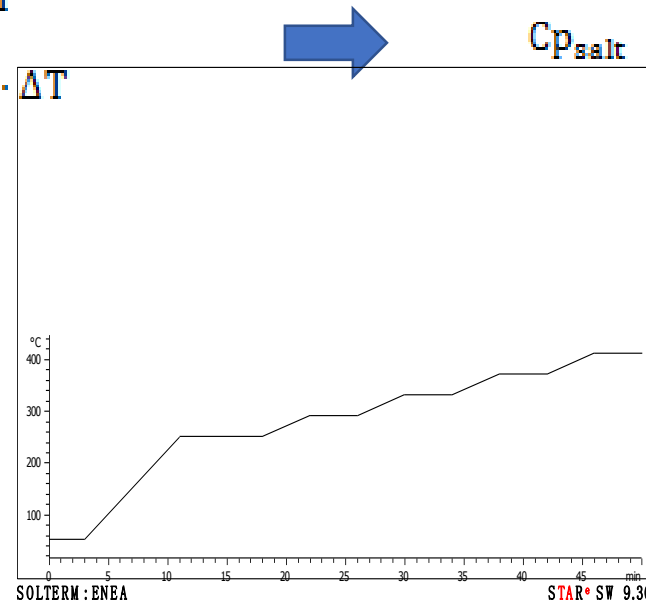
It is possible to estimate **heat capacity** values of molten salts with the use of a known heat capacity substance as reference (high purity sapphire).

$$W_z = Cp_z \cdot m_z \cdot \beta \cdot \Delta T$$

$$W_{salt} = Cp_{salt} \cdot m_{salt} \cdot \beta \cdot \Delta T$$

$$Cp_{salt} = \frac{Cp_z \cdot m_z \cdot W_{salt}}{m_{salt} \cdot W_z}$$

Mettler Toledo DSC





➤ **Viscosity is the difficulty that a mass of a fluid (a liquid or a gas) has to change in shape.**

Considering a model in which a fluid is delimited between two parallel planes and being force and surface parallel, their relationship represents a **shear stress**:

$$\tau_{xy} = \frac{\vec{F}}{\vec{A}}$$

The shear stress is proportional to the velocity \vec{u} and inversely proportional to the distance of the two plans. This dependence is called Newton's law for viscous fluids:

$$\tau_{xy} = \mu \frac{du_x}{dy}$$

in which the coefficient of proportionality μ takes the name of **dynamic viscosity** for a fluid [Pa*s].

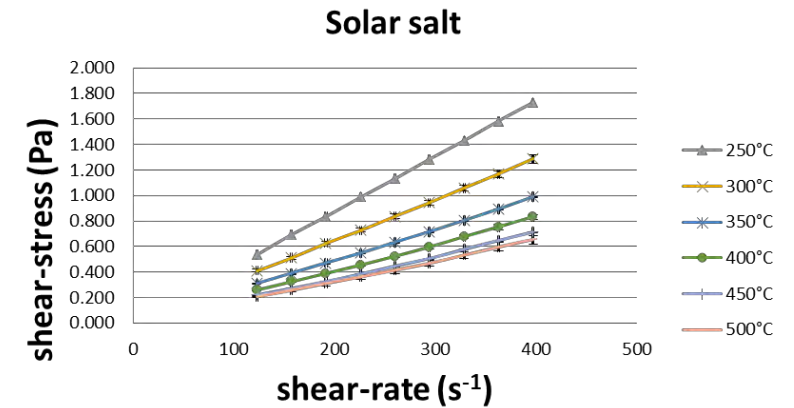
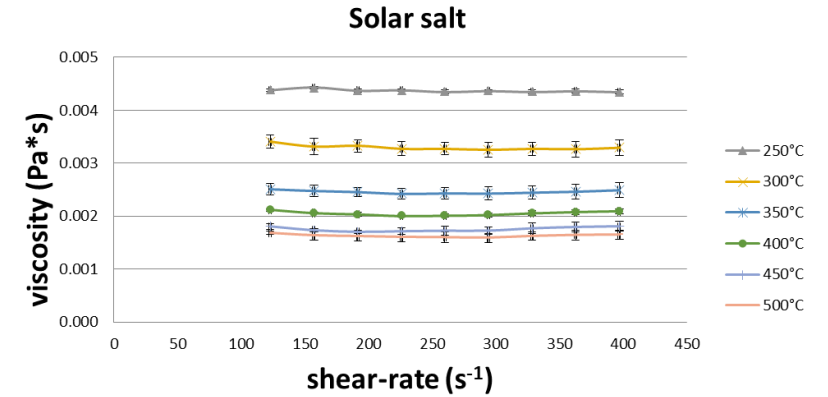
The gradient of velocity (**shear rate**) is uniform between the two planes :

$$\gamma = \frac{du_x}{dy} = \frac{u_x}{dy}$$

Then the **viscosity** is defined as:

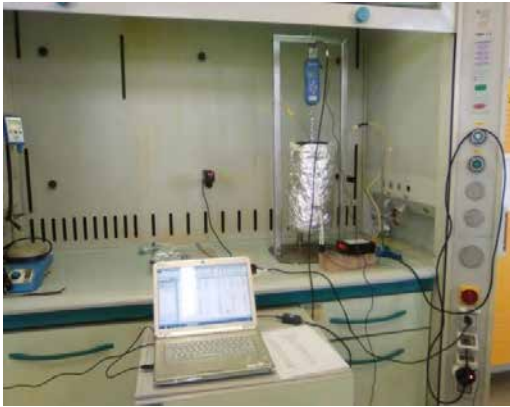
$$\mu = \frac{\text{shear stress}}{\text{shear rate}} = \frac{\tau}{\gamma}$$

If the relationship between shear stress and shear rate is a straight line passing through the axis origin, the fluid is defined Newtonian and the slope is the Viscosity



Density - heat conductivity

✓ **Density** measurements of the mixtures are performed with an *Archimedian* based test.



The method is based on the measurement of the buoyance force on a stainless steel cylinder, which is immersed into the ternary melt and is connected with a dynamometer.

✓ **Heat conductivity** : instrument based on the "hot wire" method (up to 80°C)

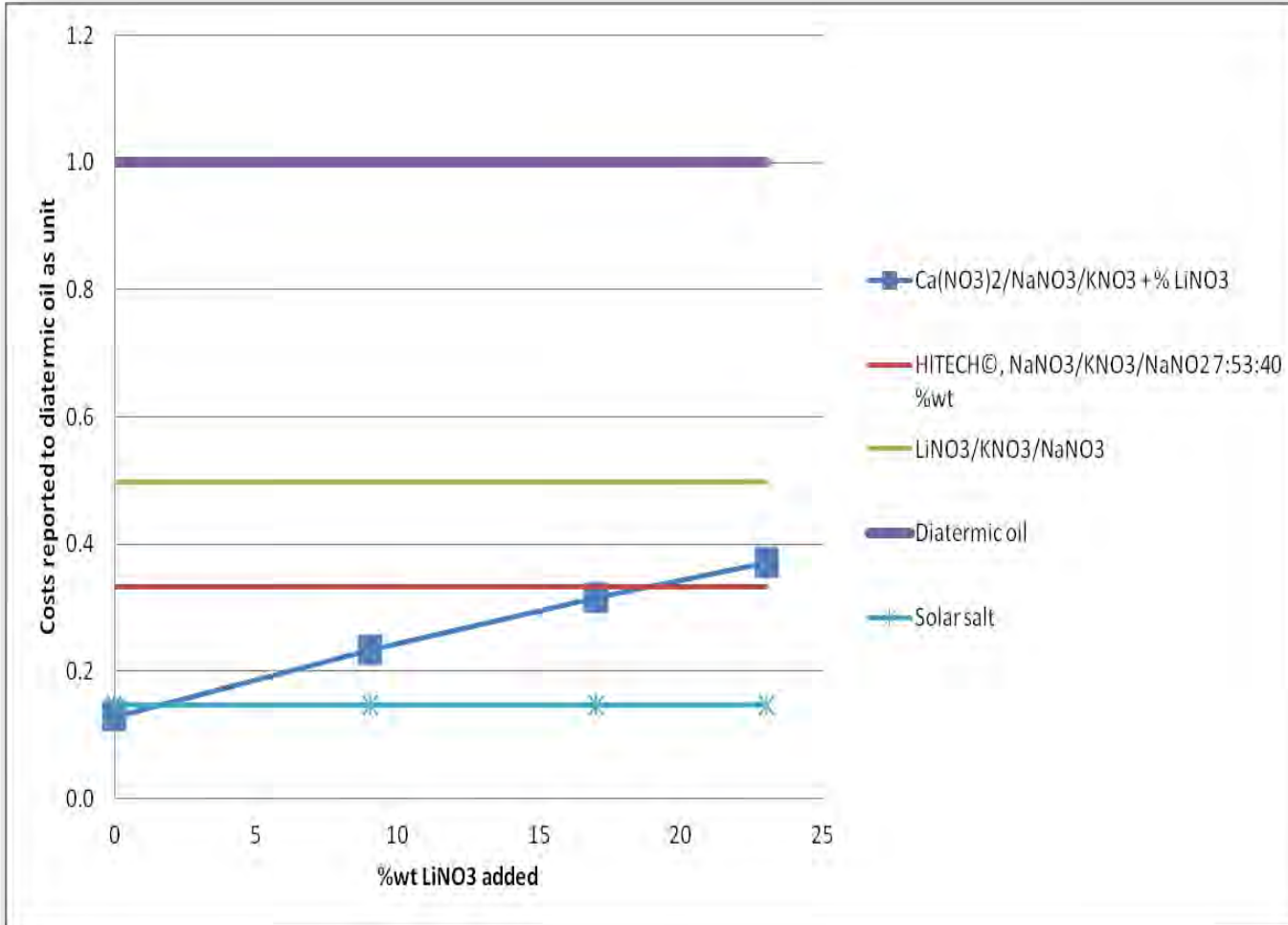
C-Therm TCi thermal conductivity analyzer.



A known current is applied to the sensor's heating element providing a small amount of heat. The heat provided results in a rise in temperature at the interface between the sensor and the sample.

The rate of increase in the sensor voltage is used to determine the thermo-physical properties of the sample material.

| | Name | Risk Phrases |
|---|------|---|
| Solar salt | M1 | H272 |
| Ternary Li/Na/K//NO3 | M2 | H272- H319 |
| Ternary Ca/Na/K//NO3 | M3 | H272 |
| Hitech® (NaNO ₃ /KNO ₃ /NaNO ₂) | M4 | H272-H301-H319-H400 |
| Quaternary Ca/Li/Na/K//NO3 | M5 | H272- H319 |
| Oil Diathermic (THERMINOL® 66) | M6 | Skin Irrit. 2 - H315 Eye Irrit. 2 - H319 Suspected of damaging fertility- H361f Aquatic Acute 1 - H400 Aquatic Chronic 1 - H410 |



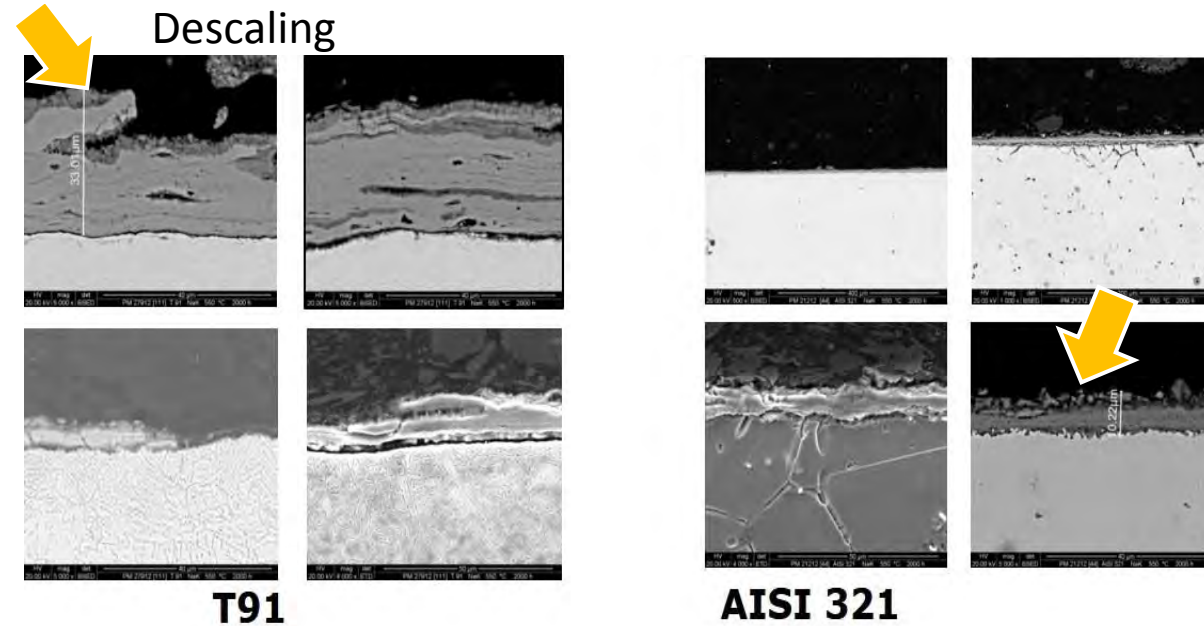
Diathermic oil as unit

- **Ternary with calcium** is the less expensive material can be an alternative especially with respect to thermal oil, which is stable at the same temperature.
- Addition of **lithium nitrate** makes the cost of the mixture more or less comparable to the "Hitech® salt"
- **Ternary with lithium** has very good thermo-physical features, including thermal stability, but can be considered **too expensive**

5) Construction materials compatibility and corrosion resistance of alloys

There are two mechanisms by which materials corrode in the presence of in molten salts: metal dissolution of the material constituents and oxidation of the metal to ions.

- ✓ The oxidation is the main degradation mechanism which causes uniform corrosion when a material is subject to molten salts like nitrate mixtures.
- ✓ The corrosion behaviour depends on the formation and stability of protective oxide layers over the material surface which impedes the material oxidation.



SEM images for the cross section of a specimen of T91 and AISI 321 after isothermal oxidation test (2000h) at 550°C in a molten salt mixtures.

❖ Binary $\text{NaNO}_3/\text{KNO}_3$ mixtures (M1).

They present low cost along with good thermophysical properties and are not toxic. Solar salt presents an acceptable freezing point ($238\text{ }^\circ\text{C}$) and it is less expensive than the eutectic mixture (freezing point around $222\text{ }^\circ\text{C}$), given the lowest KNO_3 content (the eutectic point is at Na/K//NO_3 46/54 wt%).

❖ Ternaries with lithium nitrate (M2).

The advantages are a low freezing point and a thermal stability comparable with solar salt. The main disadvantage is the high price of lithium nitrate.

❖ The addition of calcium nitrate to NaNO_3 and KNO_3 (M3)

decreases the mixture freezing point to about $110\text{ }^\circ\text{C}$, but also the upper temperature limit to around $450\text{ }^\circ\text{C}$.

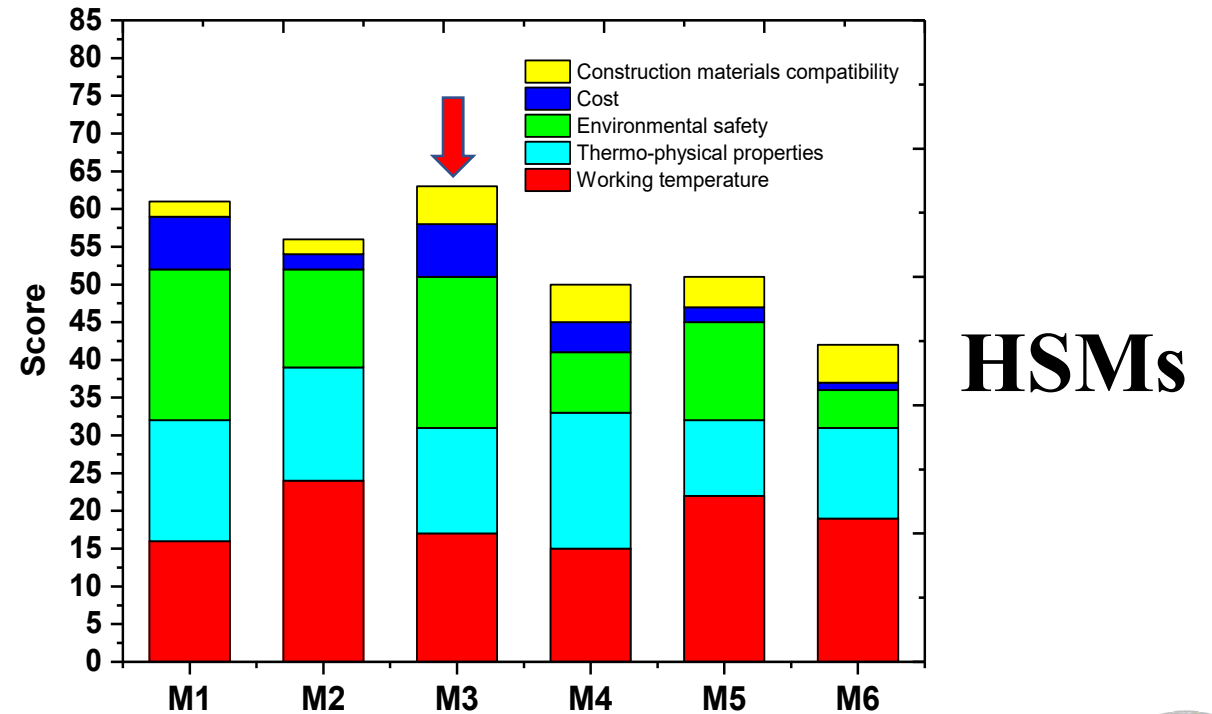
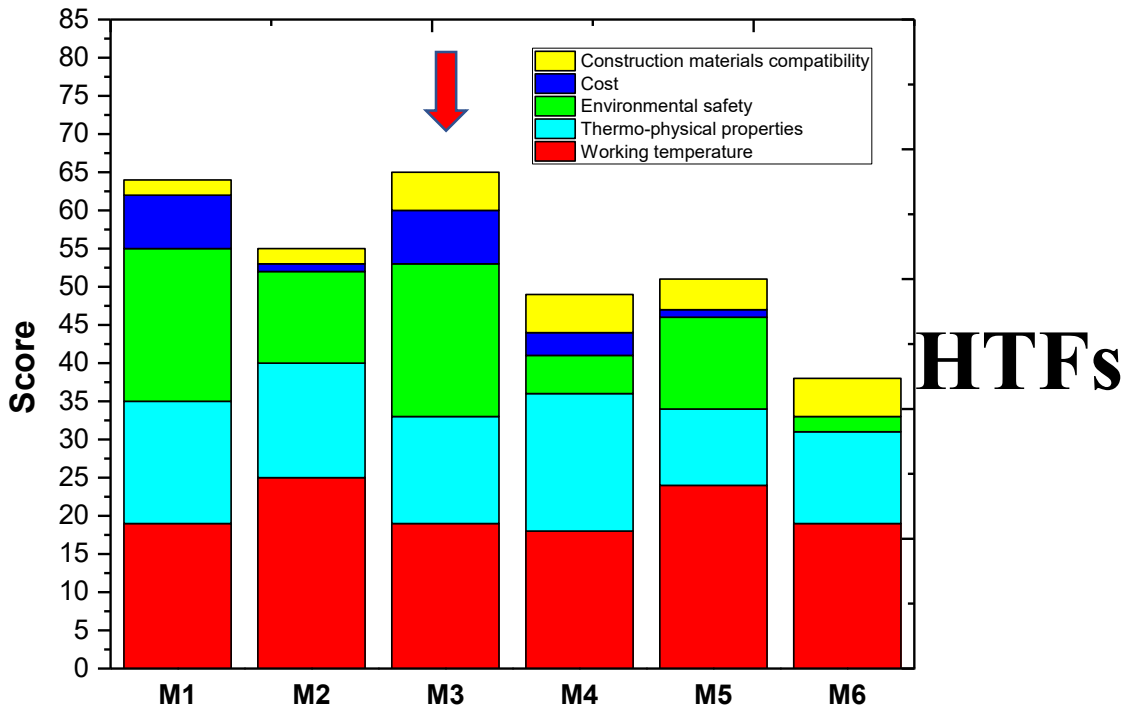
❖ Mixtures containing NaNO_2 . By far, the most used one is a commercial product named “Hitec©”, here indicated as **M4**, but they are relatively costly and toxic.

❖ Quaternary mixtures.

The choice is limited to Ca/Li/Na/K//NO_3 or $\text{Li/Na/K//NO}_3/\text{NO}_2$ systems. The former seems more significant and investigated and one formulation is taken into account (**M5**). Calcium nitrate and sodium nitrite cannot be mixed together given the formation and rapid reoxidation of calcium nitrite even at low temperatures.

| | | Tliquidus (°C) | Tdegradation (°C) | ΔT (°C) |
|--------------------------------|----|----------------|-------------------|---------|
| Solar salt | M1 | 238 | 550* | 312 |
| Ternary Li/Na/K//NO3 | M2 | 100-120 | 550* | 440 |
| Ternary Ca/Na/K//NO3 | M3 | 133 | 450 | 317 |
| Hitech® | M4 | 141 | 450 | 309 |
| Quaternary Ca/Li/Na/K//NO3 | M5 | 95 | 520 | 425 |
| Oil Diathermic (THERMINOL® 66) | M6 | -12 | 345 | 357 |

*Delise, T., Tizzoni, A.C., Ferrara, M., Corsaro, N., D'Ottavi, C., Sau, S., Licocchia, S. *Thermophysical, environmental, and compatibility properties of nitrate and nitrite containing molten salts for medium temperature CSP applications: A critical review (2019)*
Journal of the European Ceramic Society, 39 (1), pp. 92-99.



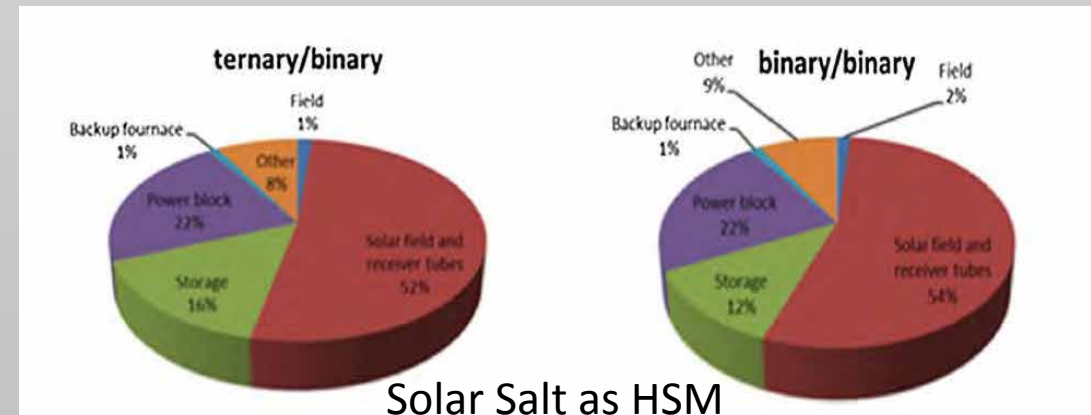
- Very useful to investigate the possible advantages of using a low melting nitrate mixture in place of the solar salt.
- The economic performance of a solar power plant is estimated by breaking down the equipment investment costs in detail, and by using common financial indicators.
- Each investment cost category is calculated based on a reference specific cost per size unit, modified by a scaling effect, a production volume effect and the price index from the reference year until now.

The total investment costs of a solar power plant with a storage system can be classified into major cost components:

- ✓ *size of the plant ground field*
- ✓ *size of the solar field*
- ✓ *heat storage materials and the tanks*
- ✓ *power block: heat generator, turbine, alternator, pre-heater, super-heater, degasser, and condenser*
- ✓ *integration back up heater*
- ✓ *civil work and infrastructure.*

Lithium ternary mixture as HTF

Solar Salt as HTF



*Sau, S., Corsaro, N., Crescenzi, T., D'Ottavi, C., Liberatore, R., Licocchia, S., Russo, V., Tarquini, P., Tizzoni, A.C. "Techno-economic comparison between CSP plants presenting two different heat transfer fluids" (2016) Applied Energy, 168, pp. 96-109. Cited 23 times.

| | Binary mixture as HTF | Ternary mixture as HTF | Measurement unit |
|--|-----------------------|------------------------|-----------------------|
| Ground field specific cost | 2.5 | 2.5 | €/m ² |
| Ground field cost | 3 449 | 3 521 | ke |
| Foundations specific cost | 10 | 10 | ke/collector |
| Solar field foundations cost | 7 600 | 7 760 | ke |
| Solar field specific cost | 275 | 261 | €/m ² |
| Specific binary mixture cost | 0.8 | | €/kg |
| Specific ternary mixture cost | | 1.6 | €/kg |
| HTF in the receiver tube cost | 2 940 | 5 497 | ke |
| Total solar field cost | 126912 | 126029 | ke |
| HSM (binary mixture) total cost | 6 736 | 6 808 | ke |
| Specific cost per storage tank | 510 | 510 | €/m ³ |
| Specific cost for melter + pumps + power system + foundations cost | 1 700 | 1 700 | €/m ³ |
| Storage tanks cost | 5 481 | 5 540 | ke |
| Melter pump's power system foundations cost | 15226 | 15390 | ke |
| Storage cost per MS (binary mixture) volume | 2 210 | 2 210 | €/m ³ |
| Intermediate HX cost | 0.0 | 8940 | €/kW h |
| Total cost for heat storage | 27 443 | 36 679 | ke |
| Total cost for heat storage without an intermediate HX | 27 443 | 27 739 | ke |
| Total cost solar field and storage | 157 803 | 166 229 | ke |
| Cost Power block | 850 | 850 | €/kW _{el} |
| Control construction, engineering and contingencies | 204.0 | 204.0 | €/kW _{el} |
| Power block | | | |
| Electric energy production cost | 52 700 | 52 700 | ke |
| Backup heater | 3000 | 2500 | ke |
| Other | 20 000 | 20 000 | ke |
| Investment cost | 233 503 | 241 429 | ke |
| Specific cost backup fuel (CH ₄) | 0.25 | 0.25 | €/m ³ |
| Fuel cost | 1 673 | 1 101 | ke/y |
| Specific O&M cost | 2 | 2 | % inv |
| O&M cost | 4 670 | 4 829 | ke/y |
| Annuality factor | 9.11 | 9.11 | |
| Depreciation rate (15 years, 7% actual discount rate) | 25 660 | 26 531 | ke/y |
| Annual cost | 32 003 | 32 460 | ke/y |
| Electric energy production | 144 607 | 145 558 | MW h _{el} /y |
| Electric energy cost | 221 | 216 | €/MW h _{el} |

Levelized Electric Energy Cost (LCOE) is defined as the total cost of a system over its lifetime divided by the expected energy output over its useful lifetime.

$$LCOE = \frac{crf \cdot C_{invest} + C_{O\&M}}{E_{net}}$$

E_{net} = annual electricity output;

$C_{O\&M}$ = annual operating and maintenance costs;

C_{invest} = total investment cost of the plant;

k_d = real debt interest rate = 8%;

n = life time = 25years;

$$crf = \text{capital recovery factor} = \frac{k_d * (1 + k_d)^n}{(1 + k_d)^n - 1}$$

*Sau, S., Corsaro, N., Crescenzi, T., D'Ottavi, C., Liberatore, R., Licoccia, S., Russo, V., Tarquini, P., Tizzoni, A.C. "Techno-economic comparison between CSP plants presenting two different heat transfer fluids" (2016) Applied Energy, 168, pp. 96-109. Cited 23 times.

- ✓ Mixtures with **Calcium nitrate** are very promising both as HSM and HTF.
- ✓ The **predictive simulation tools** have to be improved. However, it is difficult to find out parameters for other models and, for instance, some methods only consider non-ideality for the liquid state (e.g. NRTL), while it is experimentally verified that also nitrate solid mixtures present a non null enthalpy of excess. In these cases, an empirical expression can be proposed to describe the solid phase at the equilibrium.
- ✓ Regarding **corrosion data**, there is a lack especially from 400°C to 500°C and it is very important to optimize the price of the CSP construction materials.
- ✓ ENEA developed criteria for **techno-economic analysis** that are relatively rapid and easy to apply.
- ✓ Clearly, a very promising scenario is represented by the possibility **to couple sensible heat storage materials with other types of accumulation systems**, typically PCMs .

- A couple of words about the presence of the ENEA TFC-LAB in the SFERA III transnational access activities.
- An experimental set-up to investigate the chemical stability was assessed during the last SFERA II project and is present at the DTE/STSN/SCIS ENEA thermo-physical characterization laboratory. The equipment allows the determination of the produced gases and the liquid chemical composition, and permits to work in isothermal conditions and to control the reaction atmosphere.
- Moreover, the TFC labs include instrumentations specifically dedicated to the characterization of thermal fluids.



Looking forward to proposals!

THANK YOU FOR YOU ATTENTION!



- More information:

annachiara.tizzoni@enea.it

salvatore.sau@enea.it

SFERA-III

Solar Facilities for the European Research Area

1st Summer School “Thermal energy storage systems, solar fields and new cycles for future CSP plants”
WPI Capacity building and training activities
Odeillo, France, September 9th-11th 2019



“Increasing dispatchability and the capacity factor of CSP: Lessons learned from a lab-scale thermocline storage”

NETWORKING

Shahab Rohani, Fraunhofer Institute for Solar Energy Systems ISE



THIS PROJECT HAS RECEIVED FUNDING FROM THE EUROPEAN UNION'S HORIZON 2020 RESEARCH AND INNOVATION PROGRAMME UNDER GRANT AGREEMENT NO **823802**

INCREASING DISPATCHABILITY AND THE CAPACITY FACTOR OF CSP

Lessons learned from a lab-scale thermocline storage



Shahab Rohani

Fraunhofer Institute for Solar Energy
Systems ISE

SFERA III Summer School

Odeillo, 2019-09-09

www.ise.fraunhofer.de

© Abengoa

Fraunhofer ISE

At a Glance



Institute Directors:
Prof. Dr. Hans-Martin Henning
Dr. Andreas Bett

Staff: ca. 1200

Budget 2018: €94.3 million

Established: 1981



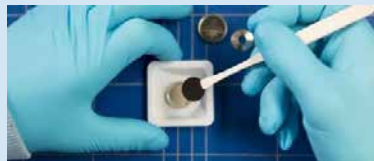
Photovoltaics



Energy Efficient Buildings



Solar Thermal Power Plants
and Industrial Processes



Hydrogen Technologies and
Electrical Energy Storage



Power Electronics, Grids
and Smart Systems

photos © Fraunhofer ISE/Guido Kirsch (1), Dirk Mahler (2,4,5,6), Simon Braungardt(3)

Business Area

Solar Thermal Power Plants and Industrial Processes



photo ©Fraunhofer ISE/Dirk Mahler

Research Themes

- Solar Thermal Power Plants
- Concentrating Solar Collectors
- Water Treatment and Separation
- Thermal Energy Storage for Power Plants and Industry
- Industry Processes and Process Heat
- Efficient Heat Exchangers

AGENDA

- Introduction to thermal storage in CSP
- Sensible heat storage
- 1-Tank thermal energy storage with stratification
- 1-Tank Storage: Prototype at Fraunhofer ISE

INTRODUCTION

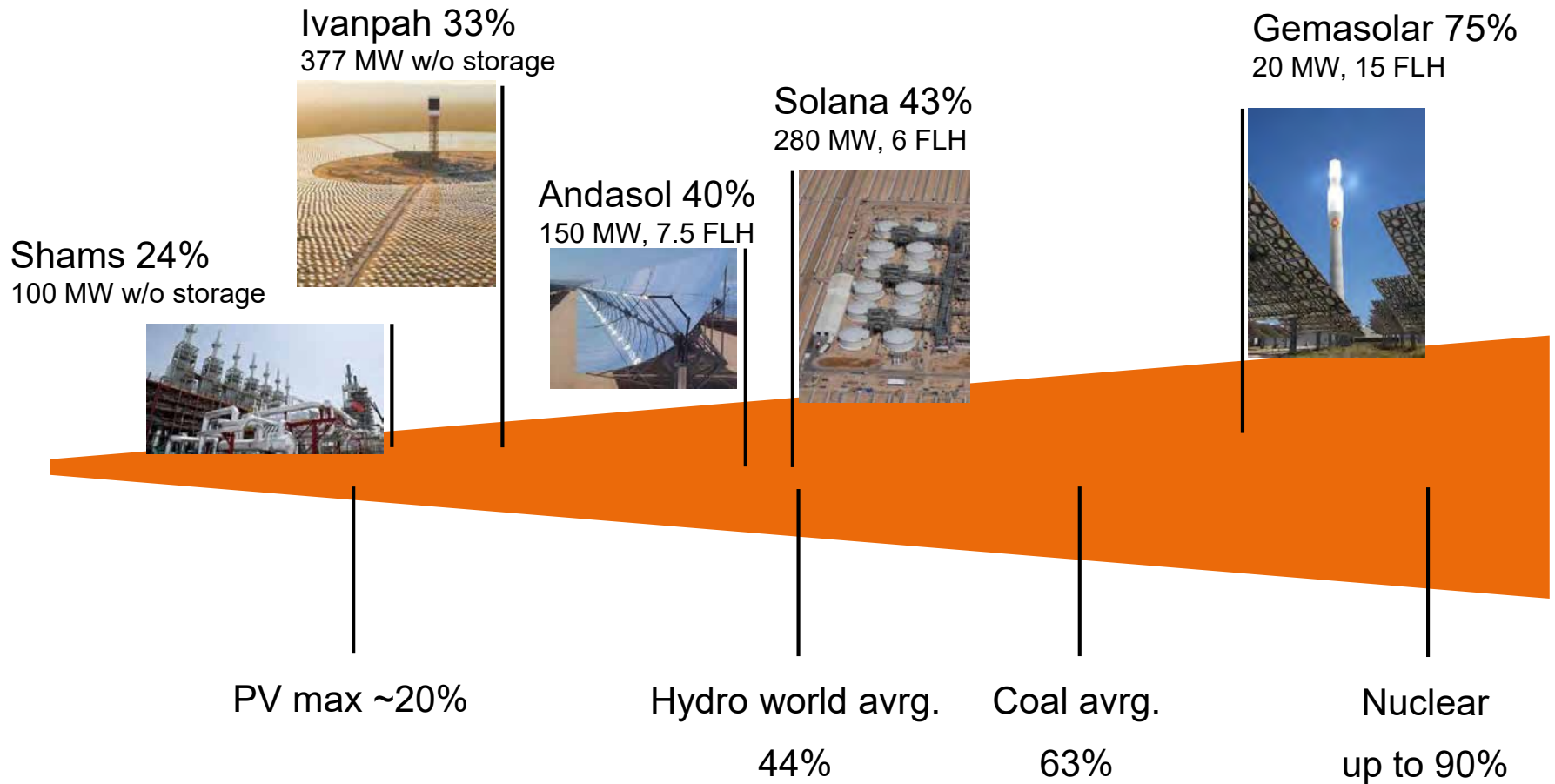
- Introduction
 - Purpose of (thermal) energy storage in CSP plants
 - Capacity factor of CSP w/ and w/o storage
 - Storage capacity, solar multiple and full load hours
 - Thermal storage classification
- Latent heat storage
- 1-tank thermal energy storage with stratification
- 1-Tank Storage: Prototype at Fraunhofer ISE

Purposes of energy storage

- Solar radiation is a fluctuating source of energy
 - Solar energy is not always available when needed
 - Solar energy is not always needed when available
- Energy storage can synchronize energy supply and demand
 - Dispatchability → Energy on demand
 - Higher revenues by load management
 - Power production can be forecasted
- Stabilize operation of power block, especially of the turbine (e.g. clouds)
- Increase power block utilization (capacity factor, CF)
 - $CF = \frac{\text{Actual annual energy production}}{\text{Nameplate capacity} * 24 \text{ h} * 365 \text{ d}}$

Capacity factors of CSP

CSP provides wide range of plant types with different CF



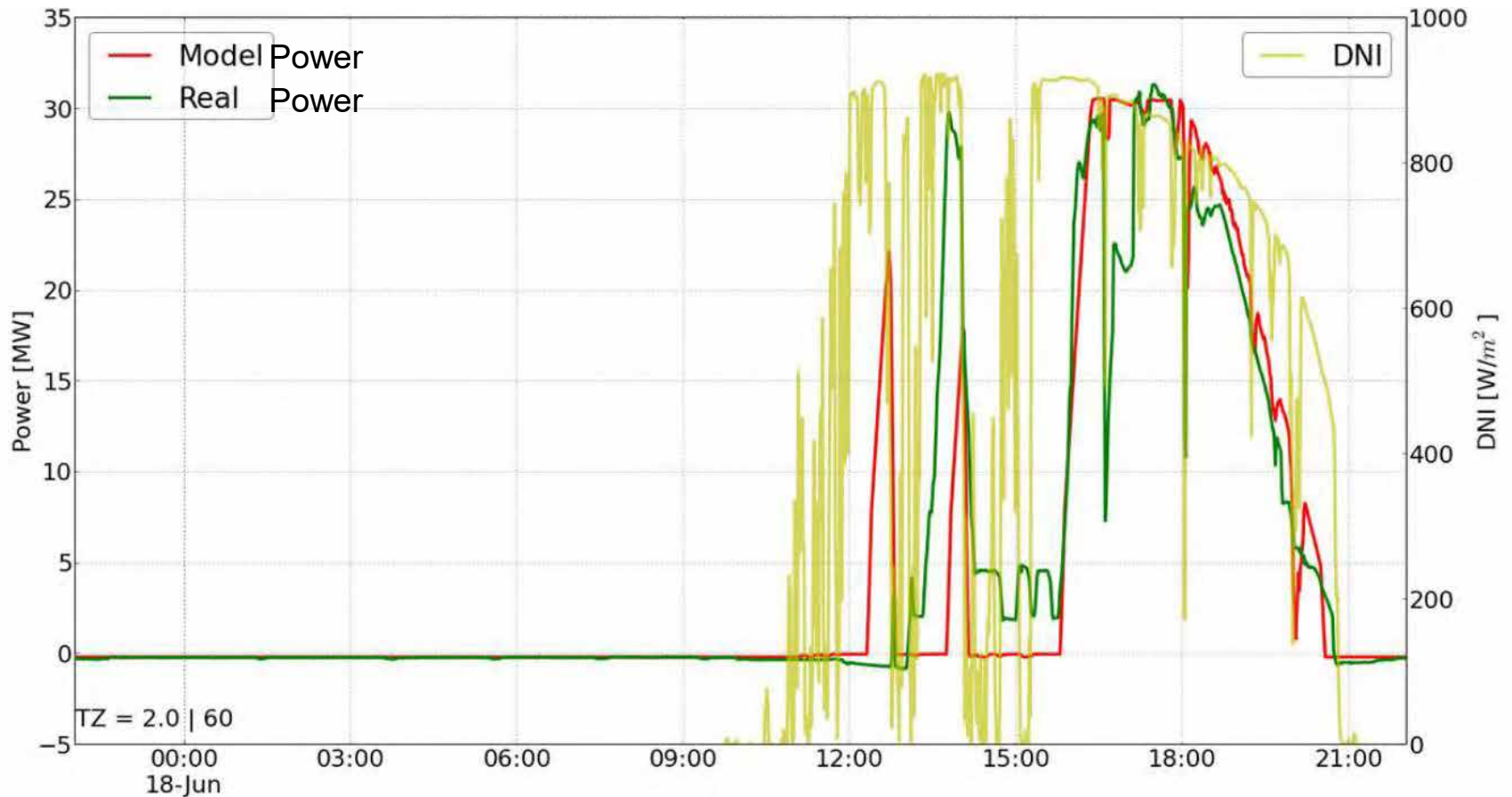
PE2: Linear Fresnel – Direct Steam Generation



Quelle: NOVATEC, SolarPACES 2014

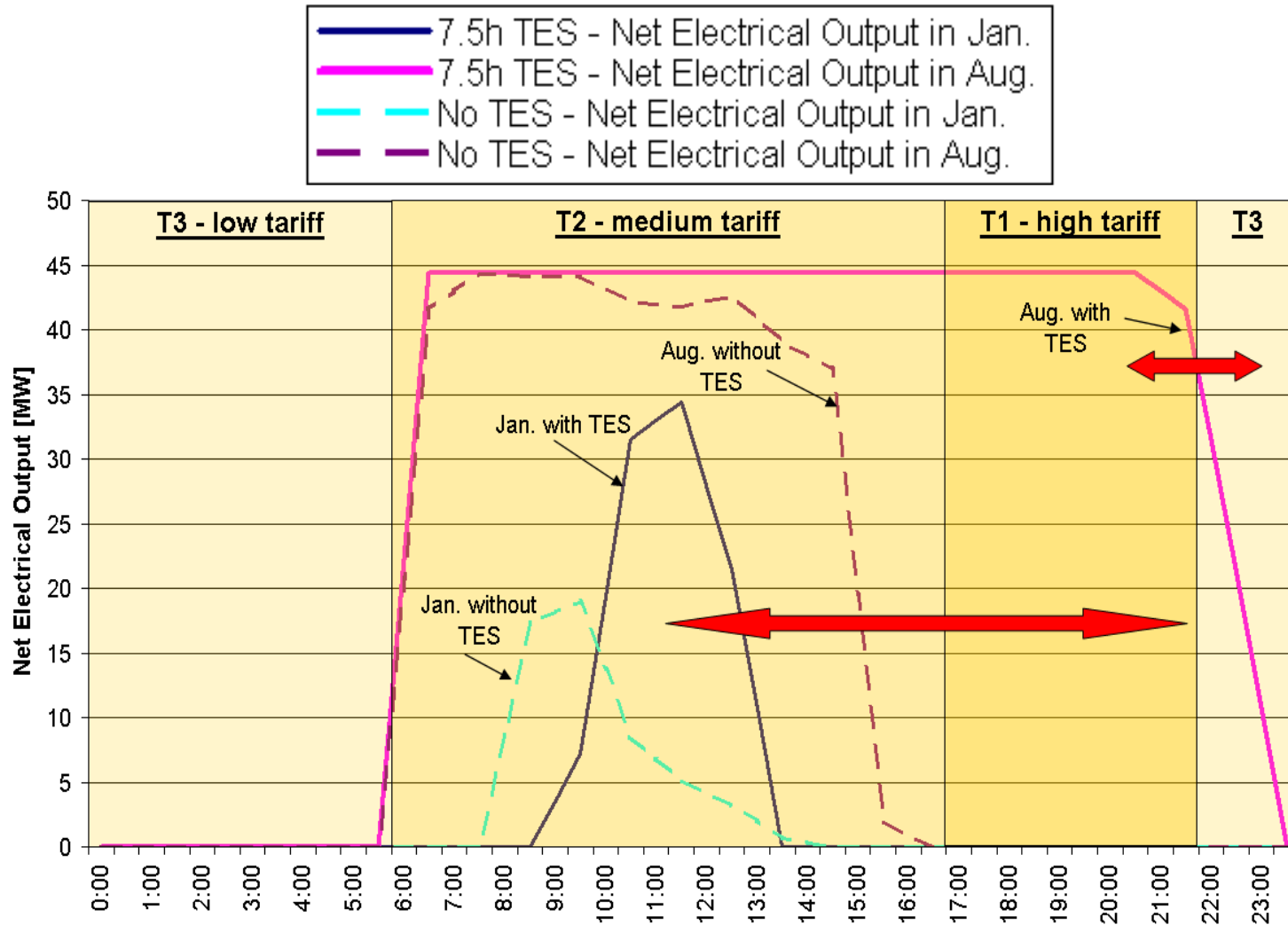
PE2 without Storage, 30 MW_{el}:

Power production on a day with volatile irradiance



Higher revenues by load management

Production is shifted to high demand & high tariff times



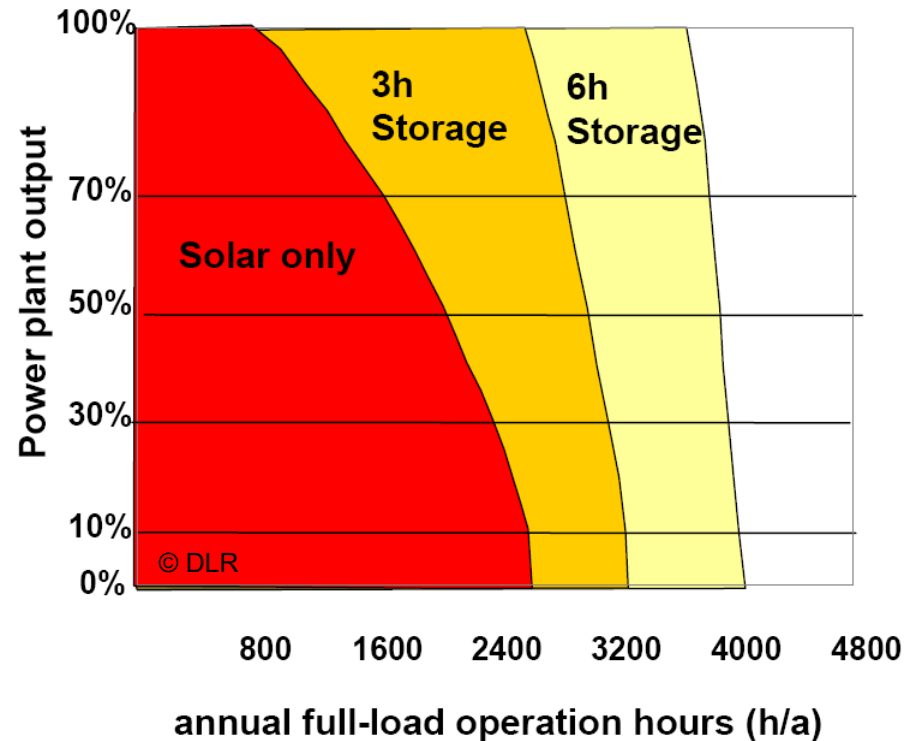
Some definitions:

Storage Capacity and Full Load Hours (FLH)

- Storage capacity: Amount of thermal energy stored
 - $Q = \text{mass} * \text{specific heat capacity} * \text{temperature difference}$ (in case of a sensible storage)
- Equivalent storage capacity: Amount of usable energy (electricity) stored
- Capacity in terms of CSP usually stated in MWh or GWh
- Full load hours (FLH) = Duration in which the plant can deliver a “full” power output through storage (nameplate capacity of turbine)

Increase of full load hours by storage

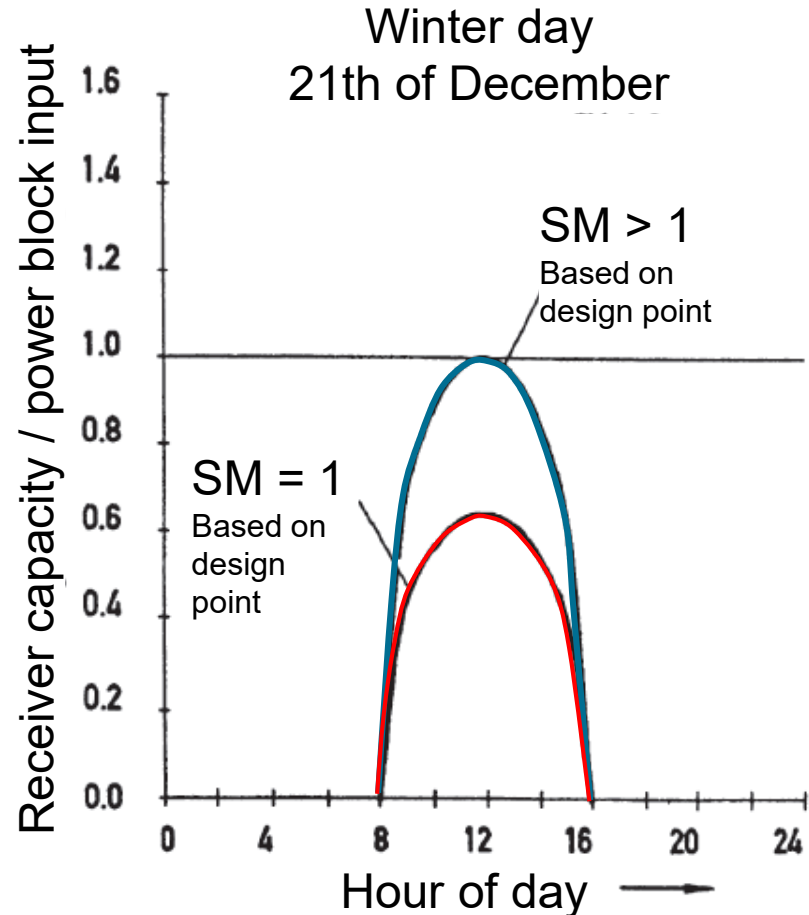
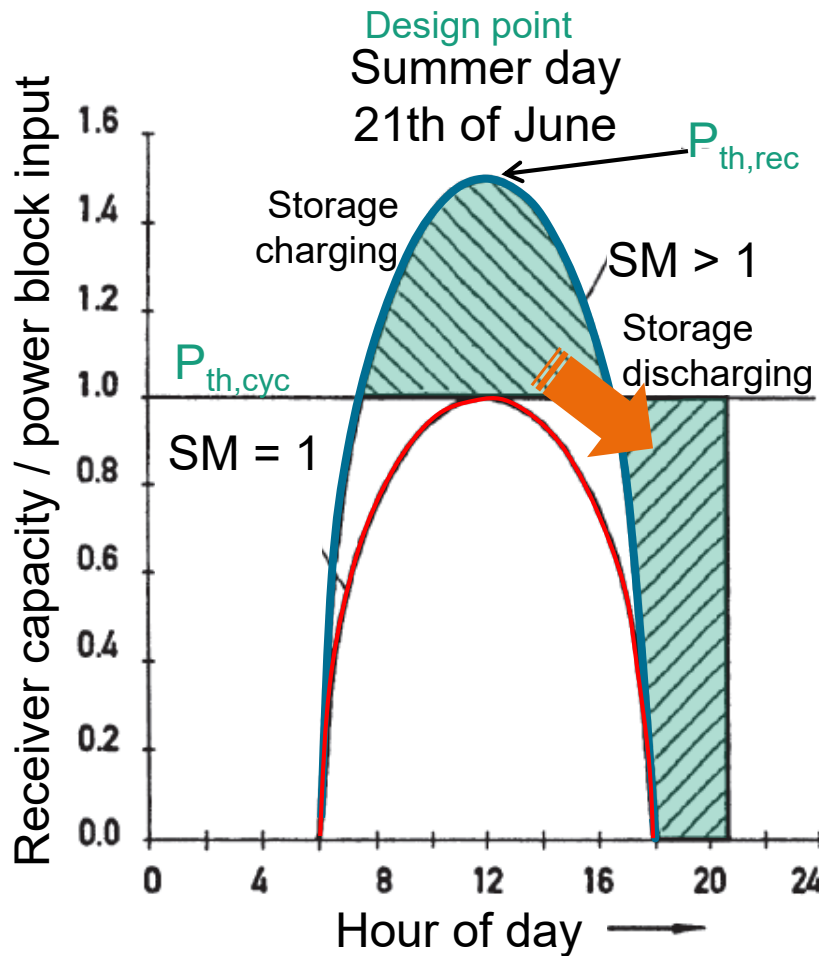
- Increase of power block utilization with storage
- Overall efficiency of the plant increases due to power conversion at **nominal load** of turbine
- Load management according to demand is possible
→ higher revenues



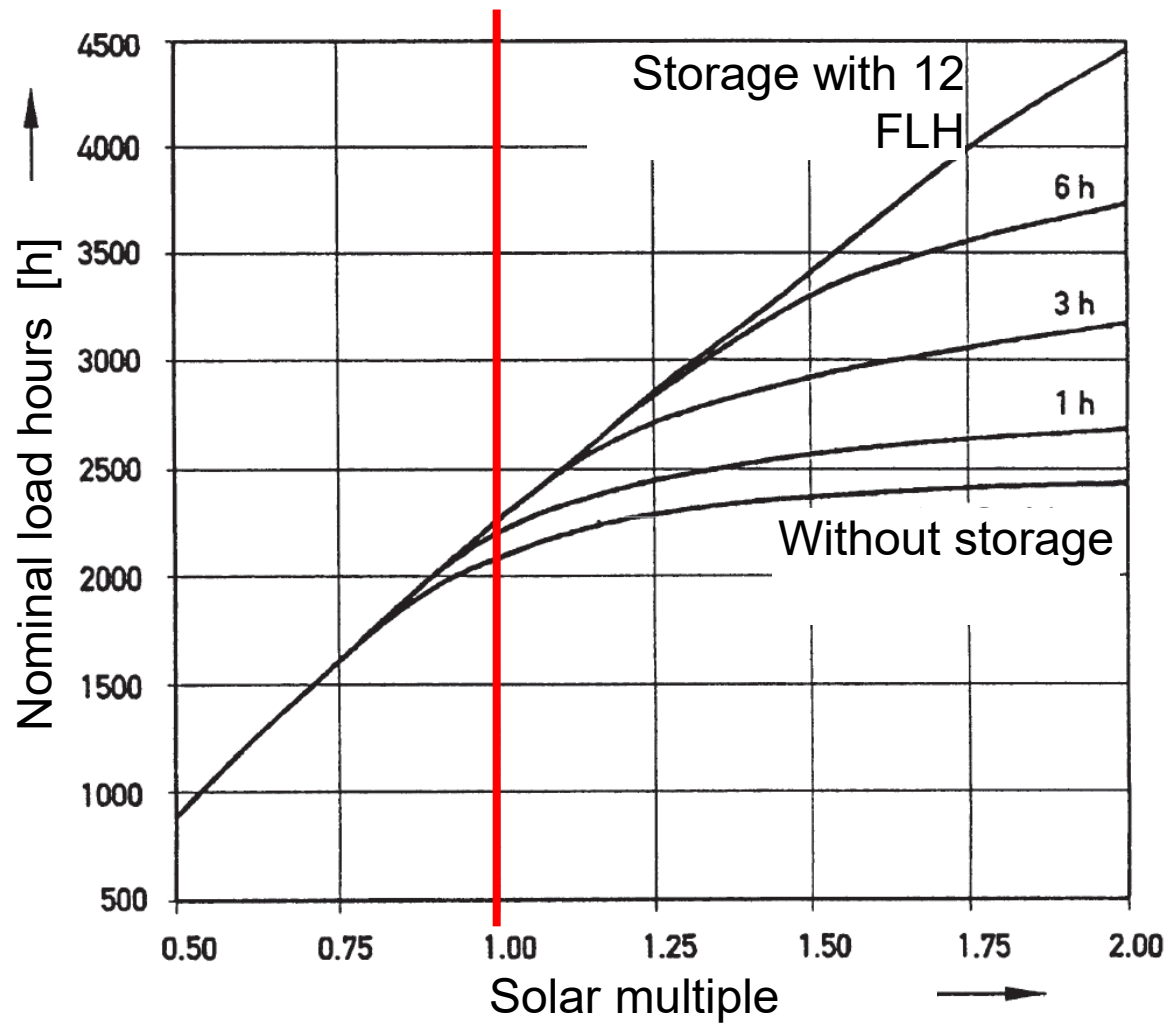
Solar multiple (SM)

$$SM = \frac{P_{th,rec}}{P_{th,cycle}}$$

Ratio of thermal receiver power ($P_{th,rec}$) at **design point** to the nominal inlet power of the power block ($P_{th,cyc}$)

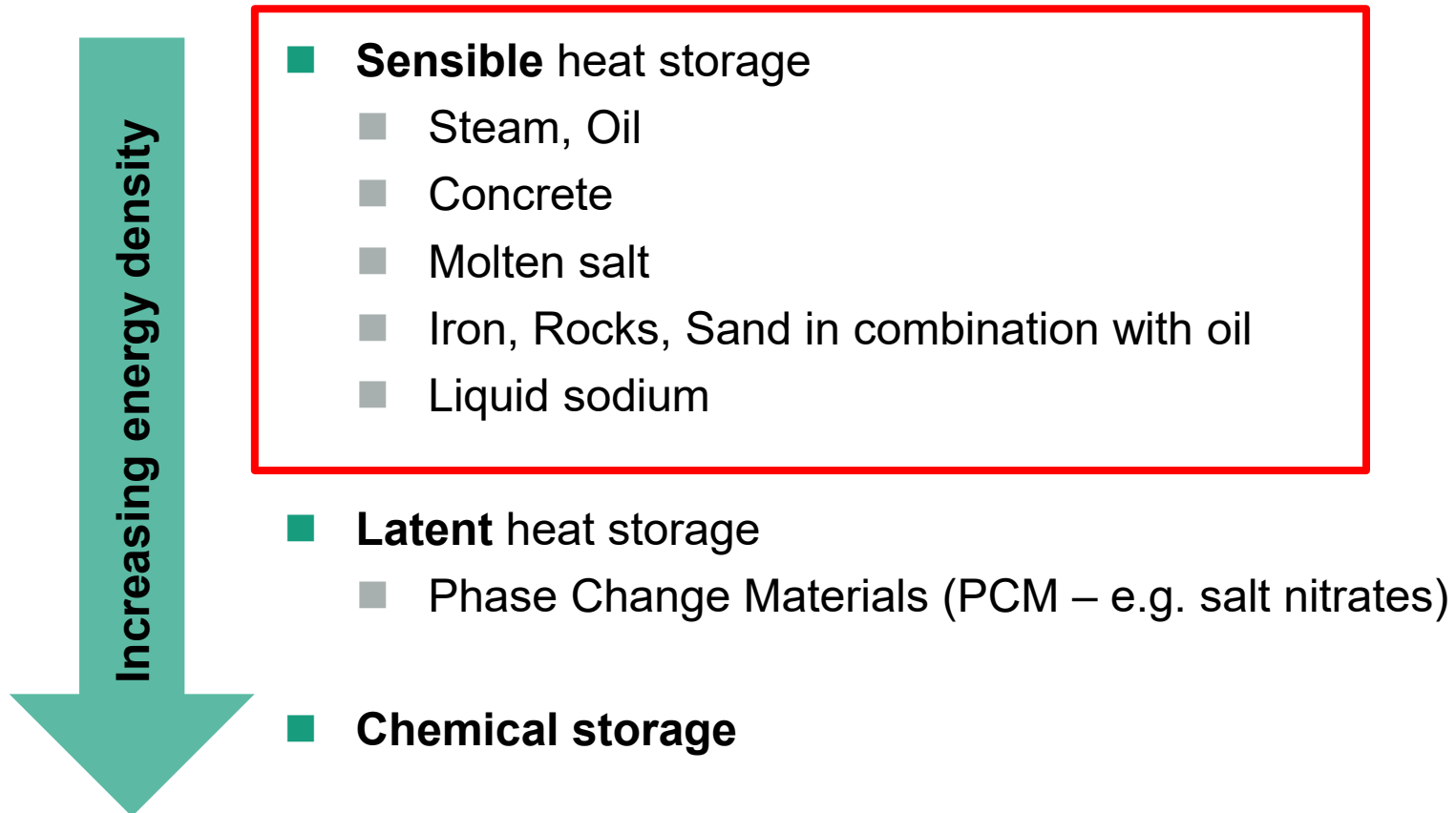


Solar multiple



edited from [1]

Classification of storage options

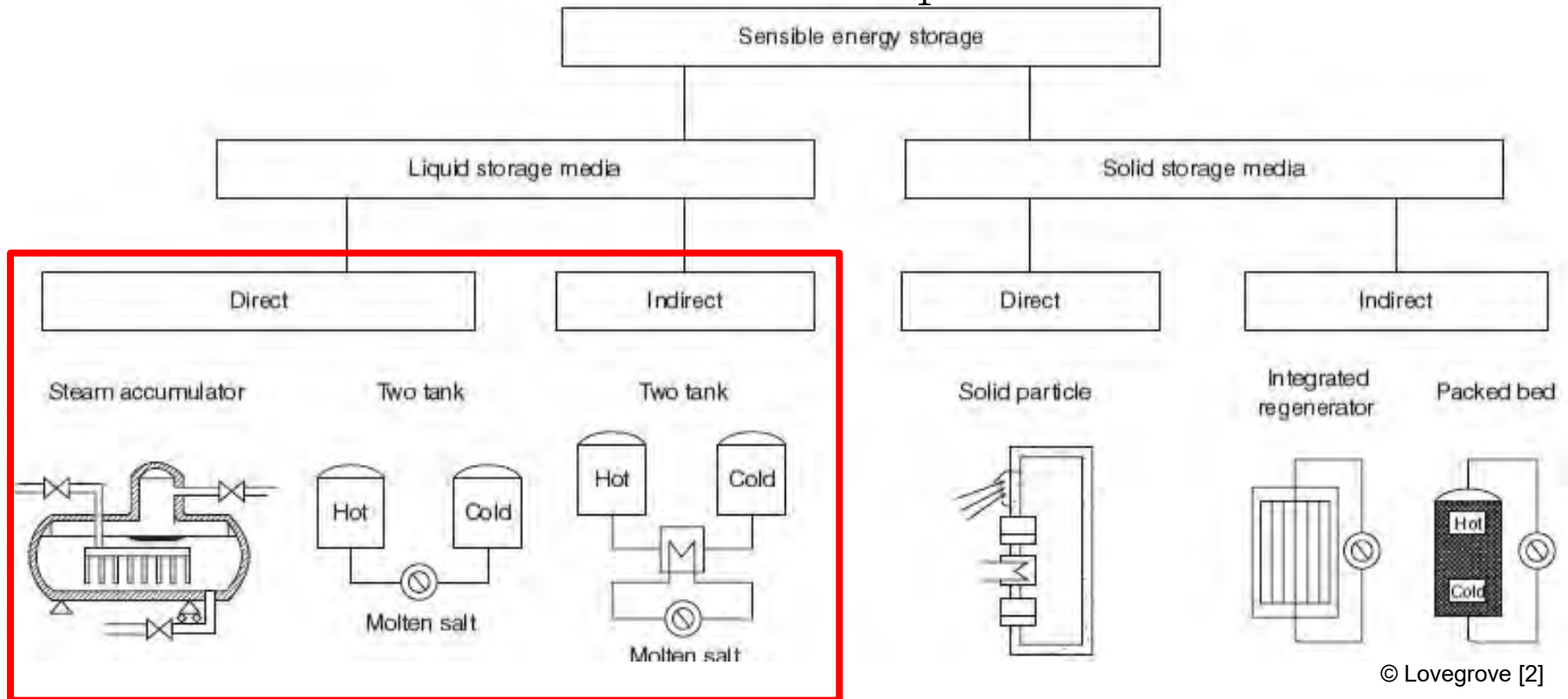


SENSIBLE HEAT STORAGE

- Introduction
- Sensible heat storage
 - Types of sensible heat storage
 - Steam accumulator
 - 2-Tank indirect
 - 2-Tank direct
 - Cost comparison
 - Realized solar thermal plants with storage (examples)
- 1-Tank thermal energy storage with stratification
- 1-Tank Storage: Prototype at Fraunhofer ISE

Overview of sensible energy storage

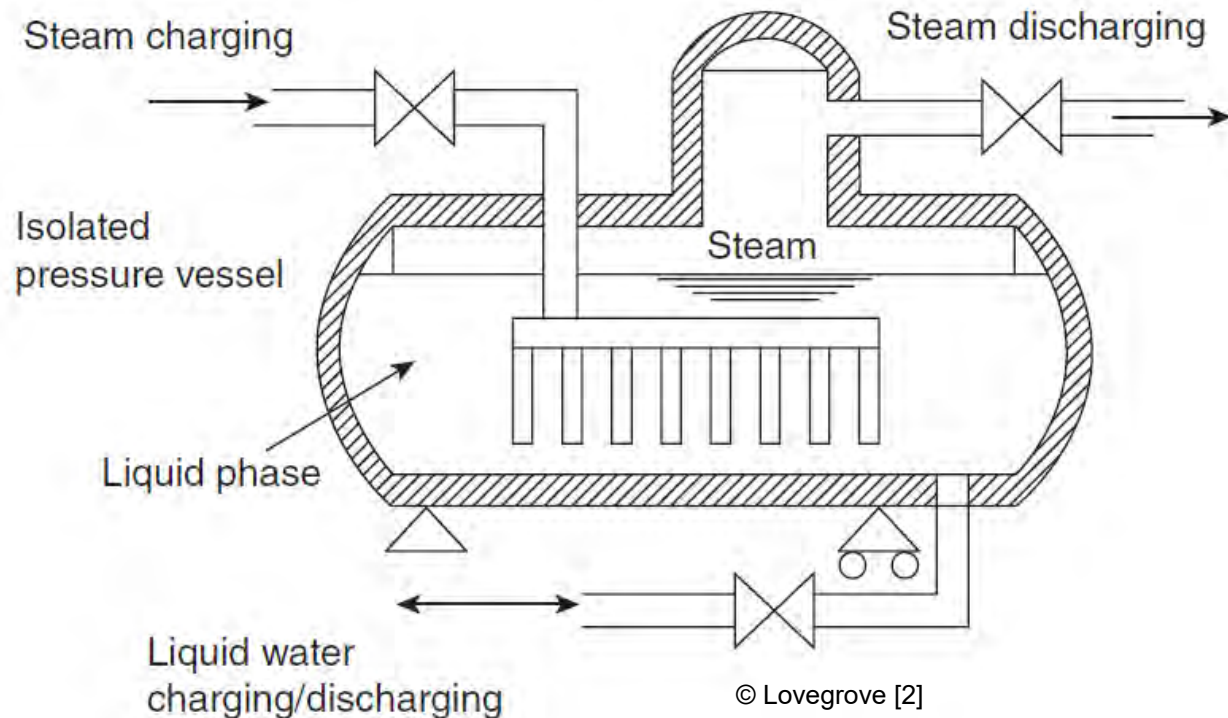
$$Q_{1,2} = m * \int_1^2 c(T) dT$$



Sensible Heat Storage

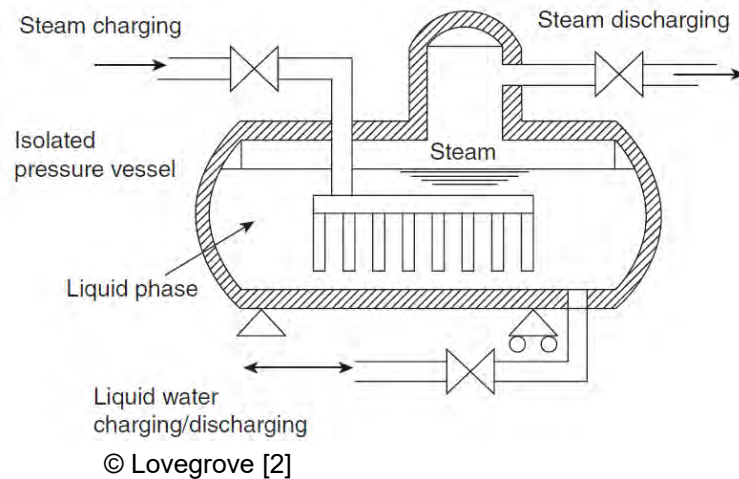
Steam Accumulator „Ruths storage“

- Only small capacity
- Short term storage
- Pressurized water as storage medium
- “Low pressure”
- Cost intensive



Sensible Heat Steam Accumulator

- **Example: PS10 (Spain)**
- 11 MW_{el}
- 50 bar / 285 °C
- Storage can run the power block for 30 Minutes



http://www.trec-uk.org.uk/images/heat_storage_tanks.jpg

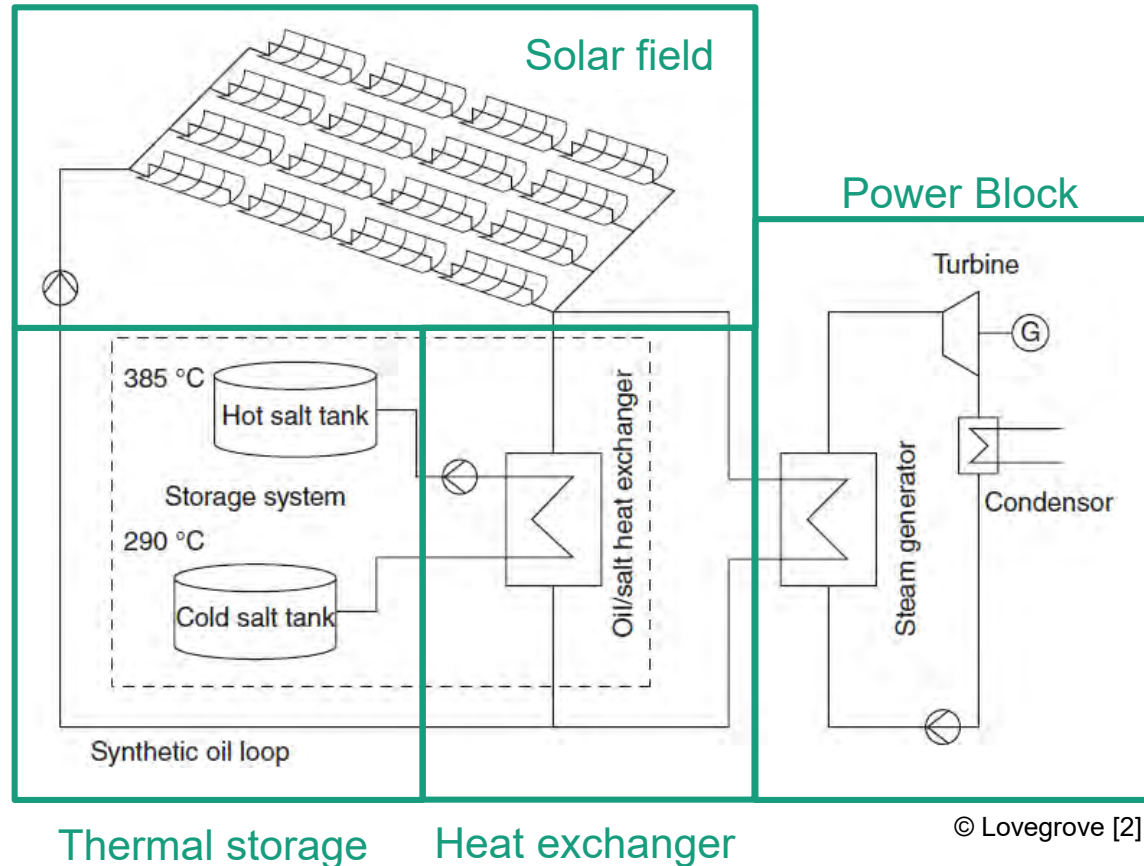


https://en.wikipedia.org/wiki/PS10_solar_power_plant

Sensible Heat

Two-tank indirect molten salt storage

- Most commonly built system
- HTF in solar field and storage medium differ
- Over-dimensioning of solar field, surplus energy is stored during the day
→ solar multiple > 1



Sensible Heat

Two-tank indirect molten salt storage

- **Example:** Andasol 3 (Spain)
- Electrical power: 50 MW
- Tank diameter: 38.5 m
- Height: 14 m
- Contents: about 28,000 m³ molten salt
- Temperatures:
cold 292°C, hot 386°C
 - $\Delta t = 94 \text{ K}$
- 7.5 full load hours

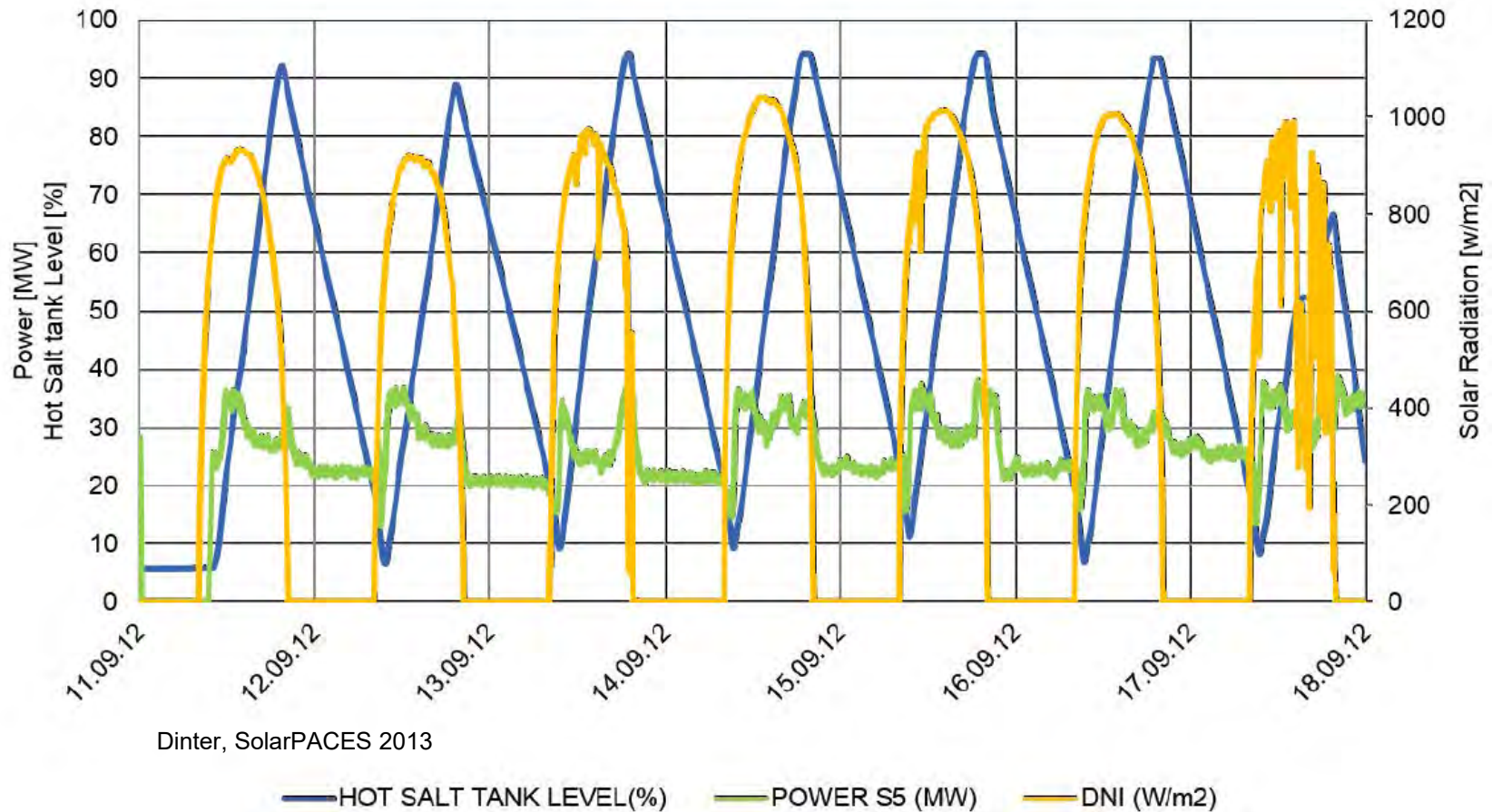


© renewableenergyfocus.com

Sensible Heat

Two-tank indirect molten salt storage

■ Example: Andasol 3



Sensible Heat

Two-tank indirect molten salt storage

- **Example 2:** Solana (USA)
- Electrical power: 280 MW (net)
- Capacity factor: 43 %
- 6 Full load hours
- Storage capacity: 1680 MWh_{el}
- **≈ 47 times** the capacity of the biggest electrical storage (December 2016)



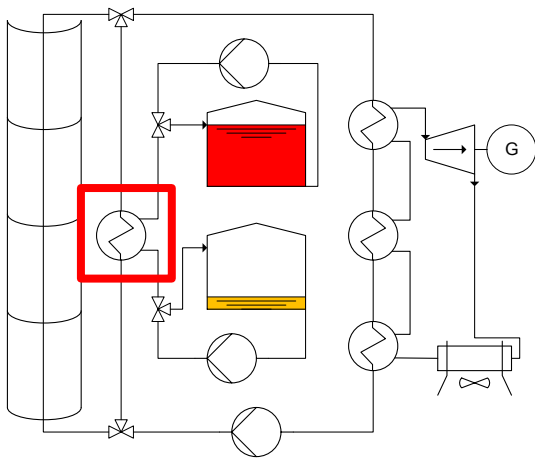
© Abengoa

Evolution of molten salt storages

The path to lower cost

Two-tank **indirect**

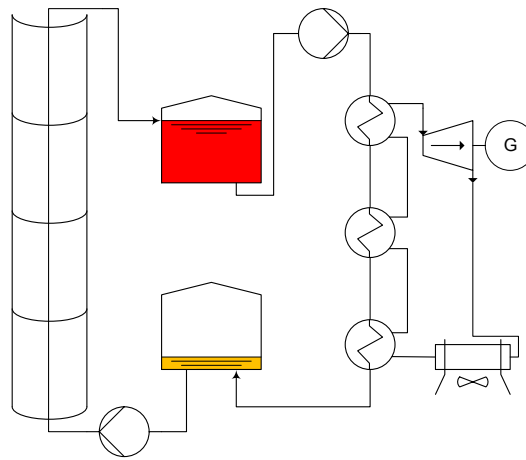
- Temperature loss due two double HX
- Temp. limited by oil
- One tank always empty



■ Andasol

Two-tank **direct**

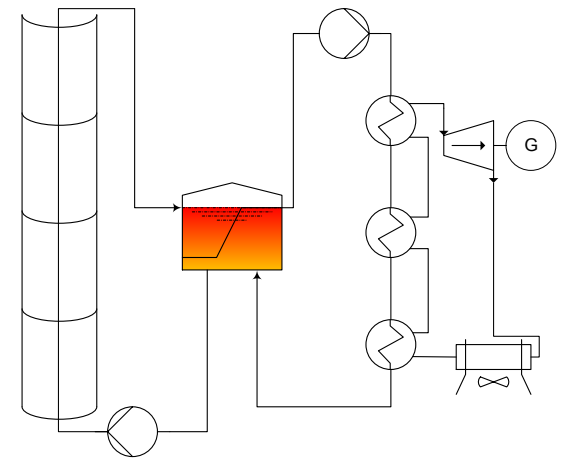
- Molten salt also in collector
- Higher temp. possible
- Less T loss & equipment



■ Gemasolar

Single thermocline tank

- One tank less
- Possible integration of HX
- Additional use of filler material reduces amount of salt

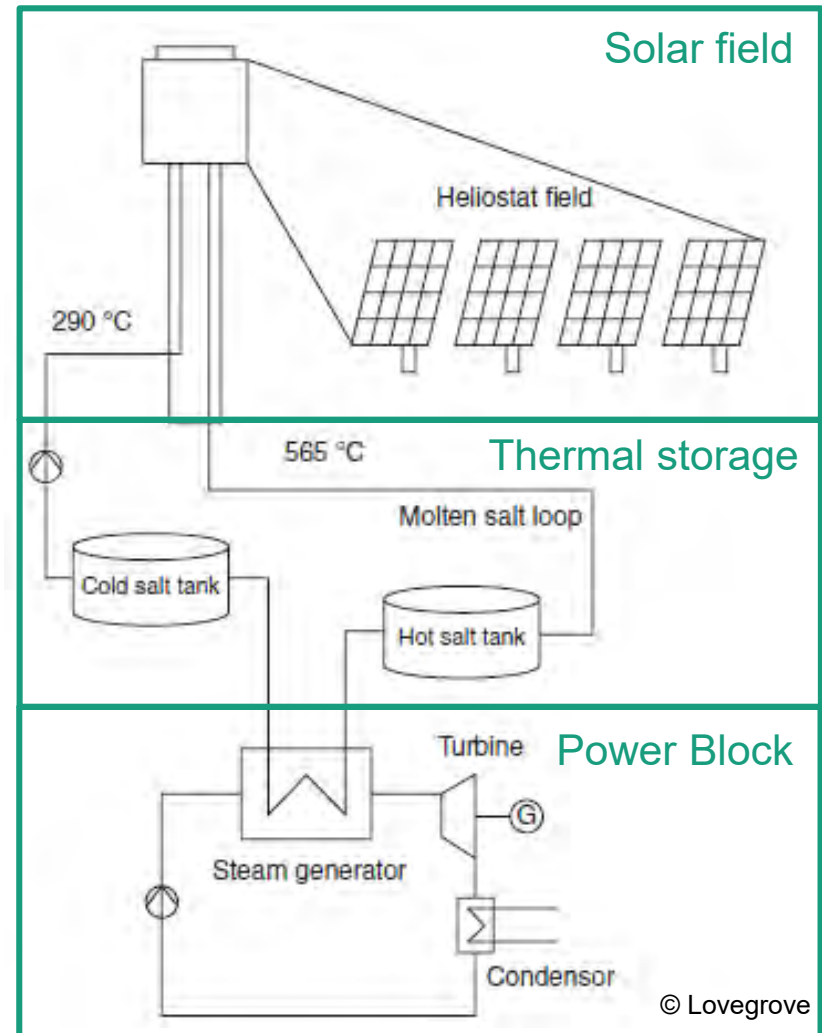


■ Testing / Pilots

Sensible Heat

Two-tank direct molten salt storage

- Trend towards direct storage
- Heat transfer fluid = Storage medium
- → No additional heat exchanger needed
 - Cost reduction, less equipment
 - Reduction of heat losses



Sensible Heat

Two-tank direct molten salt storage

- **Example:** Gemasolar (Spain)
- Storage capacity: 15 FLH
- 2650 heliostats
- Rated electrical power: 19.9 MW
- Capacity factor: 75 %
- Can produce **electricity over 24 hours a day** (during several month a year)



<http://www.torresolenergy.com>



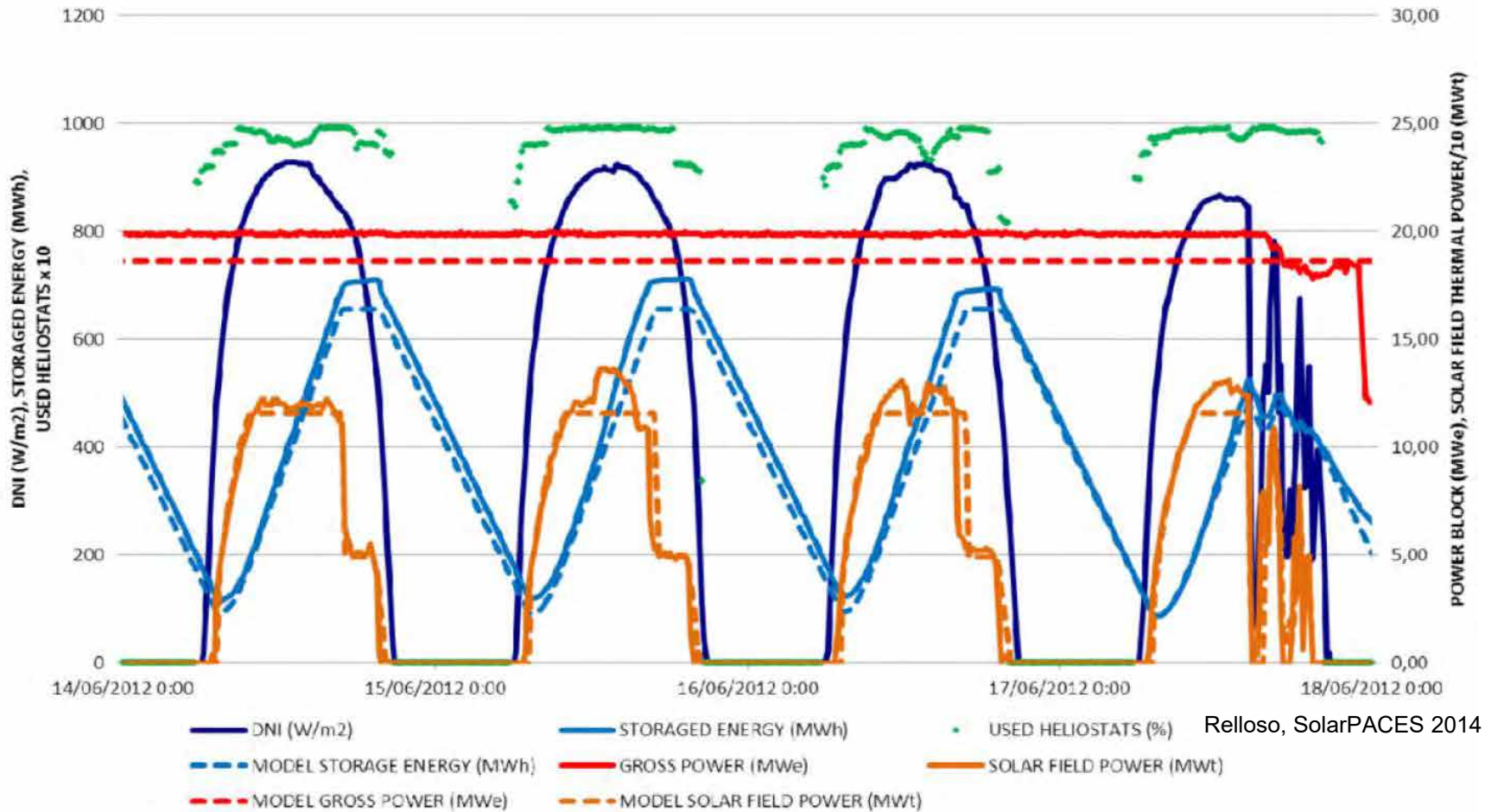
Source: Wikipedia

Location of Gemasolar in Spain

Sensible Heat

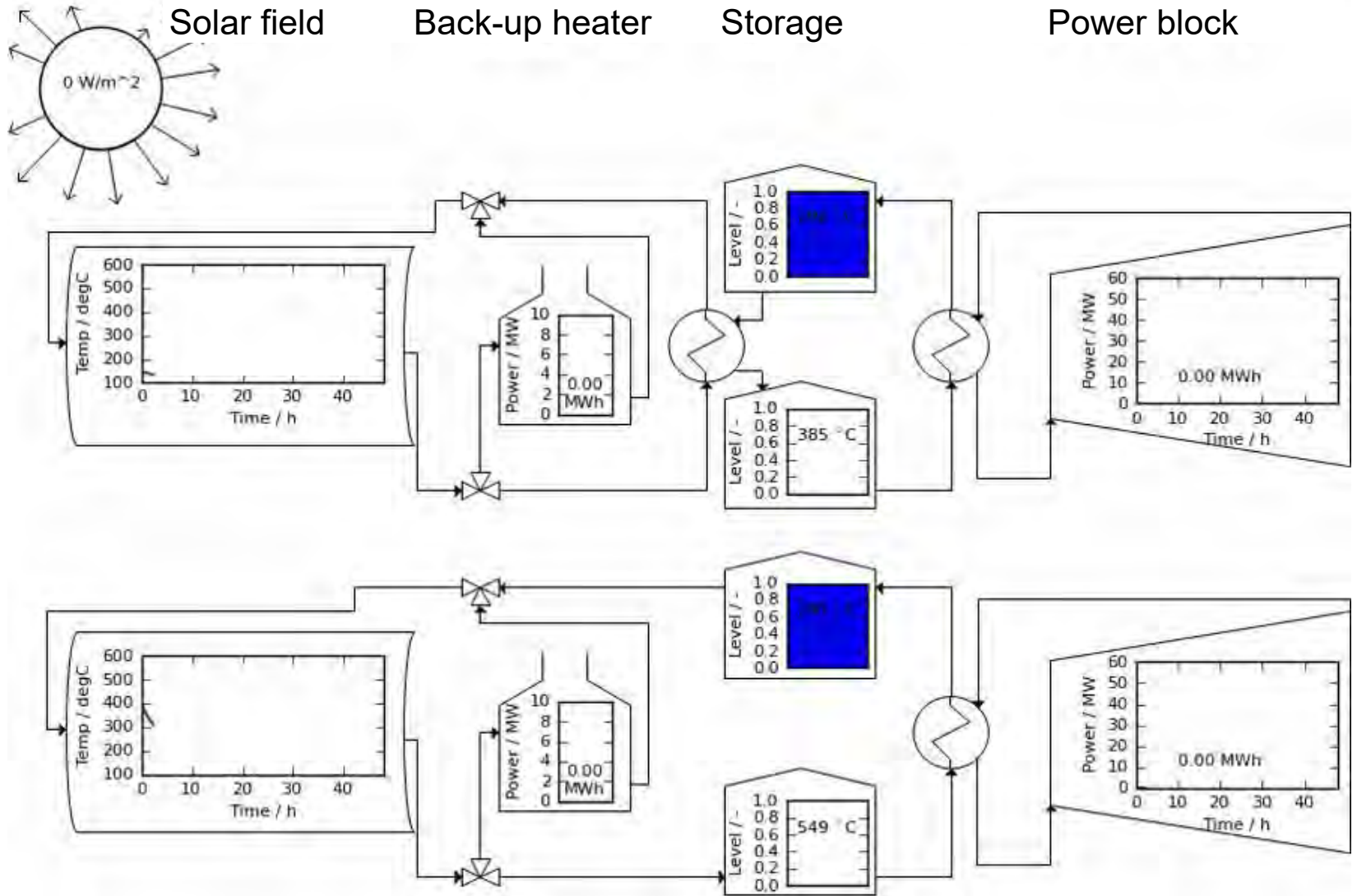
Two-tank direct molten salt storage

■ Example: Gemasolar (Spain)



Relloso, SolarPACES 2014

Direct vs. indirect storage



Different storages for different CSP systems

- There is no single type of storage solution which is available for *all* different CSP systems
 → storage material depends on operation temperature

| | |
|---|---|
| Oil parabolic trough | Two-tank molten salt storage Solid material storage Single tank thermocline molten salt storage |
| Direct steam generation parabolic trough / Linear Fresnel / Tower | Steam storage PCM storage |
| Solar tower with salt receiver | Two-tank molten salt storage Single tank thermocline molten salt storage |
| Solar tower with air receiver | Cowper storage (regenerator) Packed bed storage like a sand storage |
| Scheffler Dish | Solid block storage |

Efficiency of sensible thermal energy storage

Molten salt energy storage

- Is rather a short term storage (15 hours)
- Large quantities of storage medium is required
- Nearly no losses in the storage itself
- Thermal losses due to the piping system, heat exchanger
- Overall efficiency > 90 %

Thermal Energy Storage: Summary

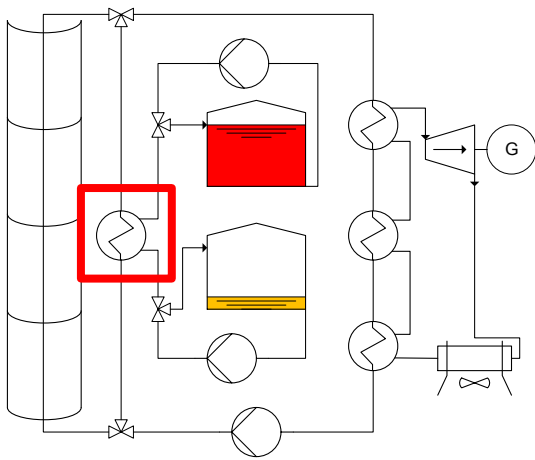
- CSP is the only solar technology that has large scale storage already today
- Implementation of storage leads to stable electricity production
 - Up to 24 hours a day
- Trend to direct storage systems
- Thermal energy storage makes CSP-plants dispatchable
 - Electricity on demand
- Thermal storage systems will become more efficient

Evolution of molten salt storages

The path to lower cost

Two-tank **indirect**

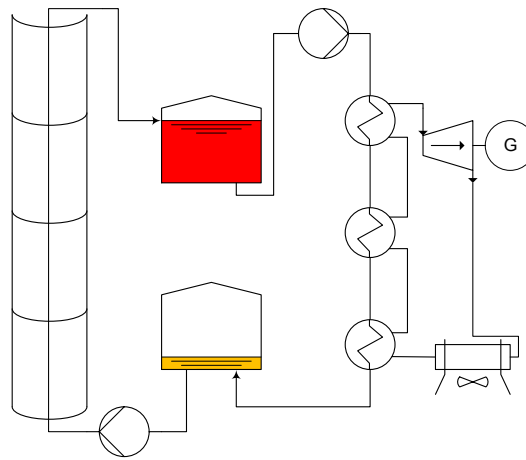
- Temperature loss due two double HX
- Temp. limited by oil
- One tank always empty



■ Andasol

Two-tank **direct**

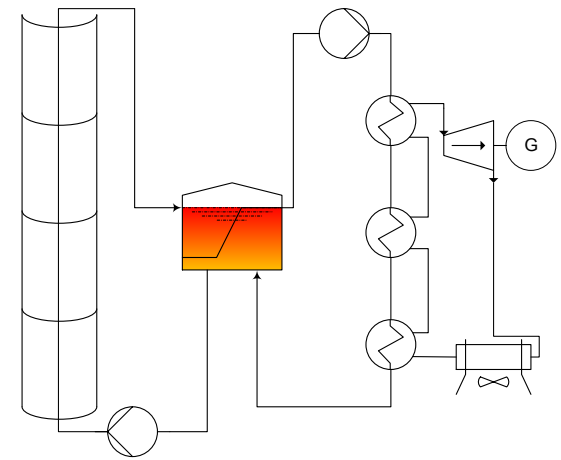
- Molten salt also in collector
- Higher temp. possible
- Less T loss & equipment



■ Gemasolar

Single thermocline tank

- One tank less
- Possible integration of HX
- Additional use of filler material reduces amount of salt



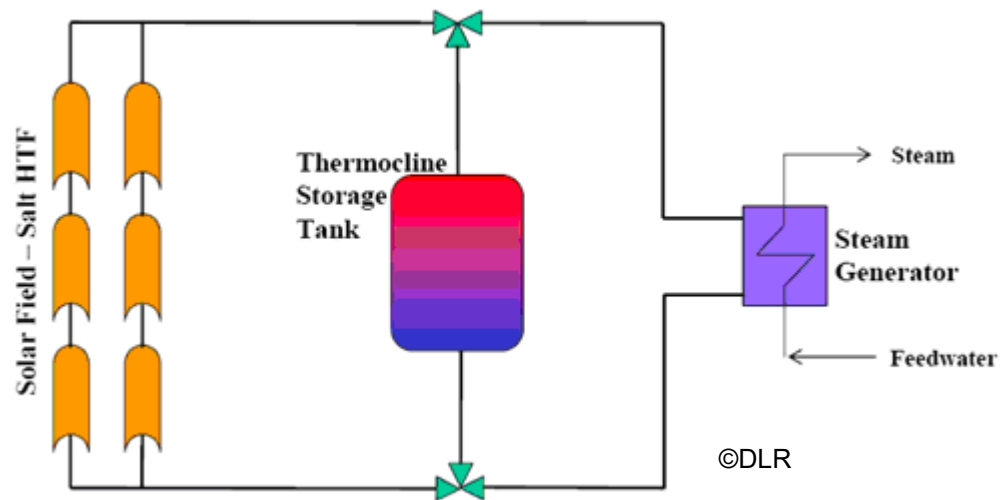
■ Testing / Pilots

1-TANK THERMAL ENERGY STORAGE

- Introduction
- Sensible heat storage
- 1-Tank thermal energy storage with stratification
 - Basics
 - Example
 - Operational characteristic
- 1-Tank Storage: Prototype at Fraunhofer ISE

Possible Options for the Future – Thermocline Storage

- Molten salt is used as heat transfer fluid in the solar collectors as well as storage fluid in the TES
- Only ONE tank is used – system is well known from domestic solar water heating systems
- Relies on thermal buoyancy
- Saves costs for 2nd storage and one oil/molten salt heat exchanger



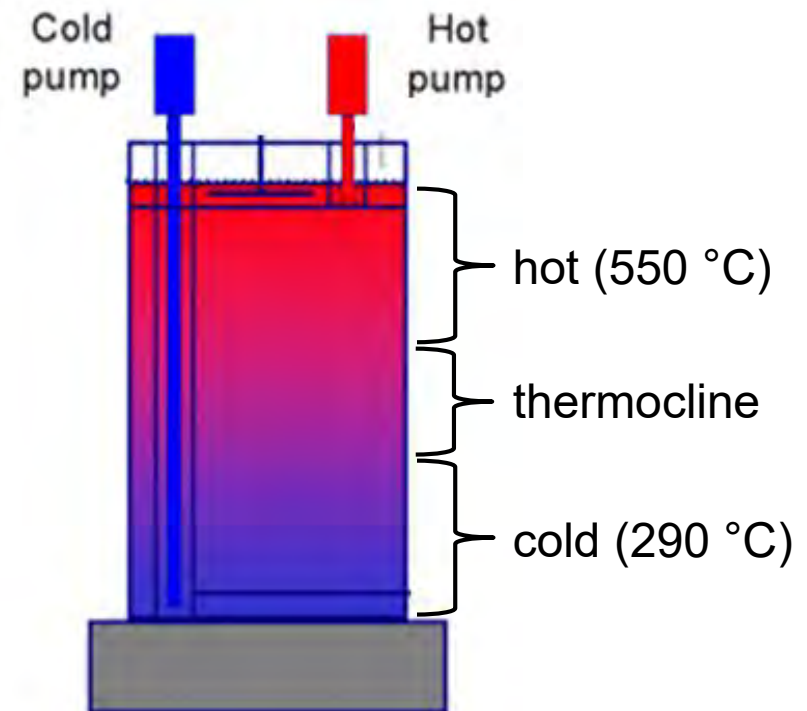
One Tank Molten Salt Storage With Stratification

■ Features

- Separation due to density difference
- Constant tank filling level
- More than 2 temperatures

■ Conventional design

- Pumping with shaft until the bottom of the tank
- External steam generator



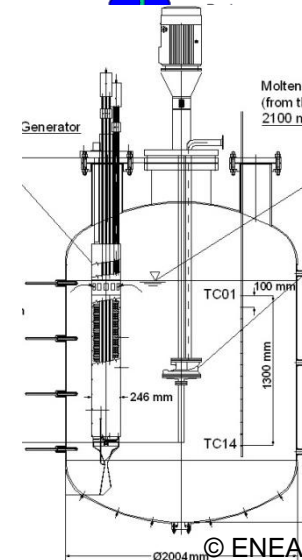
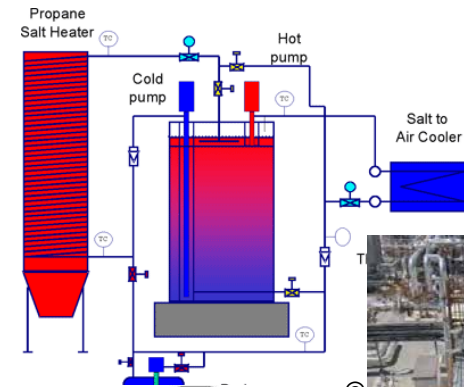
© Sandia

One Tank Storage: Basics

- Separation of hot and cold fluid due to density difference
 - Water: 20 °C – 90 °C → 998 kg m⁻³ – 965 kg m⁻³ → $\Delta\rho = 3.31\%$
 - Salt: 290 °C – 550 °C → 1905 kg m⁻³ – 1740 kg m⁻³ → $\Delta\rho = 8.66\%$
- The better the separation, the better the efficiency
- Parasitic effects for stratification
 - Mixing at the inlet (without filling material)
 - Heat exchange between molten salt and filling material

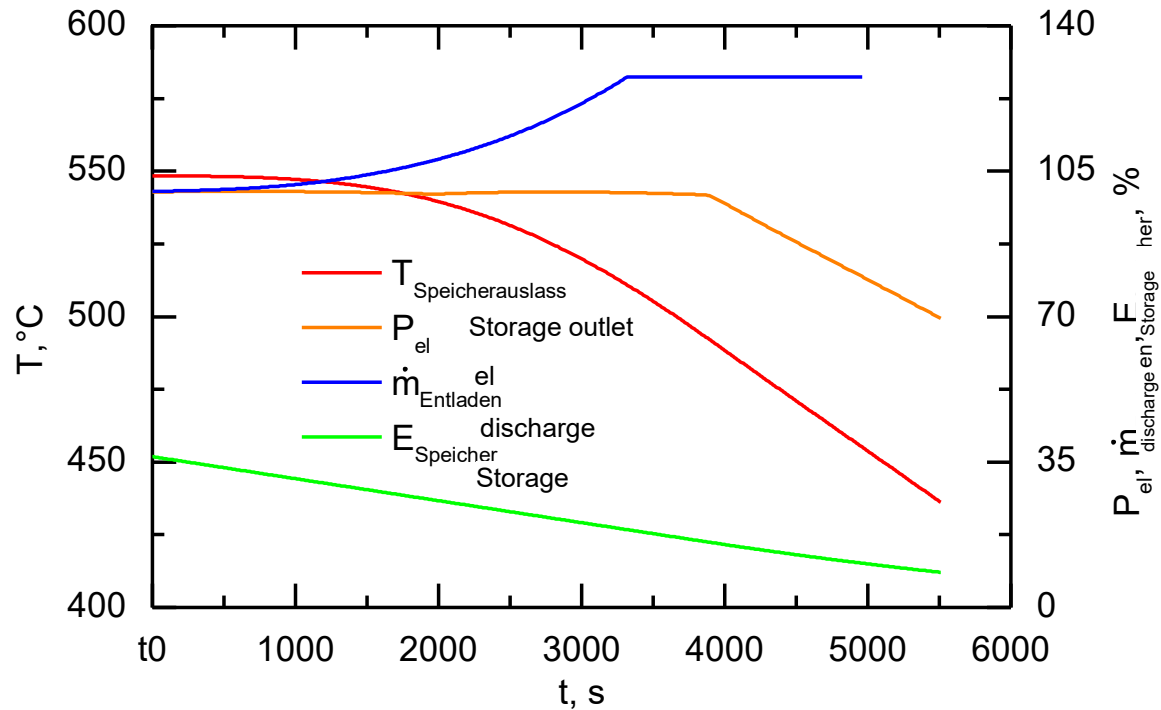
One Tank Storage: Examples

- Sandia, USA (2001): 2,3 MWh
 - T_{\max} 390 °C
 - Filling material: Stone-Sand-Mixture
- Sener, Spain (2011): 24 MWh
 - T_{\max} 390 °C
 - With separation barrier
- ENEA, Italy (2012): 1,2 MWh
 - T_{\max} 520 °C
 - Internal steam generator



One Tank Storage: Operational Characteristics

- Behavior depends on stratification
- Discharge power lowers at the end of a cycle

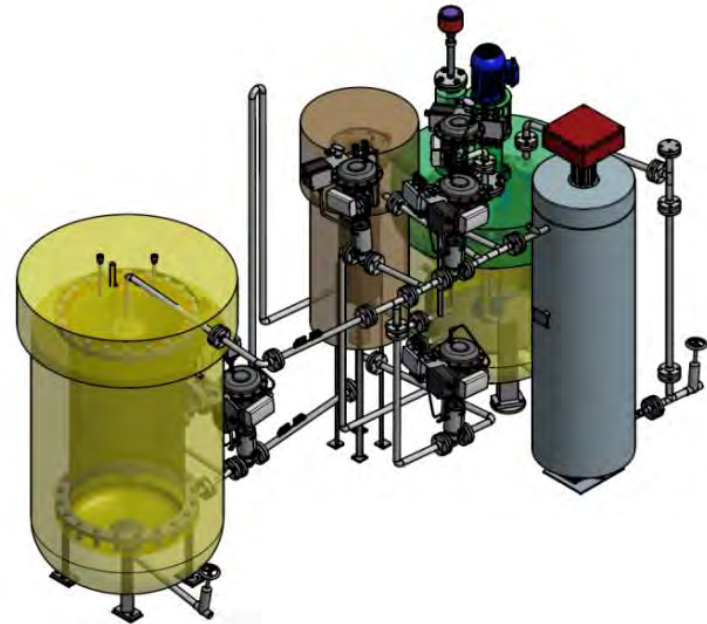


1-TANK THERMAL ENERGY STORAGE

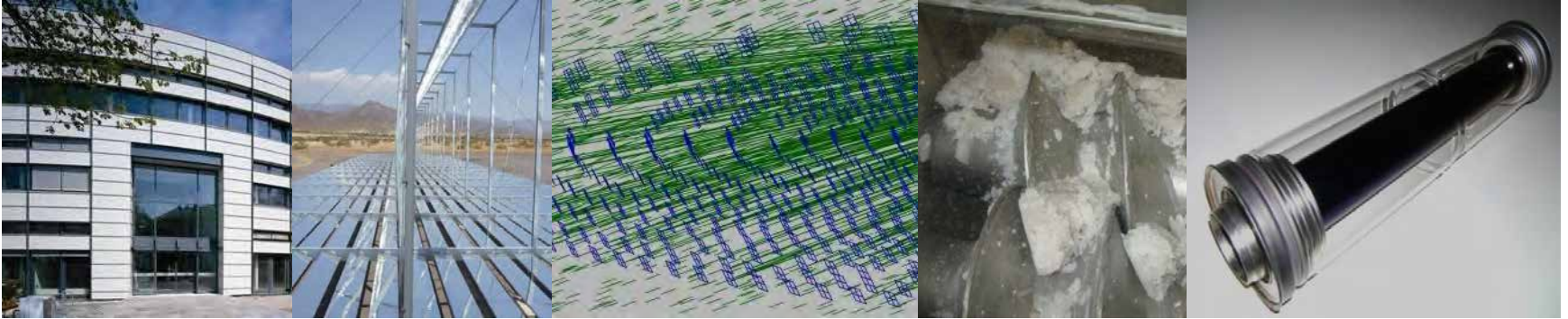
- Introduction
- Sensible heat storage
- 1-Tank thermal energy storage with stratification
- 1-Tank Storage: Prototype at Fraunhofer ISE
 - System Description
 - Qualitative Evaluation
 - Method
 - Result
 - Energetic Evaluation
 - Charging of Storage
 - Discharging of Storage
 - Conclusion and Outlook

One Tank Storage: Prototype at ISE

- Stratified storage
 - Height 1,3 m / diameter 0,6 m
 - Capacity: 72 kWh
 - Temperature: 290 °C – 550 °C
 - Heating and cooling power 60 kW
- Charge- and discharge experiments:
 - Temperature difference
 - Mass flow
- Next step: Filling material



Thank you for your attention!



Fraunhofer Institute for Solar Energy Systems ISE

Shahab Rohani

www.ise.fraunhofer.de

shahab.rohani@ise.fraunhofer.de



European Commission
FP7 Grant Agreement No:
609837



Lessons learned from a lab-scale thermocline storage

SFERA III summer school
CNRS/PROMES
September 09 – 11, 2019

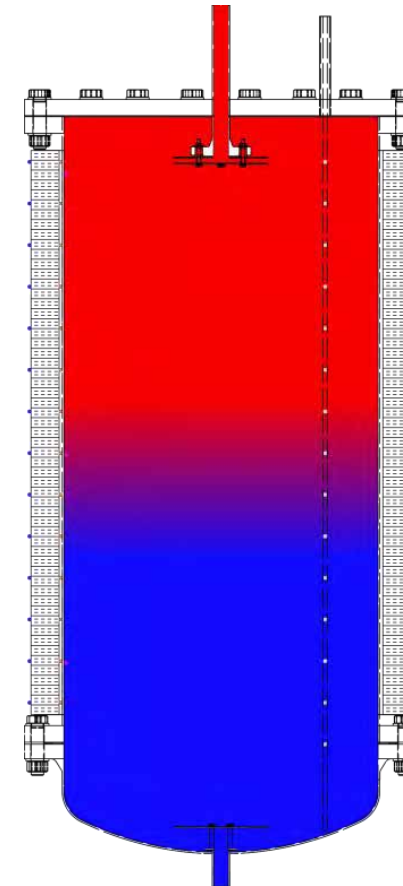
*Shahab Rohani, Martin Karl, Bernhard Seubert
Ralf Müller, Dr. Thomas Fluri, Dr. Peter Nitz
Fraunhofer ISE
Martin.karl@ise.fraunhofer.de*



www.stage-ste.eu



1. Introduction
2. System Description
3. Qualitative Evaluation
 - a) Method
 - b) Result
4. Energetic Evaluation
 - a) Charging of Storage
 - b) Discharging of Storage
5. Conclusion and Outlook



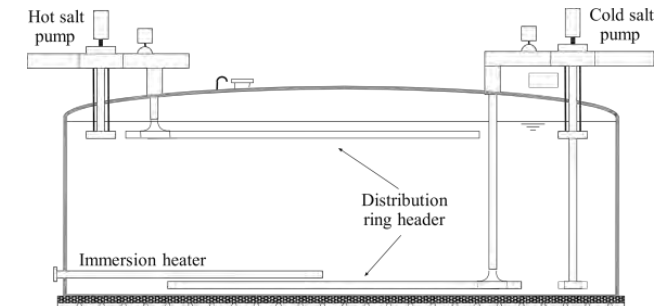
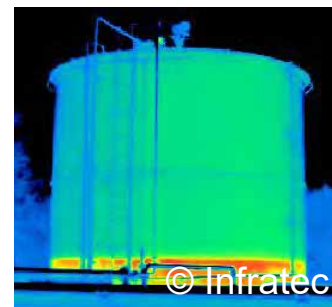
Only one tank

- Less material use
- Reduction of HTF volume
- Lower floor area demand
- Cold tank foundation
- Lower heat losses
- Reduced dead volume

Constant fill level

- Integration of filler material
- Short-shaft pumps
- **Easier tank ullage gas management**

→ Recent studies show that the CAPEX of storage systems could be reduced by up to 35 %

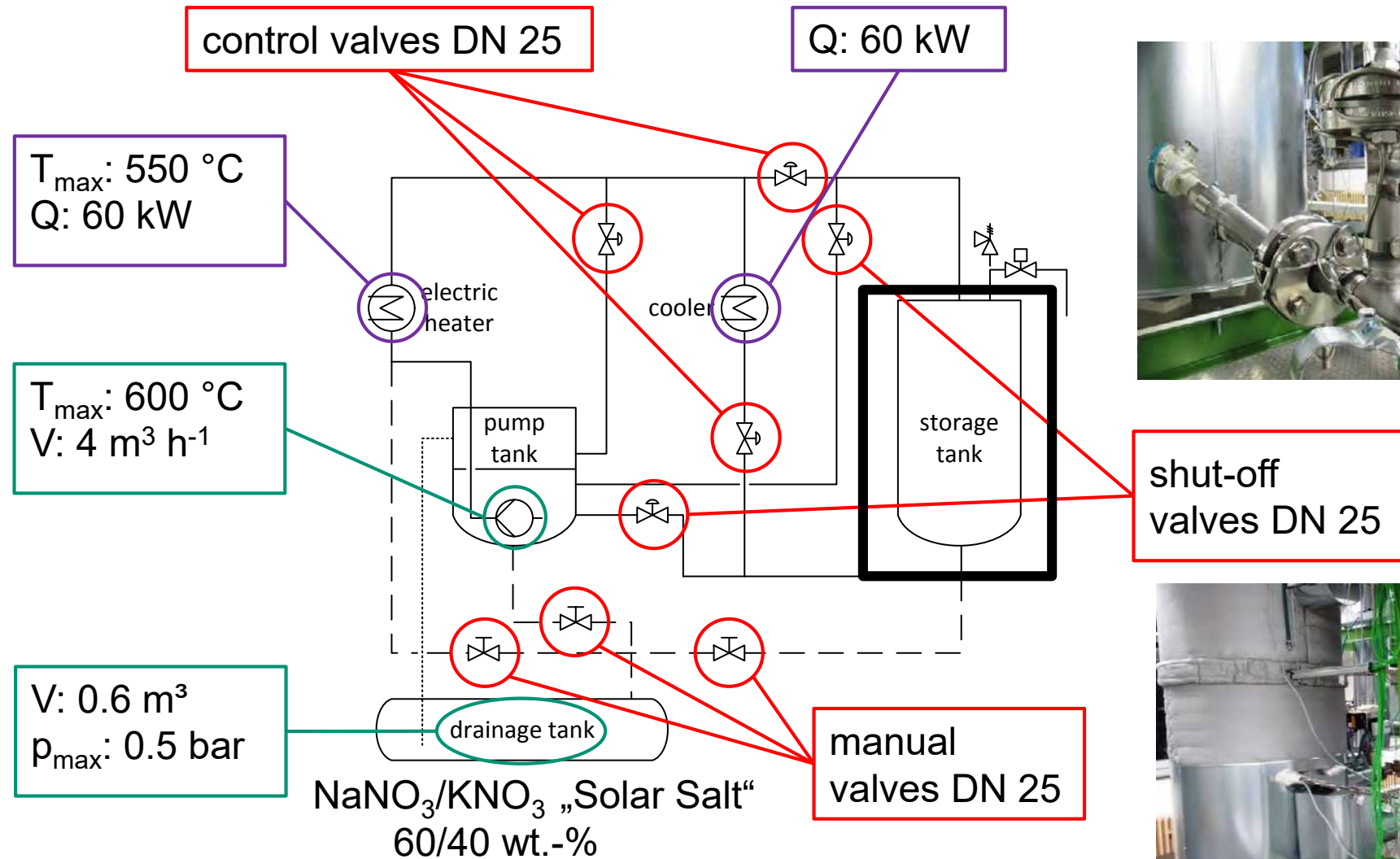


Drawback: Mixing of hot and cold layer → Loss of exergy

System Description

System Description

Main Features



shut-off valves DN 25



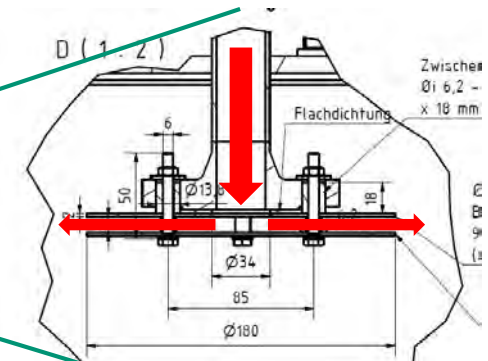
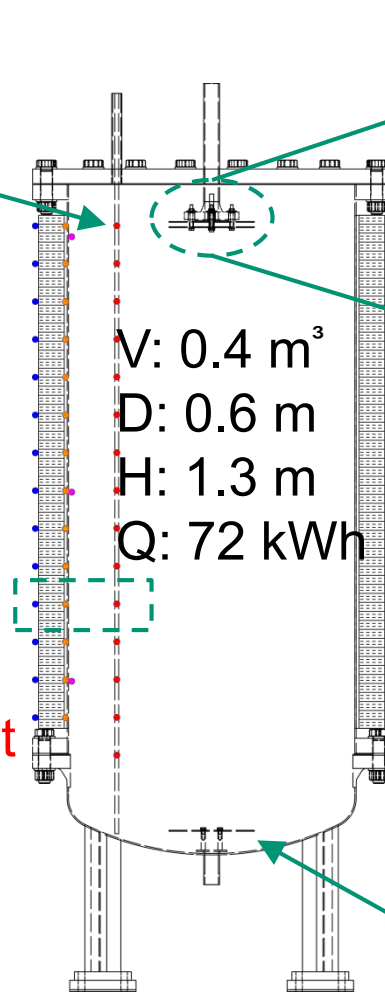
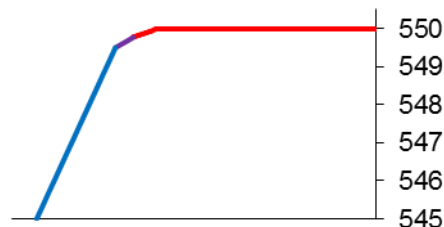
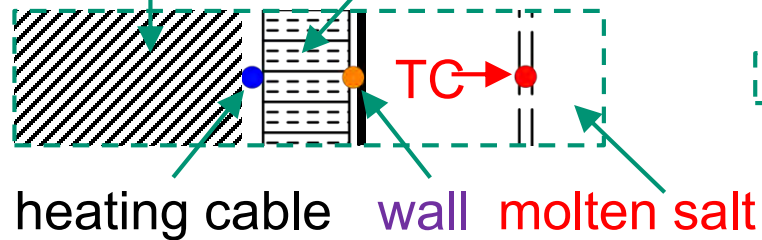
manual valves DN 25

System Description

Thermocline Tank

15 x thermocouples (TC) for measurement of stratification

secondary/main insulation primary insulation



double-plate radial diffuser
A_{inlet}: 0.0051 m²
u_{inlet}: 0.02 m s⁻¹ (@ 0.4 m³ h⁻¹)

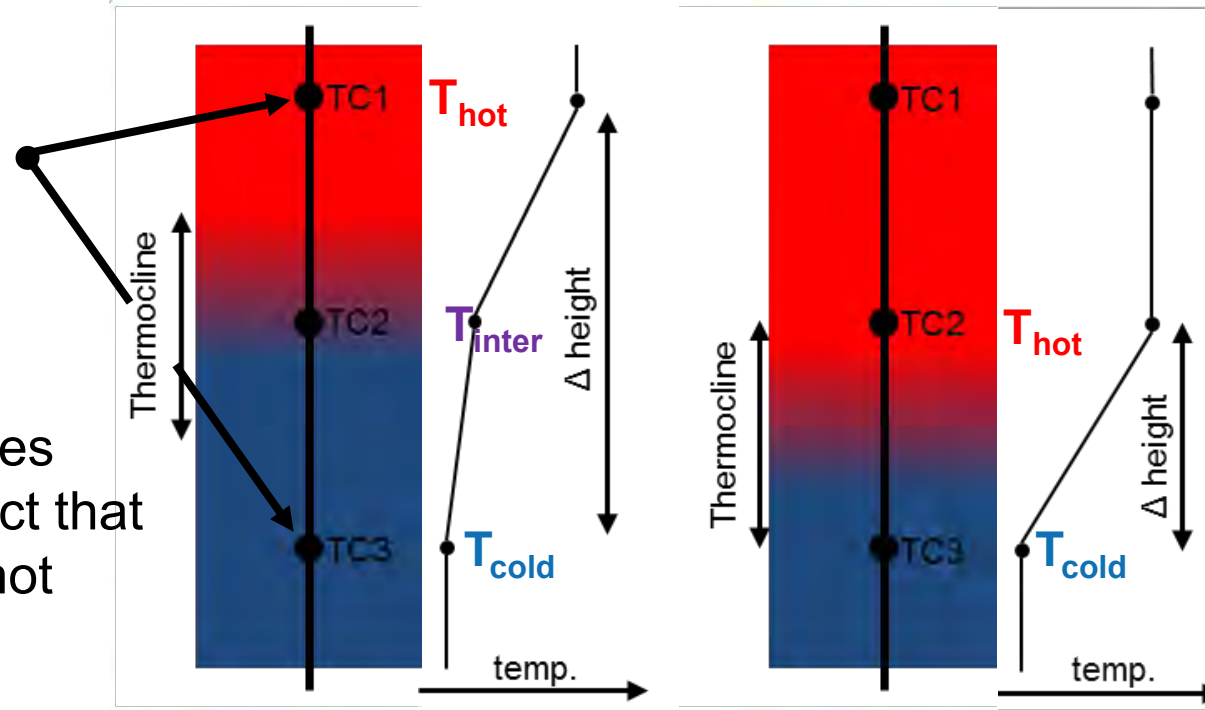
Unfavorable surface-area-to-volume-ratio -> prone to edge effects

single-plate radial diffuser



Qualitative Evaluation Method

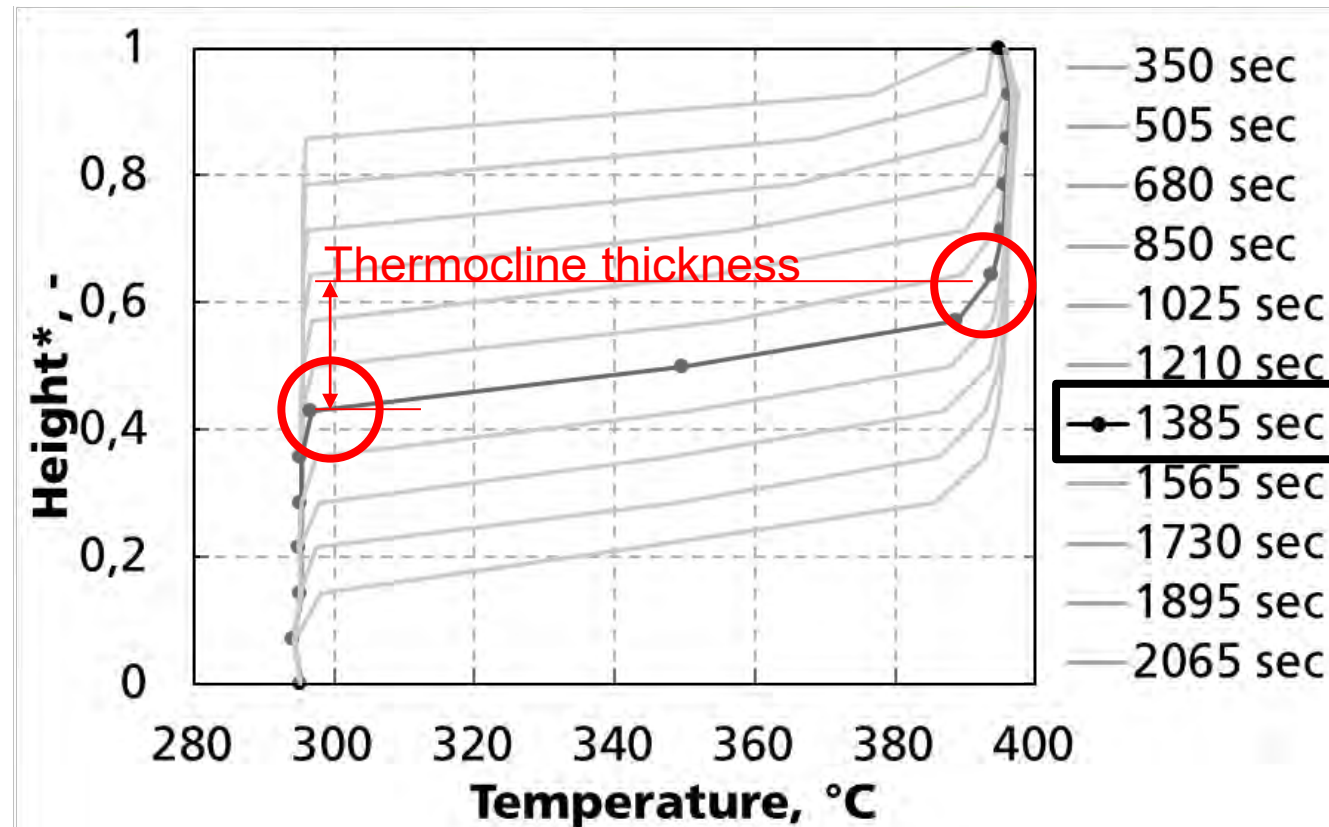
- Temperature measured by the thermocouples gives indication about the separation of cold and hot fluid → Stratification
- Only measurement values at certain vertical locations available
- The position of the thermocline changes
 - The derived thickness varies periodically, despite the fact that the “real” thickness does not change in this way



- Determination of thermocline thickness based on experimental data
 - more complex than from numerical data / simulation models
 - interpolation for thermocline thickness calculation at individual positions

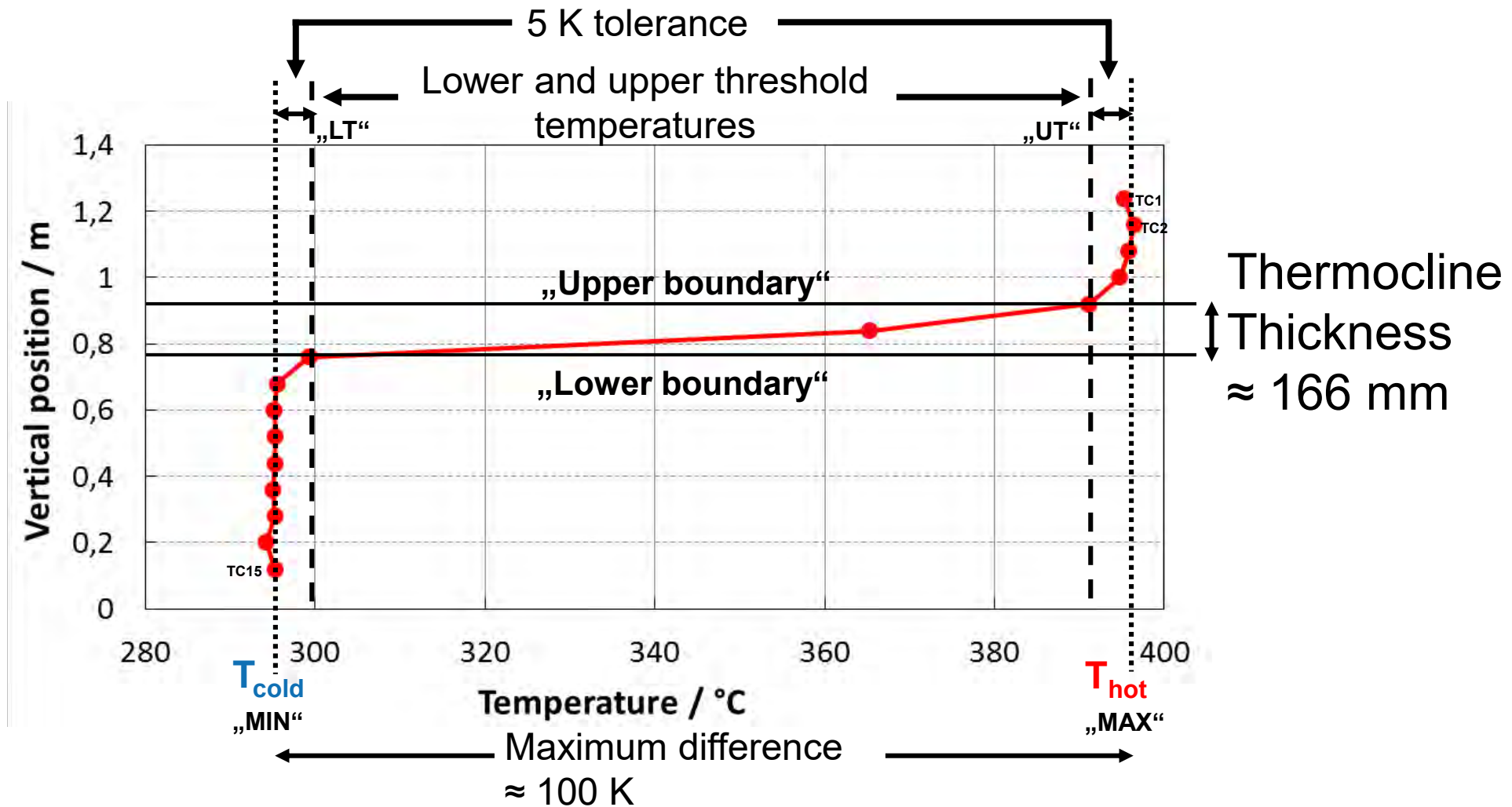
Qualitative Evaluation

Method to Measure the Thickness of the Thermocline



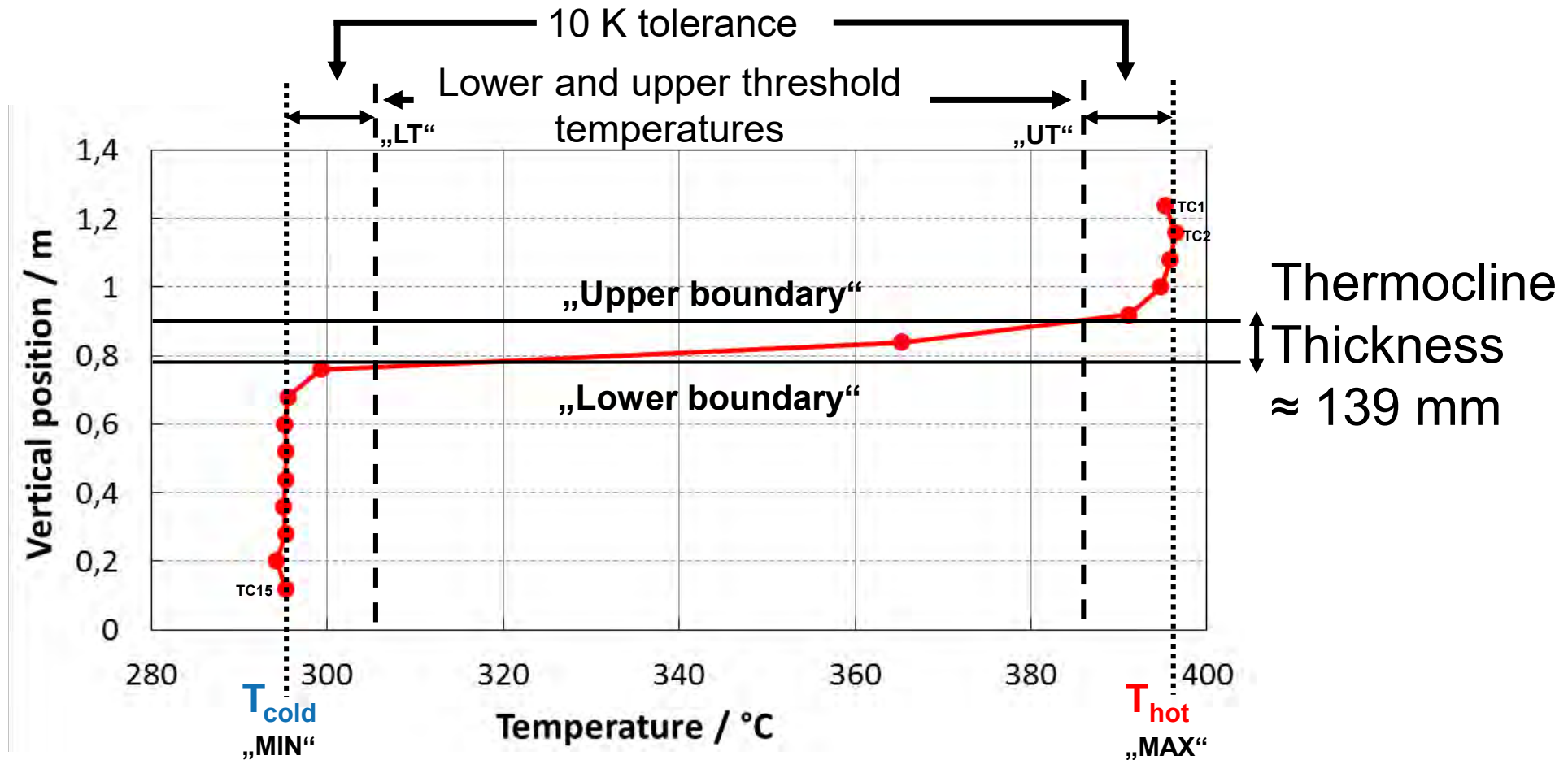
Qualitative Evaluation

Method to Measure the Thickness of the Thermocline



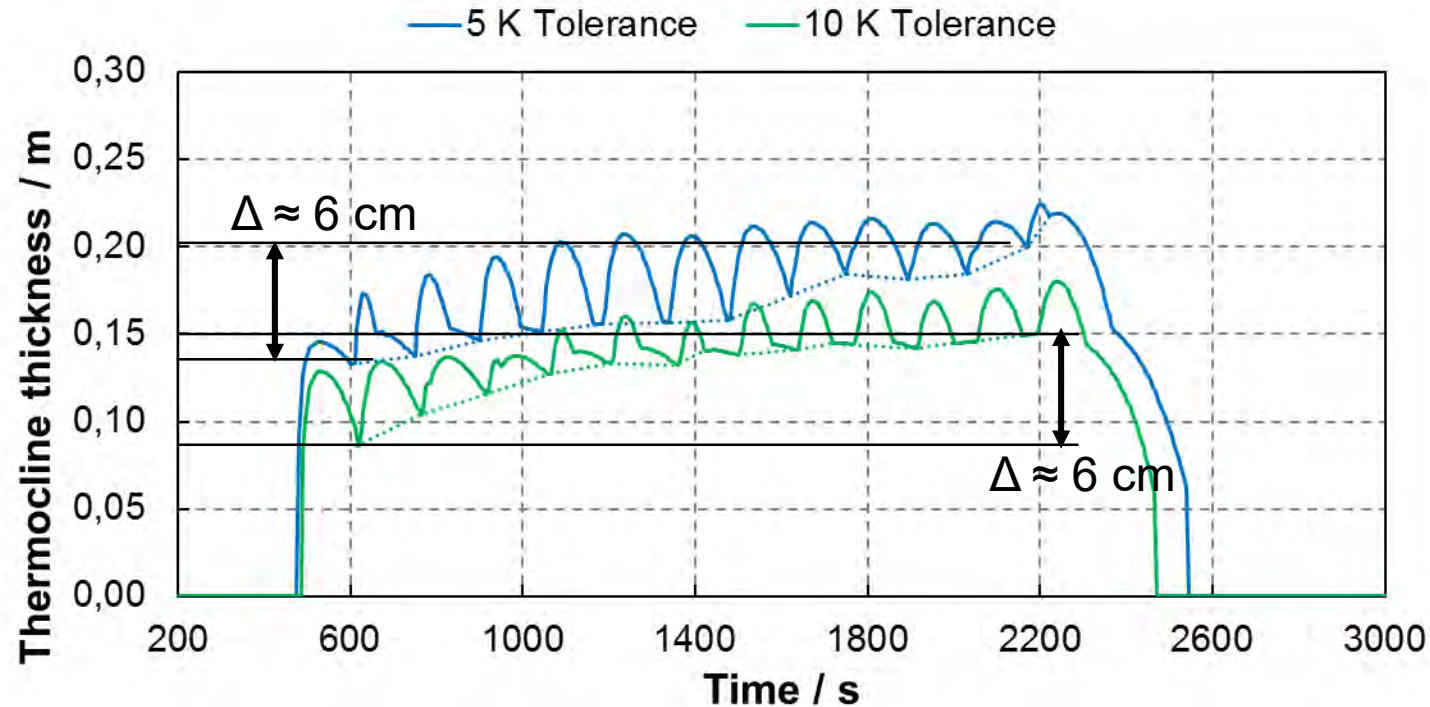
Qualitative Evaluation

Method to Measure the Thickness of the Thermocline

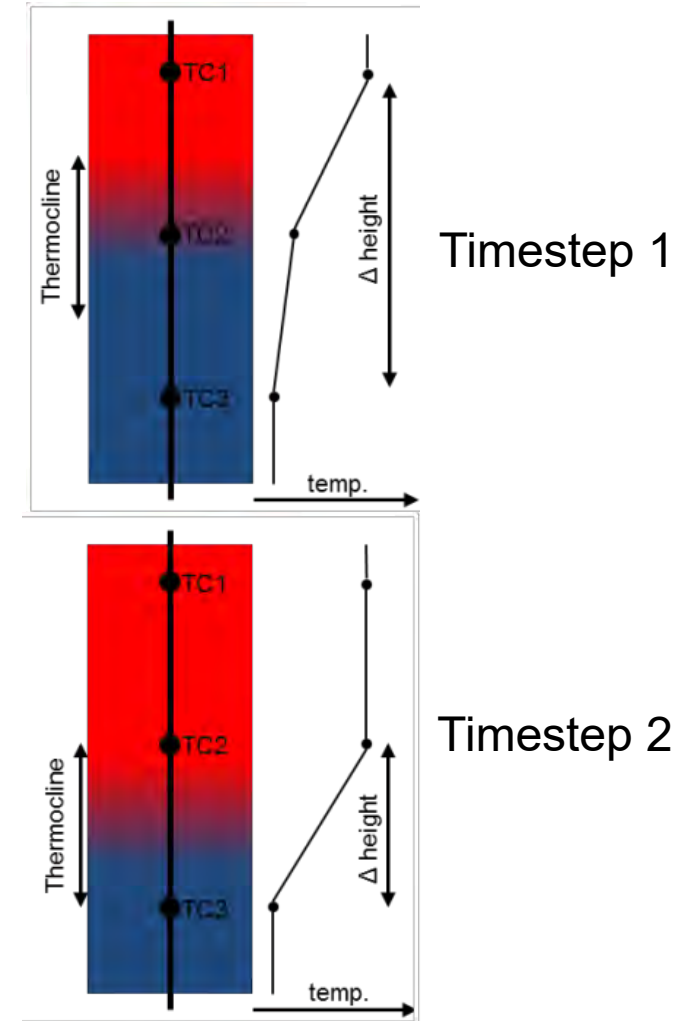


Qualitative Evaluation Results

Qualitative Evaluation Measurement Result of Thermocline Thickness



- TC thickness varies between 14 and 20 cm for 5 K tolerance (blue dotted line ---)
- .. and 9 and 15 cm for 10 K tolerance (green dotted line ---)
- → Thermocline thickness increases about 6 cm



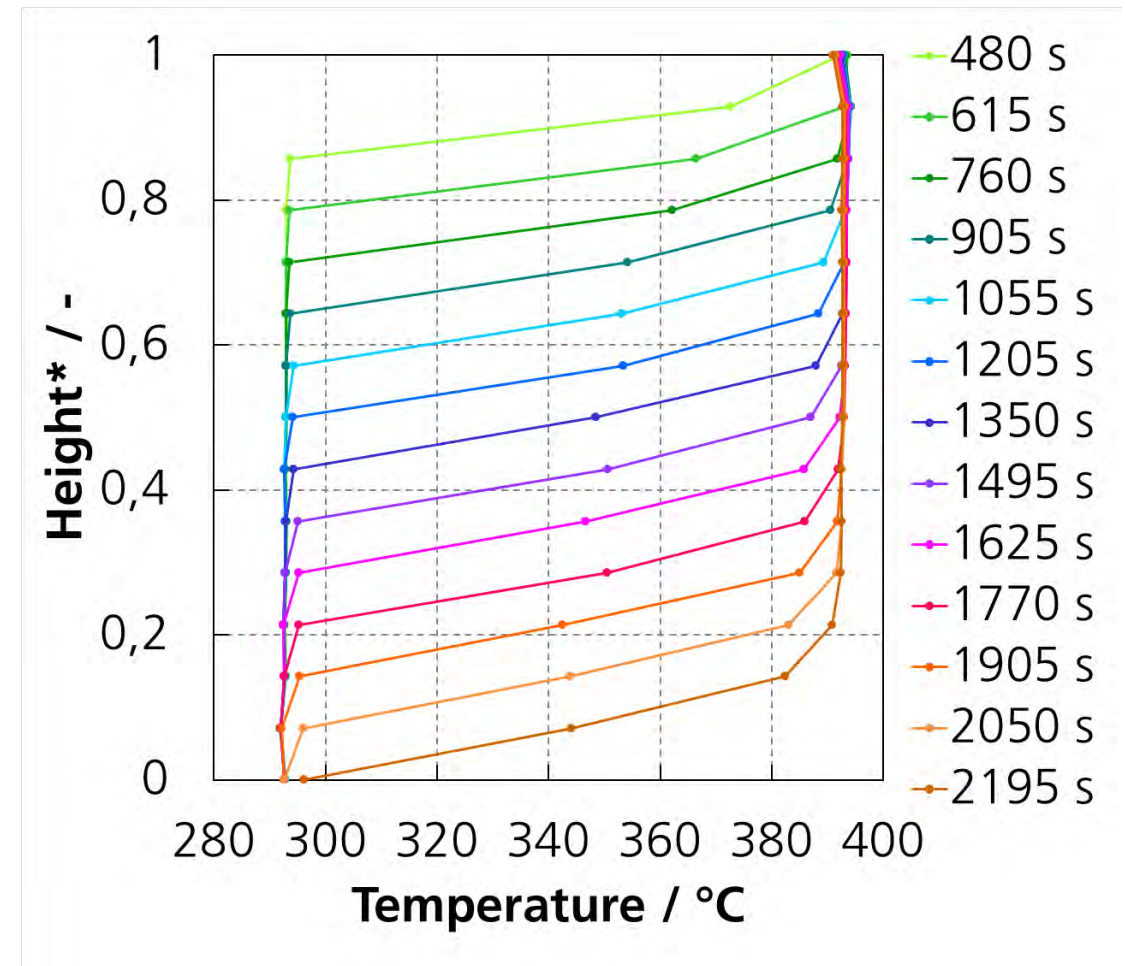
Energetic Evaluation

- Thermal power for charging and discharging of the storage by mass flow as well as inlet and outlet temperature
- Introduction of a boundary condition for charging / discharging:
“Theoretical threshold temperature”
- Storage charging / discharging limited to outlet temperature of the storage
 - Charging: Maximum inlet temperature of the solar field
 - Discharging: Minimum inlet temperature of the power block
 - Remaining heat could be used (e.g. for freeze protection or preheating)
- Comparison of actual storage capacity (charging and discharging) with theoretical values

Energetic Evaluation

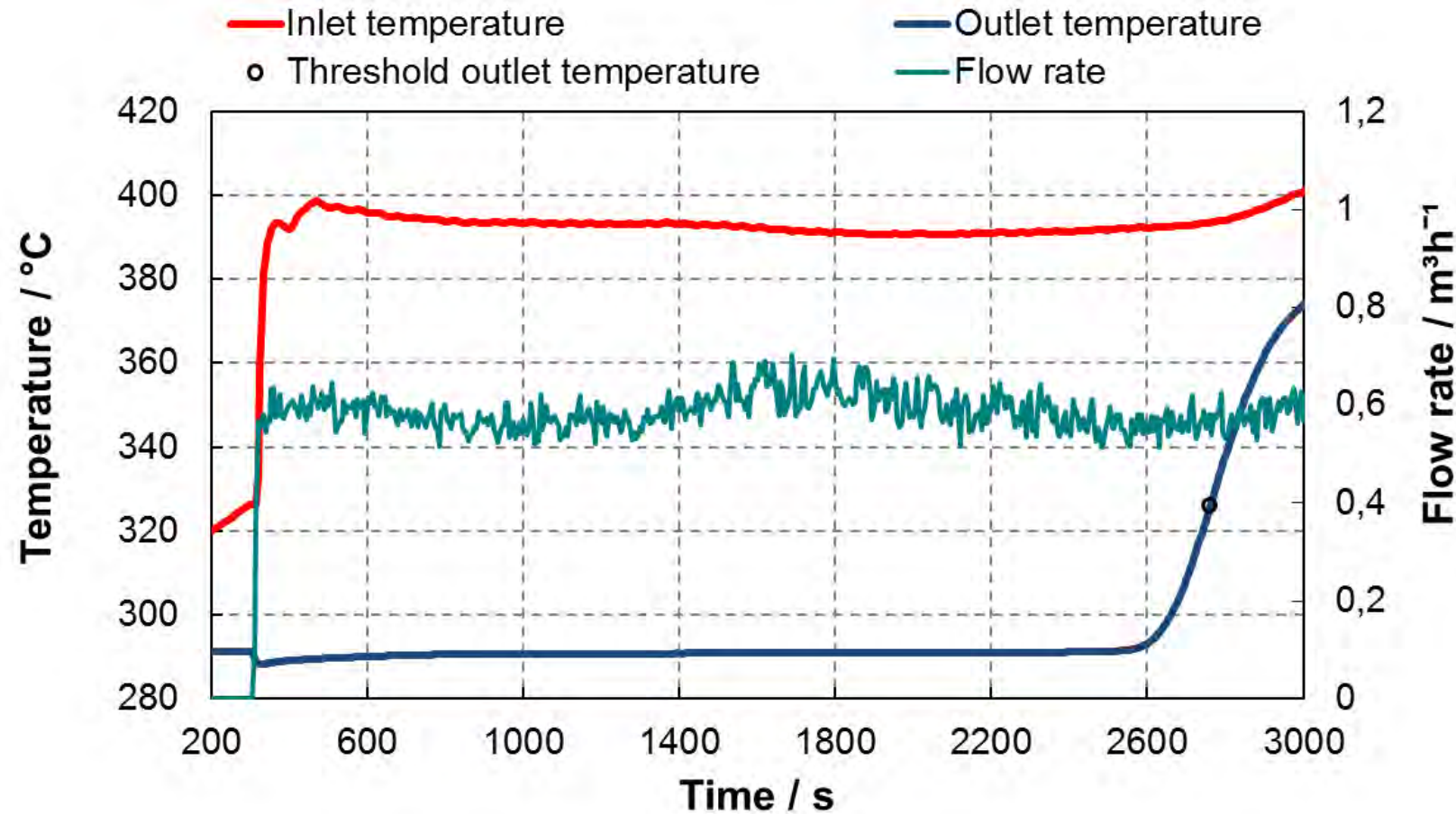
Charging of Storage

| Parameter | Value | Unit |
|---|-------|--------------------|
| Average inlet temperature | 392.3 | °C |
| Average initial tank temperature | 292.9 | °C |
| Temperature difference | 99.5 | K |
| Theoretical thermal capacity | 29.8 | kWh |
| Threshold outlet temperature (t_{th}) | 326.0 | °C |
| Thermal capacity at t_{th} | 27.94 | kWh |
| Utilization ratio | 93.8 | % |
| Average flow rate | 0.59 | m ³ / h |
| Average charging power | 38.2 | kW |



Energetic Evaluation

Charging of Storage

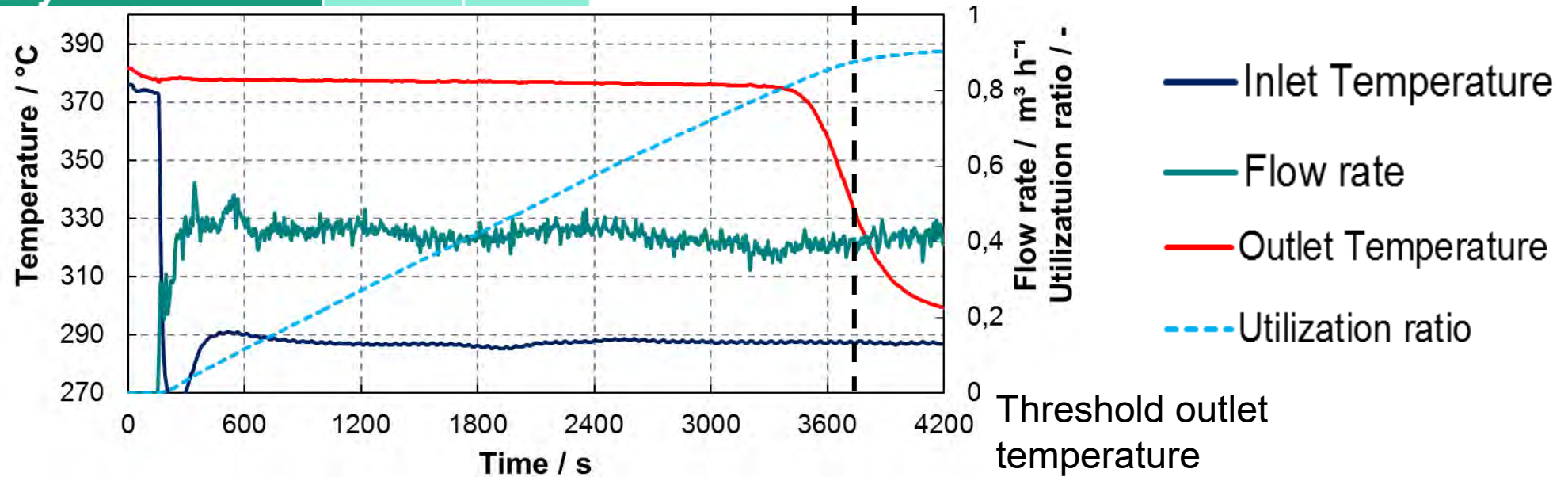


✓ Outlet temperature remains rather constant

Energetic Evaluation

Discharging of Storage

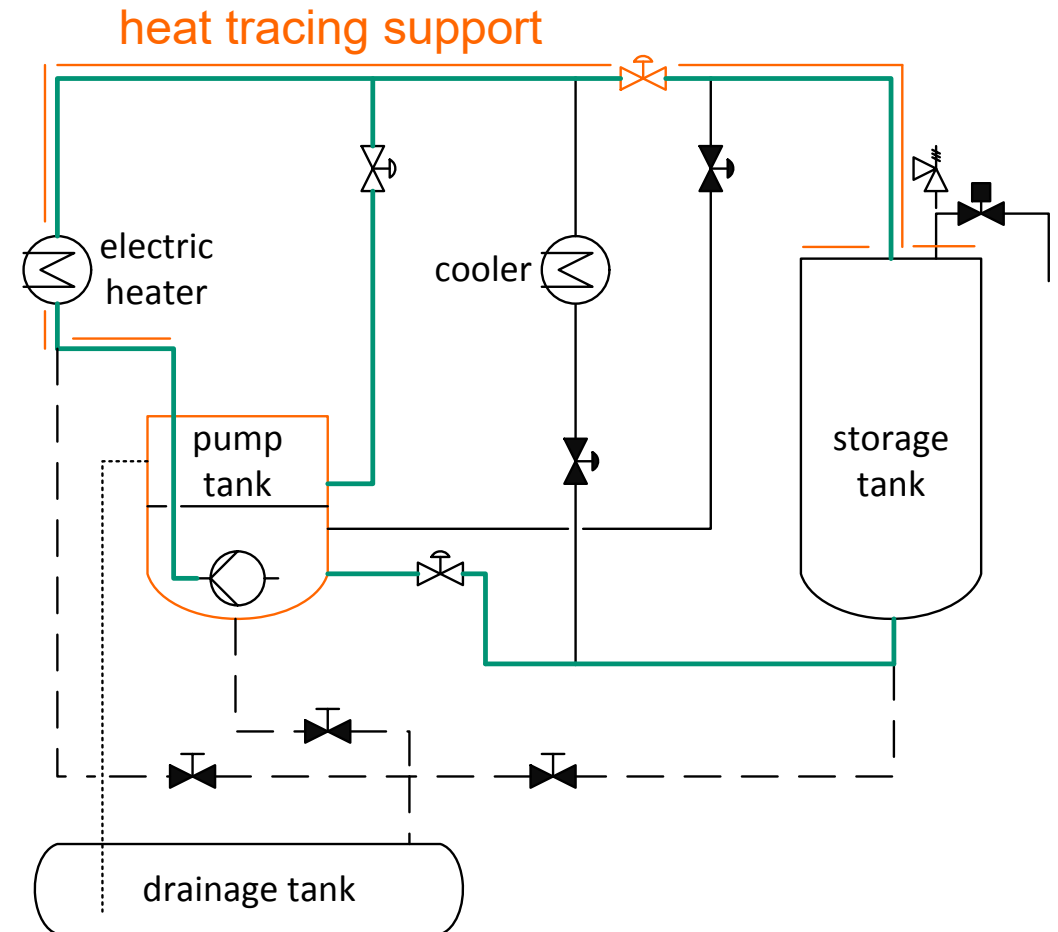
| Parameter | Value | Unit | Parameter | Value | Unit |
|----------------------------------|-------|------|---|-------|--------------------|
| Average inlet temperature | 287.0 | °C | Threshold outlet temperature (t_{th}) | 349.5 | °C |
| Average initial tank temperature | 380.7 | °C | Thermal capacity at t_{th} | 25.0 | kWh |
| Temperature difference | 93.7 | K | Utilization ratio | 86.2 | % |
| Theoretical thermal capacity | 29.1 | kWh | Average flow rate | 0.42 | m ³ / h |
| | | | Average discharging power | -26.0 | kW |



Conclusion & Outlook

Lessons Learned

- Heat tracing support for charging process
- Effect of heat loss during charging
- Good heat tracing equipment is essential in molten salt systems



- Demonstration of a stable outlet temperature of a thermocline storage with molten salt
 - → Good stratification
 - However, thermocline zone increases during charging / discharging
 - Design of diffusor and wall temperature management (for small prototype vessels) crucial for stratification
- Introduction of a method to determine the thickness of the thermocline zone at variable height positions despite fixed measurement points

- Compare introduced evaluation method with other approaches and numerical models
→ refine approach
- Performance evaluation of consecutive charging / discharging cycles
- Increase of maximum temperature and thus the temperature difference
- Investigation of different salt mixtures
- Introduction and analysis of different filler materials using a packed-bed storage tank



- Support by the EU within
 - OPTS (FP7)



- ORC-PLUS (H2020)



Thanks for Your Attention

martin.karl@ise.fraunhofer.de
shahab.rohani@ise.fraunhofer.de

SFERA-III

Solar Facilities for the European Research Area



Solar Facilities for the European Research Area

1st Summer School “Thermal energy storage systems, solar fields and new cycles for future CSP plants”
WPI Capacity building and training activities
Odeillo, France, September 9th-11th 2019

“Thermochemical thermal energy storage:
challenges and issues ”

Sylvie Rougé(CEA)‘ sylvie.rouge@cea.fr

NETWORKING



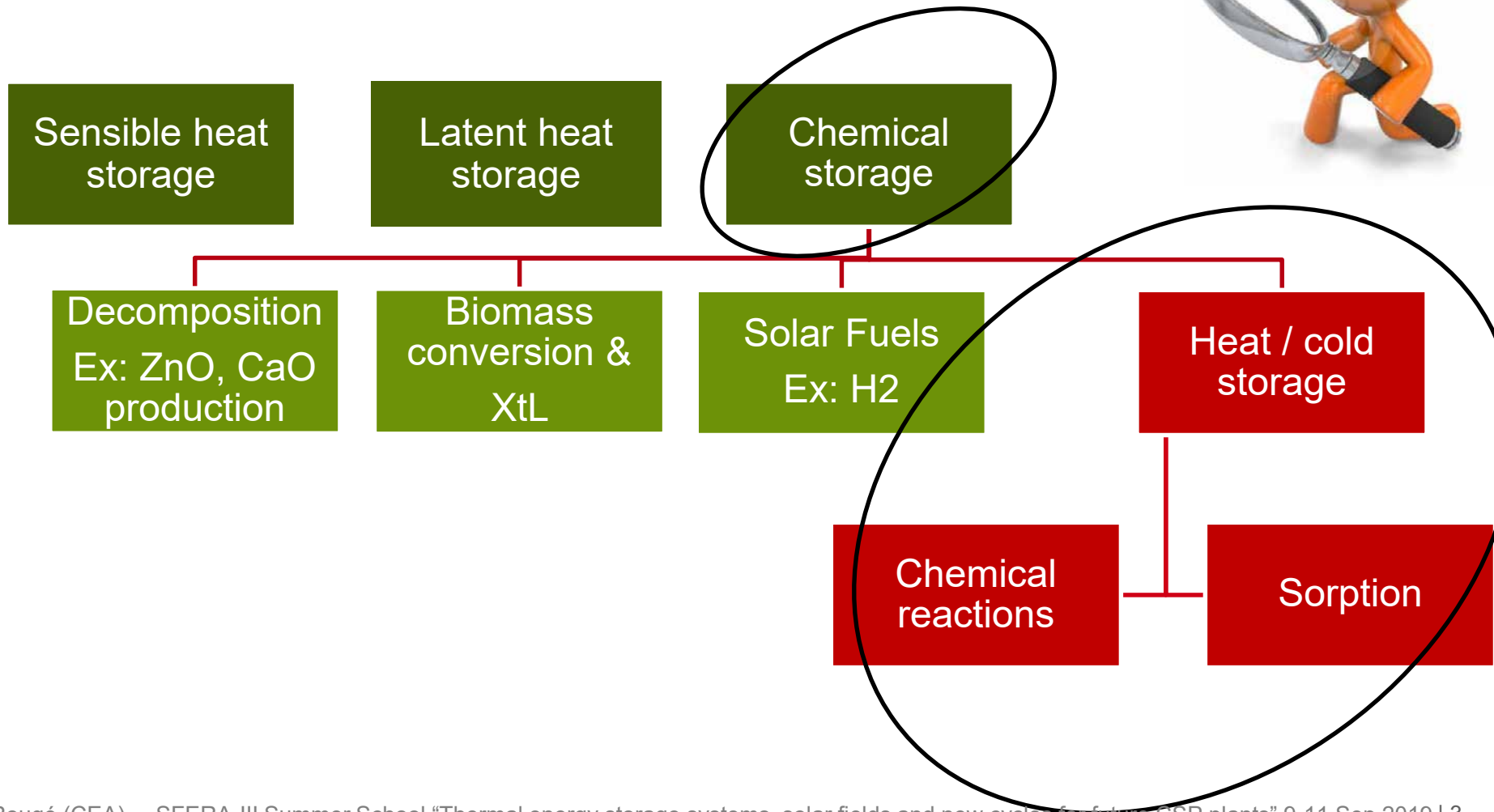
THIS PROJECT HAS RECEIVED FUNDING FROM THE EUROPEAN UNION'S HORIZON 2020 RESEARCH AND INNOVATION PROGRAMME UNDER GRANT AGREEMENT NO **823802**



- Thermochemical heat storage fundamentals
- TCS reaction selection
- Solid / gas reactor selection
- Solid material ad-equation to the reactor and process
- Reactor modelling and upscaling: 2 application cases
- Conclusion



Types of heat storage for CSP plants



■ Fundamentals:

Charge: endothermic



Discharge: exothermic

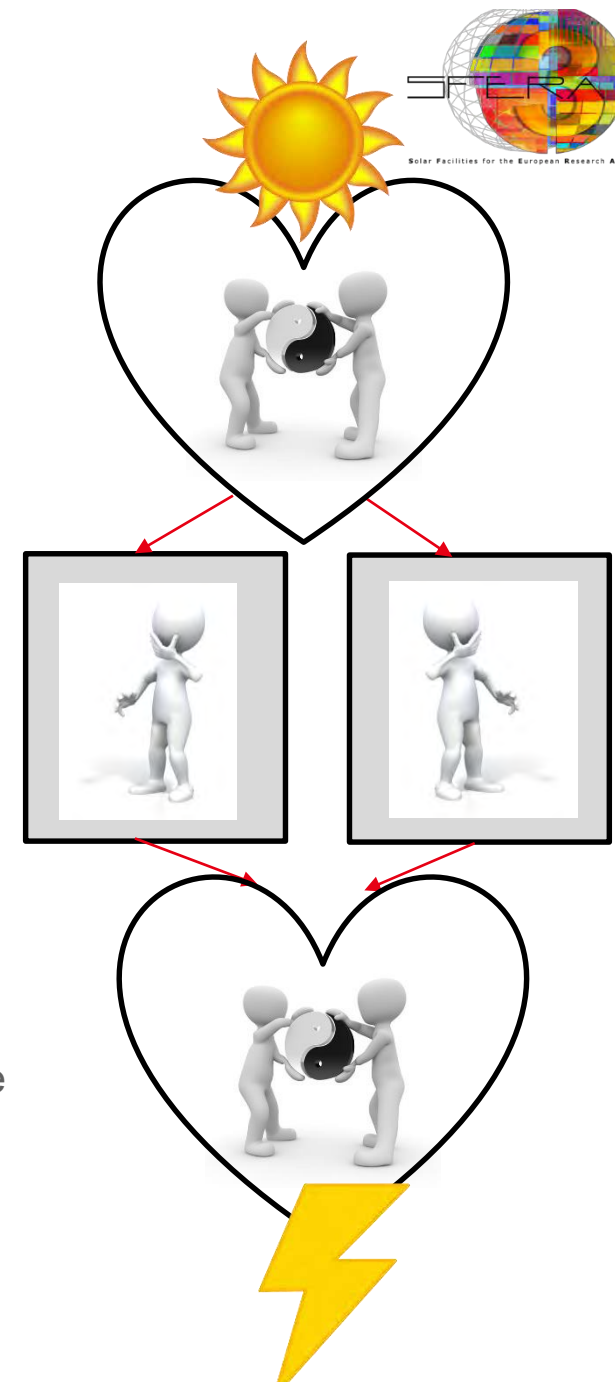


■ Advantages

- Long-term storage: chemical potential intact
- High storage volume density.

■ Required properties

- 100% reversible reaction
- Stable for hundreds of thermal cycles
- Products A and B must be easily separated for storage
- Products A, B and C are easy to store
- Products are cheap and non hazardous



- Organic reactions are rarely suitable (side reactions -> no 100% reversibility)
- Most of inorganic reactions are solid / gas reactions
 - Advantage:
 - ✓ *Easy to separate the solid from the gas*
 - Drawback :
 - ✓ *heterogeneous gas/solid reaction -> risk of mass transfer limitations*
 - ✓ *Divided solid has a low heat transfer conductivity -> risk of heat transfer limitation*
 - ✓ *gas /solid reactor , solid handling → technology is more challenging*
 - ✓ *How to store a gas at low energetic cost?*

■ Main questions to address:

- How to choose a suitable chemical reaction?
 - ✓ *Temperature criteria*
 - ✓ *Reversibility criteria*
 - ✓ *Storage density criteria*
- How to choose the reactor technology?
 - ✓ *Heat and mass transfers: intrinsic # apparent kinetics*
 - ✓ *Integration in the whole process?*
 - ✓ *Can I discharge heat at the same temperature than charge?*
 - ✓ *Can I recover sensible heat at maximal temperature?*
 - ✓ *Do I need 2 reactors for charge and discharge*
 - ✓ *How can I upscale the reactors efficiently?*
- Is the solid material perfectly adapted to the process and the reactor ?
 - ✓ *Some examples of improvements*





TCS REACTION SELECTION:

TEMPERATURE CRITERIA

REVERSIBILITY AND CYCLABILITY

STORAGE DENSITY



- Main types of reactions on the range 300-1100°C



**Metallic
hydrides
(H₂)**

**Carbonates
(CO₂)**

**Hydroxides
(H₂O)**

**Red-Ox
(O₂)**

**Ammonia
(NH₃)**

Organic

**Mg / MgH₂
Ca / CaH₂**

**PbO / PbCO₃
CaO / CaCO₃**

**MgO /
Mg(OH)₂
CaO /
Ca(OH)₂**

**CoO /
Co₃O₄
Mn₂O₃ /
Mn₃O₄**

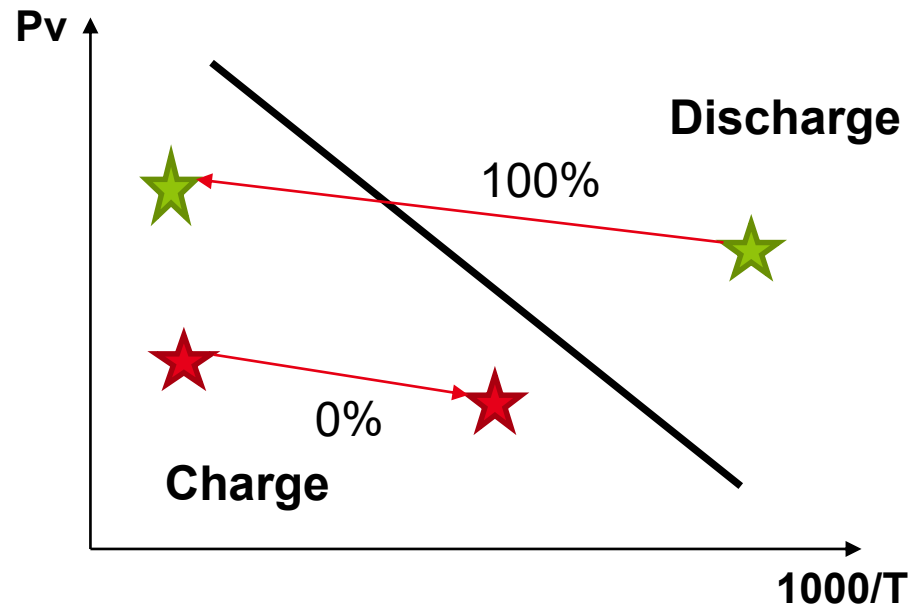
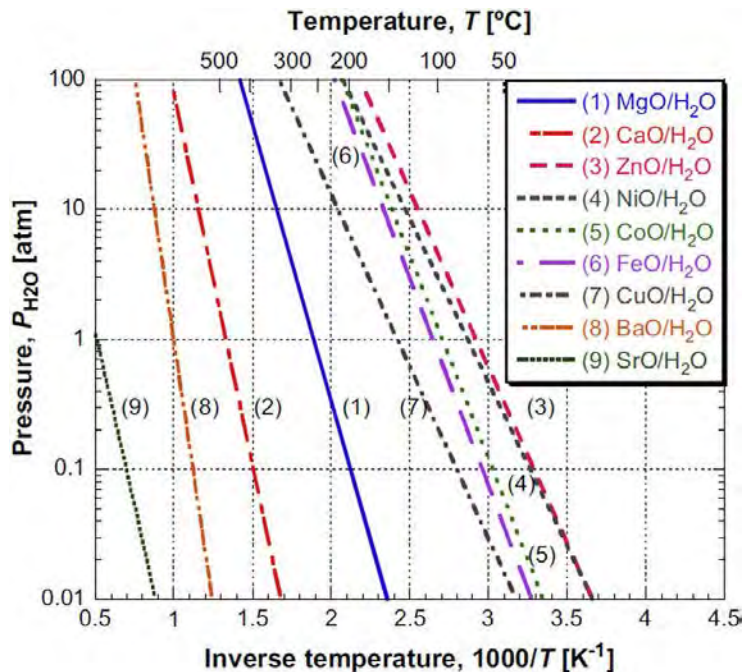
**NH₃ / N₂,H₂
HSO₄ /
NH₄SO₄**

**CH₄+H₂O
CH₄+ CO₂
C₆H₁₂
SO₃**

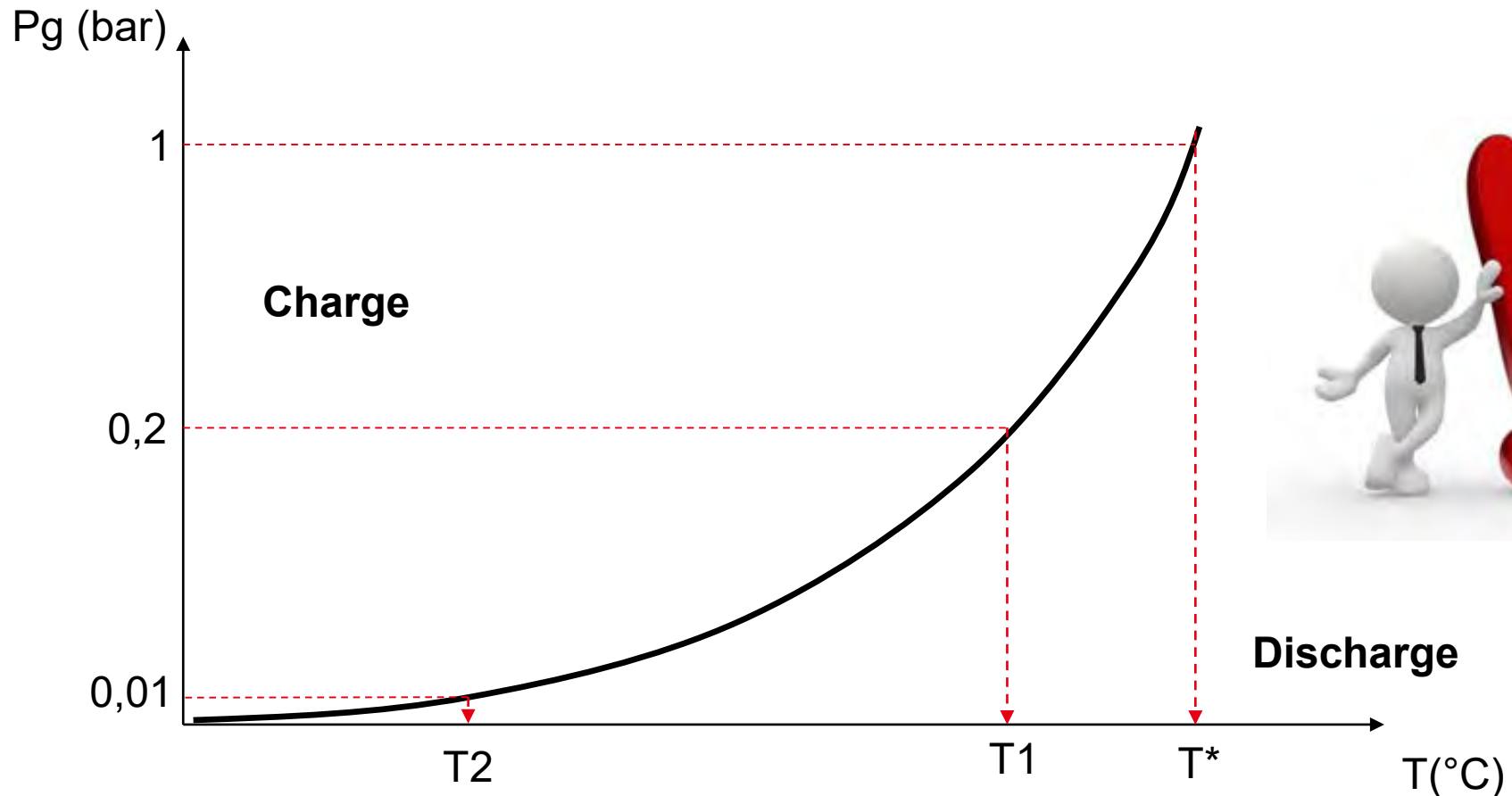
- A solid / gas reaction is generally monovariant, the equilibrium curve is derived from the Van't Hoff equation at the minimal free Gibbs energy (= no reaction):

$$\checkmark \ln(P_{g,eq}) = -\frac{DH^0}{R.T_{eq}} + \frac{DS^0}{R}$$

- As a consequence, the reaction conversion yield is 0% or 100% and the enthalpy of reaction is independent of the charge level



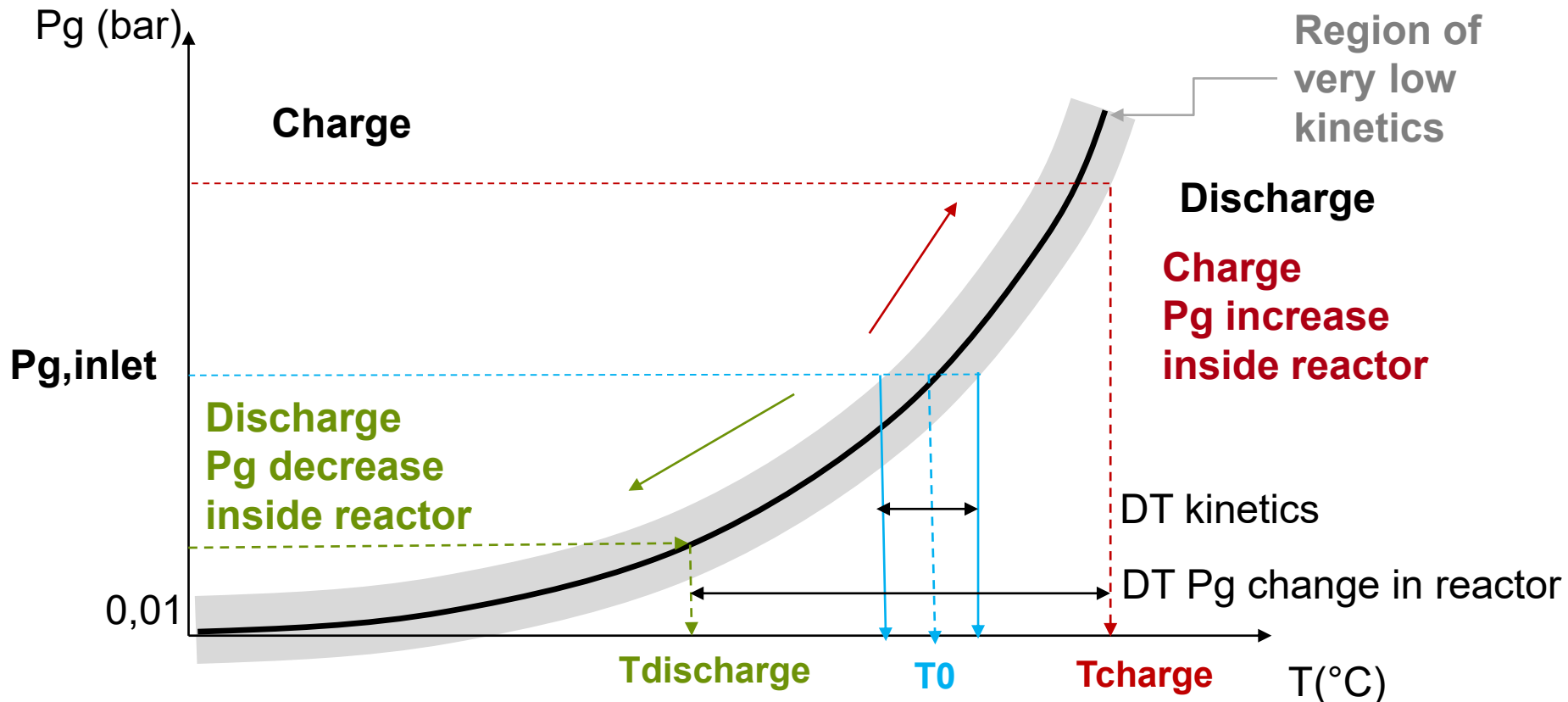
- The tuning temperature T^* (for $P=1$) cited in reviews is not always the one you need for your process!



REACTION SELECTION – TEMPERATURE CRITERIA (4)

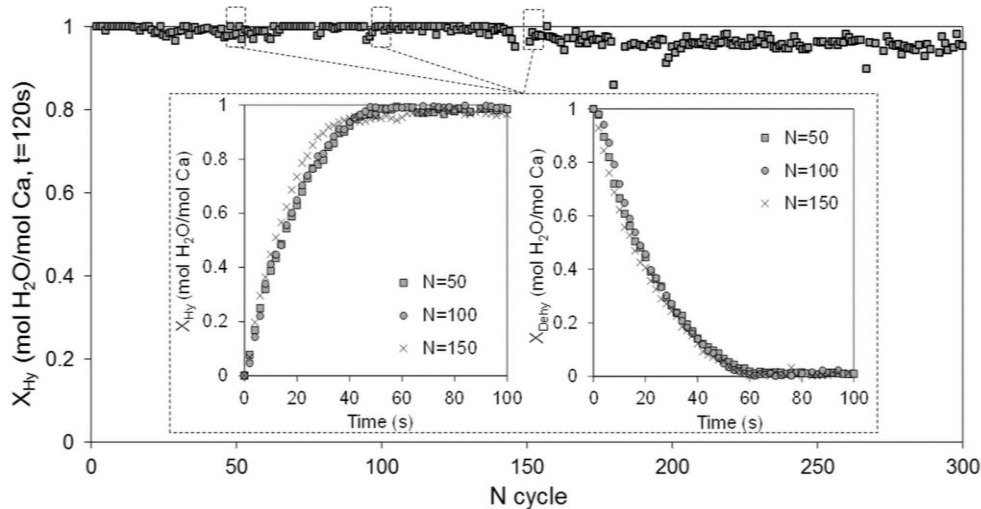


- If you operate at constant partial pressure (case of O_2 /air, steam/air...), it is not possible to have the same charging and discharging temperature at large scale:

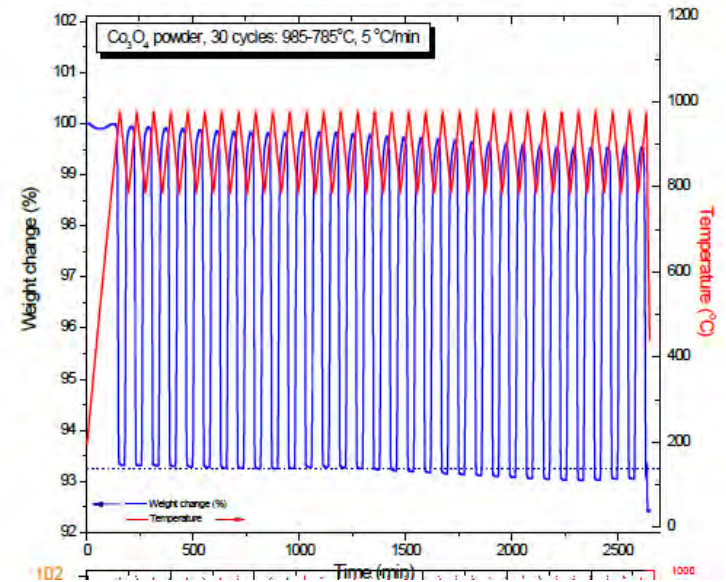


- The reaction must be reversible 100% under hundreds of thermal cycles

CaO/Ca(OH)₂ : 300 cycles under synthetic air

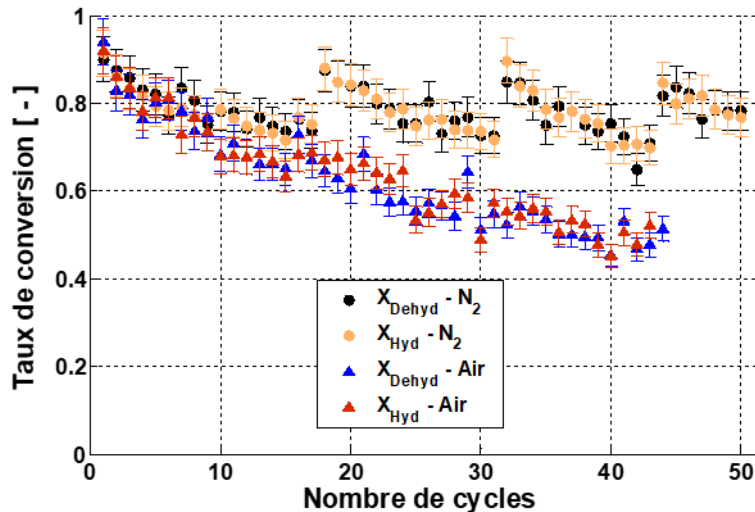


CoO / Co₃O₄ : 30 cycles



■ Main risks

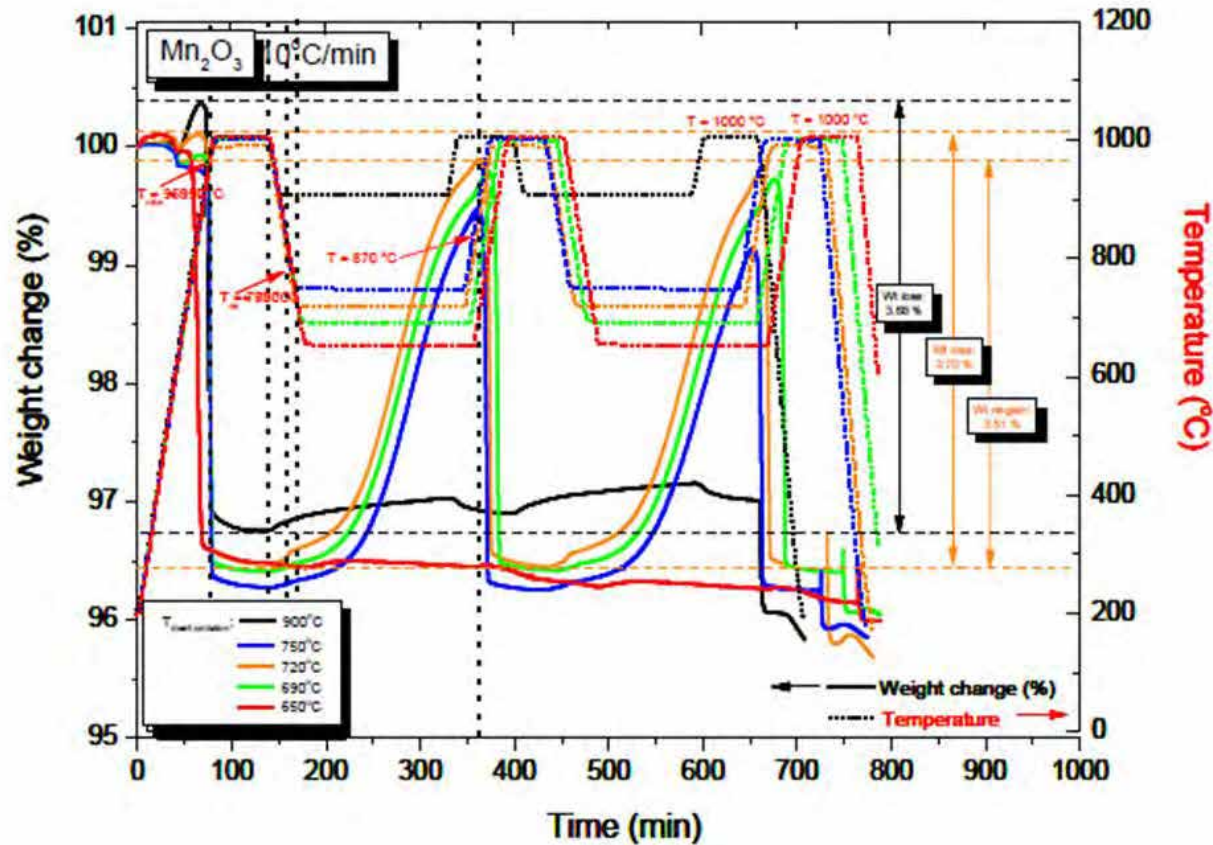
- Discharge can be at a much lower temperature than charge
 - ✓ Case of $MgO / Mg(OH)_2$ (300 / 100°C), Mn_2O_3 / Mn_3O_4 (1000 / 690-750°C)
- Charge rate can decrease after a few thermal cycles
 - ✓ Reaction sites become ineffective: $CaO / CaCO_3$, CuO / Cu_2O (shrinkage and sintering)
 - ✓ Side reactions coming from ppm in gas, for instance : $CaO / Ca(OH)_2 \rightarrow CaCO_3$ or $BaO_2 / BaO \rightarrow BaCO_3$



$CaO / Ca(OH)_2$: 50 cycles under air and N_2

Mn_2O_3 / Mn_3O_4 :

- ~1000°C for reduction
- narrow range of temperature 690-750°C for oxidation



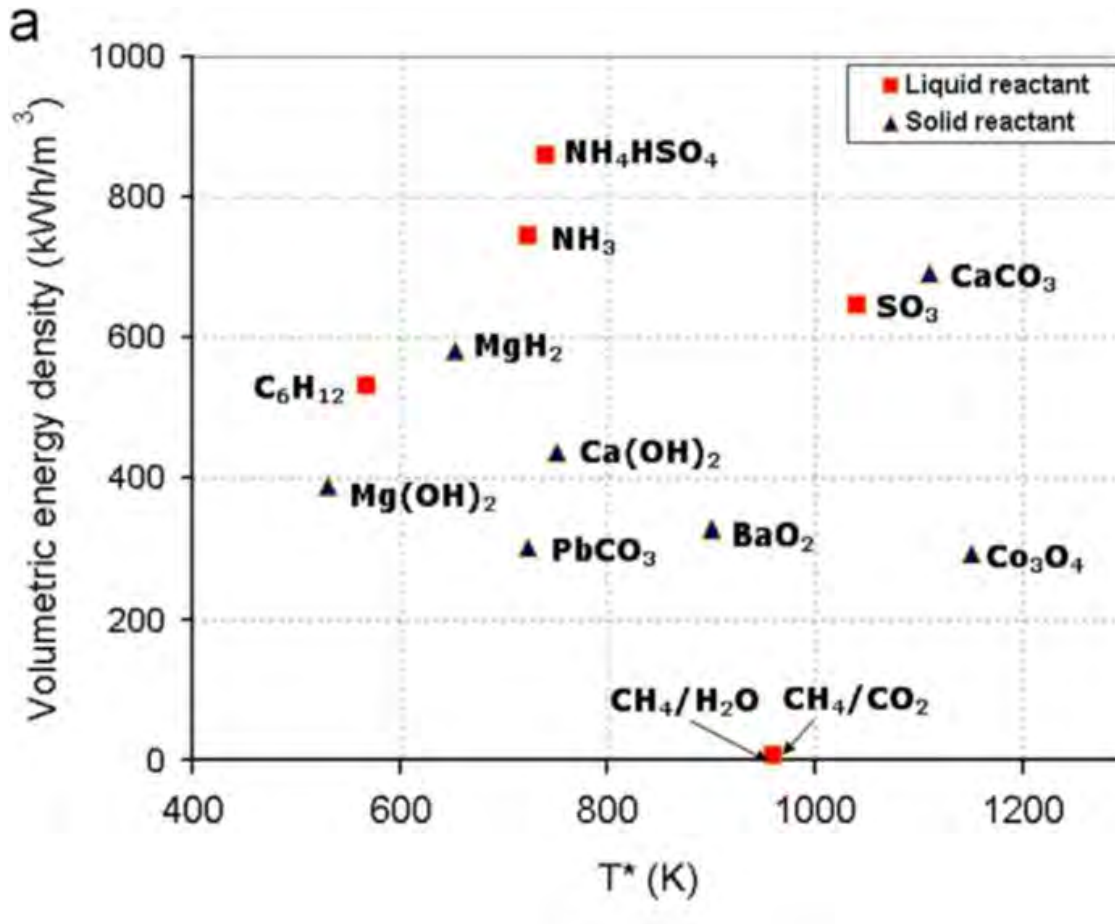
REACTION SELECTION – REVERSIBILITY CRITERIA (4)

An example of final selection for Red-Ox reactions:

Table 2.1
Metal Oxide Systems Applicable to TES Based on Thermodynamics Considerations

| Reaction | Temperature (°C) | ΔH (kJ/mole oxide) | Storage Density (kJ/kg) |
|--|------------------|----------------------------|-------------------------|
| $\text{Cr}_5\text{O}_{12} \rightarrow 2.5\text{Cr}_2\text{O}_3 + 2.25\text{O}_2$ | 110 | 126.0 | 279 |
| $2\text{Li}_2\text{O}_2 \rightarrow 2\text{Li}_2\text{O} + \text{O}_2$ | 150 | 68.2 | 1483 |
| $2\text{Mg}_2\text{O} \rightarrow 2\text{MgO} + \text{O}_2$ | 205 | 21.8 | 505 |
| $2\text{PbO}_2 \rightarrow 2\text{PbO} + \text{O}_2$ | 405 | 62.8 | 262 |
| $2\text{PtO}_2 \rightarrow 2\text{PtO} + \text{O}_2$ | 420 | 62.8 | 277 |
| $2\text{Sb}_2\text{O}_5 \rightarrow 2\text{Sb}_2\text{O}_4 + \text{O}_2$ | 515 | 92.5 | 286 |
| $4\text{MnO}_2 \rightarrow 2\text{Mn}_2\text{O}_3 + \text{O}_2$ | 530 | 41.8 | 481 |
| $6\text{UO}_3 \rightarrow 6\text{U}_3\text{O}_8 + \text{O}_2$ | 670 | 35.2 | 123 |
| $2\text{BaO}_3 \rightarrow 2\text{BaO} + \text{O}_3$ | 885 | 72.5 | 474 |
| $2\text{Co}_3\text{O}_4 \rightarrow 6\text{CoO} + \text{O}_2$ | 890 | 202.5 | 844 |
| $\text{Rh}_2\text{O}_2 \rightarrow \text{Rh}_2\text{O} + \text{O}_2$ | 970 | 249.2 | 981 |
| $6\text{Mn}_2\text{O}_3 \rightarrow 4\text{Mn}_3\text{O}_4 + \text{O}_2$ | 1000 | 31.9 | 202 |
| $4\text{CuO} \rightarrow 2\text{Cu}_2\text{O} + \text{O}_2$ | 1120 | 64.5 | 811 |
| $6\text{Fe}_2\text{O}_3 \rightarrow 4\text{Fe}_3\text{O}_4 + \text{O}_2$ | 1400 | 79.2 | 496 |
| $2\text{V}_2\text{O}_5 \rightarrow 2\text{V}_2\text{O}_4 + \text{O}_2$ | 1560 | 180.7 | 993 |
| $2\text{Mn}_3\text{O}_4 \rightarrow 6\text{MnO} + \text{O}_2$ | 1700 | 194.6 | 850 |

Volumetric energy density (kWh/m³) of some chemical reactions, calculated on the solid material base:

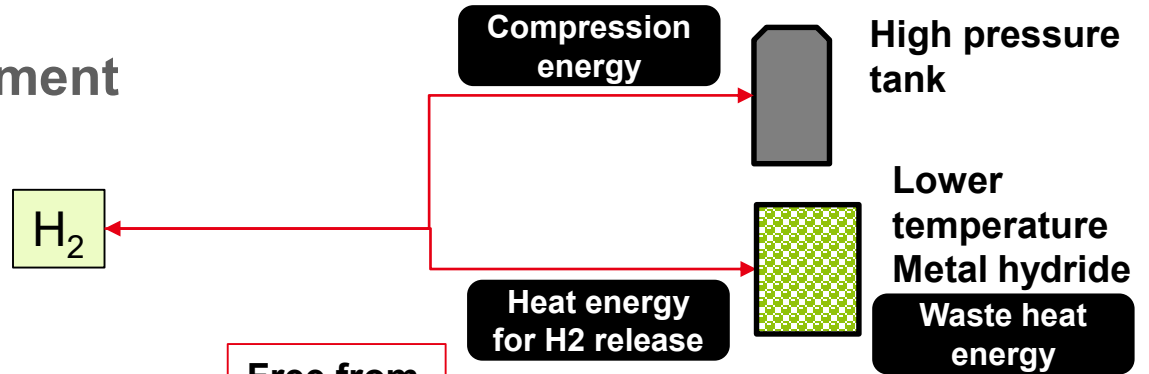


- The storage density should be estimated at process level and should integrate sensible heat aspects
 - Sensible heat stored in solids can be :
 - ✓ *An advantage :addition of sensible and chemical storage and increase of the final storage density*
 - ✓ *A drawback :waste heat for solid pre-heating*
 - Gas storage can be a main issue and a large energy sink
 - A first integration of heat and mass flows on a simplified scheme of the process allows to evaluate the **recovered heat efficiency**: $\frac{E_{end-user}}{E_{charge}+E_{parasitics}}$, this value can be far from 100%
 - This preliminary step allows to evaluate the approximate **nett volumetric storage density**

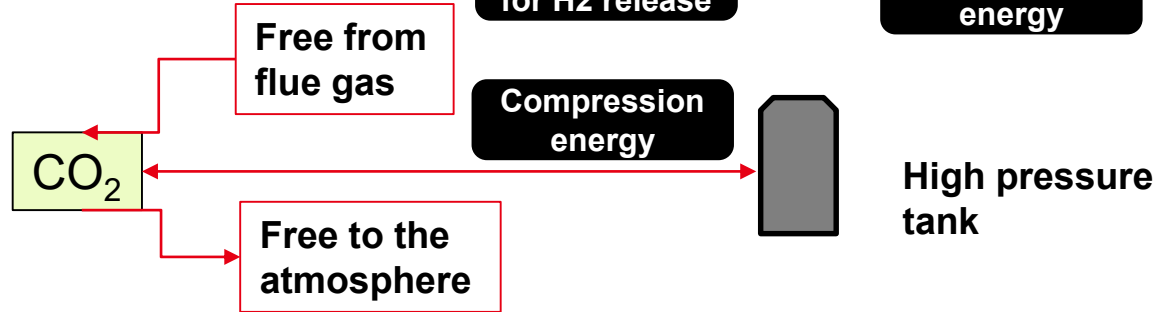


■ Gas storage management

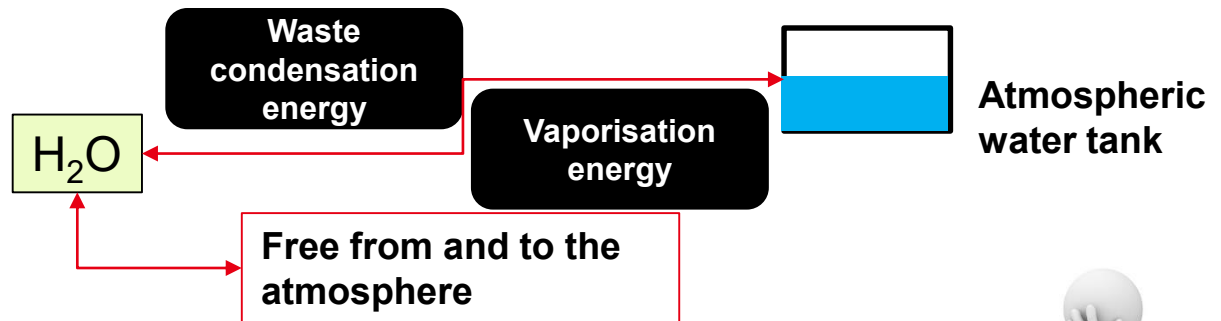
■ Di-Hydrogen



■ Carbon dioxide



■ Water steam

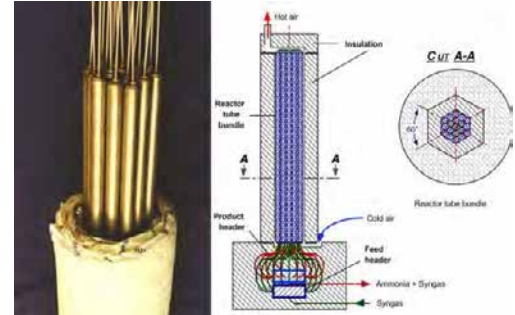
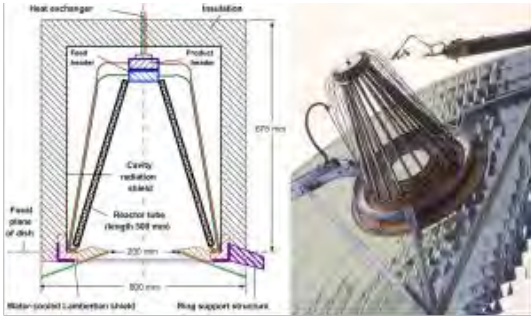


■ Di-Oxygen

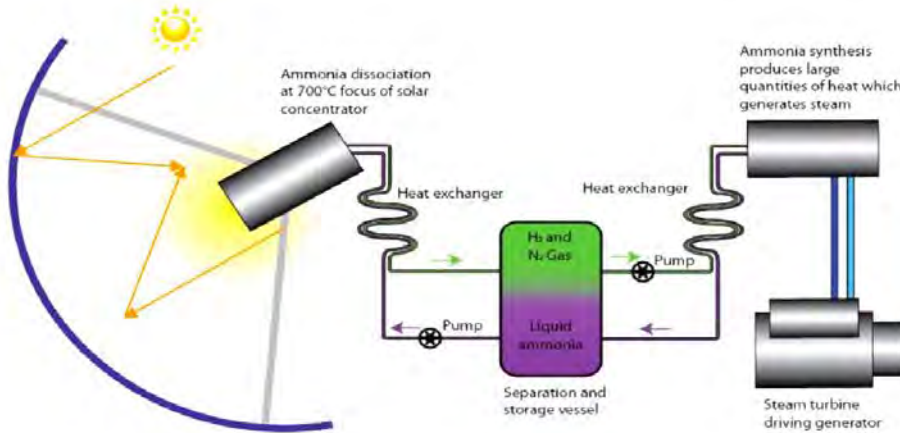


REACTION SELECTION – STORAGE DENSITY CRITERIA (4)

Ammonia dissociation: main sinks are pre-heating and compression

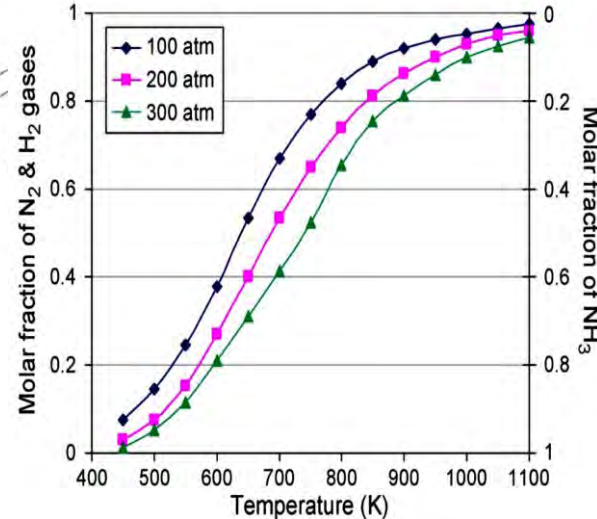


Endothermic
450°C
15 MPa



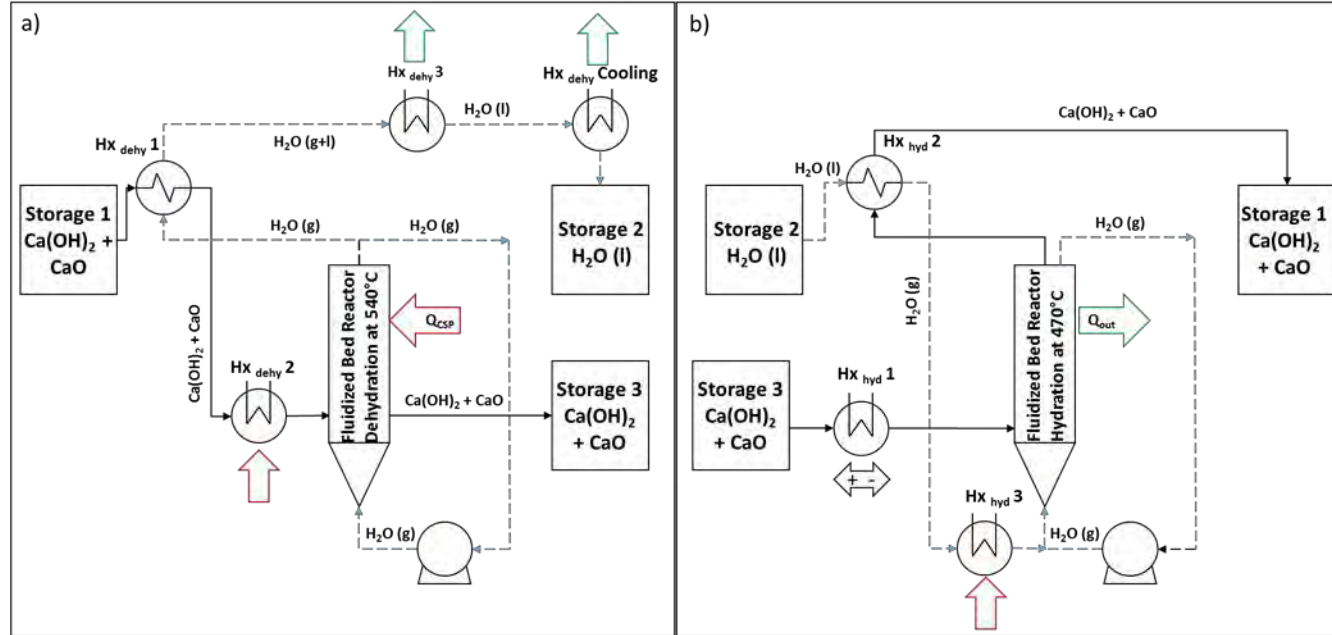
Storage tank
132°C
15 MPa

Exothermic
450°C
30 MPa

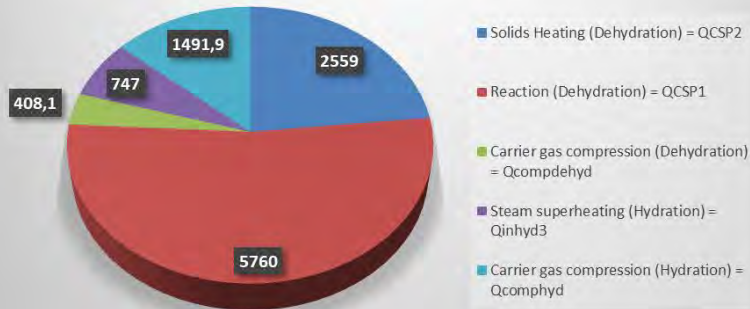


CaO/ Ca(OH)₂: main sinks are solid pre-heating and steam vapourisation

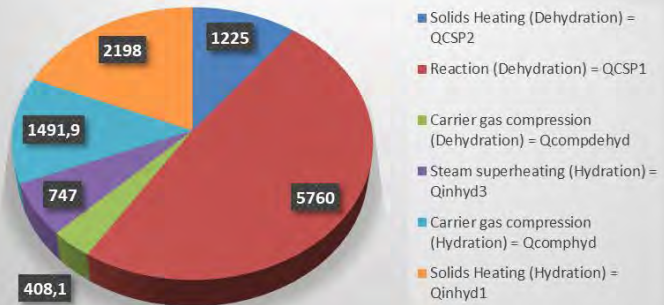
Efficiency: ~60%



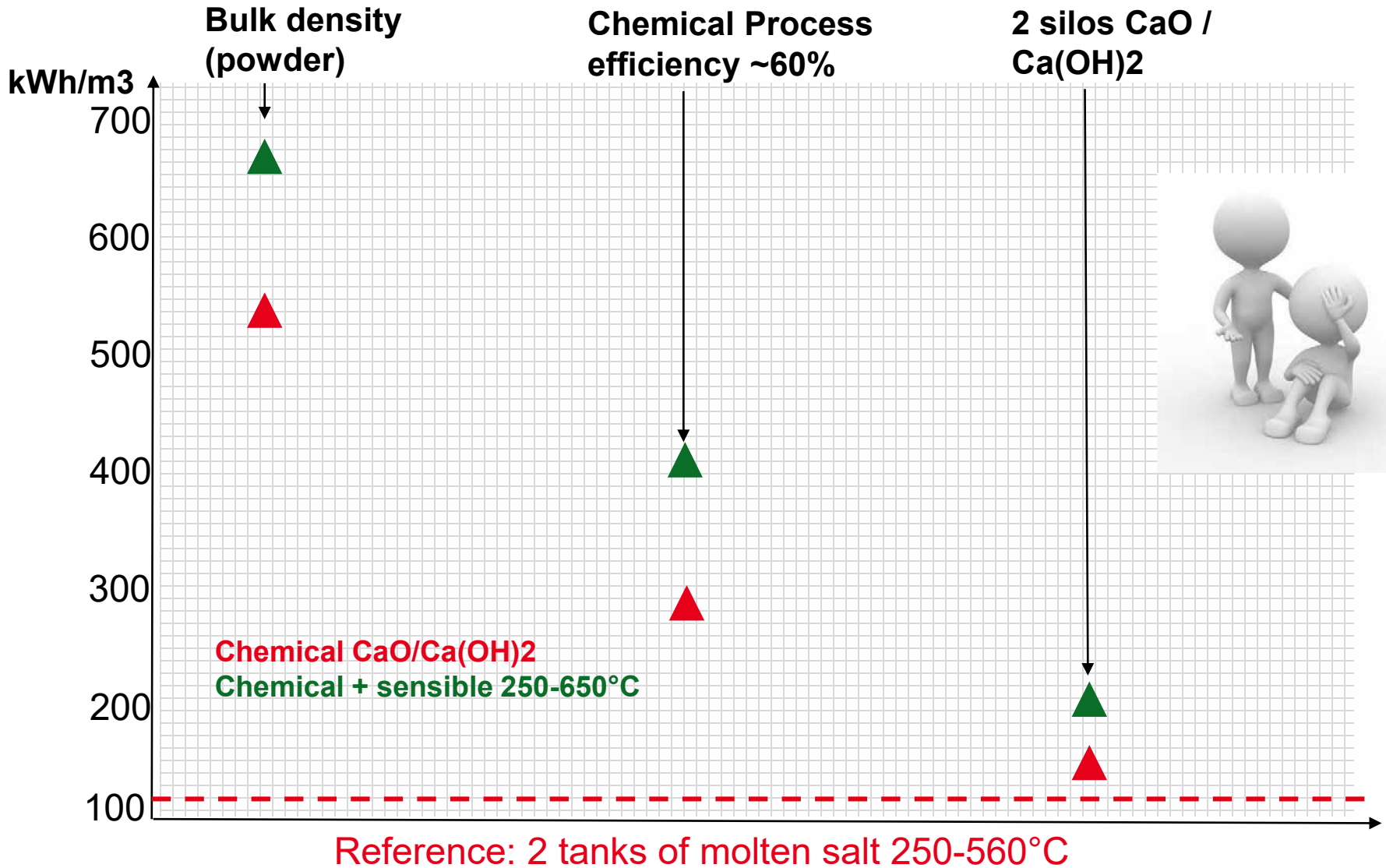
Consumed Energy in GJ for 1 cycle
Dehydration/Hydration for daily storage



Consumed Energy in GJ for 1 cycle
Dehydration/Hydration for seasonal storage



REACTION SELECTION – STORAGE DENSITY CRITERIA (5)



- **To select a suitable thermochemical reaction for heat storage**
 - Identify the range of parameters (P_g , T) on the real process
 - If the data are scarce, check the equilibrium curve
 - The temperatures of charge and discharge may be different from the tuning temperature, careful of the realistic range of partial pressure of reactant gas! Large scale reactors are not dilute systems such as thermal balances!
 - Assess the reversibility and cyclability of the reaction at particle scale
 - Perform a simplified mass and heat balance of the whole storage process to evaluate its potential interest and efficiency
 - Deduce a realistic nett volumetric storage density. It will be far away from the wonderful performances you can read in the literature, but that's life...





SOLID/GAS REACTOR SELECTION

TYPES

INTEGRATION IN PROCESS



- **Main issues for heterogeneous gas / solid reactions**

- Heat transfer
- Mass transfer
- Up-scale



- **Existing technologies:**

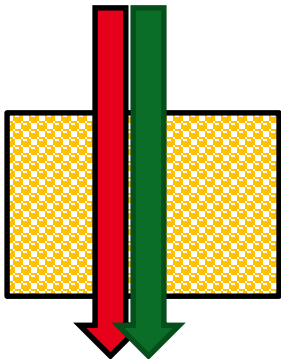
| Stacked bed | Fluidised beds | Entrained beds |
|----------------|------------------------|------------------------|
| Packed bed | Bubbling fluid. bed | Entrained flow reactor |
| Structured bed | Circulating fluid. bed | Cyclone |
| Mobile bed | Spouting fluid. bed | |
| Rotary kiln | | |
| Rotary screw | | |

■ 3 methods for heat and mass transfer



Direct:

Reactant gas part of heat transfer fluid

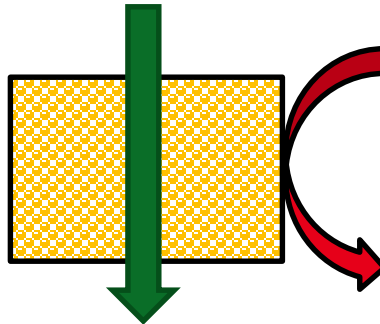


- Simple
- High heat transfer (large surface)
- Low flexibility
- Upscale medium

Ref: Fixed beds

Indirect:

Reactant gas and heat transfer fluid are different

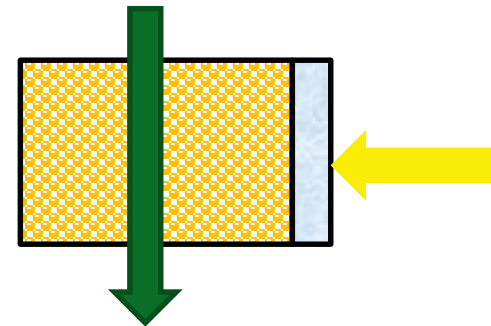


- More complex
- Indirect heat transfer: risk of low transfer
- High flexibility
- Upscale high

Ref: Fluidised beds

Direct sun:

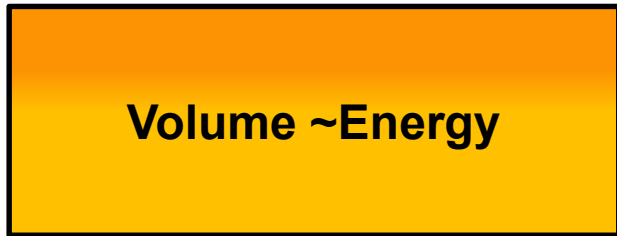
Reactant gas
No heat transfer fluid, direct irradiation



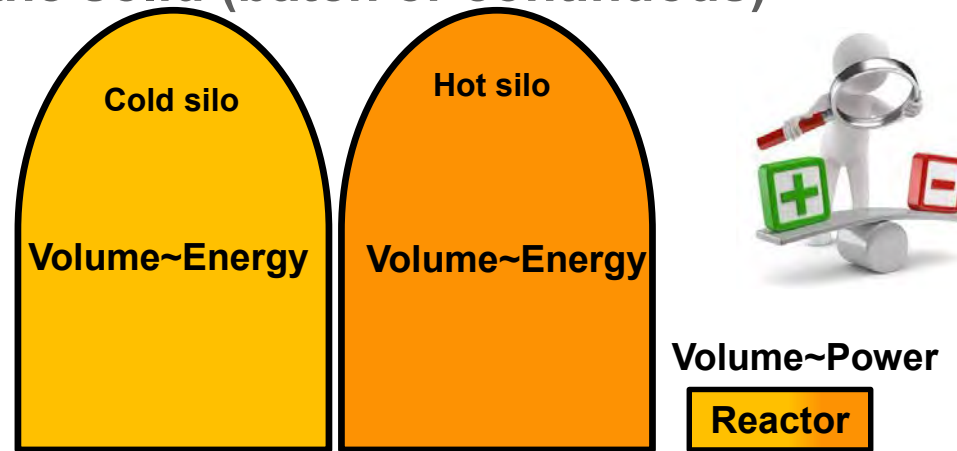
- Very complex (specific to CSP)
- High flexibility
- Upscale low to medium

Solar particle receivers

- Fixed beds are at the same time reactors and storage silos, all the other types need to transport the solid (batch or continuous)



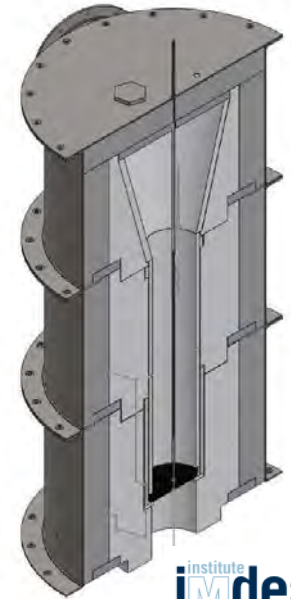
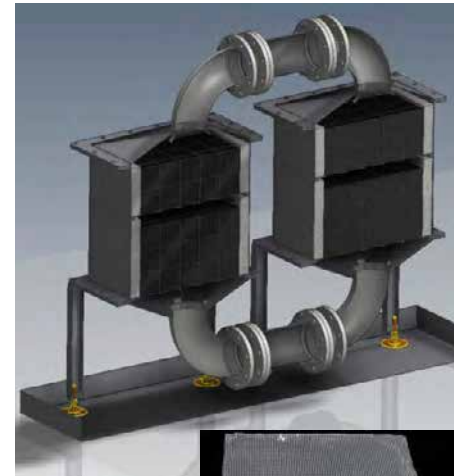
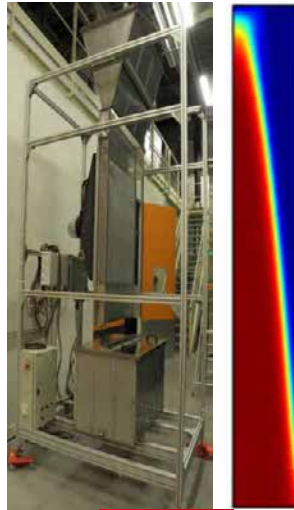
- High storage density (1 silo) but chemical conversion <100% (process temperature requirement)
- Simple technology: no solid movement
- Heat transfer very low: direct → solid/HTF/reactant compatibility; or sun → low up-scale
- Low HTF velocity → large surface, fluid distribution issue
- DP: low thickness → several beds → HTF collectors complex; or structured bed → cost?
- Larger inertia if intermittent use



- Chemical reaction can be 100% but 2 silos (storage density lower)
- Solid transport and feeding are complex, especially when hot
- The complex and expensive part is limited to a small reactor
- Any kind of heating: direct, indirect, sun
- Any kind of HTF if indirect: no chemical issue gas/HTF or solid/HTF
- Charging and discharging reactors can be different and optimised



- Direct reactors examples



Packed Bed
 $\text{SrBr}_2 / \text{SrBr}_2 \cdot \text{H}_2\text{O}$
 20-70°C

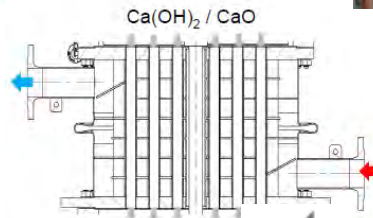
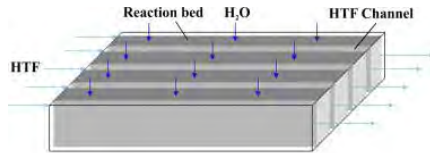
Moving Bed
 $\text{MgBr}_2 / \text{MgBr}_2 \cdot 6\text{H}_2\text{O}$
 70-140°C

Packed bed
 RD Silica gel
 20-60°C

Structured bed
 $\text{Co}_3\text{O}_4 / \text{CoO}$
 800-1000°C

Fluidised bed
 $\text{Mn}_2\text{O}_3 / \text{Mn}_3\text{O}_4$
 650-1200°C

- Indirect reactors examples



BFB batch
CaO/Ca(OH)₂
300-550°C

BFB continuous
CaO/Ca(OH)₂
300-600°C

Packed bed / plate heat-exchanger
CaO/Ca(OH)₂
300-600°C

Moving bed
CaO/Ca(OH)₂
300-600°C

BFB
CaO/Ca(OH)₂
300-700°C
7 bars

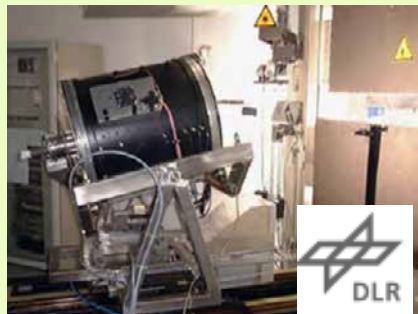
Solar particle receivers

Direct irradiation

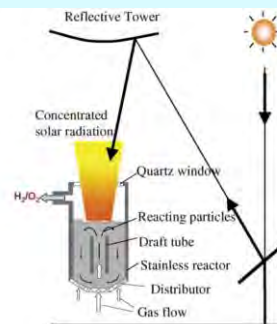


**Free falling curtain
(Sensible heat)**

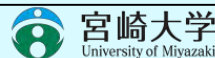
Irradiation Via quartz window



**Kiln
CaCO₃
calcination**



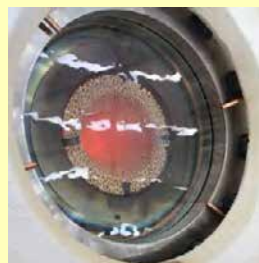
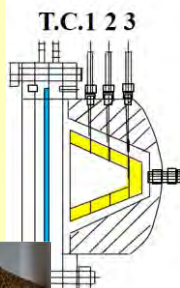
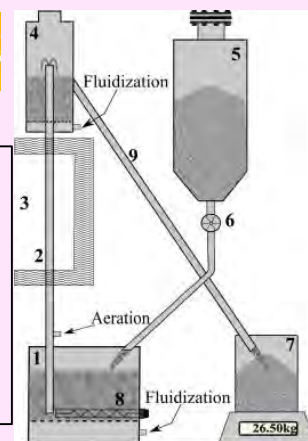
**BFB
CaCO₃ calcination**



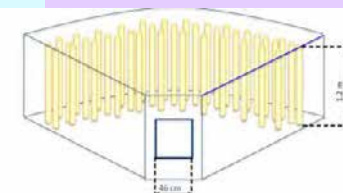
Heating Via walls



**BFB
dense in
tubes
(sensible
heat)**



**Fixed
structured bed
H₂ production**

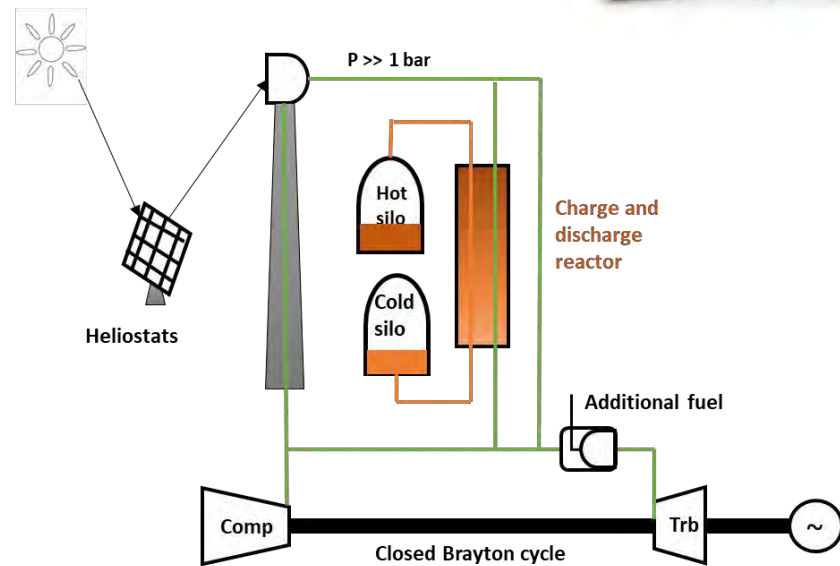
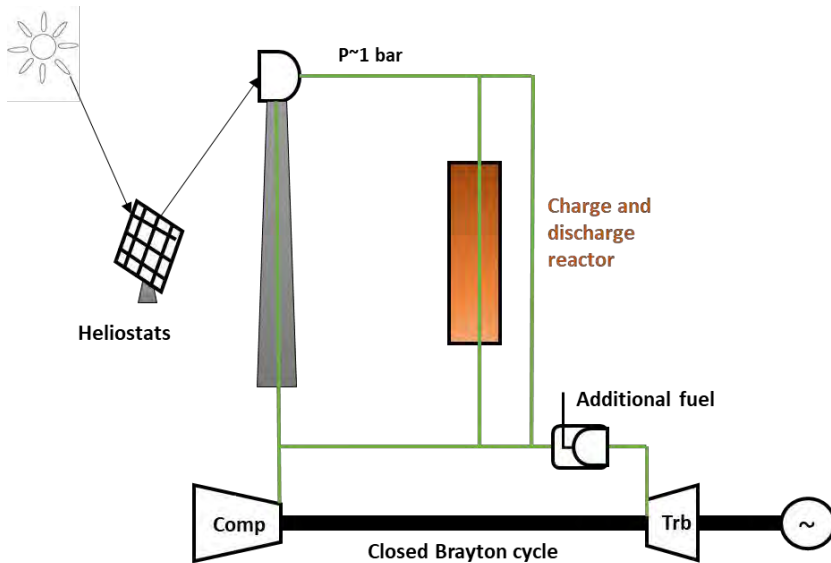


**Pellets in Al
tubes
H₂ production**



- The charge reactor may be different from the discharge reactor: it is /process / solar HTF / power block HTF/ dependant:

Example with one single reactor for charge and discharge:

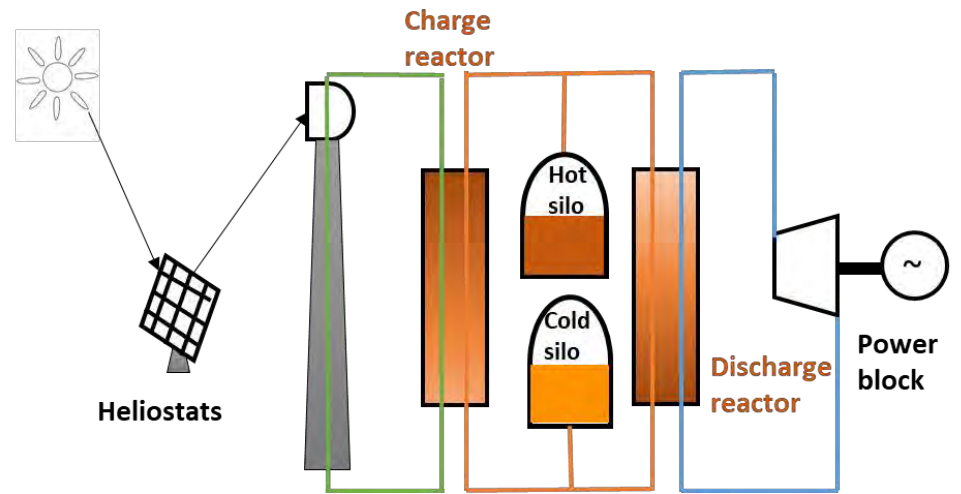
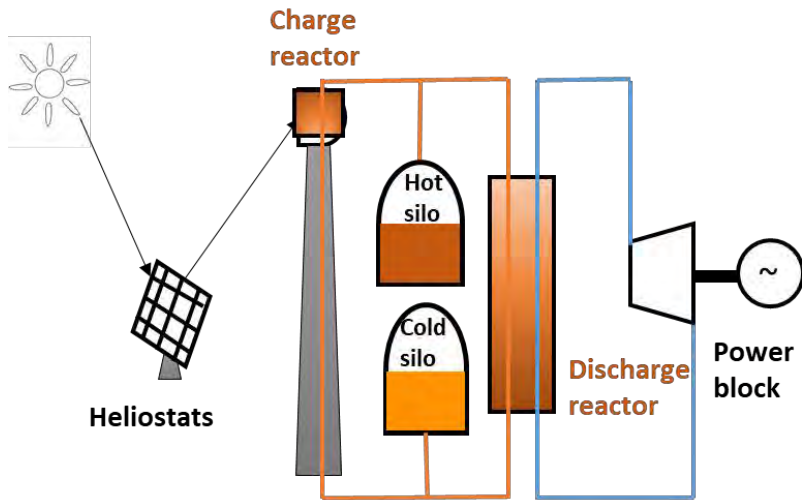


Packed or structured bed

SOLID/GAS REACTOR SELECTION – INTEGRATION IN PROCESS (2)



Example with two reactors for charge and discharge:



Solar particle receiver

- **There is no ideal reactor: there is a best compromise selection that must take into account**
 - ✓ *Material properties,*
 - ✓ *Reaction kinetics,*
 - ✓ *Heat transfer fluid,*
 - ✓ *Reactant gas,*
 - ✓ *Industrial scale target: 1MWh, 10 MWh, 100 MWh or 1000 MWh*
 - ✓ *Process integration,*
 - ✓ *...*

- **The best technology is not the simplest one!!! Look for industrial technologies, industrials look for the best techno-economic compromises. There are many BFB and CFBs in the range 50-500MW and no fixed beds for instance...**





SOLID MATERIAL AD-EQUATION TO THE REACTOR TYPE AND PROCESS



■ Solid material can:

- ✓ *Change volume through reaction (swelling)*
- ✓ *Form a crust after chemical cycles (hydration in fixed bed)*
- ✓ *Change mechanical strength through thermal of chemical cycles (break)*
- ✓ *Sinter, agglomerate (operation T too close from softening T)*
- ✓ *Suffer attrition (case of FB but also pneumatic transport)*
- ✓ *Have a poor flowability / pourability (case of mobile beds)*
- ✓ *Fluidise with difficulty (see Geldart classification)*
- ✓ *Have chemical properties that are not optimal : for instance T discharge too low compared to T charge*
- ✓ *...etc*

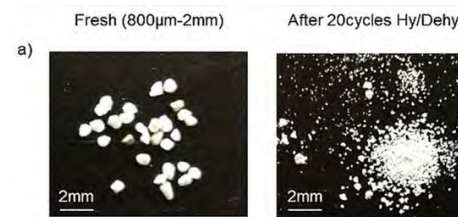
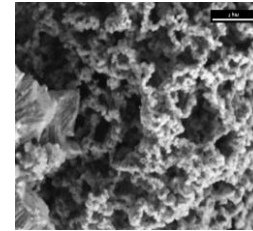


■ The material can be improved to fit better to the reactor / process specifications (careful of the final cost!)

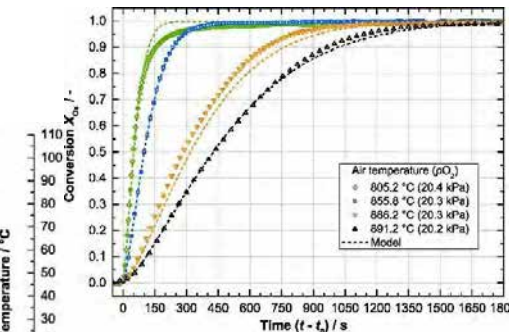
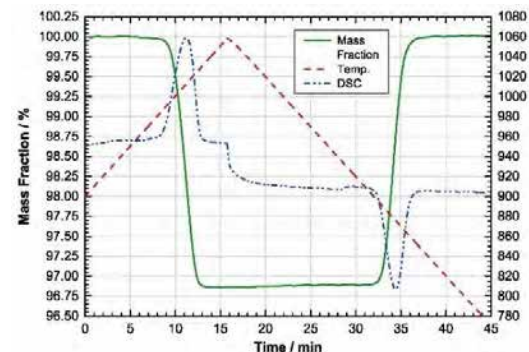


Some exemples

- Lime nano-coating (SaltX process) → improve pourability and fluidisation
- Lime-clay composite → improve mechanical strength
- Cobalt oxide shaping → improve heat transfer and pressure drop
- Mn_2O_3 doping with Fe oxide: (Fe/Mn 1:3 mol) → Red: 988°C & Ox 895°C



Very important to collaborate between material & reactors specialists for TCS storage





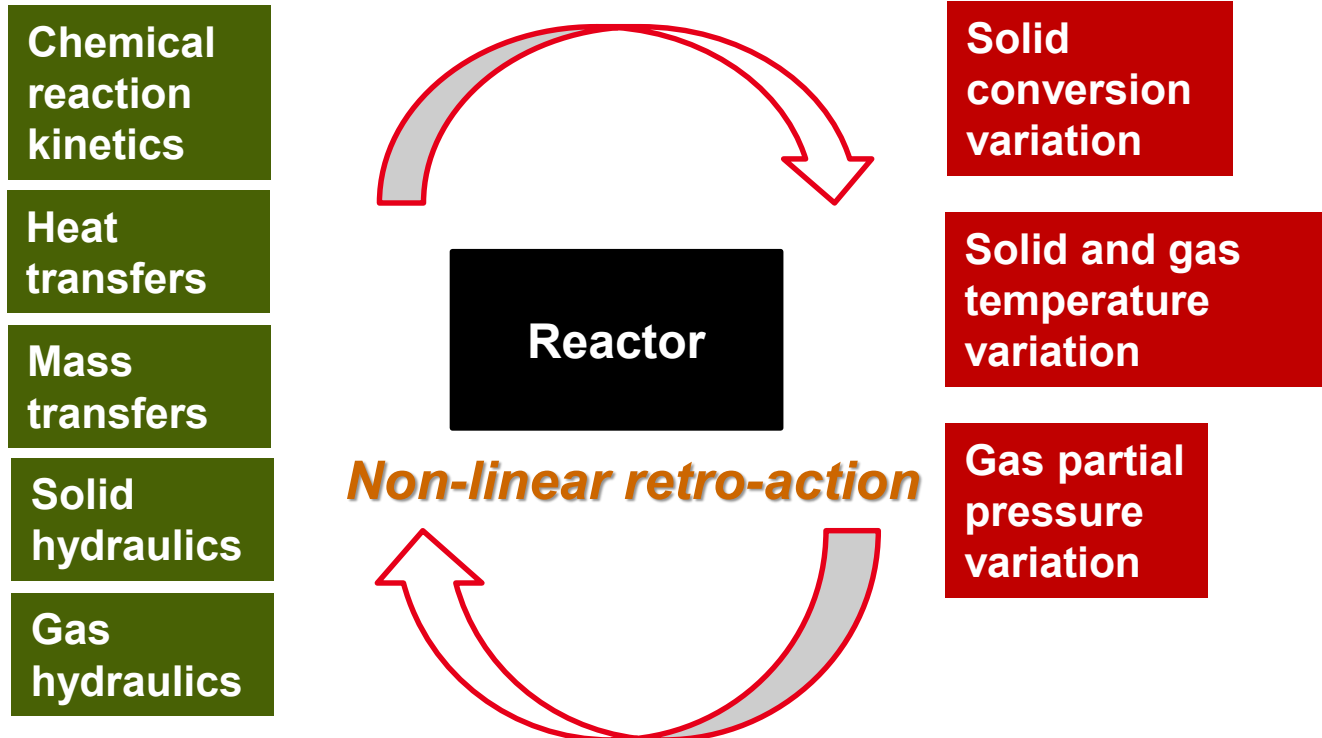
REACTOR MODELLING AND UP SCALING

CASE OF BFB AND CAO/CA(OH)_2

CASE OF PACKED BED AND SORPTION

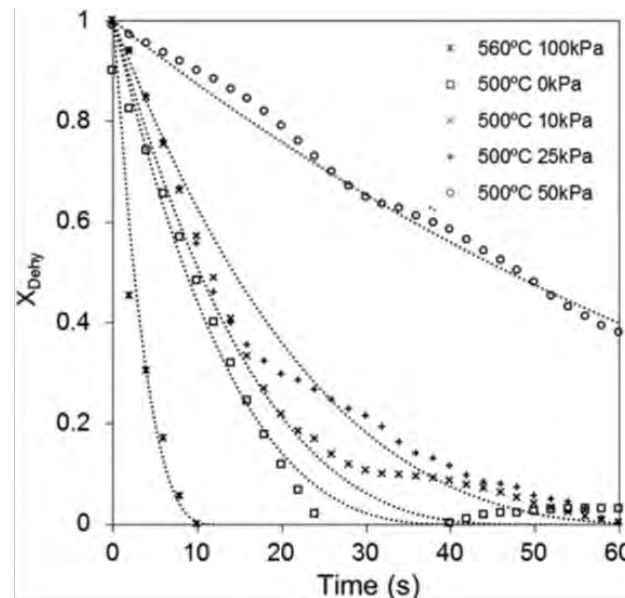
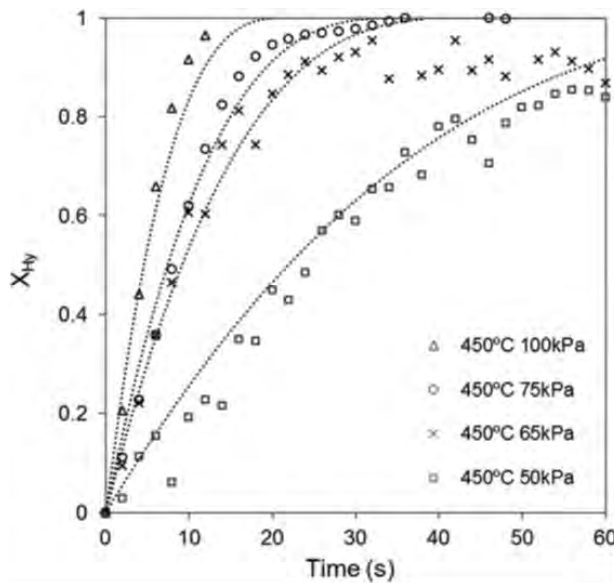


- Why modelling is so important for TCS reactors?
 - Comprehension of experimental data at pilot scale is complex
 - Transposition from pilot to industrial scale is not straight
 - Need of upscaling tool



- 1st example: CaO/ Ca(OH)₂
- The reaction is fast and allows to select a FB reactor
 - General industrial criteria for FB: 500 to 1000 kW/m² → low parasitics
 - The intrinsic kinetics of the reaction has a standard form:

$$\checkmark \frac{dX}{dt} = k_o * \exp\left(\frac{-Ea}{R*T}\right) * (P_v - P_{v,eq})^n * (1 - X)^m$$

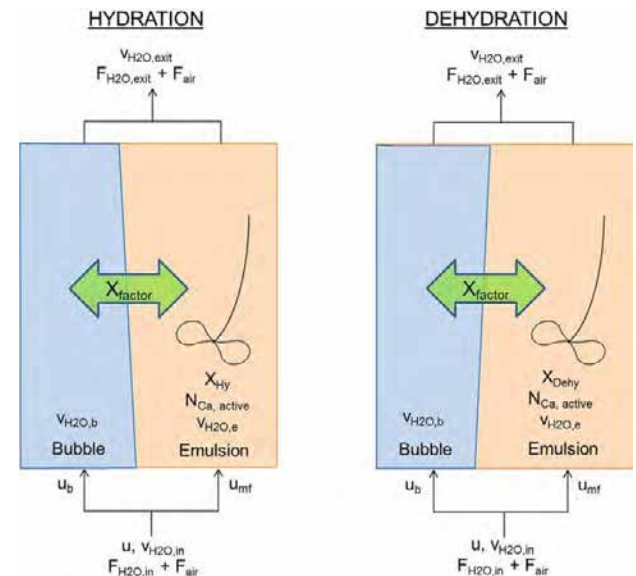
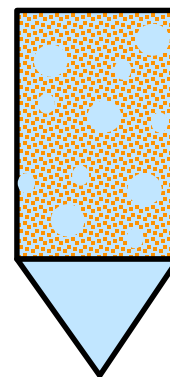


- At pilot scale, the reactor is a perfectly mixed reactor:
 - Same temperatures everywhere in the bed
 - Variation of gas pressure along the height of the bed → conversion varies
 - Far away from the minimum velocity of fluidisation, 2 phases of bubble and emulsion → mass transfer limitations between the gas phases are possible

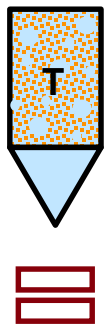
Experimental tests in batch and continuous BFB validate this limitation when kinetics is fast -> Xfactor ~5



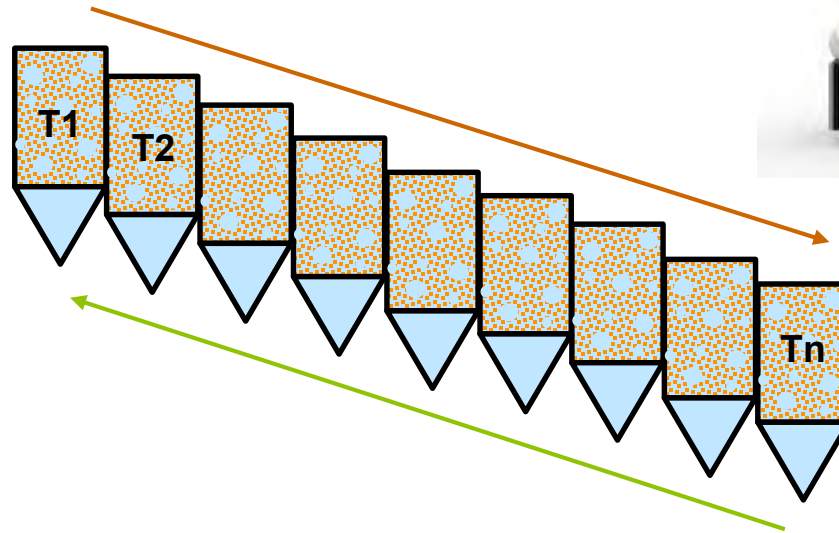
CEA batch and continuous BFB reactors



- At industrial scale the objective is to recover both sensible heat and chemical heat
 - Sensible heat can cover 20 to 30% of the stored energy



Perfectly mixed
No sensible heat recovery

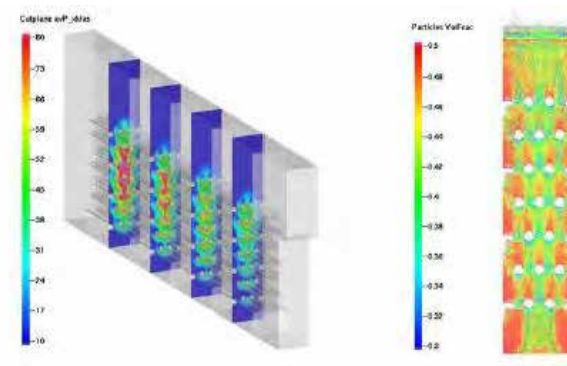
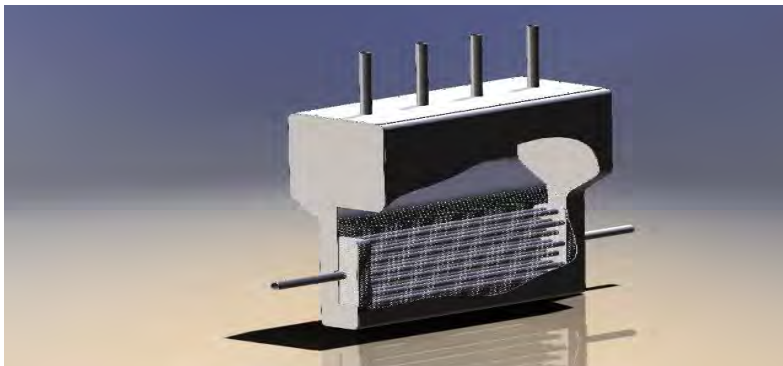


■ The industrial concept is:

- A tube-calander heat exchanger BFB reactor with indirect exchange between the tubes (HTF) and the calander (gas-solid emulsion)
- The emulsion is flowing from one end to the other

■ The model is simplified :

- 1D model along the length of reactor
- Pure steam (no vertical profile in each section)
- Perfect mixing in each section in the tube bundle (CFD validation, many data)
- Plug-flow of emulsion along the length

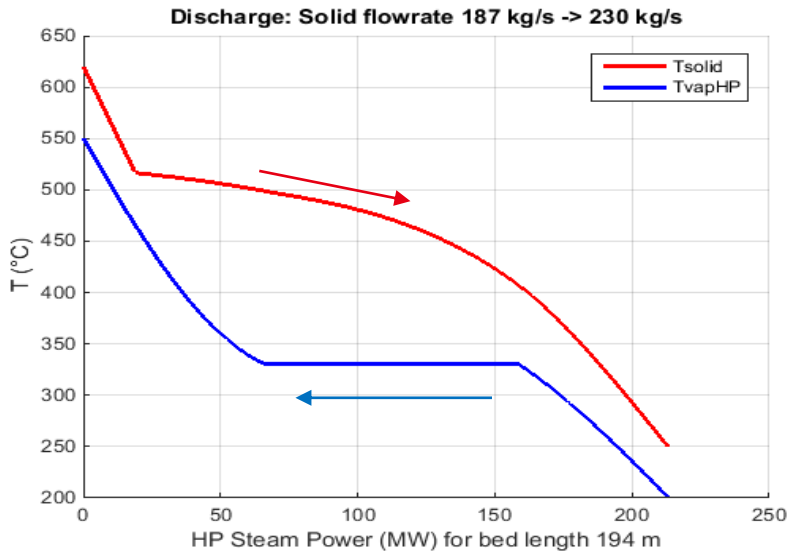


Example for hydration reactor:

- 210 MWth
- HTF: HP water 110 bar, 200→550°C
- Inlet solid: Pure CaO, 600→250°C

Result:

- 187 kg/s CaO + inert (25%)
- 100% conversion at the end
- Length: 194 m
- Section: 1,15 x 1,20 (700 tubes)

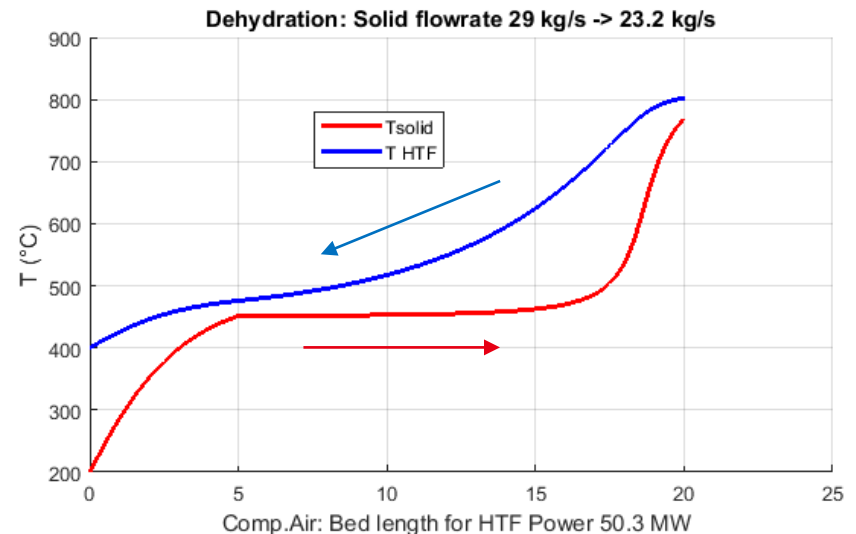


Example for dehydration reactor:

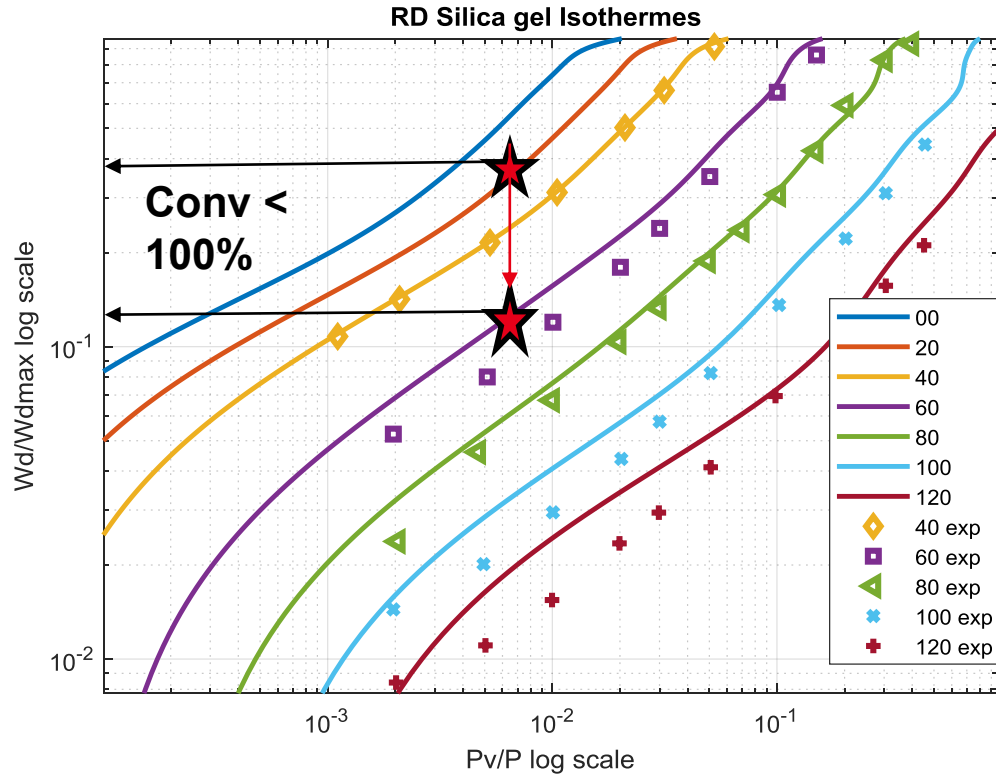
- 50 MWth
- HTF: air 20 bar, 800→400°C
- Inlet solid: Pure Ca(OH)₂, 200→780°C

Result:

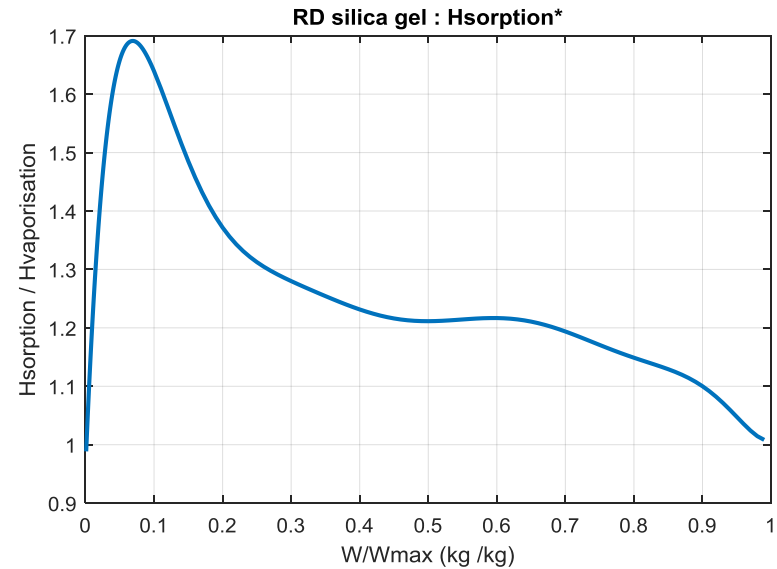
- 29 kg/s Ca(OH)₂ + inert (25%)
- 100% conversion at the end
- Length: 20 m
- Section: 1,8 x 2 m (945 tubes)



- **2nd case : sorption for cold storage**
 - Adsorption is exothermic and desorption is endothermic
 - Sorption is a surface reaction. The gas molecule must leave the surface site to have it active again → the sorption kinetics is very fast but controlled by the diffusion inside the sorbant grains (Knudsen and Surface diffusion) which is slow
 - The reaction is bi-variant : 3 parameters are relied: partial pressure of gas, temperature and level of sorbant charge X (kg reactant/kg sorbant)
 - The adsorption and desorption are not complete
 - The enthalpy of sorption is close to the enthalpy of vaporisation for water sorption → steam must be 'free' for steam sorption (atmospheric moisture)
 - The enthalpy of sorption varies with the level of charge of the solid sorbant

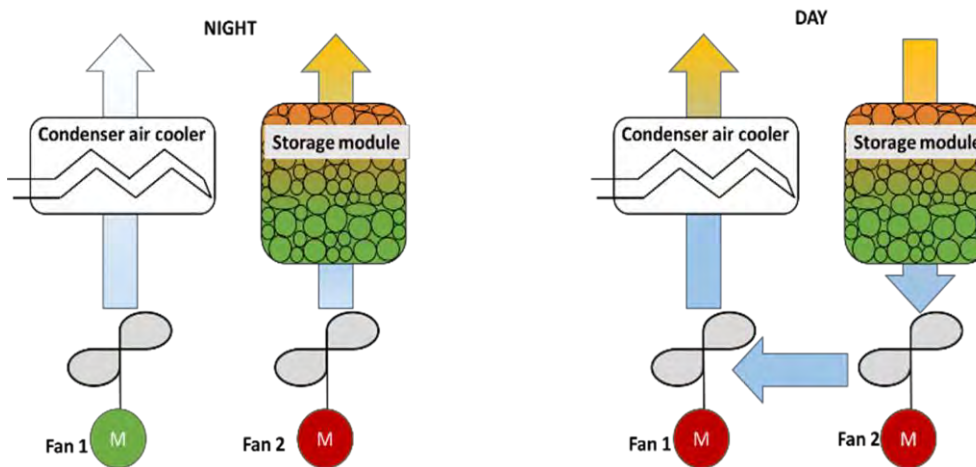
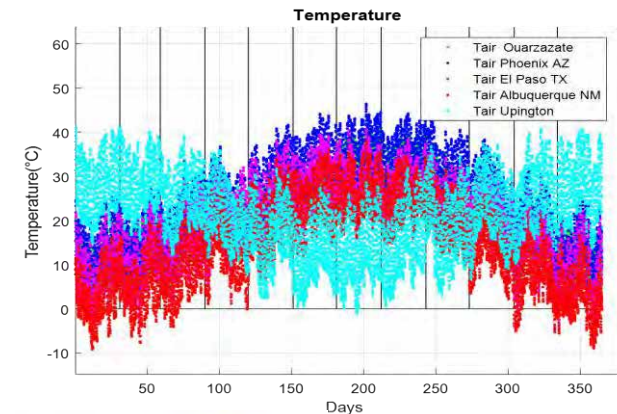
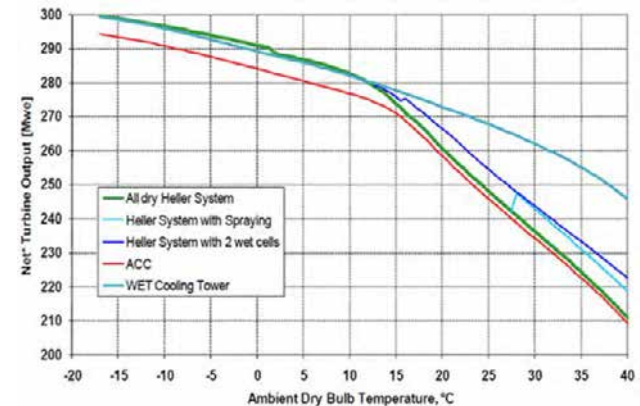


**RD silica gel
properties**

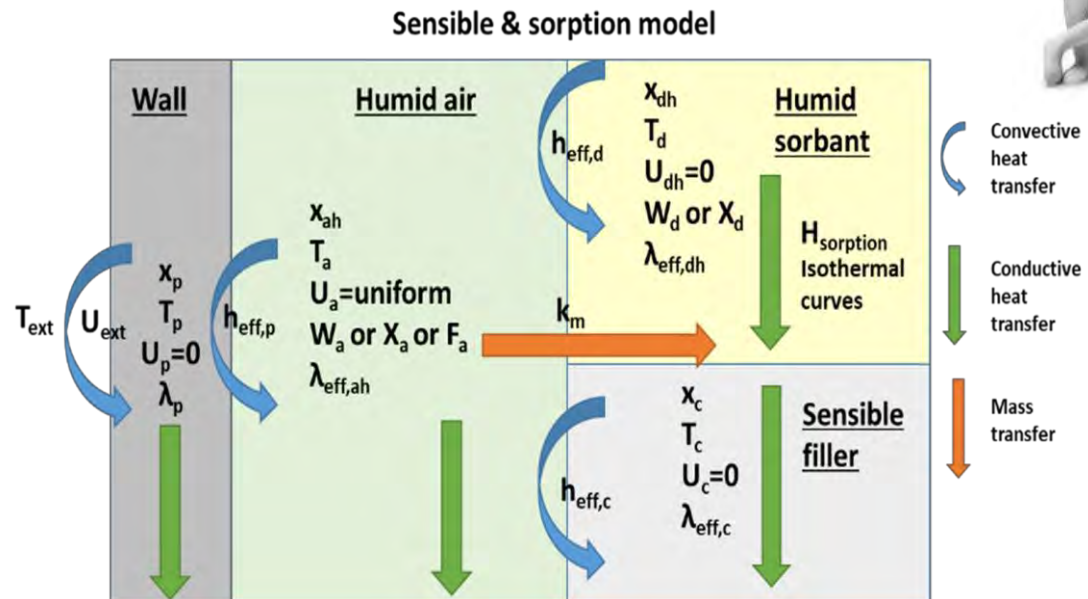


What is the use for CSP plants?

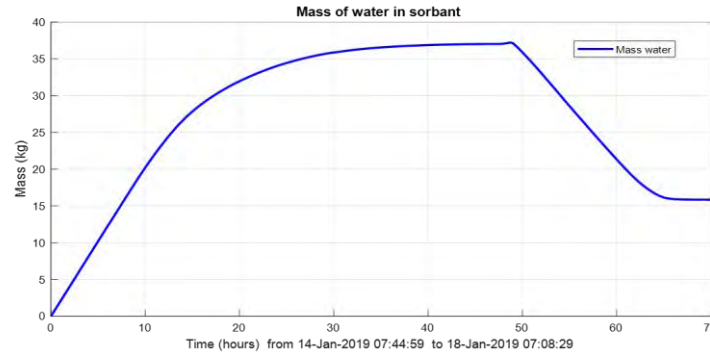
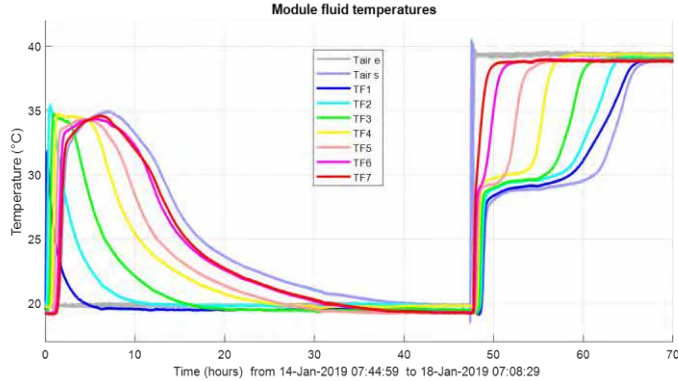
- Thermodynamic power plants waste 1 to 4 m³/MWh of water, 90% for the condenser cooling.
- A solution for arid regions is air cooling.
- Steam Turbine Output decreases fast when ambient air is hotter than 15°C whereas Ambient air can reach 40-45°C during hot periods in arid regions
- The idea is to store cold and moisture of ambient air during nights (adsorption) and cool hot air during days (desorption)



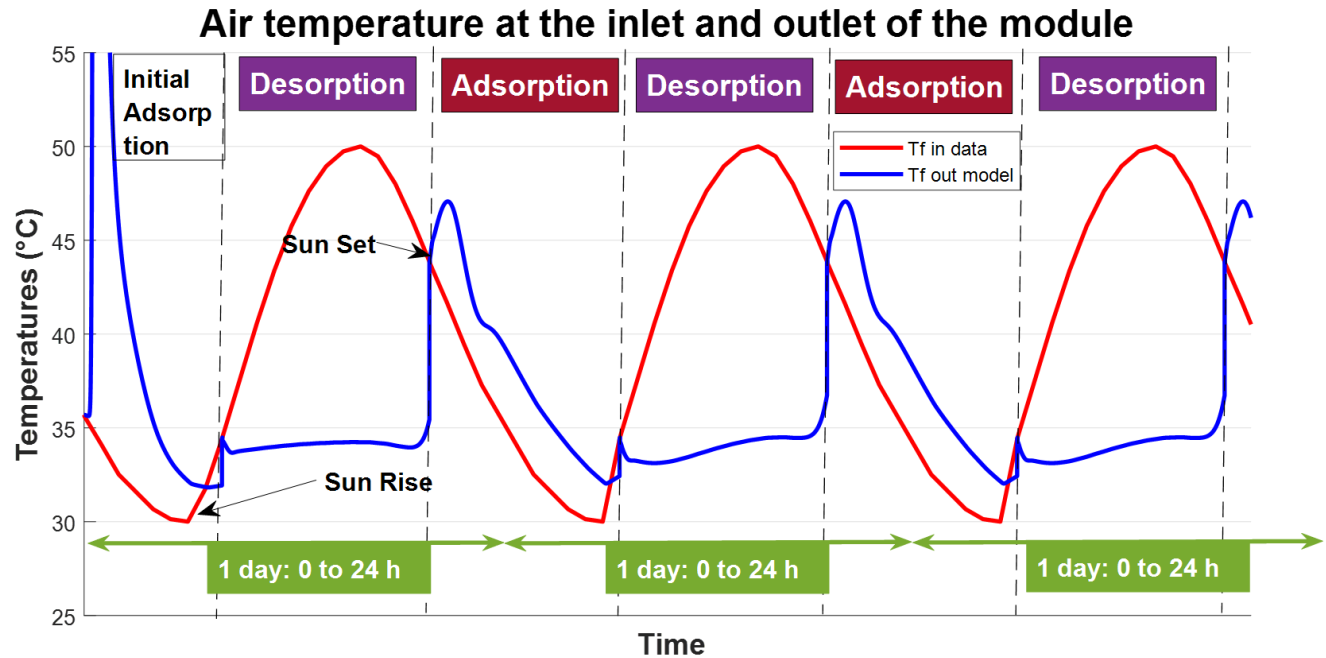
- Sorption selection: desorption $< 50^{\circ}\text{C}$ \rightarrow RD silica gel or zeolite Z01, 02 or 05
- Low DP + sensible storage : sensible material (lass beads at pilot scale)
- Reactor: slow kinetics + ambient air \rightarrow packed bed of sorbant and sensible material
- Model of packed bed: 6 phases, 4 temperatures



Exp results of a sorption at $Pv/P=0,007$, $T_{ad}=20^{\circ}\text{C}$ $T_{des}=40^{\circ}\text{C}$



Model prediction
 Air $30 \rightarrow 50^{\circ}\text{C}$
 $Pv/P \sim cte$





CONCLUSION



- **Developing a TCS concept for CSP is a challenging and iterative process that must identify and characterise:**
 - A chemical reaction
 - The range of realistic operations
 - The integration in the whole CSP process, the links with solar HTF, power block HTF, solid storage, gas storage, minimize heat wastes....
 - One or 2 reactors technologies
 - The ad-equation of the solid properties with the whole process
 - A model coupling chemical reaction, heat and mass transfers and hydraulics: very needed for understanding and upscaling
 - Evaluate the storage process at economic and environmental level: what is the final advantage?

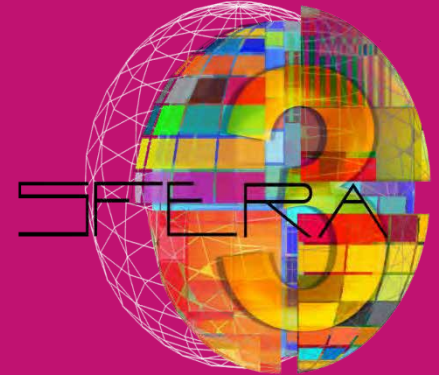
- **This is very important to have close relationship between material, reactors and process experts.**

- **When applying TCS to a process, never forget the main advantages:**
 - Long-term chemical storage (a few weeks to a few month)
 - Sensible heat stored longer in a solid (low conductivity, no convection)
 - Sensible heat temperature can be high ($\sim 800^{\circ}\text{C}$ for lime, $>1000^{\circ}\text{C}$ for RedOx)
 - Heat easy to transport = transport of a solid \rightarrow many transverse applications are possible (ex: industry \rightarrow District heating)
 - Higher storage density \rightarrow useful when space is limited

Thank you for your attention!

SFERA-III

Solar Facilities for the European Research Area



Solar Facilities for the European Research Area

1st Summer School “Thermal energy storage systems, solar fields and new cycles for future CSP plants”

WPI Capacity building and training activities

Odeillo, France, September 9th-11th 2019

Thermal Energy Storage Performance Assessment

Pierre Garcia, CEA-LITEN

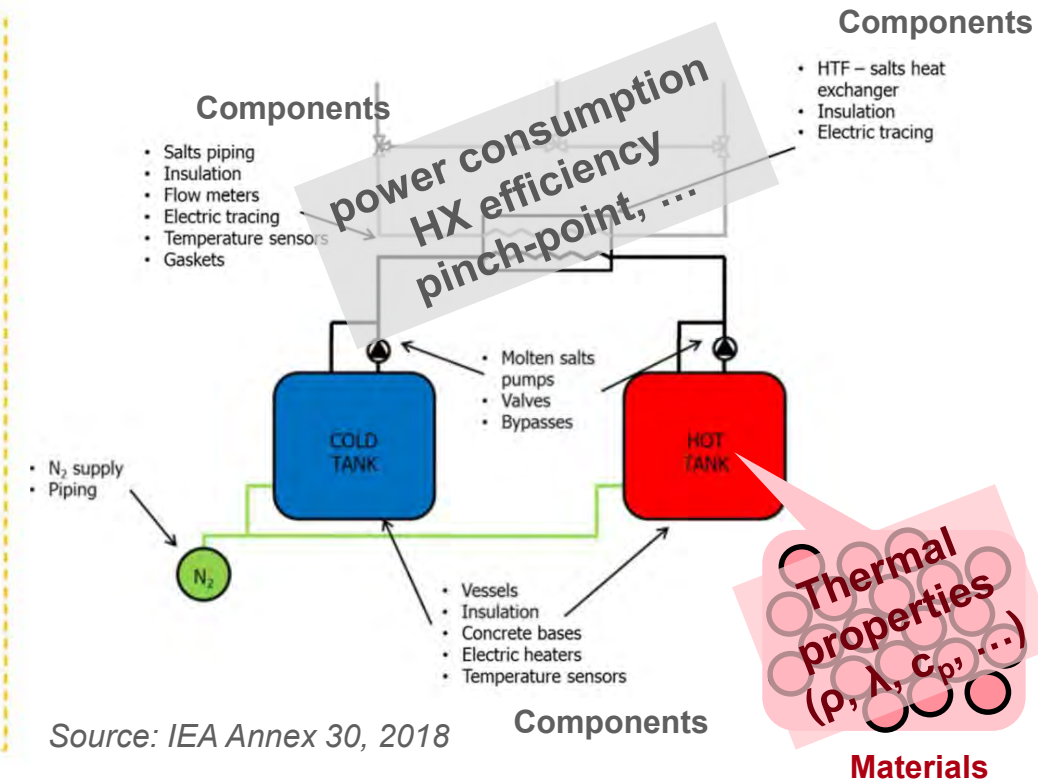
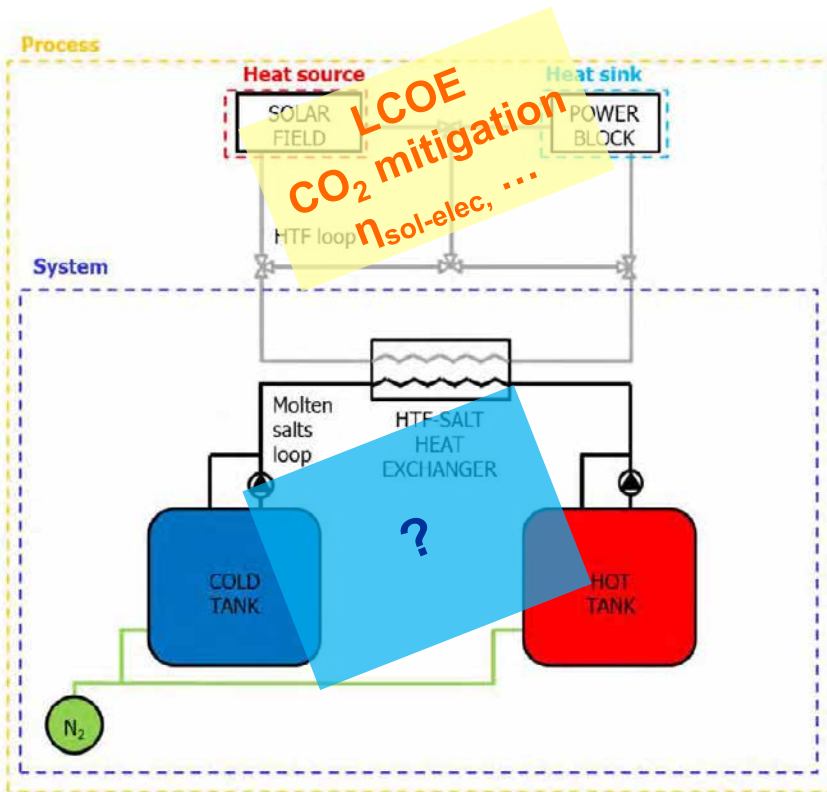
NETWORKING



THIS PROJECT HAS RECEIVED FUNDING FROM THE EUROPEAN UNION'S HORIZON 2020 RESEARCH AND INNOVATION PROGRAMME UNDER GRANT AGREEMENT NO **823802**

- **Scope of this presentation**
- **KPI from the end-user perspective**
- **Technical performance indicators**
- **Case study: latent heat storage with PCM**
- **Durability issues**

- Performance indicators are required everywhere
 - In research calls for proposal,
 - In CSP plants invitations to tender,...
- From process level to material level



Source: IEA Annex 30, 2018

- This presentation deals with performance indicators at **system level**

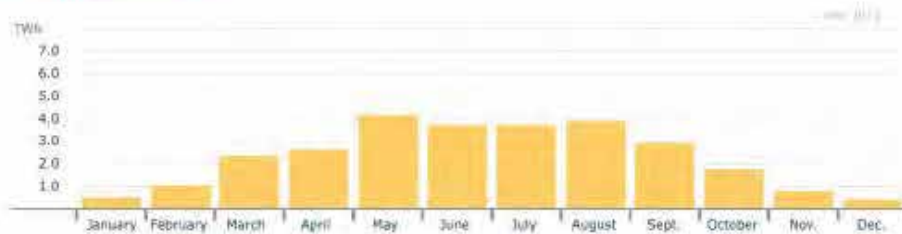
- Depend on the stakeholder perspective

| KEY PERFORMANCE INDICATORS | | | |
|----------------------------|-------------------------------------|--------------------|-----------------------------------|
| Stakeholder: | CSP plant operator | Electric utility | Policy-maker |
| KPI 1: | Storage capacity | Dispatchable power | CO ₂ mitigation |
| KPI 2: | Power | Response time | Increased use of renewable energy |
| KPI 3: | Lifetime | | Grid stability |
| KPI 4: | Reduced LCOE | | |
| KPI 5: | Boosted energy efficiency (process) | | |

KPI selection per stakeholder for integration of TES into a CSP plant (IEA Annex 30, 2018)

- TES make CSP production **Dispatchable**
 - Dispatchable generation = sources of electricity that can be delivered on demand to grid operators
 - “Peak-shaving” ability (time-shifted operation)
 - Reduced need for peak-load fossil generating capacities

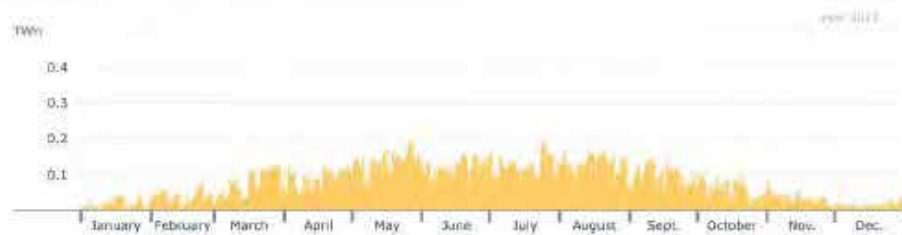
Monthly Production Solar



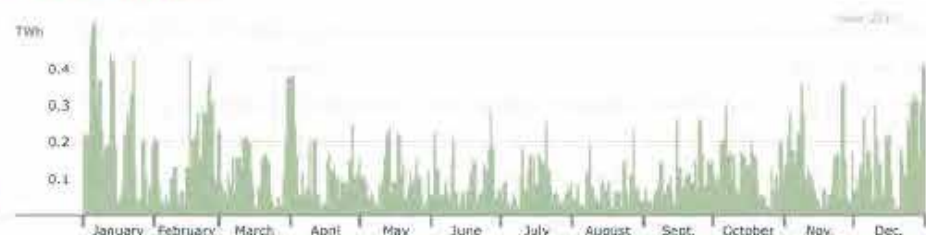
Monthly Production Wind



Daily production Solar



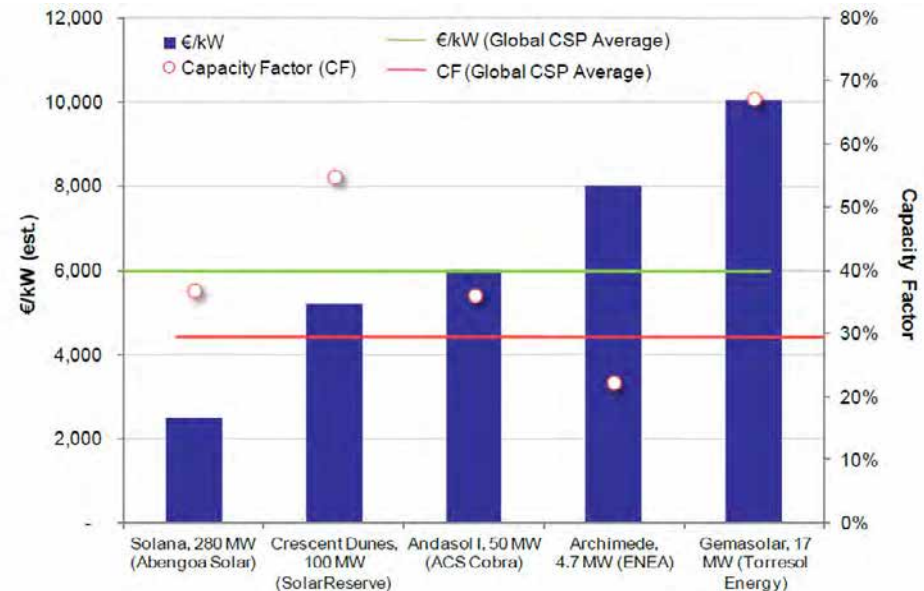
Daily production Wind



- TES make CSP production **Reliable**
 - Increases plant utilization and capacity factor F_c

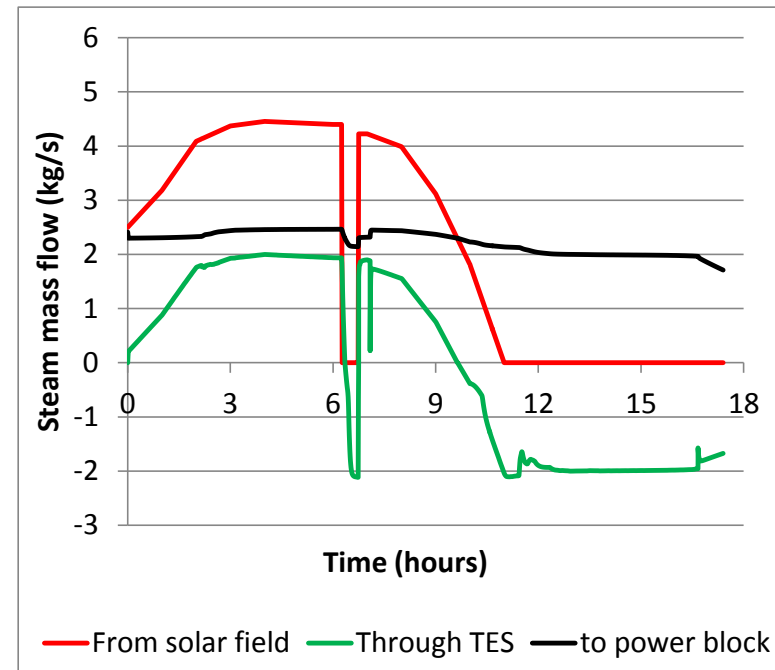
$$F_c = \frac{\text{power output during time } t \text{ (MWh)}}{t \times \text{rated power (MW)}}$$

- Improves plant controllability and operability
 - expanding the range of possible operating strategies
- If adequately designed, improves
 - the value of the produced electricity
 - the profitability of the project



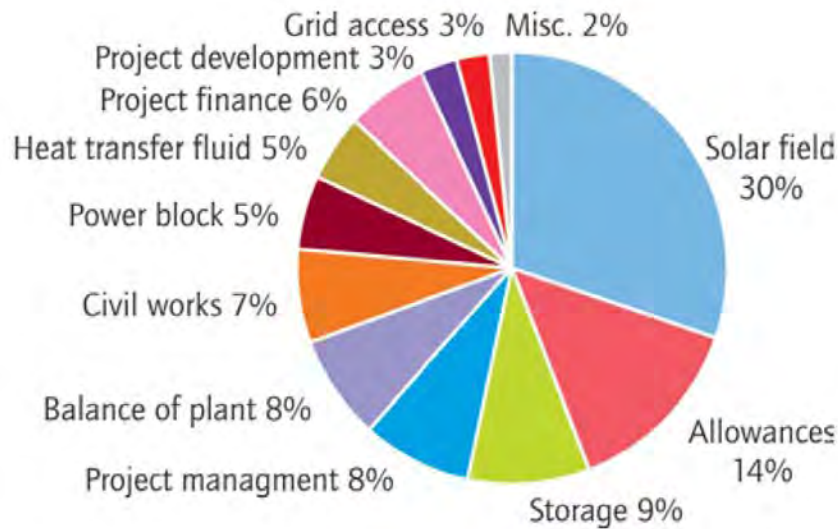
Reference capital costs and capacity factors of CSP plants with TES
(Emerging Energy Research, 2010)

- TES make CSP production **Stable**
 - Smoothes load variation of the power block
 - Power generation kept almost constant during cloud transients
 - Part load operation and start-stop cycles are reduced
 - Improving thermal cycle efficiency
 - Extends lifetime of equipment
 - Reducing the number of start-stop cycles

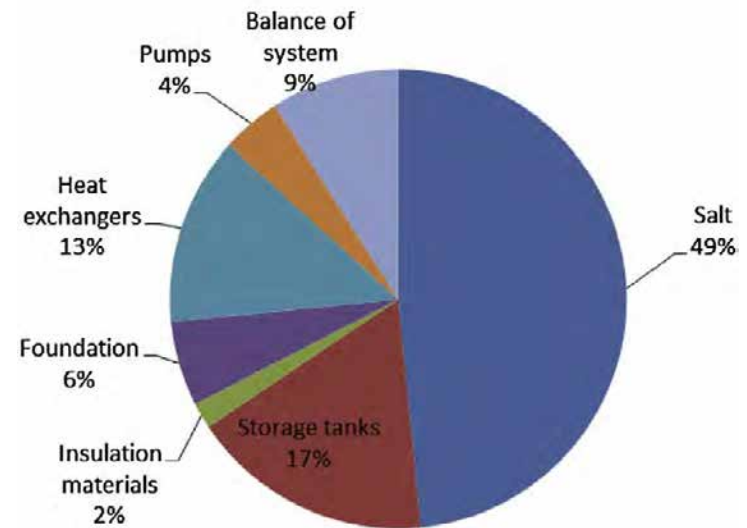


Simulated steam mass flow in a DSG plant with TES (CEA)

- Storage costs

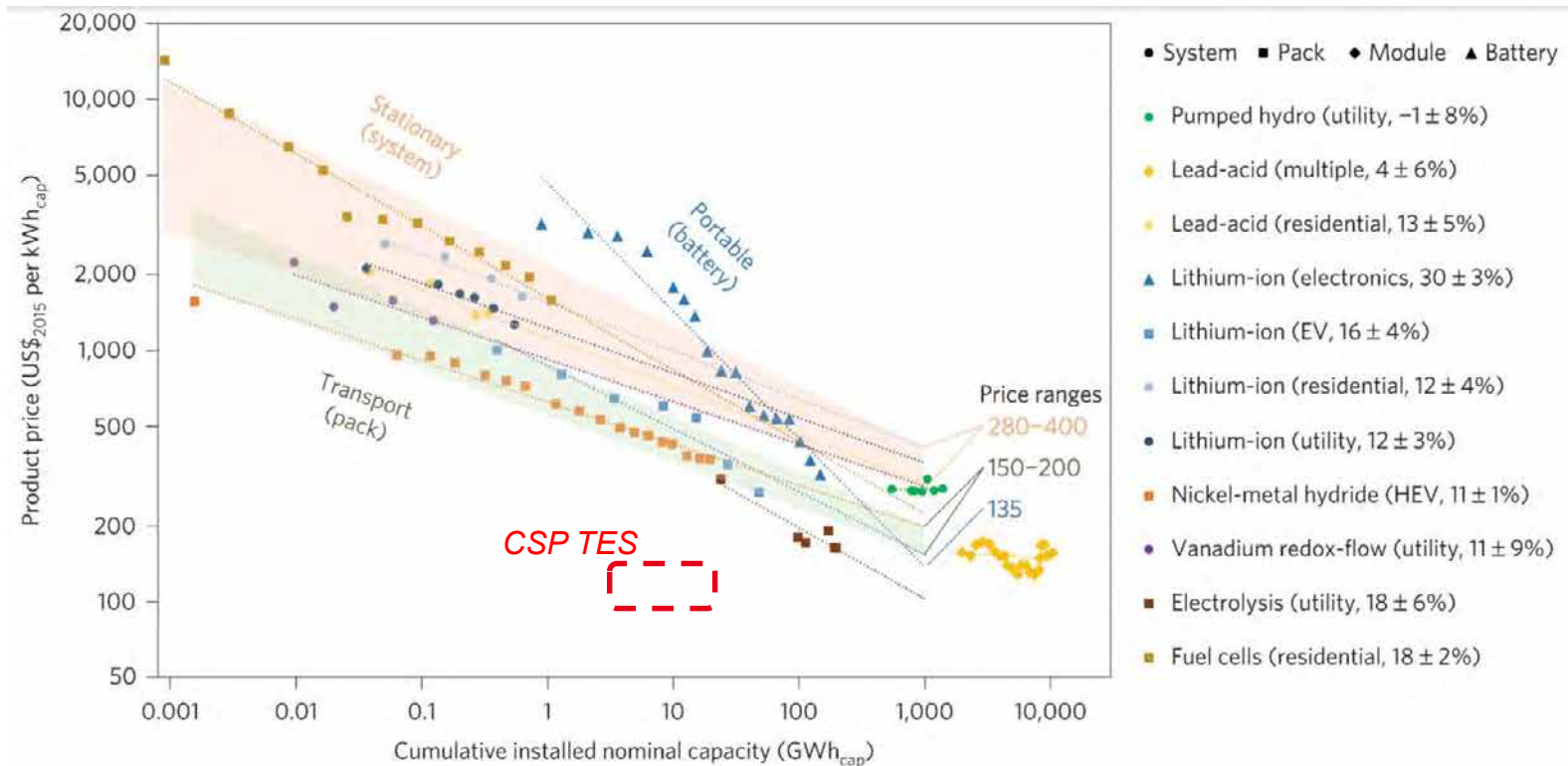


Investment costs breakdown of a 50 MWe PTC plant with indirect 7-hour storage (Source: IES STE roadmap 2010)



Detailed breakdown of the TES system (Source: IRENA 2012)

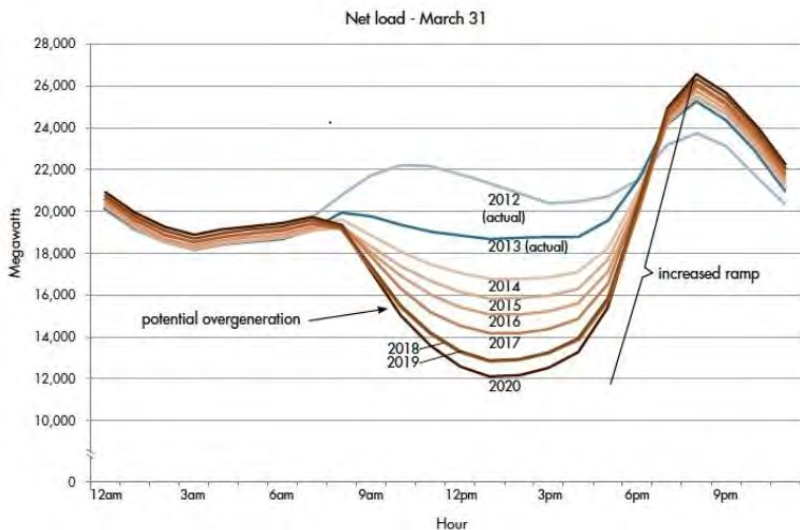
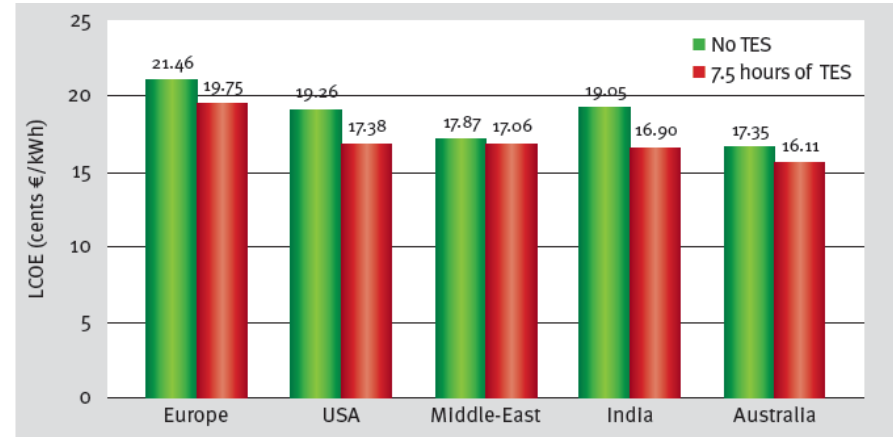
- Storage costs
 - From 20 to 33 USD/kWh_{th} (NREL 2017)  about 100 USD/kWh_{el}
 - Lower than the other energy storage solutions



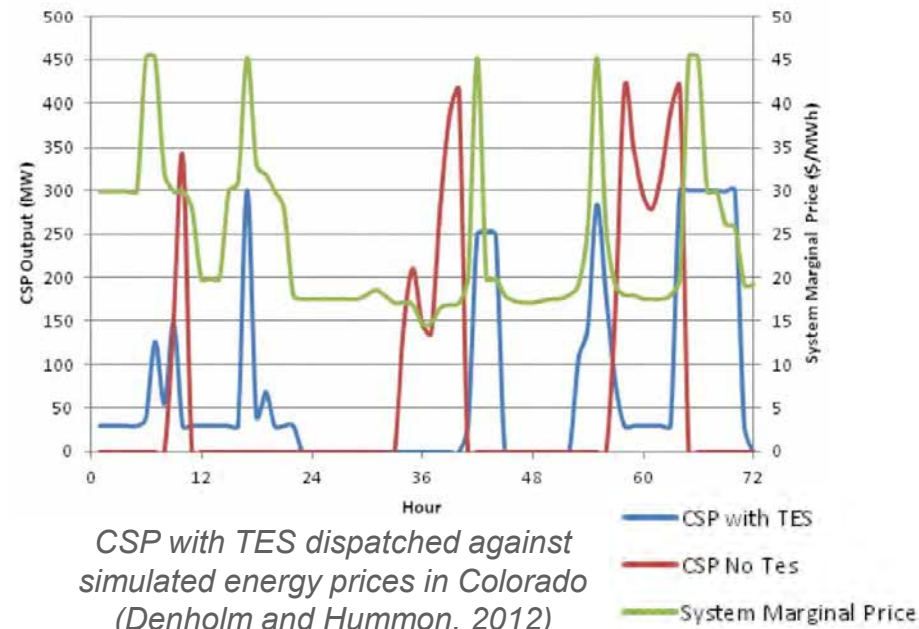
Future cost of electrical energy storage technologies at 1 TWh cumulative capacity (Schmidt, 2017)

- Levelized Cost Of Electricity
- TES costs have low influence on LCOE
 - Extra investments → more \$\$
 - Extra production → more kWh
- TES Value
 - + \$6/kWh_e compared to PV under 40% renewable penetration in California (NREL, 2017)

(NREL, 2017)



The Duck Curve (California Independent System Operator)



CSP with TES dispatched against simulated energy prices in Colorado (Denholm and Hummon, 2012)

**TECHNICAL PERFORMANCE INDICATORS
TES SYSTEM**

- Reference documents

- IEE standard (draft)
- AENOR standard (draft)
- ASHRAE standards
- Handbooks SFERA and SFERA III
- SolarPACES Task III TES WG
- Report of IEA ECES Annex 30

About 30 indicators proposed
Different definitions
Additional basic definitions needed!

- Basic principles

- Measurements always done in HTF side
 - HTF may be different from the storage medium
- Initial and final state are characterized by enthalpy levels
 - Temperature levels are only applicable to sensible storage

Indicators

| | |
|---|----------------------------------|
| 1 | Storage capacity |
| 2 | Utilization rate |
| 3 | Nominal Thermal power |
| 4 | Thermal losses |
| 5 | Storage efficiency |
| 6 | Stratification index degradation |

+ Durability aspects

• Definition

- Amount of **useful thermal energy** that the thermal storage system can supply by **full discharge** under certain starting and ending conditions.

$$SC = \int_{\text{initial conditions}}^{\text{full discharge conditions}} [\dot{m}(h_{\text{outlet}} - h_{\text{in}})] dt$$

Comments

- A charge capacity can also be defined ($SC_{\text{ch}} \neq SC$)
- SC depends on the initial conditions in the storage

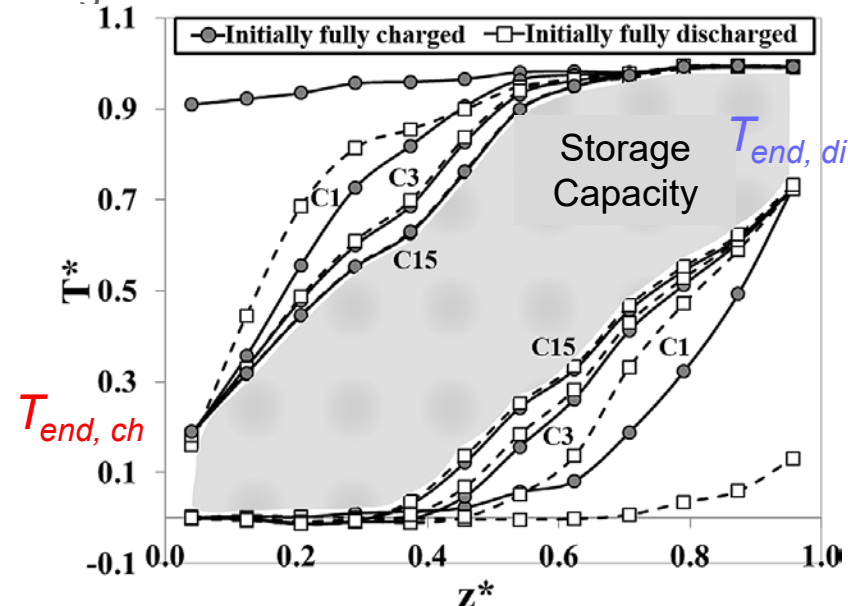


Having a given value of $h_{\text{HTF,out}}$ does not ensure to have the same SC / SC_{ch}

- Storage level = $\frac{SC_{\text{present conditions}}}{SC_{\text{nominal}}}$

• Test procedures (to assess SC_{nominal})

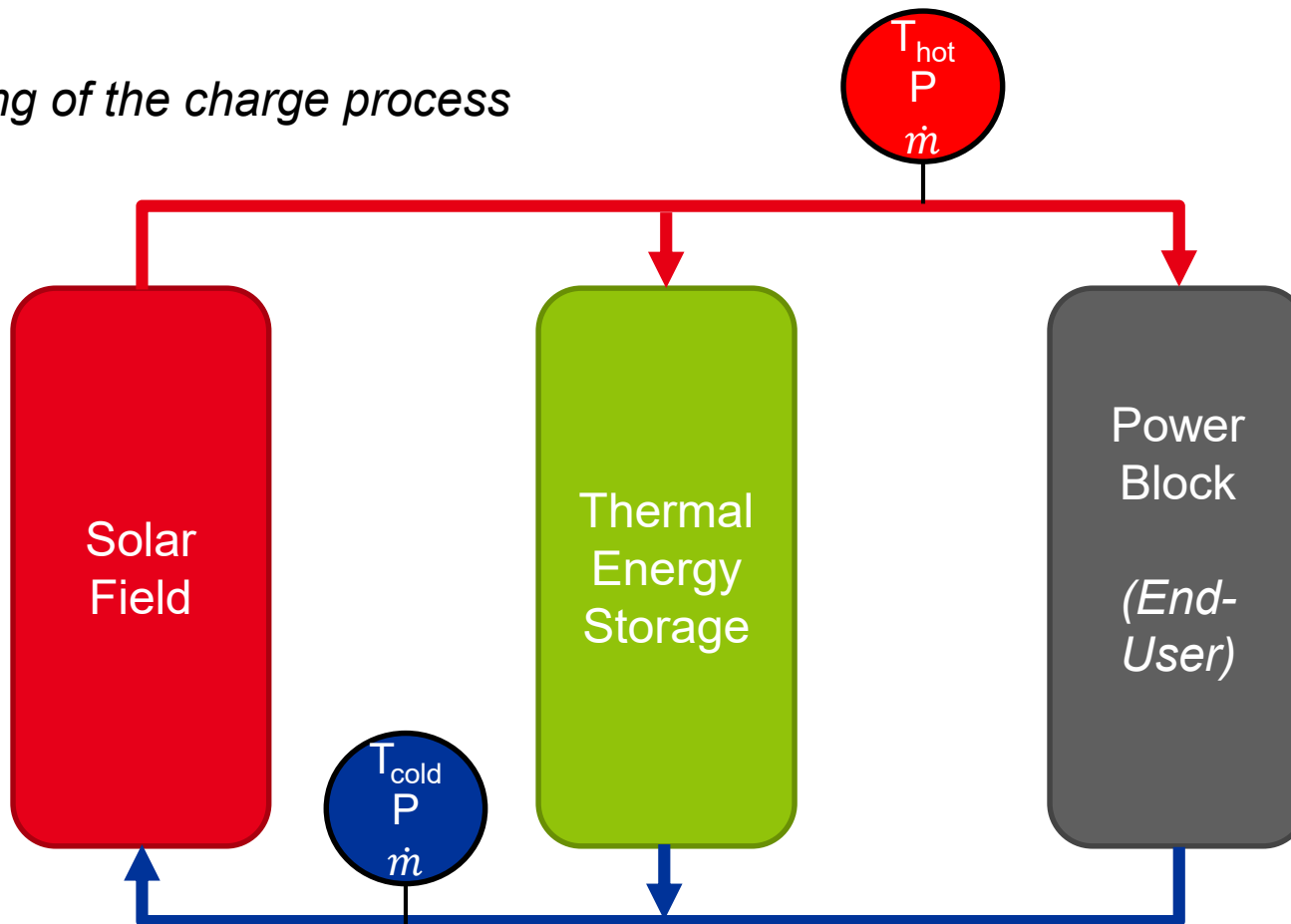
- Option A: Initial conditions with a given uniform temperature in the storage media
- Option B: After a given number of charge-discharge cycles



Influence of storage initial state on thermocline cyclic behavior; Temperature profiles; "Cn" refers to the n^{th} repetition of the cycle (Bruch, 2017) | 13

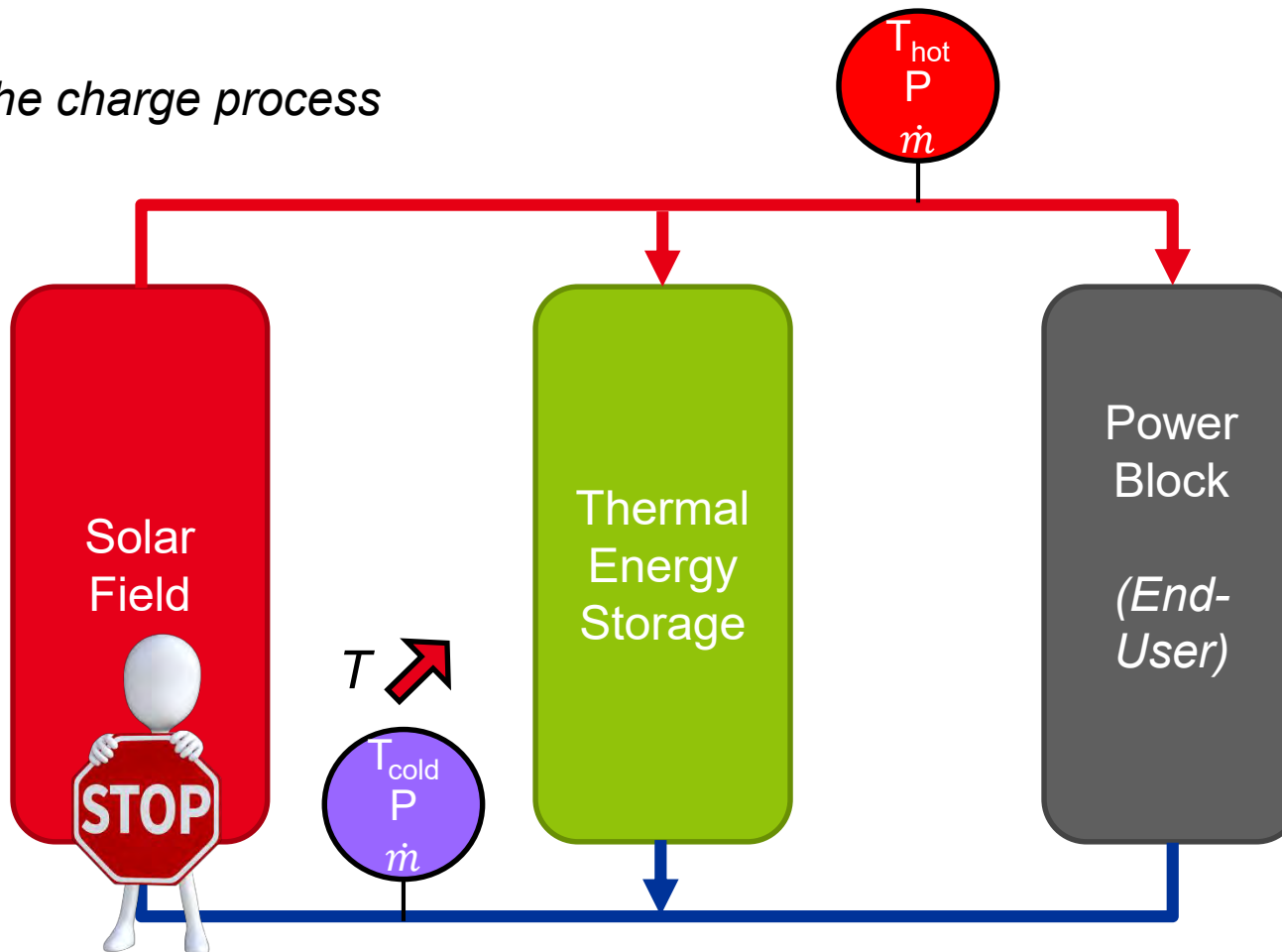
- **Full charge state:** after a charge process made under nominal conditions
 - End of full charge is obtained when the TES outlet HTF flow reaches the maximum solar field inlet conditions.

Beginning of the charge process



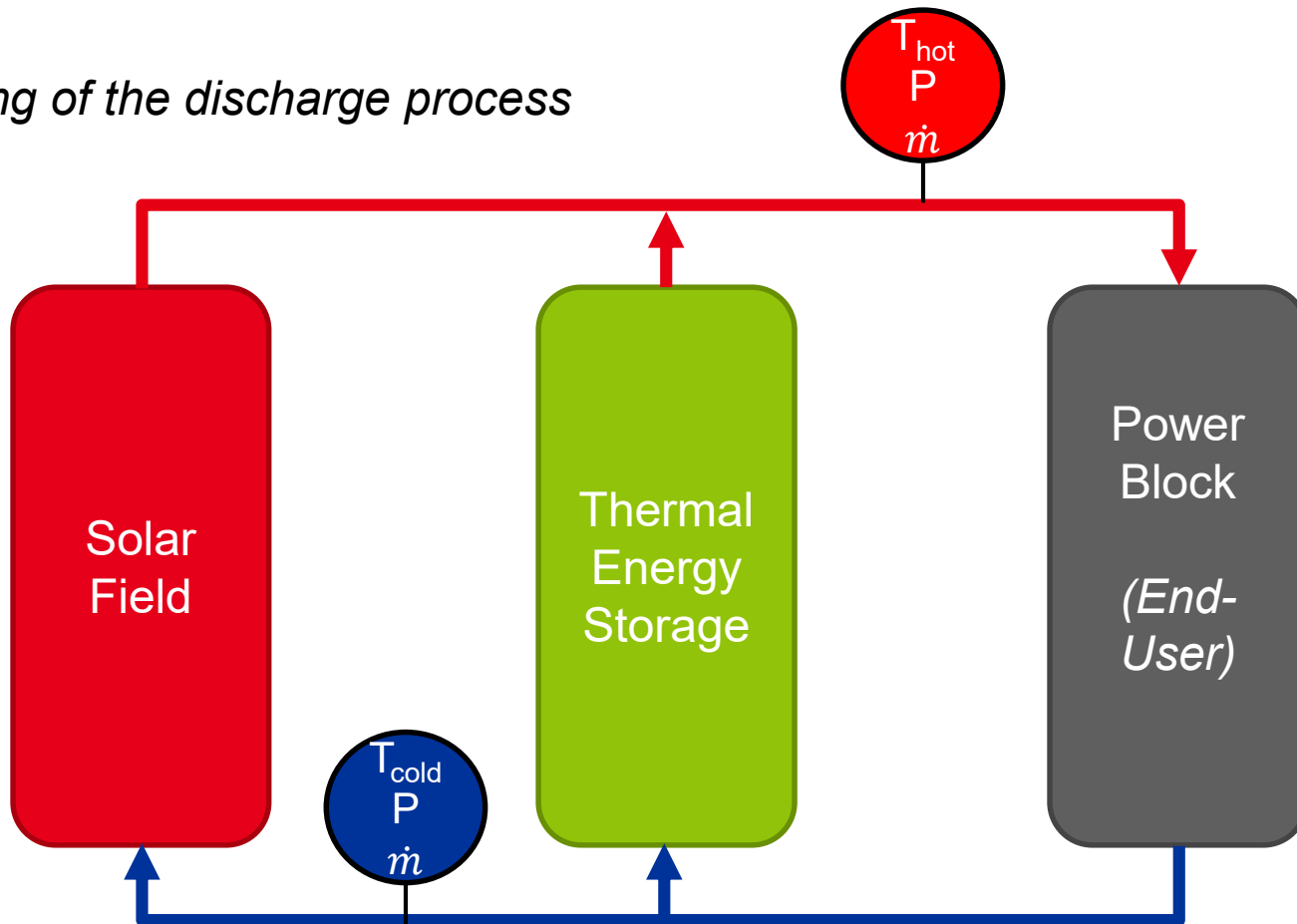
- **Full charge state:** after a charge process made under nominal conditions
 - End of full charge is obtained when the TES outlet HTF flow reaches the maximum solar field inlet conditions.

End of the charge process



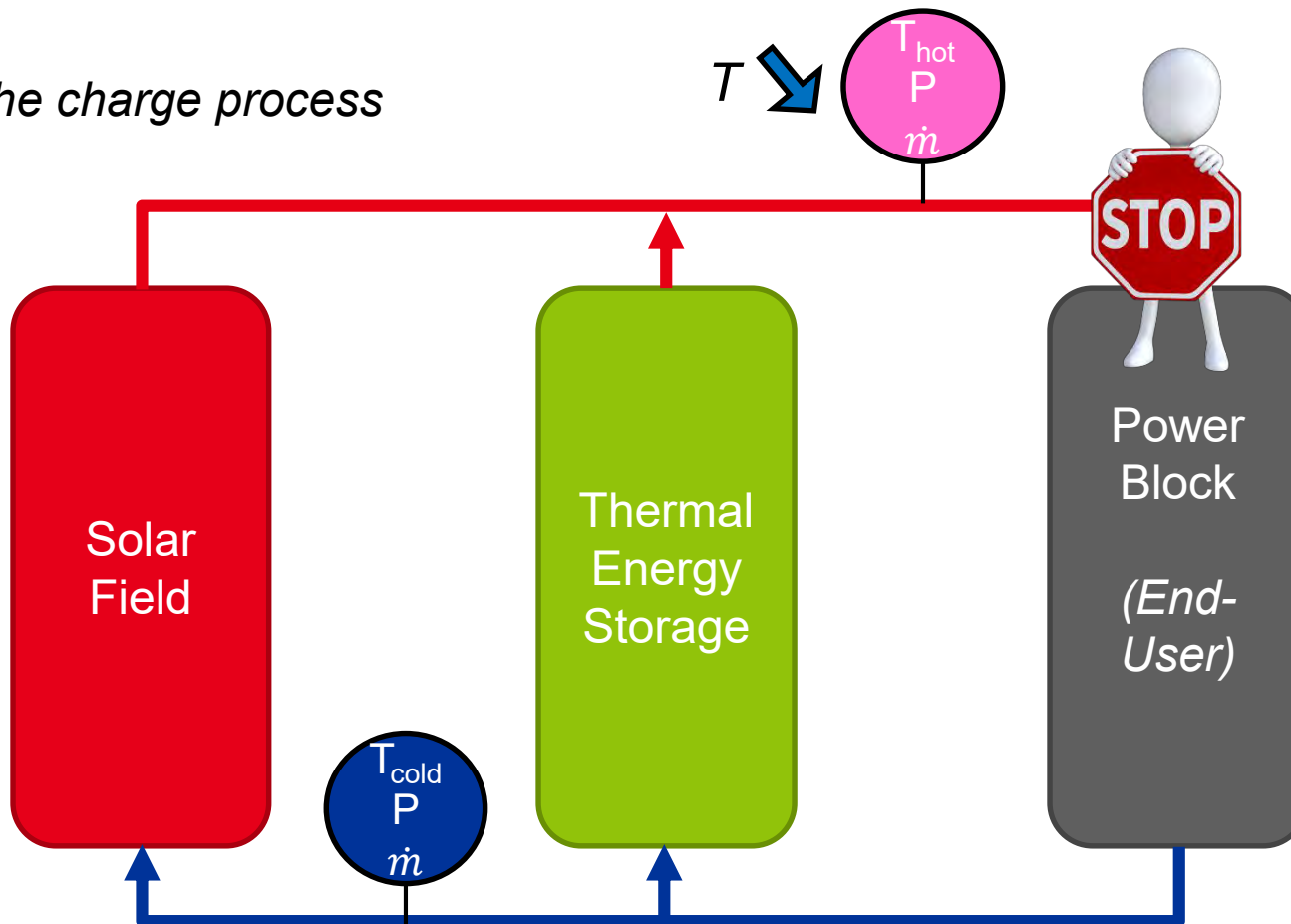
- **Full discharge state:** after a discharge process made under nominal conditions
 - End of full discharge is obtained when the TES outlet HTF flow reaches the minimum power block inlet conditions.

Beginning of the discharge process



- **Full discharge state:** after a discharge process made under nominal conditions
 - End of full discharge is obtained when the TES outlet HTF flow reaches the minimum power block inlet conditions.

End of the charge process



- Definitions

- Theoretical storage capacity (SC_{th}):** amount of energy that can be accumulated by the storage medium
- $SC_{th} = \sum_{storage\ materials} m (h_{charge,nominal} - h_{discharge,nominal})$
- Utilization Rate** = $\frac{SC}{SC_{th}}$

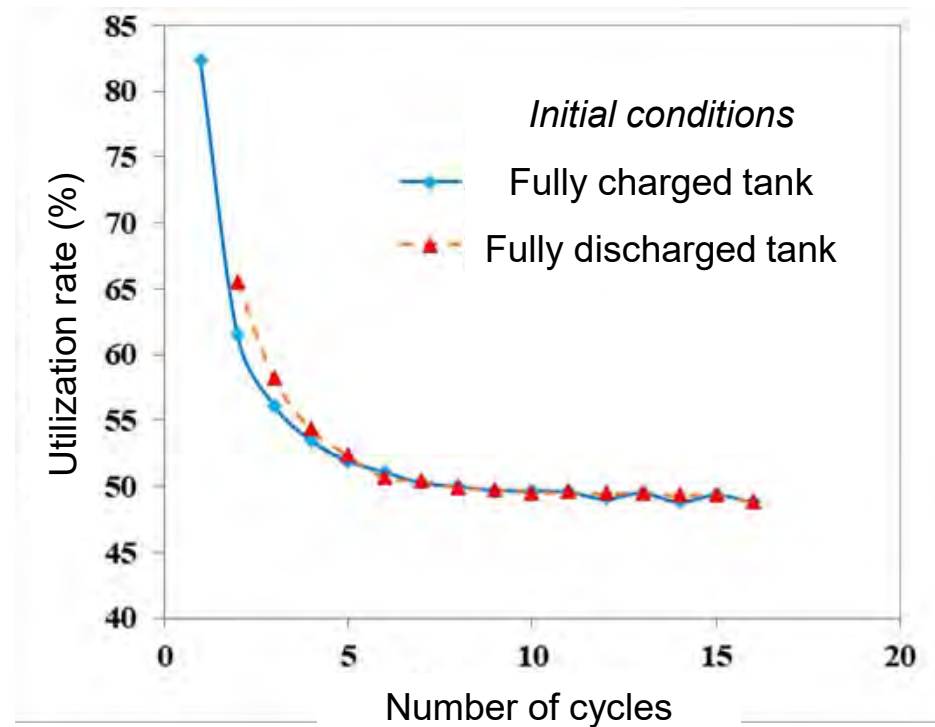
- Comments

- Like SC, UR depends on TES initial state and evolves from cycle to cycle.
- Alternative definition for sensible heat storage (Bruch 2017):

$$UR = \frac{\left(\int_{L_{tank}} T dz\right)_{charge} - \left(\int_{L_{tank}} T dz\right)_{discharge}}{(T_{charge} - T_{discharge})L_{tank}}$$

- Test procedure

- SC_{th} is calculated from literature material characteristics.
- The utilization rate can be evaluated from any storage capacity test.



Influence of storage initial state on thermocline cyclic behavior: Utilization rate

- Definition

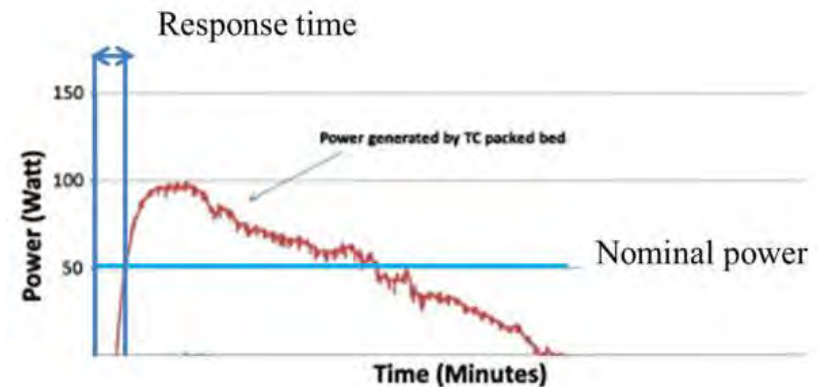
- P_{nom} is the nominal thermal power of the discharge. If relevant for the TES system, the nominal power of the charge ($P_{nom, ch}$) can be indicated next to the discharge value, clearly stating which belongs to charge and which to discharge.

- Comments

- It is a mean value all over the discharge process
- P_{nom} can be limited by
 - The maximum mass flow rate of the storage pumps
 - The maximum allowable pressure drop in the TES system
 - The heat transfer rate between the HTF and the storage material (ex PCM)
- Directly linked to the nominal discharging time ($t_{discharge}$) and charging time (t_{charge})
 - $t_{discharge} = \frac{SC}{P_{nom}}$ & $t_{charge} = \frac{SC_{ch}}{P_{nom, ch}}$

- Test procedure

- P_{nom} can be estimated from SC and $t_{discharge}$ under nominal discharge conditions



- Definition
 - Energy lost by the thermal storage system during time "t" from the instant at which it is at storage level A, without charging or discharging.
- Comments
 - Thermal losses can hardly be extrapolated from small to large systems.
 - Difficult to estimate
 - Order of magnitude:
 - A few degrees decrease per hour for lab-scale TES
 - A few degrees decrease per day for industrial-scale TES
- Test procedures (examples)
 - Isothermal test
 - Losses offsetting with heat tracing
 - No fluid flow
 - Energy balance at constant temperature
 - Balance between inlet and outlet enthalpies at constant inlet conditions after temperature stabilization
 - Comparison between two standardized charging-discharging tests
 - With and without idle time between end of charge and beginning of discharge

- Definition

- In consecutive charge and discharge:

$$\eta_{TES} = \frac{E_{discharge}}{E_{charge}}$$

- When considering full discharge conditions:

$$\eta_{TES} = \frac{SC}{SC_{ch}}$$

- Comments

- η_{TES} depends on TES initial state and varies from cycle to cycle in case of repetitive cycles.
 - This is a 1st law of thermodynamics approach.
 - Energy quality (exergy) degradation is not taken into account.

- Test procedure

- Derived from SC and SC_{ch} values obtained from consecutive charge and discharge cycles

- Definition

- Indicates the degree of thermal stratification in a storage device.
- Generated entropy ΔS can be a representative value of the thermal stratification

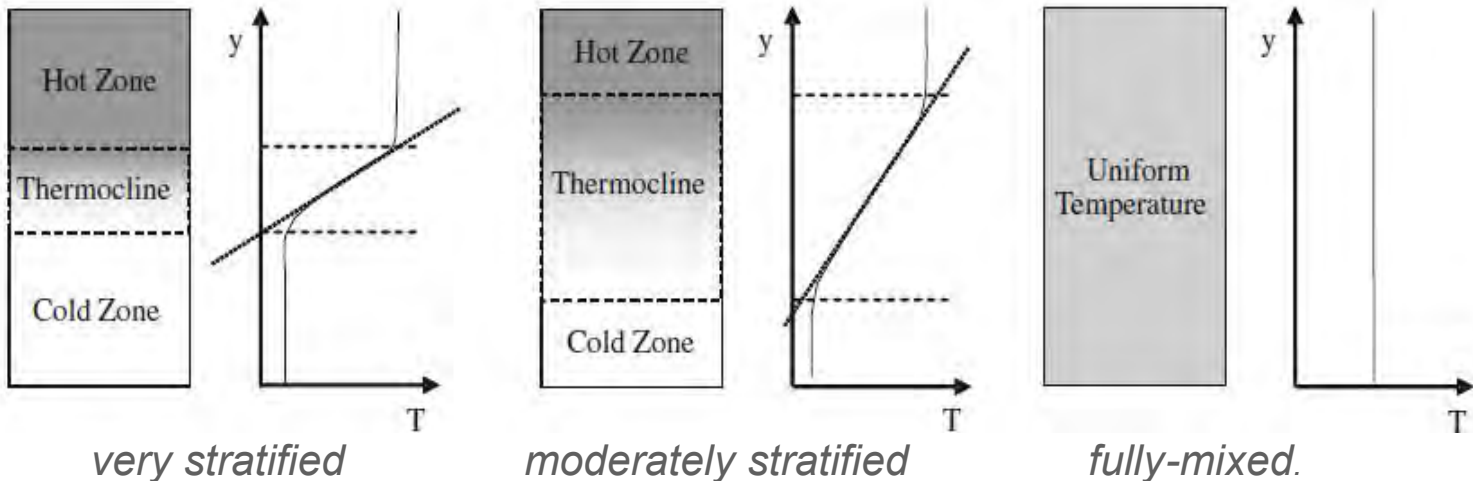
$$\Delta S_{fully-mixed} > \Delta S_{real} > \Delta S_{stratified}$$

- No agreed definition for this concept

- Comments

Only for thermocline or regenerative storage
Measured on storage media side

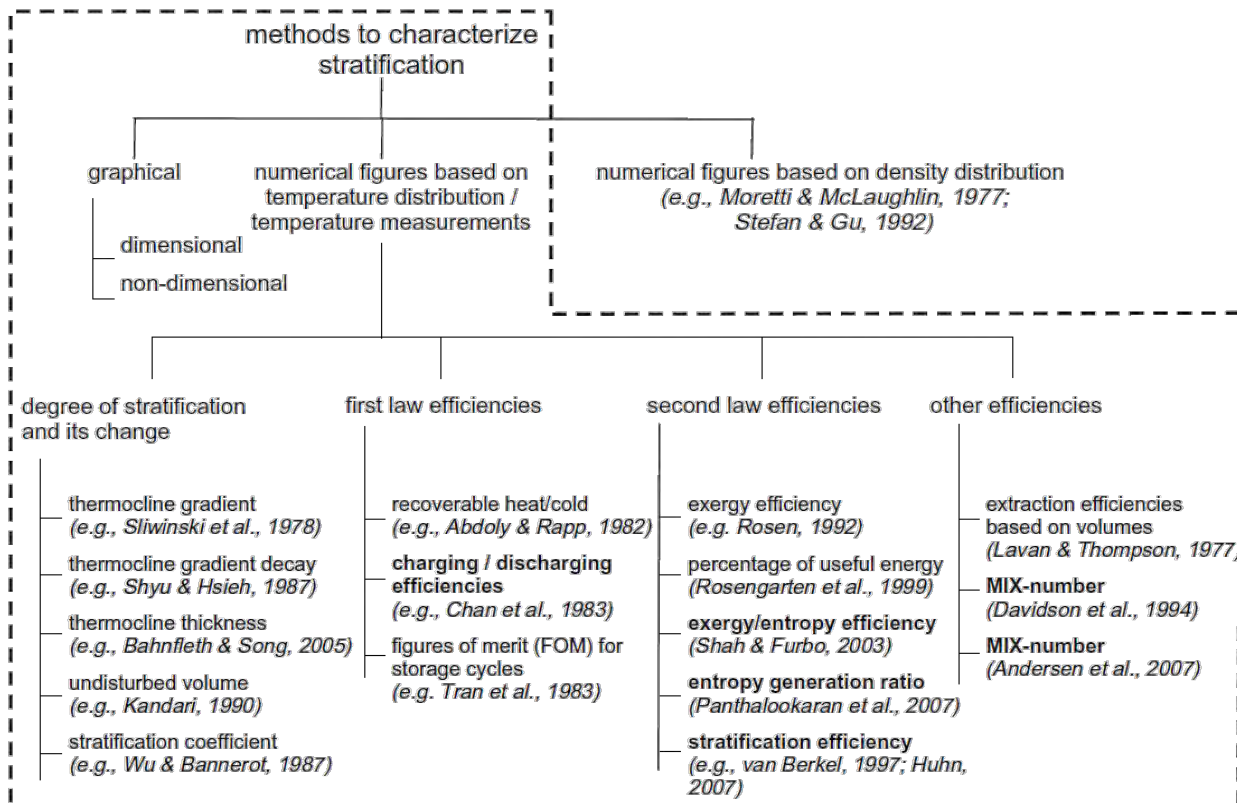
- Thorough instrumentation of the tank is needed



Different stratification degrees in a tank with the same energy content (Haller et al., 2009)

- Possible test procedures

- Thermocline thickness evaluation (Bahnfleth, 2005)
- MIX-number (Andersen, 2009)
- Stratification efficiency (Huhn 2007, Haller 2010): $\eta_{strat} = 1 - \frac{\Delta S_{irr*}^{exp}}{\Delta S_{irr*}^{mix,0}}$



- Is **storage density** a KPI for CSP plants?
 - Area needed for storage \ll Area needed for solar field
 - Storage density is critical for other applications
 - In buildings
 - If heat must be transported



Density of the
storage media



Density of the
storage tank



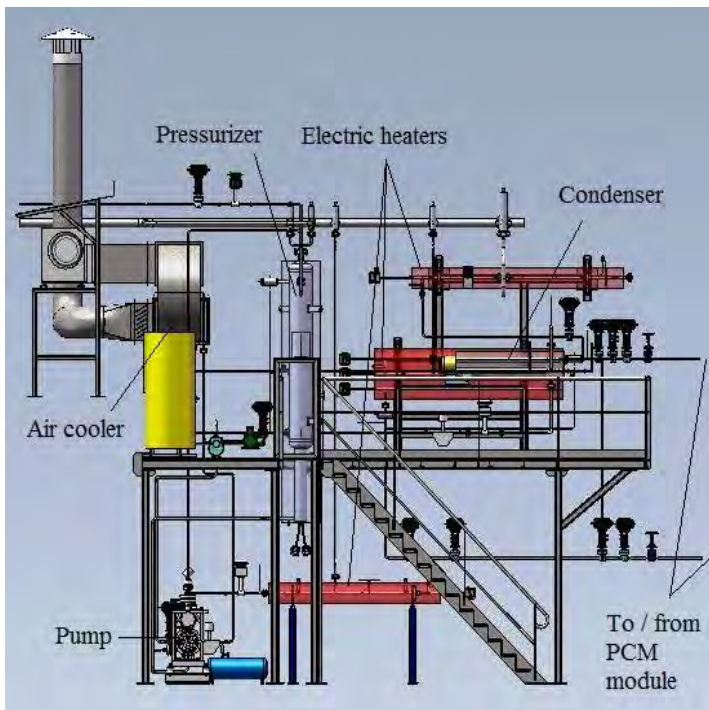
Density of the
storage system

- Response time
- Auxiliary energy ratio
- Minimum cycle length
- Partial load suitability

CASE STUDY

**LATENT HEAT STORAGE
PERFORMANCE ASSESSMENT**

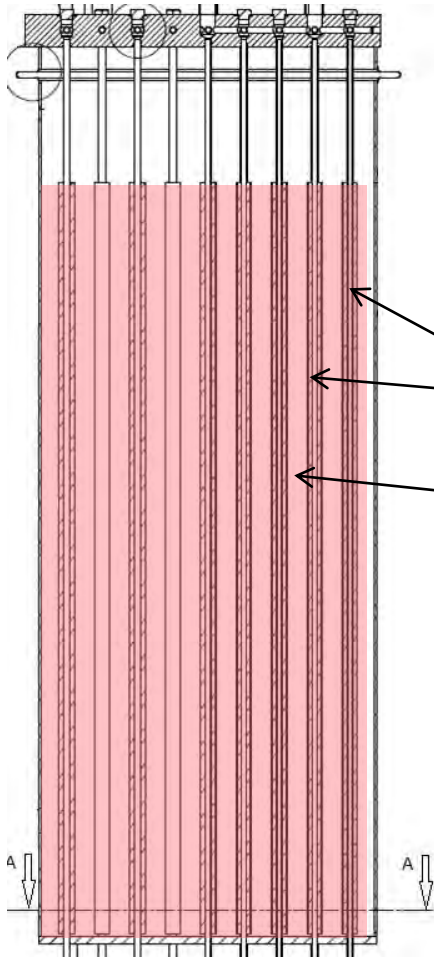
- LHASSA experimental facility at the CEA Grenoble
 - operating conditions similar to those of commercial CSP DSG plants (145 bar, 350 °C)
 - high pressure water-steam closed loop
 - wide range of charge and discharge transients



LHASSA test facility



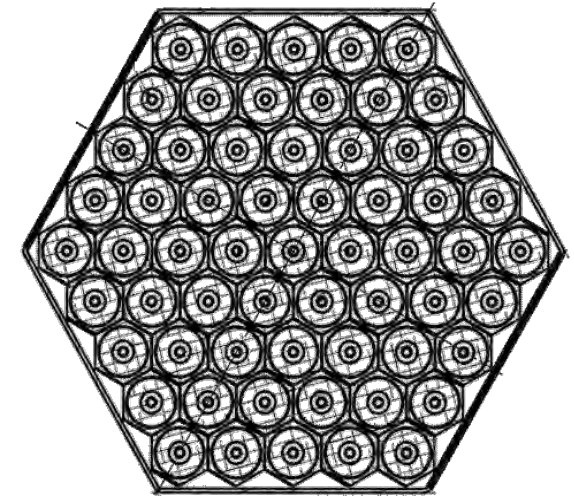
PCM module



Vertical bundle of parallel tubes with high pressure steam/water inside and a static PCM volume outside

Finned tubes

PCM volume

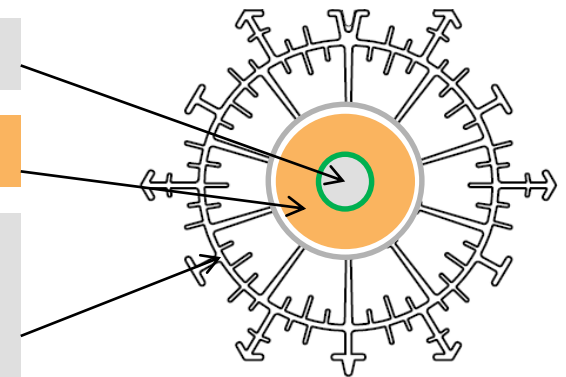


A-A section

Tubes

Fins

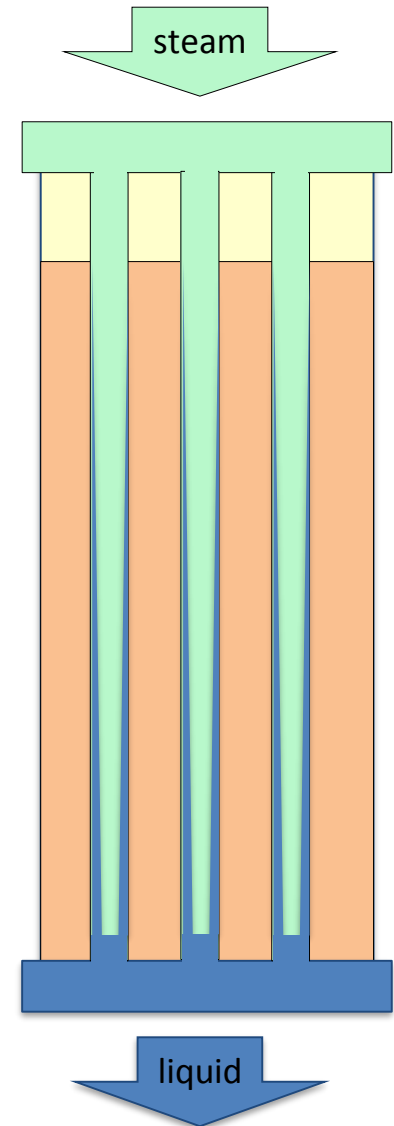
Heat transfer enhancement by aluminum inserts around the vertical finned tubes



- Objectives : validating the thermo-hydraulic behavior of the storage module under realistic operating conditions
 - Inlet mass flow is set by the operator
- Two control strategies
 - Sliding pressure
 - Controlled pressure to keep water level constant
 - Fixed pressure (in charge)
 - With variable water level in the tubes
- In **charging mode**
 - Low liquid water level in the test section
 - Steam condenses causing the melting of the PCM



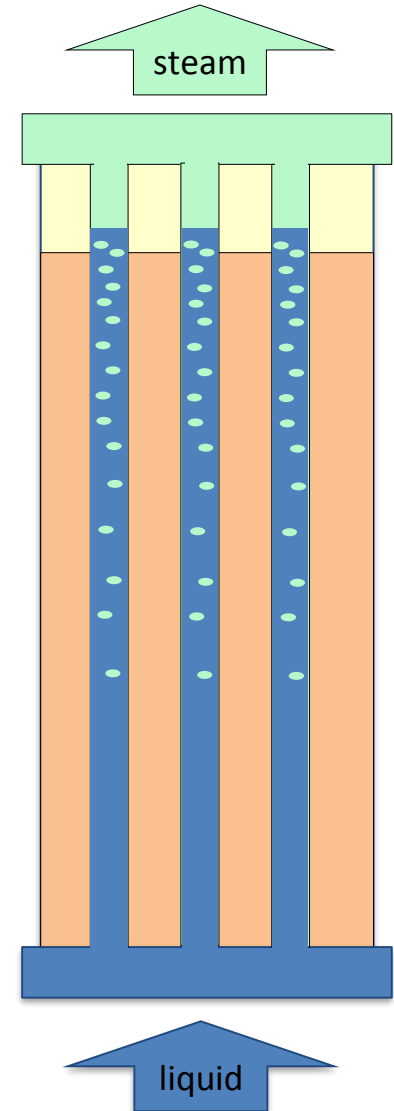
Full charge process compatible with the storage charging time of a commercial CSP plant on summer days



- Objectives : validating the thermal performances of the storage module under realistic operating conditions
 - Inlet mass flow is set by the operator
- Two control strategies
 - Sliding pressure
 - Controlled pressure to keep water level constant
 - Fixed pressure (in charge)
 - With variable water level in the tubes
- In **discharging mode**
 - High liquid water level in the test section
 - Liquid PCM solidifies causing the evaporation of the liquid water



Full discharge process corresponds to a typical discharging time when storage is used during peak loads after sunset



- Calculated on HTF side

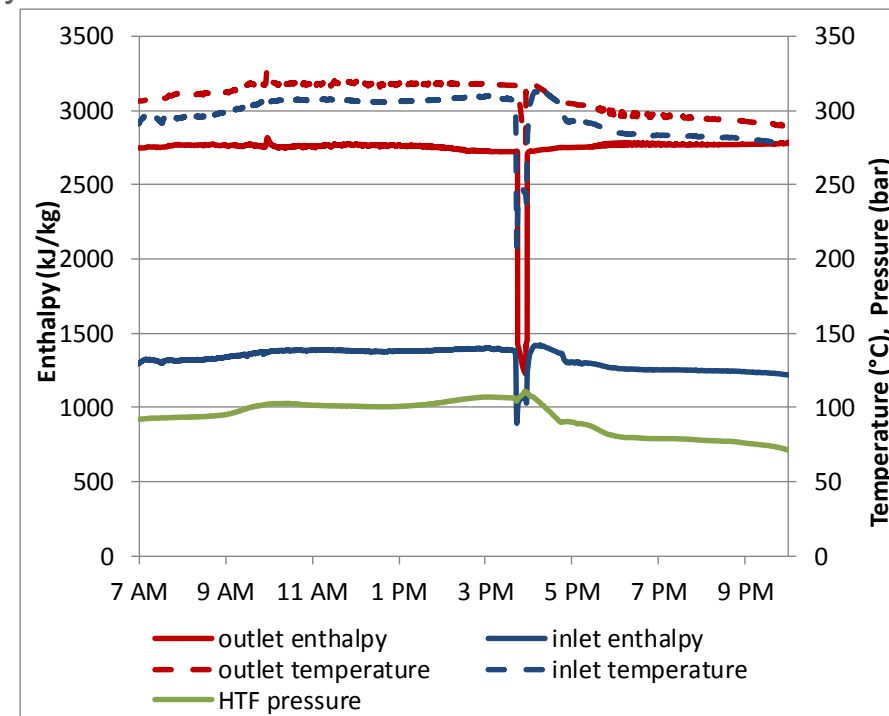
- $$SC = \int_{initial\ conditions}^{full\ discharge\ conditions} [\dot{m}(h_{outlet} - h_{in})] dt$$
- Inlet: liquid water
 - $h_{in} = \text{enthalpy}(T_{in}, P_{in})$
- Outlet: steam
 - If $T_{out} > T_{sat} + 2^{\circ}\text{C}$, $h_{out} = \text{enthalpy}(T_{out}, P_{out})$
 - Else, h_{out} is calculated thanks to an energy balance at the condenser boundaries

- Discharge

- Initial state: $T_{PCM} \sim 310^{\circ}\text{C}$
- Inlet temperature: $T_{sat} - 10^{\circ}\text{C}$

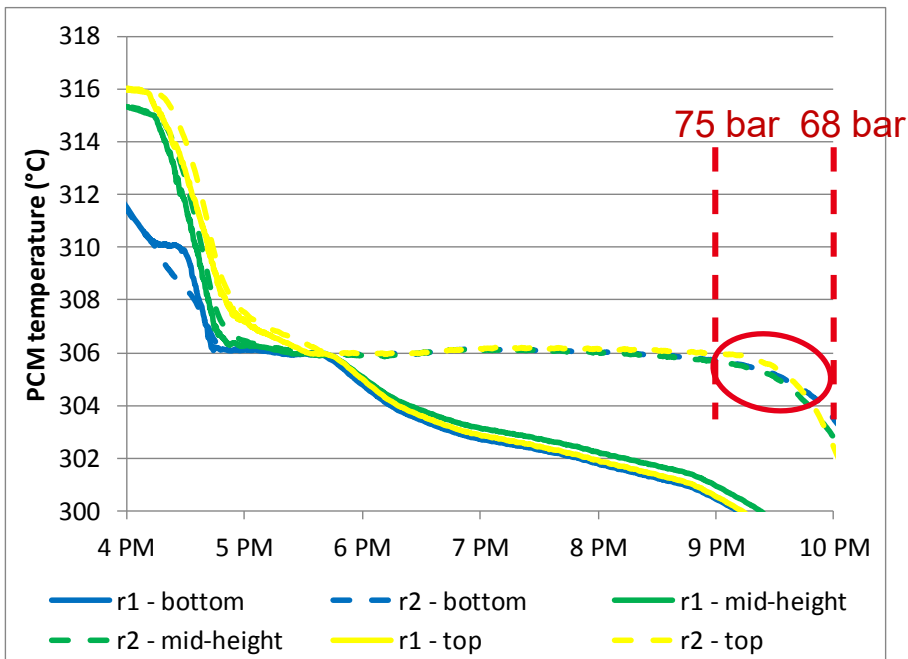
- SC results

- End of discharge @ 75 bar
255,6 kWh
- End of discharge @ 68 bar
316,5 kWh

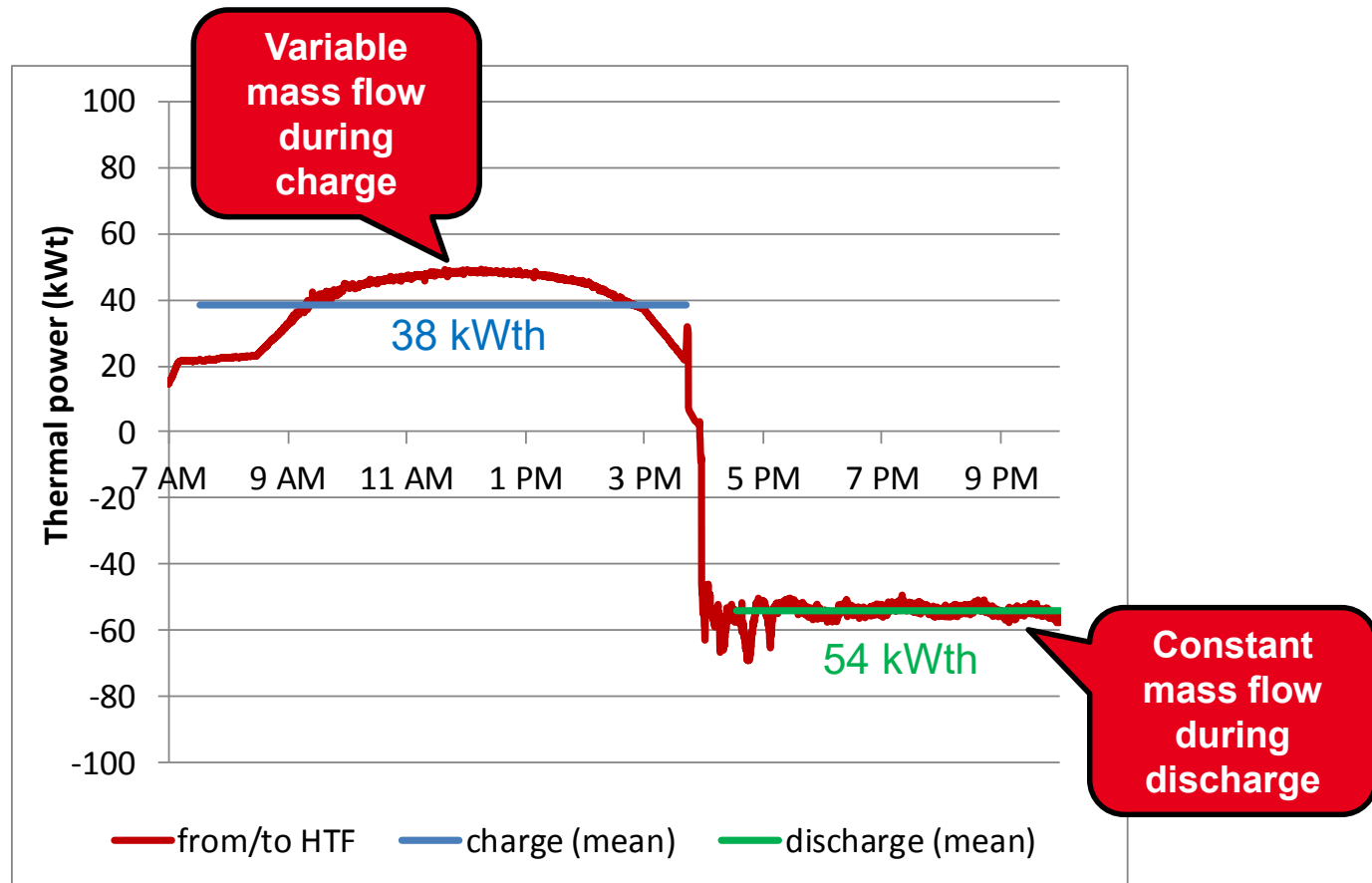


- Theoretical storage capacity (SC_{th})
 - Depends on temperature references!

| | | | | |
|-------------------------------------|-------------|------------|------------|------------|
| PCM total mass | kg | 6330 | | |
| PCM latent heat | kJ/kg | 172 | | |
| Total latent heat | kWht | 302 | | |
| Phase change temperature | °C | 306 | | |
| Design hot temperature | °C | 315 | 310 | 310 |
| Design cold temperature | °C | 295 | 294 | 301 |
| Total sensible heat (PCM) | kWht | 58 | 48 | 26 |
| Total sensible heat (metal) | kWht | 16 | 13 | 7 |
| Theoretical storage capacity | kWht | 376 | 363 | 336 |
| % sensible heat | | 20% | 17% | 10% |



- Utilization rate
 - End of discharge @ 75 bar
mean $T_{PCM} \sim 301^{\circ}\text{C}$
UR = 76%
 - End of discharge @ 68 bar
mean $T_{PCM} \sim 294^{\circ}\text{C}$
UR = 87%

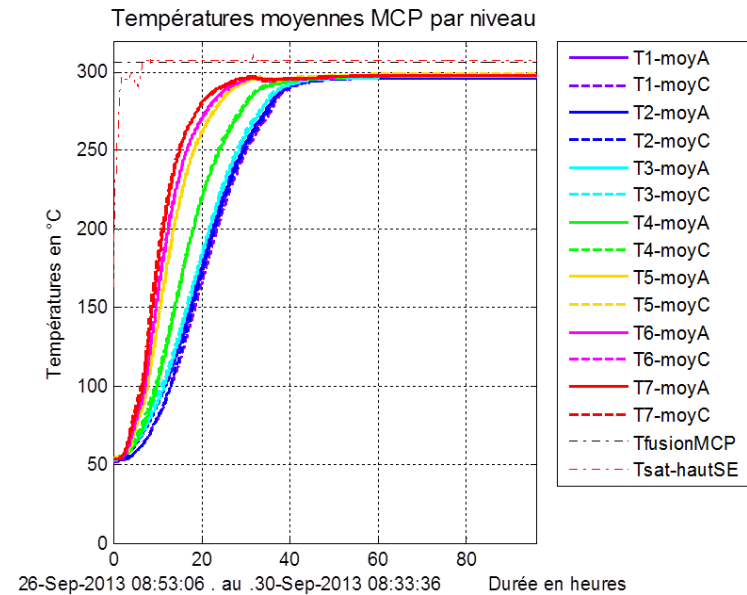
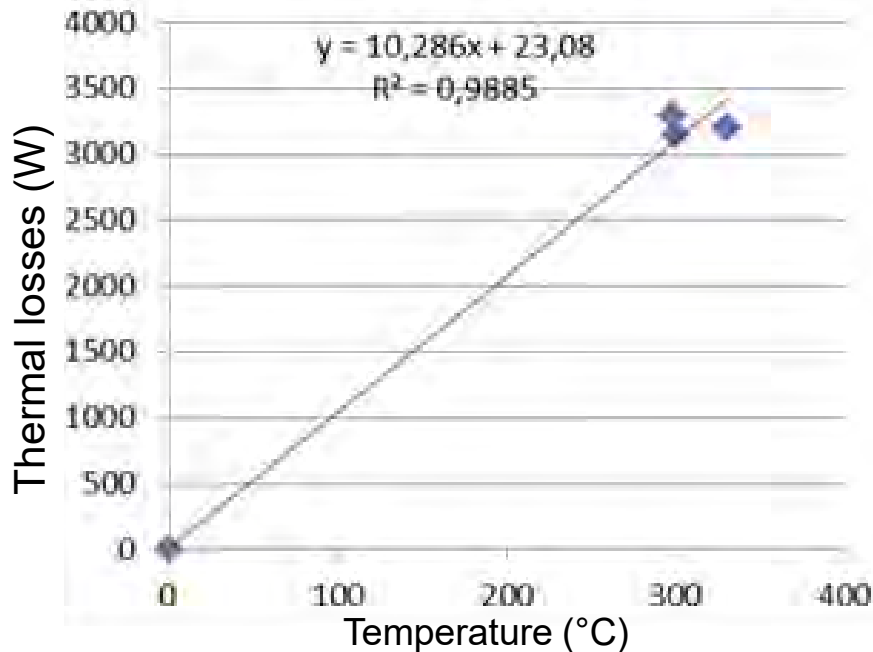


- Repeated isothermal tests
 - Temperature maintained constant
 - Thanks to electrical heat tracing

$$P_{\text{losses}} = P_{\text{elec}}$$

Results

- 2,88 kW_{th} at 300 °C
- About 5% of P_{nom}



| TEST | CHARGE | | | | DISCHARGE | | | |
|---------------|-----------|--|----------|----------------------|-----------|----------------------------|--------------|----------------------|
| | Mass flow | Charge state (Ec/E _{latent}) | Duration | Final pressure (bar) | Mass flow | Storage efficiency (Ed/Ec) | Duration | Final pressure (bar) |
| Partial load | Variable | 49,9% | 4h18 | 94,1 | Constant | 90,1% 100,0% | 3h06 3h23 | 75,0 73,6 |
| Partial load | Constant | 28,4% | 1h46 | 101,6 | Constant | 89,5% | 1h38 | 75,0 |
| Complete load | Variable | 107,5% | 8h11 | 104,8 | Constant | 75,7% 94,2% | 4h44 5h51 | 75,0 68,1 |



- η_{TES} should be estimated in « cycling conditions »
 - With storage conditions at the end of discharge equal to those at the beginning of charge
 - If not respected, storage efficiency may > 100%

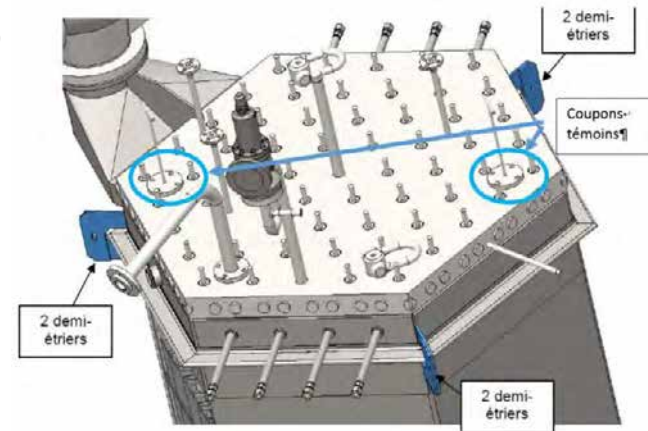
- **TES performance depends strongly on the end-user!**
 - Basic technical KPI cannot be defined independently from the whole process
- **Many KPI vary depending on the initial state of the TES system**
 - e.g. for thermocline TES, the initial state depends on previous charge-discharge cycles until stable initial conditions are reached
- **Calculation on the HTF side, but you need information from inside the tanks...**
- **Test procedures for KPI estimation should be thoroughly described**
 - Initial and final conditions
 - Inlet and outlet flow conditions (mass flow, pressure, temperatures, ...)

DURABILITY ISSUES

- TES Lifetime is another KPI
 - Expected lifetime in CSP plants is about 20 to 30 years
 - Difficult to demonstrate
 - Durability and corrosion tests must be performed
- Issues
 - Performance degradation
 - Safety issues: risk of failure
- Specific indicators
 - Degradation of the above-mentioned performance indicators
 - Corrosion mechanisms of metals by HTF and storage media
 - Passivation
 - Intergranular / Pit corrosion
 - Composition and thermo-physical properties of the storage media

CASE STUDY: PCM STORAGE

- Direct measurement on tubes and fins: *corrosion rate*
 - From a representative sample removed when the salt is liquid
 - Metal loss rate assessment (weighting, thickness measure)
 - SEM and XRD measurements
- Indirect measurement on PCM: *Fe release due to corrosion and salt purity*
 - ICP analysis for Fe release
 - Calorimetry measurement (NaNO₃ Vs NaNO₂)
- Indirect measurement on gases: *initial composition and composition evolution*
 - O₂ / N₂ measurements to monitor chemical equilibriums



MERCI POUR VOTRE ATTENTION

THANKS FOR YOUR ATTENTION

Commissariat à l'énergie atomique et aux énergies alternatives
17 rue des Martyrs | 38054 Grenoble Cedex
www-liten.cea.fr

Établissement public à caractère industriel et commercial | RCS Paris B 775 685 019

- IEA Solar Thermal Electricity Technology Roadmap, OECD/IEA, Paris, 2014.
- P. Denholm, Y.-H. Wan, M. Hummon and M. Mehos, "An Analysis of Concentrating Solar Power with Thermal Energy Storage in a California 33% Renewable Scenario," NREL Report No. TP-6A20-58186, National Renewable Energy Laboratory, Golden, CO, 2013.
- IEA Technology Roadmap: Concentrating Solar Power, OECD/IEA, Paris, 2010.
- W.-D. Steinmann, Thermal energy storage systems for concentrating solar power (CSP) technology, in Advances in Thermal Energy Storage Systems. In Woodhead Publishing Series in Energy, Woodhead Publishing, 2015, Pages 511-531.
- NREL, Survey of Thermal Storage for Parabolic Trough Power Plants, NREL/SR-550-27925, 2000.
- Goldstern, Walter Steam storage installations. Springer-Verlag OHG, Berling / Göttingen / Heidelberg, 1970.
- NREL website, <https://www.nrel.gov/csp/solarpaces>.
- IRENA Renewable energy technologies: cost analysis series, Concentrating Solar Power, June 2012.
- NREL Technical Report, Concentrating Solar Power Gen3 Demonstration Roadmap, TP-5500-67464, January 2017.
- P. Denholm and M. Hummon, Simulating the Value of Concentrating Solar Power with Thermal Energy Storage in a Production Cost Model. Technical Report NREL/TP-6A20-56731, November 2012.
- U. Herrmann and D. W. Kearney, Survey of thermal energy storage for parabolic trough power plants, J Sol Eng, 124:145, 2002.
- P. Garcia, M. Olcese, S. Rougé, Energy Procedia 69, 842 – 849 (2015).
- Laing D, Bahl C, Bauer T, Lehmann D, Steinmann WD. Thermal energy storage for direct steam generation. Solar Energy 85; 2011. p. 627–633.
- M. Haller, C Cruickshank, W. Streicher, S. Harrison, E. Andersen, S. Furbo: Methods to determine stratification efficiency of thermal energy storage processes - Review and theoretical comparison. In: Solar Energy 83 (2009), Oct, Nr. 10, S. 1847–1860. – ISSN 0038–092X
- Zavattoni, S.A., Barbato, M.C., Zanganeh, G., Pedretti, A., High temperature thermocline TES – Effect of system pre-charging on thermal stratification. AIP Conference Proceedings Volume 1734, 31 May 2016, 21st International Conference on Concentrating Solar Power and Chemical Energy Systems, SolarPACES 2015; Cape Town; South Africa.
- Andersen E., Furbo S., Fan J., Multilayer fabric stratification pipes for solar tanks. Solar Energy 81 (2007) 1219–1226.
- A. Bruch, S. Molina, T. Esence, J.F. Fourmigue, R. Couturier, Experimental investigation of cycling behaviour of pilot-scale thermal oil packed-bed thermal storage system, Renewable Energy 103 (2017) 277-285
- Applications of Thermal Energy Storage in the energy transition, benchmarks and developments: Public Report of IEA ECES Annex 30, September 2018

SFERA-III

Solar Facilities for the European Research Area

1st Summer School “Thermal energy storage systems, solar fields and new cycles for future CSP plants”
WPI Capacity building and training activities
Odeillo, France, September 9th-11th 2019



Next generation of CSP plants: technology developments and market opportunities

Manuel Romero, IMDEA Energy, Spain

Institute
IMdea
energy

NETWORKING





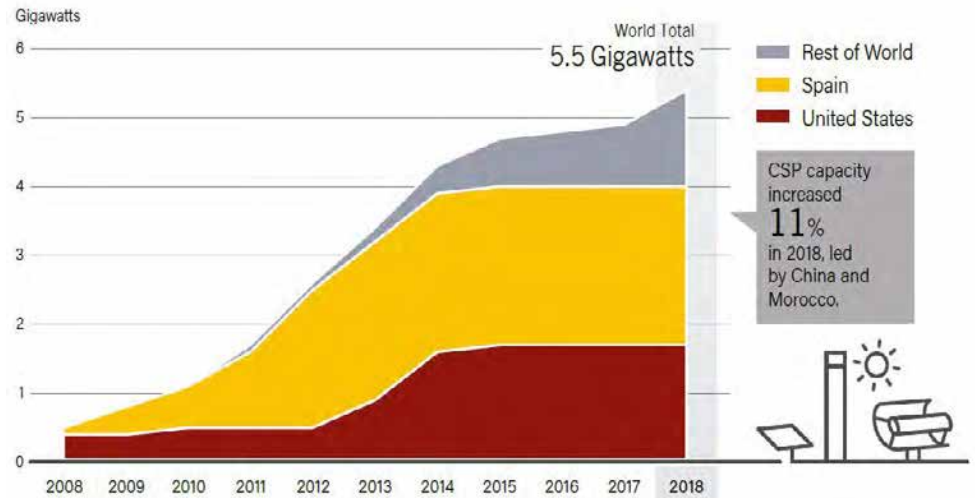
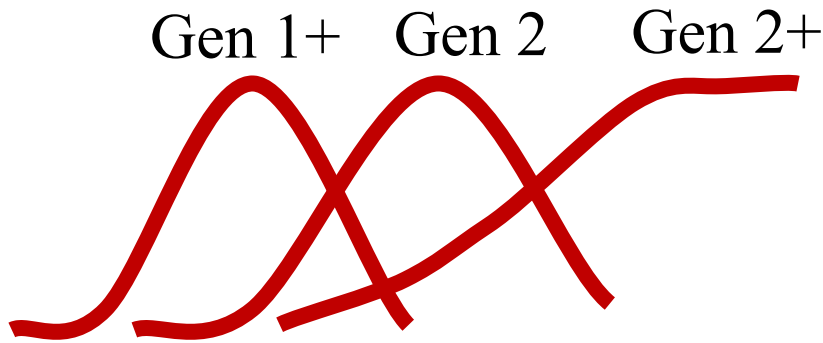
Structure presentation

-Where are we coming from?

- Where are we now?

-Where are we going to?

Three market waves in few years! CSP market experience mostly happened in just 13 years



Spain 2007-2013

- Early market
- Routine operation
- Industrial network
- 50 MW units
- Storage/capacity factor
- Feed-In-Tariff (FIT)

USA 2013-2015

- Scaling-up
- 100-400 MW
- Utility PPA
- Dispatchability value
- Environmental impact

World 2015-2022

- Globalization (MENA, SA, Chile, India, China)
- Indigenization
- Market competition
- Hybridization (CSP/PV, Bio, Fossil)

There are few projects in the short term pipeline but ambitious programs are expected when a thorough approach for the Energy Transition will be done in Sunbelt countries

Evolución de la potencia instalada termosolar a nivel mundial



FRANCE

Slowly, almost imperceptibly, the platform bearing a handful of white powder rose until it reached the focal point of the parabolic mirror overhead. Then, before the eyes of

scientists and engineers at the recent Mont-Louis solar energy symposium, the powder suddenly burst into white heat brighter than any diamond.

The powder was zirconium oxide with a melting point

steel daily for it will turn solar heat into the equivalent of 1,000 kilowatts of electrical energy.

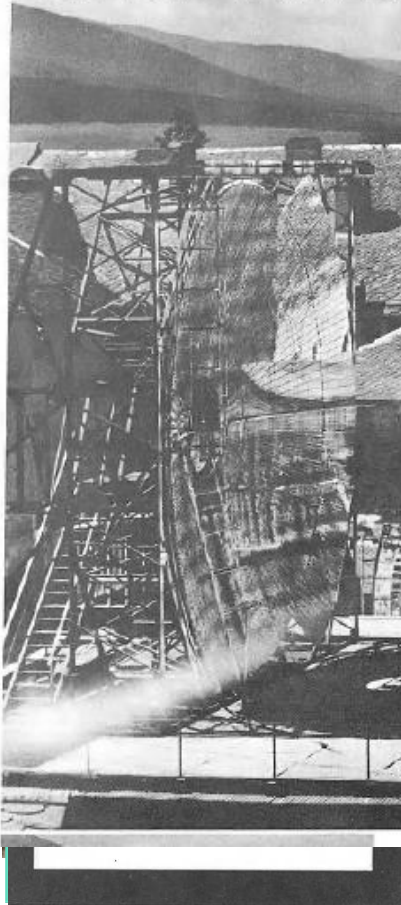
Prof. Trombe, who gave these facts in an interview, is a tall, lean man in his forties and far more at home tinkering with a parabolic mirror than presiding over an international symposium. This probably explained the success of the symposium—where tea was brewed in laboratory beakers and the future of solar energy discussed in a handsome 17th century room heated by the crackling logs of a huge fireplace.

s, CNRS,

an fifty
ont-Louis, a

THE WORLD'S FIRST SUN-OPERATED INDUSTRIAL PLANT

SOLAR FURNACE FRESH WATER



ISRAEL

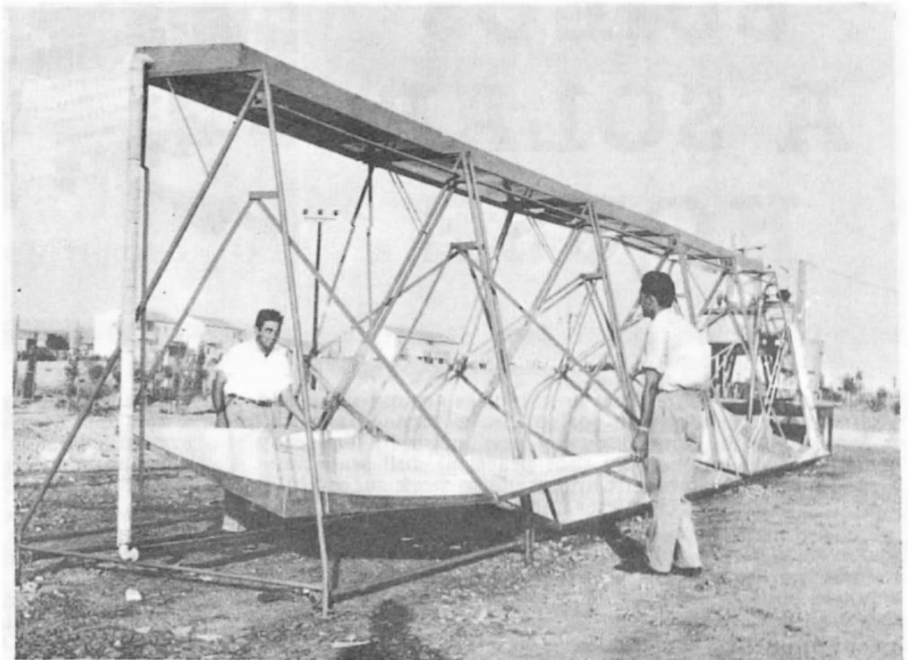
The world's first industrial plant operating on solar energy is now under construction in Israel at ancient Beersheba, the home of the Negev Institute for Arid Zone Research.

This is one of the applications of the solar energy programme which Israel is now carrying out on a broad front described by Dr. Harry Tabor, director of the National Physical Laboratory in Jerusalem and one of the fifty scientists and engineers who participated in the Mont-Louis Solar Energy Symposium.

A lean, alert man who obviously has little use for the "science fiction" approach to solar energy, Dr. Tabor methodically traced, in an interview, the practical steps which his sun-baked country is taking to put the sun to work.

"We are trying to answer four questions at the Negev Institute", he stated, and then he ticked them off:

- Can we use solar energy to cool houses?
- Can we use solar energy to generate steam for a factory?
- Can we use it to run a small power unit for farmers?
- What are the long-term prospects of building a solar power station?



Israel National Research Council

FUEL-POOR BUT SUN-RICH, Israel has embarked on a broad programme of solar energy research including the development of steam for industries and the production of small power units. At the Negev Research Institute, Israeli scientists have built the new type of solar energy collector unit shown above. This consists of simple curved mirrors which reflect heat upwards to collectors fixed overhead. Use of black surfaces cuts heat losses by about four fifths, enabling unit to compete with more expensive systems. Five hundred units will save about 500 tons of fuel oil a year.

Gen 1 → Gen 1+

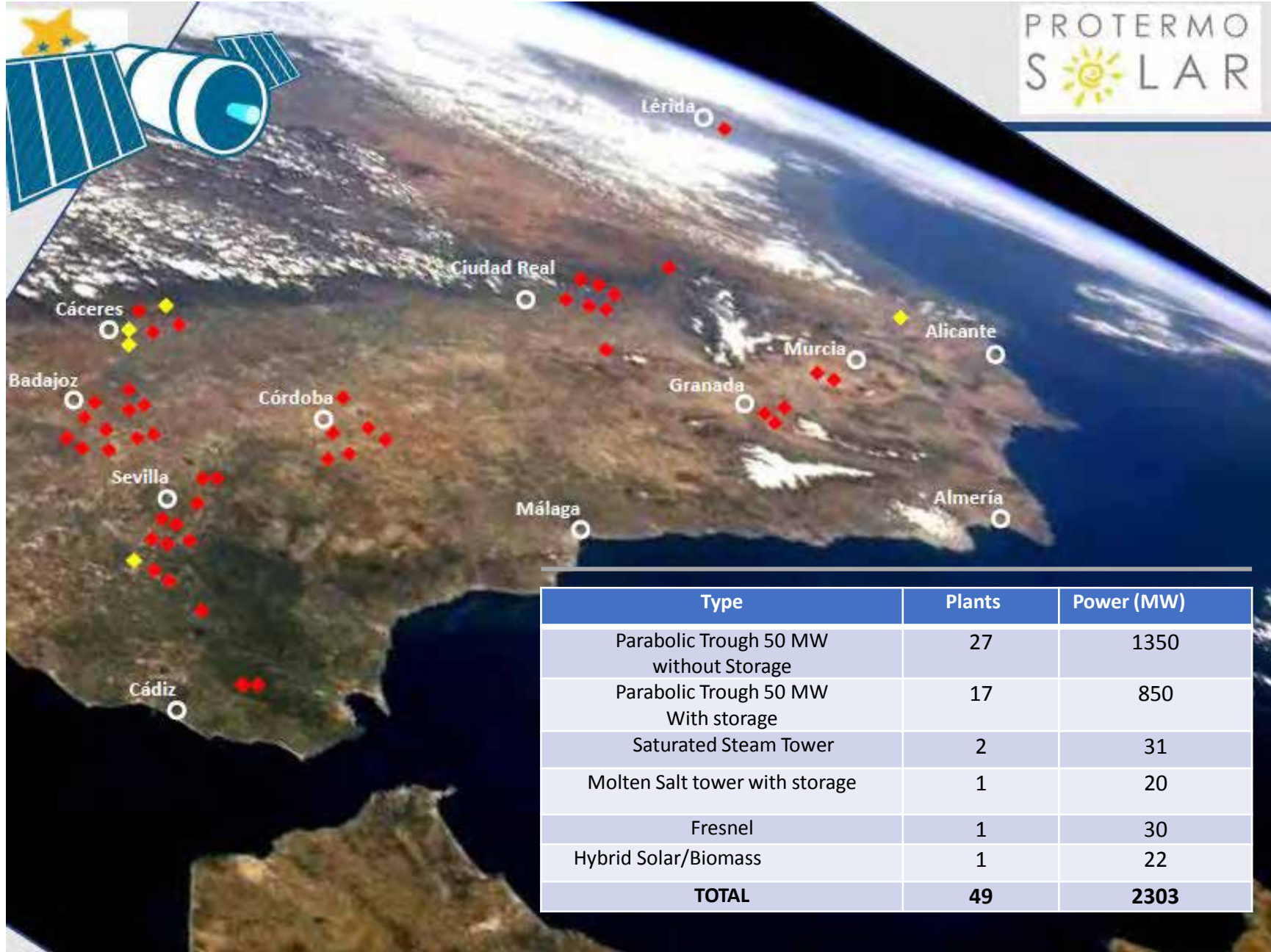
Decades of R&D leading to early markets



Spain 2007-2013



Early market
Routine operation
Industrial network
50 MW units
Storage/capacity factor
Feed-In-Tariff (FIT)



| Type | Plants | Power (MW) |
|--|-----------|-------------|
| Parabolic Trough 50 MW without Storage | 27 | 1350 |
| Parabolic Trough 50 MW With storage | 17 | 850 |
| Saturated Steam Tower | 2 | 31 |
| Molten Salt tower with storage | 1 | 20 |
| Fresnel | 1 | 30 |
| Hybrid Solar/Biomass | 1 | 22 |
| TOTAL | 49 | 2303 |

75-MW Solar Thermal Power Plant in Nevada



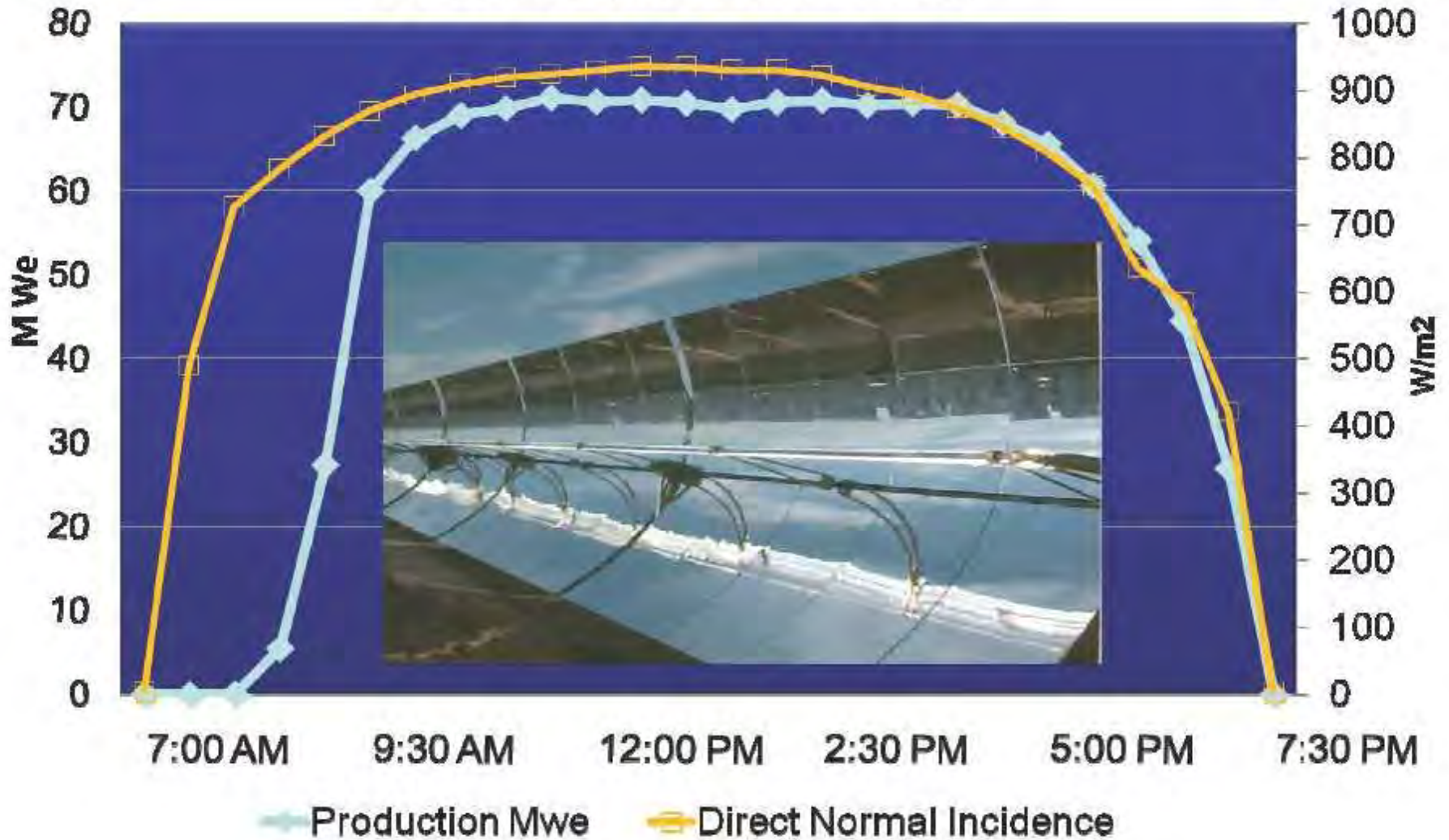
**SOLAR FIELD : 60% COMPLETED BY
THE END OF SEPTEMBER 2006**

Nevada Solar One – 75 MW



NEVADA SOLAR ONE – ACCIONA SOLAR POWER

NEVADA SOLAR ONE JUNE 12 2007



Acciona/ Mitsubishi Corp (Alvarado, Badajoz)



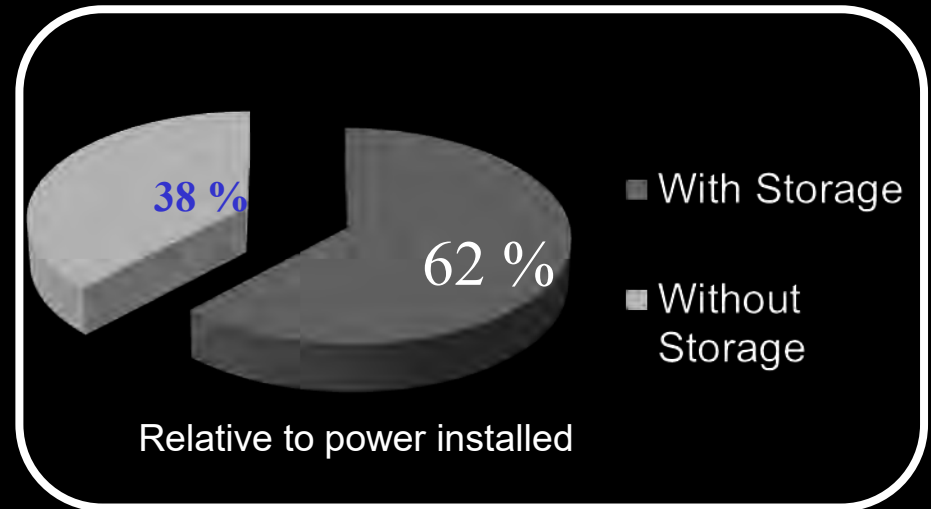
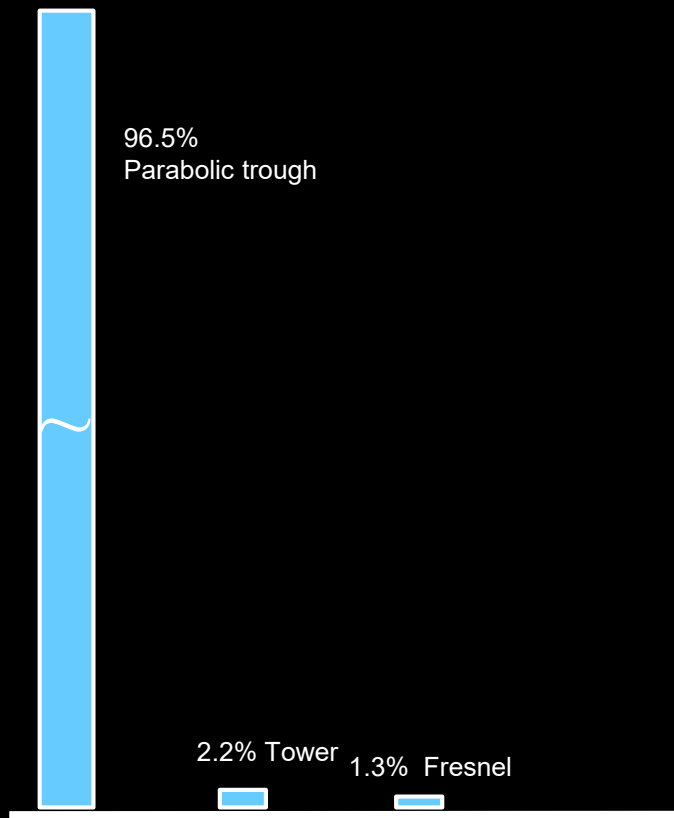
Break Ground Date December 2007

Start Production Date June 2009

La Risca, Alvarado

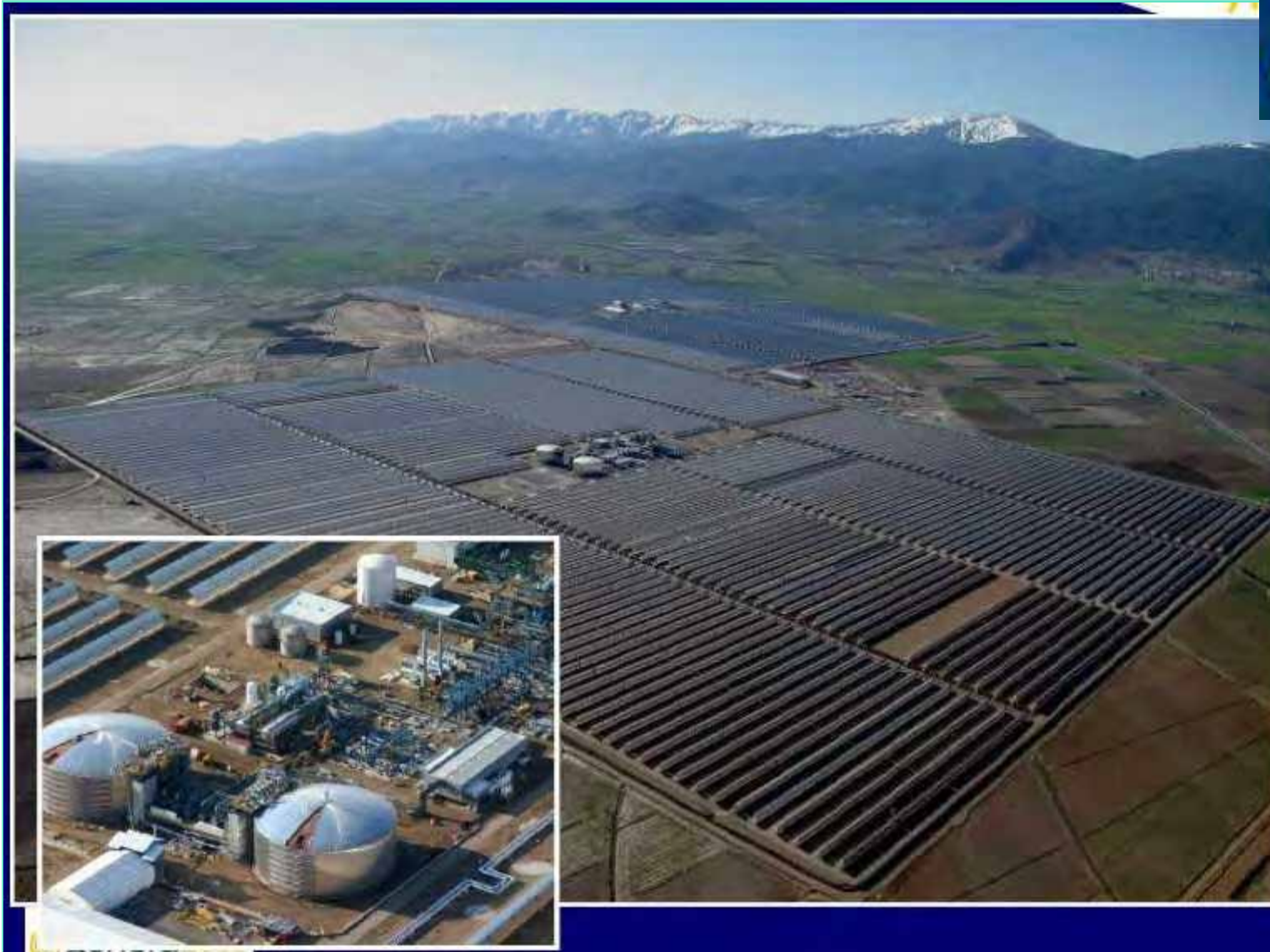
DISPATCHABILITY:

Breakdown of CSP plants in Spain



Power: 2303 MW
Production: 4500 GWh/year
CO₂ Emissions avoided: 4 Mt/year

Andasol 1 and 2: Thermal storage with molten salts



ANDASOL 1
and
ANDASOL 2



Break Ground Date July 3, 2006
Start Production Date November 26, 2008



Steam Storage System

Nominal Rate Operation

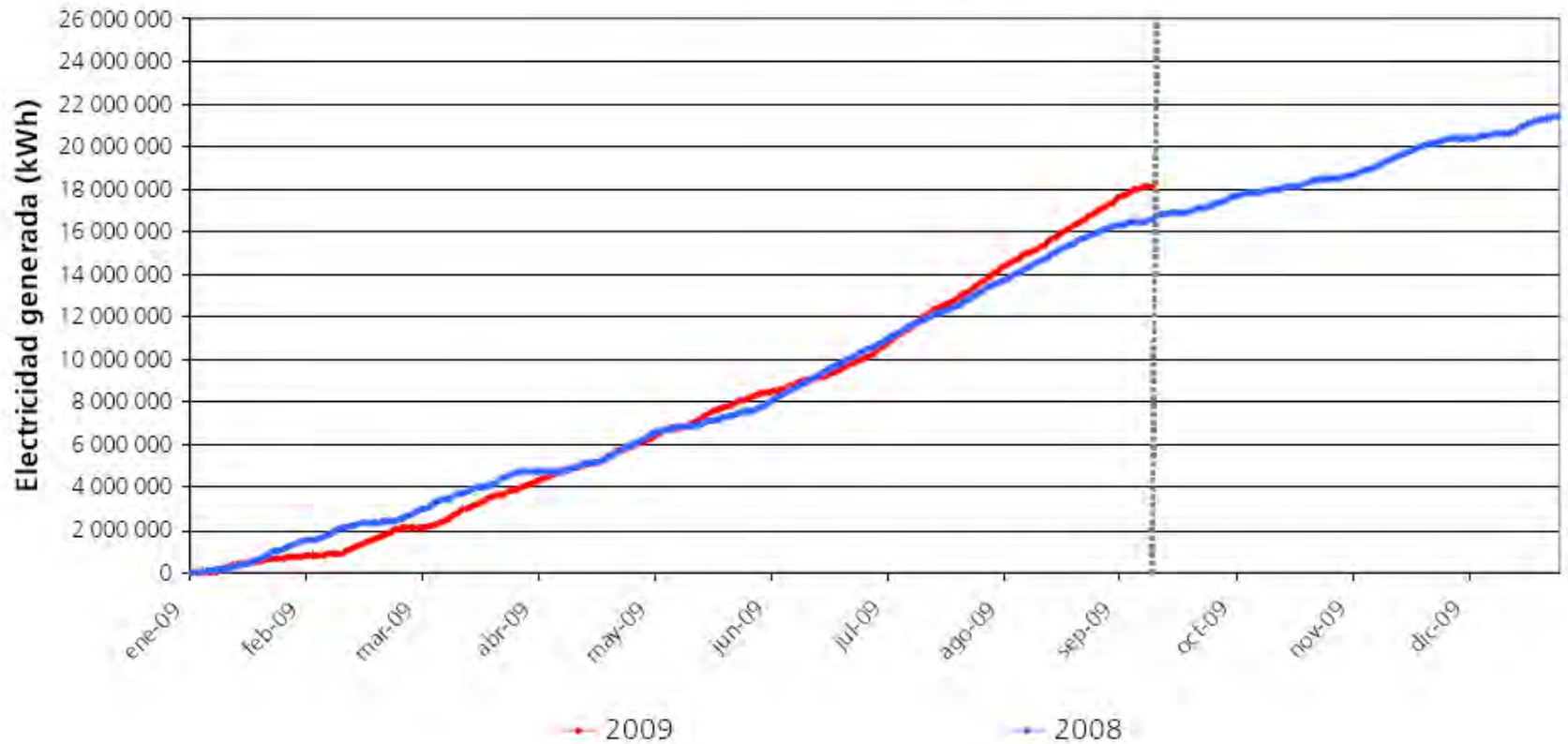
| | | |
|--|-------|------------------|
| Optical Efficiency | 77.0% | 67.5MW -> 51.9MW |
| Receiver and Heat Handling Efficiency | 92.0% | 51.9MW -> 47.7MW |
| Thermal Power to Storage | | 11.9MW |
| Thermal Power to Turbine | | 35.8MW |
| Thermal Pow. -> Electric Pow. Efficiency | 30.7% | 35.8MW -> 11.0MW |
| Total Efficiency at Nominal Rate | | 21.7% |

Energetical Balance in Annual Basis

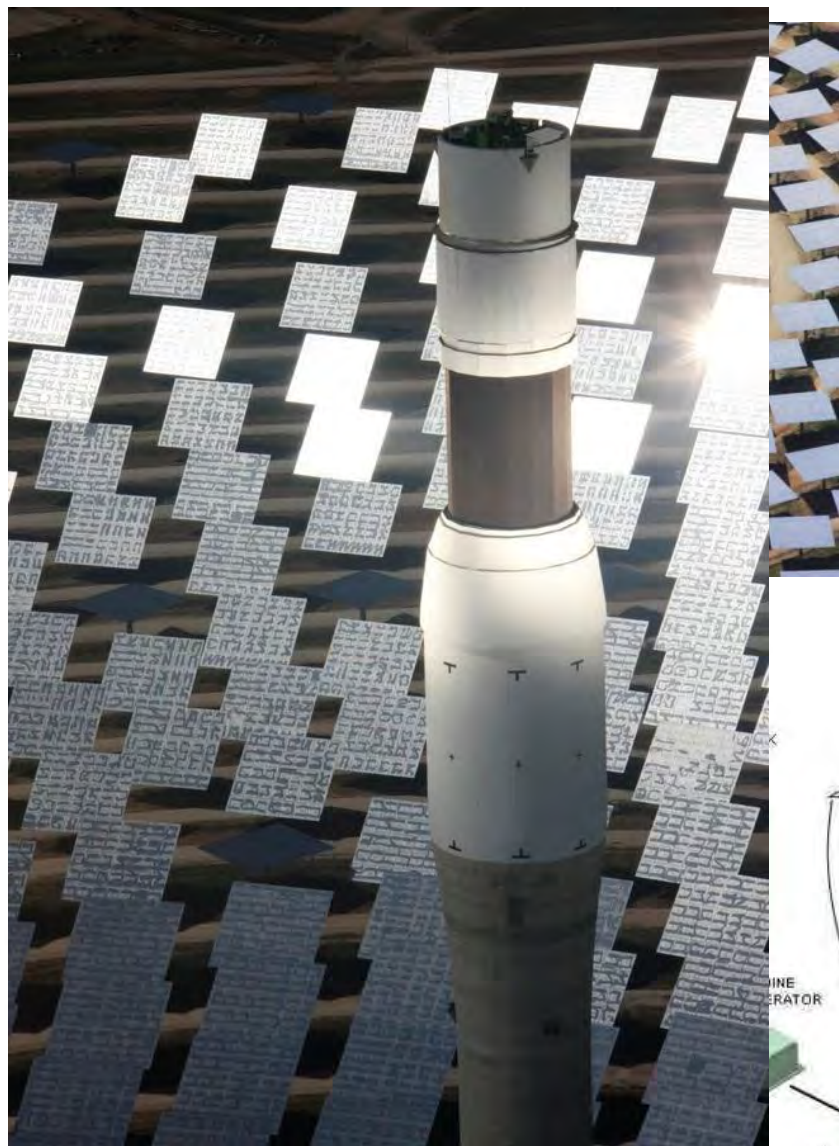
| | | |
|--|-------|-------------------------------|
| Mean Annual Optical Efficiency | 64.0% | 148.63GWh(useful) -> 95.12GWh |
| Mean Annual Receiver&Heat Handling Efficiency | 90.2% | 95.12GWh -> 85.80GWh |
| Operational Efficiency (Starts Up/Stops) | 92.0% | 85.80GWh -> 78.94GWh |
| Operational Efficiency (Breakages, O&M) | 95.0% | 78.94GWh -> 75.00GWh |
| Mean Annual Thermal Ener. -> Electric Efficiency | 30.6% | 75.00GWh -> 23.0GWh |
| Total Annual Efficiency | | 15.4% |



ión Eléctrica PS10



Solar Towers and storage: Gemasolar plant

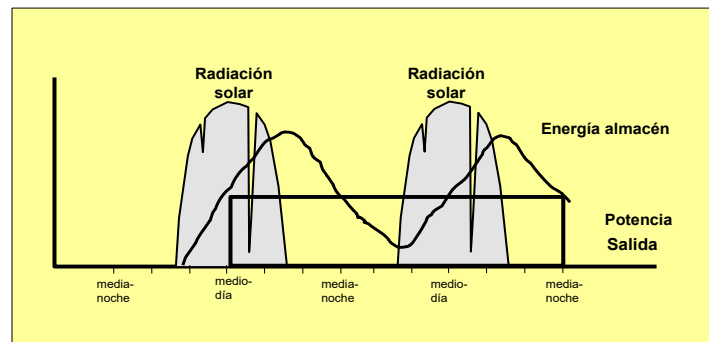


DESIGN PARAMETERS

| | |
|---------------------------------------|------------------------------|
| Total Reflective Area | 304.750 m² |
| Number of heliostats | 2650 |
| Total Area covered by Heliostat Field | 195 ha |
| Thermal output of the Receiver | 120 MW |
| Tower height | 140 m |
| Heat Storage Capacity | 15 hours |
| Steam Turbine power gross | 19.9 MWe |

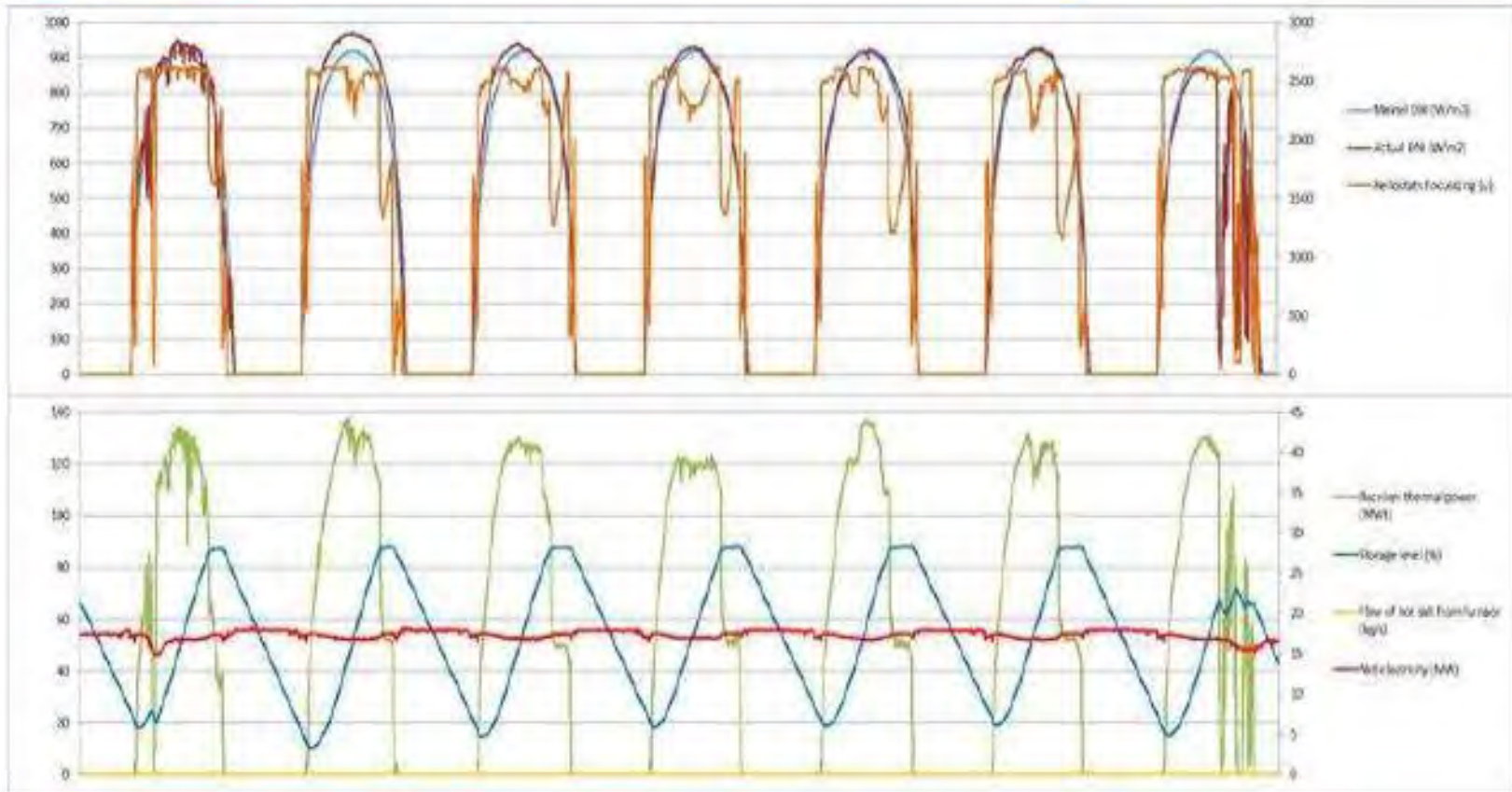
Projected Operative Figures

| | |
|-------------------------|-------------------------------|
| Annual solar irradiance | 2062 kWh/m² |
| Annual Energy sales | 80,000 MWh |
| CO2 savings | 30.000 t/y |
| Capacity factor | 55% |
| | |





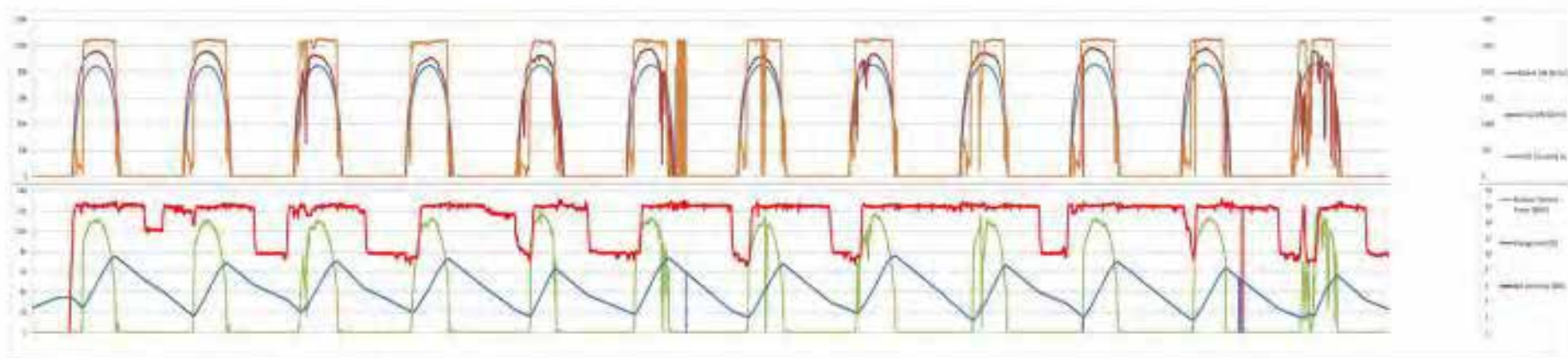
Plant operation



- Turbine at nominal power continuously running in summer



Plant operation



- Non-stop operation in winter time.

Gen 1+ → Gen 2

Where are we coming from?



USA 2013-2015

Scaling-up
100-400 MW
Utility PPA
Dispatchability value
Environmental impact

Second wave: USA the Scaling-Up



| Project | Ivanpah | Genesis | Solana | Crescent Dunes | Mojave |
|------------|--------------|------------|--------------------|------------------------|------------|
| Utility | SCE + PG&E | PG&E | APS | NVE | PG&E |
| State | California | California | Arizona | Nevada | California |
| Size | 390 MW | 250 MW | 280 MW | 110 MW | 280 MW |
| Technology | Power Tower | Trough | Trough/ Storage | Power Tower/Storage | Trough |
| Price kWh | ? | ? | \$0.14 | \$0.135 | ? |
| Cost | \$2.18 B | \$1.20 B | \$2.00 B | \$0.91 B | \$1.6 B |
| Company | BrightSource | NextEra | Abengoa | SolarReserve | Abengoa |

Total CSP in operation 1,804 MW

Second wave: USA the Scaling-Up

- Large plants: 100-400 MW per unit
- Land: Solana occupies 774 hectares; Ivanpha 1600 ha.
- Typical Power Purchase Agreement with utilities (Time of Delivery value) with selling price \$0.14/kWh
- Commissioning and routine operation more complex (3-4 years from groundbreaking to start up)
- Environment: Visual impact, glint and glare, birds, water

Prospects

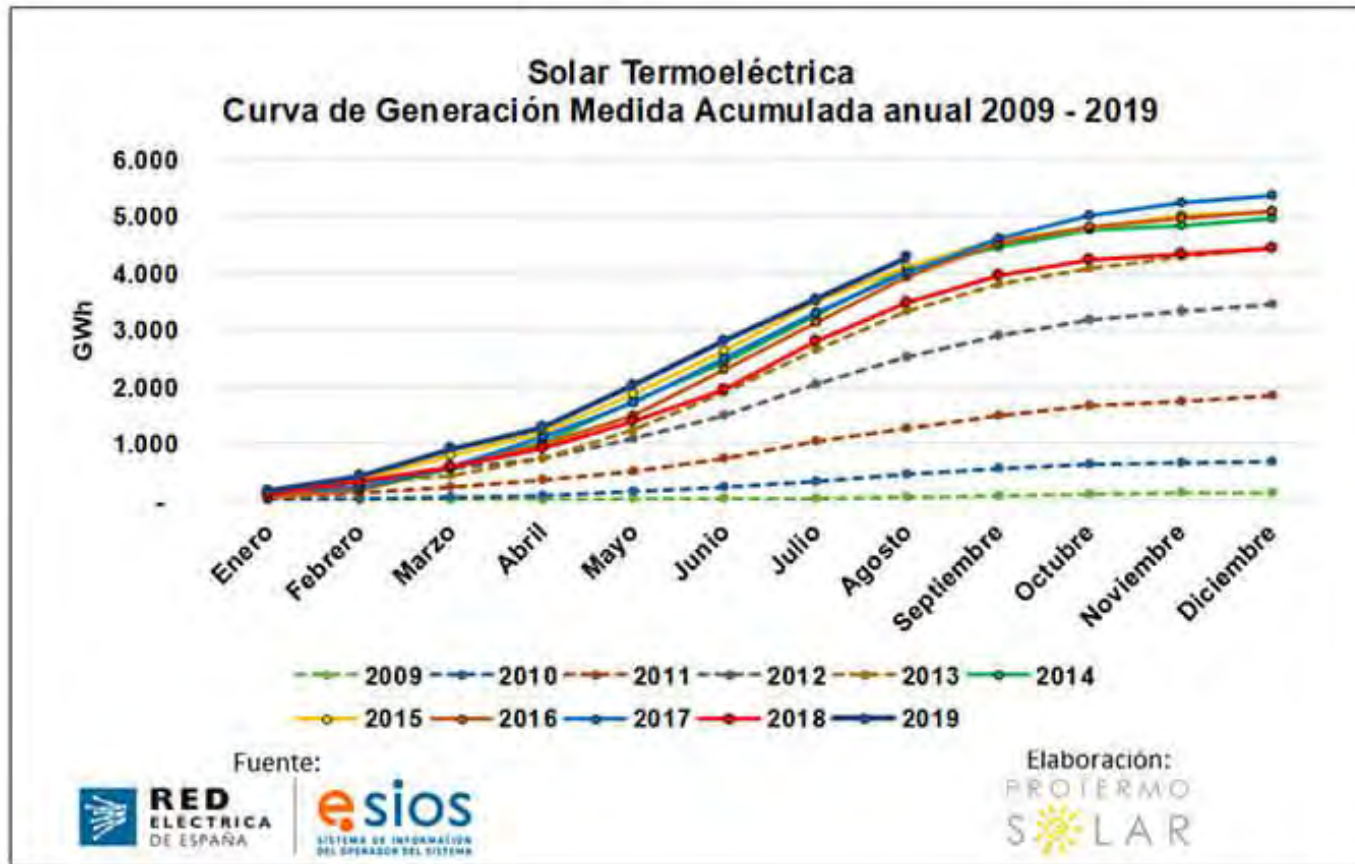
- Strong competition with PV at the short term
- Future STE plants will depend on the position of the utilities regarding dispatchability.



- Routine operation of Gen 1+ in Spain
- Early feedback from Gen 2 in US
- Aggresively fighting for globalization (Gen 2+)

Routine operation of Gen 1+ in Spain

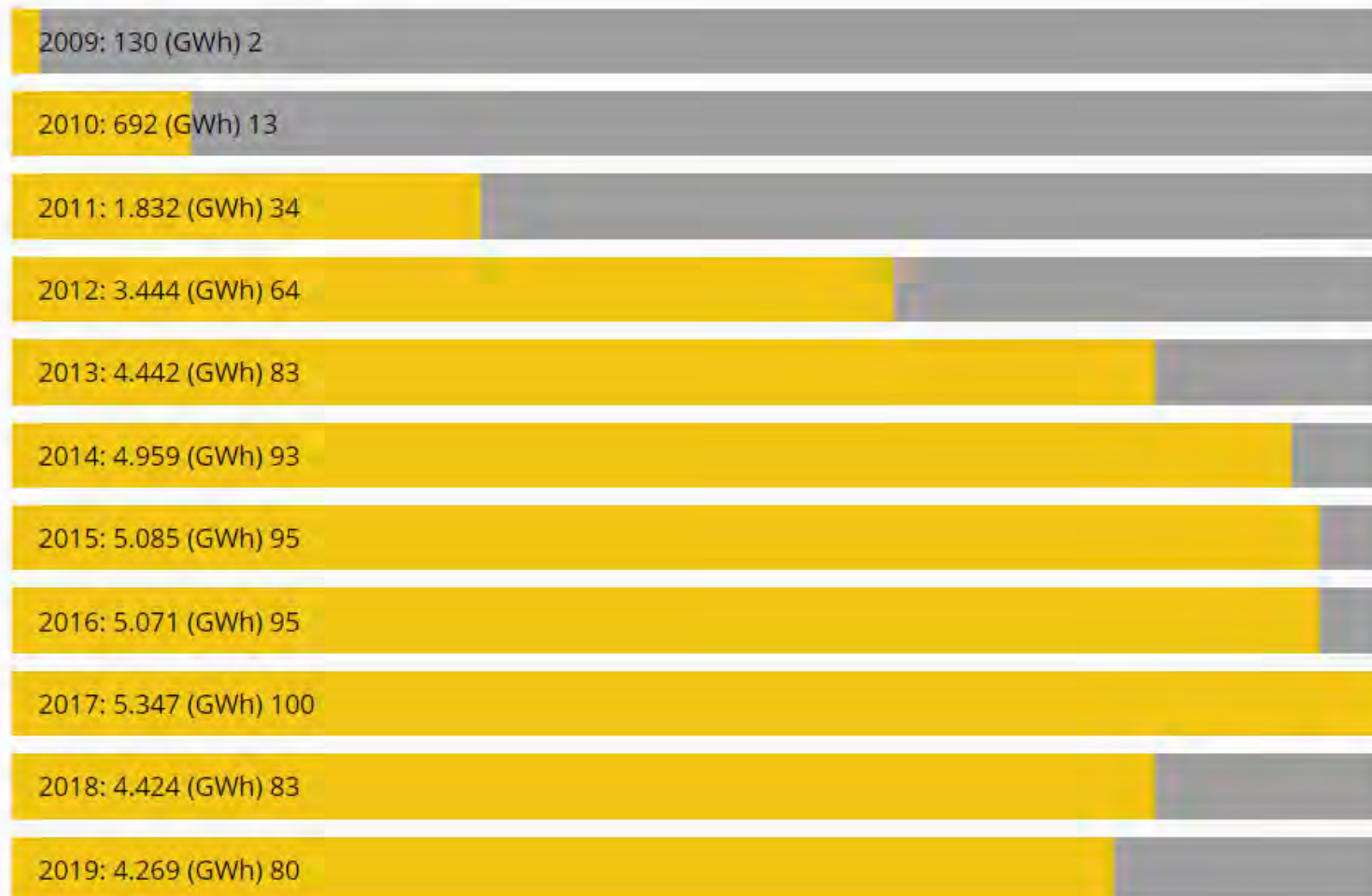
- The plants don't show degradation signs and they are continuously breaking specific records. 2019 is getting the maximum cumulative yield
- Lessons learned on specific operational issues are part of the knowhow of the Spanish companies for design and operation of future plants



Routine operation of Gen 1+ in Spain

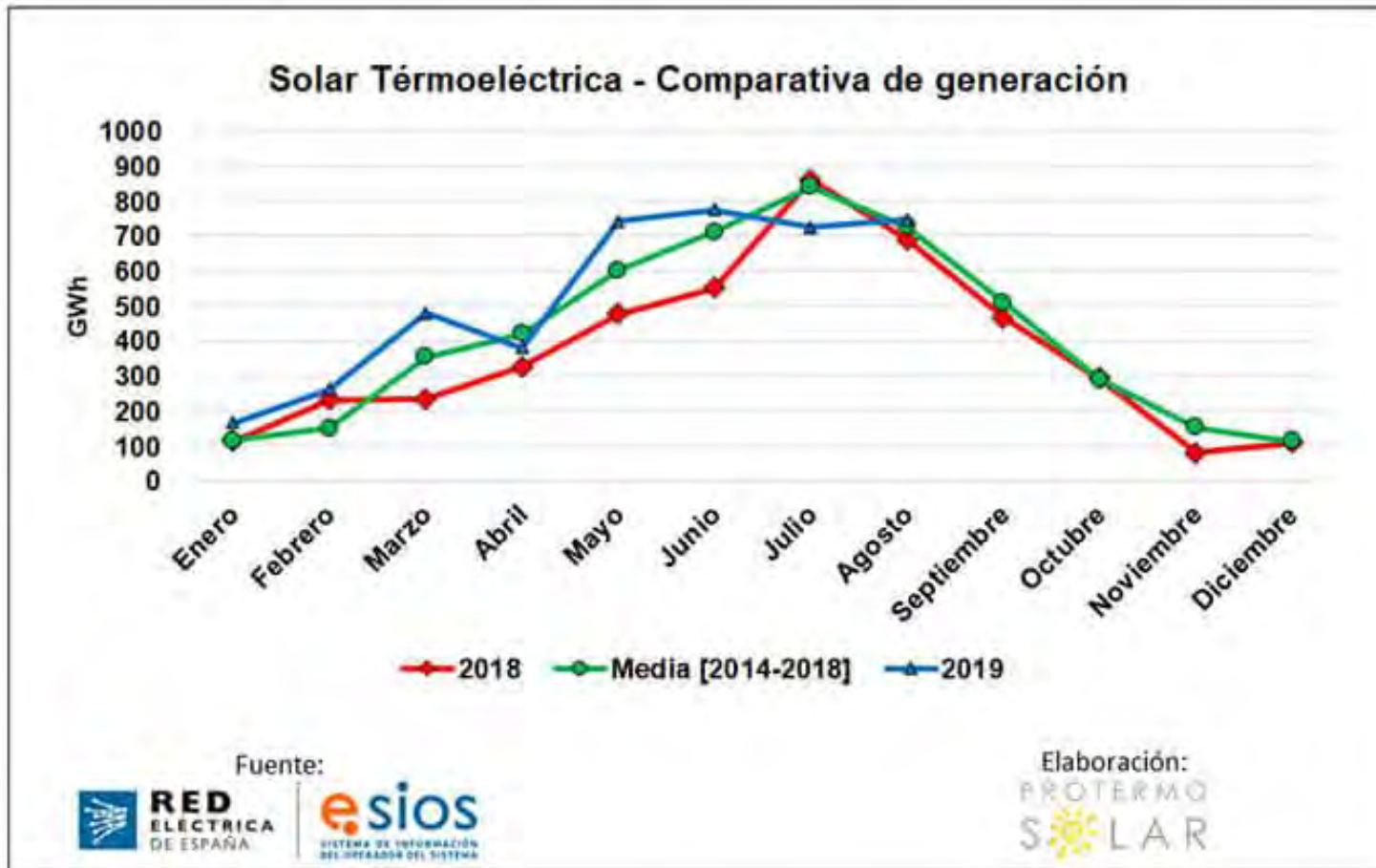


GENERACIÓN ANUAL (GWh)



Operational Experience in Spain

- ✓ 10% of instantaneous contribution has been achieved. 8% is oftenly achieved in summer months. 5% daily max achieved.
- ✓ 3 weeks have been running some plants in a non stop 24/7 mode. Gemasolar, in particular, reached 36 non stop days at nominal power
- ✓ Montly contribution raised 3.65% in August 2019.
- ✓ 5,300 direct employment in 2017.



First market wave: Features

- Performing as planned
- Typical size 50 MW (land > 1 km²)
- Already 6-7 hours nominal storage

BUT.....

- 96.5% installed capacity in parabolic troughs
- Efficiencies below 20% nominal solar to electricity,
- Only feasible with FIT of 27 c€/kWh
- High water consumption (0.5-1 million m³ per year and plant),
- The limitation to reach the temperatures needed for thermochemical routes of solar fuels.



Extresol 1 and 2 (ACS/Cobra)



Nevada Solar One 75 MW (Acciona)



Early feedback from Gen 2 in US



science alert

Trending



5bharris/WikiCommons

NATURE

This Solar Plant Accidentally Incinerates Up to 6,000 Birds a Year

JOSH HRALA 15 SEP 2016

A solar power plant in California is accidentally killing up to 6,000 birds every year, with staff reporting that the birds keep flying into its concentrated beams of sunlight, and spontaneously bursting into flames.

The problem has been going on since the site opened in 2014, and the team says it's trying everything to save the birds from a fiery fate. But so far, the perfect solution has eluded them.

TABLE 1. Number of avian detections at ISEGS during the first year of monitoring.¹⁰

| Cause | Number of Detections | | | | Total |
|--------------|----------------------|------------|------------|------------|------------|
| | Winter | Spring | Summer | Fall | |
| Singed | 27 | 100 | 42 | 147 | 316 |
| Collision | 14 | 15 | 10 | 45 | 84 |
| Other* | 5 | 5 | 2 | 3 | 15 |
| Unknown | 51 | 82 | 61 | 94 | 288 |
| Total | 97 | 202 | 115 | 289 | 703 |

* Includes detections in ACC buildings without evidence of singeing or collision effects.

Ho. CK, AIP Conference Proceedings **1734**, 070017 (2016)



IN THIS LIST

ELECTRIC POWER

SolarReserve's CSP technology with storage struggles to stay online

COMMODITIES | ENERGY |
ELECTRIC POWER | EMISSIONS |
RENEWABLES | LNG | NATURAL GAS
| OIL | CRUDE OIL | REFINED
PRODUCTS | PETROCHEMICALS

Market Movers Europe, Sep
2-6: Oil and carbon
conferences set the tone for
commodities in September

ELECTRIC POWER

Platts M2MS-Power

COMMODITIES | ENERGY |
ELECTRIC POWER | RENEWABLES |
BANKING | INFRASTRUCTURE &
UTILITIES

Financing US Power
Conference, 21st Annual

AGRICULTURE

Brazil's Aug soybean exports

ELECTRIC POWER — 02 Aug 2019 | 19:01 UTC — Houston

SolarReserve's CSP technology with storage struggles to stay online



Author **Jeffrey Ryser** ✉

Editor **Richard Rubin** ✉

Commodity **Electric Power**

HIGHLIGHTS

110-MW Crescent Dunes facility out most of Q1

Company offers no comments about current operations

The 110-MW Crescent Dunes Concentrated Solar Power facility near Tonopah, Nevada, was offline most of the second quarter of this year 2019,

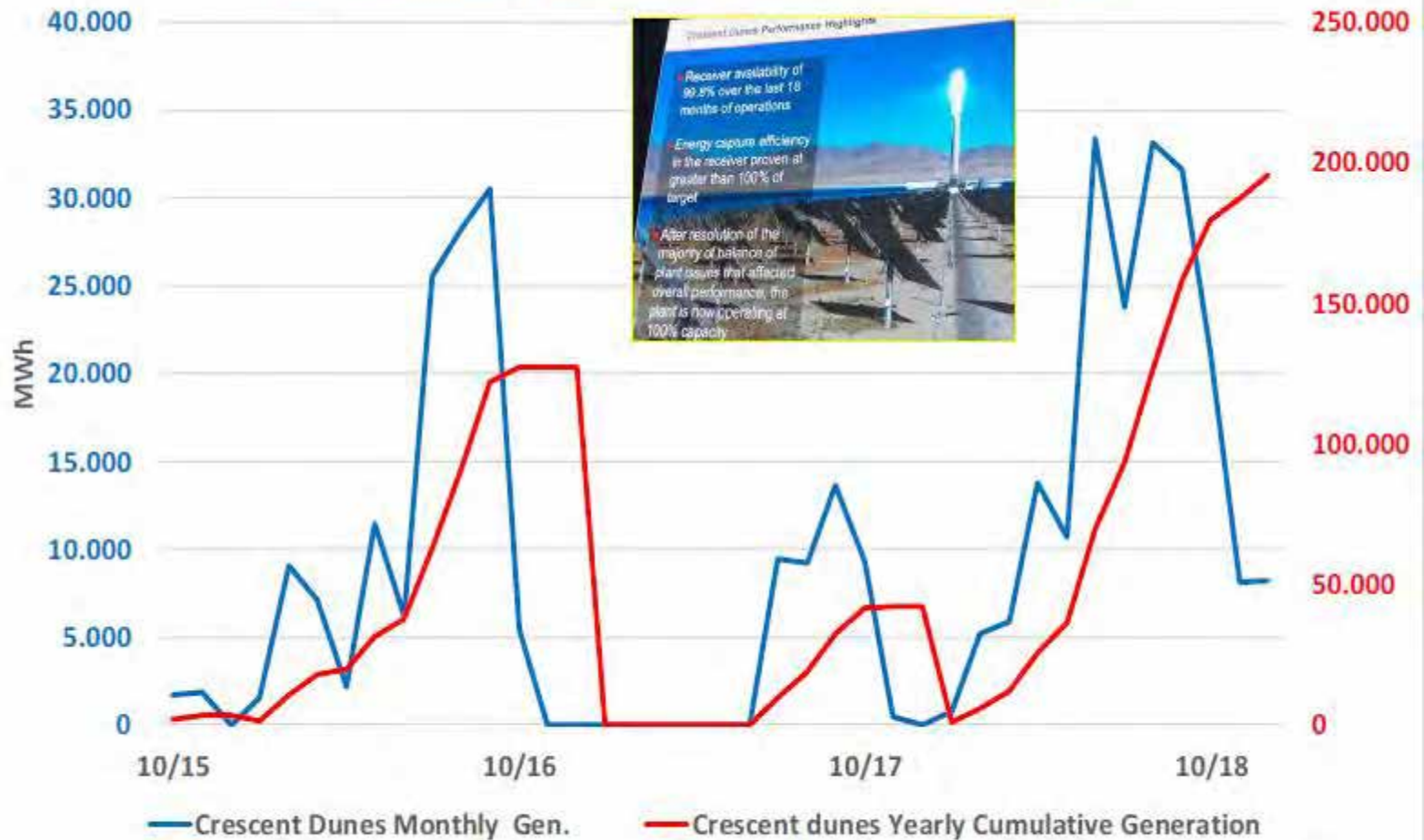
The facility has experienced outages before. It reported no wholesale sales in November and December 2016 after a leak in a tank filled with molten salt forced a shutdown.

It also has a 25-year power purchase agreement with NV Energy subsidiary Nevada Power for power priced at 13.5 cents/kWh. An NV Energy spokeswoman on Friday declined to comment on the status of the Crescent Dunes facility.

Solar Reserve's subsidiary Tonopah Solar Energy, which owns the facility, reported no wholesale power sales to FERC in the entire first half of 2017. It had a slow operational rebound, with capacity factors of just 4% and 5% in Q4 2017 and Q1 2018, respectively.

The facility's highest average quarterly capacity rates have come in the summer of 2016 and 2018. Its record high quarterly capacity average was 36.7% in Q3 2018.

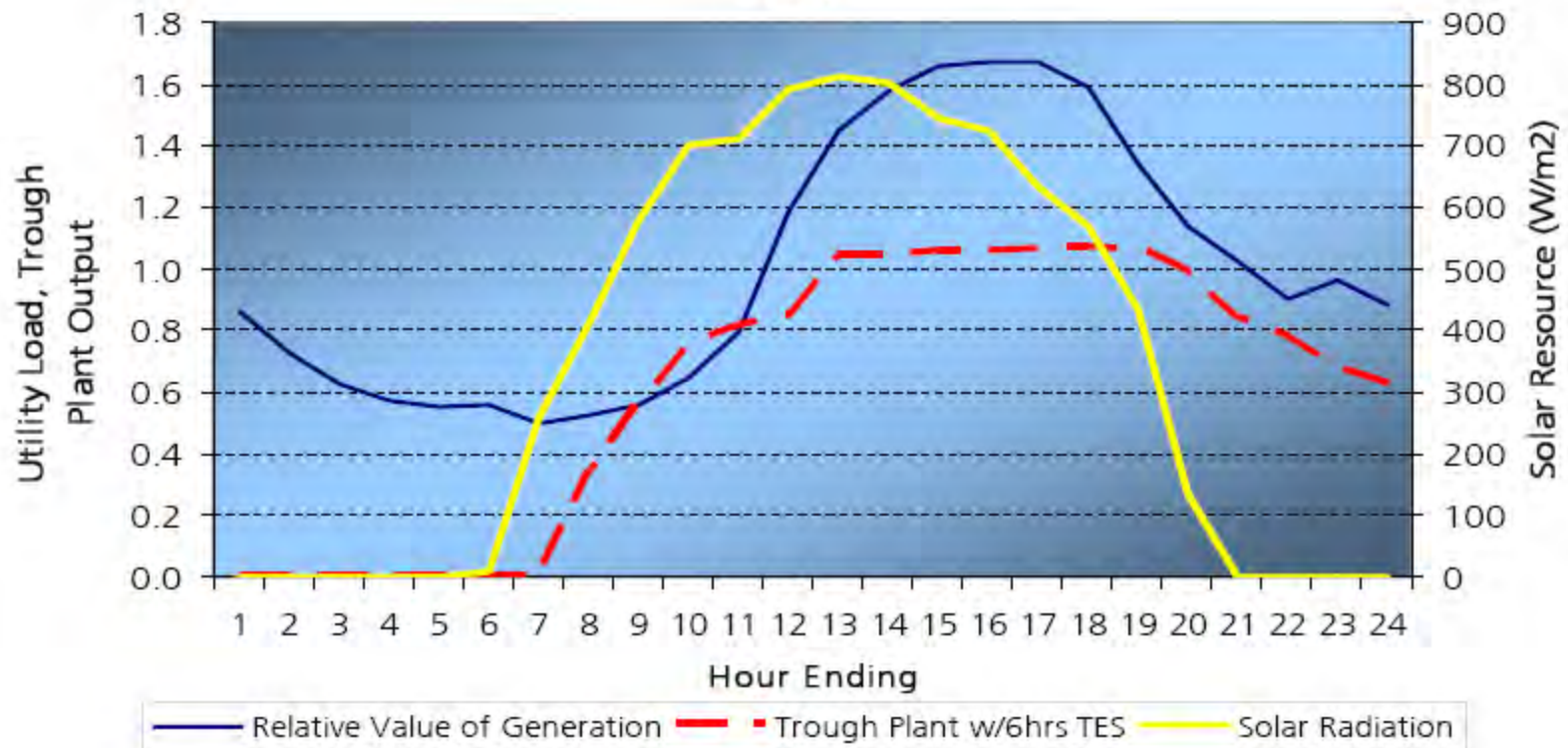
CSP Plant CRESCENT DUNES monthly generation over the last 2 years



Solana (280 MW) in Arizona

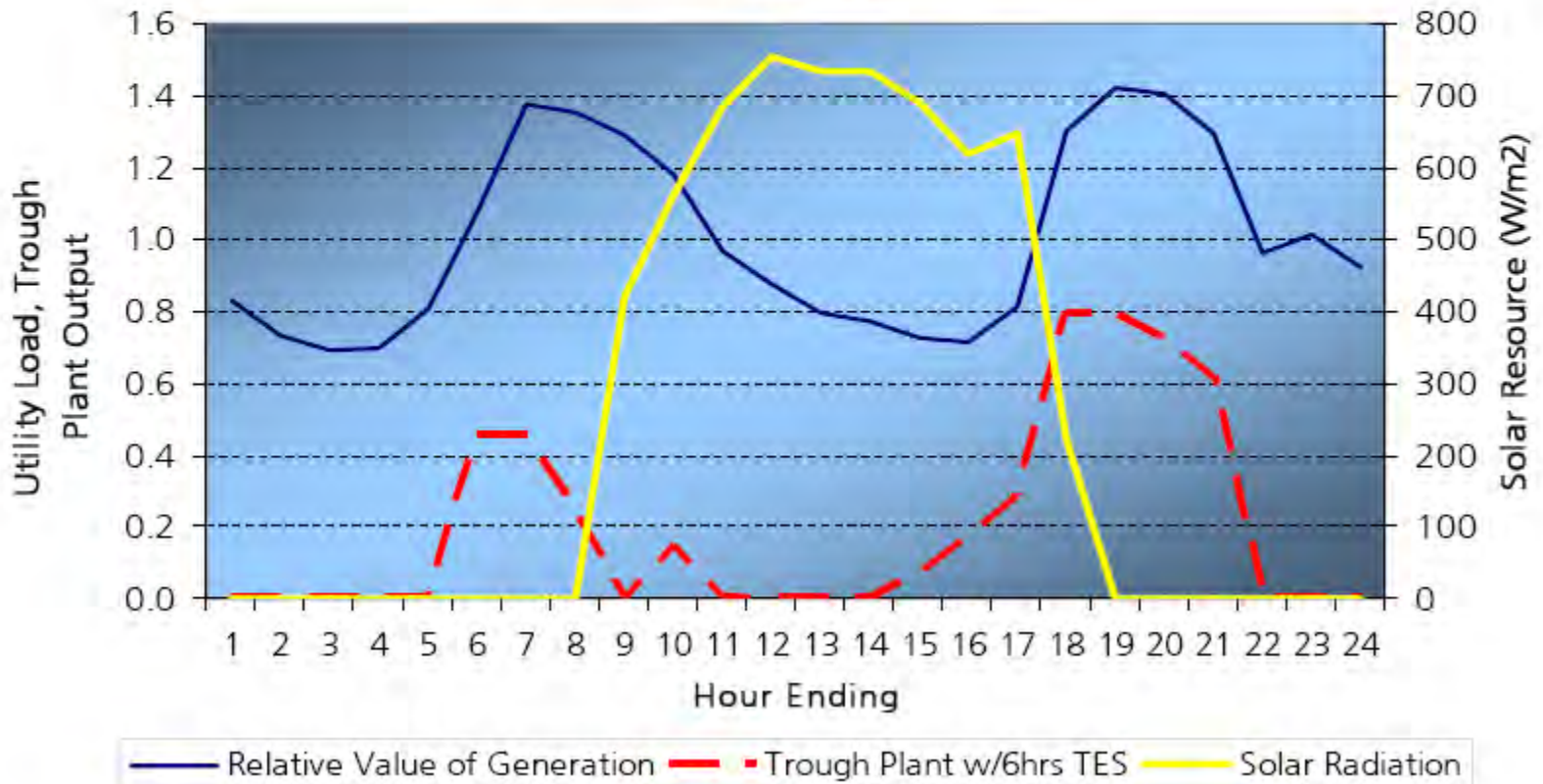


Solar Plant With Storage vs. Utility System Load July



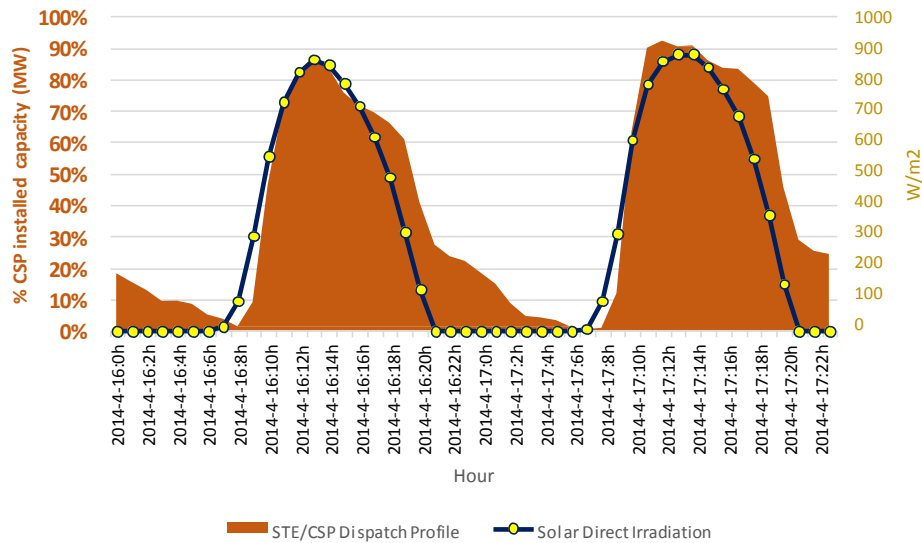


Solar Plant With Storage vs. Utility System Load January



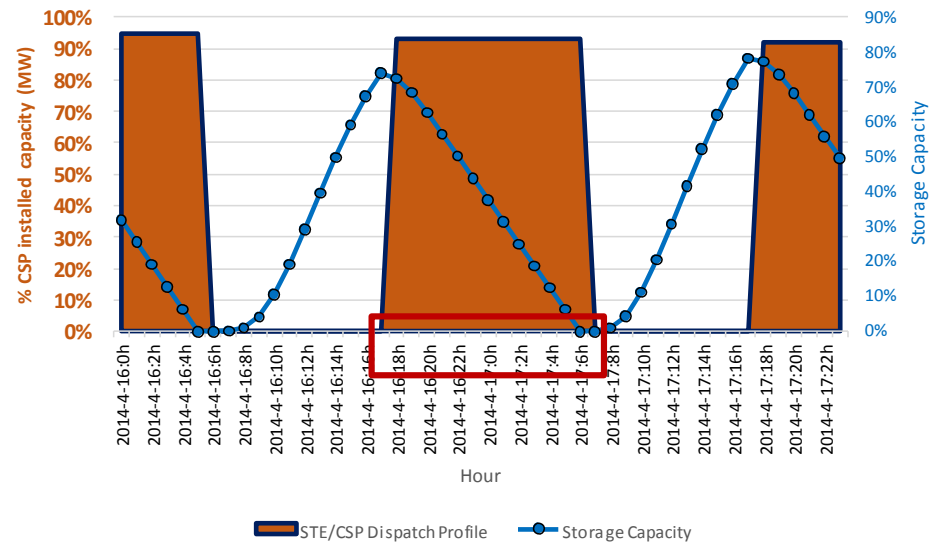
Current and – most likely – future STE/CSP dispatch profiles by year 2030 (Spanish Case)

Current STE/CSP fleet dispatch profile - Spring example

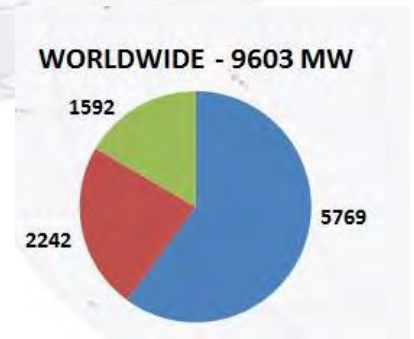
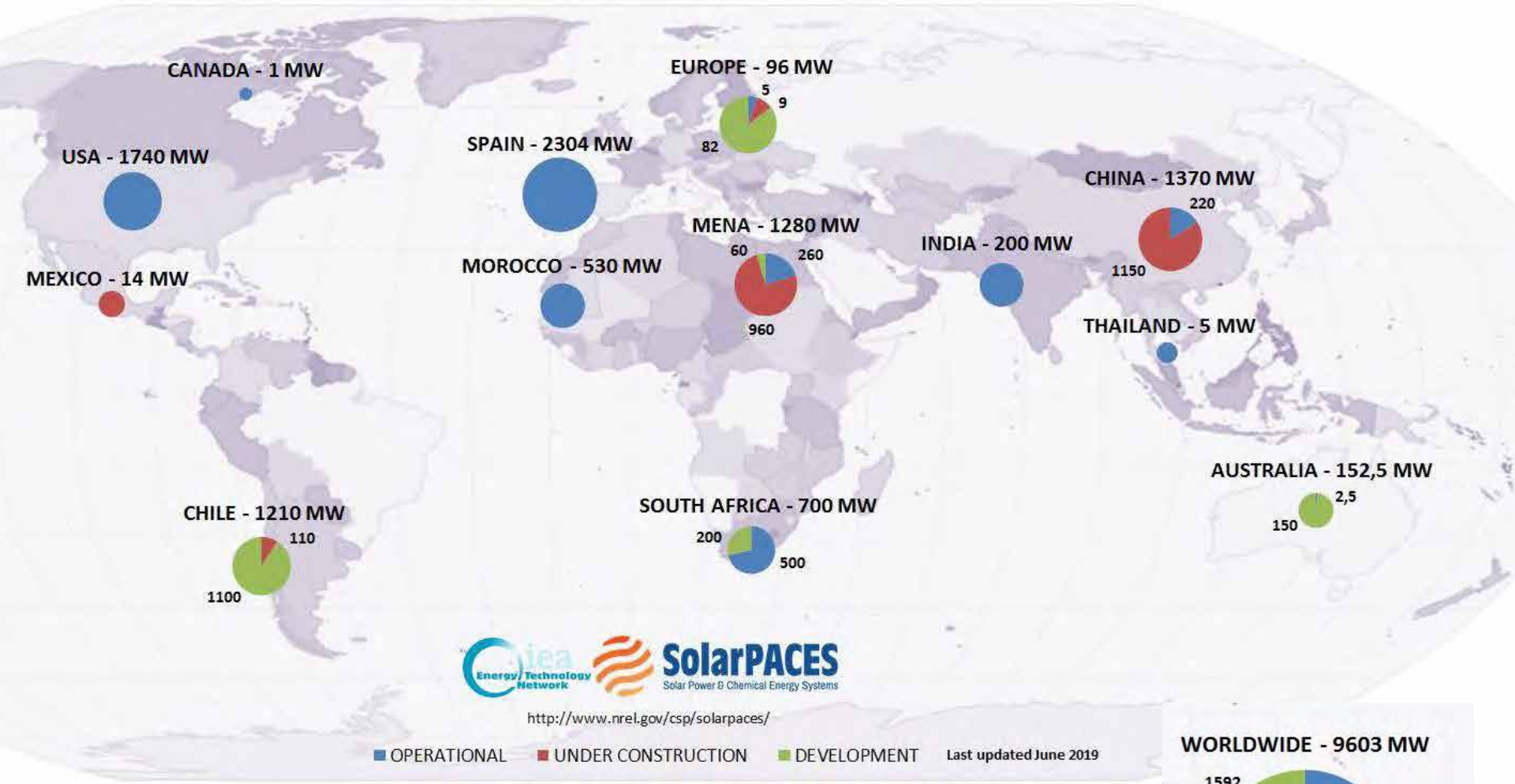


Current fleet consist of 1/3 plants with 7,5 hours of storage and 2/3 without storage

Proposed STE/CSP fleet dispatch profile - Spring example



Future CSP plants would be constructed with 10 – 12 hours of storage



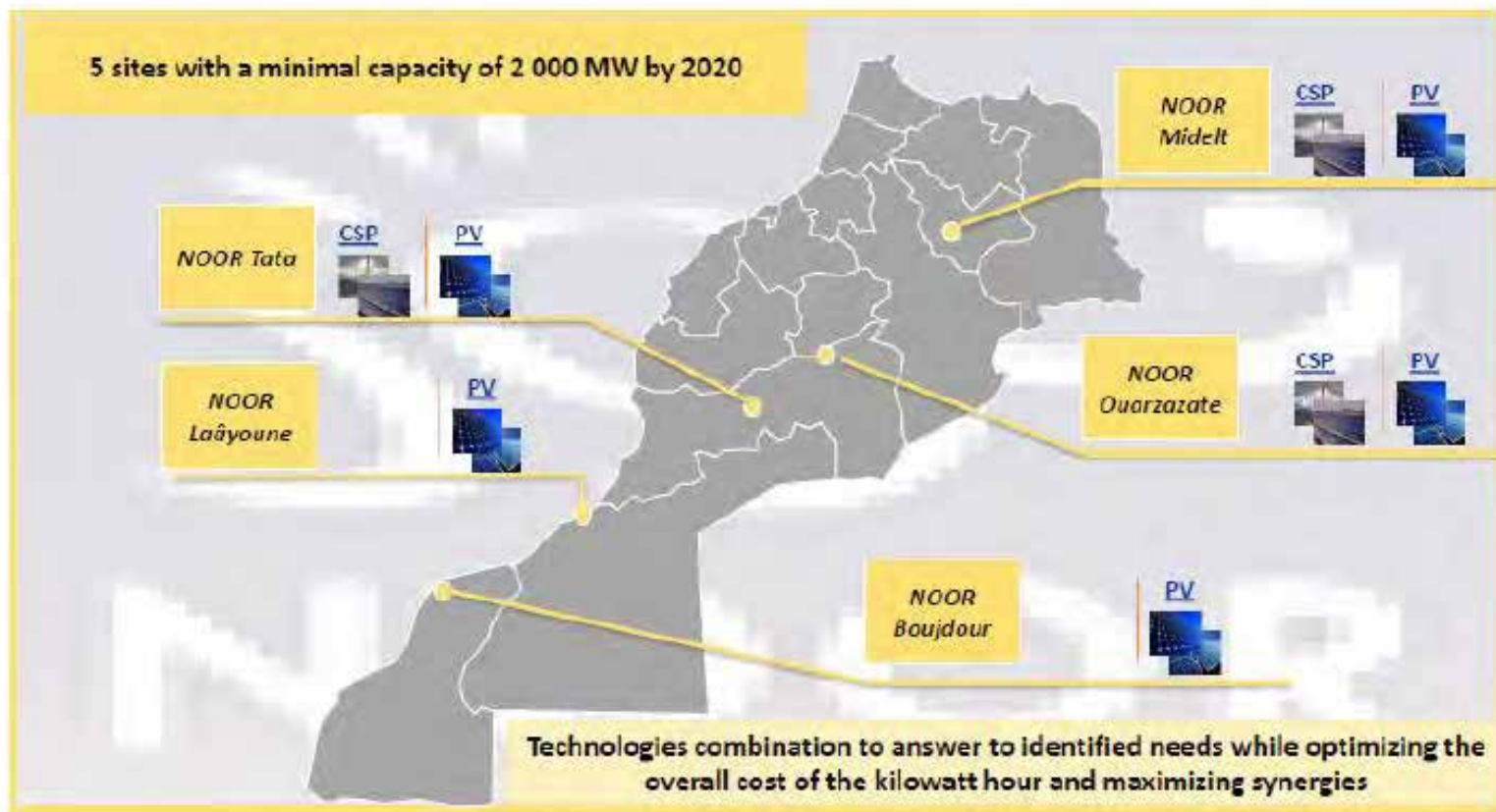
Globalization (Gen 2+) or just China/MENA receiving the baton?



CSP in Chile: Market

- CSP projects have participated in energy tenders for distribution companies:
 - Abengoa (Tender 2015-02)
 - Won a contract for 38,8 GWh/yr at a price of 97 US\$ MW/h
 - Weighted average price of the tender was 79,3 US\$/MWh
 - Solar Reserve (Tender 2015-01)
 - Offered 67,86 USD/MWh for 8.360 GWh/yr
 - Didn't win energy blocks
 - Offer was 5,97 US\$/MWh, below the average of LNG and coal offers.
 - Weighted average price of the contracts that were awarded was 47,6 US\$/MWh

NOOR, A MULTI-SITE AND MULTI-TECHNOLOGY PLAN



New developers in the field

NOOR₀ I PLANT IN OPERATION



Techno.

Concentrated Solar Power using parabolic trough

Capacity

160 MWe Gross Capacity

Storage

3 hours Thermal Energy Storage

Financial Institutions



New EPCs in the field

NOOR₀ II, UNDER CONSTRUCTION *Techno.*



| | |
|-----------------|---|
| Techno. | Concentrated Solar Power using parabolic trough |
| Capacity | 200 MW Gross Capacity |
| Storage | > 7 hours |

| |
|------------------|
| Developer |
| EPC |

| |
|--|
| |
| |
| |

Financial Institutions

| | | |
|--|--|--|
| | | |
| | | |

New EPCs in the field

NOOR_o III, UNDER CONSTRUCTION



Techno.

Concentrated Solar Power using tower

Capacity

150 MW Gross capacity

Storage

> 7 hours

Developer

ACWA POWER

SENER 山东电建

POWERCHINA

EPC

Financial Institutions



KFW



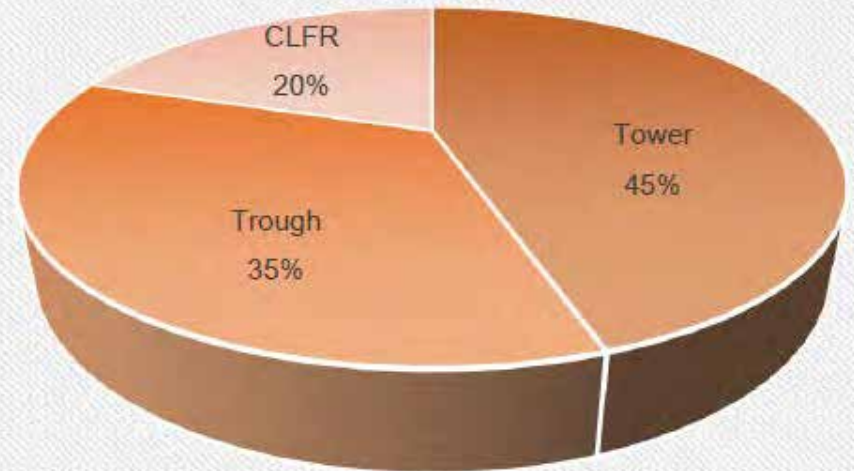
THE WORLD BANK



China National Solar Thermal Energy Alliance

- 1.3 GW/ 20 demonstration Projects
- 200MW already grid connected in 2018

Technology—China 1st Batch of CSP Pilot Projects
(Sept., 2016)



The first batch of CSP demonstration projects which are completed and put into operation by December 31, 2018, will have on-grid price of RMB 1.15/kWh (inclusive of taxes).

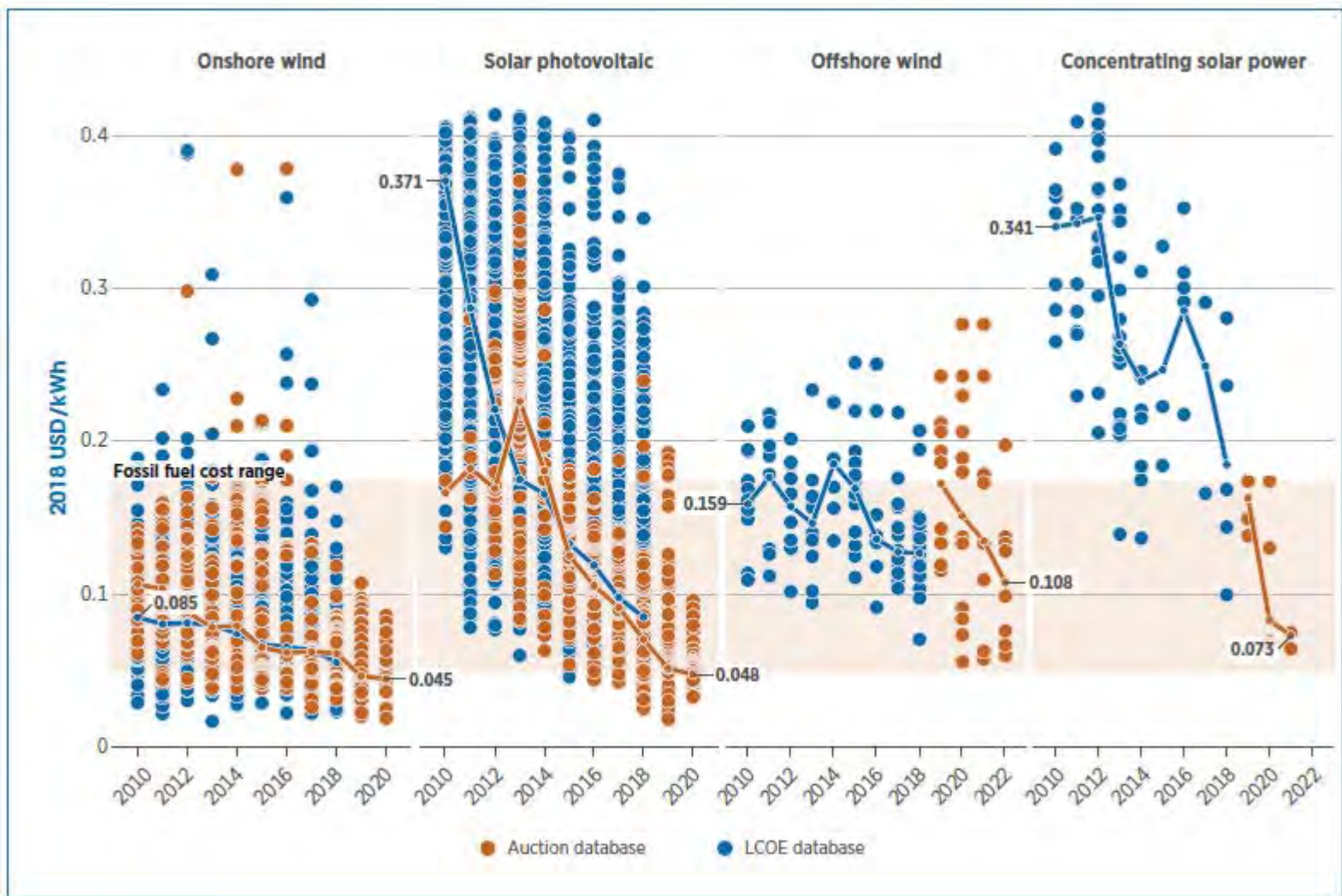
- An electricity price reduction mechanism for overdue projects in operation:
 - since January 1, 2019 1.14 RMB /kWh,
 - since January 1, 2020 till December 31, 2021 1.10 RMB/kWh.
 - It's expected there'll be 6 projects (350MW) put into operation in 2019.

China National Solar Thermal Energy Alliance

200MW were completed and connected to the grid, in one year (2018):

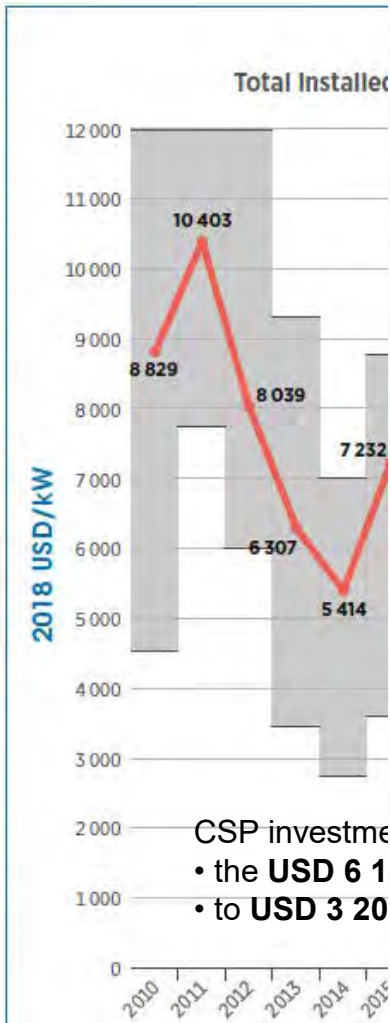
- CGN Delingha 50MW Parabolic Trough CSP project—June 30th
- Shouhang Dunhuang 100MW Molten Salt Tower CSP project—December 28th
- SUPCON Delingha 50MW Molten Salt Tower CSP project—December 30th



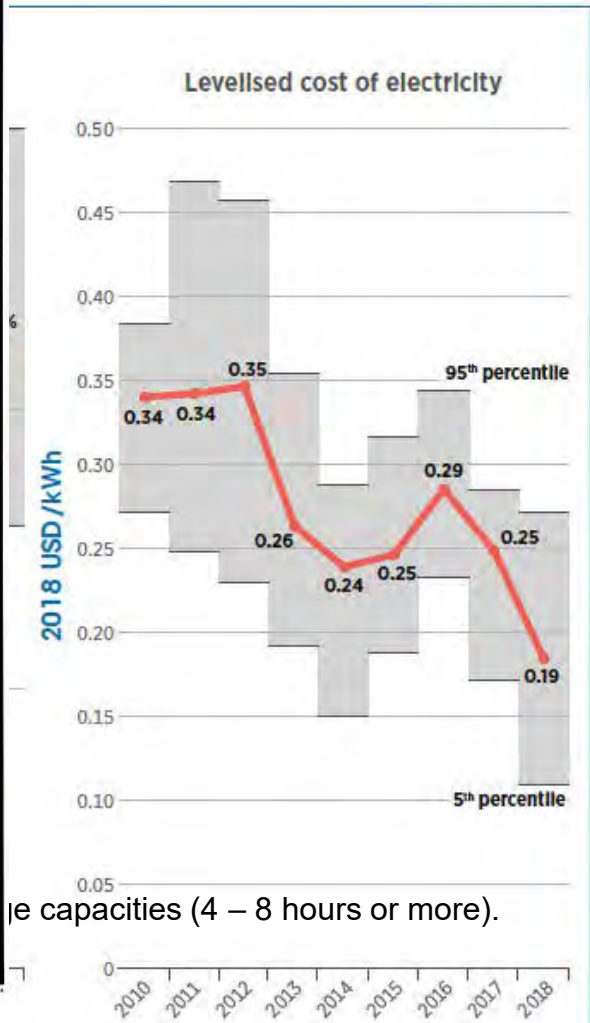


In 2018, around 500 MW of new concentrating solar power was commissioned – predominantly in China, Morocco and South Africa. The global weighted average LCOE in 2018 was USD 0.185/kWh – 26% lower than in 2017 and 46% lower than in 2010.

Global weighted average total installed costs, capacity factors and LCOE for CSP, 2010–2018



CSP investment
 • the **USD 6.1**
 • to **USD 3.20**



...for large capacities (4 – 8 hours or more).

What Does the Future Look
Like for CSP?
That's anybody's guess!

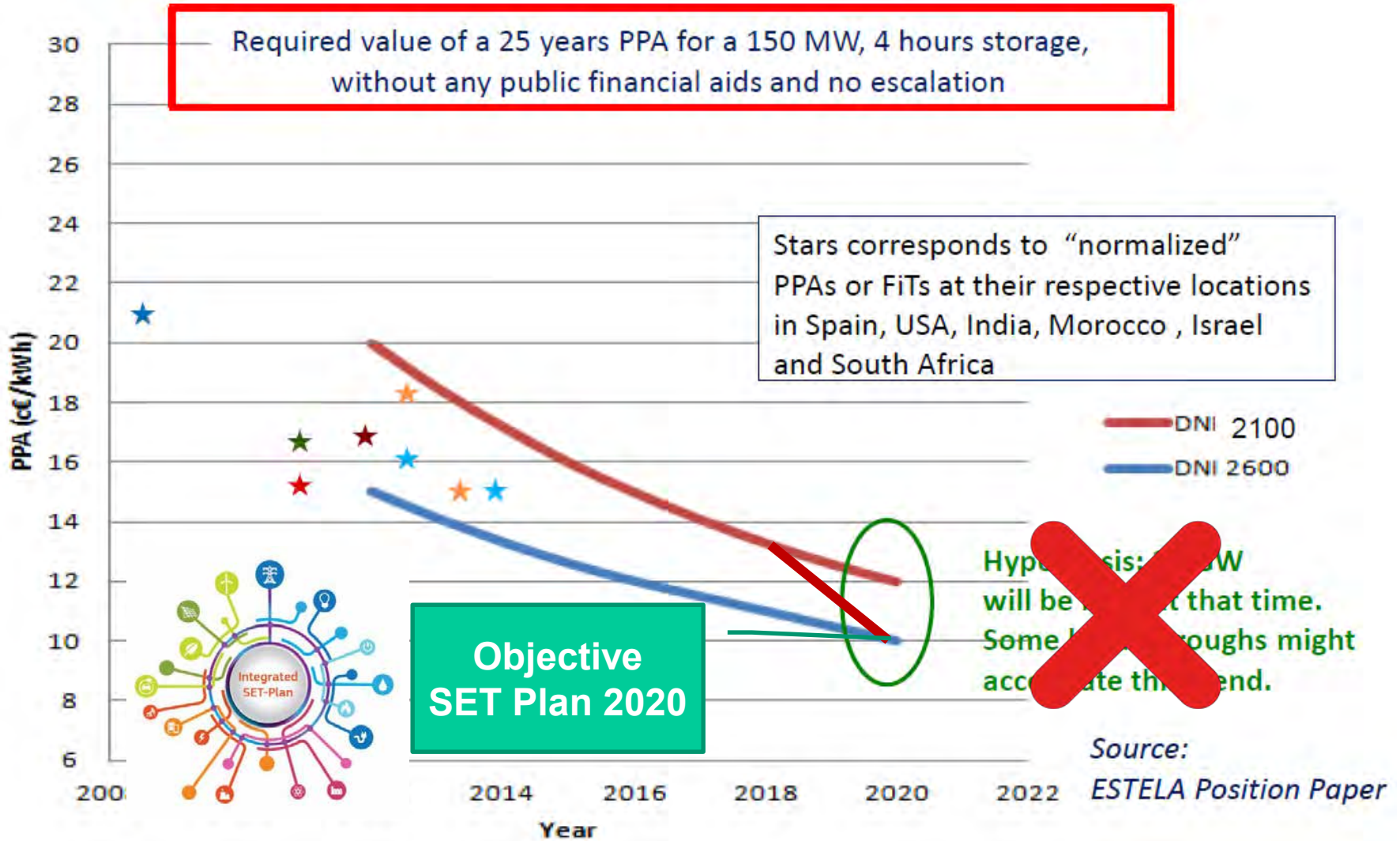


Gen 2++ or Gen 3?

Roadmaps: “The EU style”



Cost reduction estimations: The view from the European Industry





Initiative for Global Leadership in Concentrated Solar Power Implementation Plan

1. Advanced **Linear Concentrator Fresnel** technology with direct molten salt circulation as HTF and for high temperature thermal energy storage
2. **Parabolic Trough** with Molten Salt
3. **Parabolic Trough** with Silicon Oil
4. Solar Tower Power Plant to commercially scale-up and optimize the core components of the **Open Volumetric Air Receiver** technology
5. Improved **Central Receiver Molten Salt** technology
6. **Next Generation of Central Receiver** power plants
7. **Pressurized Air Cycles** for high efficiency solar thermal power plants
8. Multi-Tower Central Receiver **Beam Down** System
9. Thermal Energy **Storage**
10. Development of innovative concepts for **supercritical turbine** trains for CSP
11. Development of advanced concepts for **improved flexibility in CSP** applications
12. Development and Field Test of **CSP Hybrid Brayton Turbine Combined Cycle sCO₂** System

O&M TARGET
\$40/kW-yr plus \$3/MWh

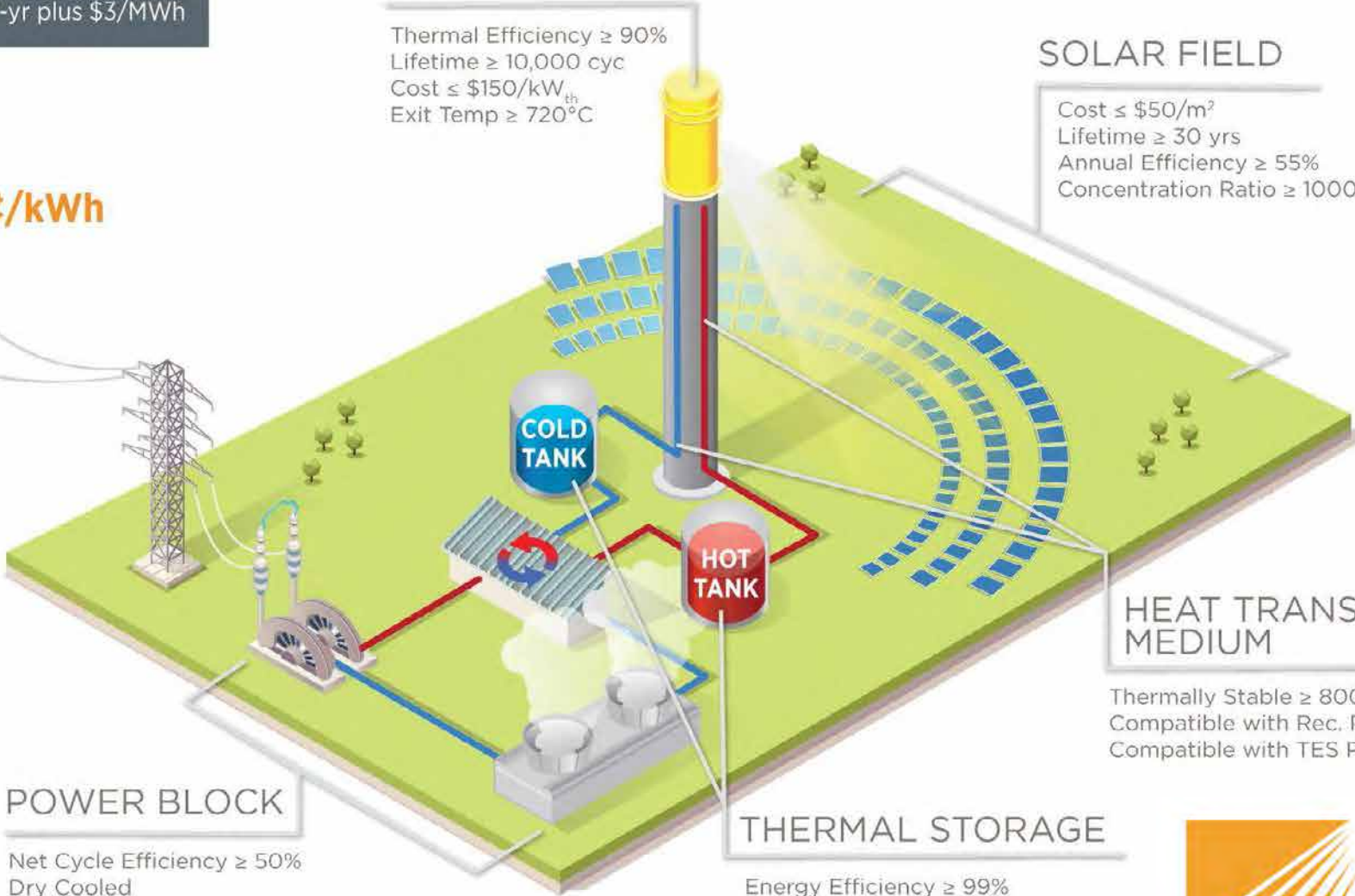
5¢/kWh

RECEIVER

Thermal Efficiency $\geq 90\%$
Lifetime $\geq 10,000$ cyc
Cost $\leq \$150/\text{kW}_{\text{th}}$
Exit Temp $\geq 720^\circ\text{C}$

SOLAR FIELD

Cost $\leq \$50/\text{m}^2$
Lifetime ≥ 30 yrs
Annual Efficiency $\geq 55\%$
Concentration Ratio ≥ 1000 Suns



HEAT TRANSFER MEDIUM

Thermally Stable $\geq 800^\circ\text{C}$
Compatible with Rec. Performance
Compatible with TES Performance

POWER BLOCK

Net Cycle Efficiency $\geq 50\%$
Dry Cooled
Cost $\leq \$900/\text{kW}_e$

THERMAL STORAGE

Energy Efficiency $\geq 99\%$
Exergetic Efficiency $\geq 95\%$
Cost $\leq \$15/\text{kWh}_{\text{th}}$
Power Cycle Inlet Temp $\geq 720^\circ\text{C}$

US DOE's vision 2030



Concentrating Solar Power Gen3 Demonstration Roadmap (Technical Report.NREL/TP-5500-67464 January 2017)

| | Collector Field | | |
|--|---|--|--|
| | <ul style="list-style-type: none"> • Cost <\$75/m² • Concentration ratio >50 | <ul style="list-style-type: none"> • Operable in 35-mph winds | <ul style="list-style-type: none"> • Optical error <3.0 mrad • 30-year lifetime |
| | Molten Salt | Falling Particle | Gas Phase |
| Receiver | <ul style="list-style-type: none"> • Similarities to prior demonstrations • Allowance for corrosive attack required | <ul style="list-style-type: none"> • Most challenging to achieve high thermal efficiency | <ul style="list-style-type: none"> • High-pressure fatigue challenges • Absorptivity control and thermal loss management |
| <ul style="list-style-type: none"> • Cost < \$150/kW_{th} • Thermal Efficiency > 90% • Exit Temperature > 720°C • 10,000 cycle lifetime | | | |
| Material & Support | <ul style="list-style-type: none"> • Potentially chloride or carbonate salt blends; ideal material not determined • Corrosion concerns dominate | <ul style="list-style-type: none"> • Suitable materials readily exist | <ul style="list-style-type: none"> • Minimize pressure drop • Corrosion risk retirement |
| <ul style="list-style-type: none"> • Cost < \$1/kg • Operable range from 250°C to 800°C | | | |
| Thermal Storage | <ul style="list-style-type: none"> • Direct or indirect storage may be superior | <ul style="list-style-type: none"> • Particles likely double as efficient sensible thermal storage | <ul style="list-style-type: none"> • Indirect storage required • Cost includes fluid to storage thermal exchange |
| <ul style="list-style-type: none"> • Cost < \$15/kW_{th} • 99% energetic efficiency • 95% exergetic efficiency | | | |
| HTF to sCO ₂ Heat Exchanger | <ul style="list-style-type: none"> • Challenging to simultaneously handle corrosive attack and high-pressure working fluid | <ul style="list-style-type: none"> • Possibly greatest challenge • Cost and efficiency concerns dominate | <ul style="list-style-type: none"> • Not applicable |
| | | | |
| Supercritical CO ₂ Brayton Cycle | | | |
| | <ul style="list-style-type: none"> • Net thermal-to-electric efficiency > 50% | <ul style="list-style-type: none"> • Power-cycle system cost < \$900/kW_e | <ul style="list-style-type: none"> • Dry-cooled heat sink at 40° C ambient • Turbine inlet temperature ≥ 700°C |

Various pathways for CSP Gen3 technology. No one pathway through all sub-systems exists without at least one significant technical, economic, or reliability risk.

Does it make sense to build large plants?

Solana was built large to take advantages of economies of scale.

- Economy of scale achieved in solar field assembly.
- Economy of scale not achieved as well in other areas:
 - Two 140 MW steam turbines
 - Four steam generators – two 50% trains per steam turbine
 - 6 parallel thermal energy storage (TES) units
 - 8 solar fields and 2 HTF pump groups
- The HTF system is large and complex
 - Twice the HTF per m² of collector area relative to 50 MW plant.
- Schedule – Took almost 3 years to build
- O&M – Large complex plant
 - Lots of equipment to operate and maintain
 - Takes time to get around.

 **Build smaller plants in a power park configuration**

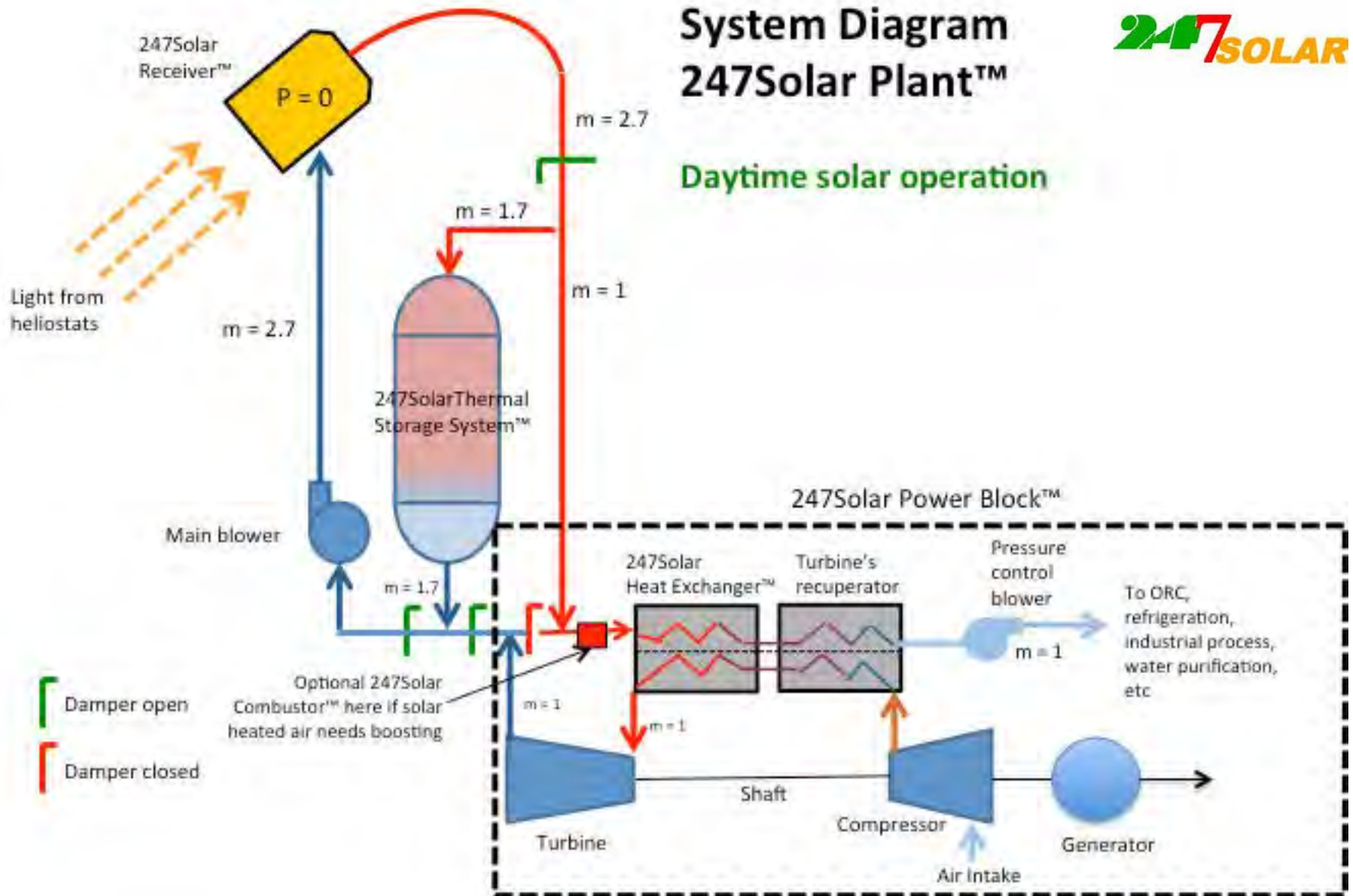
Modularity: Multitowers



System Diagram 247Solar Plant™



Daytime solar operation



50MW Beam-down molten salt tower in Yumen, Gansu



- 15 mirror field Modules, and each module consists of 17MWth solar field and one beam-down tower, totaling 50MWe.
- One 9-hour molten salt thermal storage system & steam turbine set are also equipped in the project.

It is expected that No.1-3 Modules will be completed and connected to the grid in September 2019.



Solar Thermal Electricity

... to Market Implementation of Advanced Technologies

- Efficiency (high-temperature /high-flux/new HTF/solar receivers)
- Integration in advanced cycles and direct conversion systems



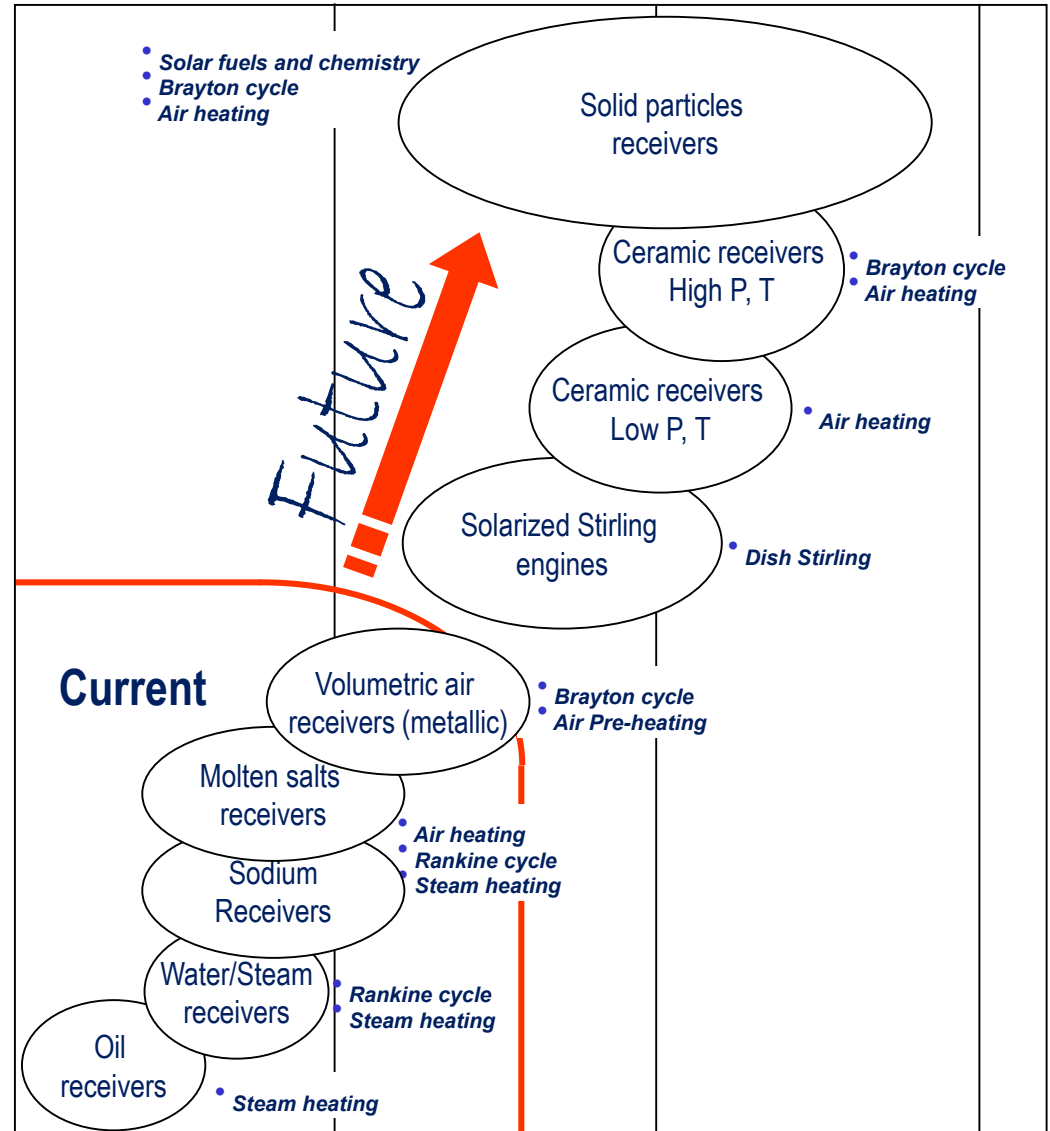
SPAIN
AORA
SOLAR ENERGY. LOCAL POWER.



WILSON
SOLARPOWER

Advanced concepts

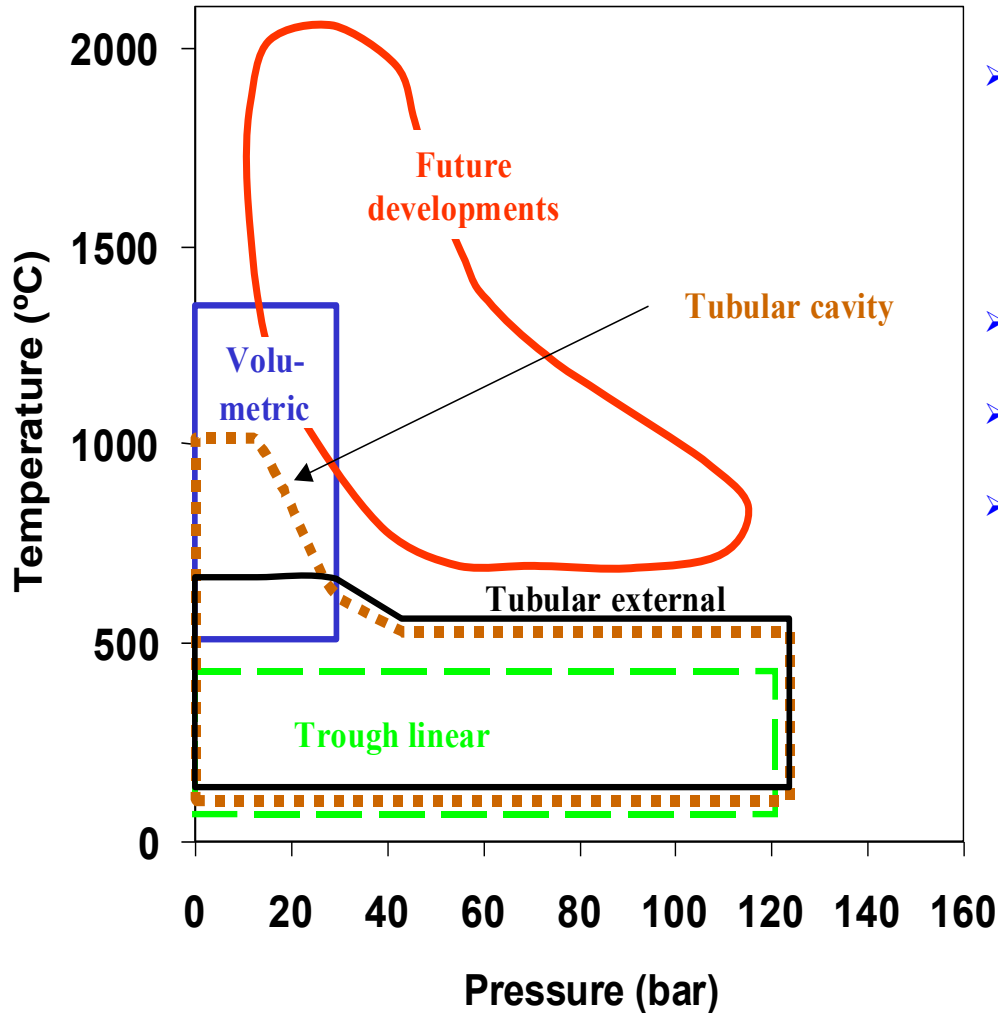
Present concepts



Source: IMDEA Energia

Temperature (thermal fluid)

Solar receiver: Reliable black-body is the key



- All should accumulate operational experience and long-term endurance tests.
- Volumetric
- Particle receivers
- Pressurized

Thank you very much for your attention!



institute
imdea
energy

SFERA-III

Solar Facilities for the European Research Area

1st Summer School “Thermal energy storage systems, solar fields and new cycles for future CSP plants”
WPI Capacity building and training activities
Odeillo, France, September 9th-11th 2019



“New concepts of line focus and point focus
concentrators”

Diogo Canavarro, University of Évora

NETWORKING

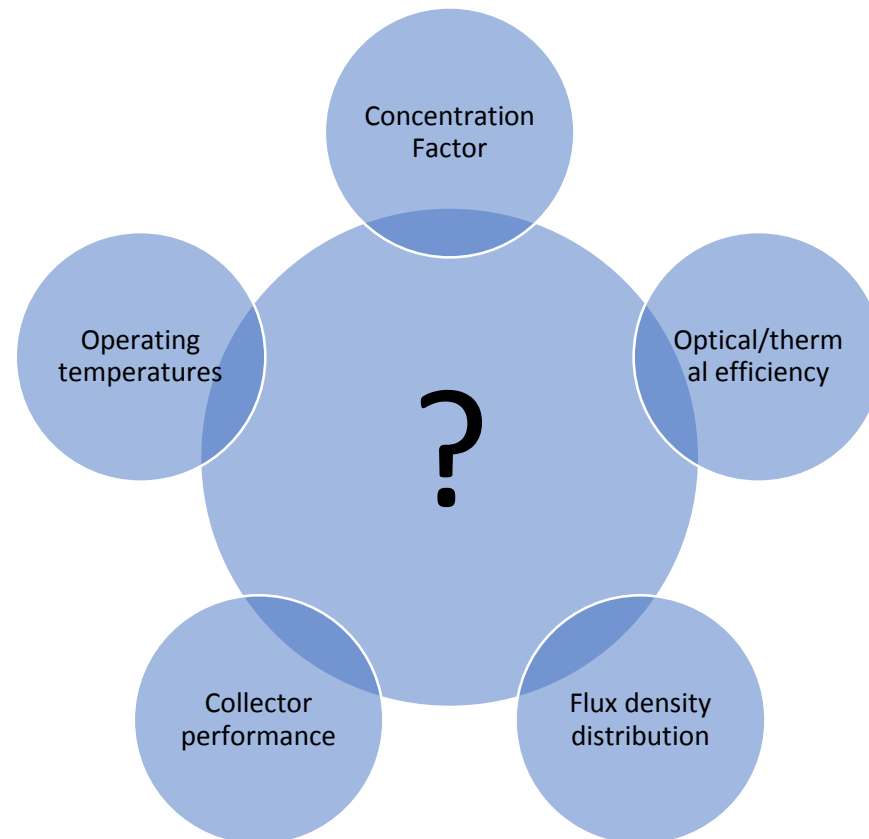


THIS PROJECT HAS RECEIVED FUNDING FROM THE EUROPEAN UNION'S HORIZON 2020 RESEARCH AND INNOVATION PROGRAMME UNDER GRANT AGREEMENT NO **823802**

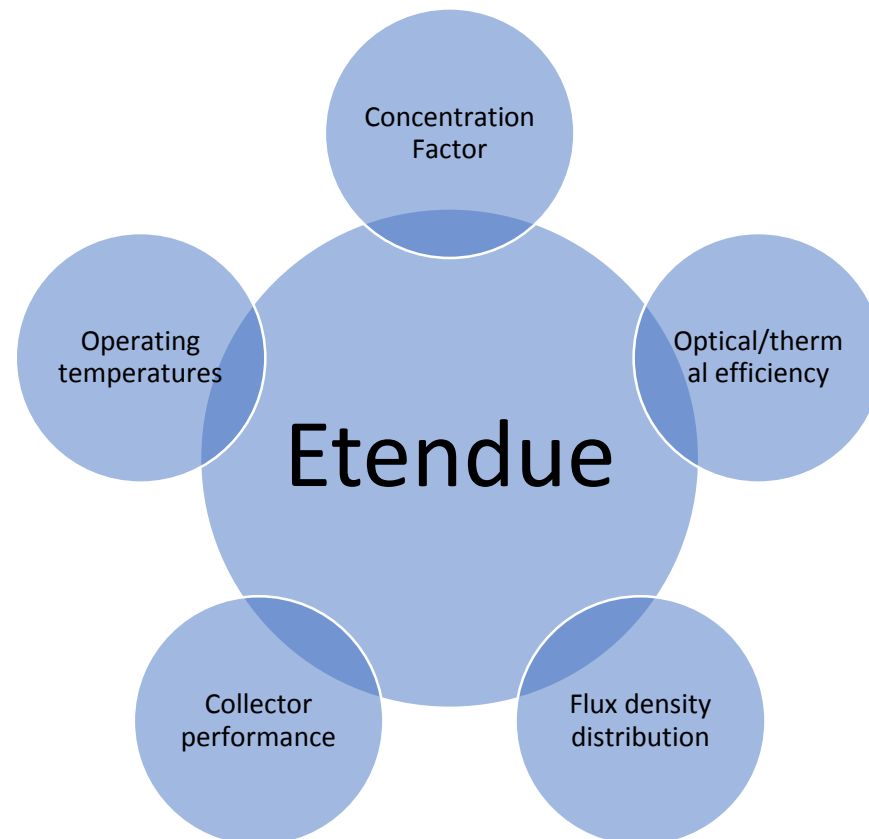
Outline

- The main guiding idea of solar concentration
- The limits of concentration and non-imaging optics
- Line focusing concentrators
 - Parabolic trough concentrators
 - Linear Fresnel concentrators
- Point focusing concentrators
 - Parabolic dish concentrators
 - Central Tower concentrators
- Future developments and trends
- Conclusions
- References

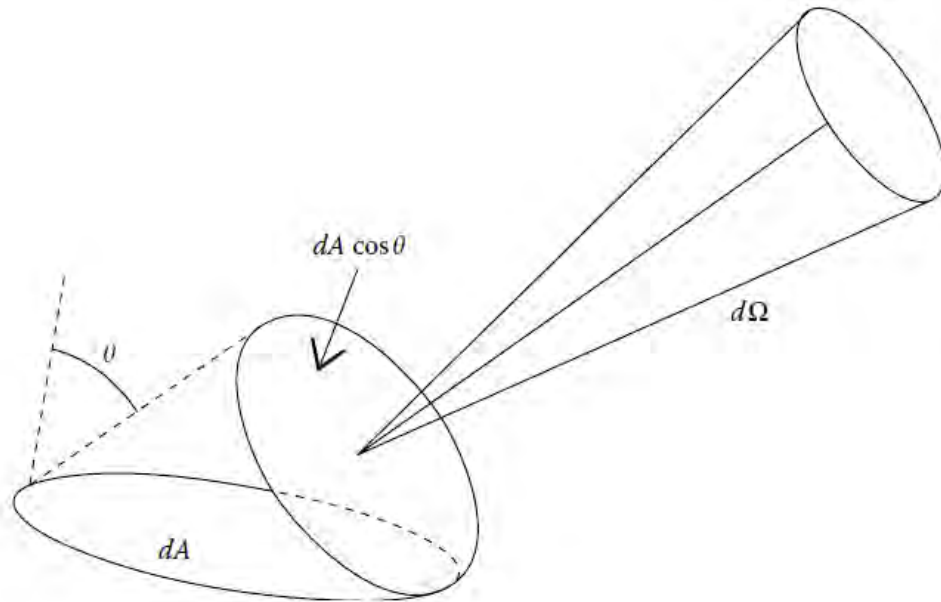
What is the main guiding idea of solar concentration?



The main guiding idea of solar concentration



The concept of Etendue



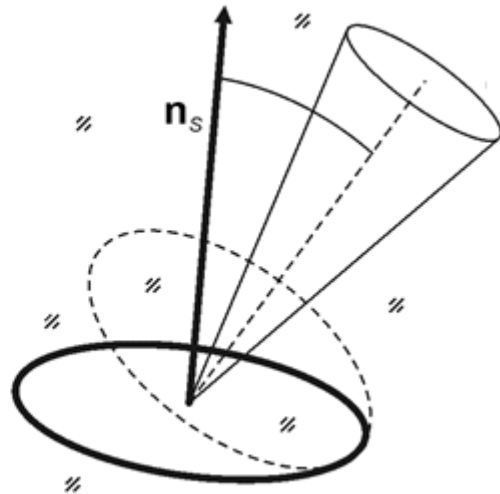
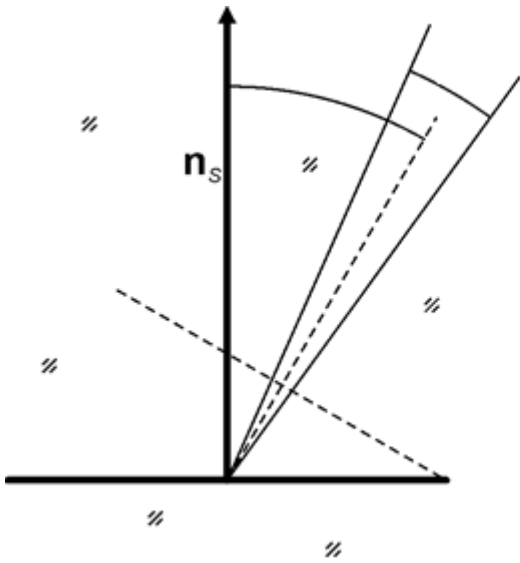
Etendue is a geometrical quantity that measures the amount of “room” available for light to pass through

- **Spatial room** (light crosses dA in direction θ): $dA \cos \theta$
- **Angular room** (from within the solid angle): $d\Omega$



$$dU = n dA \cos \theta d\Omega$$

The concept of Etendue



Etendue for a differential surface element in 2D (left) and 3D (right)

- In 2D-systems:

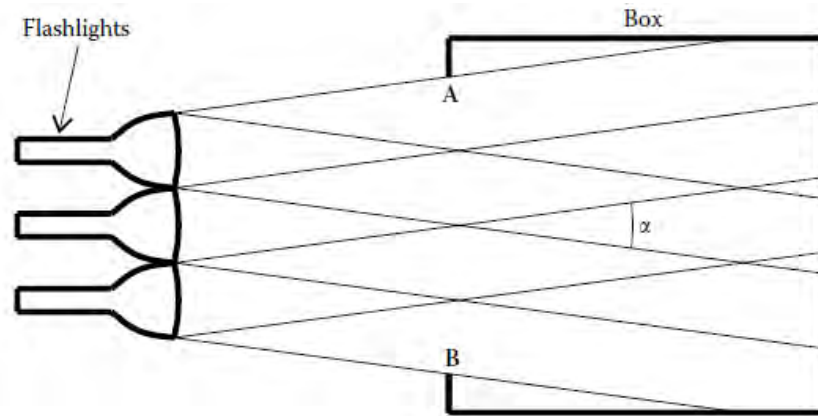
$$dU = n dA \cos \theta d\Omega$$



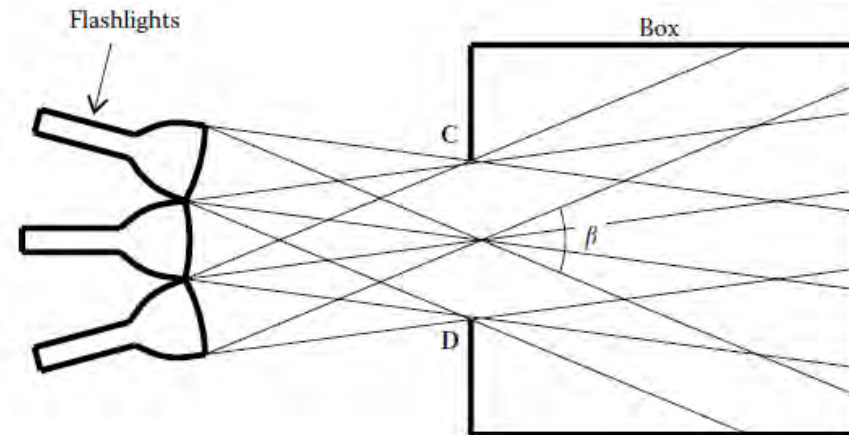
$$U = nA \int_{-\theta}^{+\theta} \cos \theta d\theta = 2nA \sin \theta$$

Which corresponds to the etendue of the light crossing a length A within a solid angle $\pm\theta$

The concept of Etendue



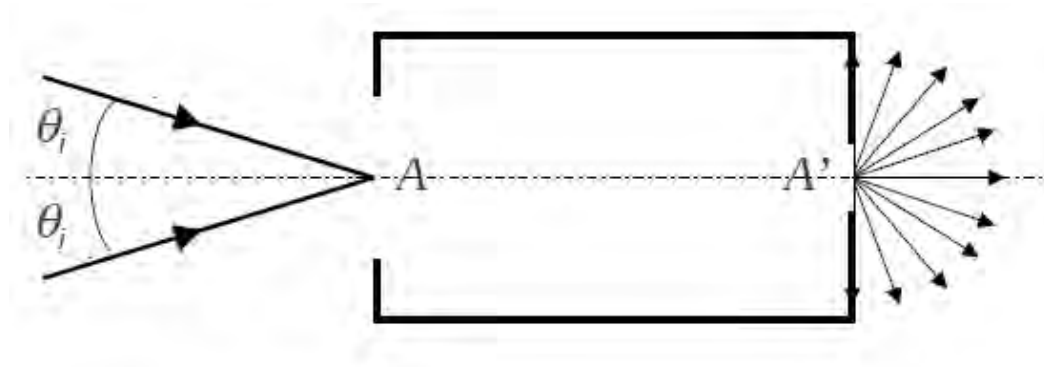
$$U_1 = 2n[\mathbf{A}, \mathbf{B}] \sin \alpha$$



$$U_2 = 2n[\mathbf{C}, \mathbf{D}] \sin \beta$$

From the conservation of the étendue ($U_1 = U_2$) $\rightarrow \beta > \alpha$

Conservation of etendue and maximum concentration



Etendue incident on a aperture A within a solid angle $\pm\theta_i$ and exiting through a surface A' . What is the maximum concentration $C = A/A'$ possible?

- The etendue at entrance A , U_A , is given by:

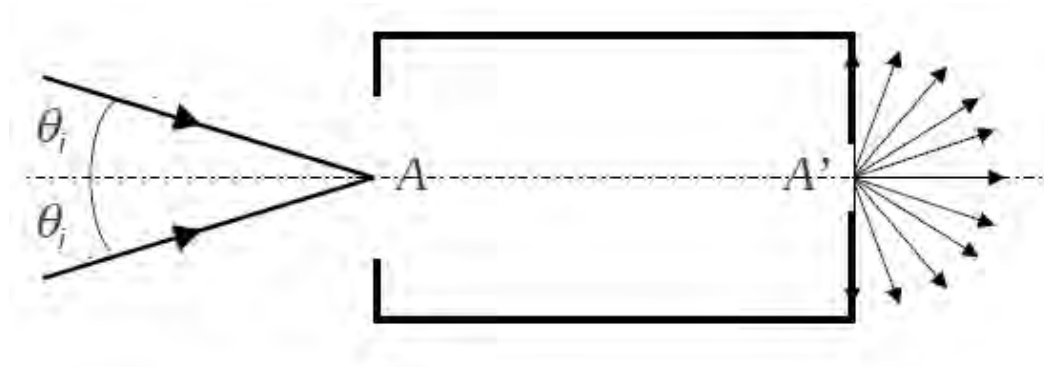
$$U_A = 2nA \sin \theta_i$$

- The etendue at exit A' , $U_{A'}$, is given by:

$$U_{A'} = 2nA' \sin \theta_e$$

- Conservation of etendue implies $U_A = U_{A'}$

Conservation of etendue and maximum concentration



Etendue incident on a aperture A within a solid angle $\pm\theta_i$ and exiting through a surface A' . What is the maximum concentration $C = A/A'$ possible?

- We want the maximum etendue (maximum concentration) at the exit. Therefore, $\theta_e = \pi/2$ and for a uniform medium $n=1$:

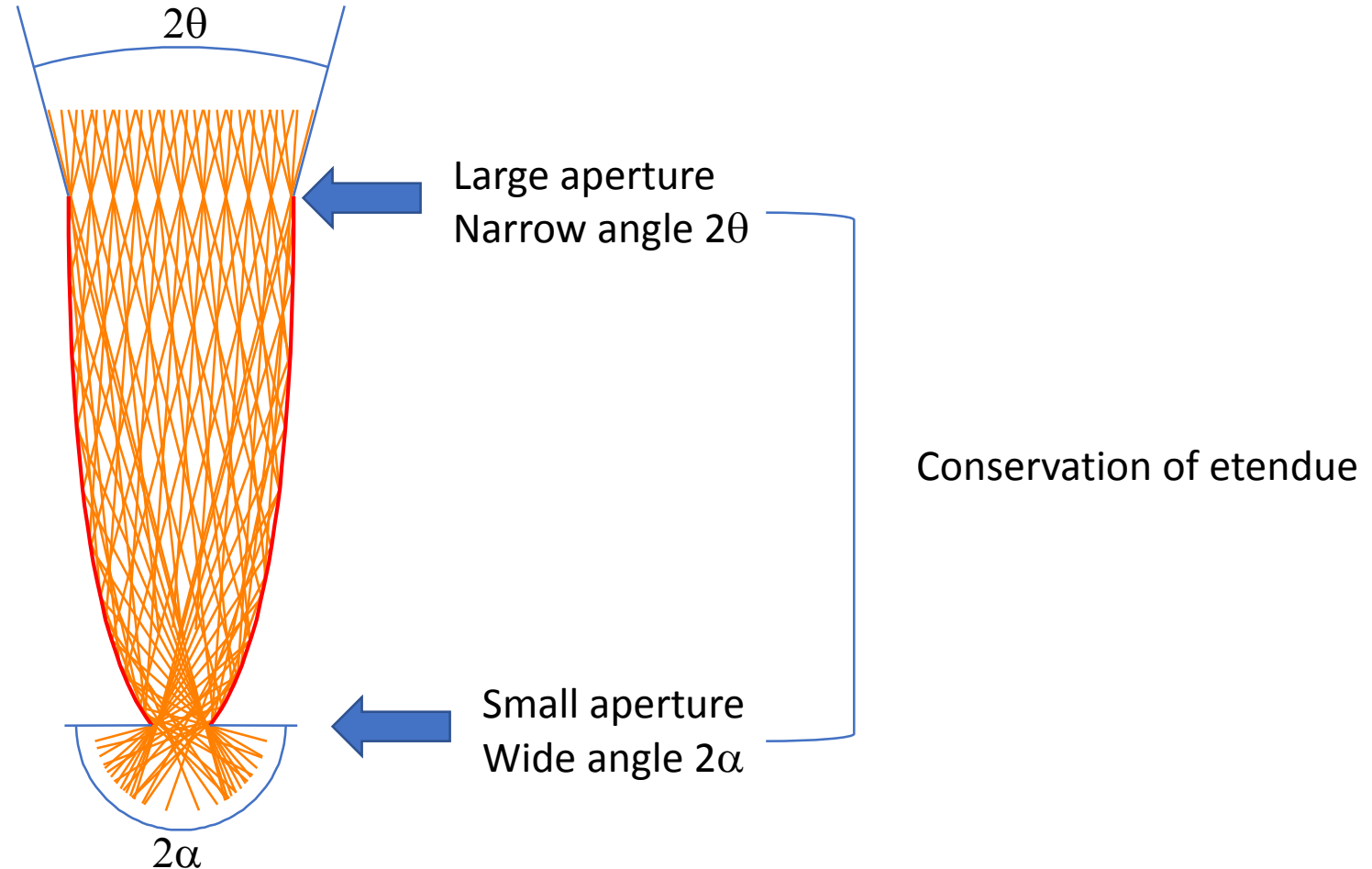
$$2A \sin \theta_i = 2A'$$

$$\frac{A}{A'} = C = \frac{1}{\sin \theta_i}$$

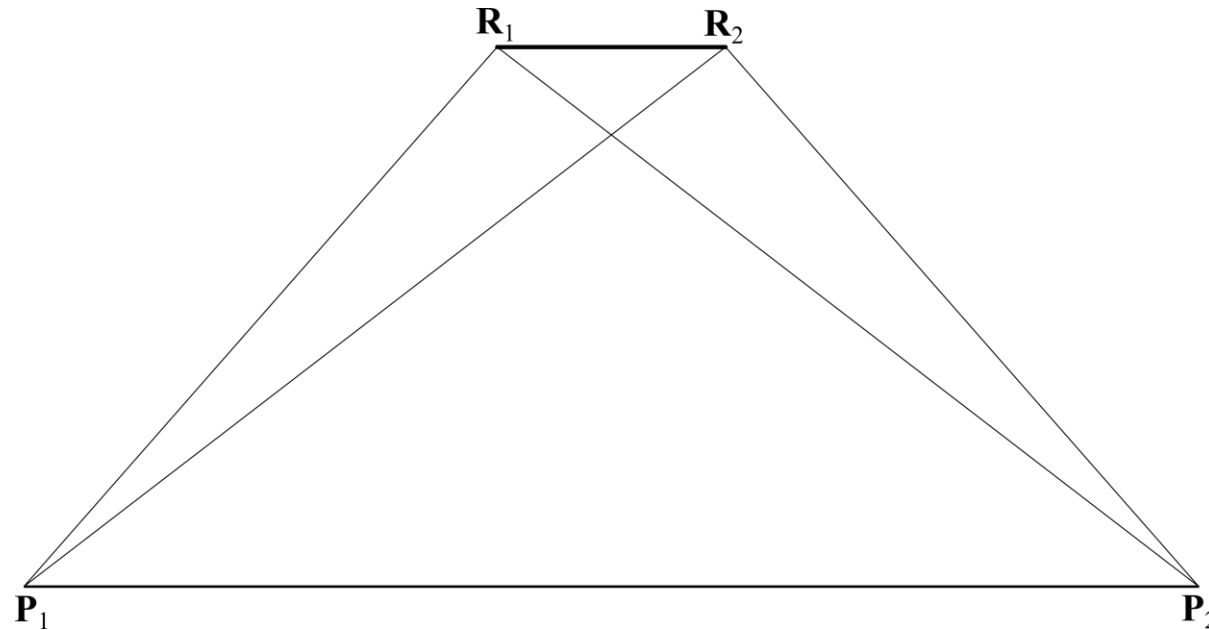
Maximum concentration for 2D-systems

SFERA-III

Solar Facilities for the European Research Area

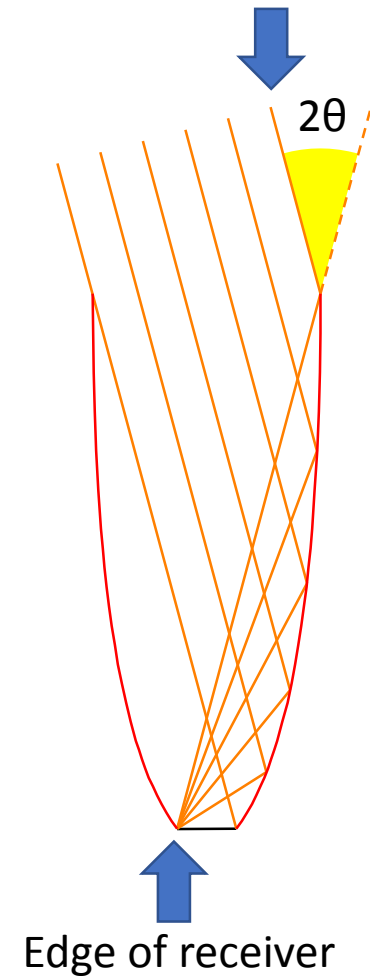
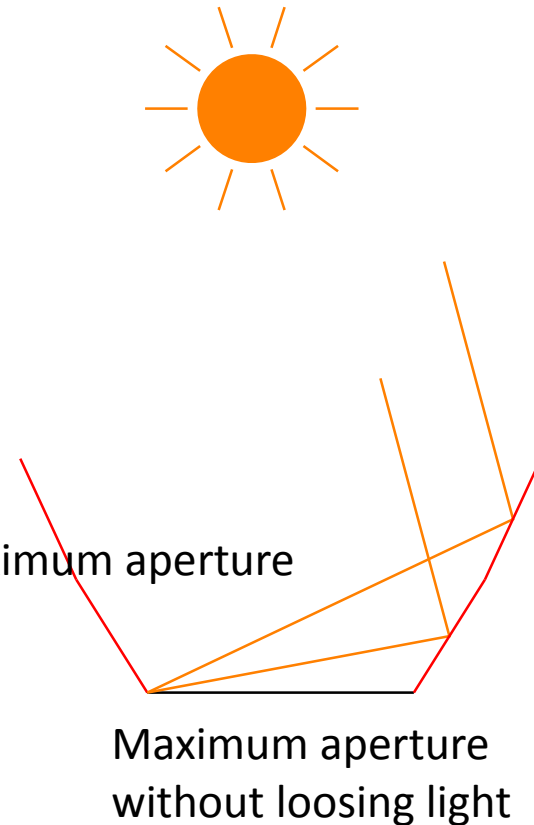
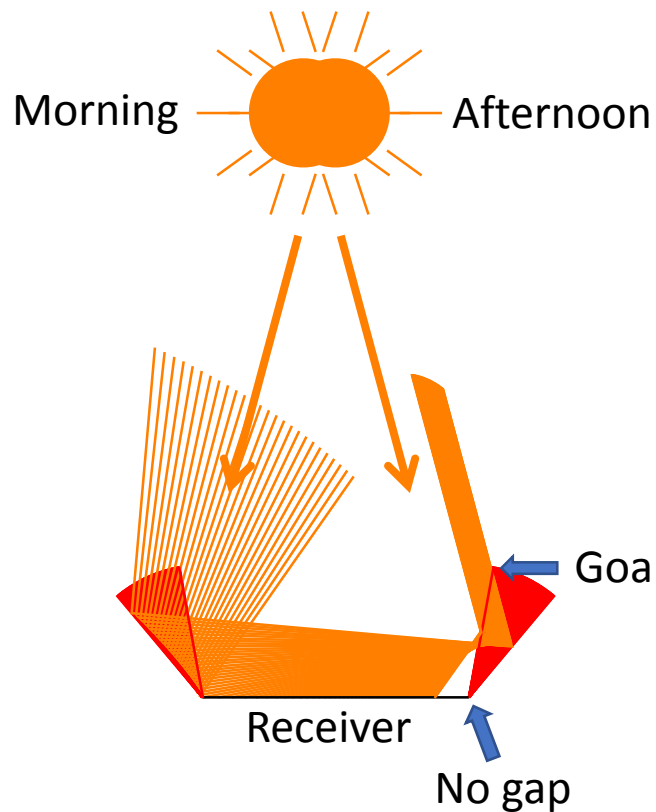


A trade-off: **The Hottel's string method.** The etendue exchanged between two surfaces can be given by the difference of the optical path length.



$$U_{P_1P_2-R_1R_2} = [P_1, R_2] + [P_2, R_1] - [R_1, P_1] - [R_2, P_2]$$

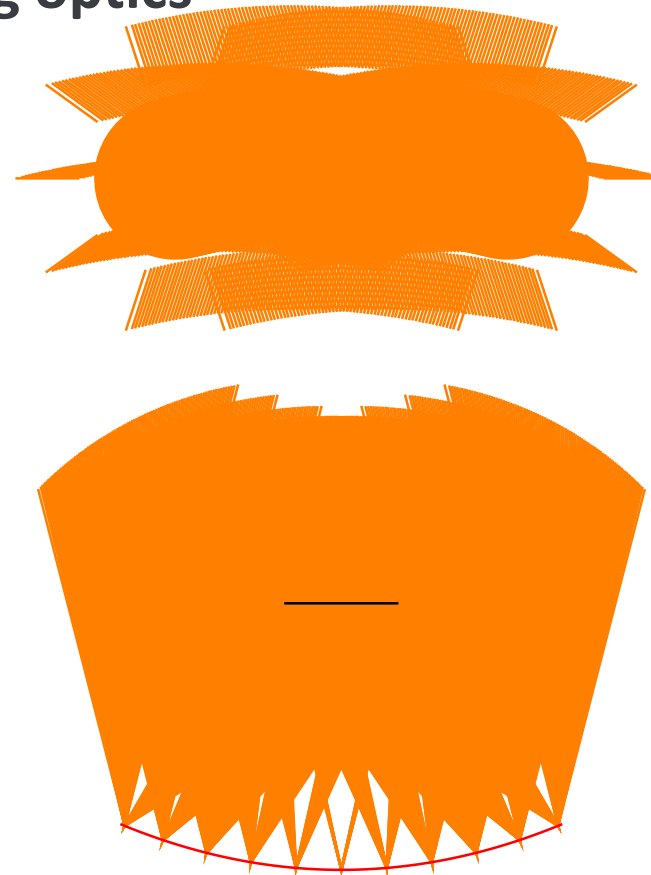
The limits of concentration and non-imaging optics



Edge-Ray Principle:
Edge rays of the incoming radiation are redirected to the edges of the receiver.

The limits of concentration and non-imaging optics

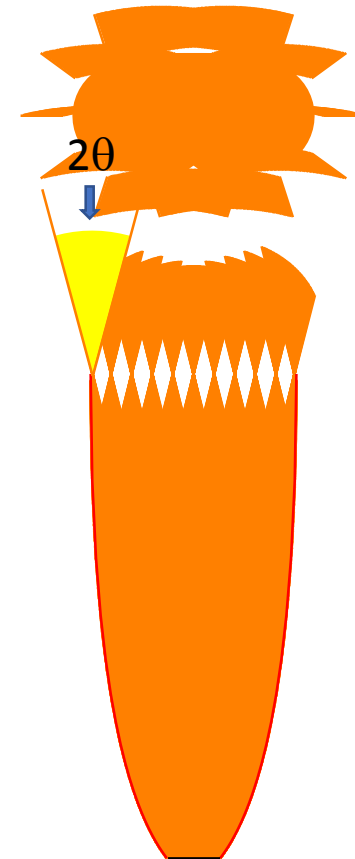
Imaging optics such as parabolas, lens, etc., tend to violate the Edge-Ray Principle. They form image(s) somewhere between $\pm\theta$ but not at the maximum acceptance angle.



Small acceptance angle!

The limits of concentration and non-imaging optics

Non-Imaging optics such as CPC, Trumpet, etc., respect the Edge-Ray Principle. They form image(s) at maximum acceptance but not in between $\pm\theta$.

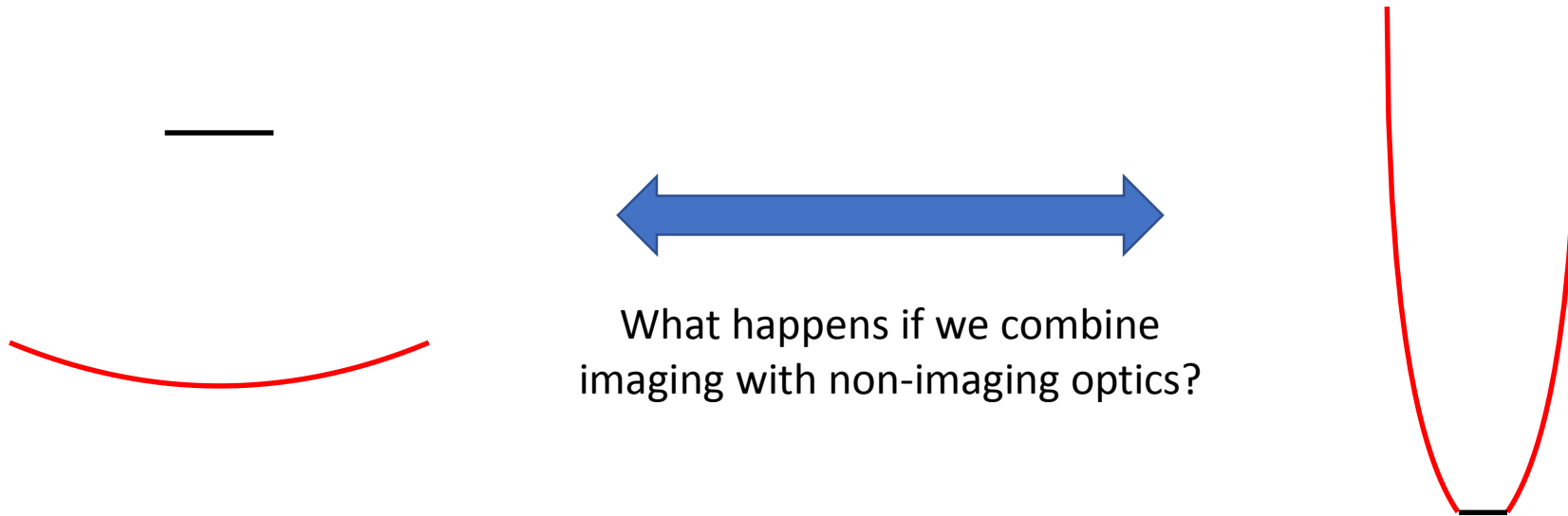


Maximum acceptance angle!

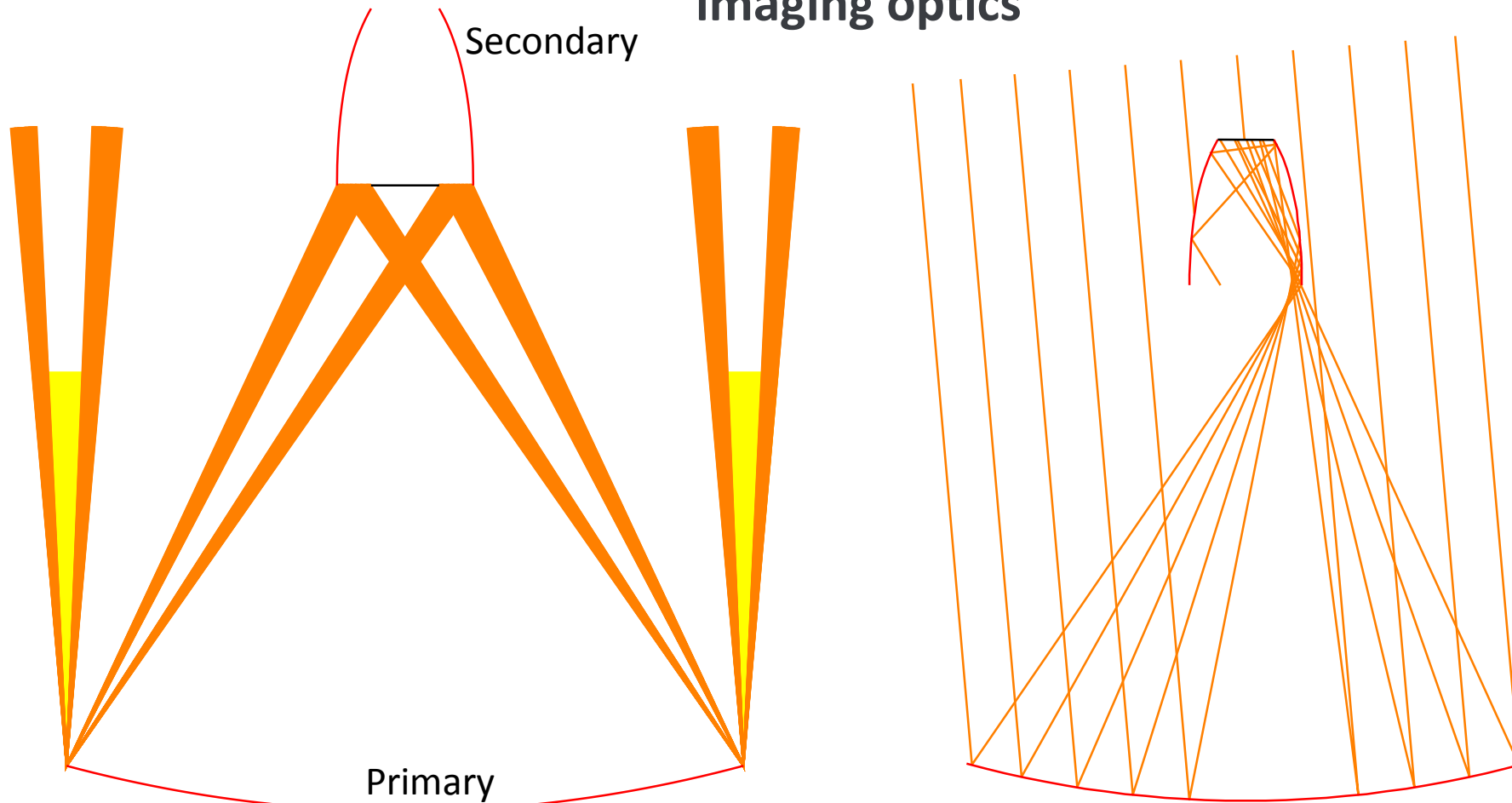
The limits of concentration and non-imaging optics

Imaging optics usually fall short from the theoretical limits (small acceptance-angle for a given concentration factor). However, they are compact (low f-number)

Non-Imaging optics usually reach the theoretical limits (maximum acceptance-angle for a given concentration factor). However, they are not compact (high f-number)



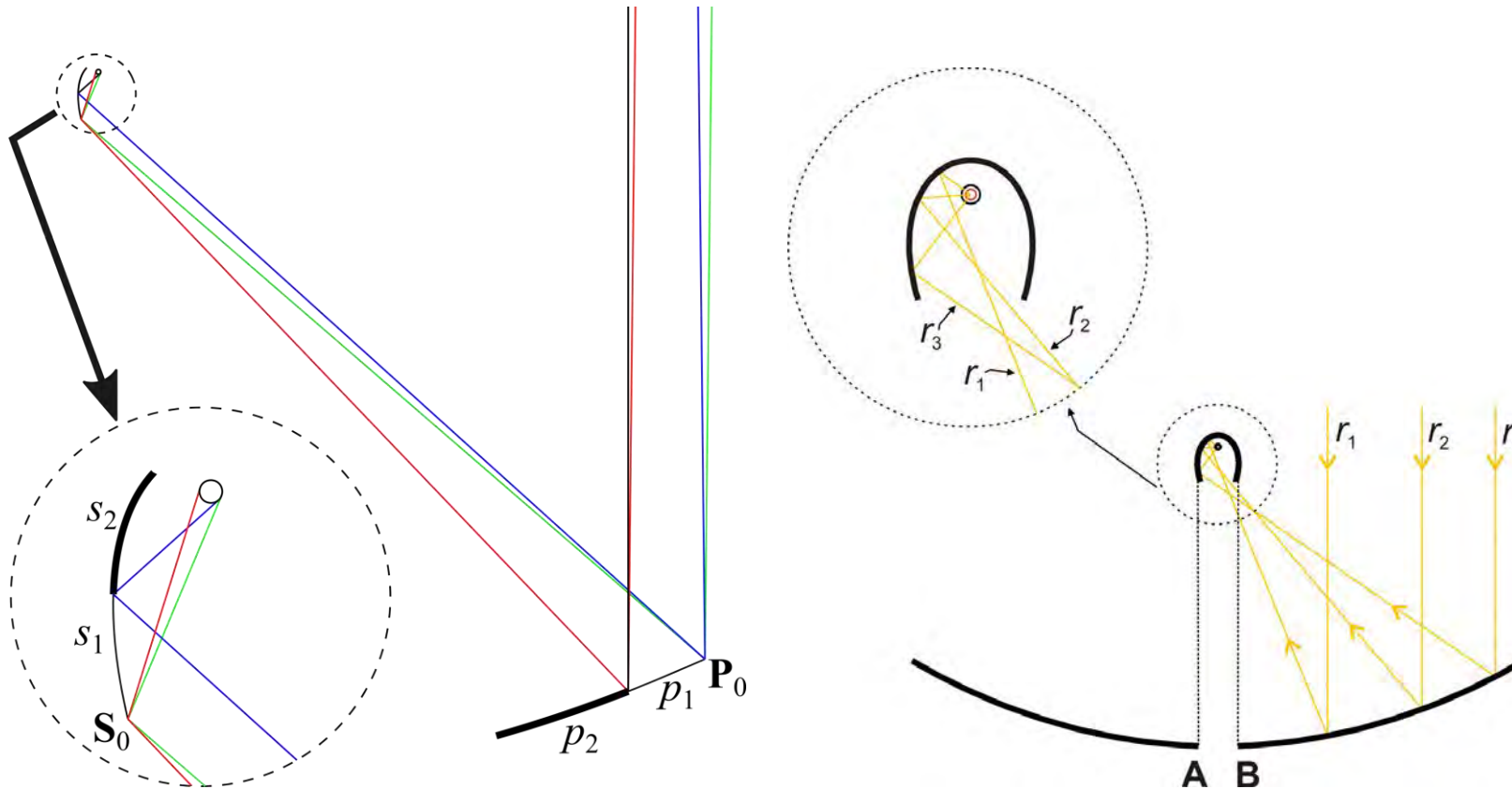
The limits of concentration and non-imaging optics



Compared to CPC:
Trades some acceptance for compactness

Compared to the parabola:
Trades some compactness for acceptance

Line Focusing Concentrators – Parabolic Trough concentrators



- Simultaneous Multiple Surface method with double reflective mirrors (XX SMS)
- Designed for maximum concentration (etendue conservation and edge-ray principle)
- Light enters perpendicularly to the receiver to reduce Fresnel losses.

Line Focusing Concentrators – Parabolic Trough concentrators

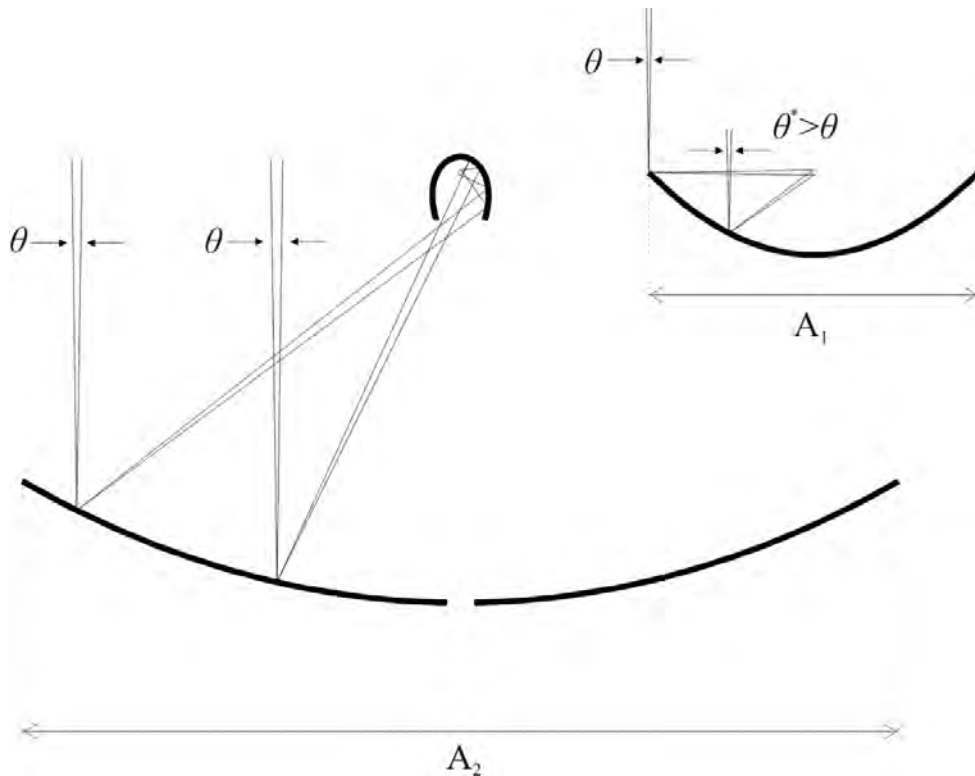
A comparison with PT concentrators

| | Aperture size (m) | Receiver radius (m) | Aspect ratio (Height/Width) | φ (deg) | Cg (X) | θ (deg) | CAP | η_{opt0} |
|--------|-------------------|---------------------|-----------------------------|-----------------|--------|----------------|------|---------------|
| PT | 5,77 | 0,035 | 0,30 | 80,3 | 26,24 | 0,694 | 0,32 | 0,81 |
| XX SMS | 11,08 | 0,035 | 0,51 | 55 | 50,38 | 0,694 | 0,61 | 0,72 |

| Optic | DNI Faro, Portugal (kWh/m ²) | Collected Energy per aperture area (kWh/m ²) | Total amount of collected energy (kWh)* |
|--------|--|--|---|
| PT | 2234 | 1304 | 7524 |
| XX SMS | | 1150 | 12742 |

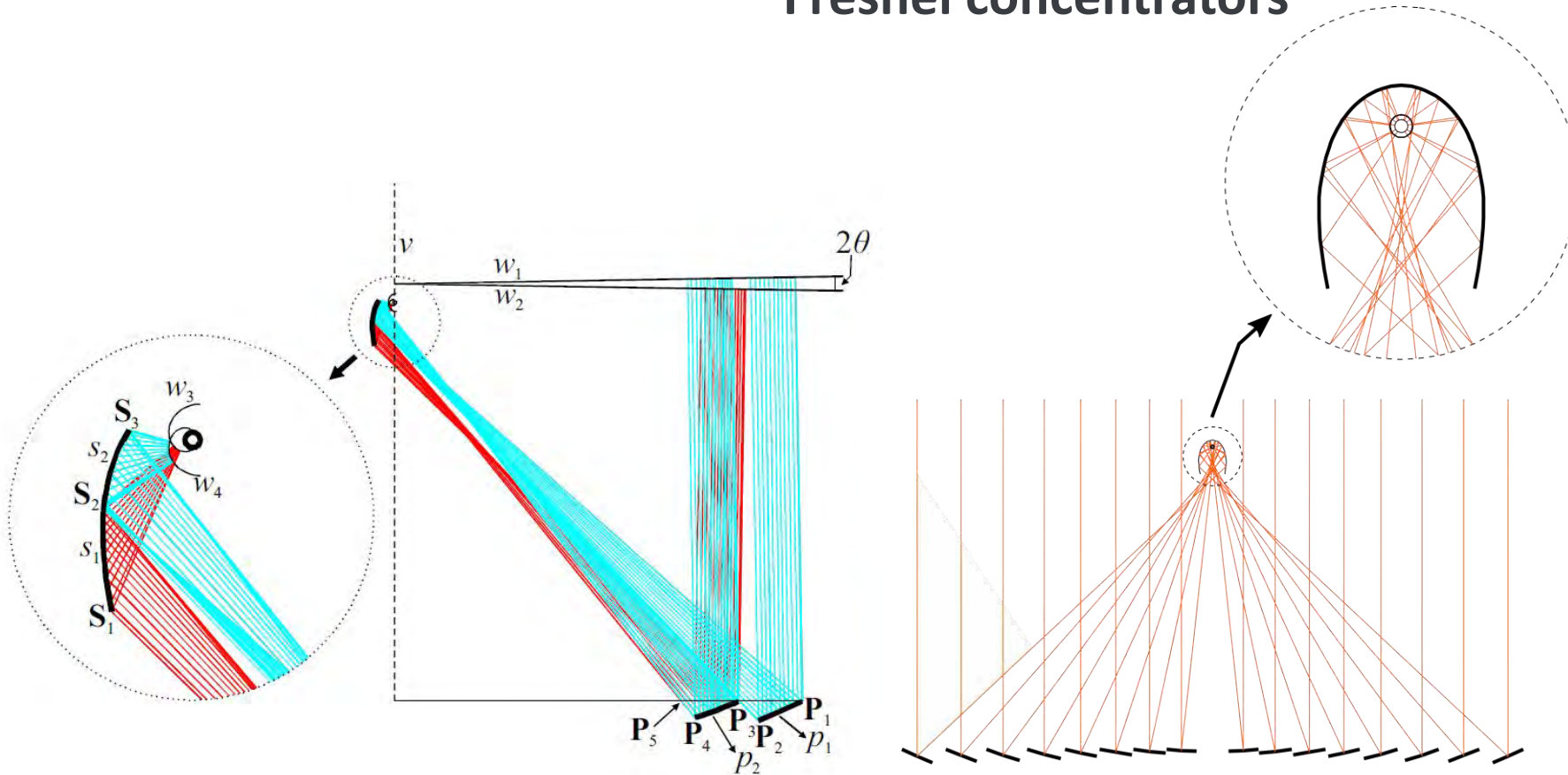
* - For a length of 1m. Calculations done using a raytracing technique.

Line Focusing Concentrators – Parabolic Trough concentrators



$A_2 \gg A_1$! The XX SMS has a much **LARGER** aperture width for the same acceptance-angle of the PT concentrator.

Line Focusing Concentrators – Linear Fresnel concentrators



- Linear Fresnel XX SMS (similar to the previous XX SMS)
- Maximum concentration
- Maximum compactness of heliostats

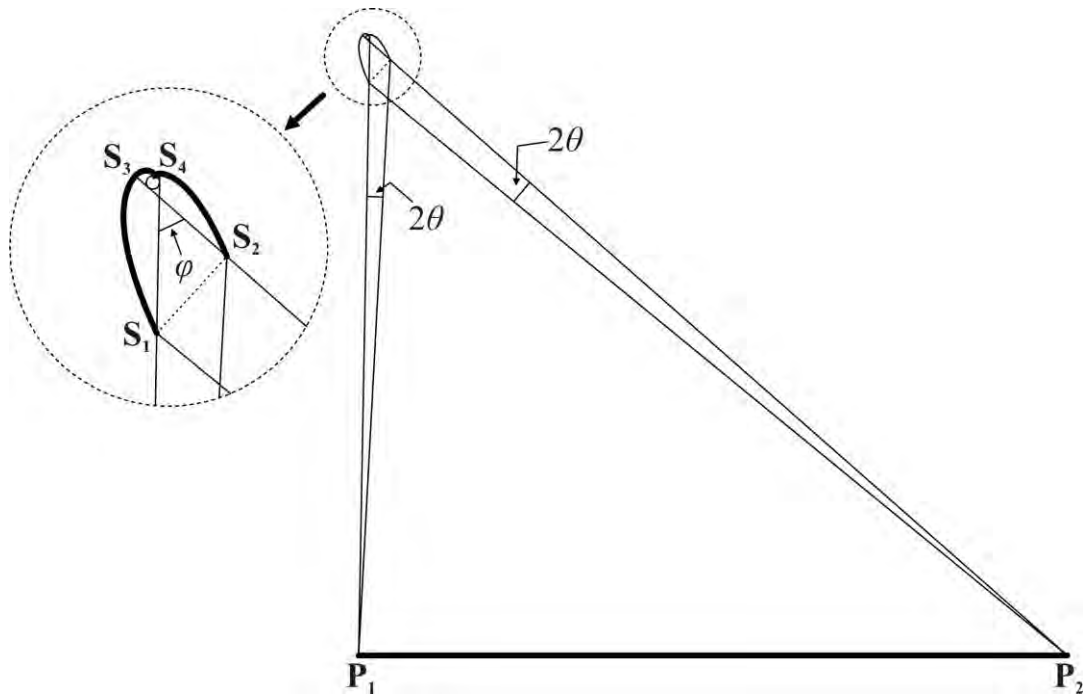
Line Focusing Concentrators – Linear Fresnel concentrators

A comparison with PT concentrators and Fresnel with CPC concentrators

| Optic | DNI Faro, Portugal (kWh/m2) | Cg (X) | θ (°) | CAP | η_{opt0} | Collected Energy (kWh)* |
|-------------------|-----------------------------|--------|--------------|------|---------------|-------------------------|
| Fresnel CPC | 2234 | 48.21 | 0.44 | 0.38 | 0.68 | 11361 |
| Fresnel XX SMS #1 | | 73.71 | 0.44 | 0.57 | 0.68 | 15122 |
| PT | | 26.24 | 0.69 | 0.32 | 0.81 | 7527 |
| Fresnel XX SMS #2 | | 52.95 | 0.69 | 0.64 | 0.66 | 10622 |

* - For a length of 1m. Calculations done using a raytracing technique.

Line Focusing Concentrators – Linear Fresnel concentrators



The etendue, U , exchanged between P_1 and P_2 is given by:

$$U = [P_1, S_2] + [P_2, S_1] - [P_1, S_1] - [P_2, S_2]$$

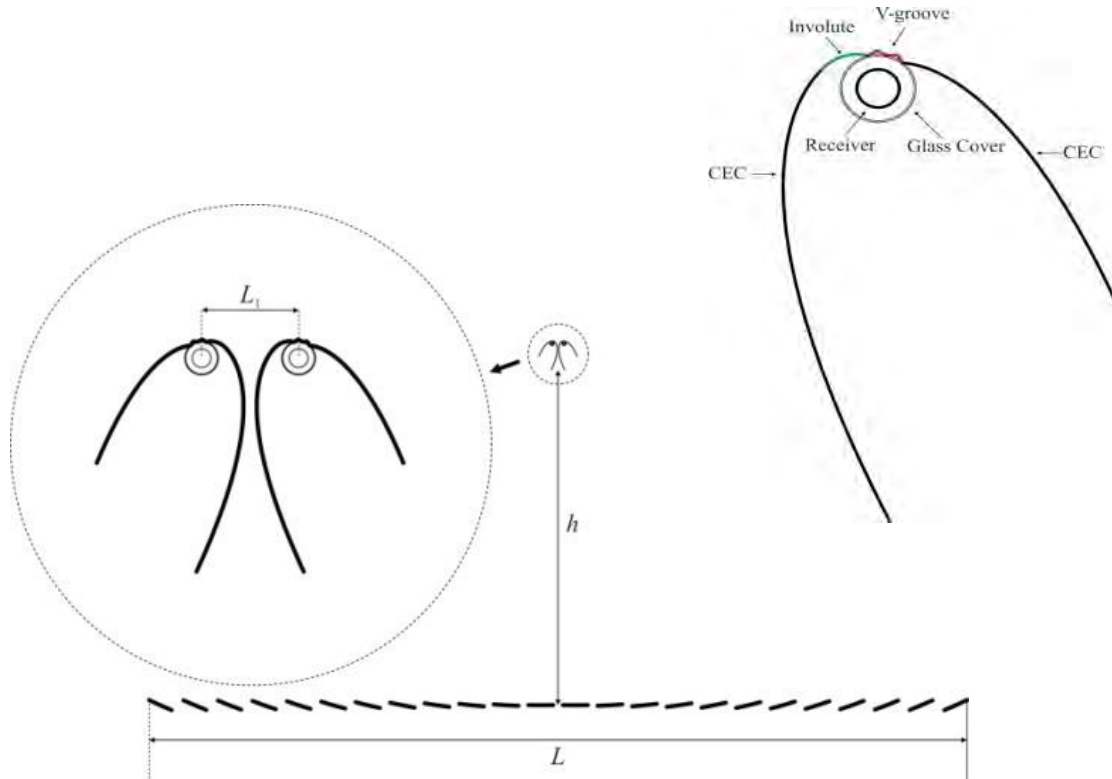
The maximum etendue capture by the receiver, U_R , is given by (r is the radius):

$$U_R = 4\pi r$$



$$r = \frac{U}{4\pi}$$

Line Focusing Concentrators – Linear Fresnel concentrators



- Compact system with two receivers placed at the same tower with a low distance ($L_1 < 0.5\text{m}$) between them.
- Asymmetric set of primary/secondary stage CEC combinations
- It uses a very large primary ($L > 20\text{m}$) contributing for the reduction of rows in the total field;
- The two evacuated tubular receivers can be fed by a single pipe and merge in a single exit pipe.

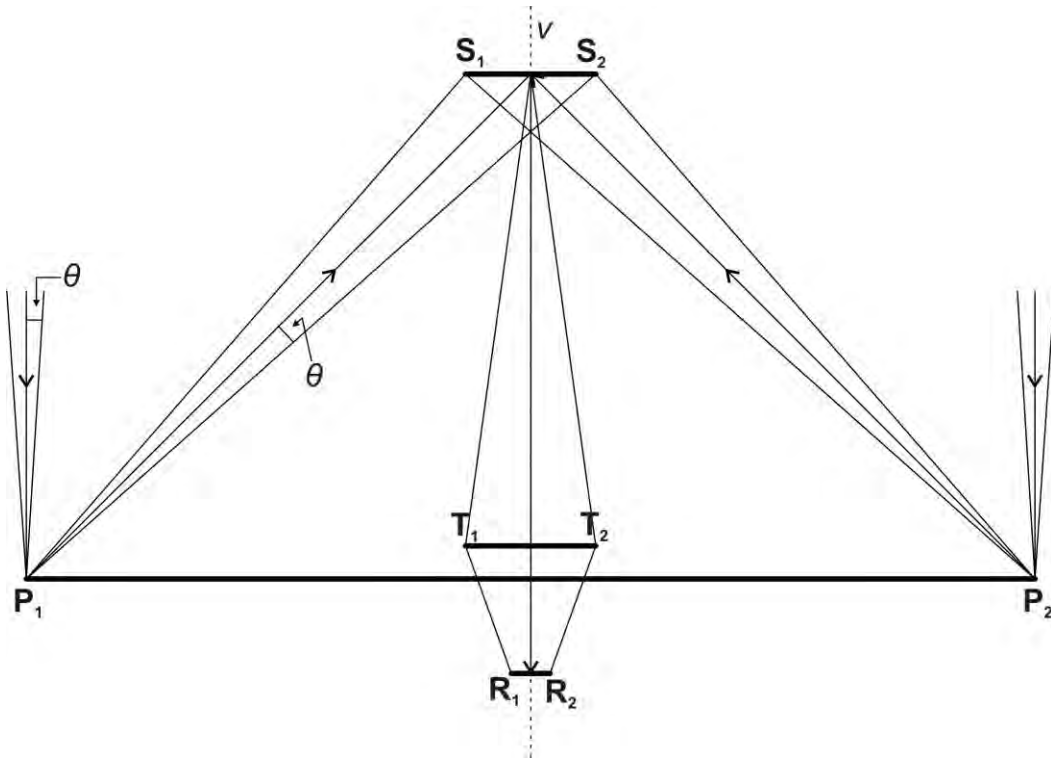
Line Focusing Concentrators – Linear Fresnel concentrators

Geometric data and performance estimation

| Optic | Aperture width (m) | Total mirror aperture width (m) | Receiver radius (m) | Receiver height (m) | Number of mirrors | Mirror width (m) | Cg (X) | φ (°) |
|--------------------------------------|--------------------|---------------------------------|---------------------|---------------------|-------------------|------------------|--------|---------------|
| Dual Asymmetric CEC LFR Concentrator | 26 | 22 | 0.035 | 10.8 | 22 | 1 | 45 | 49.73 |

| Location | Thermal Energy delivered (kWh) | Electricity produced (kWh) | Total average yearly efficiency (kWh) |
|-----------------|--------------------------------|----------------------------|---------------------------------------|
| Faro, Portugal | 2.11×10^8 | 8.38×10^7 | 0.14 |
| Hurgahda, Egypt | 3.02×10^8 | 1.22×10^8 | 0.16 |

Point Focusing Concentrators – Parabolic dish concentrators



The etendue reaching the primary $\mathbf{P}_1\mathbf{P}_2$, $U_{\mathbf{P}_1\mathbf{P}_2}$, is given by:

$$U_{\mathbf{P}_1\mathbf{P}_2} = 2[\mathbf{P}_1, \mathbf{P}_2] \sin \theta$$

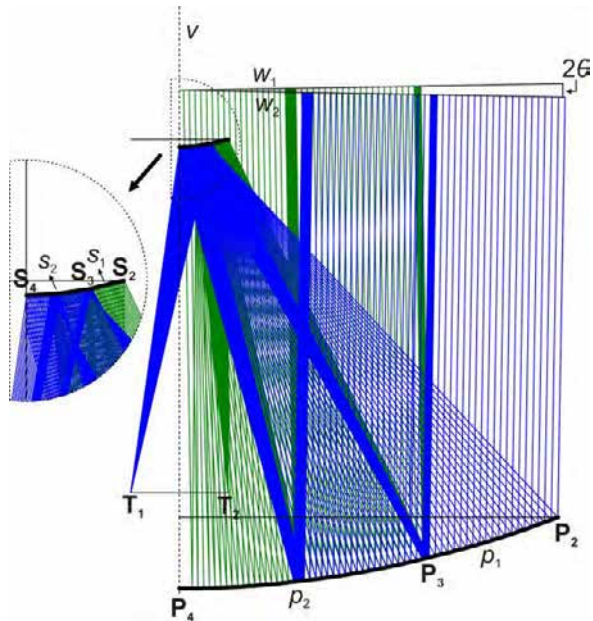
$$U_{\mathbf{P}_1\mathbf{P}_2-\mathbf{S}_1\mathbf{S}_2} = [\mathbf{P}_1, \mathbf{S}_2] + [\mathbf{P}_2, \mathbf{S}_1] - [\mathbf{S}_1, \mathbf{P}_1] - [\mathbf{S}_2, \mathbf{P}_2]$$

$$U_{\mathbf{S}_1\mathbf{S}_2-\mathbf{T}_1\mathbf{T}_2} = [\mathbf{S}_1, \mathbf{T}_2] + [\mathbf{S}_2, \mathbf{T}_1] - [\mathbf{S}_1, \mathbf{T}_1] - [\mathbf{S}_2, \mathbf{T}_2]$$

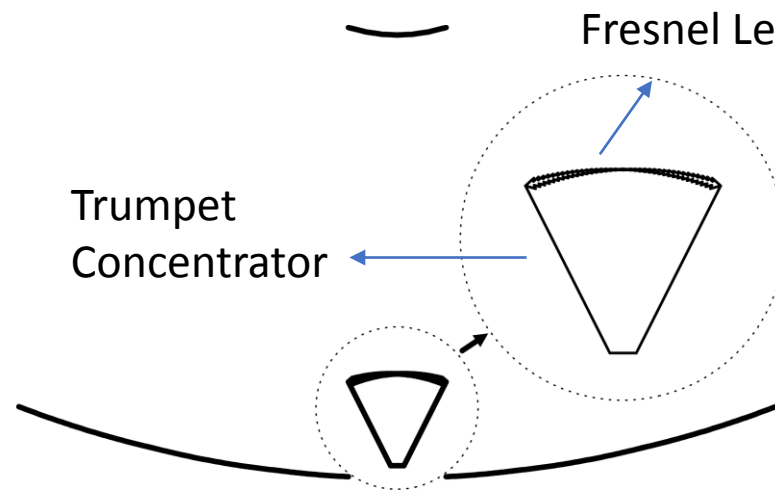
$$U_{\mathbf{T}_1\mathbf{T}_2-\mathbf{R}_1\mathbf{R}_2} = [\mathbf{T}_1, \mathbf{R}_2] + [\mathbf{T}_2, \mathbf{R}_1] - [\mathbf{T}_1, \mathbf{R}_1] - [\mathbf{T}_2, \mathbf{R}_2]$$

The conservation of the etendue implies that $U_{\mathbf{P}_1\mathbf{P}_2} = U_{\mathbf{S}_1\mathbf{S}_2-\mathbf{T}_1\mathbf{T}_2}$ and the same between $\mathbf{T}_1\mathbf{T}_2$ and $\mathbf{R}_1\mathbf{R}_2$.

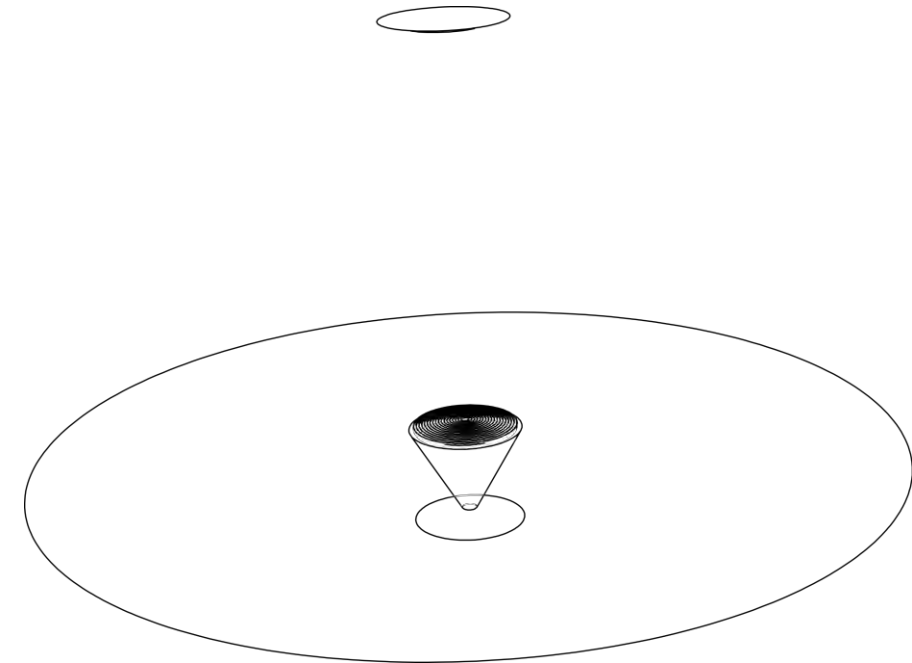
Point Focusing Concentrators – Parabolic dish concentrators



Design



2D-version



3D-version

Point Focusing Concentrators – Parabolic dish concentrators

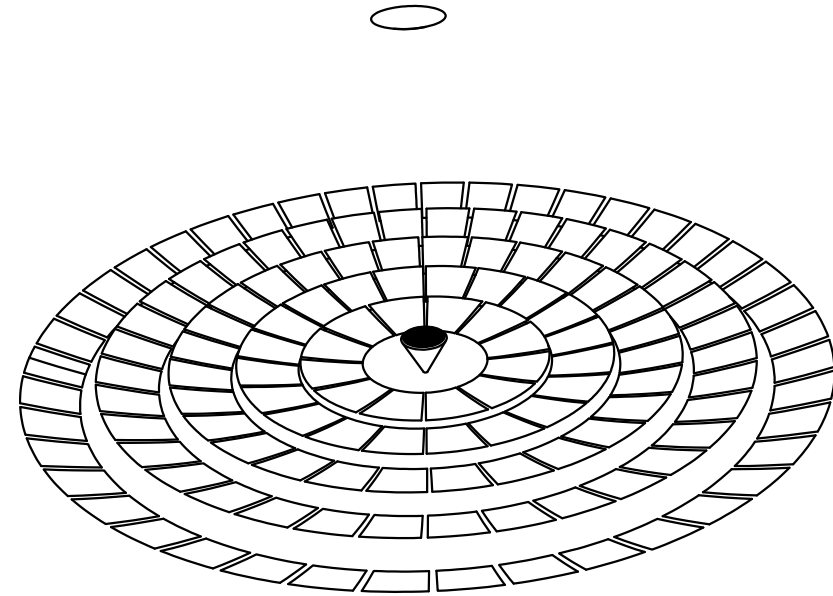
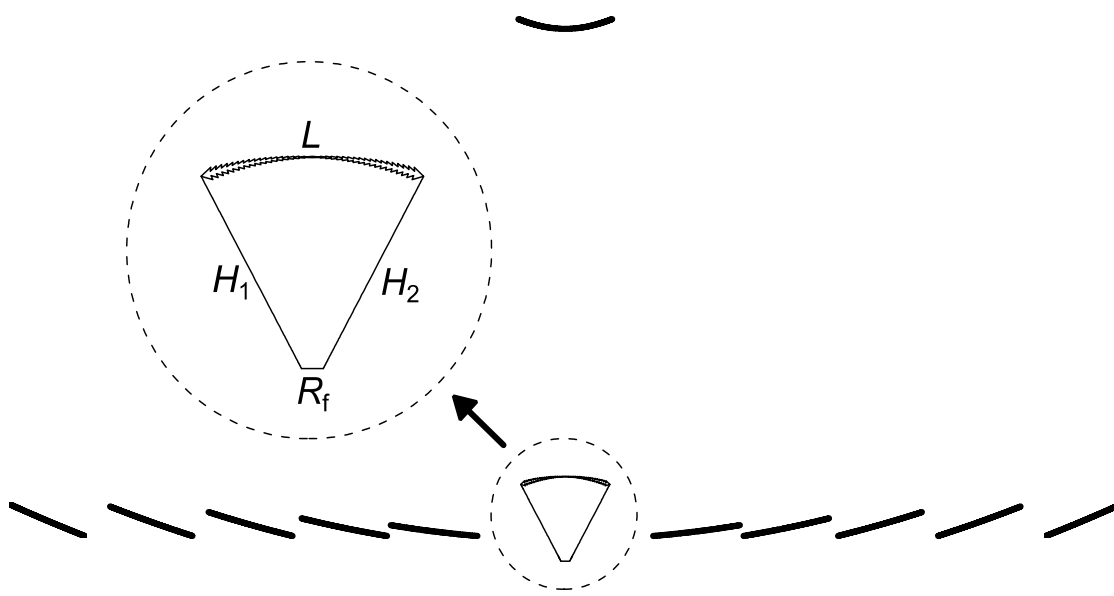
Geometric data and expected performance (using a raytracing method). Materials used: 92% of reflectivity, 90% of absorptivity, 90% of transmissivity and 1.48 of refractive index (lens).

| Aperture width (m) | Receiver Height (m) | Fresnel Lens width (m) | Receiver width (m) | η_{opt} | C_g (X) | θ (deg) | CAP | Peak Power @ DNI 1000W/m ² |
|--------------------|---------------------|------------------------|--------------------|--------------|-----------|----------------|------|---------------------------------------|
| 7 | 4.1 | 0.91 | 0.12 | 0.5 | 2339 | 0.58 | 0.49 | 20kW |

- Advantages: Practical configuration with a interesting CAP value;
- Drawbacks: The tertiary touches the receiver + multiple reflections inside of the trumpet leading to lower optical efficiencies.

Point Focusing Concentrators – Central Tower concentrators

The same ideas can be applied to Central Tower Concentrators



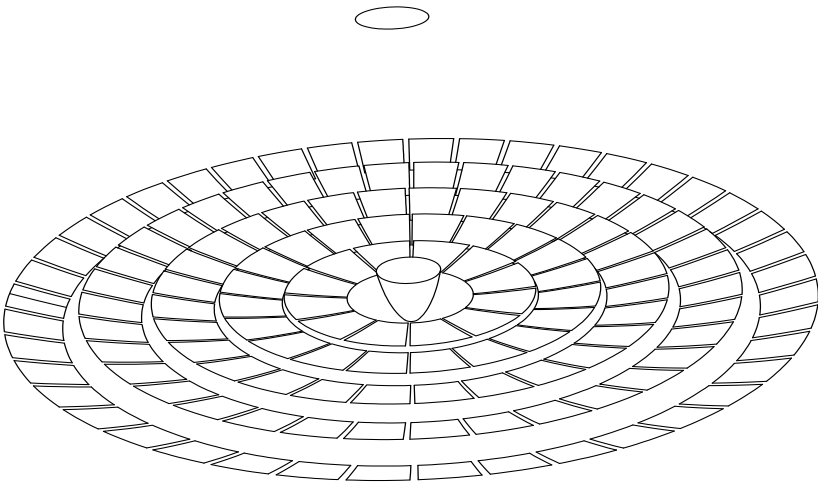
Point Focusing Concentrators – Central Tower concentrators

Geometric data and expected performance (using a raytracing method). Materials used: 92% of reflectivity, 90% of absorptivity, 90% of transmissivity and 1.48 of refractive index (lens).

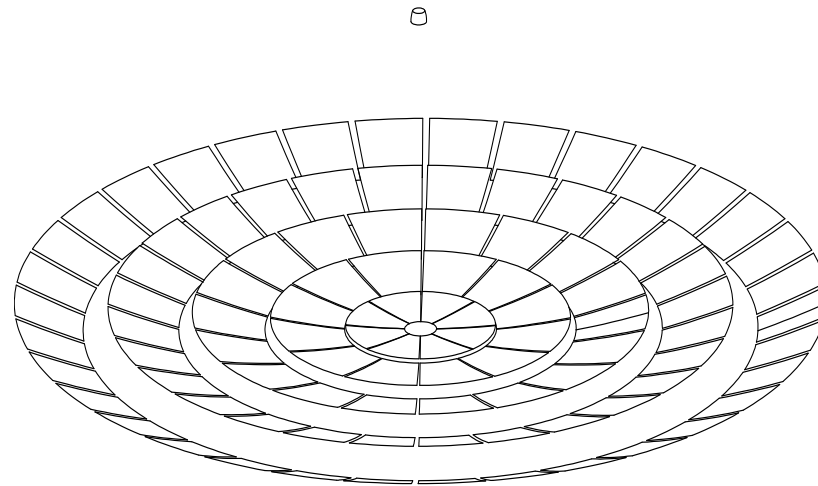
| Optic | Total reflective Area (m ²) | Number of heliostats | Receiver height (m) | Secondary mirror area (m ²) | Terceary cavity volume (m ³) | Receiver area (m ²) | C _g (X) | θ (deg) | η _{opt0} | CAP _{3D} | Peak Power @ DNI 1000W/m ² |
|---|---|----------------------|---------------------|---|--|---------------------------------|--------------------|---------|-------------------|-------------------|---------------------------------------|
| ST Beam Down with Trumpet+ Fresnel lens terceary concentrator | 3407 | 112 | 95 | 57 | 38 | 1.01 | 2300 | 0.55 | 0.5 | 0.46 | 1.7 MW |

Point Focusing Concentrators – Central Tower concentrators

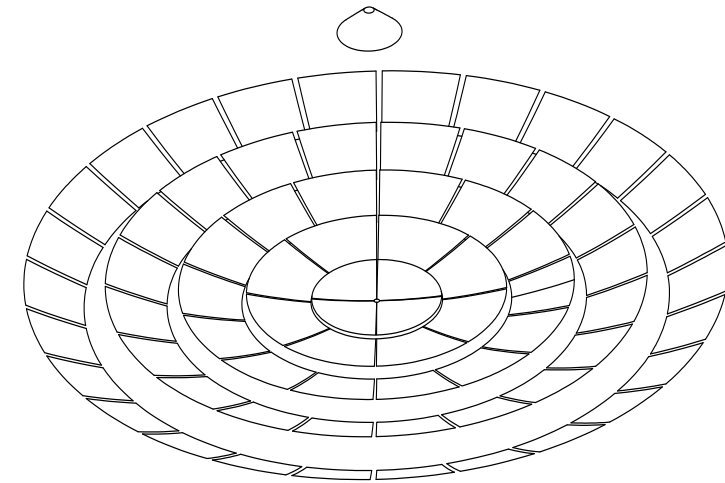
Other configurations are possible...



CT beam-down with CEC-type tertiary



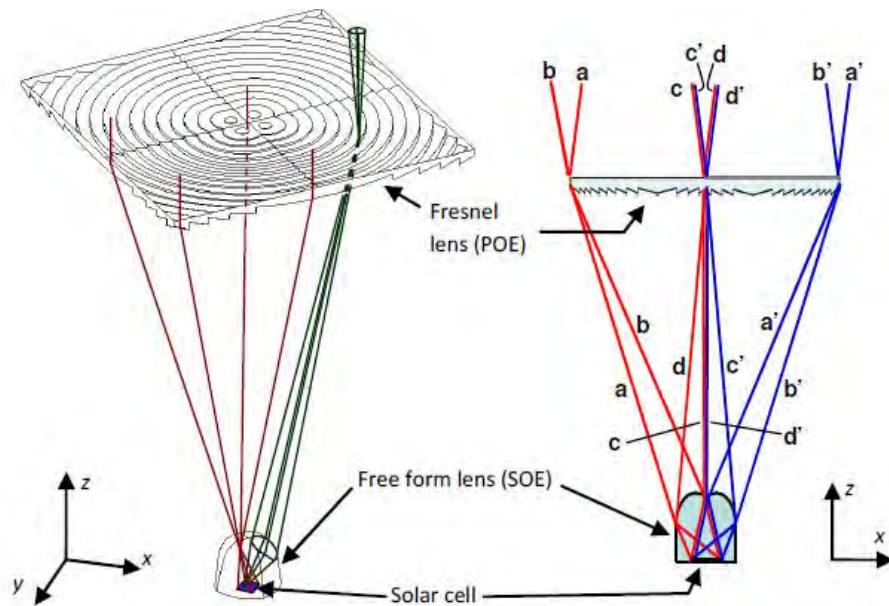
CT with CEC-type secondary



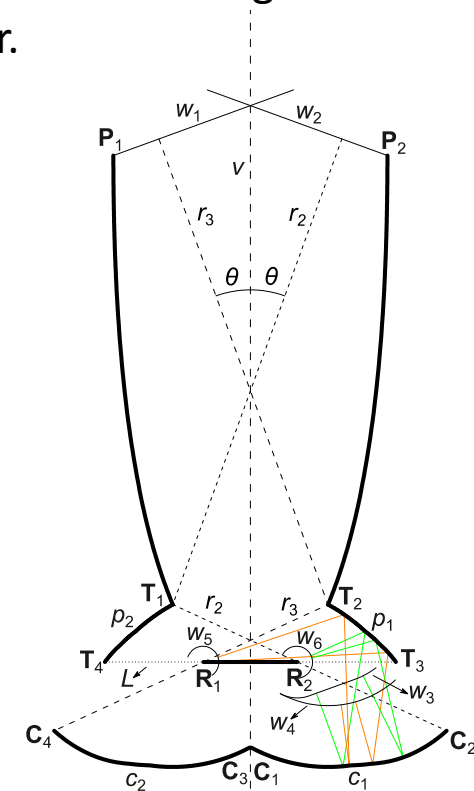
CT with TERC secondary

Future developments and trends

These configurations have two main problems: The non-uniform distribution of the light over the receiver and the thermal short-circuits due to the no gap between the mirrors and the receiver.



Fresnel Kohler lens for better uniformization of the light



Ideal concentrators with gaps

Conclusions

- Etendue-coupling is the main guiding idea of solar concentration
- Imaging optics fall short from the theoretical limits but they can be improved using non-imaging optics
- Multiple configurations for line-focus and point-focus are possible but the principles are the same: etendue-conservation and edge-ray principle.
- These optics achieve higher CAP values, hence improving of the overall performance of these systems
- There is still room from improvements, especially regarding the light distribution over the receiver and gap-losses control.

References

- Chaves, J., Introduction to nonimaging optics, CRC Press, Taylor and Francis Group
- Winston, R., Miñano, J.C., Benítez, P., (contributions by Shatz, N., Bortz, J.,C.), Nonimaging Optics, Elsevier Academic Press, Amsterdam, 2005.
- Canavarro, D. et al, “New second-stage concentrators (XX SMS) for parabolic primaries; Comparison with conventional parabolic trough concentrators”, Solar Energy Volume 92, June 2013, Pages 98-105, <https://doi.org/10.1016/j.solener.2013.02.011>
- Canavarro, D., et al, “Simultaneous Multiple Surface method for Linear Fresnel concentrators with tubular receiver”, Solar Energy Volume 110, December 2014, Pages 105-116, <https://doi.org/10.1016/j.solener.2014.09.002>
- Canavarro, D. et al, “New dual asymmetric CEC linear Fresnel concentrator for evacuated tubular receivers”, AIP Conference Proceedings 1850, 040001 (2017); <https://doi.org/10.1063/1.4984397>
- Canavarro, D., et al., “Simultaneous multiple surface method for the design of new parabolic dish-type concentrator using a Cassegranian approach”, AIP Conference Proceedings 2126, 050001 (2019); <https://doi.org/10.1063/1.5117584>

SFERA-III

Solar Facilities for the European Research Area

THANK YOU FOR YOUR ATTENTION!
ANY QUESTIONS?



SFERA-III

Solar Facilities for the European Research Area

1st Summer School “Thermal energy storage systems, solar fields and new cycles for future CSP plants”
WPI Capacity building and training activities
Odeillo, France, September 9th-11th 2019



“New concepts of heliostats for solar tower systems”
José González-Aguilar, IMDEA Energy Institute

NETWORKING



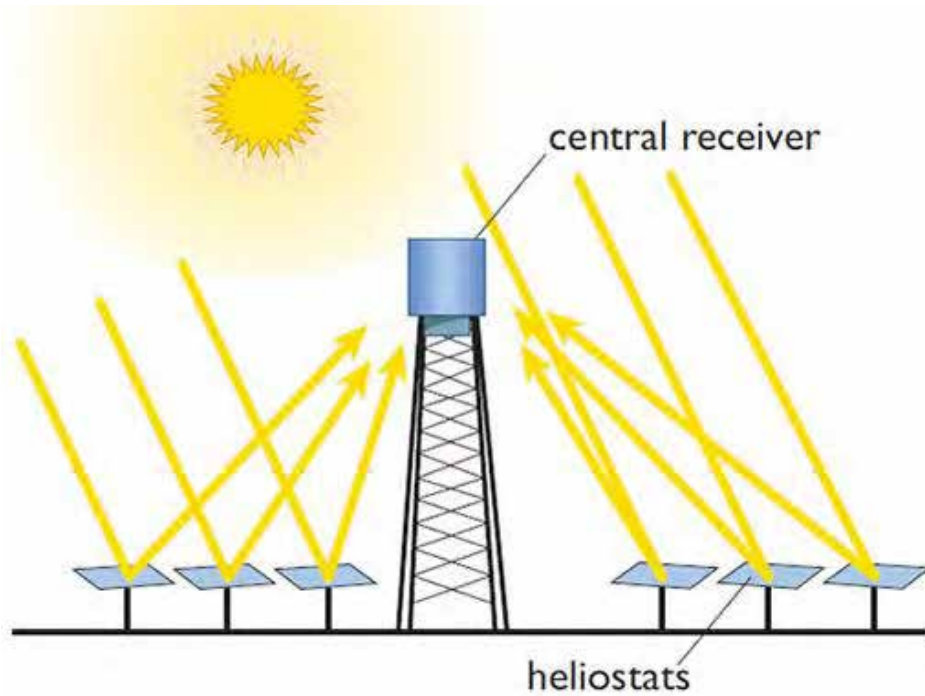
THIS PROJECT HAS RECEIVED FUNDING FROM THE EUROPEAN UNION'S HORIZON 2020 RESEARCH AND INNOVATION PROGRAMME UNDER GRANT AGREEMENT NO **823802**

Outline

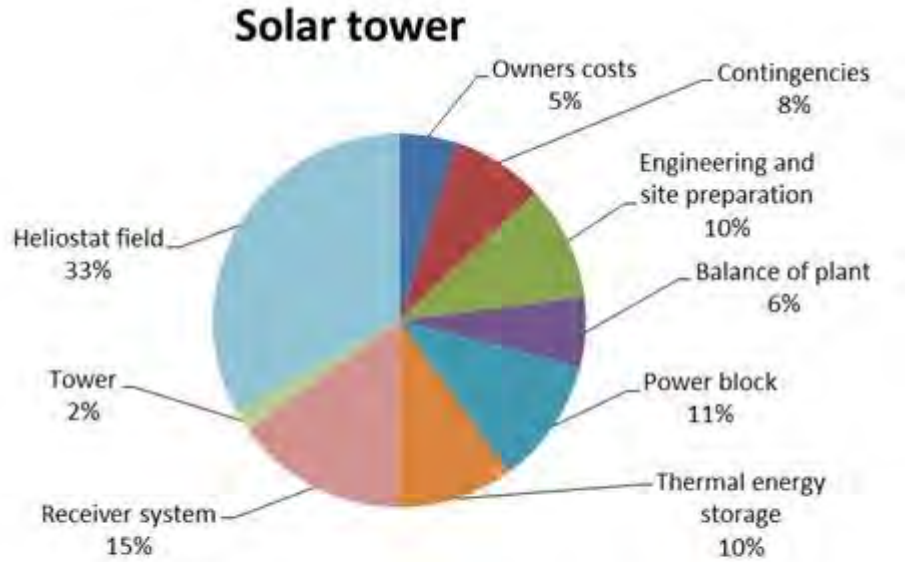
- Context
- Heliostats design
- Big vs. small heliostats
- Current concepts under development (attention, may be your heliostat is missing)
- Conclusions and perspectives

SFERA-III

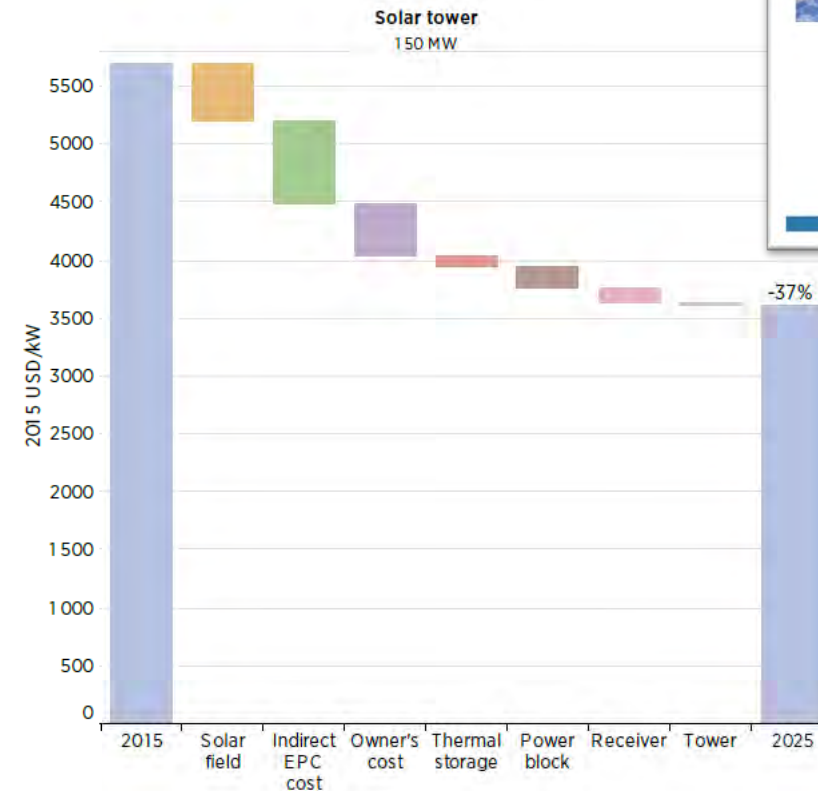
Solar Facilities for the European Research Area



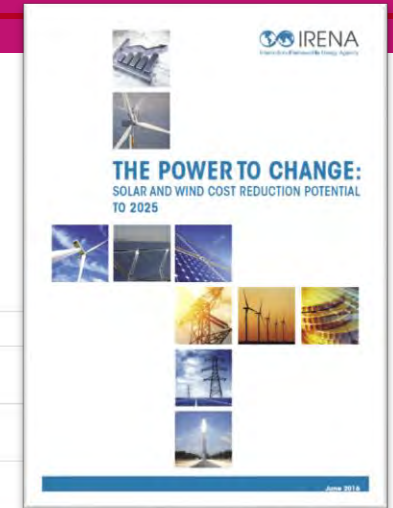
Impact of heliostats cost in solar thermal power plants



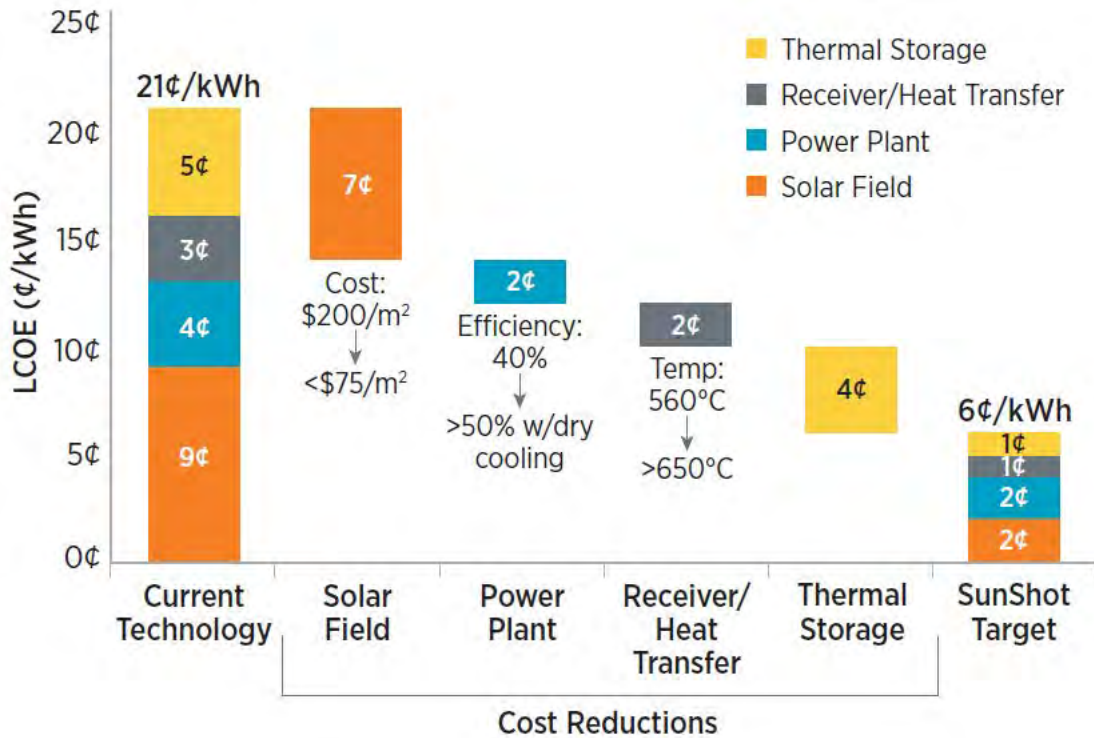
SOURCE: FICHTNER, 2012



Source: IRENA and DLR, 2016.



Impact of heliostats cost in solar thermal power



SunShot CSP Progress and Goals

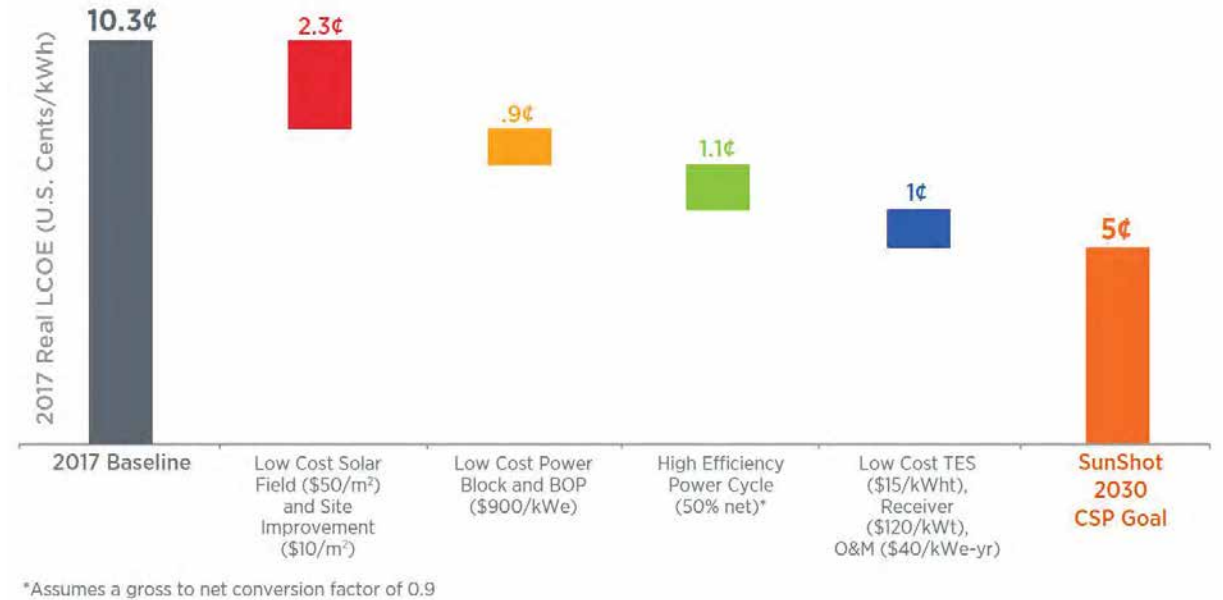
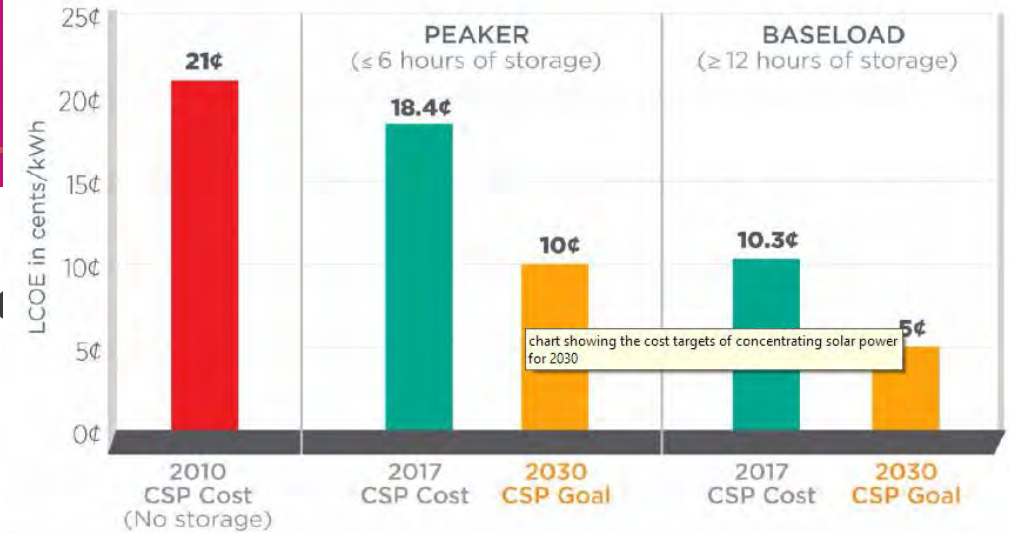


Figure 5. Example modeled pathway toward 5¢/kWh for baseload CSP.

SFERA-III

Solar Facilities for the European Research Area

| CSP SunShot Awards (2011) | Component | 2012 | 2013 | 2014 | 2015 | 2016 | 2017 |
|-------------------------------|-----------|------|------|------|-------------|------|------|
| BrightSource Energy | Collector | | | | \$4,795,284 | | |
| Boston University | Collector | | | | \$730,340 | | |
| 3M Company | Collector | | | | \$4,886,359 | | |
| University of Arizona | Collector | | | | \$1,480,935 | | |
| Pennsylvania State University | Collector | | | | \$248,377 | | |
| Jet Propulsion Laboratory | Collector | | | | \$2,343,330 | | |



| Funding Program | Year Announced | Amount Awarded |
|--|----------------|----------------|
| Concentrating Solar Power: Concentrating Optics for Lower Levelized Energy Costs (CSP: COLLECTS) | 2016 | \$9M |

SOLAR DYNAMICS LLC

Project Name: Drop in, Ring of Power Heliostat for Collects

Location: Broomfield, CO

SunShot Award Amount: \$2,062,246; **Awardee Cost Share:** \$850,436

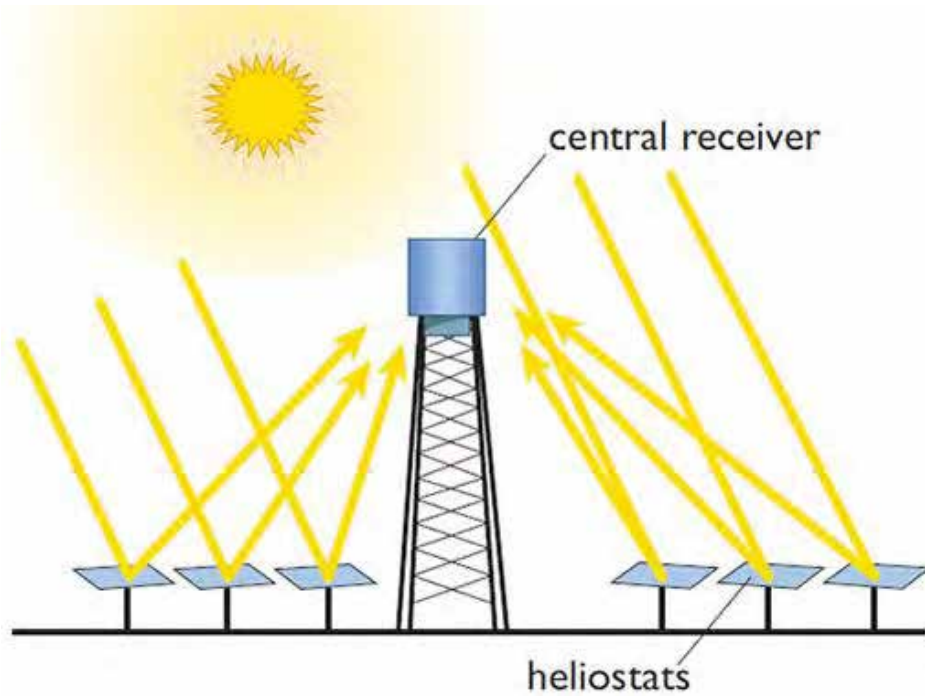
Project Summary: Solar Dynamics is building on heliostat technology developed under a previous award in the Baseload CSP funding program to develop the DROP C (Drop-in, Ring-Of-Power Heliostat for COLLECTS). The new design allows the heliostats to be dropped into a location with drastic reduction of the preparation of the site location, which enables a reduction in costs and improves financing terms. The addition of a wide base and protected drives, which permit heliostats to move and reflect sun at the best angle, allows lower manufacturing costs, reduced costs for the structure's support, and increased protection from high winds. These improvements, coupled with wireless control of the heliostats, support lower cost targets well beyond the SunShot 2020 goals.

Target on reduction of heliostats cost

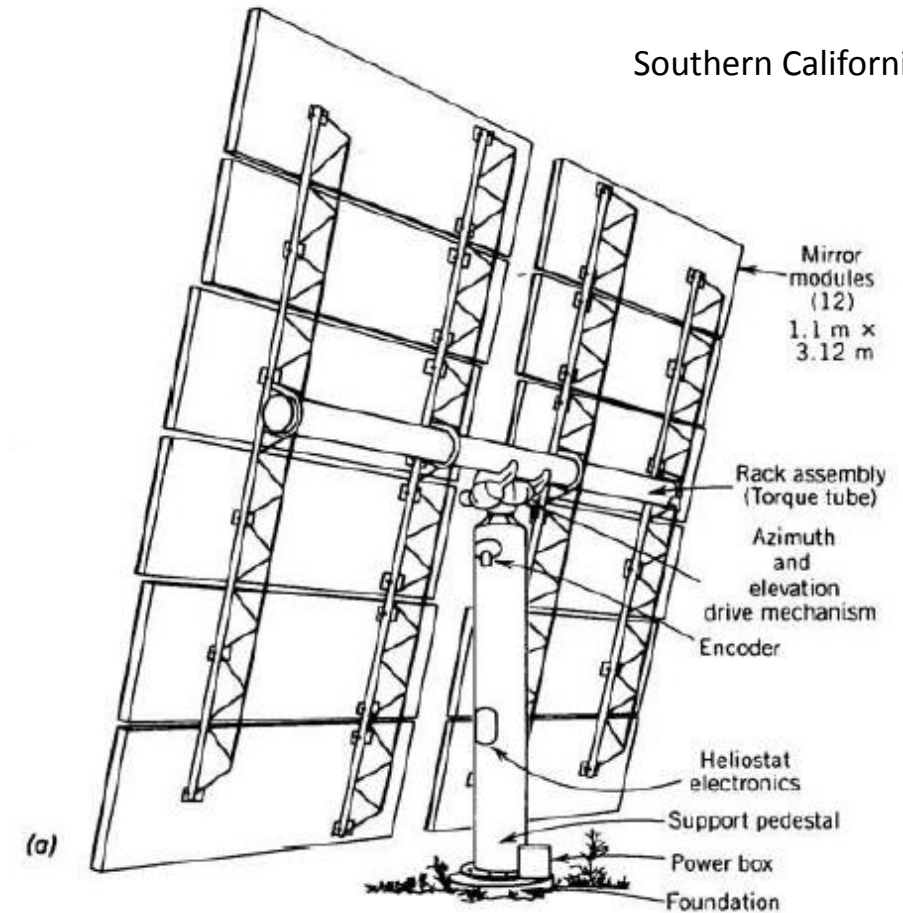
- USA, SunShot, 50 \$/kWh, 75 \$/m²
- Australia, Australian Solar Thermal Research Initiative, ASTRI, 90 AUD/m²
- South Africa
- EU, STAGE-STE KPI, 100 €/m²

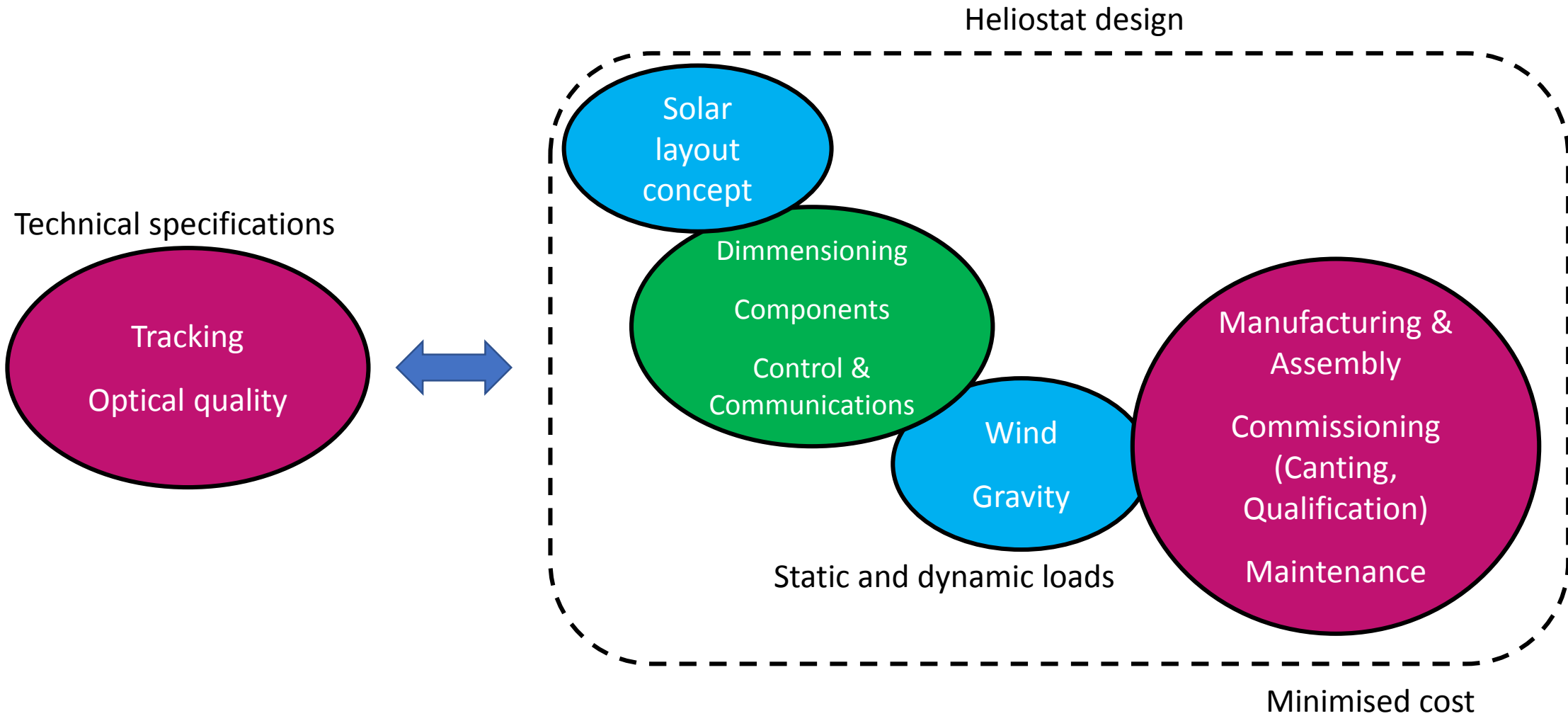
SFERA-III

Solar Facilities for the European Research Area



| Heliostat component | Sub-elements |
|---------------------|---|
| Reflecting module | <ul style="list-style-type: none"> Mirror modules / facets Frame / rack assembly |
| Foundation | <ul style="list-style-type: none"> Foundation / Ground anchorage |
| Structure | <ul style="list-style-type: none"> Support structure |
| Drive mechanism | <ul style="list-style-type: none"> Azimuth and elevation drive Gear box Cabling |
| Control | <ul style="list-style-type: none"> Position sensor Interface with power system and heliostat field controller Drive controller Wiring Master control interface electronics for heliostat local control Time base, computers, software |
| Support equipment | <ul style="list-style-type: none"> Handling equipment Maintenance trucks and equipment Heliostat washing equipment Operating procedures (including offset error corrections, ...) Maintenance Procedures |





Primary factors for heliostat definition

- The size (e.g. area of reflective surface) directly impacts other critical parameters for the design and for the cost such as the weight, wind load, time of construction and installation.
- The optical design covers the general design of the heliostat: nature of the reflective material (e.g. silvered glass, aluminum, polymer-based silver film, etc.), number of facets, shape (e.g. curvature), and orientation (e.g. elevation-azimuth vs. tilt-azimuth, target-aligned vs. zenith axis).Tracking

Secondary factors

- Mechanical structure and pedestal
 - General design (mast anchorage to the ground, beam, girder, box vs. truss...)
 - Material (steel, aluminum, concrete...)
 - Assembly (welding, bolts, rivets, glue...)
- Motors and drives
 - Main power supply (electric vs. hydraulic or pneumatic)
 - Type of motor (DC motors, synchronous motors, asynchronous motors, stepping motors)
 - Reduction step (direct drive, gear box, drive belt, chains, cable)
 - Actuator type (linear vs. rotating)
- Tracking controls, security systems
 - Open-loop vs. closed-loop
 - Local controller vs. central controller
 - Wireless communication vs. wired system
 - Heliostat concept connections (autonomous vs. grid connected)

SFERA-III

Solar Facilities for the European Research Area

Reflecting module

- Mirror: silvered glass, aluminum, polymer-based silver film...
- Mirror support structure (fixing mirror shape): Connection of glass mirrors to steel frames, Stamped mirror facet support structure, Sandwich panel mirror facets, stretched membrane,

Pylon and foundations (ground connection)

- Steel reinforced concrete piers, pile driving, ground anchor, and ballast type foundations

Structure (degrees of freedom)

- T-type (open, closed)
- Pitch/roll, rim drive, carousel

Drive mechanism

- Rotary electromagnetic motors, Hydraulic actuators
- Worm gears, spur gears, screw and nut, chain and pinion, harmonic drive configuration gears (“strain wave gears”), planocentric drives, rack and Pinion, linear drives, friction wheels, capstan drives.

Control

- Local to each heliostat (field wiring to a central system); autonomous heliostats (PV panels, wireless communication)



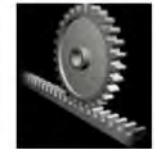
Spur gear



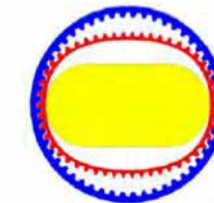
Worm gear



Screw and nut



Rack and pinion



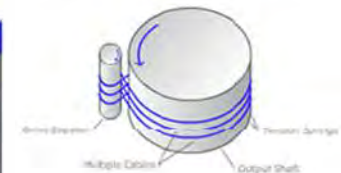
Harmonic drive



Chain and pinion



Planocentric drives



Capstan drive

Big vs. small heliostats

- Big heliostats - few parts and foundations are needed for an equivalent mirror area
- Small heliostats – low wind speeds (low height) and then low weight per mirror area

F. Téllez, M. Burisch, C. Villasente, M. Sánchez, C. Sansom, P. Kirby, P. Turner, C. Caliot, A. Ferriere, C A. Bonanos, C. Papanicolas, A. Montenon, R.Monterreal, J. Fernández, 2014. **State of the art in heliostats and definition of specifications – survey for a low cost heliostat development.** STAGE-STE EU Project, Deliverable 12.1.

A. Pfahl, J. Coventry, M. Röger, F. Wolfertstetter, J. F. Vásquez-Arango, F. Gross, M. Arjomandi, P. Schwarzbözl, M. Geiger, Ph. Liedkejk, **Progress in heliostat development**, Solar Energy 152 (2017) 3–37

J. Coventry, J. Campbell, Y. Peng Xue, C. Hall, J.-S. Kim, J. Pye, G. Burgess, D. Lewis, G. Nathan, M. Arjomandi, W. Stein, M. Blanco, J. Barry, M. Doolan, W. Lipinski, A. Beath, **Heliostat Cost Down Scoping Study Final Report** ANU document reference: STG-3261 Rev 01 (2016)



Sener's 178 m2 heliostat with hydraulic drives and concrete pylon

Abengoa ASUP 140

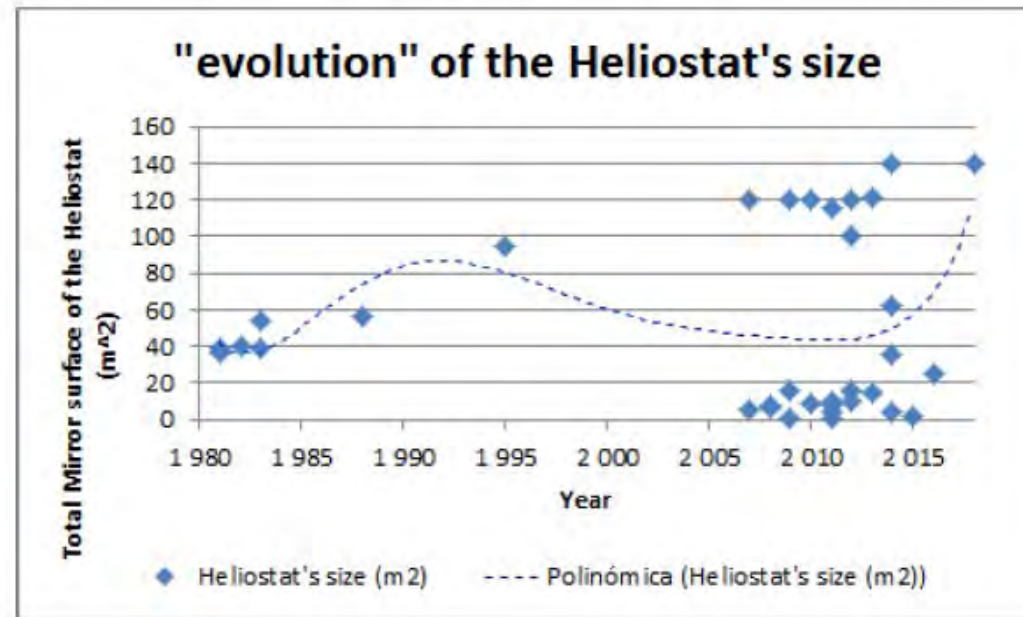


Figure 15. Temporal evolution of the size of the heliostats deployed commercially.

Trends – Titan Tracker

- Heliostat with carousel based azimuth drive
- 150m² - heliostat size
- Carousel design enables cost effective heliostat design
- Gear 3F AC motor.
- Jack – worm gear for elevation
- Lower than 100 €/m²

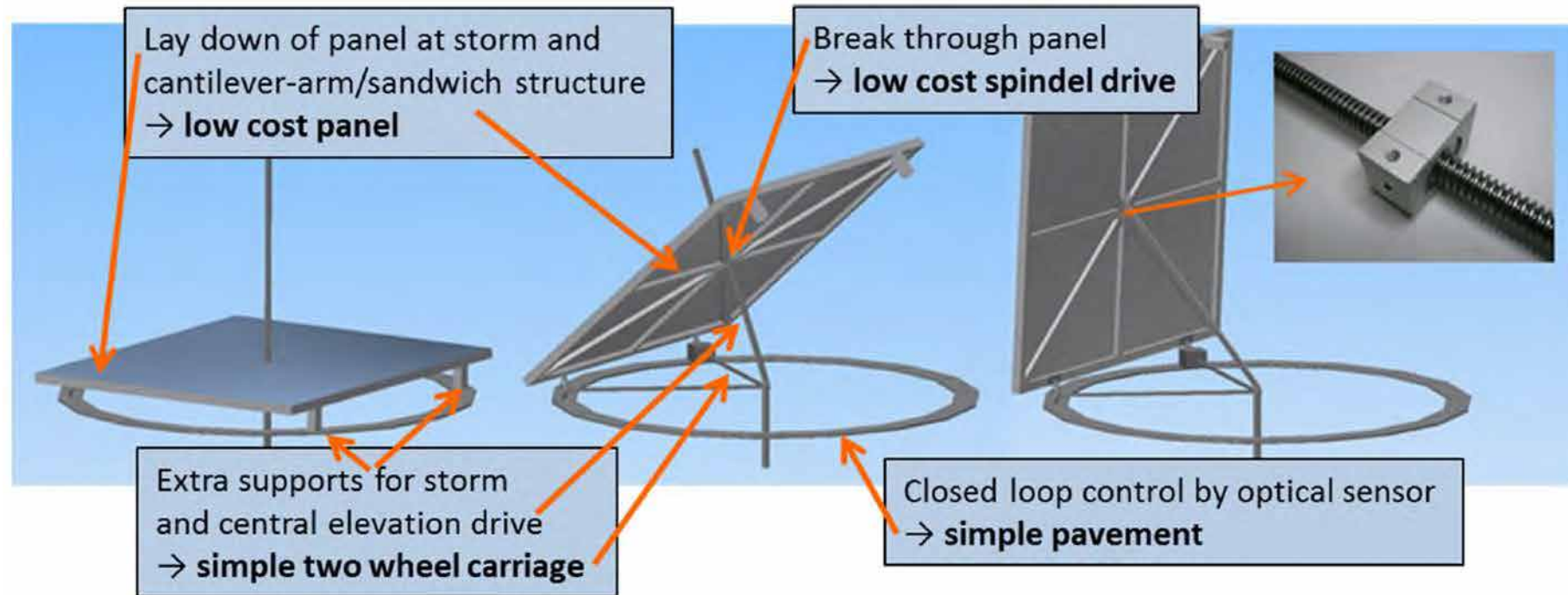
N. Goel et al. Energy Procedia, Volume 57, 2014, Pages 301-310



DLR carrousel

A. Pfahl et al. AIP Conference Proceedings 2033, 040030 (2018)

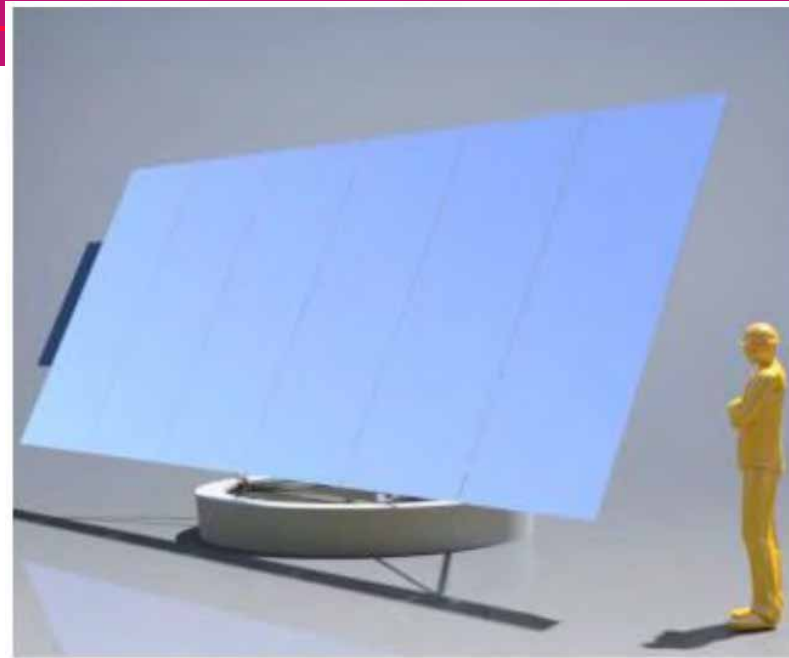
A. Pfahl et al. AIP Conference Proceedings 2126, 030042 (2019)



Drop-C – SolarDynamics

- Drop-C heliostat
 - Evolution of the Abengoa Solar’s Ring-of-Power (ROP) heliostat (Colorado office award #EE0003596, Installed cost, 114 \$/m²)
 - 76 \$/m² installed cost estimate
 - Efficient space frame support system
 - Azimuth drive/idler wheels transmit all load to foundations (no central ground anchor required)
 - Ballast foundation
 - Drop-in place installations
 - Reduced civil work, permitting, and geotechnical risk in solar field

- Wireless Mesh Network and Rapid Calibration System



Drop-C: Front View

| Drop-C Heliostat Key Metrics | |
|------------------------------|---------------------------|
| Reflective area | 27 m ² |
| Overall dimensions | 8.46 m wide x 3.21 m tall |
| Aspect ratio | 2.6 (width/height) |
| Stow height | 1.98 m |
| Mirror shape | Flat, no-canting |
| Foundation | Ballast |
| Power | PV plus battery |
| Control | Wireless |

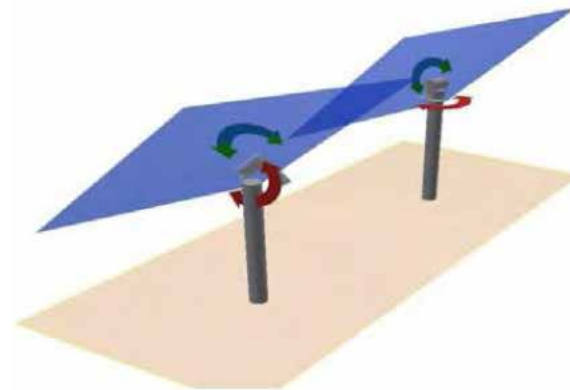
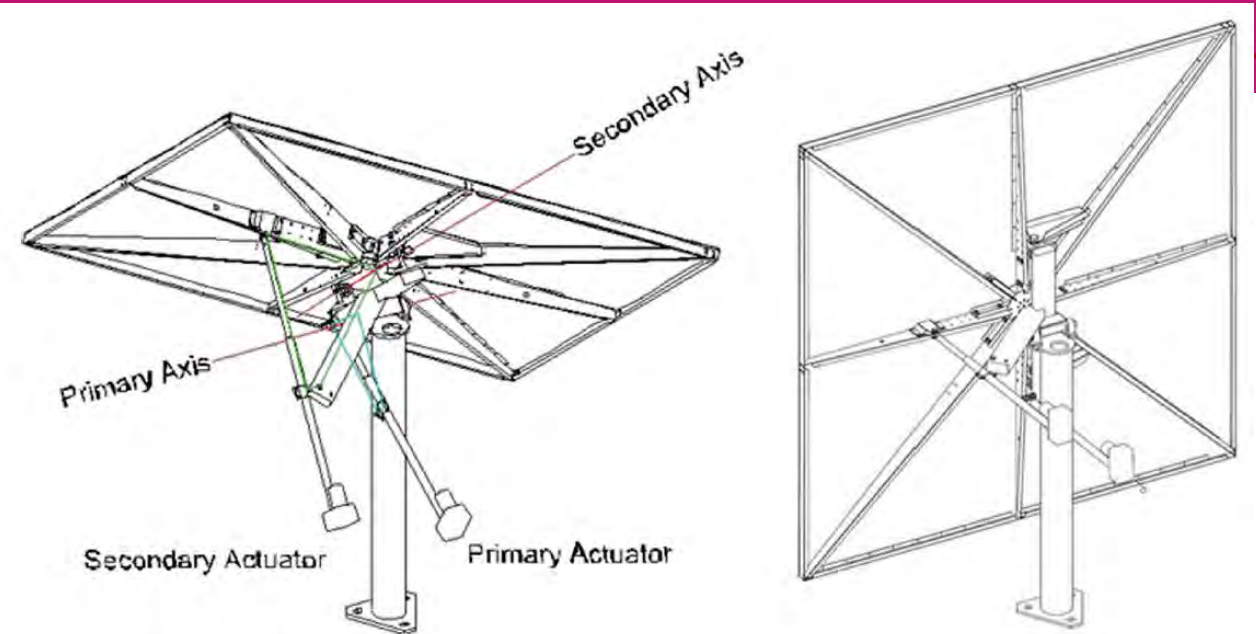


SFERA-III

Solar Facilities for the European Research Area

CSIRO

- 4.5 m² (2.44 m x 1.84 m)
- Linear driven horizontal primary axis



Trends – SBP Stellio

- Schaich Bergermann Partner
- 48 m²
- Compact round-like form
- Linear drives

F. Arbes et al. AIP Conference Proceedings 1734, 160002 (2016)

F. von Reeken et al. AIP Conference Proceedings 1734, 160018 (2016)

T. Keck et al. Hami – The first Stellio solar field. AIP Conference Proceedings 2126, 030029 (2019)

D. Nieffer et al. AIP Conference Proceedings 2126, 030039 (2019)

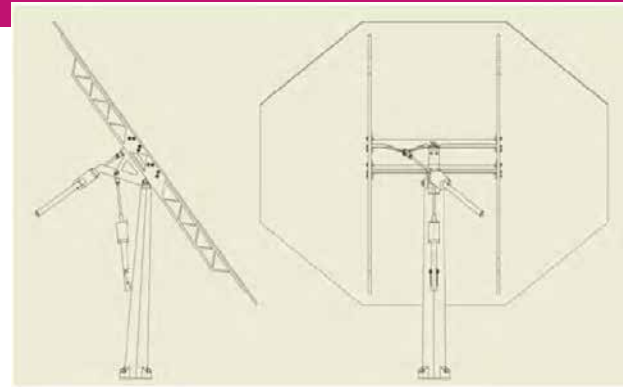


an Research Area

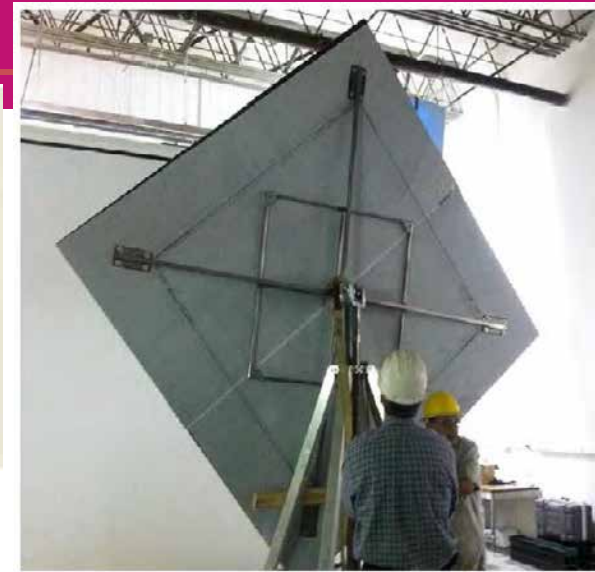
...and more



Aora m² heliostat



Heliotower's 36m² heliostat



NREL 6m² heliostat

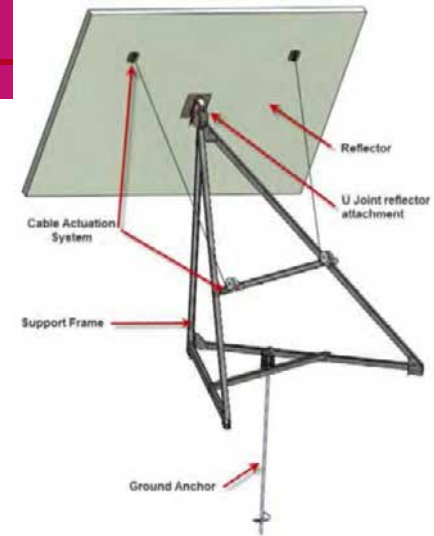


Diagram of prototype heliostat frame

The Google heliostat



Solaflect's 16 m² 'suspension heliostat'. 16 x 1 m² glass facets held in position by cables tensioned from a compression element perpendicular and central to the mirror panels



Heliosystems's 9m² "Passive Adjustment Toroidal Heliostat" (PATH),



UNAM heliostat



SFERA-III

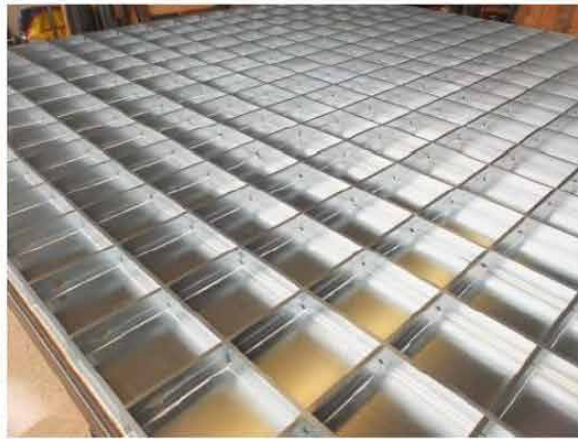
Solar Facilities for the European Research Area

Trends – DLR heliostat



P. Liedke et al. AIP Conference Proceedings 2033, 040021 (2018)

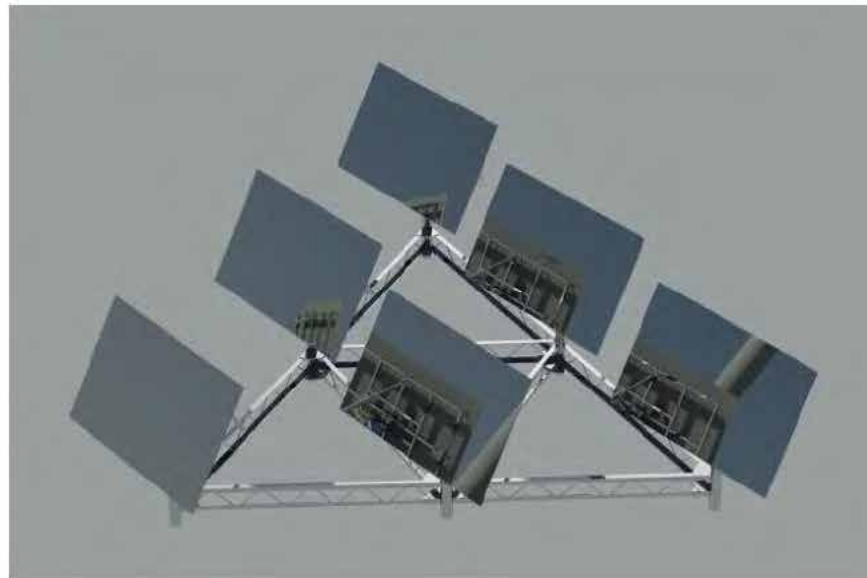
P. Liedke et al. AIP Conference Proceedings 1734, 020014 (2016)



Helio 100

J. N. Larmuth AIP Conference Proceedings 1734, 020013 (2016)

C. -A. Domínguez-Bravo et al. AIP Conference Proceedings 1734, 070006 (2016)



Mini-facets heliostats

- C. Hall. AIP Conference Proceedings 1850, 110005 (2017)

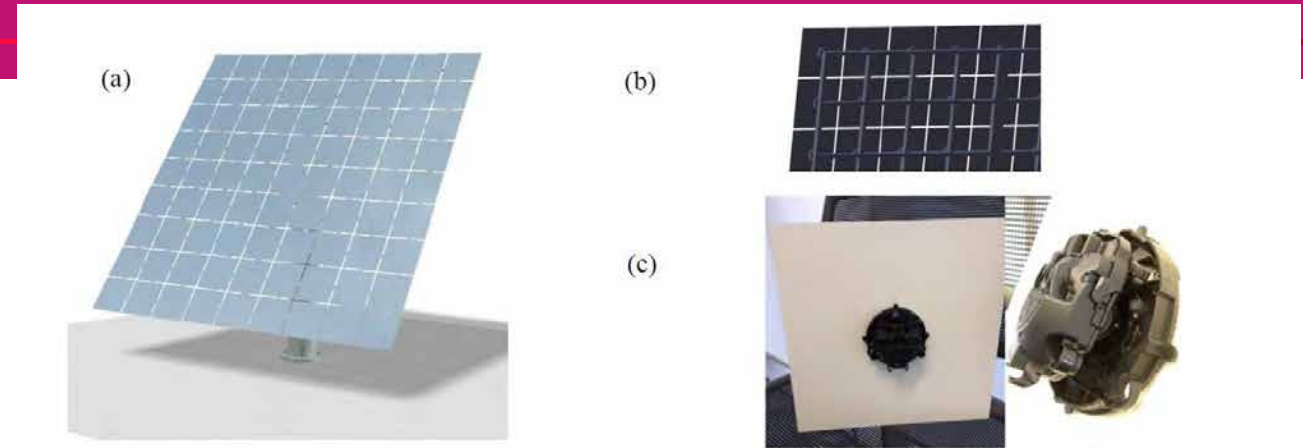


FIGURE 1. (a) Mini-facet concept image. (b) close up of rear. (c) proposed actuator as used in automotive industry mounted to glass mirror panel and close up of the mini-actuator.

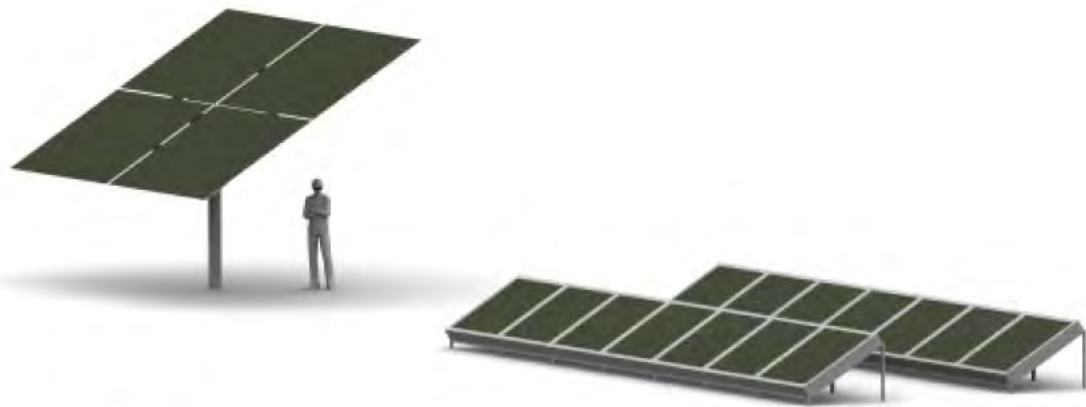


FIGURE 1. Standard heliostat (left), micro-heliostat (MH) (right)

Heliostat concepts - Micro heliostats

M. Y. Lazardjani et al. AIP Conference Proceedings 1734, 020028 (2016)

Pitch-Roll heliostats

- Amrita University, India
- The pitch/roll heliostat is particularly well suited to smaller designs which can use very low-cost electric linear actuators produced in large quantities for a wide variety of operations and purposes around the world.
- The primary disadvantage of the pitch/roll heliostat is the significantly more complicated kinematics of such a structure.

J. Freeman. AIP Conference Proceedings 1850, 030018 (2017)

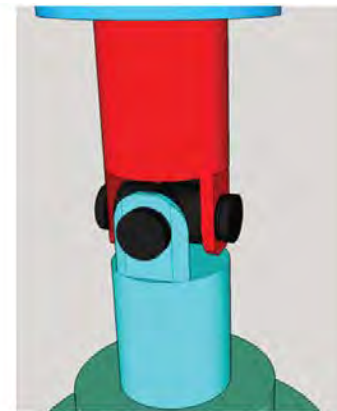
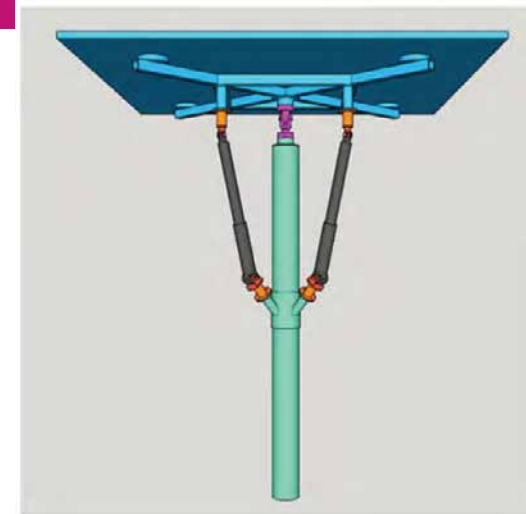


FIGURE 2. CAD model of the simple Hooke's joint, with co-incident axes of rotation

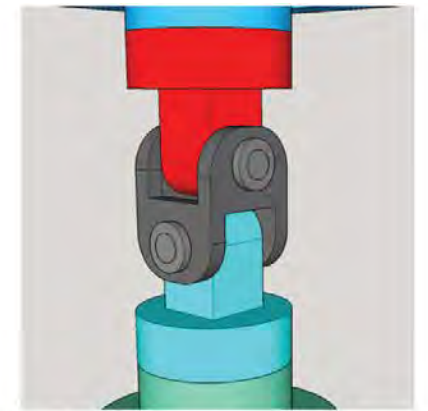


FIGURE 3. CAD model of a modified Hooke's joint with non-zero distance between pivot axes

Heliostat concepts – Ganged heliostats

- Multiple heliostats are combined where they share structures and components, particularly pedestals and rotational drives. These ganged heliostats can be connected via two or more tensioned cabling systems to facilitate structural rigidity and actuation.
- The reduced number of pedestals and drives can reduce the overall cost since these make up the majority of the heliostat cost at approximately 40-50%.
- Challenges for ganged heliostats, which can vary in cabling designs, include oscillation and vibration affects from wind loads that can detrimentally impact performance as well as causing structural damage at particular resonant frequencies.
- 75 \$/m²

K. M. Armijo. AIP Conference Proceedings 2126, 060001 (2019)

J. Yellowhair et al. Mechanical and Optical Performance Evaluation of the Skysun Tensile Ganged Heliostat Concept. SAND2017-7101 (2017)



Trends - Stamping

- **Stamping** is attractive as a low-cost and scalable manufacturing method, enabling simple fabrication of the support structure of mirror facets. The mirror and support are bonded together on a mould to fix the desired curvature. Stamped facets efficiently use thin sheet metal to form a high-stiffness geometry. This constrains mirror deformation to achieve high optical accuracy.
- Topography optimisation is a promising tool for the design of lightweight stamped mirror facets.
- Concepts optimised for a severe wind load showed the best performance, with distinct bead structures that maximised facet stiffness compared to the finer structures optimised for the evenly-distributed gravity load. Survival during severe winds limits weight reduction, with low gravity-induced shape errors observed at minimum thicknesses to prevent failure.
- Results suggest optimising for minimum weight and evenly-distributed support stress during severe winds is a promising approach for facet design.
- Incremental sheet forming was used to develop a rapid-prototyping method which is accessible and low-cost. The
- ISF process imposes additional geometry constraints, exhibits wall-thinning, and has lower dimensional accuracy compared to stamping.
- Incremental forming may offer a low-cost solution for pilot-scale plants or small run heliostat installations.

N. Rumsey-Hill et al. AIP Conference Proceedings 2126, 030048 (2019);

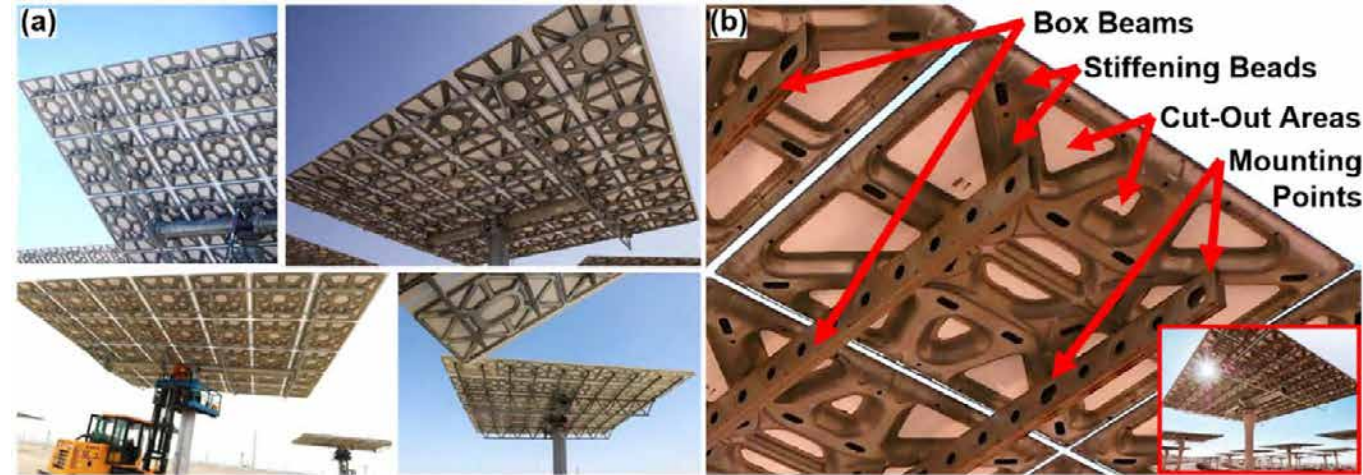
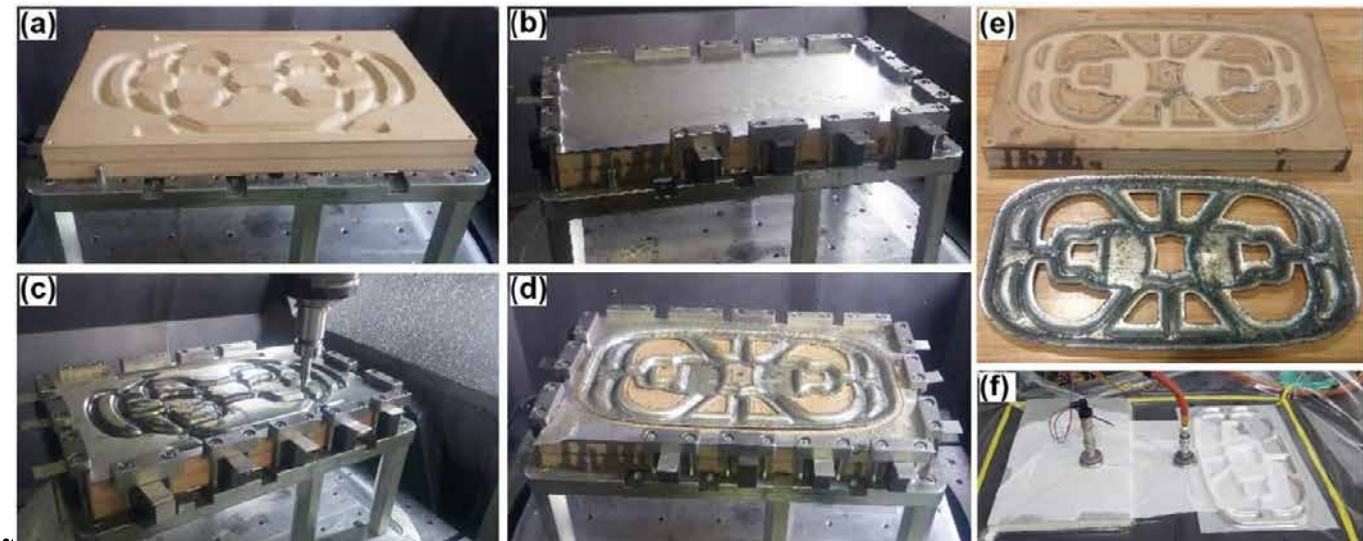


FIGURE 1. (a) Commercial multi-facet heliostats with stamped facets. Clockwise from top left: Crescent Dunes⁶, Gemasolar⁷, Dunhuang⁸, and Suncan CSP plants⁹. (b) NOOR III heliostat incorporating stamped mirror supports¹⁰.



Conclusions

- Heliostat technology is currently considered mature (beam quality smaller than 2.9 mrad, 20-years durability)
- Main target focuses on cost reduction
- “Any clever solution (even if crazy) is a cheap solution”
- No preferential size: low (1-5 m²), medium (40-50 m²) and large (120-180 m²) heliostats coexist
- Any new technological advance is rapidly implemented in heliostat technology (material, hardware, software)

Thanks for your attention

SFERA-III

Solar Facilities for the European Research Area

1st Summer School “Thermal energy storage systems, solar fields and new cycles for future CSP plants”
WPI Capacity building and training activities
Odeillo, France, September 9th-11th 2019



“Raytracing software and design tools for heliostats fields”

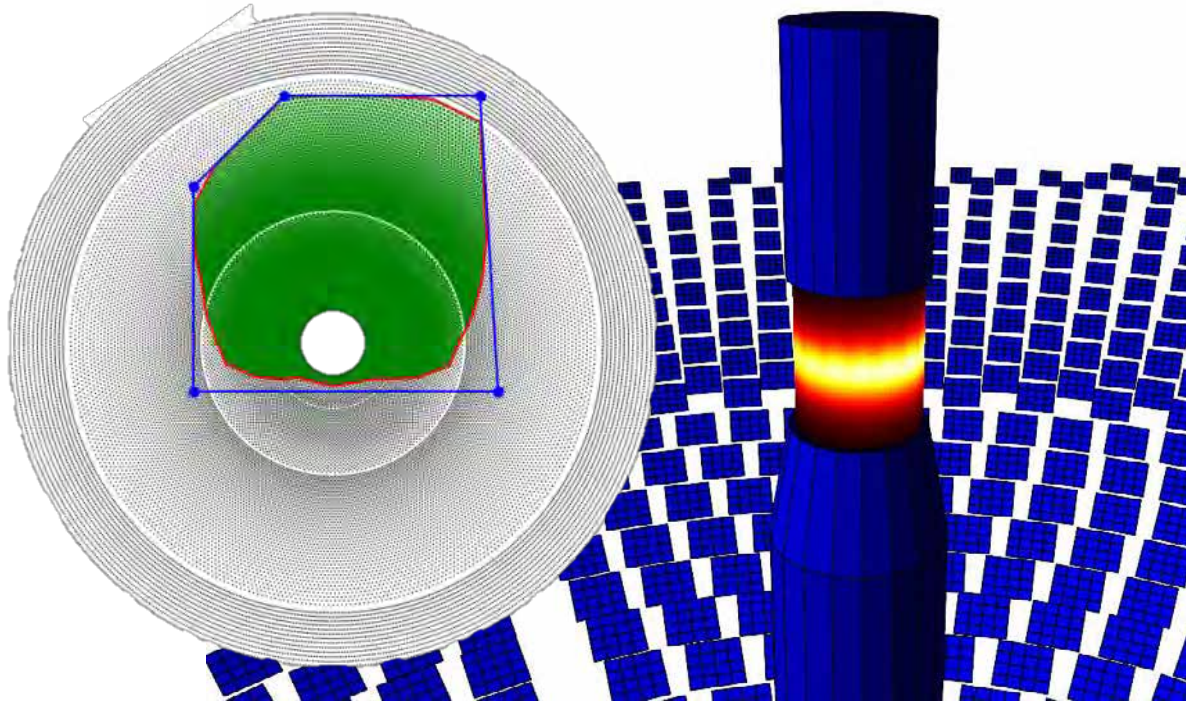
Shahab Rohani, Fraunhofer Institute for Solar Energy Systems ISE

NETWORKING



THIS PROJECT HAS RECEIVED FUNDING FROM THE EUROPEAN UNION'S HORIZON 2020 RESEARCH AND INNOVATION PROGRAMME UNDER GRANT AGREEMENT NO **823802**

RAYTRACING SOFTWARE AND DESIGN TOOLS FOR HELIOSTATS FIELDS



Shahab Rohani, Peter Schöttl

Fraunhofer Institute for Solar Energy Systems ISE

SFERA III Summer School

Odeillo, Sep. 9-11 2019

www.ise.fraunhofer.de

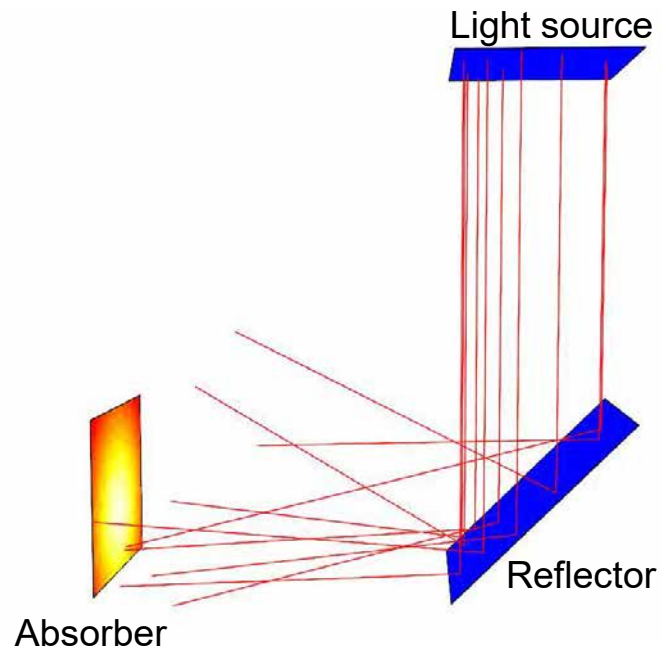
AGENDA

- Raytrace3D
 - Basics
 - Simulation acceleration
 - Angle-dependent reflectance for soiling modeling
 - Individual heliostat assessment
 - Sky discretization for fast annual assessment
 - Coupling to dynamic receiver simulation
- Heliostat field design/optimization
 - Heliostat field layout algorithms
 - Heliostat selection based on polygon optimization

Raytrace3D

Principle

Monte-Carlo forward ray tracing



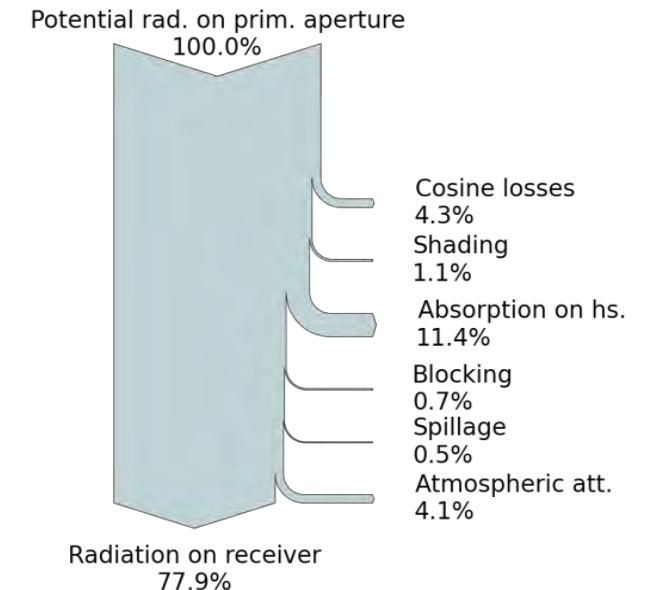
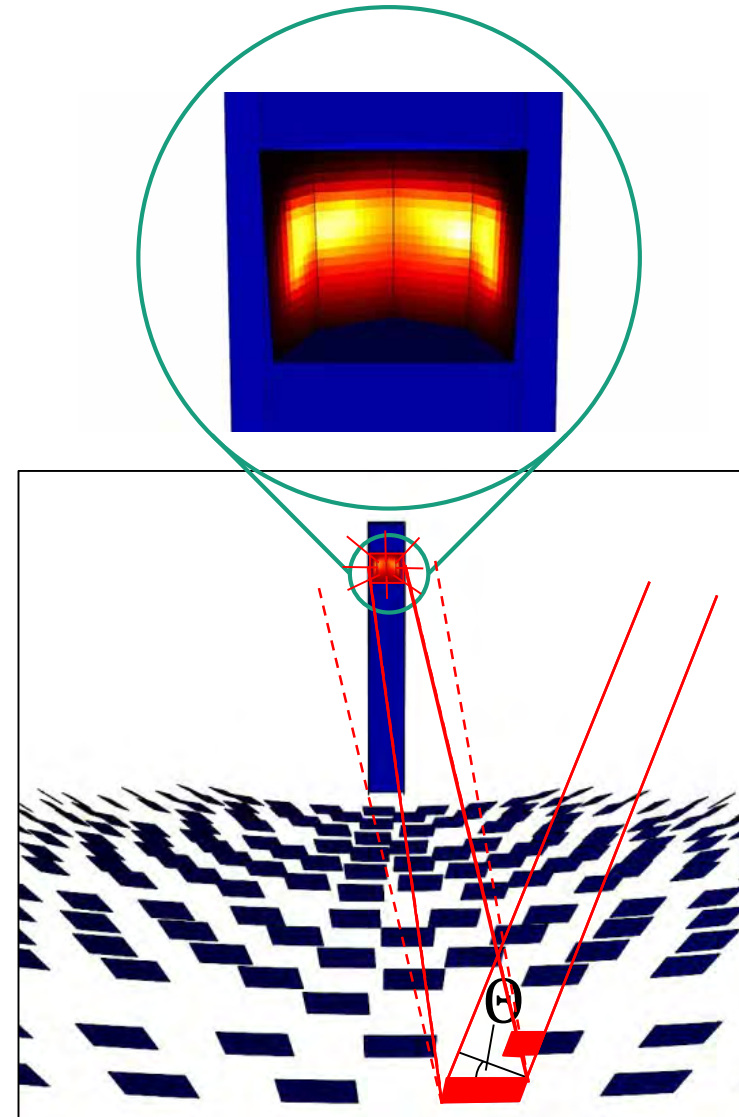
Features

- Comprehensive library of geometries/materials/light sources
→ sophisticated modeling of solar applications
- Fully object-oriented
→ readily extensible
- Number crunching in C++
+ Pre/Postprocessing in Python
→ Fast and versatile
- Parallelized
→ Run on simulation servers

Raytrace3D

Heliostat field losses

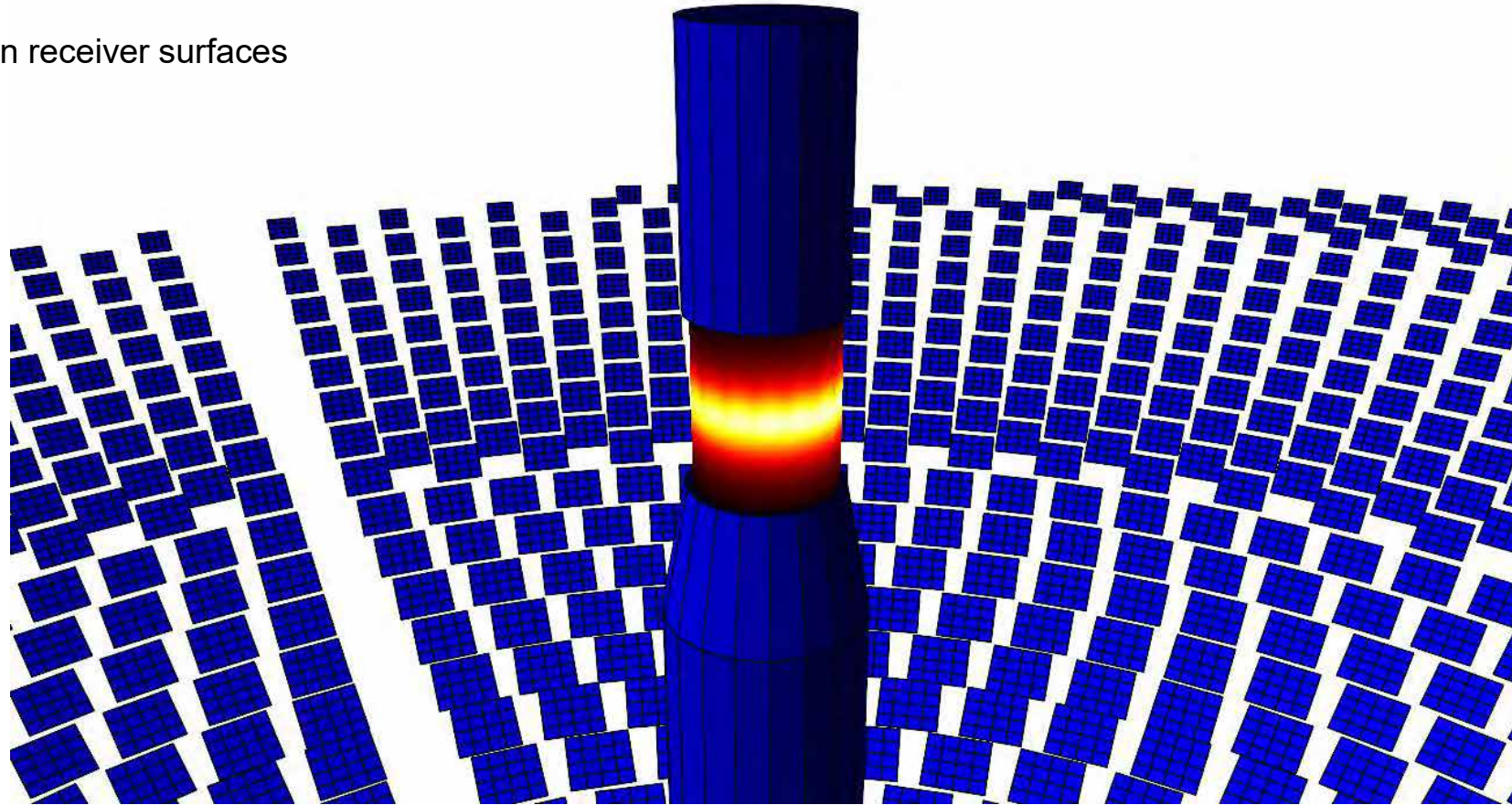
- Monte-Carlo ray tracing:
Fraunhofer ISE tool *Raytrace3D*
 - Cosine losses
 - Shading
 - Absorption on heliostats
 - Blocking
 - Atmospheric attenuation
 - Spillage
 - Reflection from receiver
- Flux distribution
on receiver surfaces [1]



Raytrace3D

Graphical postprocessing

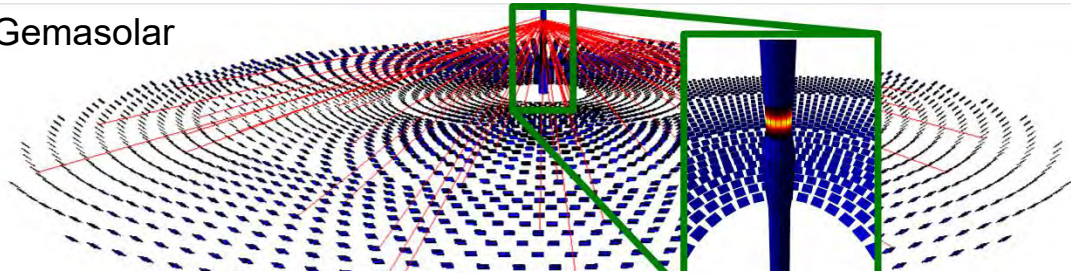
Gemasolar system
Fluxmaps depicted on receiver surfaces



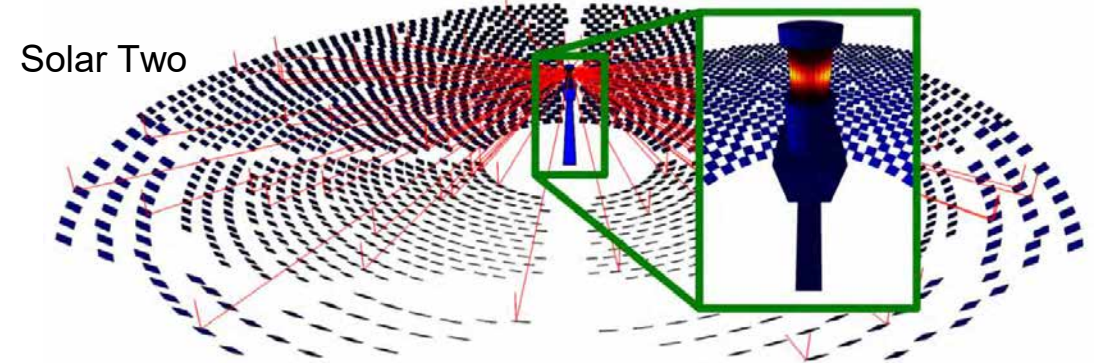
Raytrace3D

Simulation of solar towers

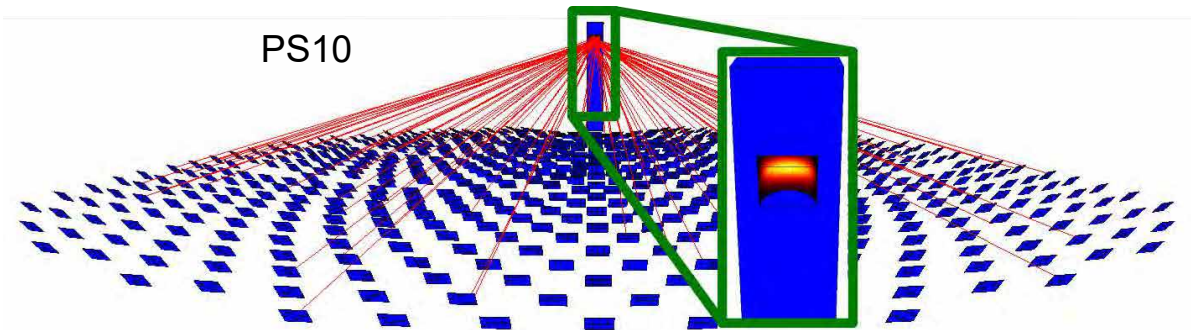
Gemasolar



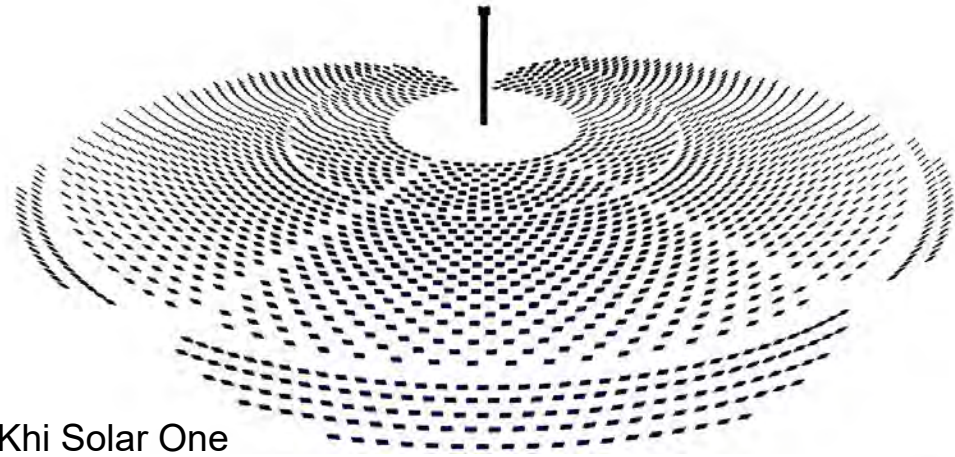
Solar Two



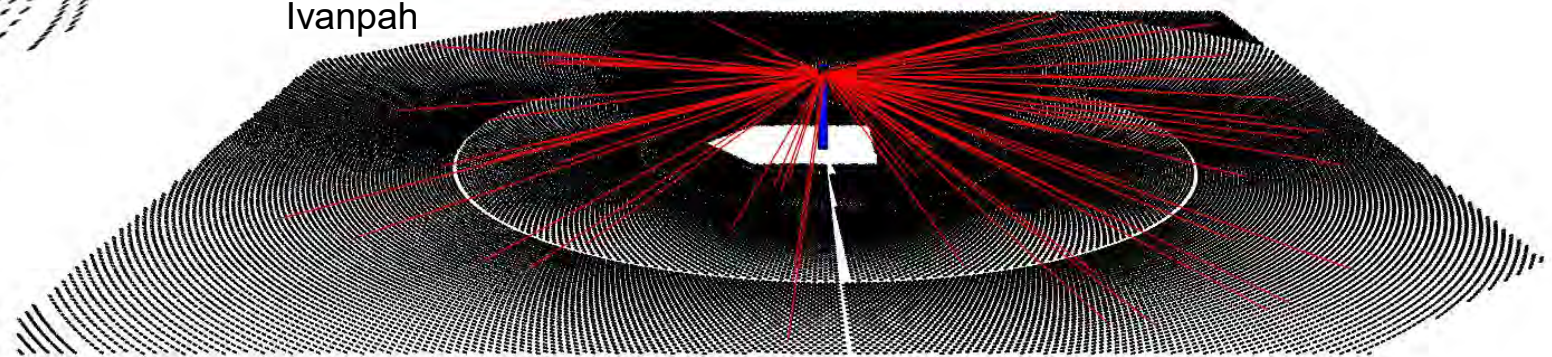
PS10



Khi Solar One



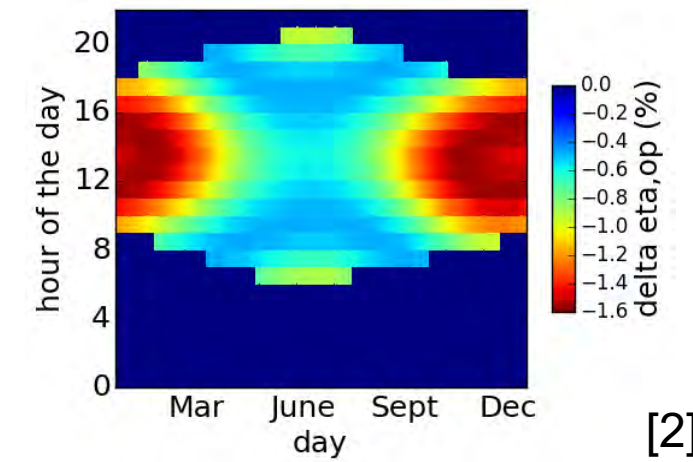
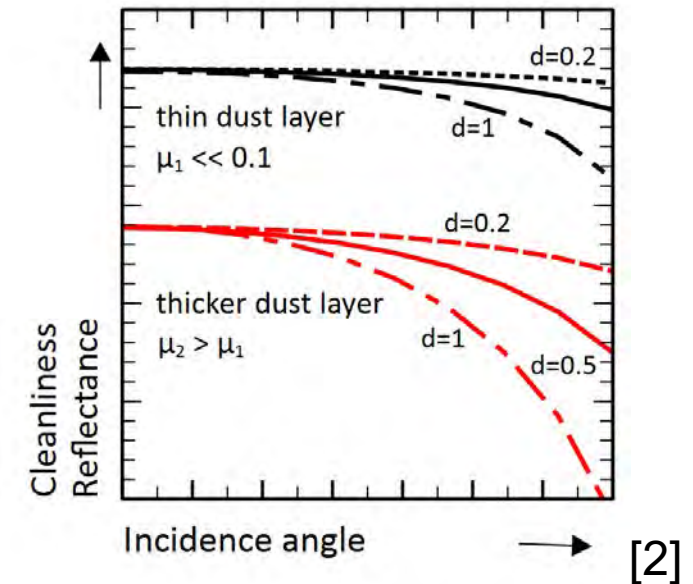
Ivanpah



Raytrace3D concepts

Angle-dependent reflectance for soiling modeling

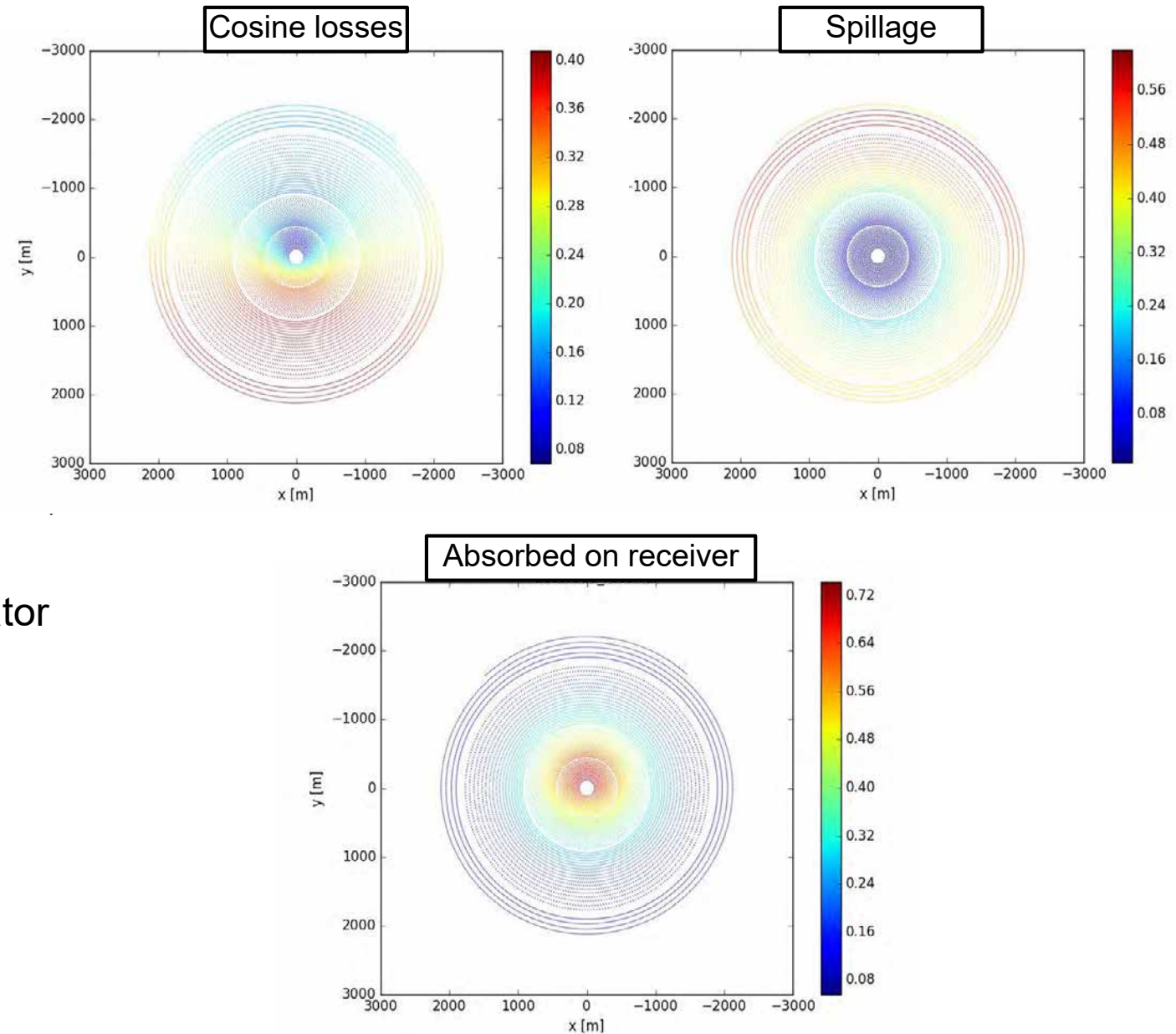
- Clean mirrors → weak incidence angle dependency of reflectance
- Soiled mirrors → strong incidence angle dependency of reflectance
- Raytrace3D: incidence angle dependent reduction of reflectance
- Reduction of solar yield
- Improved yield prediction
- Optimization of cleaning cycles



Raytrace3D concepts

Individual heliostat assessment

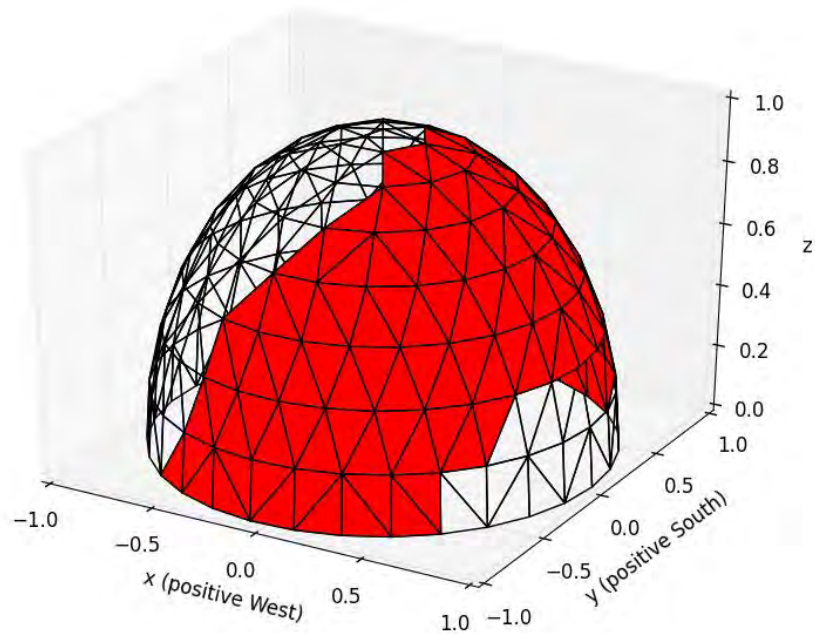
- Built-in routine for evaluating ray history
 - Per-unit assessment of primary aperture (heliostats)
 - Evaluation of different loss mechanisms (cos shading, ...)
 - (Optional) integration of secondary concentrator
- Full insight in heliostat field loss mechanisms
- Input for field design



Raytrace3D concepts

Sky discretization for fast annual assessment [2,3]

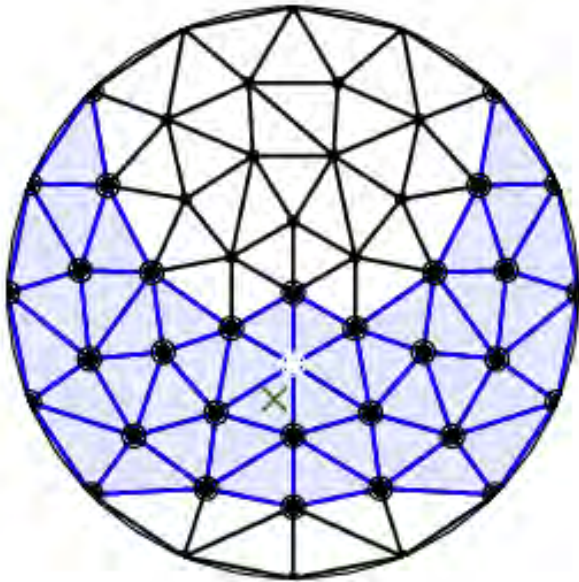
- Uniform discretization of the sky hemisphere



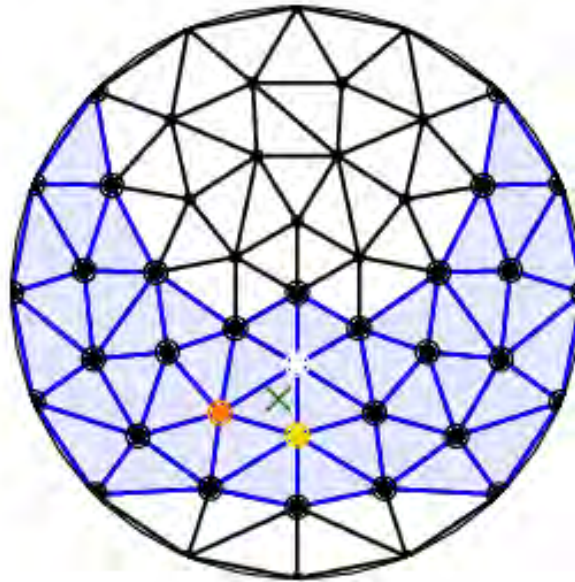
Raytrace3D concepts

Sky discretization for fast annual assessment [2,3]

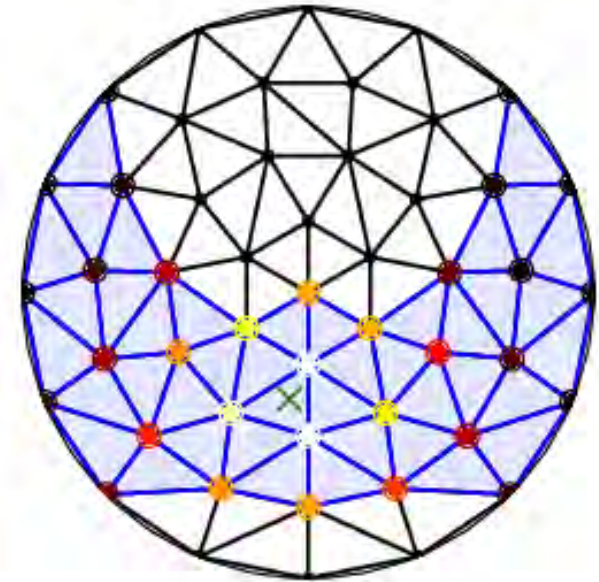
Nearest neighbor



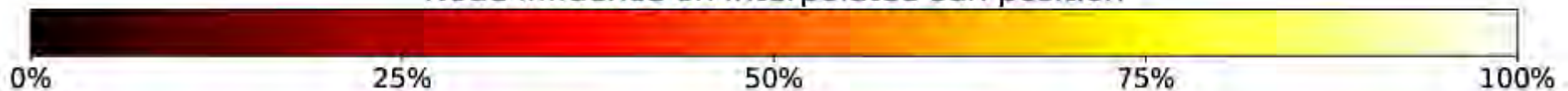
Spherical barycentric



Radial basis function network



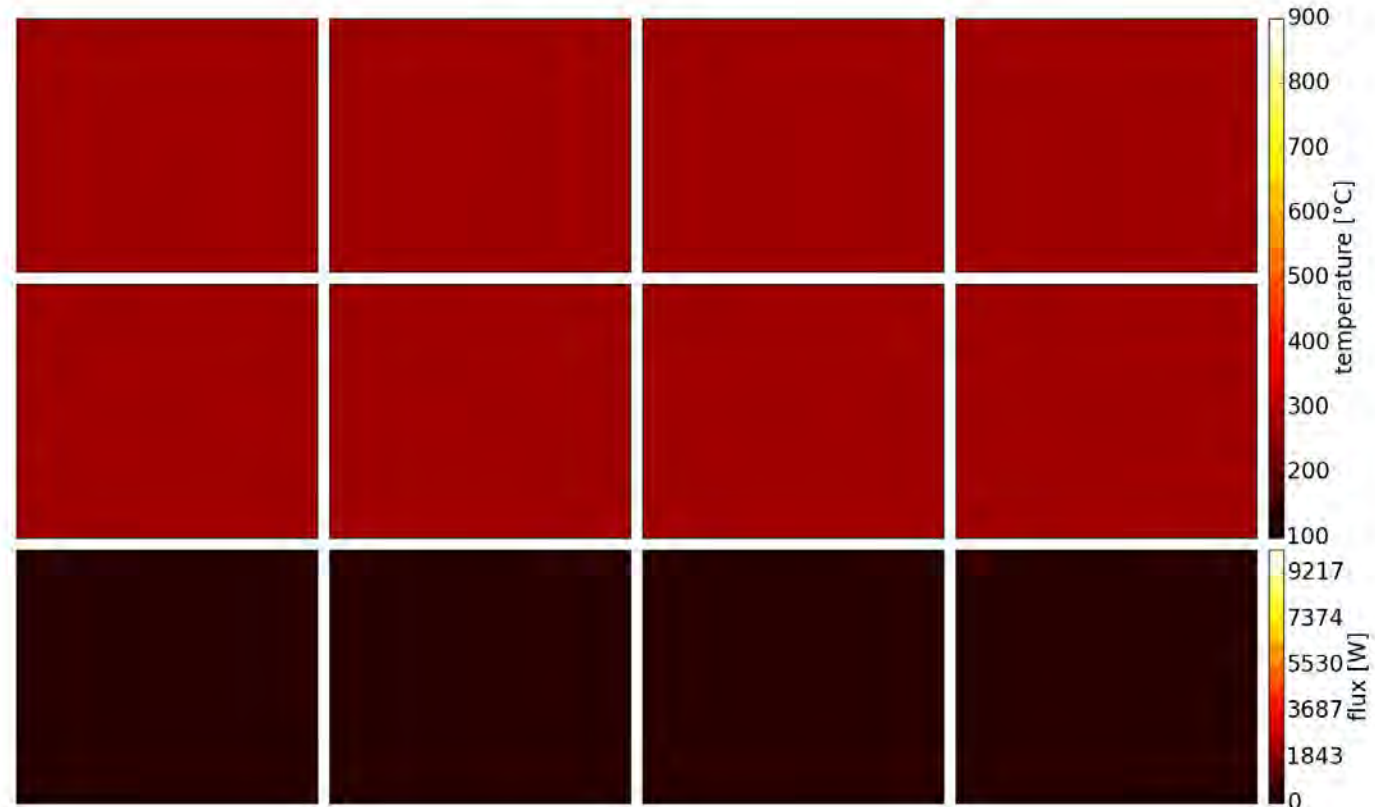
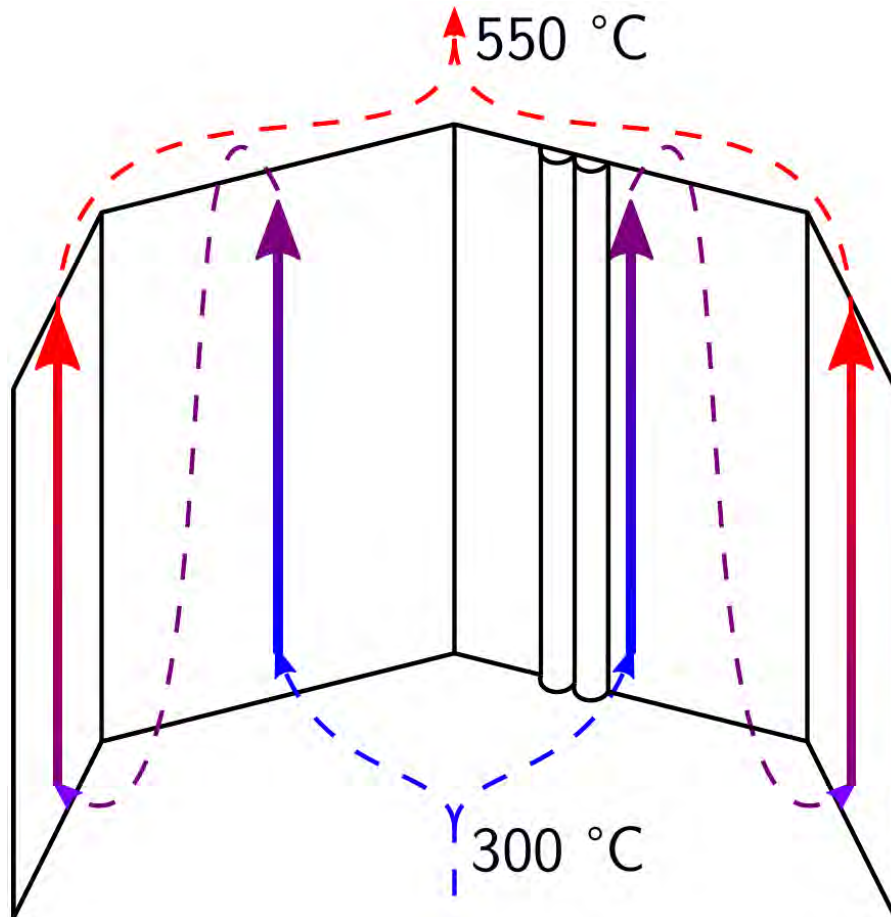
Node influence on interpolated sun position



Raytrace3D concepts

Coupling to dynamic receiver simulation

time: 2010-06-20 06:10:00



Top row: Temperature distribution [°C] in the fluid
Center row: Temperature distribution [°C] on the panel surface
Bottom row: Flux distribution [W] on the panel surface

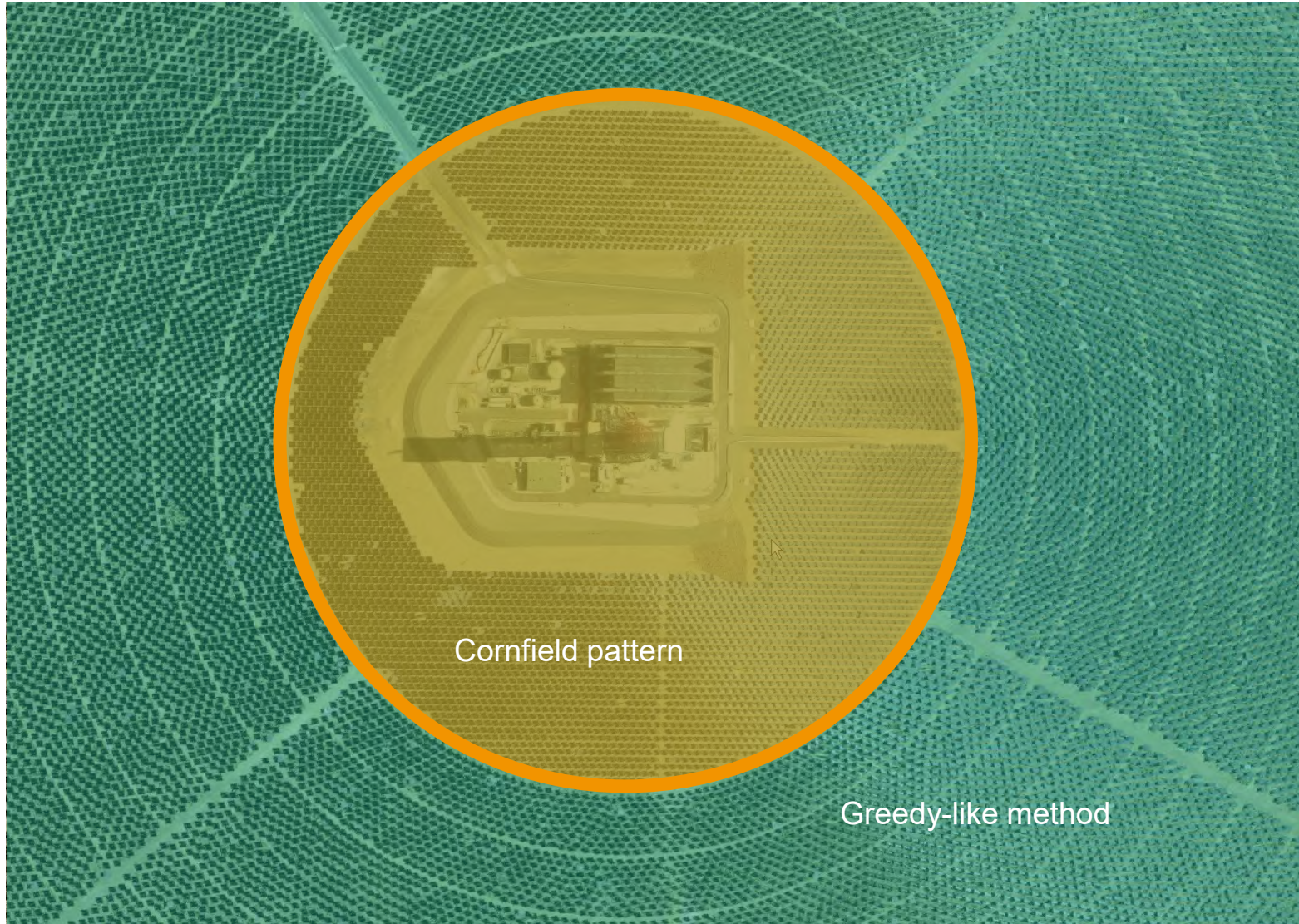
AGENDA

- Raytrace3D
 - Basics
 - Simulation acceleration
 - Angle-dependent reflectance for soiling modeling
 - Individual heliostat assessment
 - Sky discretization for fast annual assessment
 - Coupling to dynamic receiver simulation
- Heliostat field design/optimization
 - Heliostat field layout algorithms
 - Heliostat selection based on polygon optimization

Heliostat field design/optimization

Patterns-based algorithms

- Layout algorithms based on underlying pattern
- Base cases: radially staggered vs. cornfield
- Several free parameters
- Advantages:
 - Fast creation of large fields
 - Construction and maintenance easier in a regular layout
- Disadvantage:
 - Difficult to adapt to uneven terrain

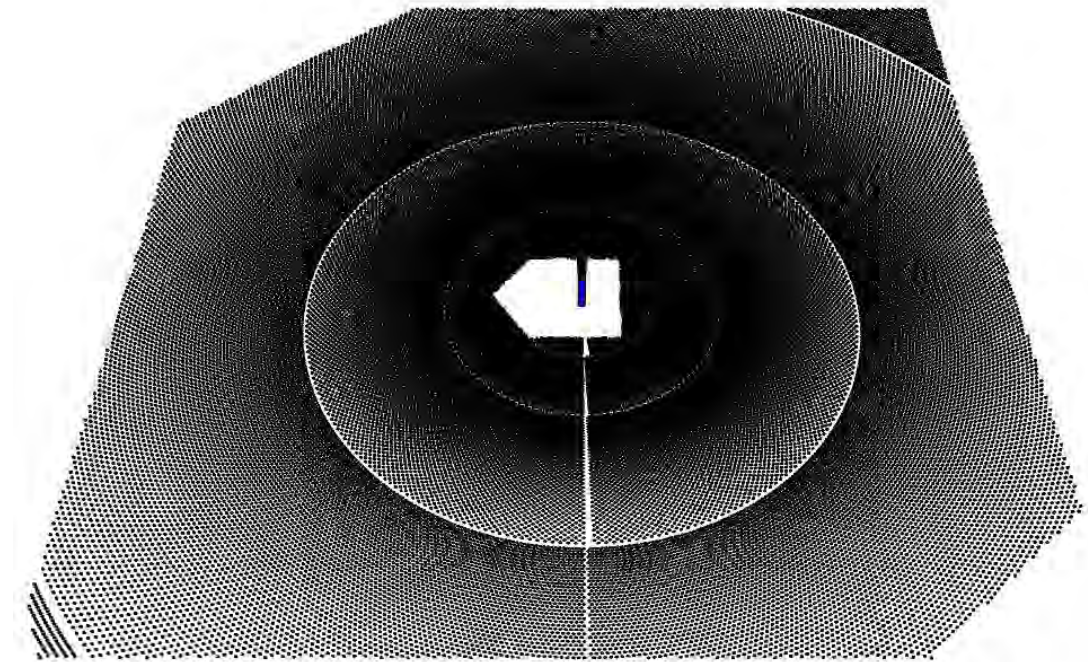


Part of Ivanpah field (source: Google Maps)

Heliostat field design/optimization

MUEEN layout

- Aim: no blocking
- Radially staggered
- Re-grouping for denser field
- Original algorithm [6] extended by Fraunhofer ISE [5]

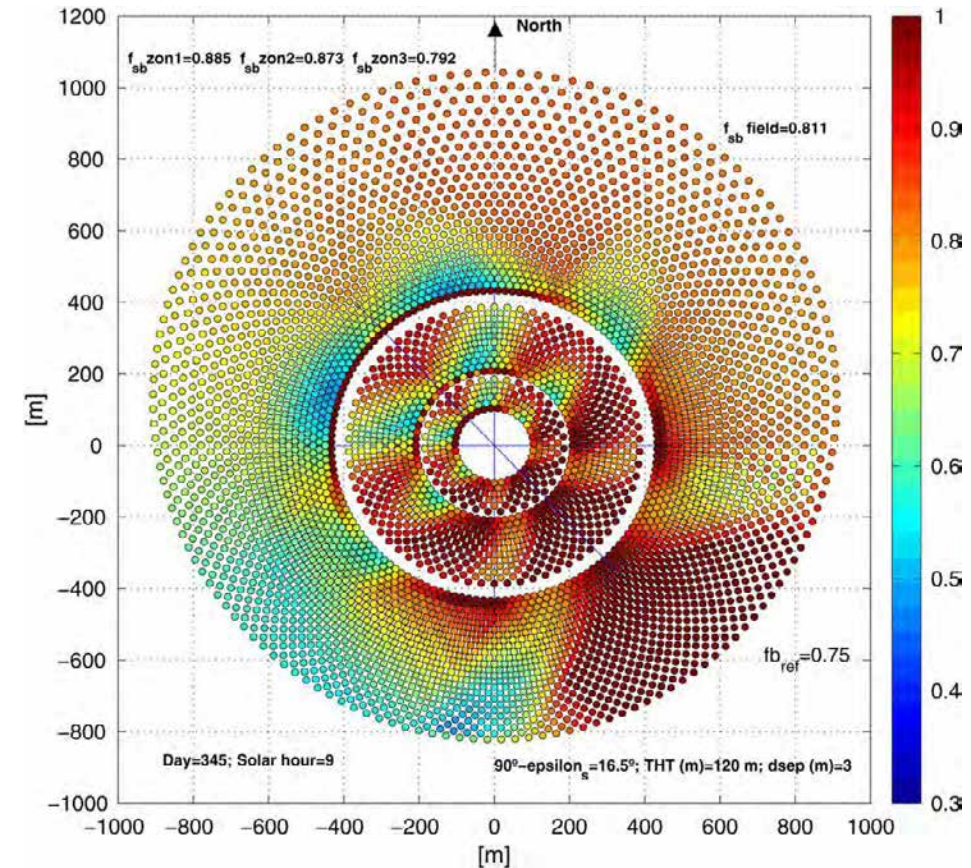


Re-modeling of Ivanpah heliostat field with *Fraunhofer ISE MUEEN* algorithm and field boundaries

Heliostat field design/optimization

CAMPO layout [7]

- Radially staggered
- Creation of densest possible field
- Azimuthal and radial stretching (local!) to reduce shading and blocking

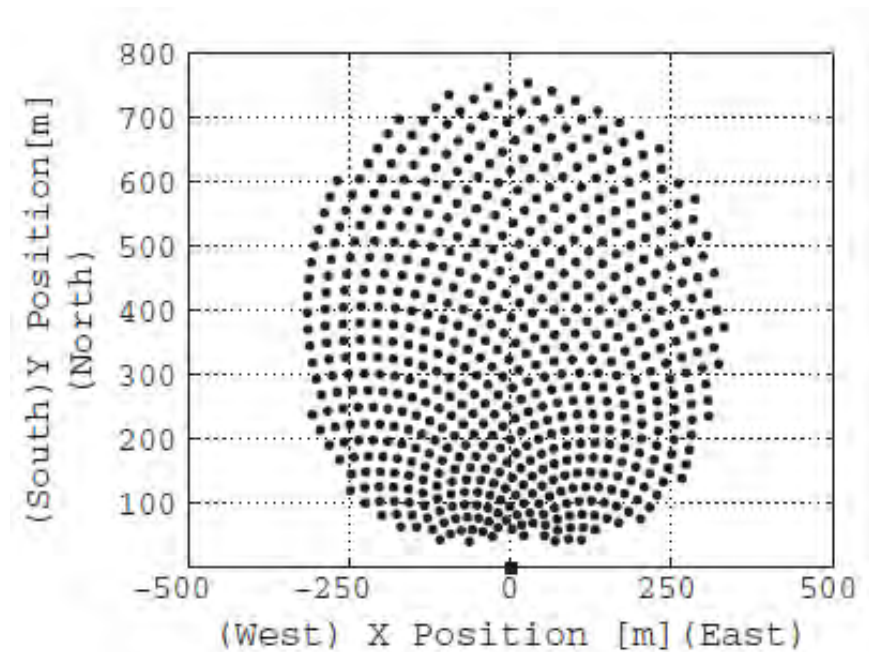


Field generated with CAMPO algorithm (plot from [7])

Heliostat field design/optimization

Biomimetic layout [8]

- Biomimetic phyllotaxis disc pattern
→ sunflower
- Angular distribution is related to the golden ratio $(1 + \sqrt{5})/2$
- Optimization of free parameter



Field generated with biomimetic algorithm (plot from [8])

Heliostat field design/optimization

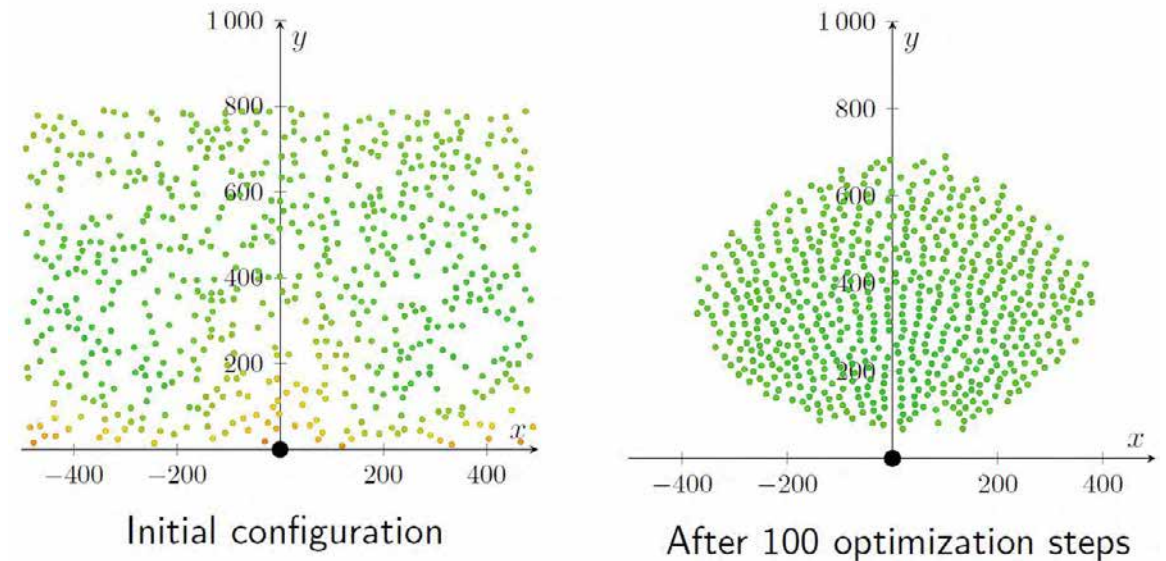
Pattern-free algorithms

- No underlying pattern
- Heliostat placement based on some heuristic
- Advantages:
 - Easily applicable to uneven terrain
- Disadvantage:
 - Field creation very complicated and computationally intensive

Heliostat field design/optimization

Genetic algorithm [9]

- Random generation of initial heliostat base points
- Genetic algorithm (cross-over, mutation, selection) to optimize field

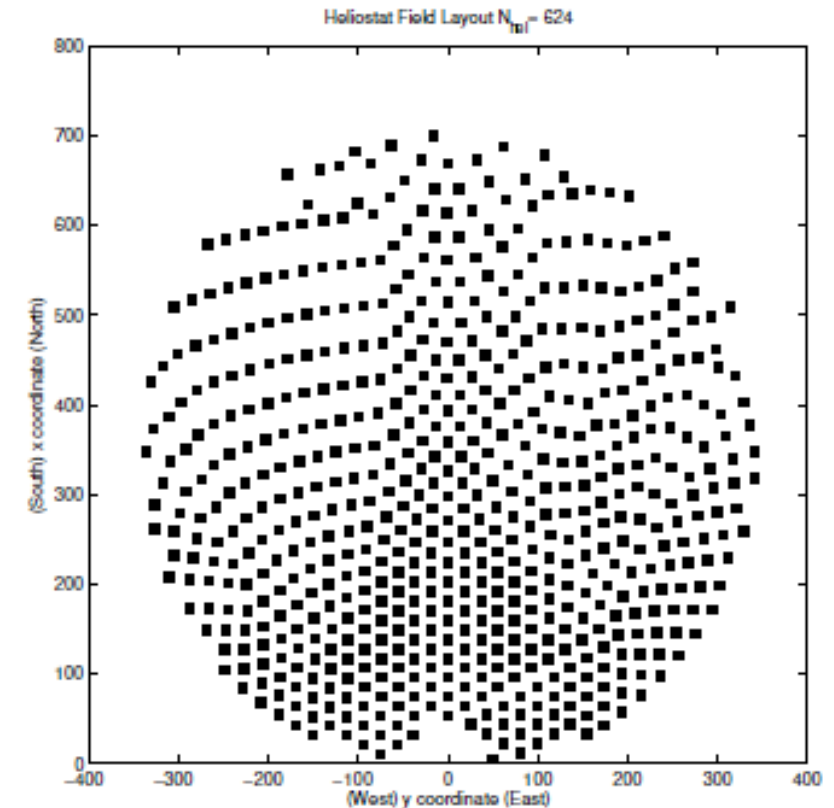


Field optimization with genetic algorithm (plot from presentation related to [9])

Heliostat field design/optimization

Greedy algorithm [10]

- Iterative growth of the heliostat field
- Every new heliostat is placed at the currently best position in the available area
- Different implementations available



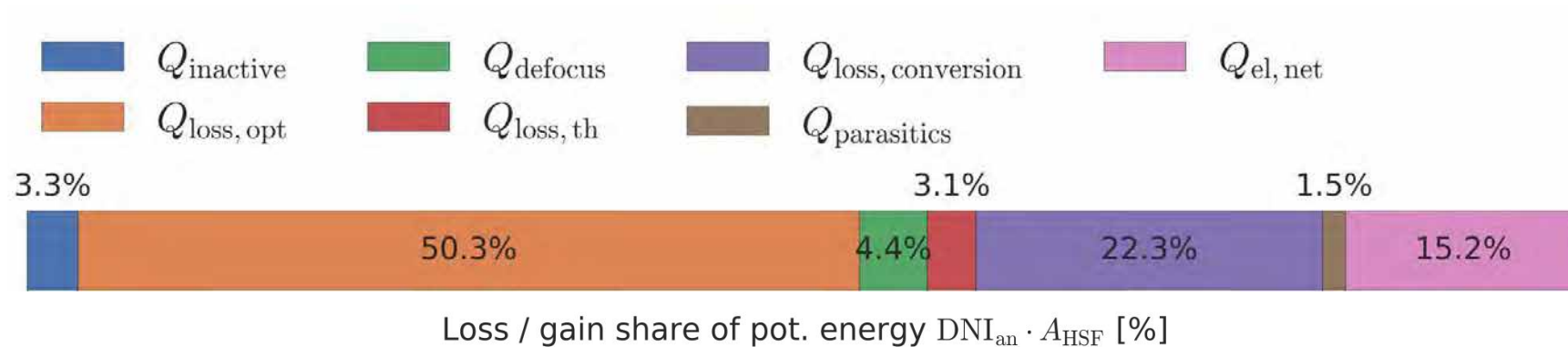
Field optimization with greedy algorithm (plot from [10])

HELIOSTAT SELECTION BASED ON POLYGON OPTIMIZATION

- Motivation
- Problem Description
- Methodology
- Application
- Summary & Outlook

Motivation

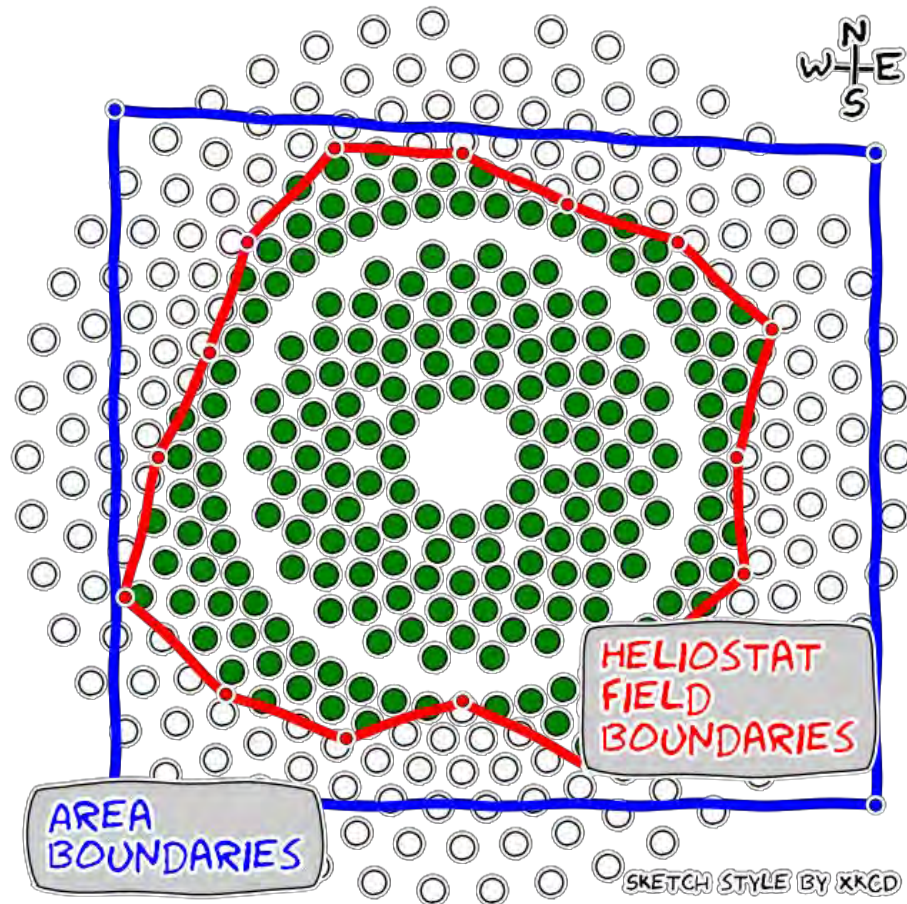
- Heliostat field represents about 40% of CAPEX of entire plant [1]
- Typical loss composition for a 600 MW_{th} Solar Tower plant [3]



- Field design for **high annual efficiency** and **low cost** is crucial

Heliostat selection based on polygon optimization

Problem description: Heliostat Selection from Oversized Field



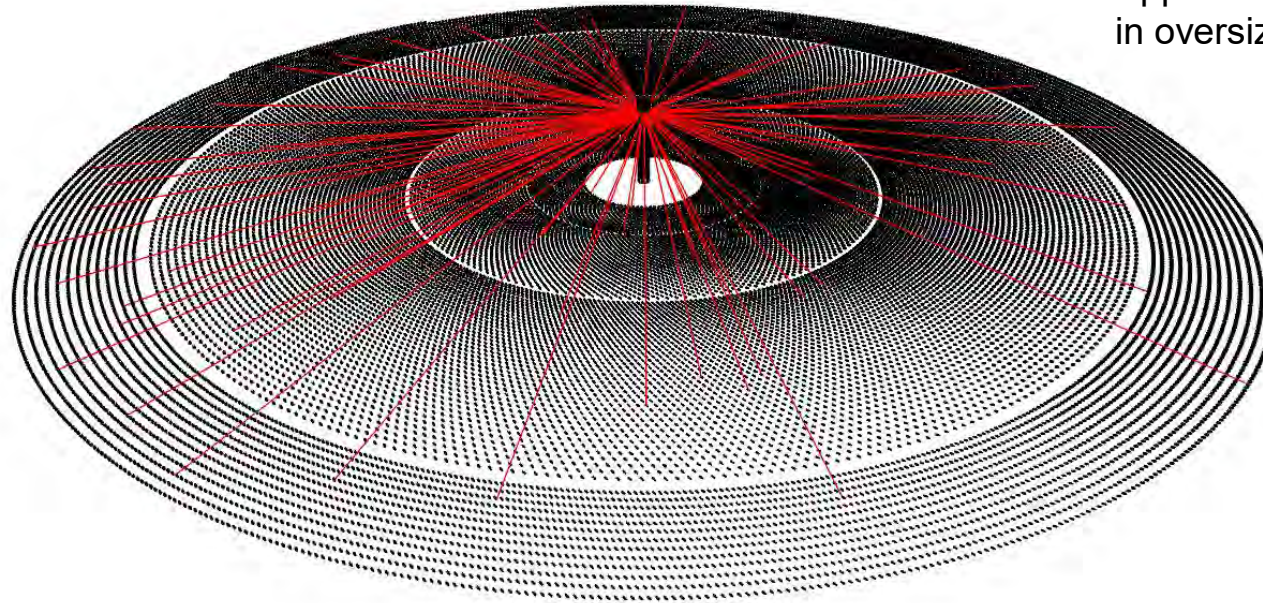
- Respect area boundaries
- Meet flux requirements
- Optimize for given objective function
- Coherent field, feasible w.r.t. construction and maintenance

HELIOSTAT SELECTION BASED ON POLYGON OPTIMIZATION

- Problem Description
- Methodology
 - Oversized Field
 - Polygon-Based Selection
 - Area Boundaries
 - Evolutionary Optimization Algorithm
- Application
- Summary & Outlook

Methodology

Oversized Field



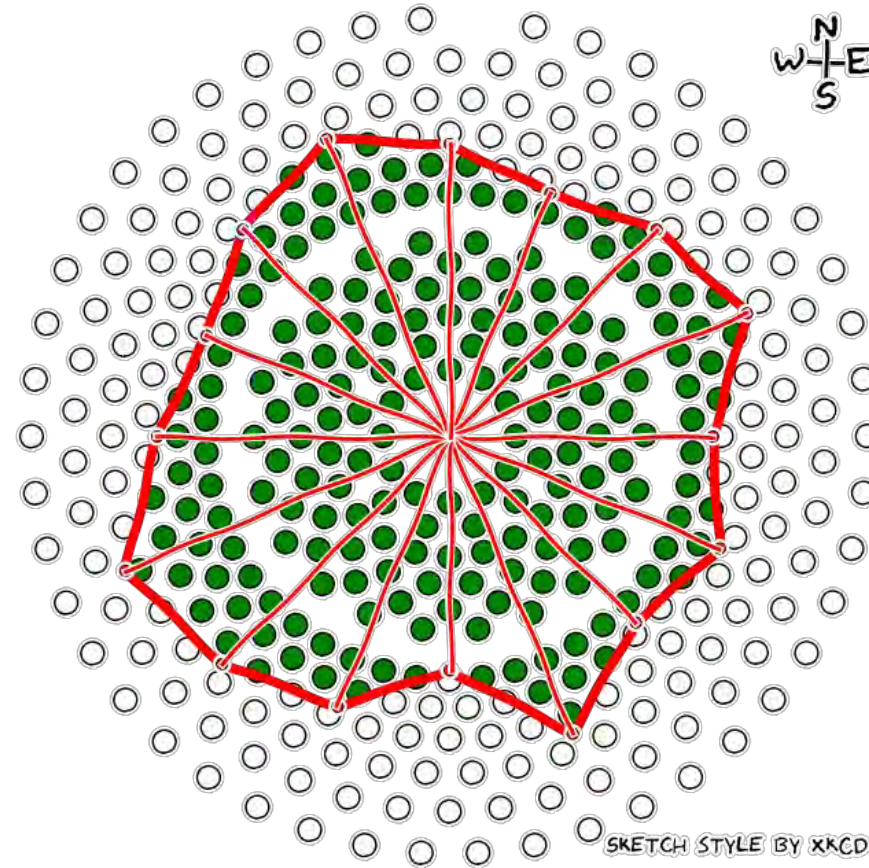
Approx. 35k heliostats
in oversized field

- Generation with **extended MUEEN algorithm [4]**
- Assessment with **Raytrace3D [5]**

Methodology

Polygon-Based Selection

- Equi-angular vertices
- Centered around tower base
- Only vertex radii as free parameters in optimization
- Coherent field boundaries
- Evaluation of objective function on entire field
- For polar field, limit angular range



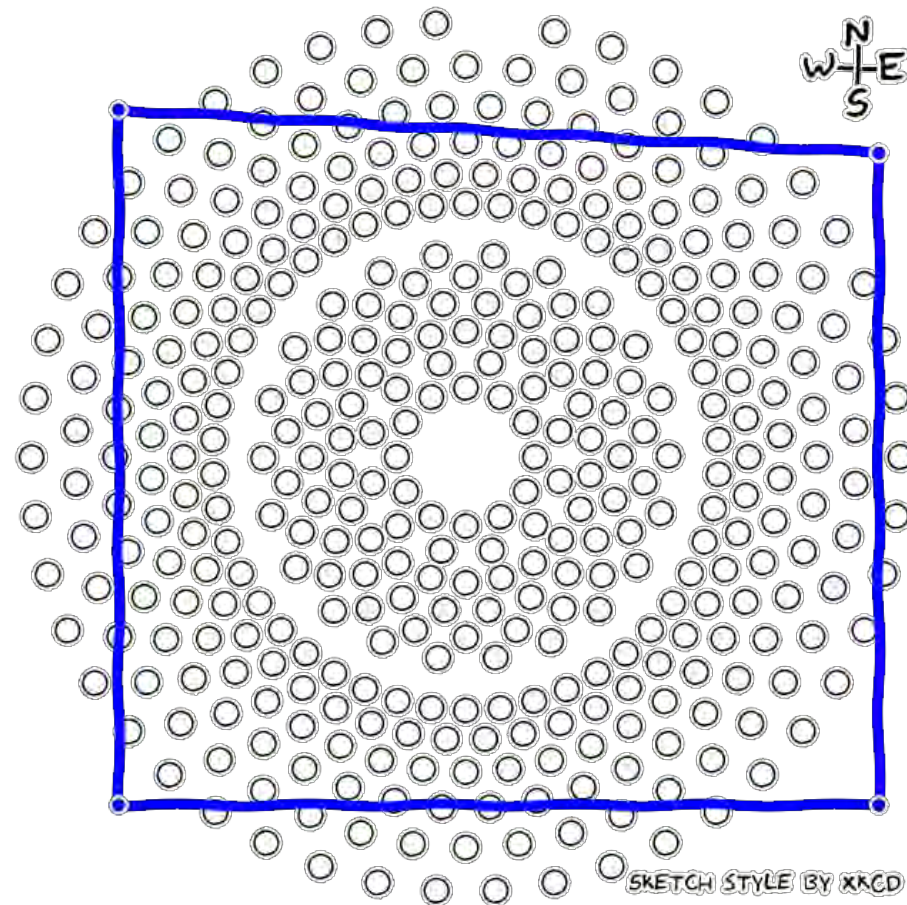
Methodology

Area Boundaries

- Yet another polygon
- Move relative to tower base
- Two additional degrees of freedom: Δx , Δy

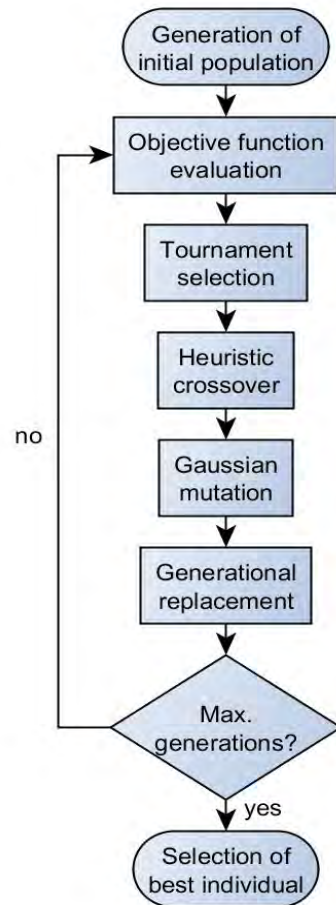
Area boundaries are

- ~~Large, not constraining~~
- Large enough, constraining
- ~~Too small~~



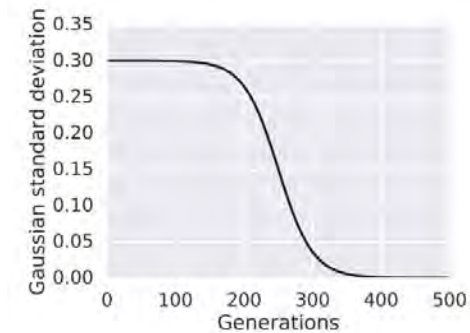
Methodology

Evolutionary Optimization Algorithm



Problem-specific tweaks

- Penalty on not reaching required flux at design point
- Mutation range decreases with sigmoid function



- Small tournament size of 3
- Full generational replacement, no elitism
- low selection pressure, no premature convergence

HELIOSTAT SELECTION BASED ON POLYGON OPTIMIZATION

- Problem Description
- Methodology
- Application
 - Base Scenario
 - Objective Function
 - Examples
- Summary & Outlook

Application

Base Scenario

| Parameter | Value [6] |
|--|----------------------|
| Site | Seville, Spain |
| Absorbed power at design point | 55.27 MW |
| Tower height | 100.5 m |
| External receiver diameter | 14 m |
| External receiver height | 12 m |
| Number of heliostats in oversized field | 35000 |
| Heliostat area (square) | 8 m ² |
| Minimum radial heliostat distance to tower | 80 m |
| Design point | Winter solstice |
| Design DNI | 850 W/m ² |

Application

Objective function

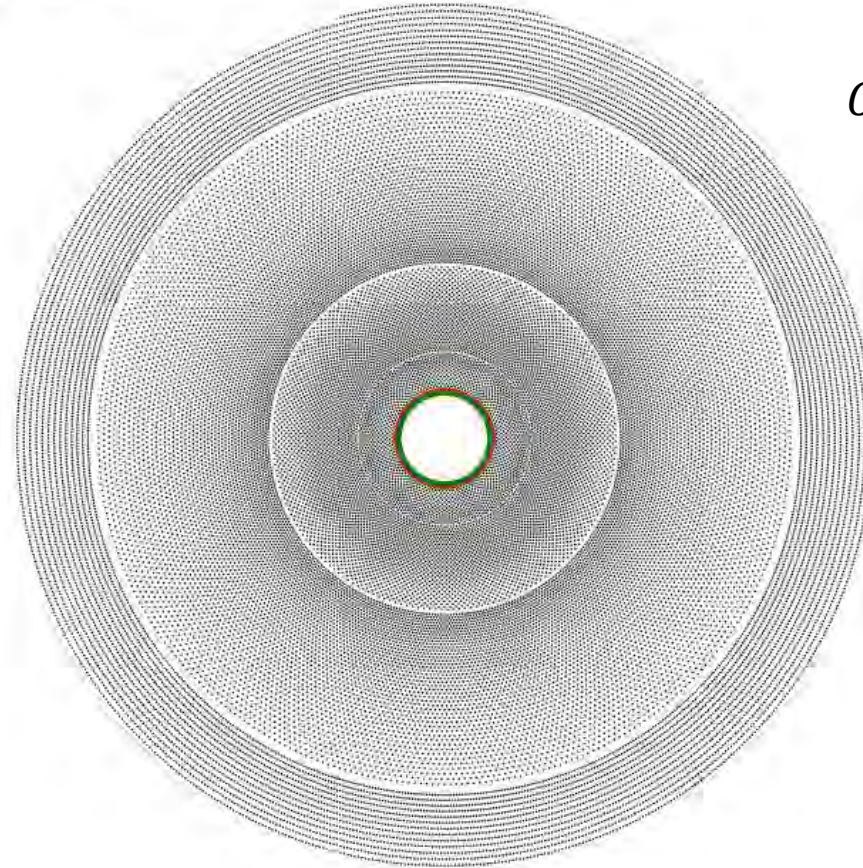
Objective function maximizes yield per cost [6]:

- annual optical efficiency η_{an} of the entire field
- ground area A_{ground} being the convex hull of all heliostats
- cumulative mirror area A_{HSF} of all heliostats
- cost ratio $k = \frac{k_{ground}}{k_{HSF}}$ of ground area to mirror area
- Cumulative annual direct normal irradiance DNI_{an}

Application

No Area Boundaries, Cost Ratio $k=0\%$

Generation 0



$$OF = \frac{\eta_{an}}{k \cdot \frac{A_{ground}}{A_{HSF}} + 1} = \eta_{an}$$

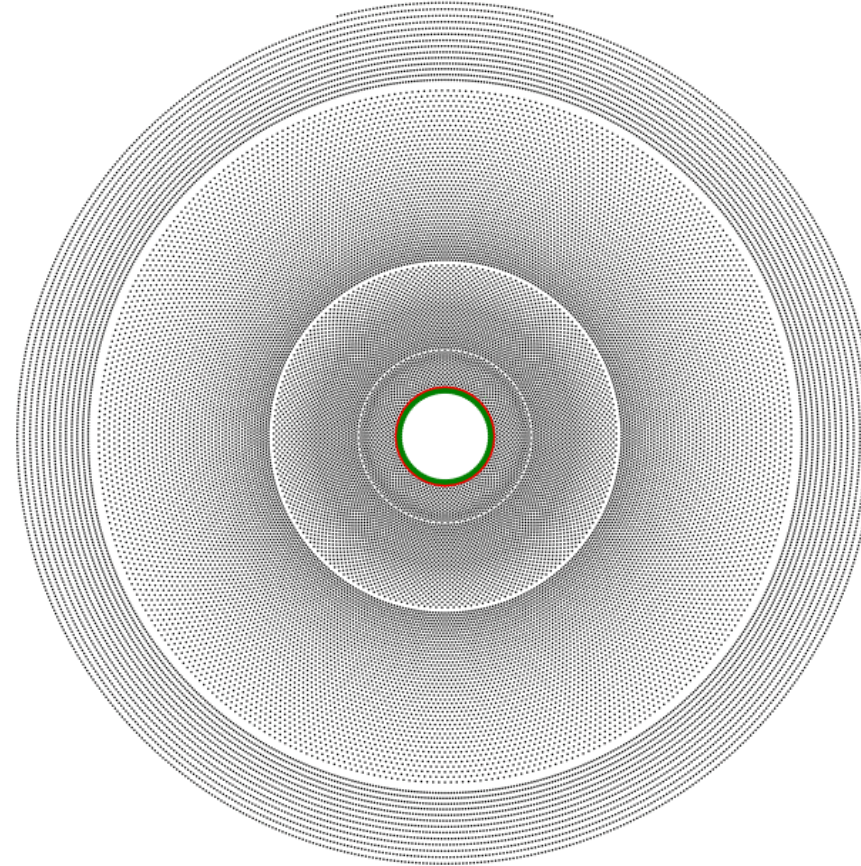
Animations showing best candidate every ten generations

Application

No Area Boundaries, Cost Ratio $k=0\%$

Generation 0

$$OF = \eta_{an}$$

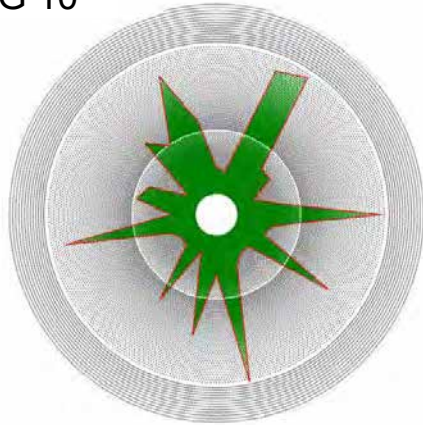


Application

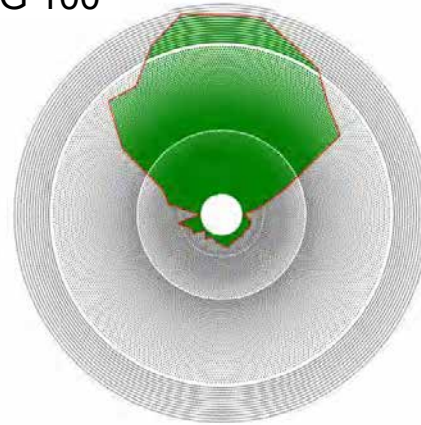
No Area Boundaries, Cost Ratio $k=0\%$

$$OF = \eta_{an}$$

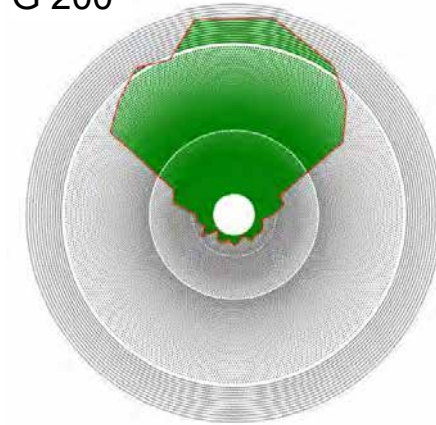
G 10



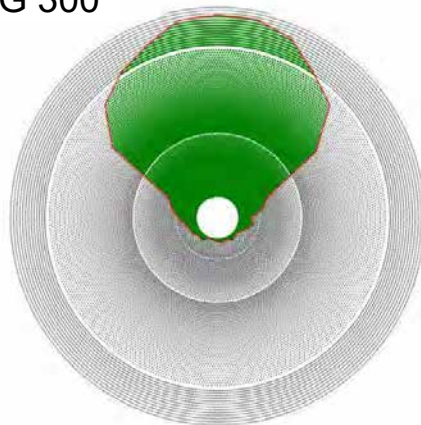
G 100



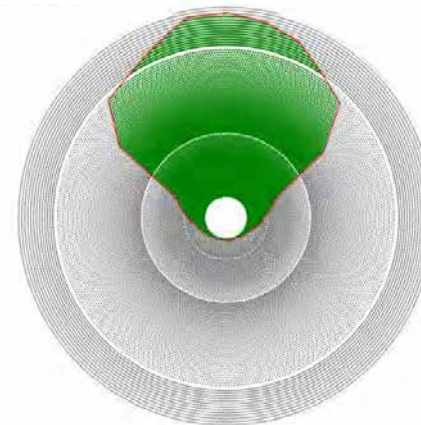
G 200



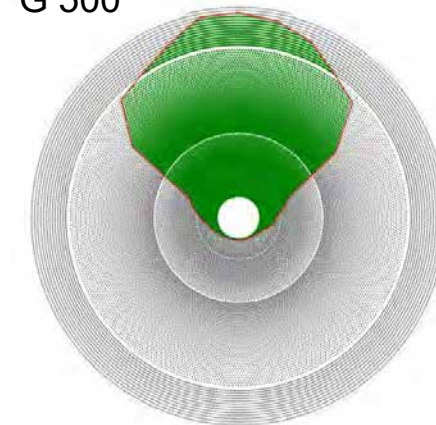
G 300



G 400



G 500

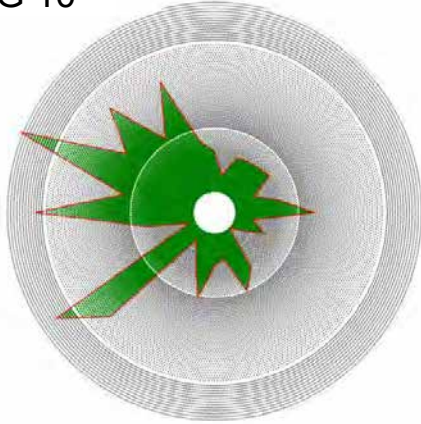


Application

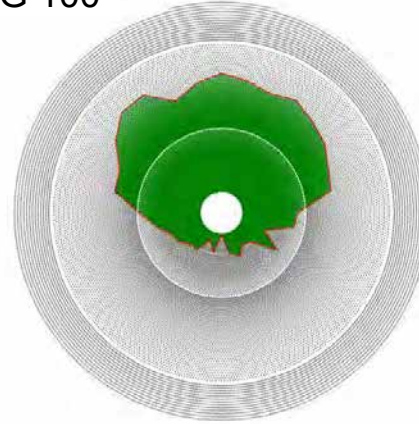
No Area Boundaries, Cost Ratio $k=4\%$

$$OF = \frac{\eta_{an}}{k \cdot \frac{A_{ground}}{A_{HSF}} + 1}$$

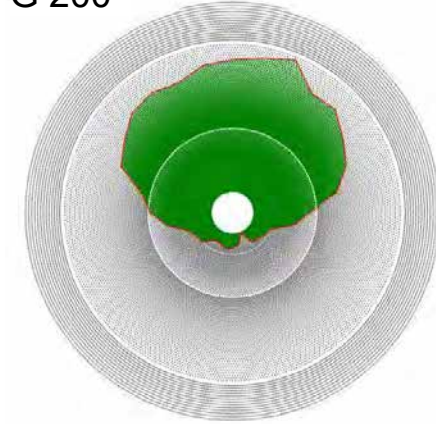
G 10



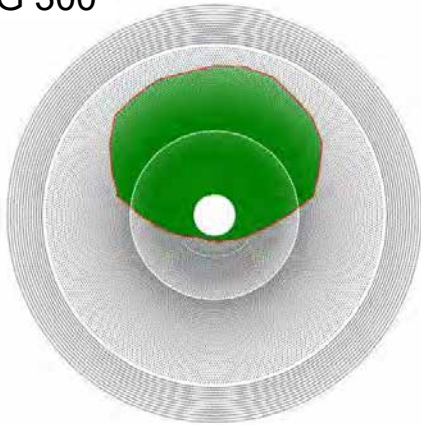
G 100



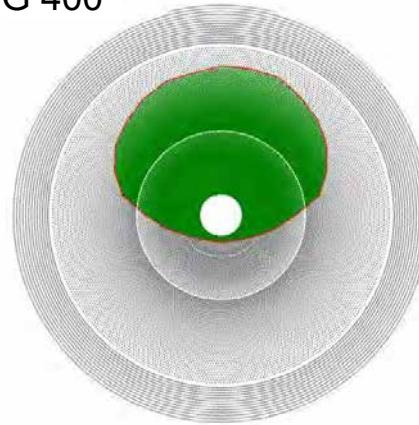
G 200



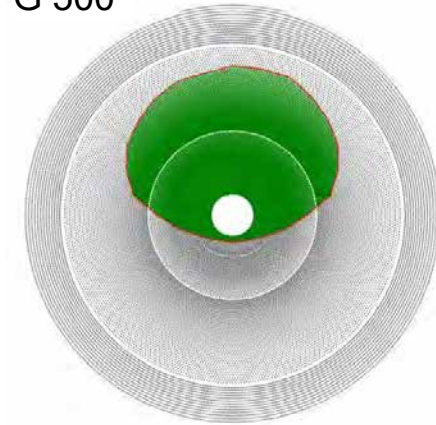
G 300



G 400



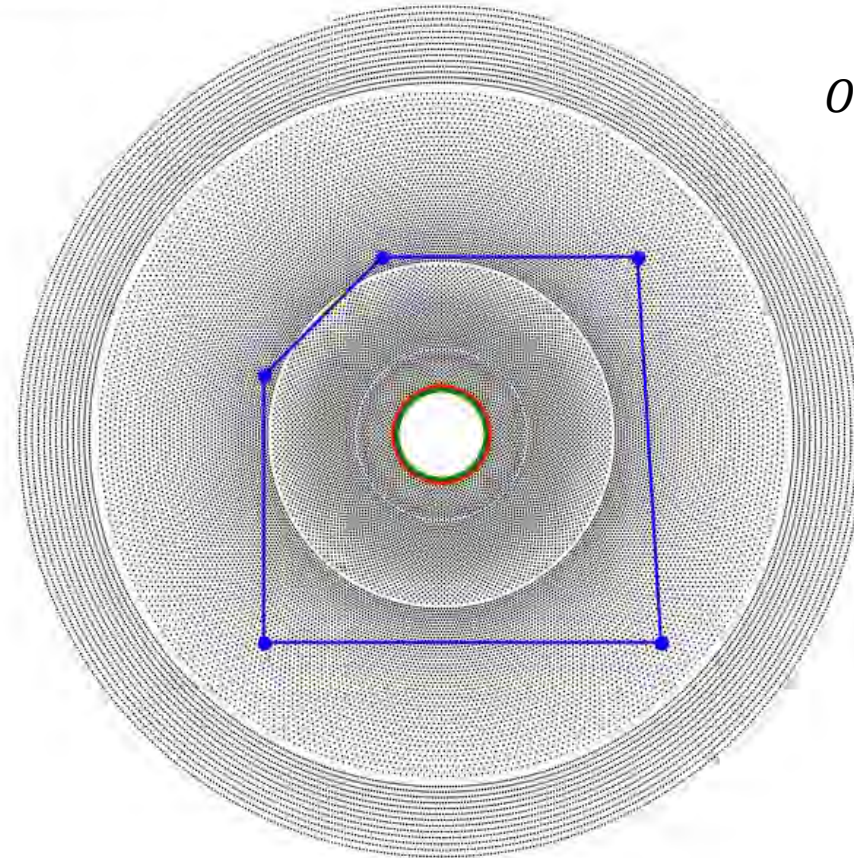
G 500



Application

Complex Area Constraints, Cost Ratio $k=0\%$

Generation 0

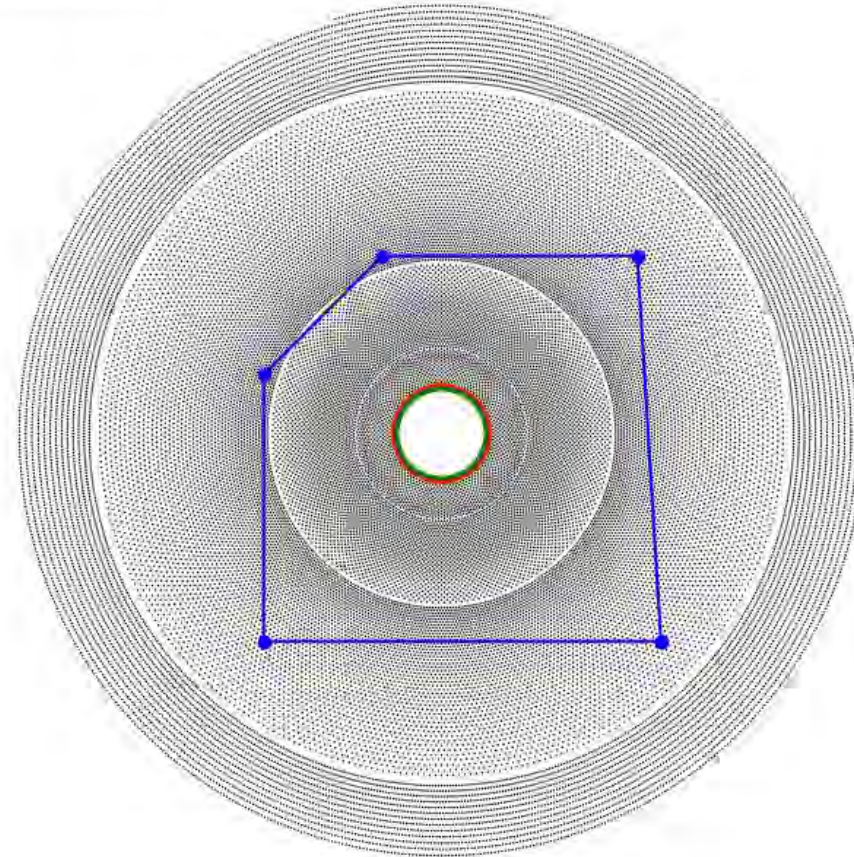


$$OF = \frac{\eta_{an}}{k \cdot \frac{A_{ground}}{A_{HSF}} + 1} = \eta_{an}$$

Application

Complex Area Constraints, Cost Ratio $k=0\%$

Generation 0



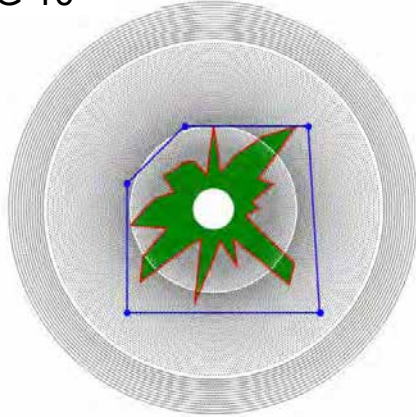
$$OF = \eta_{an}$$

Application

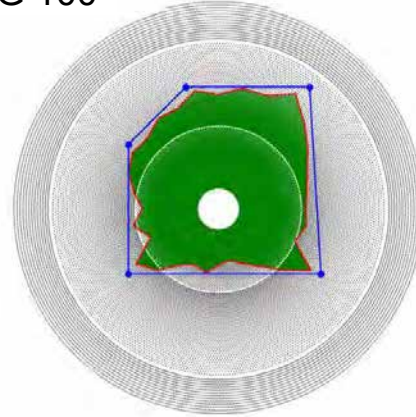
Complex Area Constraints, Cost Ratio $k=0\%$

$$OF = \eta_{an}$$

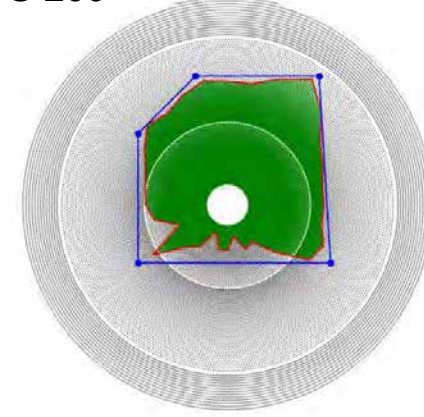
G 10



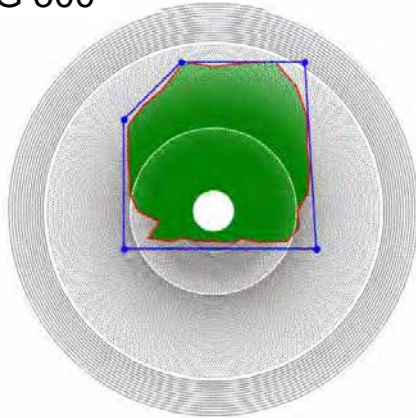
G 100



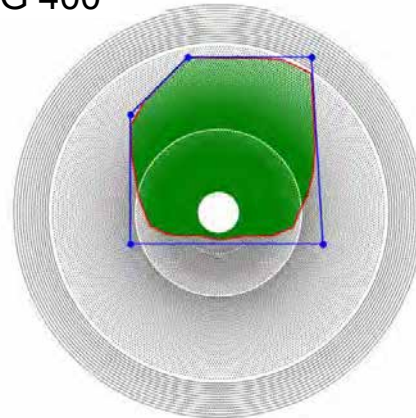
G 200



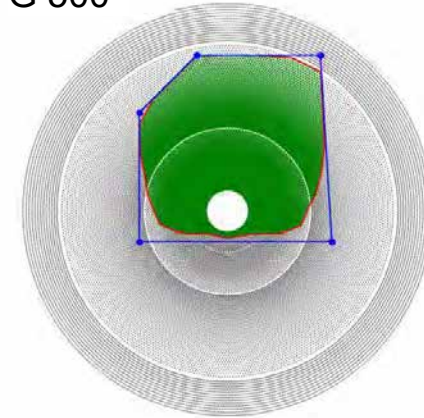
G 300



G 400

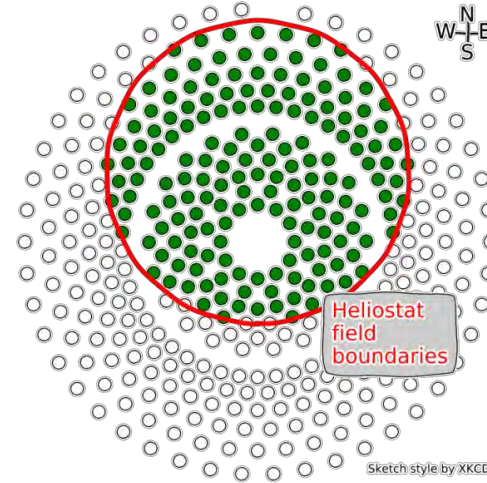


G 500



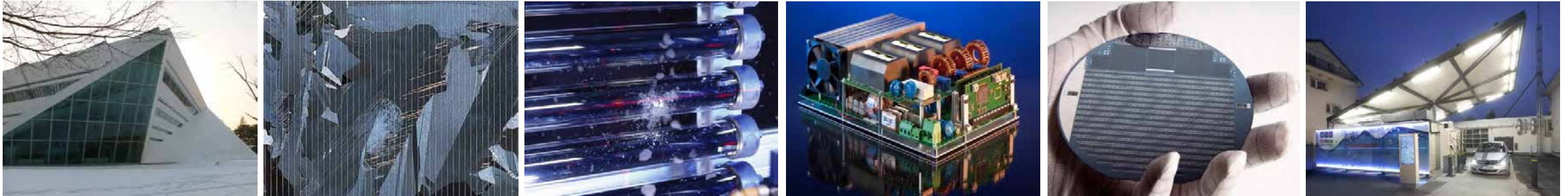
Summary & Outlook

- Method: solar field heliostat selection based on polygon optimization and boundaries
 - Coherent fields
 - Area boundaries
 - Flexible objective function
-
- Quantitative comparison to other approaches
 - Allowable flux limits in objective function
 - Area boundaries with undercuts, holes and hilly terrain



Ashalim Power Station, BrightSource Industries Israel (source: <https://inhabitat.com/>)

Thank you for your Attention!



Fraunhofer Institute for Solar Energy Systems ISE

Shahab Rohani, Peter Schöttl

www.ise.fraunhofer.de

shahab.rohani@ise.fraunhofer.de

peter.schoettl@ise.fraunhofer.de

CASE STUDY

surrounding versus north fields

Heliostats fields, understanding the influence of latitude

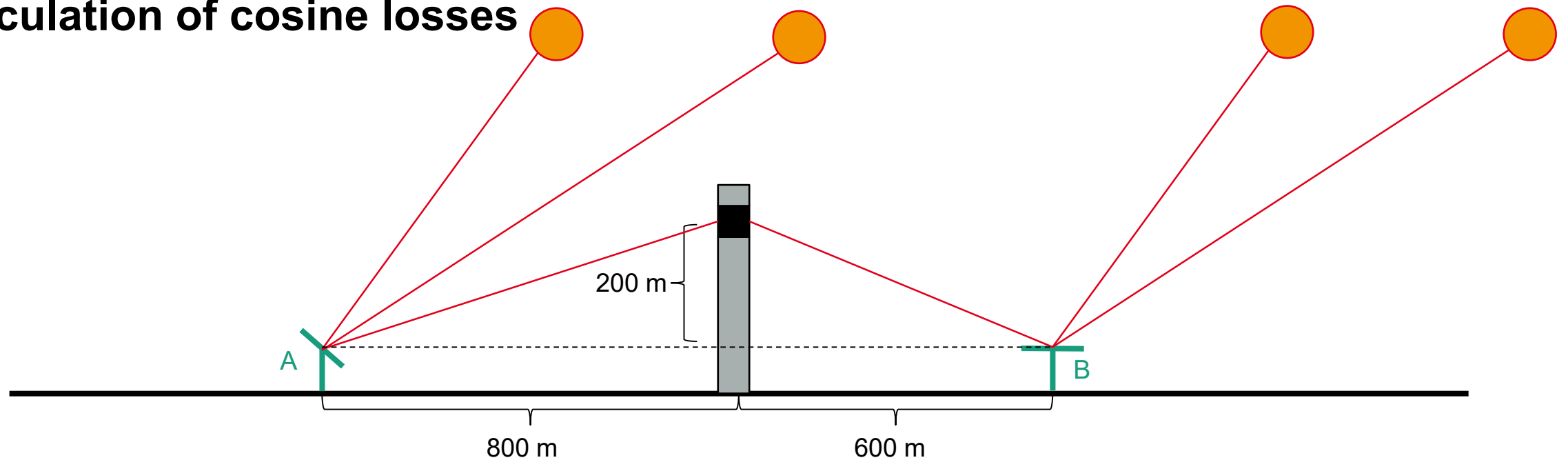
AGENDA

- Interactive
 - Summer/winter solstice sun position
 - Calculation of cosine losses
- Latitude effects on surround/polar heliostat fields
 - Reference scenarios
 - Methodology recap
 - Result discussion

Summer/winter solstice sun position

- Location: Odeillo, France
- www.suncalc.org
- Summer (S) solstice: solar zenith $\theta_{s,S} = 19.1^\circ$, solar elevation $\alpha_{s,S} = 70.9^\circ$
- Winter (W) solstice: solar zenith $\theta_{s,W} = 65.9^\circ$, solar elevation $\alpha_{s,S} = 24.1^\circ$

Calculation of cosine losses

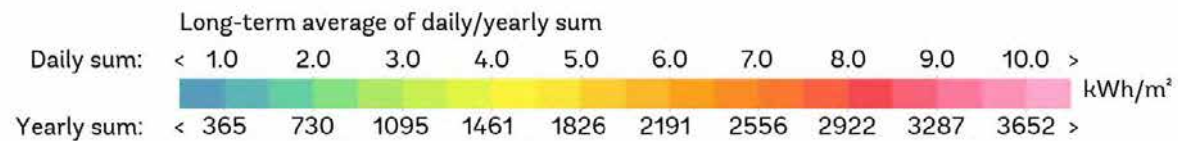
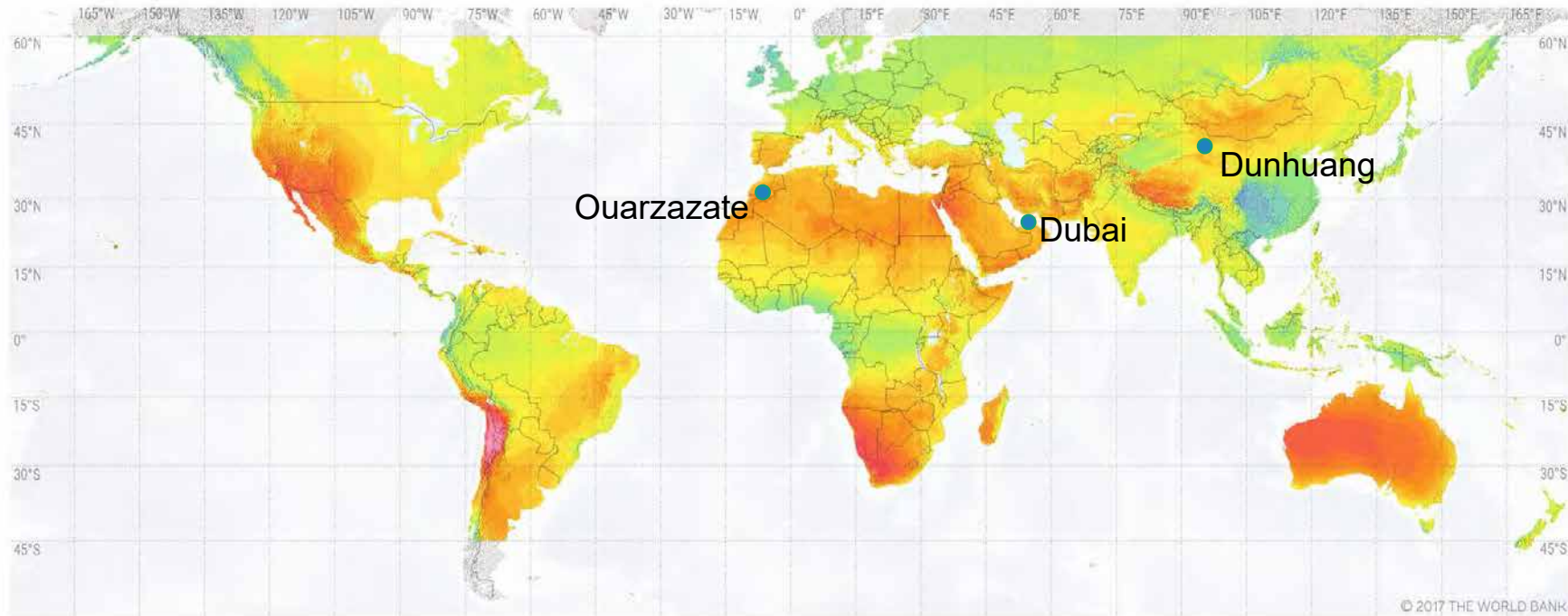


- Heliostat-tower angles: $\beta_A = \tan^{-1} \frac{200}{800} = 14.0^\circ$, $\beta_B = \tan^{-1} \frac{200}{600} = 18.4^\circ$
- Summer solstice: $\theta_{inc,A} = \frac{|\alpha_{s,S} - \beta_A|}{2} = \frac{|70.9^\circ - 14.0^\circ|}{2} = 28.5^\circ$, $\theta_{inc,B} = \frac{|180^\circ - \alpha_{s,S} - \beta_B|}{2} = 45.4^\circ$
Cosine losses: $1 - \cos \theta_{inc,A} = 0.12$, $1 - \cos \theta_{inc,B} = 0.30$
- Winter solstice: $\theta_{inc,A} = 5.1^\circ$, $\theta_{inc,B} = 68.8^\circ$
Cosine losses: $1 - \cos \theta_{inc,A} = 0$, $1 - \cos \theta_{inc,B} = 0.64$

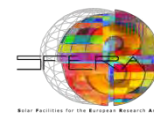
Reference scenarios

Sites

SOLAR RESOURCE MAP DIRECT NORMAL IRRADIATION



This map is published by the World Bank Group, funded by ESMAP, and prepared by Solargis. For more information and terms of use, please visit <http://globalsolaratlas.info>.



Reference scenarios

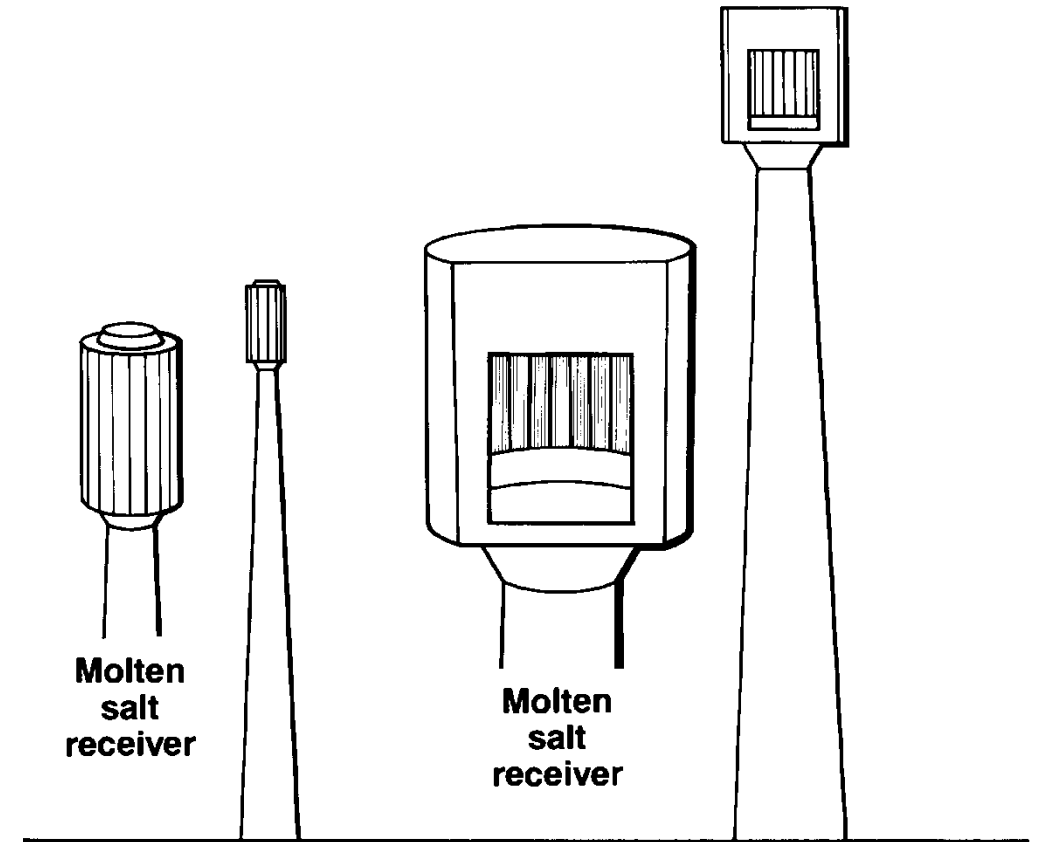
Parameters

| | Dubai | Ouarzazate | Dunhuang |
|------------------------|--|---------------------------|---------------------------|
| Location | 24.8 °N, 55.4 °E | 31.0 °N, 6.9 °W | 39.8 °, 92.7 °E |
| Annual DNI | 2.15 MWh/m ² a | 2.92 MWh/m ² a | 2.13 MWh/m ² a |
| Design point DNI | 800 W/m ² at summer solstice | | |
| Tower height | 140 m | | |
| Receiver design power | 120 MW _{th} | | |
| Receiver absorber area | 521.5 m ² (cavity), 260.8 m ² (external) | | |
| Heliostat mirror area | 115.7 m ² | | |
| Heliostat beam quality | 3 mrad | | |
| Heliostat reflectance | 93% | | |

Reference scenarios

External vs cavity

- Cavities combined with higher towers than external receivers
 - ignored
- Cavities larger than external receivers
 - $A_{abs,cavity} = A_{abs,external} \cdot 2$
 - Higher costs!



Source: P. K. Falcone, *A HANDBOOK FOR SOLAR CENTRAL RECEIVER DESIGN*. SAND-86-8009. Livermore, CA (USA), 1986.

Methodology recap

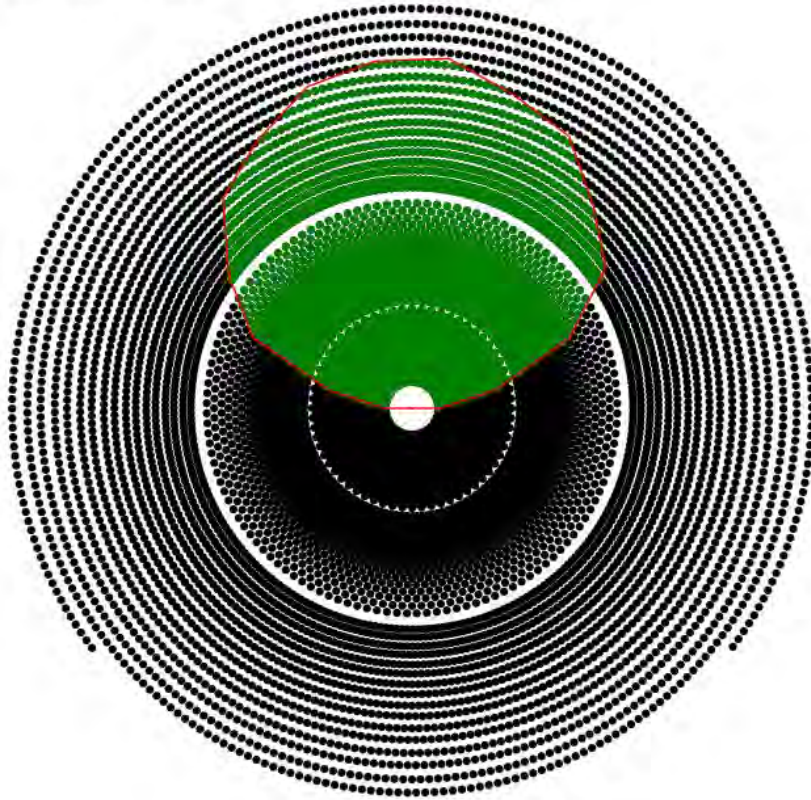
1. Create oversized MUEEN field
2. Assess heliostat annual efficiencies with Raytrace3D
3. Assess heliostat design point efficiencies with Raytrace3D
4. Select best-performing heliostats with polygon-based approach

Result discussion

Dubai: selected fields

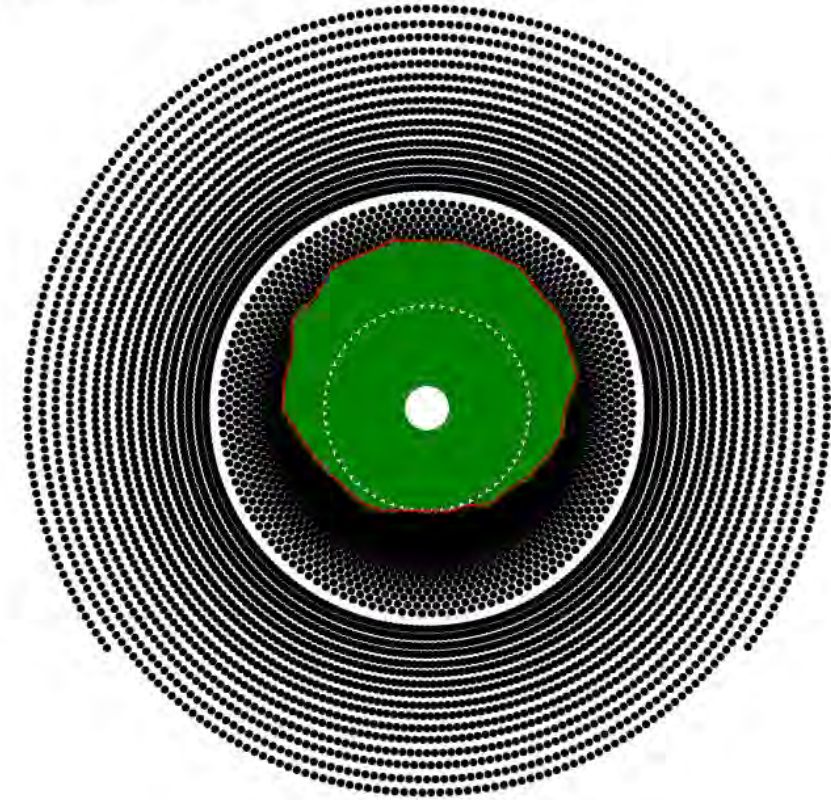
Cavity

Generation 500



External

Generation 500

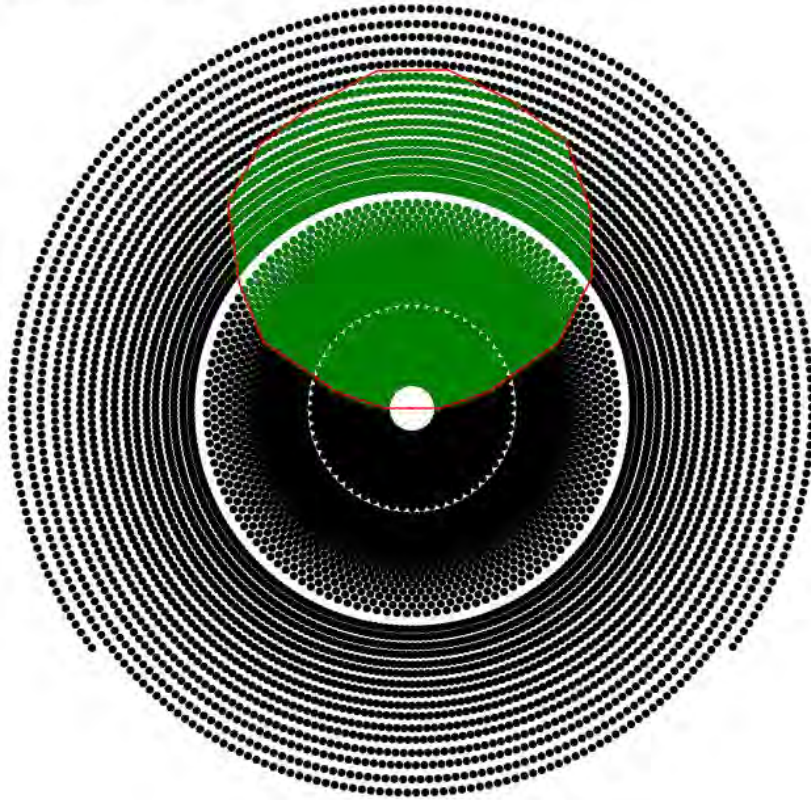


Result discussion

Ouarzazate: selected fields

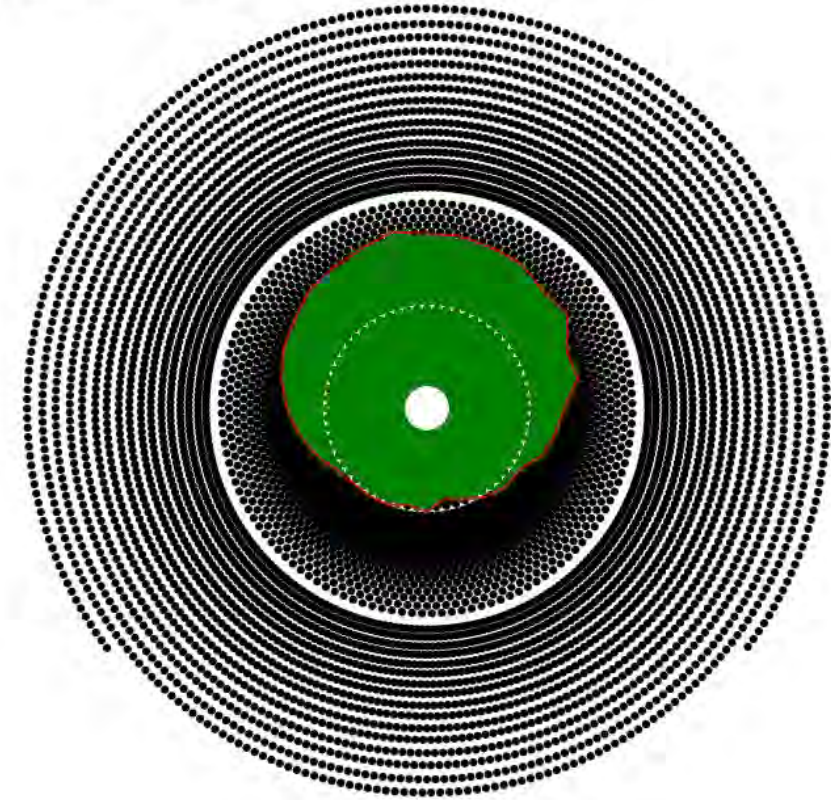
Cavity

Generation 500



External

Generation 500

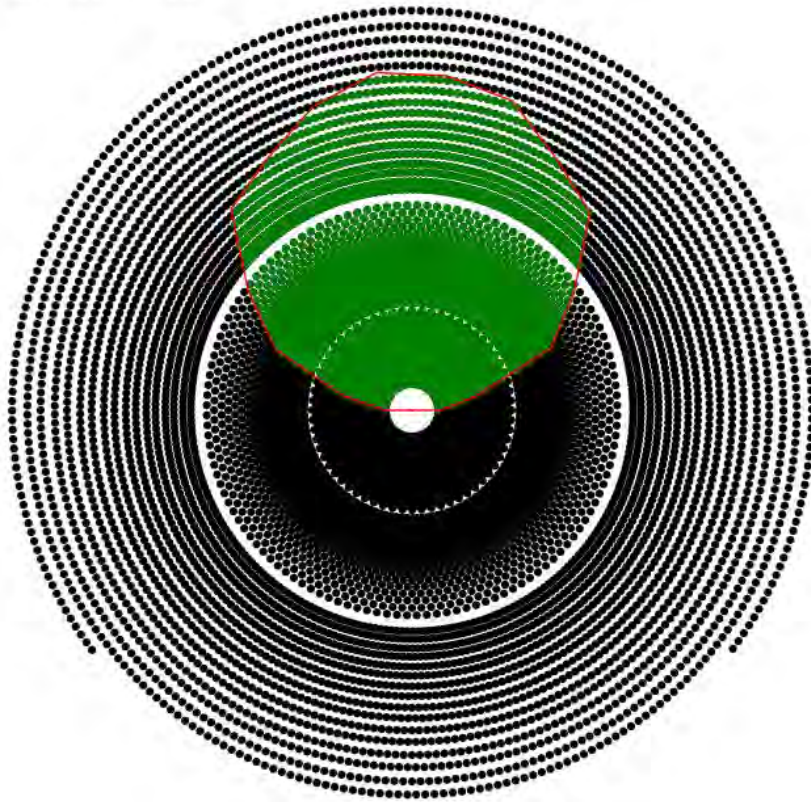


Result discussion

Dunhuang: selected fields

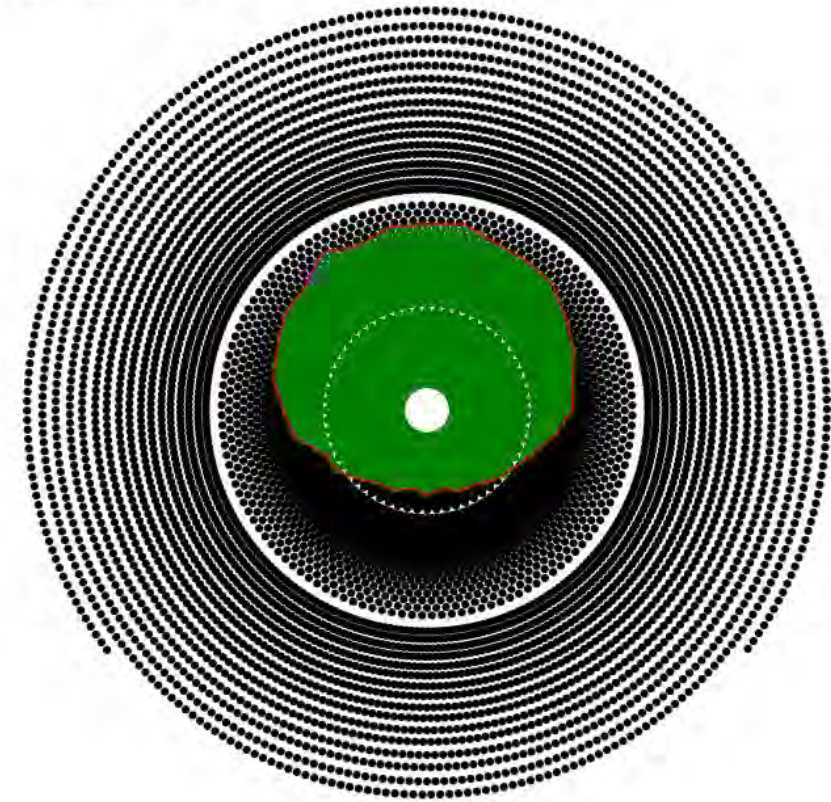
Cavity

Generation 500



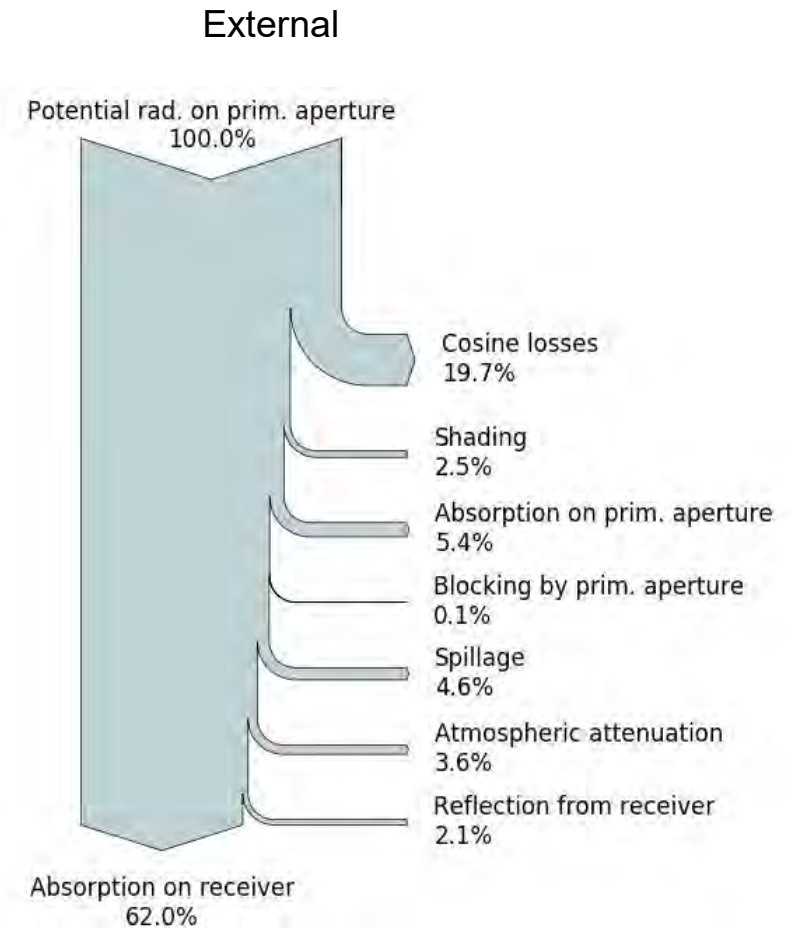
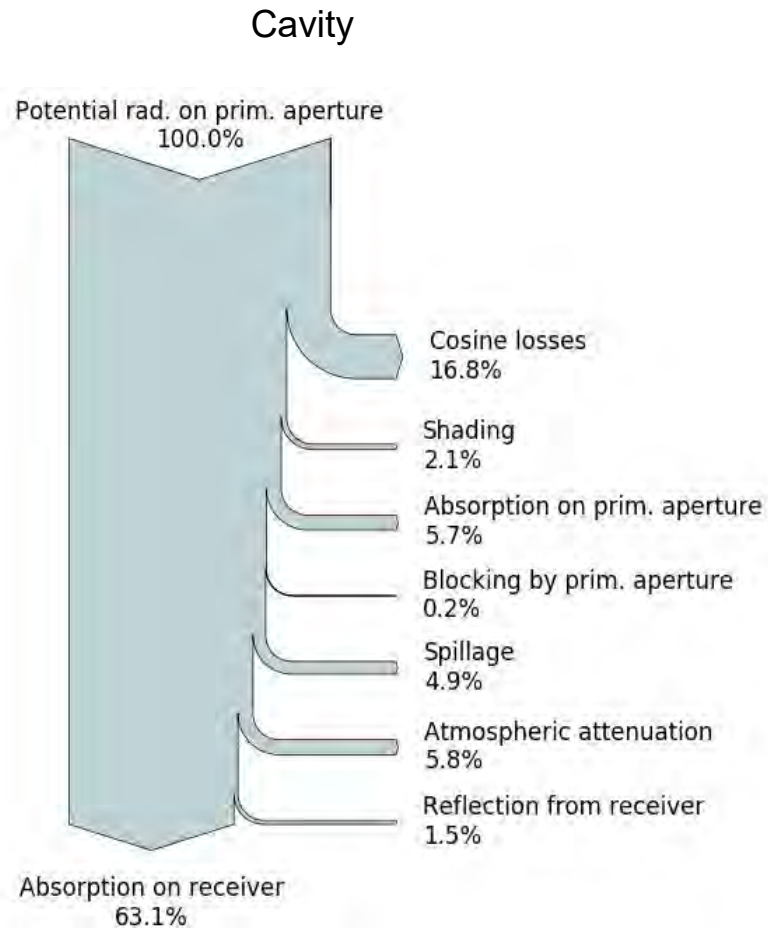
External

Generation 500



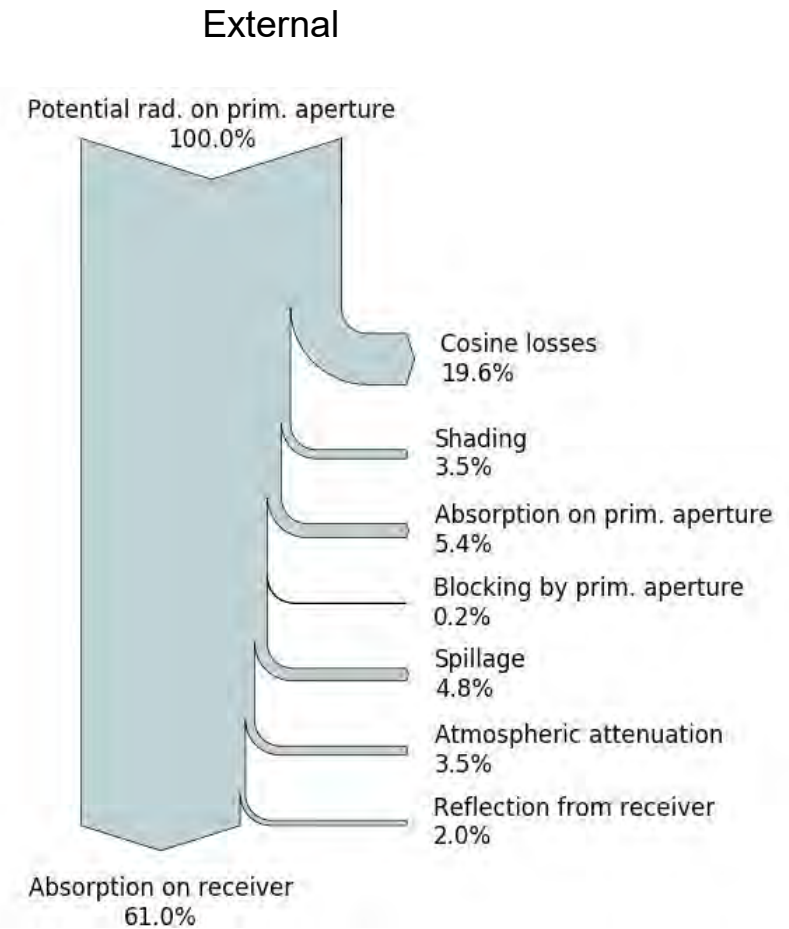
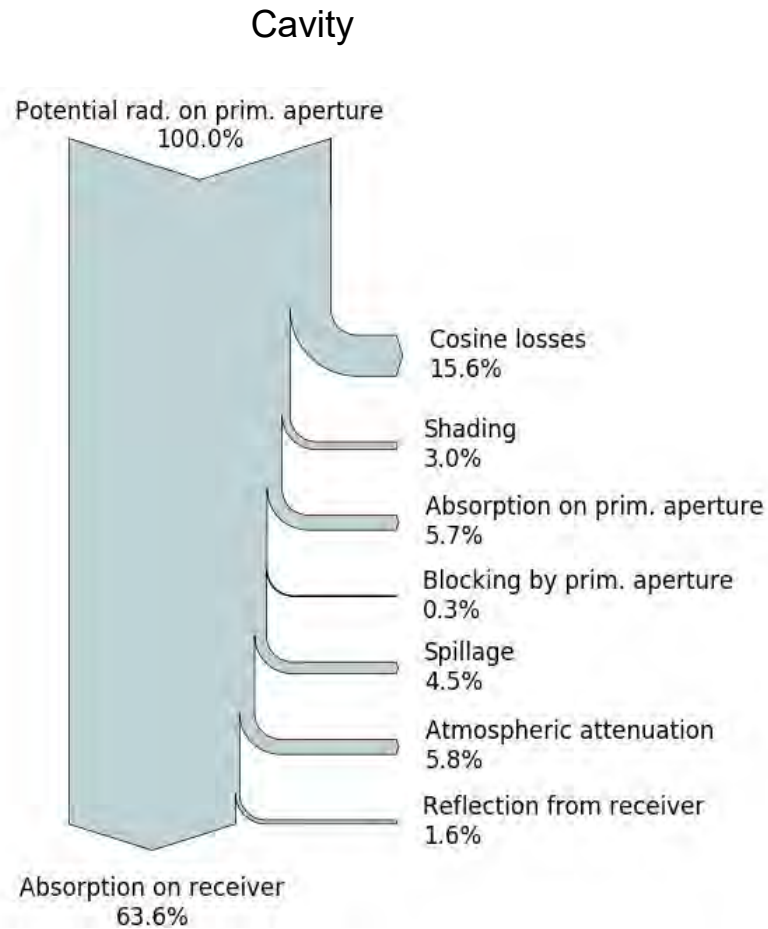
Result discussion

Dubai: optical losses



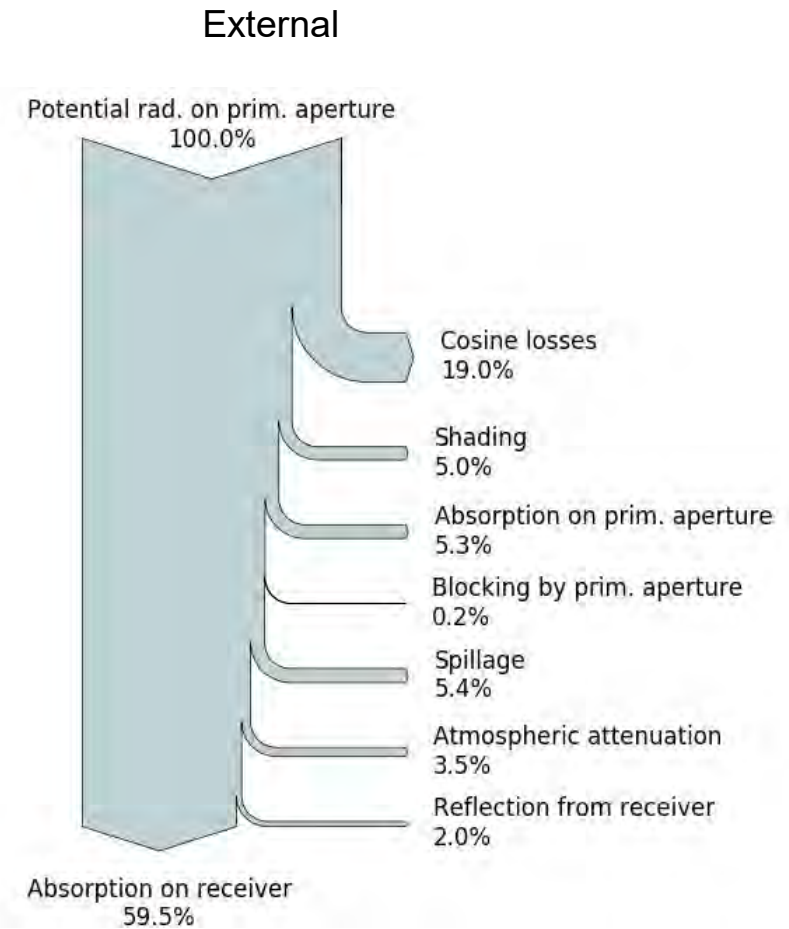
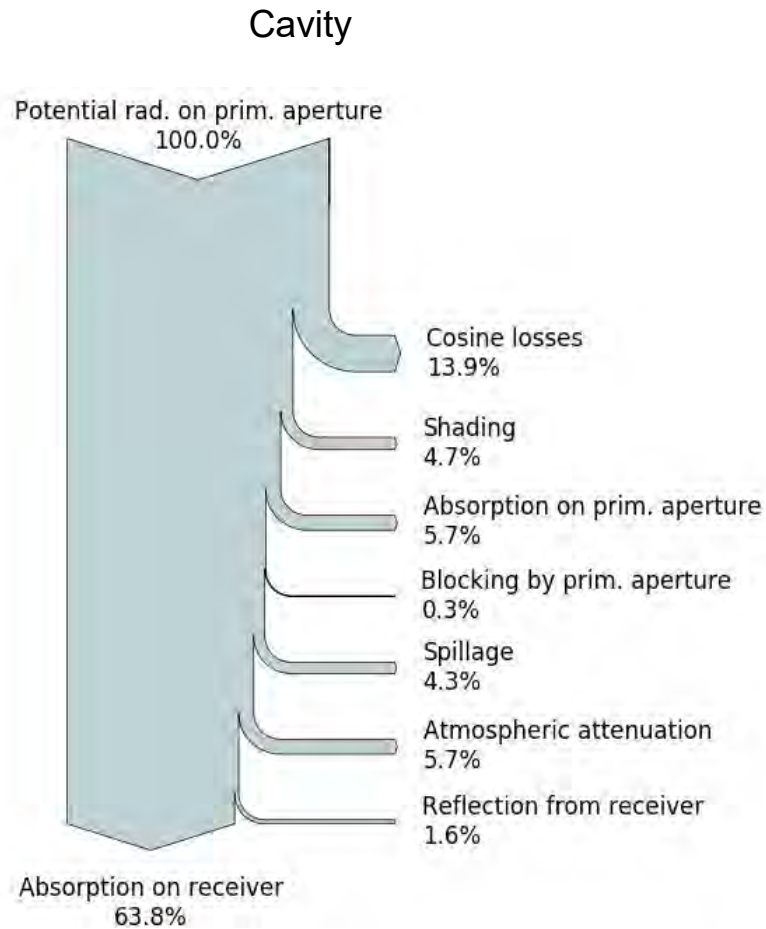
Result discussion

Ouarzazate: optical losses



Result discussion

Dunhuang: optical losses

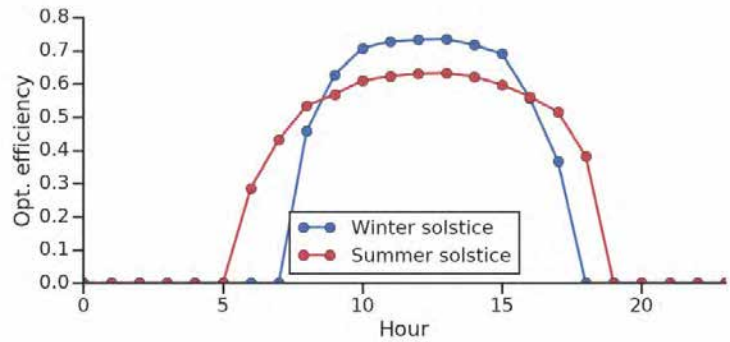


Result discussion

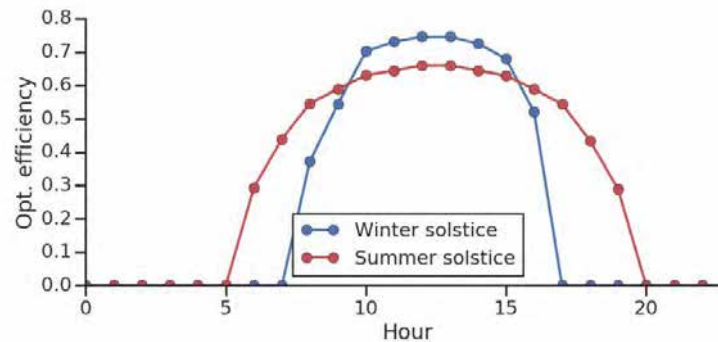
Summer/winter solstice

Cavity

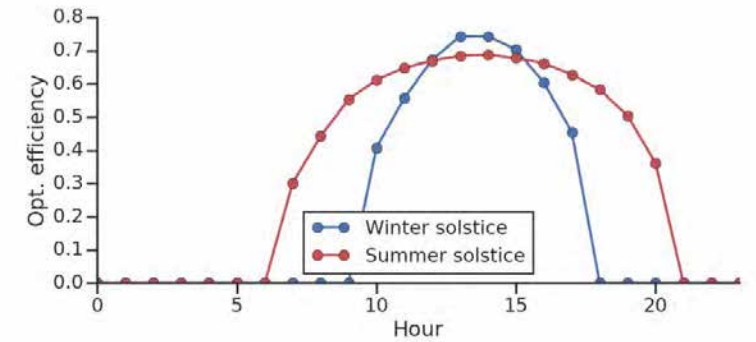
Dubai



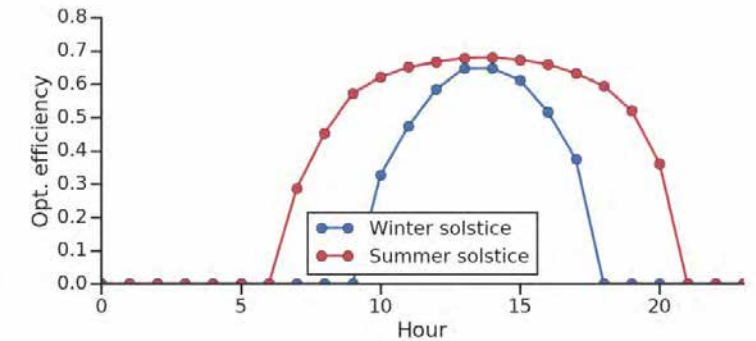
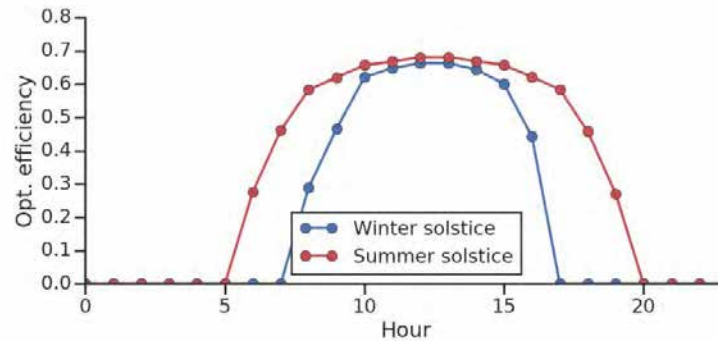
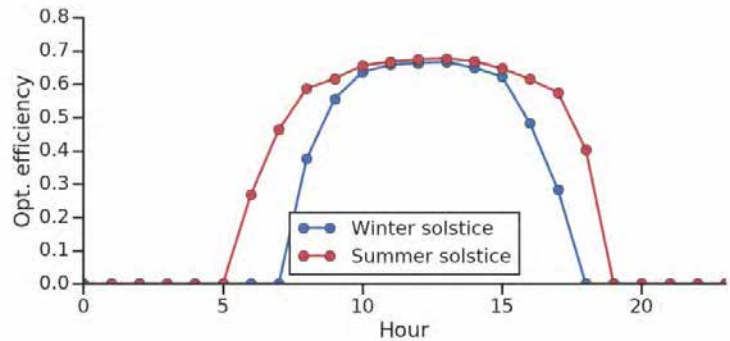
Ouarzazate



Dunhuang

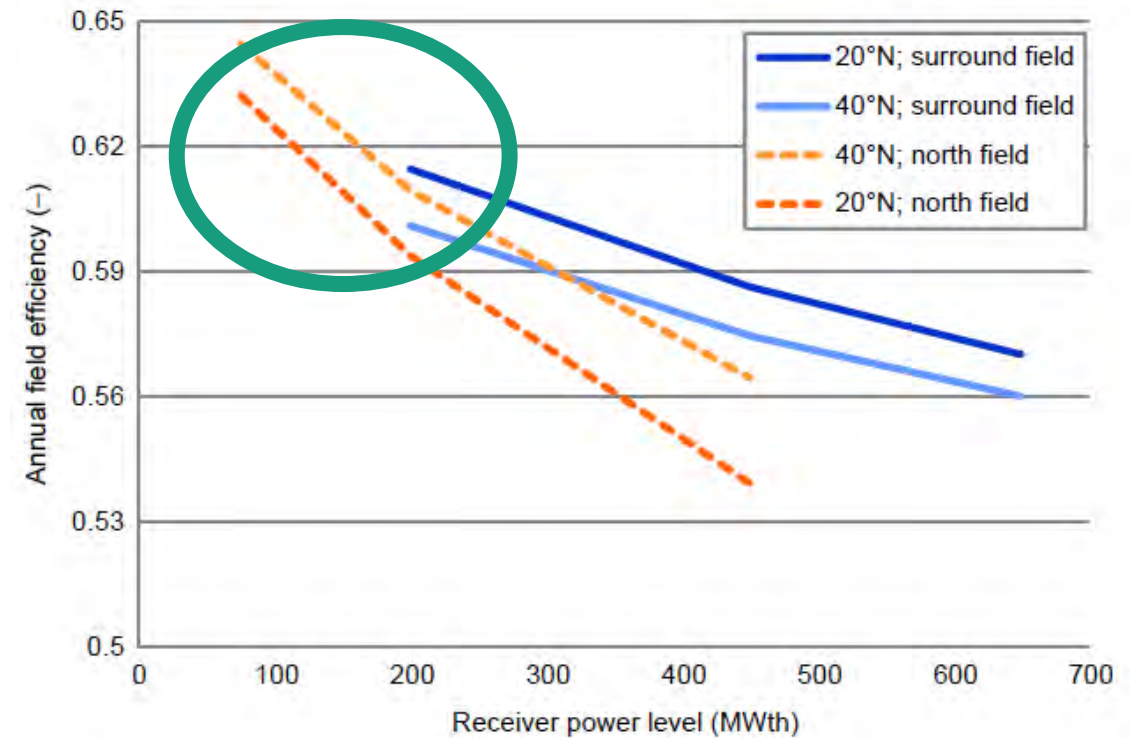
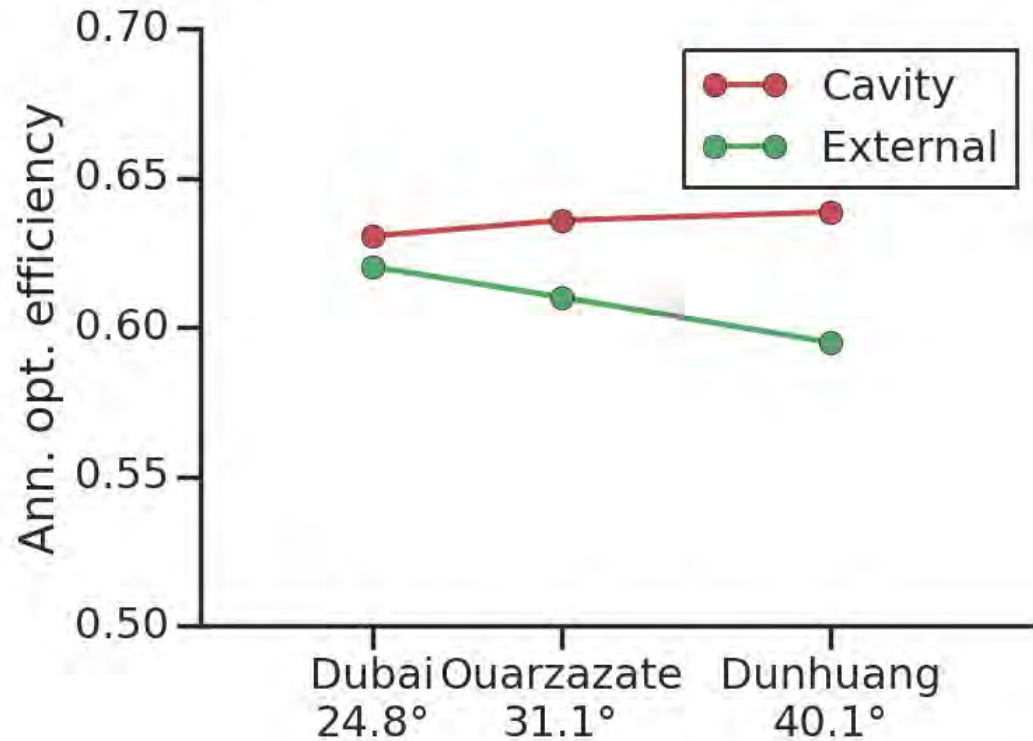


External



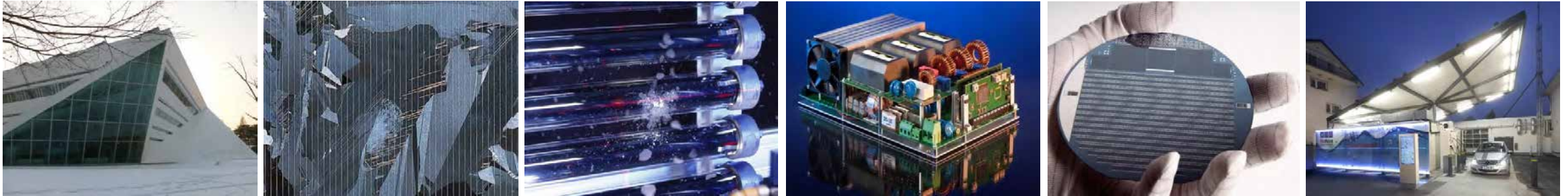
Result discussion

Annual optical efficiency



Source: R. Buck and P. Schwarzbözl, "4.17 Solar Tower Systems," in *Comprehensive Energy Systems*: Elsevier, 2018, pp. 692–732.

Thank you for your Attention!



Fraunhofer Institute for Solar Energy Systems ISE

Shahab Rohani, Peter Schöttl

www.ise.fraunhofer.de

shahab.rohani@ise.fraunhofer.de

peter.schoettl@ise.fraunhofer.de

SFERA-III

Solar Facilities for the European Research Area

1st Summer School “Thermal energy storage systems, solar fields and new cycles for future CSP plants”
WPI Capacity building and training activities
Odeillo, France, September 9th-11th 2019



“Power Cycles for CSP/STE Plants”

Eduardo Zarza, CIEMAT-PSA (Spain)

NETWORKING



THIS PROJECT HAS RECEIVED FUNDING FROM THE EUROPEAN UNION'S HORIZON 2020 RESEARCH AND INNOVATION PROGRAMME UNDER GRANT AGREEMENT NO **823802**



SFERA-III
1st Summer School
September, 9th- 10th, 2019
CNRS- PROMES, Odeillo, France

Power Cycles for CSP/STE Plants

Dr. Eduardo Zarza Moya
Plataforma Solar de Almería (PSA)
R+D Unit for Concentrating Solar Thermal Systems
E-mail: eduardo.zarza@psa.es

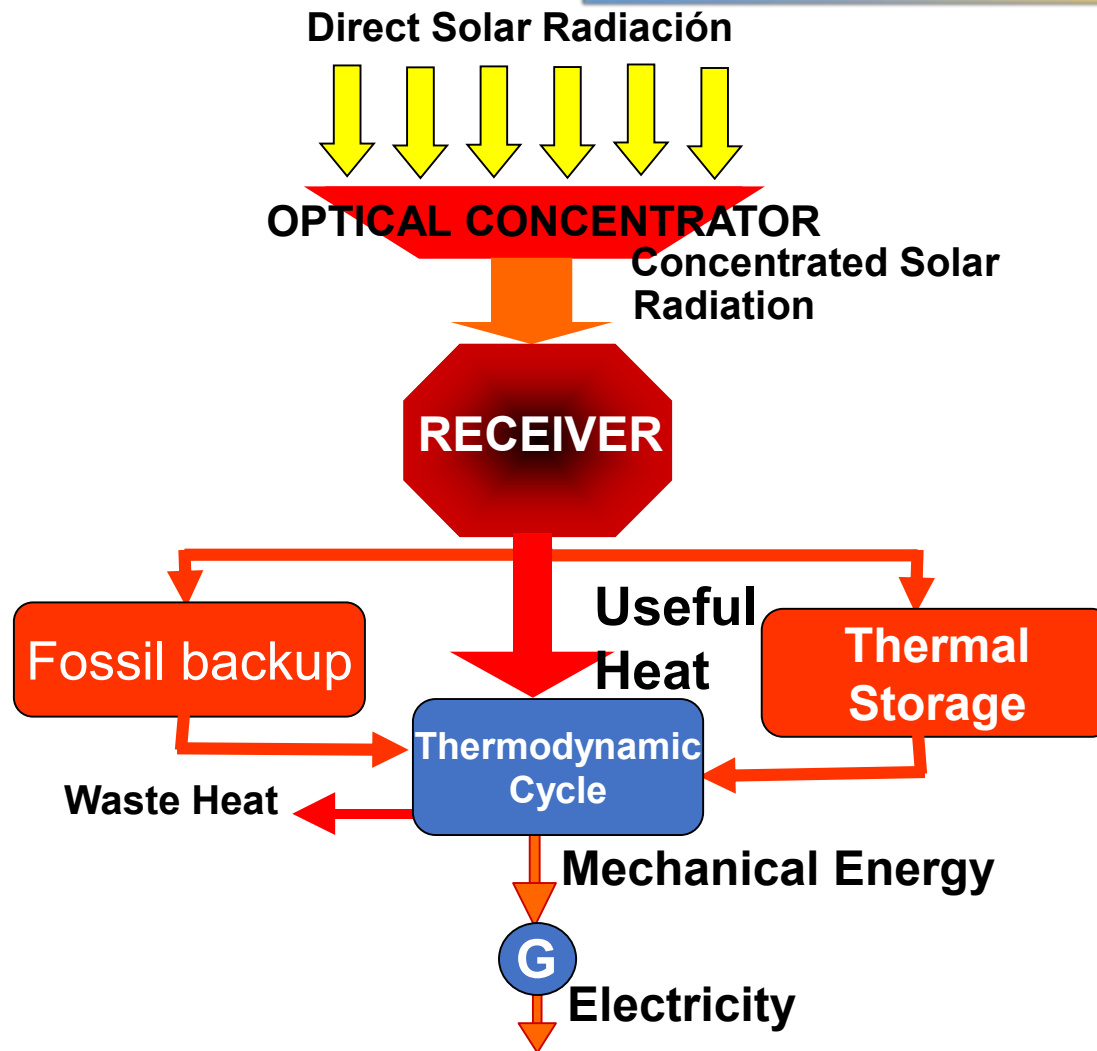


Power Cycles for STE Plants

Content

- ✦ Introduction to Thermodynamic Cycles
- ✦ Power Cycles used in STE Plants
 - Rankine Cycle
 - Organic Rankine Cycle
 - Brayton Cycle
 - Combined Cycle
 - Supercritical Cycles
 - Stirling Cycle

Schematic diagram of a Solar Thermal Electricity Plant



(Ref. M. Romero, 2009)

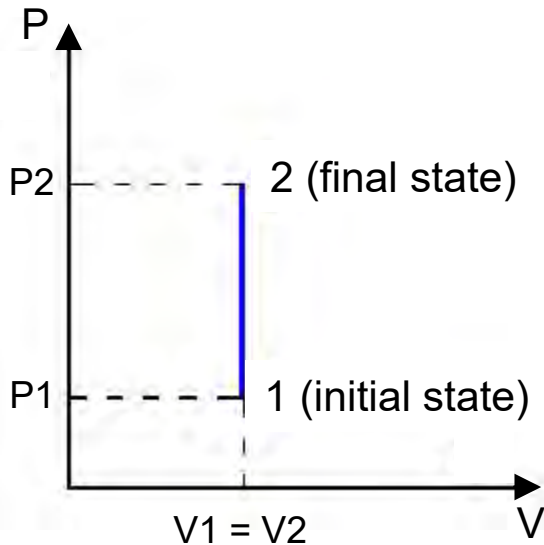
Basic Terms: Thermodynamic Processes

- **Thermodynamic Process:** is any process in which a system changes its thermodynamic properties (e.g., temperature, pressure, mass and volume, mainly). The properties at the beginning of the process are the “*Initial Parameters*” and those at the end of the process are the “*Final Parameters*”
- **Types of Thermodynamic Processes:** depending on the properties changing along the process and the way they change, there are different processes:
 - + Adiabatic process: the process takes place without heat or mass transfer
 - + Isothermal process: the temperature of the system remains constant, $\Delta T=0$
 - + Isochoric process: the volume of the system remains constant, $\Delta V=0$
 - + Isobaric process: the system pressure remains constant, $\Delta P=0$
 - + Reversible process: the system is continuously in equilibrium with its surrounding all along the process and both the system and its surrounding can be restored to their initial states. It is an ideal process that never occurs in the nature
 - + Isentropic process: is a reversible and adiabatic process (it is therefore an ideal process). The entropy remains constant, $\Delta S=0$

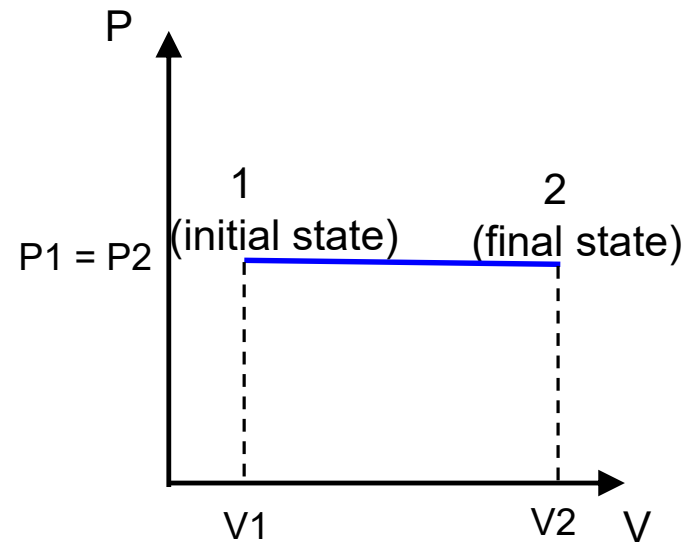
Basic Terms: Thermodynamic Processes

Graphical representation of Thermodynamic Processes (I)

Thermodynamic processes are represented using a Cartesian coordinate system. The parameters assigned to the axis are selected according to the process:



Isochoric process



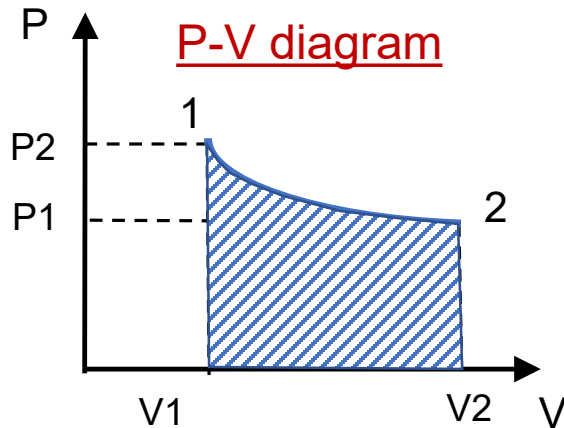
Isobaric process

Basic Terms: Thermodynamic Processes

Graphical representation of Thermodynamic Processes

Thermodynamic processes are represented using a Cartesian coordinate system. The more usual graphical representations are:

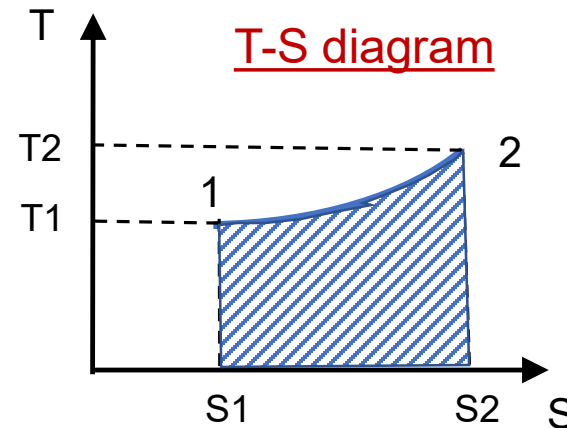
a) Pressure-Volume (P-V)



It is very useful to visualize the amount of work exchanged with the surrounding, W :

$$W = \int_1^2 P \cdot dV$$

b) Temperature-Entropy (T-S)

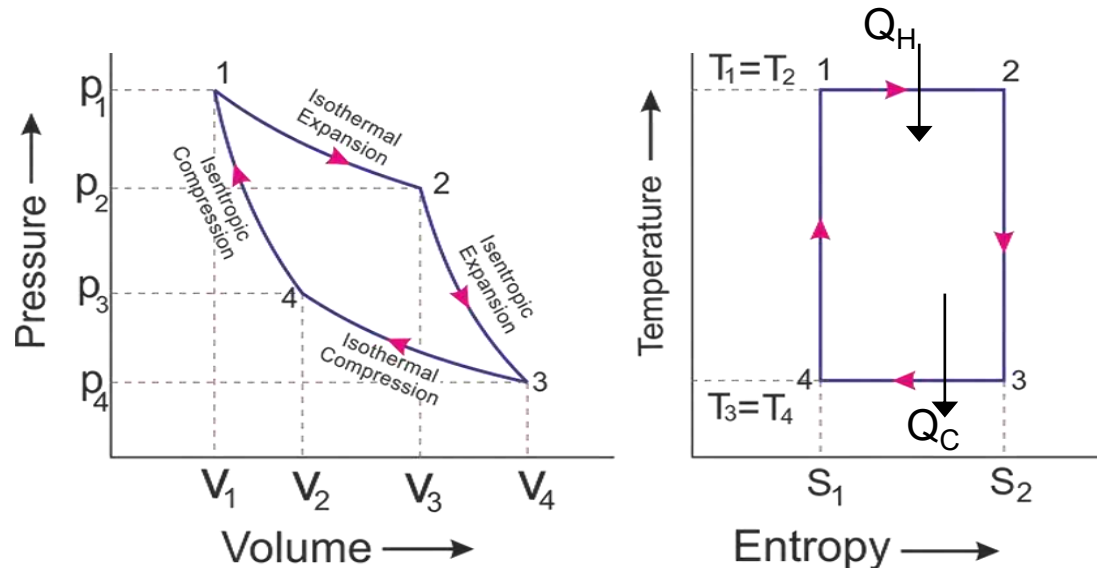


It is very useful to visualize the amount of heat exchanged with the surrounding, Q :

$$Q = \int_1^2 T \cdot dS$$

Basic Terms: Thermodynamic Cycle

- A **thermodynamic Cycle** is composed of a series of thermodynamic processes performed in a way that the system is returned to its initial state (i.e., the initial and final parameters are the same). The graphical representation in a Cartesian coordinate system is a closed shape



Graphical representation
of a thermodynamic cycle
(Carnot cycle)

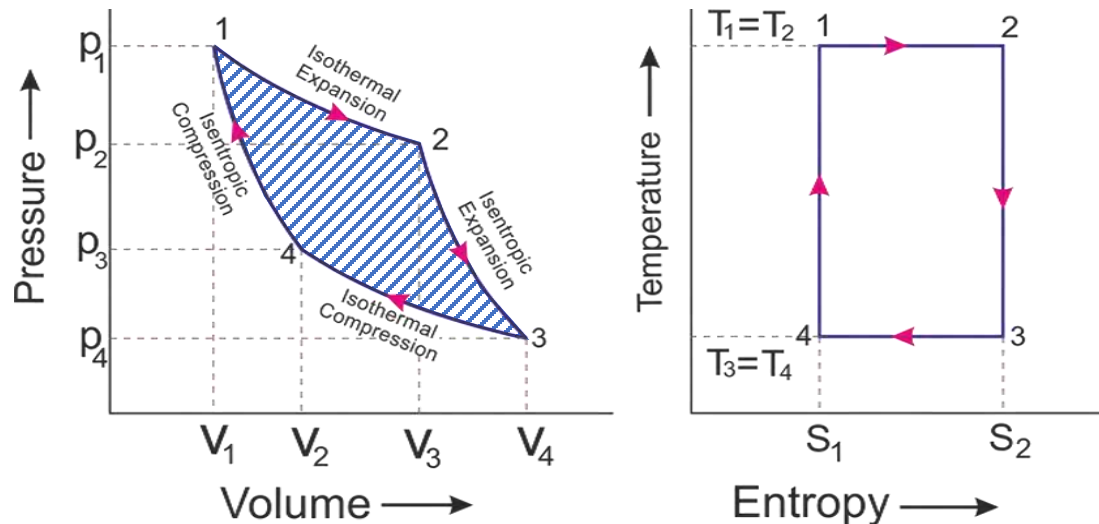
- During a thermodynamic cycle **the system can exchange heat and/or mechanical energy (work)** with its surrounding

Basic Principles of Thermodynamic Cycles

Some Basic Principles

- In those cycles used to convert thermal energy into mechanical energy (work) **the amount of work produced is proportional to the area enclosed** by the geometrical shape of the cycle in the P-V diagram.

Taking the Carnot cycle as a reference, it means that the higher the temperature difference $T_1 - T_4$, the more mechanical work will be produced.



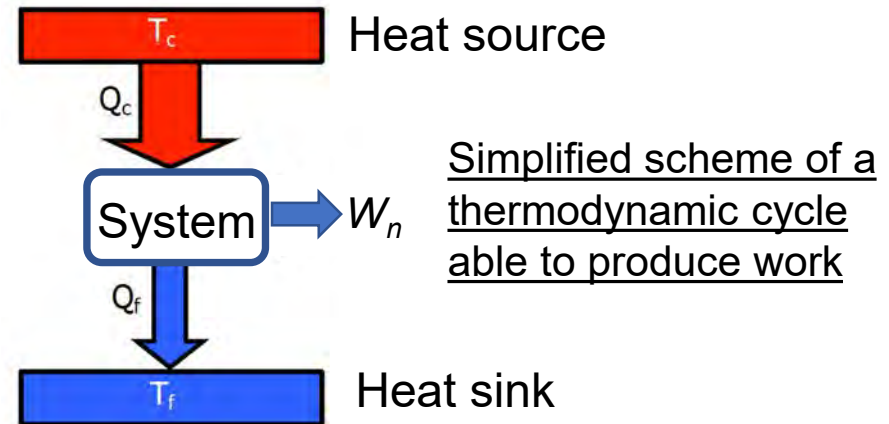
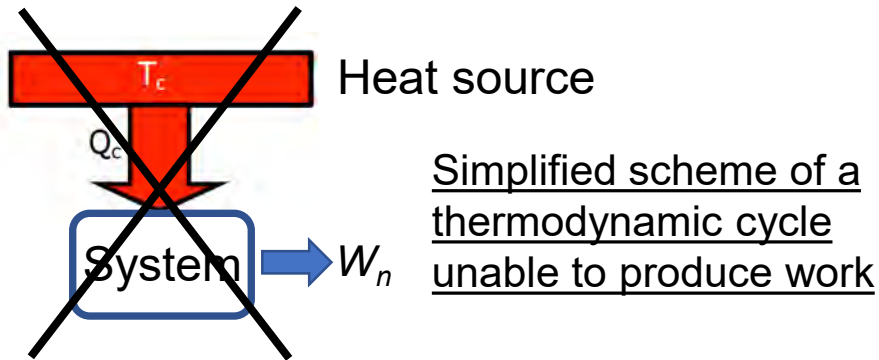
Basic Principles of Thermodynamic Cycles

Some Basic Principles

- In those cycles used to convert thermal energy into mechanical energy (work) **the amount of work produced is proportional to the area enclosed** by the geometrical shape of the cycle in the P-V diagram.

Taking the Carnot cycle as a reference, it means that the higher the temperature difference $T_1 - T_4$, the more mechanical work will be produced.

- Kelvin principle:** It is impossible to produce work with a thermodynamic system in contact with only one heat source/sink



Basic Principles of Thermodynamic Cycles

Some Basic Principles

- In those cycles used to convert thermal energy into mechanical energy (work) **the amount of work produced is proportional to the area enclosed** by the geometrical shape of the cycle in the P-V diagram.

Taking the Carnot cycle as a reference, it means that the higher the temperature difference $T_1 - T_4$, the more mechanical work will be produced.

- **Kelvin principle:** It is impossible to produce work with a thermodynamic system in contact with only one heat source/sink
- Due to the **First Law of Thermodynamic** the amount of energy (mechanical energy + thermal energy) delivered by the system to its surrounding is equal to the amount of energy (mechanical + thermal) received from its surrounding

$$\sum Q_i + \sum W_i = 0$$

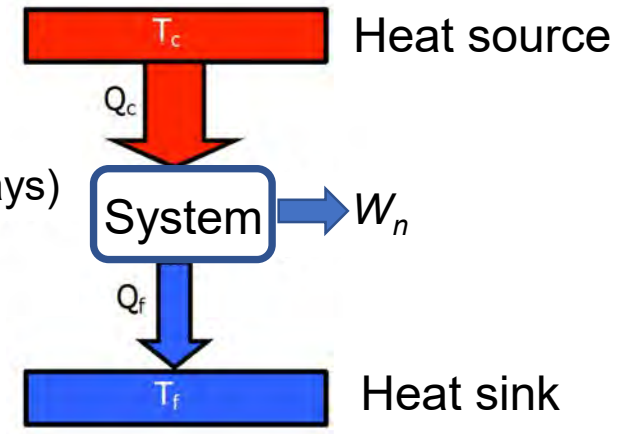
- **Hierarchy principle:** The fraction of thermal energy that can be transformed into work (mechanical energy) increases with the temperature difference between the hot source and the cold sink ($T_1 - T_4$ in the Carnot Cycle)

Thermodynamic Power Cycles

- A Power Cycle is a **thermodynamic cycle aimed at transforming thermal energy into mechanical energy, which is then converted into electricity** with an electricity generator
- According to Kelvin principle, **a heat source and a heat sink are needed**
- **The efficiency, η , of a Power Cycle** is the quotient between the net mechanical energy produced, W_n , and the thermal energy consumed, Q_c

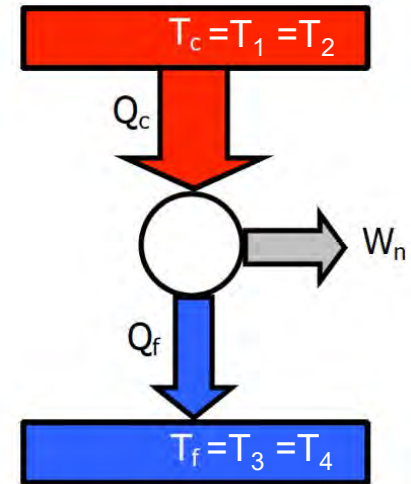
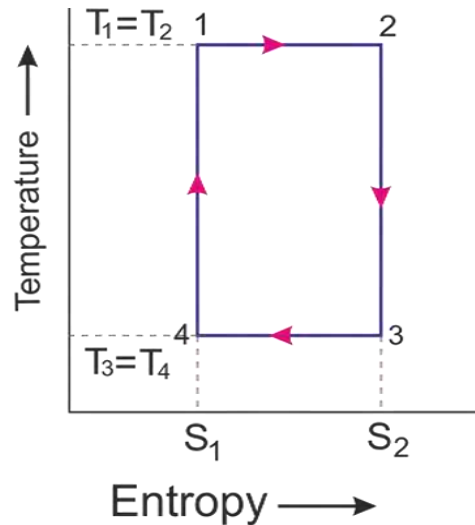
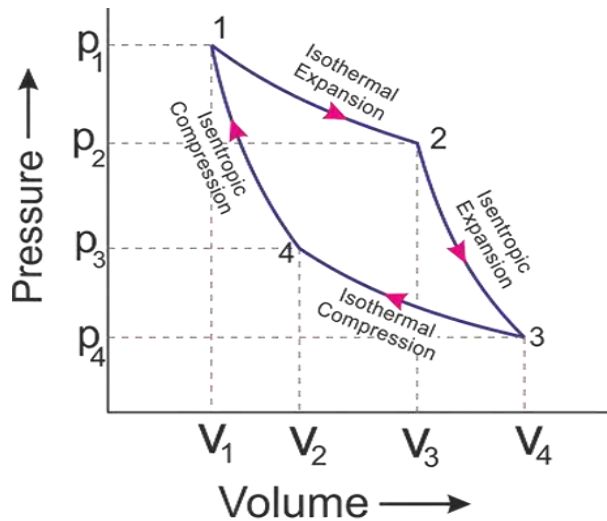
$$\eta = \frac{W_n}{Q_c} = \frac{Q_c - Q_f}{Q_c} = 1 - \frac{Q_f}{Q_c} < 1 \text{ (always)}$$

1st Law of Thermodynamic



The Ideal Power Cycle: the Carnot Cycle

The Carnot cycle is an ideal thermodynamic cycle composed of four reversible processes (1 isothermal expansion + 1 isentropic expansion + 1 isothermal compression and 1 isentropic compression), taking heat from a heat source, delivering heat to a heat sink at lower temperature and producing mechanical work



Since the four processes are reversible, this cycle is the cycle with the maximum possible efficiency for a thermodynamic cycle connected to the same heat source and heat sink:

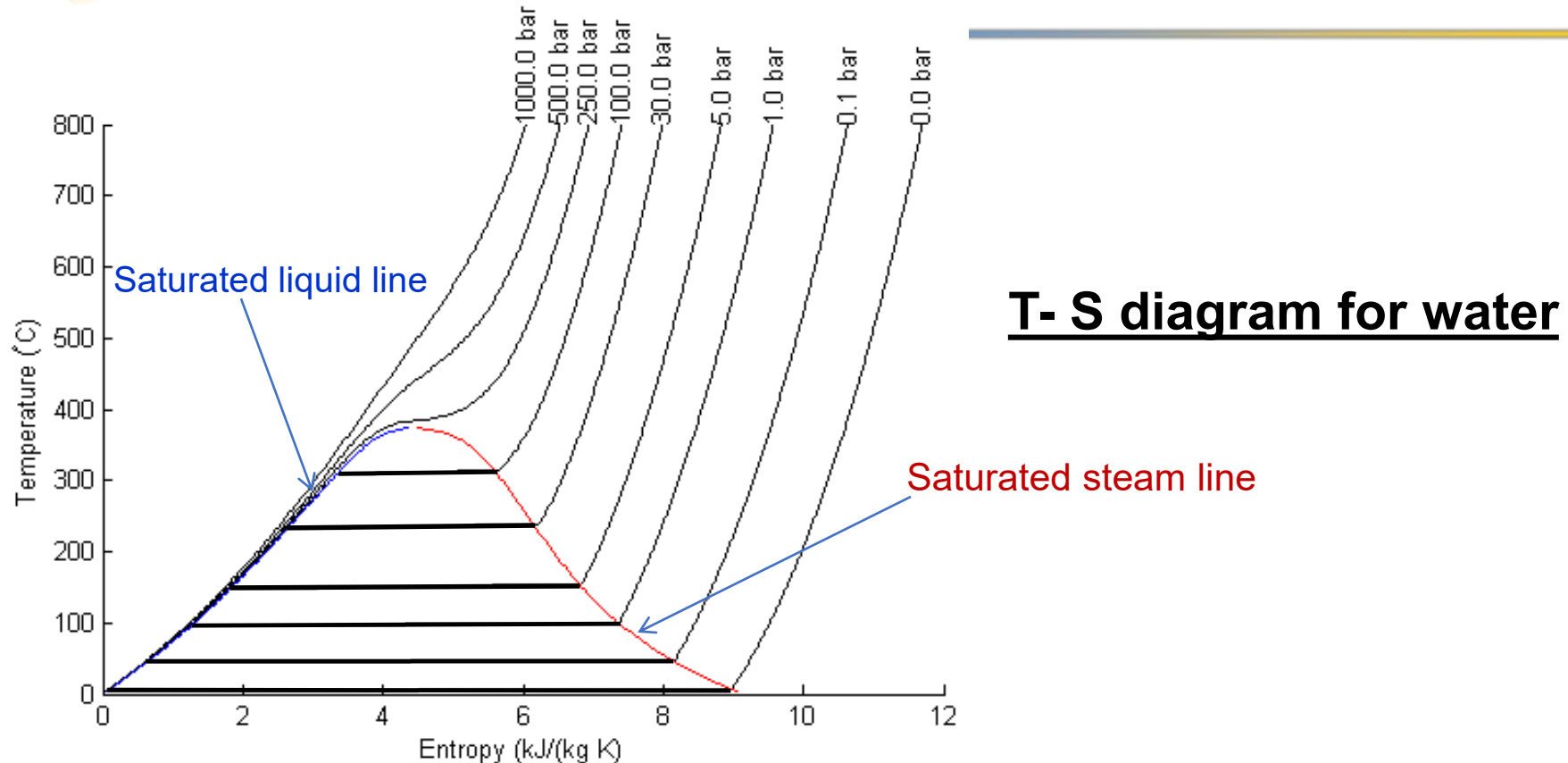
$$\eta_{\text{Carnot}} = \eta_{\text{max.}} = 1 - \frac{T_f}{T_c} < 1$$

Power Cycles for STE Plants

Content

- Introduction to Thermodynamic Cycles
-  Power Cycles used in STE Plants
 -  Rankine Cycle
 - Organic Rankine Cycle
 - Brayton Cycle
 - Combined Cycle
 - Supercritical Cycles
 - Stirling Cycle

“Temperature – Entropy” diagram of Water

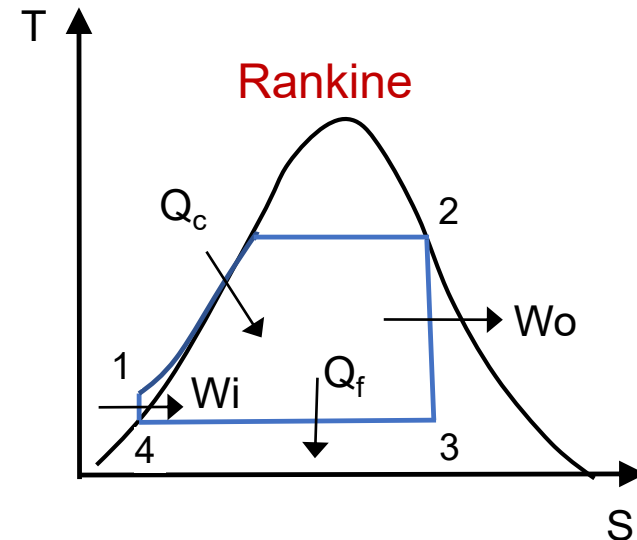
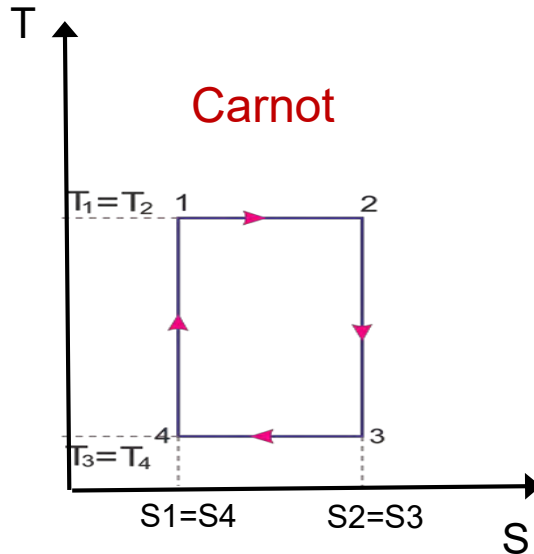


T- S diagram for water

When liquid water is heated at constant pressure, the water increases its temperature until the saturation temperature is reached. At that moment, water starts boiling and passing from liquid to steam phase without increasing its temperature (liquid+steam). When all water is in gas phase it increases its temperature (superheated steam)

Basic Rankine Cycle

The Rankine cycle is an approximation to the ideal Carnot cycle, changing the isothermal processes (1-2 and 3-4) by isobaric processes with water

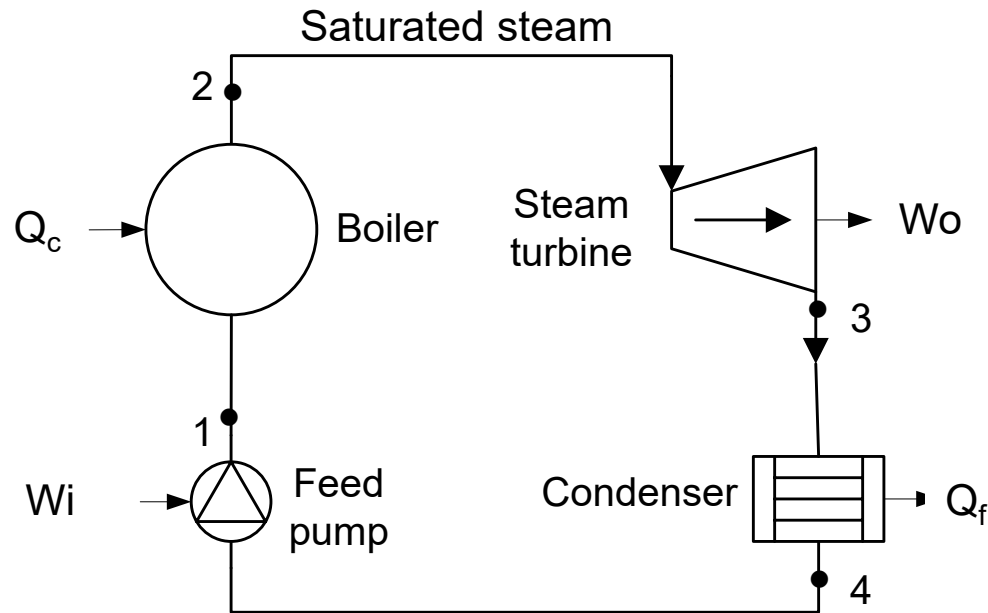
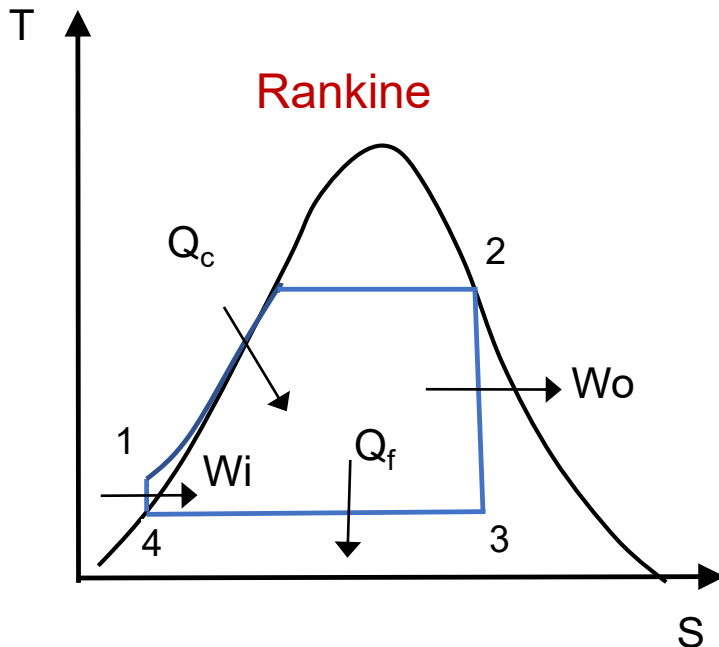


- 1–2: Isobaric evaporation of water (boiler, heat source of the cycle)
- 2–3: Isentropic expansion of the steam (turbine, mechanical work obtained)
- 3–4: Isobaric steam condensation (condenser, heat sink of the cycle)
- 4–1: Isentropic compression of liquid water (boiler feed pump, mechanical work consumed).

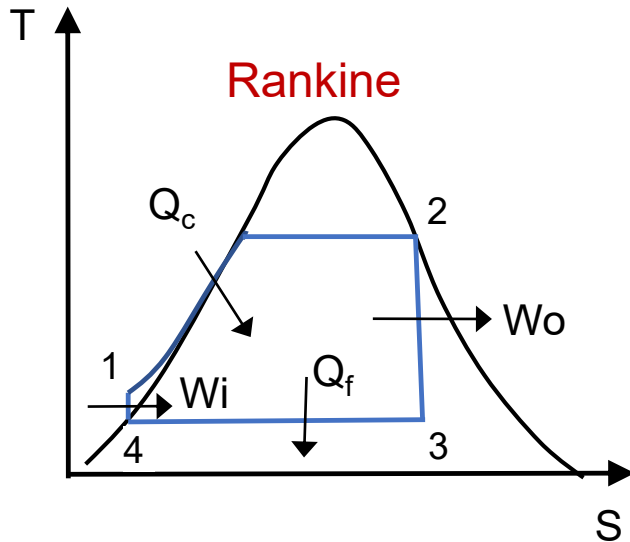
Basic Rankine Cycle

Physical Implementation of a Basic Rankine Cycle

Pressurized liquid water is evaporated in a boiler where thermal energy is given to the cycle (process 1-2). The saturated steam thus produced is expanded in a turbine (process 2-3) and then condensed (process 3-4). Once condensed the liquid water is pressurized and sent to the boiler (process 4-1) to start the cycle again.



Basic Rankine Cycle



Efficiency:

$$\eta = \frac{W_{net}}{\dot{Q}_c} = \frac{\dot{W}_o - \dot{W}_i}{\dot{Q}_c} = \frac{(h_2 - h_3) - (h_1 - h_4)}{h_2 - h_1}$$

Example:

$$P_2 = 100 \text{ bar}, T_2 = 311^\circ\text{C}$$

$$P_3 = 0.05 \text{ bar}$$

$$\text{steam fraction}_3 = 0.65$$

$$\eta \approx 21\%$$

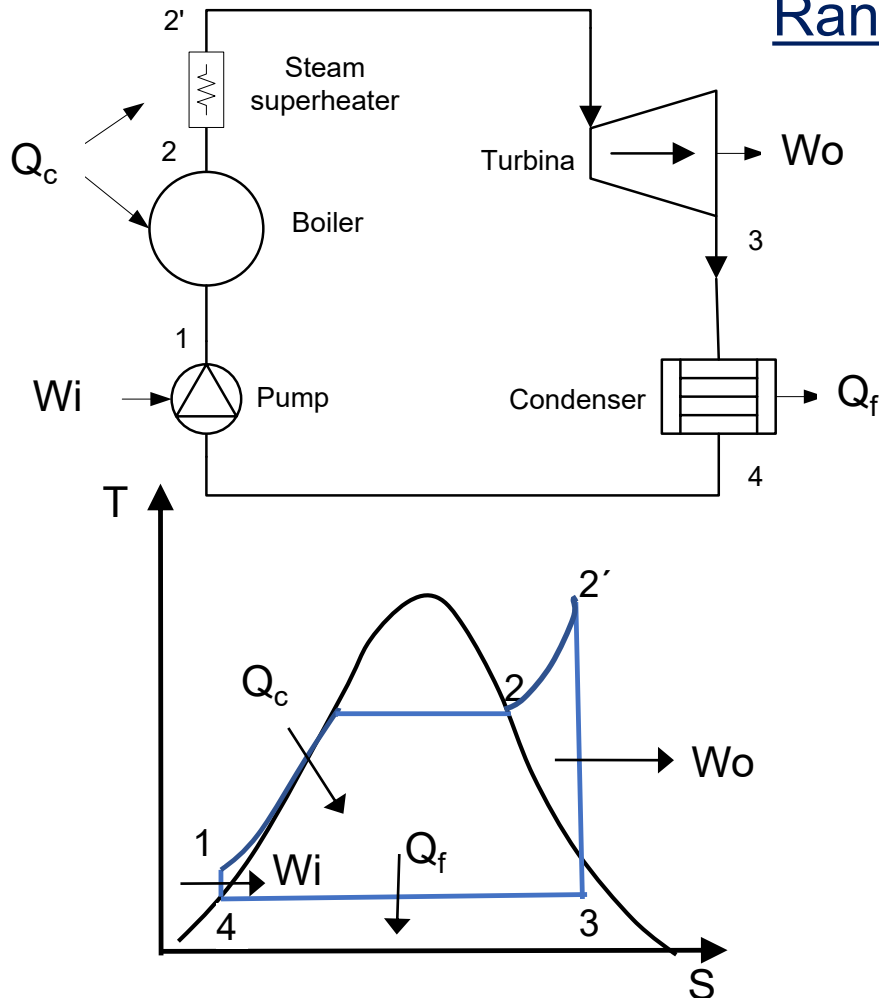
Main problems of the basic Rankine Cycle:

- Low steam fraction → erosion problems in the blades of the turbine
- Moderate efficiency if the maximum pressure is not very high

Improved Rankine Cycles

Rankine cycle with steam superheating

The temperature of the steam is increased before its expansion in the turbine. It has two benefits: a) the efficiency is increased, and b) less erosion in the blades of the turbine due to a higher steam quality at the turbine exit



Efficiency:

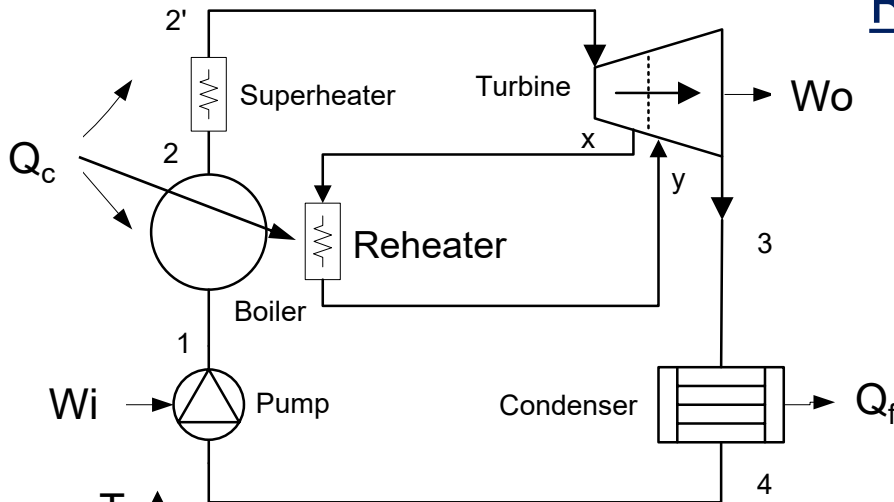
$$\eta = \frac{W_{net}}{\dot{Q}_c} = \frac{\dot{W}_o - \dot{W}_i}{\dot{Q}_c} = \frac{(h_{2'} - h_3) - (h_1 - h_4)}{h_{2'} - h_1}$$

Example:

$$\left. \begin{array}{l} P_2 = 100 \text{ bar}, T_{2'} = 450^\circ\text{C} \\ P_3 = 0.05 \text{ bar} \\ \text{steam fraction}_3 = 0.85 \end{array} \right\} \eta \approx 34\%$$

Improved Rankine Cycles

Rankine cycle with steam reheating



The steam is reheated before it completes its expansion in the turbine. The benefits are: less erosion inside the turbine and higher η

To increase the efficiency: $T_{2'} - T_x < T_x - T_3$

Efficiency:

$$\eta = \frac{W_{net}}{\dot{Q}_c} = \frac{\dot{W}_o - \dot{W}_i}{\dot{Q}_c} = \frac{(h_{2'} - h_x) + (h_y - h_3) - (h_1 - h_4)}{(h_{2'} - h_1) + (h_y - h_x)}$$

Example:

$$P_2 = P_{2'} = 100 \text{ bar}, T_{2'} = 450^\circ\text{C}$$

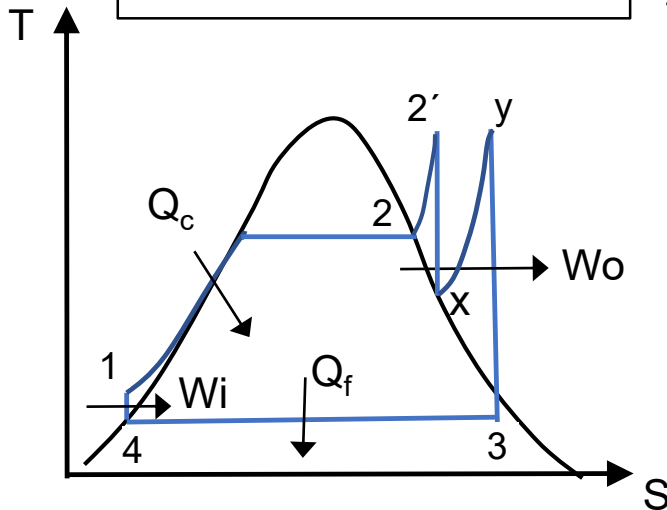
$$P_x = P_y = 10 \text{ bar}, T_y = 250^\circ\text{C}$$

$$P_3 = 0.05 \text{ bar}$$

$$\text{steam fraction}_x = 1.0$$

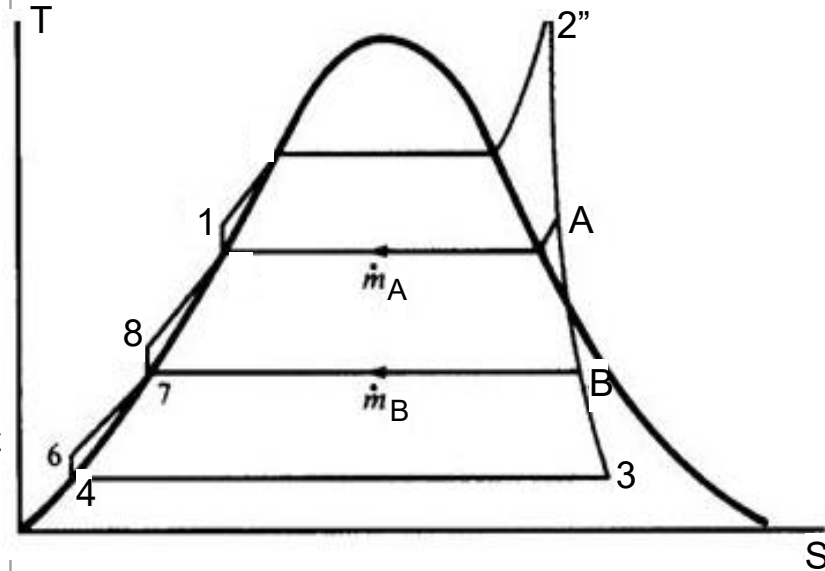
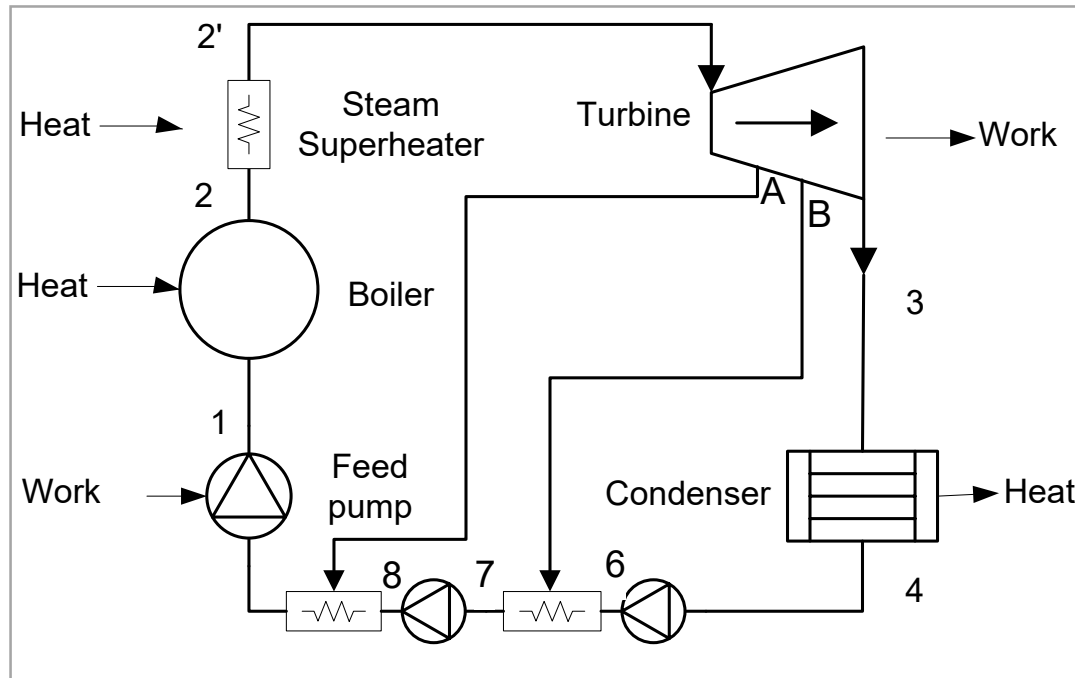
$$\text{steam fraction}_3 = 0.85$$

$$\eta \approx 37\%$$



Improved Rankine Cycles

Regenerative Rankine cycle



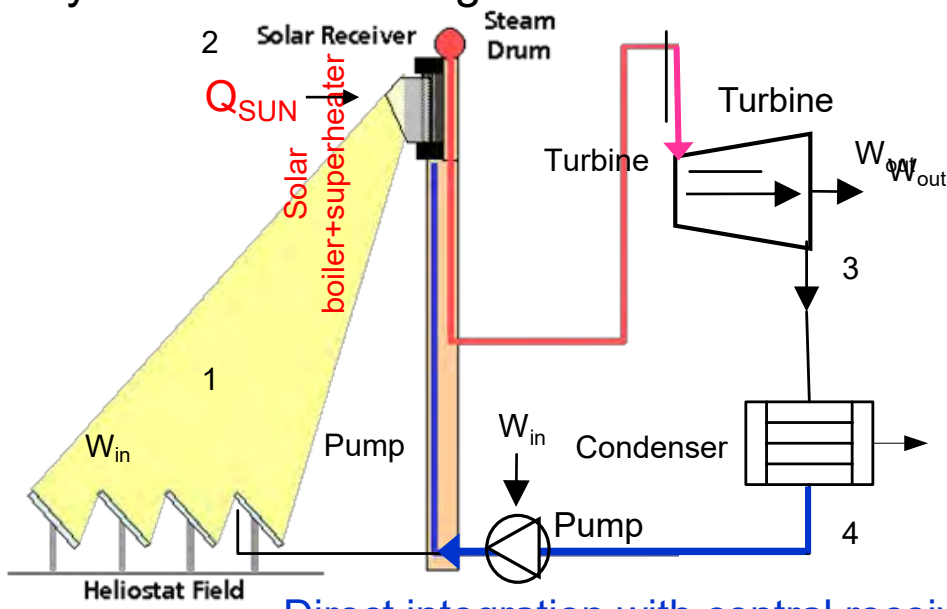
The **cycle efficiency is increased by raising the mean cycle input temperature**. The working fluid in the cycle is heated by steam extractions from the turbine. Although the more steam extractions the higher the efficiency, **there are practical limitations** due to the cost of the regenerators.

Integration of a Rankine Cycle in STE Plants

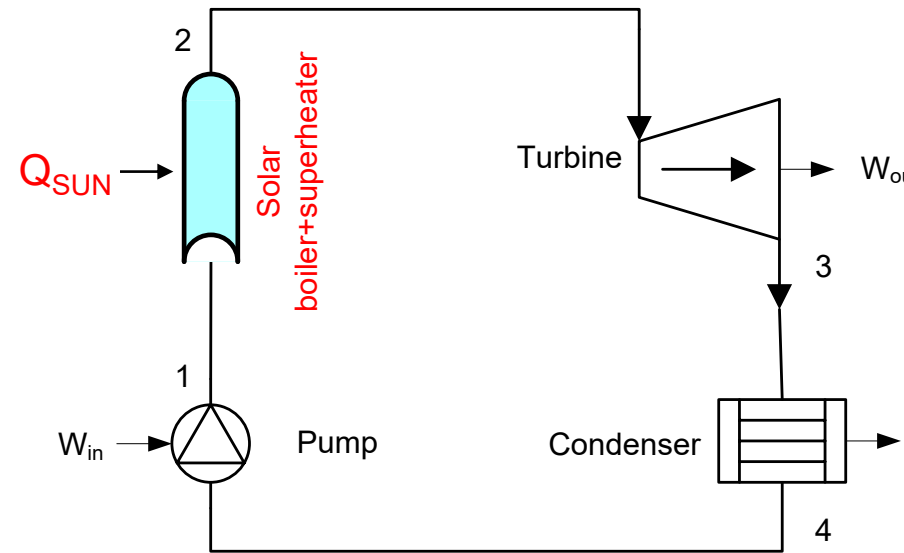
Direct Integration

Liquid water is directly heated and converted into steam by the concentrated solar Radiation in the receiver. This integration is called **Direct steam generation (DSG)**. It can be implemented with either central receivers or parabolic troughs.

The main limitation is the maximum steam temperature/pressure, which are limited by the receiver design and materials due to stress ($P < 150\text{bar}$, $T < 575^\circ\text{C}$)



Direct integration with central receiver
Direct integration in Rankine cycle

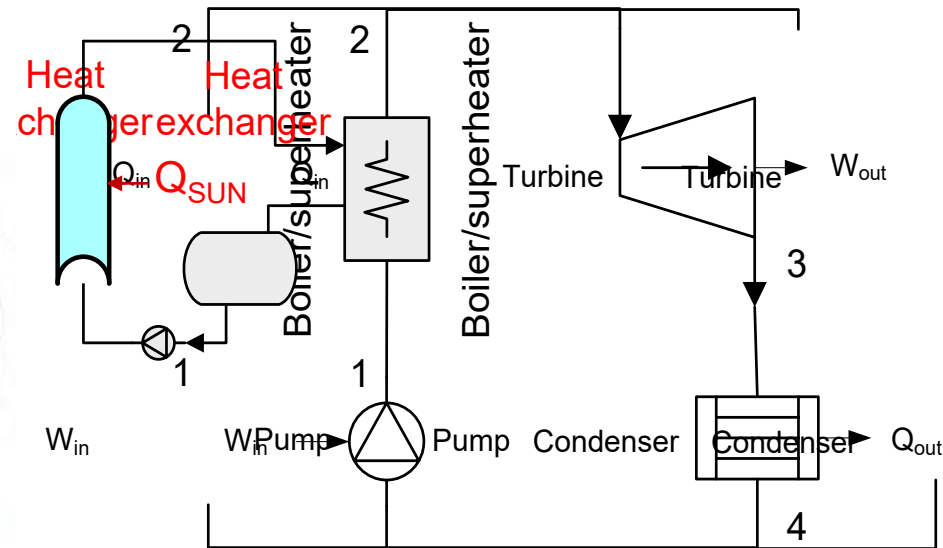
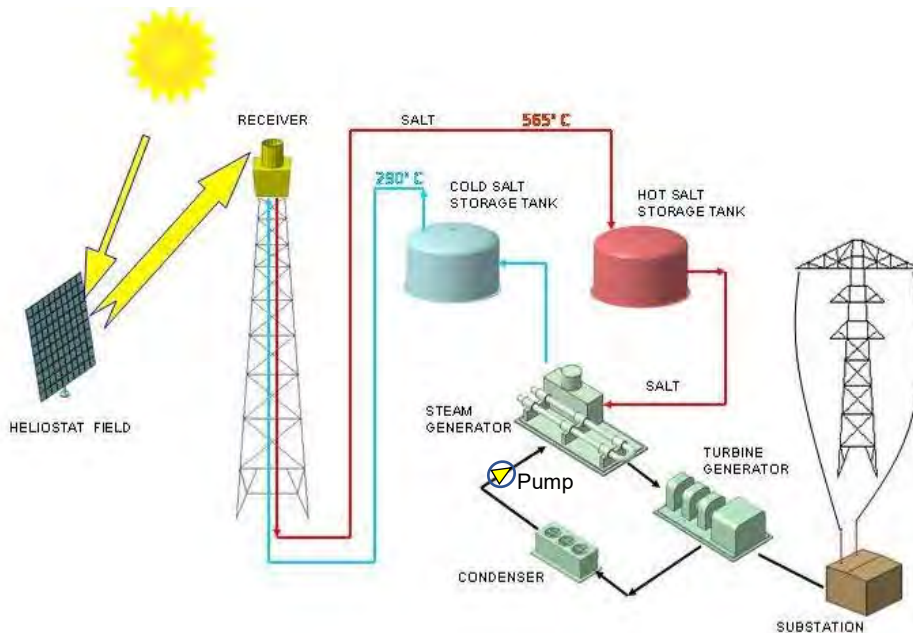


Direct integration with parabolic troughs
Direct integration in Rankine cycle

Integration of a Rankine Cycle in STE Plants

Indirect Integration

A Heat Transfer Fluid (HTF) is heated by the solar field and the steam is produced in a heat exchanger with the thermal energy delivered by the HTF. This integration can be implemented with either central receivers or parabolic troughs. The main limitation is the maximum HTF temperature: 400°C (Oil), 565°C (Molten salts)

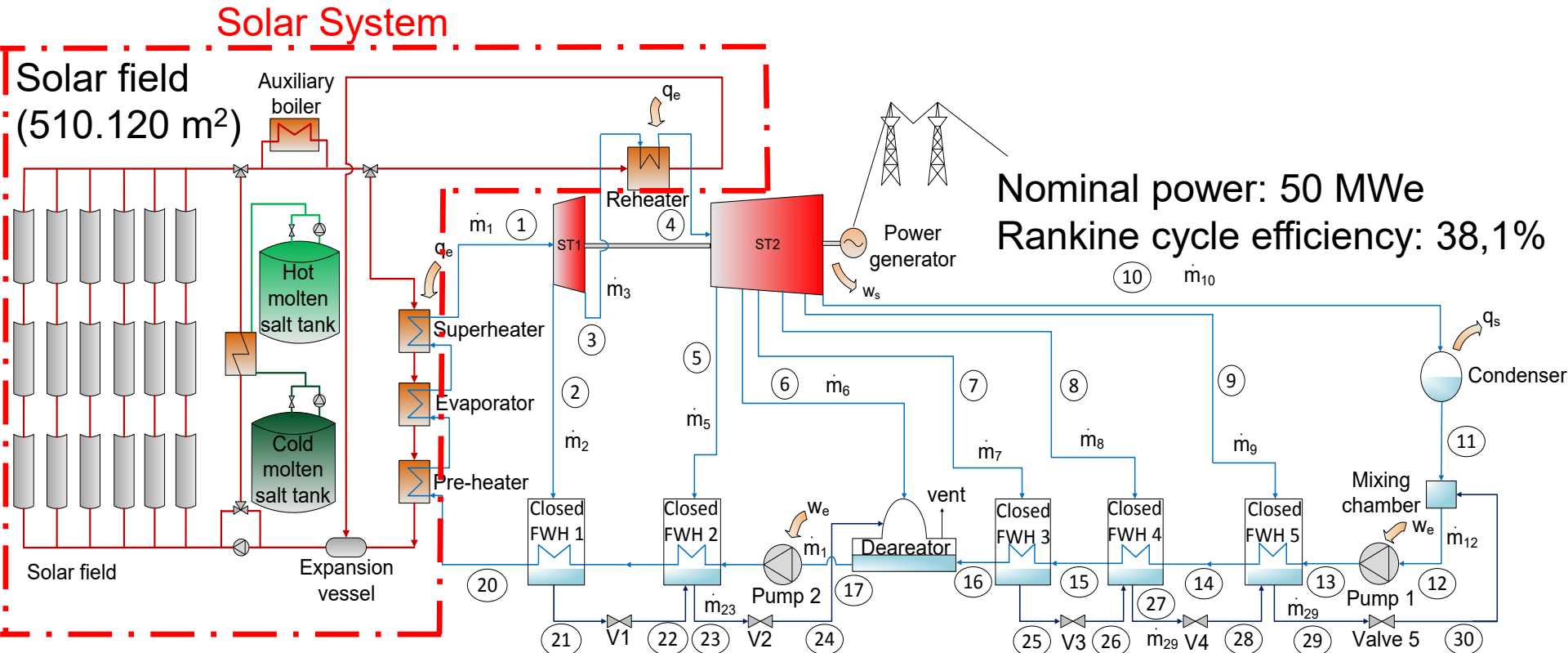


Unfired boiler configuration (indirect)

Typical Rankine Cycle used in STE Plants

Simplified scheme of a 50 MWe STE plant

Regenerative (6 steam extractions) Rankine cycle with steam reheating and superheated steam

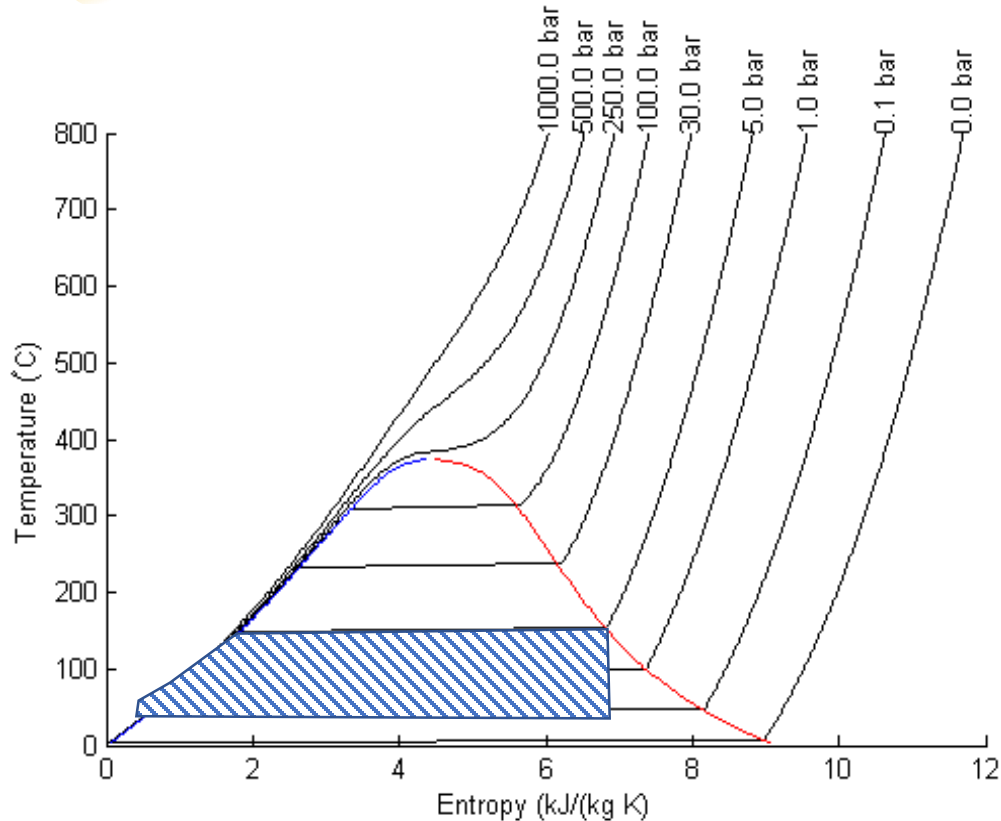


Power Cycles for STE Plants

Content

- Introduction to Thermodynamic Cycles
-  Power Cycles used in STE Plants
 - Rankine Cycle
 -  Organic Rankine Cycle
 - Brayton Cycle
 - Combined Cycle
 - Supercritical Cycles
 - Stirling Cycle

Organic Rankine Cycle (ORC)



When the temperature of the heat source available is low ($T < 150^{\circ}\text{C}$) the use of water for a Rankine cycle is not good because of two main problems:

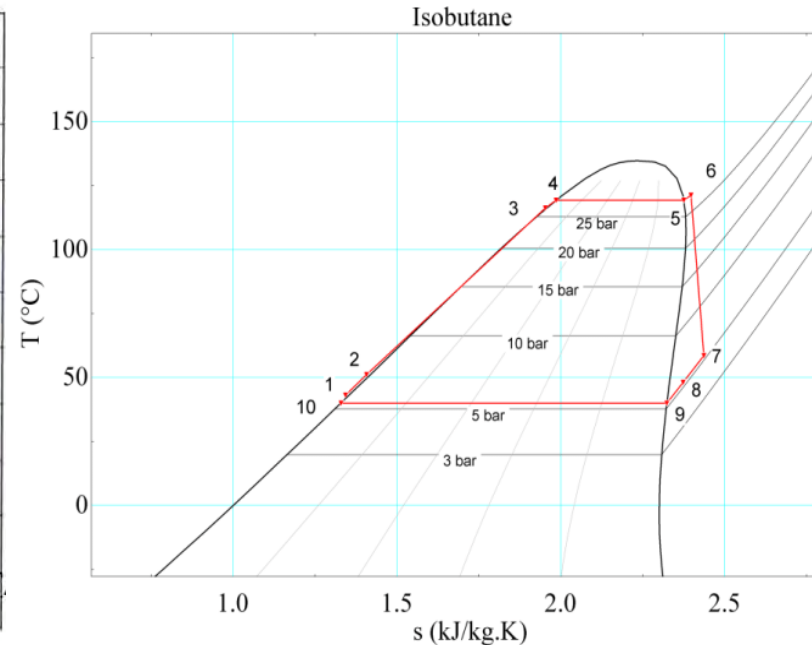
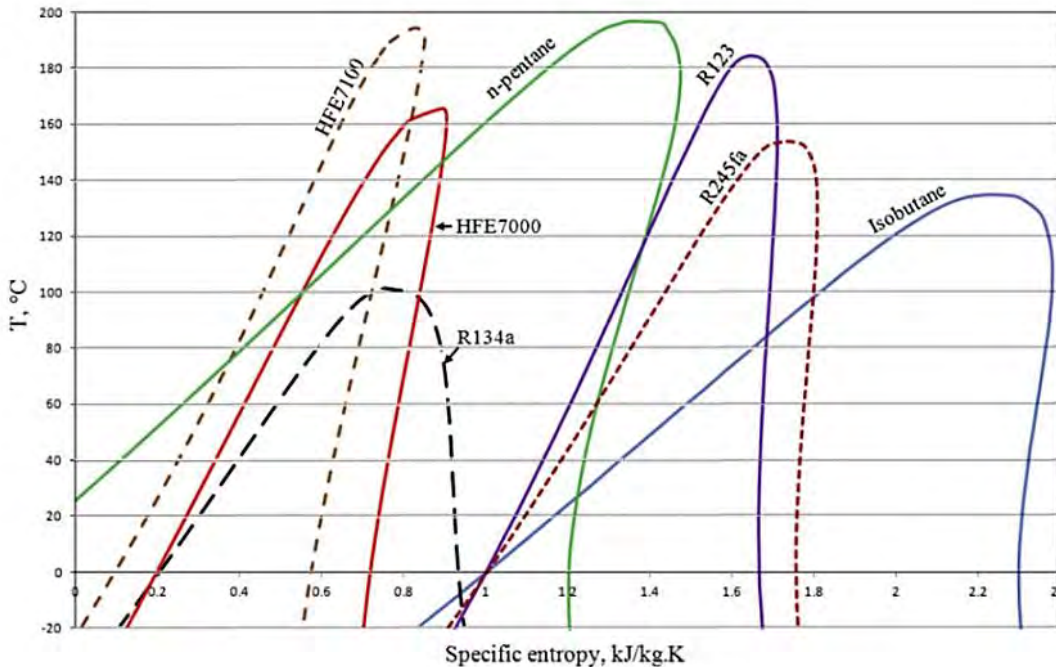
- Superheating or reheating is not feasible → **low cycle efficiency**
- Low steam quality at the end of the expansion → **dangerous for the turbine**

T- S diagram for water

In this case, replacement of water by a hydrocarbon is a good option → **Organic Rankine Cycle (ORC)**

Organic Rankine Cycle (ORC)

The hydrocarbons used in ORCs have a positive slope of their saturated vapor curve

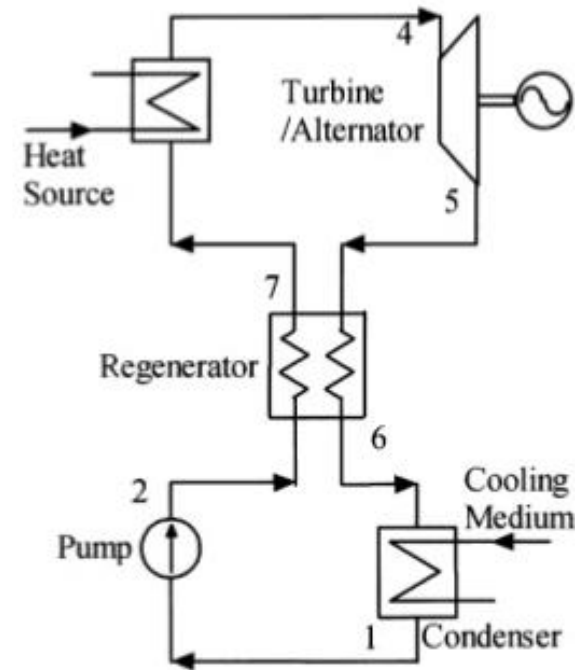
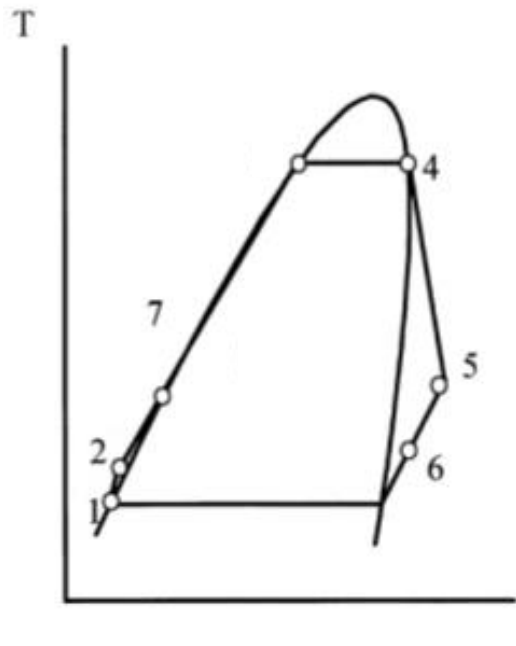


Source: <http://heatcatcher.com>

Benefits of the Organic Rankine Cycles

BENEFITS:

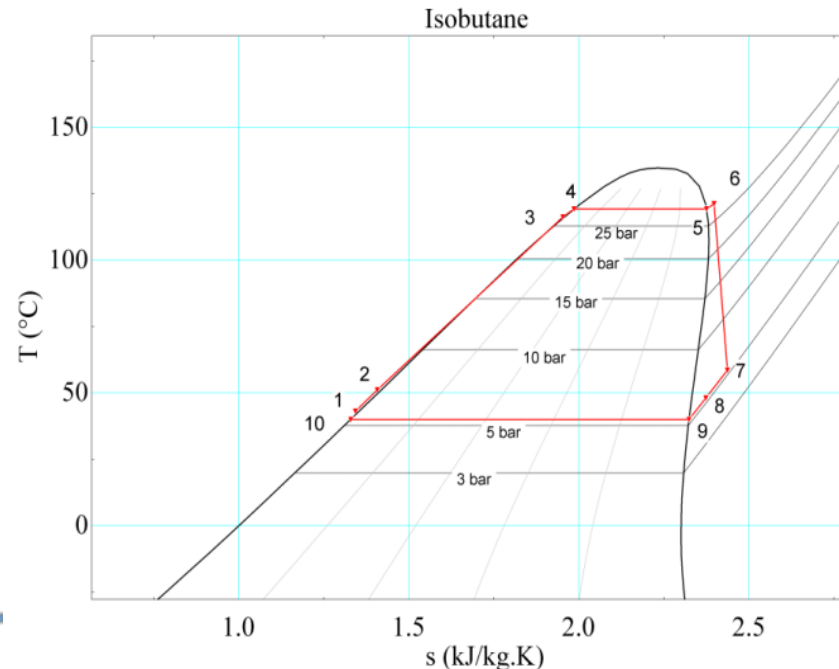
- Higher efficiency than a standard Rankine Cycle using water with the same temperature of the heat source ($\sim 15\%$ for $T=150^\circ\text{C}$)
- Simple configuration: pump + evaporator + turbine + regenerator + condenser



Benefits of the Organic Rankine Cycles

BENEFITS:

- Higher efficiency than a standard Rankine Cycle using water with the same temperature of the heat source ($\sim 15\%$ for $T=150^\circ\text{C}$)
- Simple configuration: pump + evaporator + turbine + regenerator + condenser
- No need for superheating or reheating to achieve a high steam quality, thus achieving a reasonable efficiency without risk for the turbine



Drawbacks of the Organic Rankine Cycles

DRAWBACKS

- Low thermal stability of the hydrocarbons used (low maximum temperatures)
- Compatibility of the fluids with raw materials and lub oil
- Fluid decomposition may produce gases that reduce the heat transfers in the condenser and increase corrosion

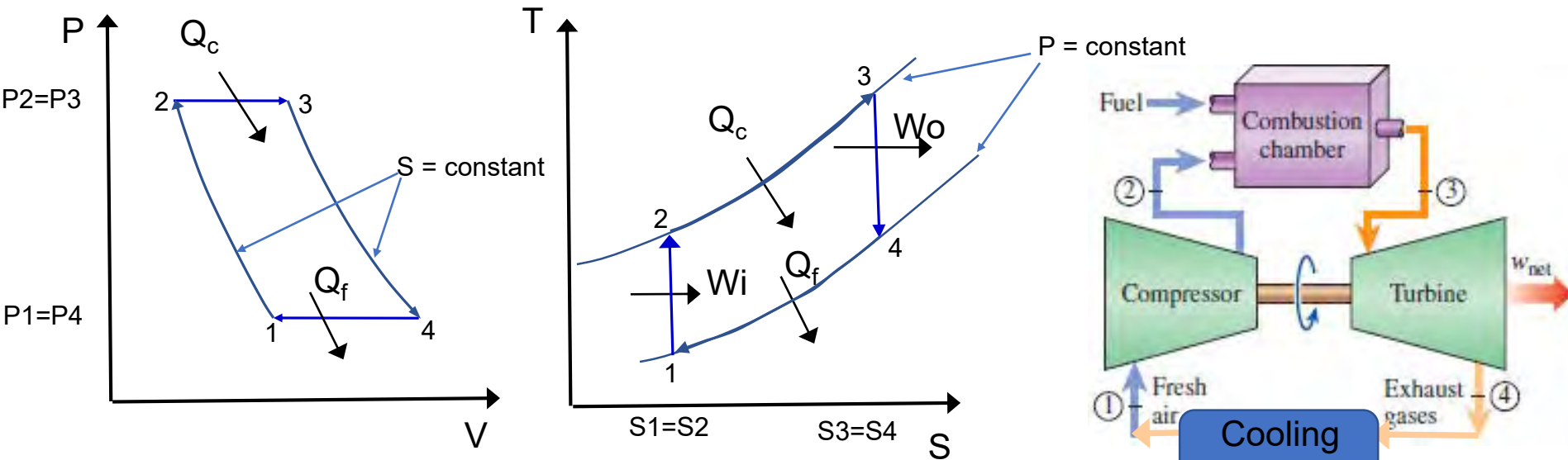
Power Cycles for STE Plants

Content

- Introduction to Thermodynamic Cycles
-  Power Cycles used in STE Plants
 - Rankine Cycle
 - Organic Rankine Cycle
 -  Brayton Cycle
 - Combined Cycle
 - Supercritical Cycles
 - Stirling Cycle

The (ideal) Brayton Cycle

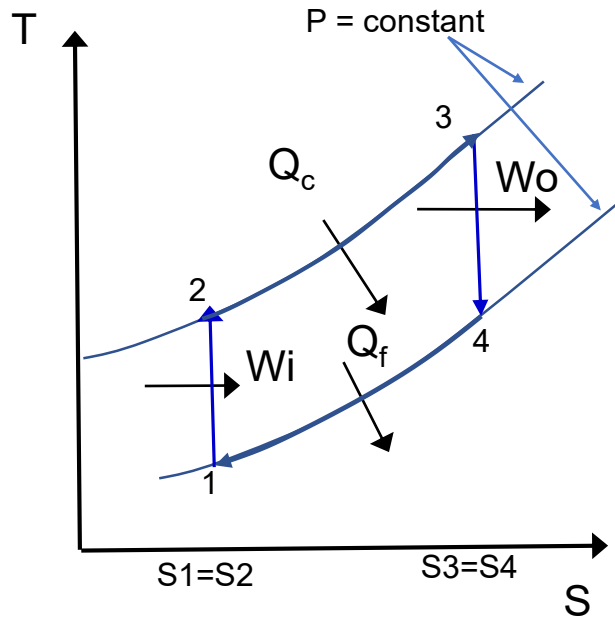
- This cycle was designed by the American engineer George Brayton en 1870.
- The working fluid is gas (usually air)



This cycle is composed of four processes:

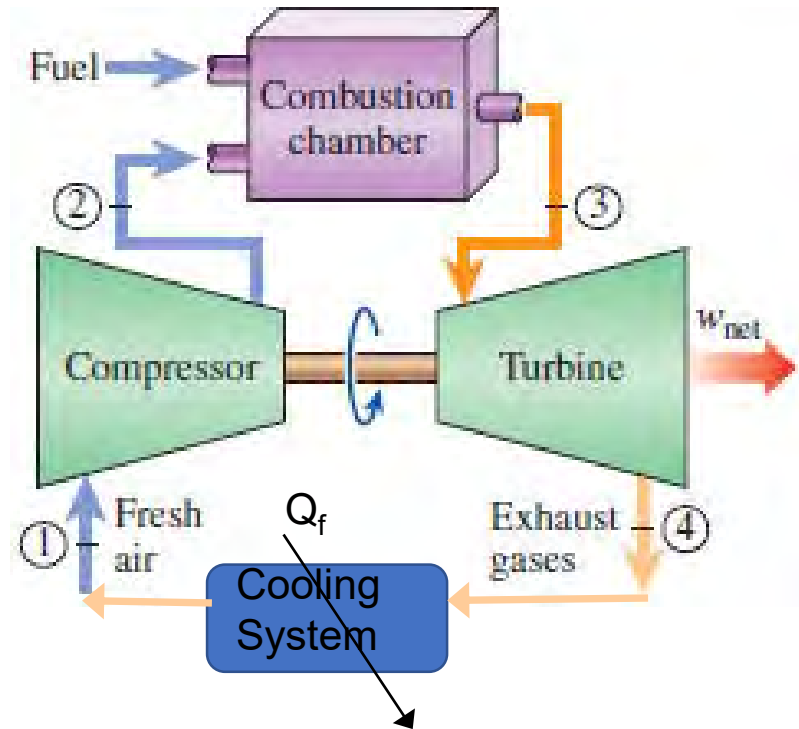
- 1–2: Isentropic compression (Gas compressor)
- 2–3: Isobaric heating (Combustion chamber)
- 3–4: Isentropic expansion (Gas turbine)
- 4–1: Isobaric heat rejection (gas rejection to the atmosphere)

Parameters of the (ideal) Brayton Cycle



Compression thermal ratio $\lambda = \left(\frac{P_2}{P_1}\right)^{\frac{\gamma-1}{\gamma}}$

$\gamma = C_p / C_v > 1$



Temperature ratio $\tau = \frac{T_3}{T_1}$

Pressure ratio $r_p = P_2/P_1$

Efficiency of the (ideal) Brayton Cycle

The efficiency, η , is calculated assuming that the working gas behaves as an ideal gas with constant heat capacity all through the cycle:

$C_p = \text{constant}$

$$\sum Q_i + \sum W_i = 0$$

$$\eta = \frac{W_{net}}{\dot{Q}_c} = \frac{\dot{W}_o - \dot{W}_i}{\dot{Q}_c} = \frac{(h_3 - h_2) - (h_4 - h_1)}{h_3 - h_2} = 1 - \frac{(h_4 - h_1)}{h_3 - h_2} = 1 - \frac{C_p(T_4 - T_1)}{C_p(T_3 - T_2)} = 1 - \frac{T_4 - T_1}{T_3 - T_2}$$

$$\eta = 1 - \frac{(T_4 - T_1)}{T_3 - T_2} = 1 - \frac{T_1 \left[\left(\frac{T_4}{T_1} \right) - 1 \right]}{T_2 \left[\left(\frac{T_3}{T_2} \right) - 1 \right]} = 1 - \frac{T_1}{T_2}$$

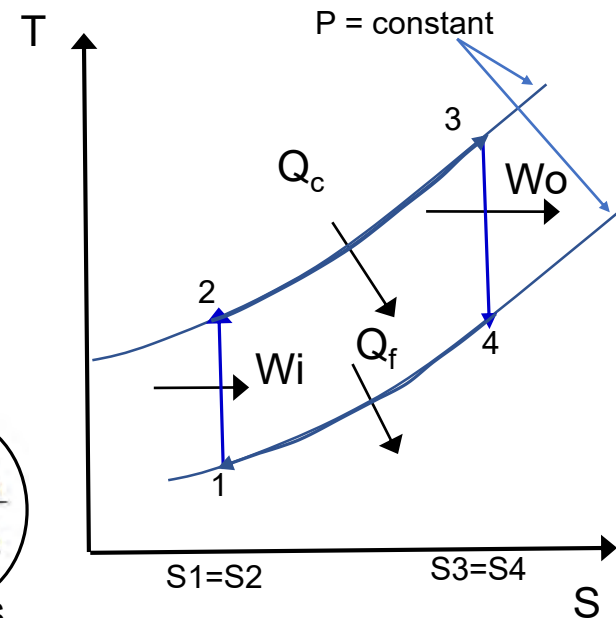
Adiabatic process for ideal gases: $TP^\gamma = Cte$

Process 3-4 $T_4 P_4^{1-\gamma} = T_3 P_3^{1-\gamma}$

Process 1-2 $T_1 P_1^{1-\gamma} = T_2 P_2^{1-\gamma}$

2-3 and 4-1 are Isobaric processes

$$\frac{T_4}{T_1} \left(\frac{P_4}{P_1} \right)^{1-\gamma} = \frac{T_3}{T_2} \left(\frac{P_3}{P_2} \right)^{1-\gamma} \rightarrow \frac{T_4}{T_1} = \frac{T_3}{T_2}$$



Efficiency of the (ideal) Brayton Cycle

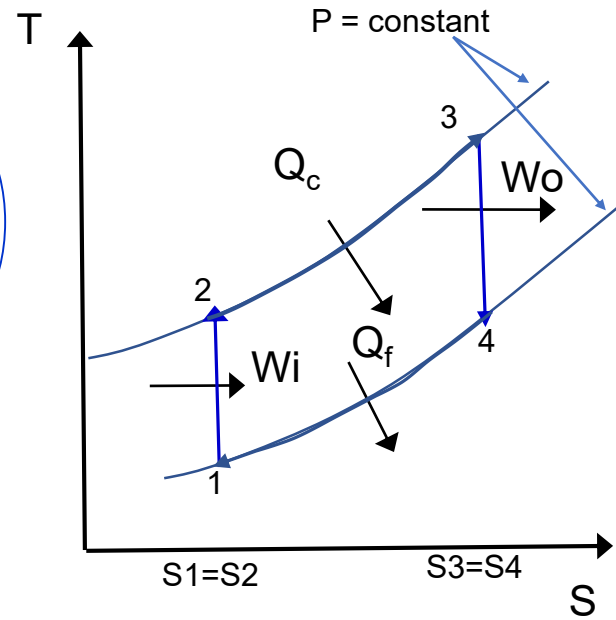
The efficiency, η , can be expressed in different ways:

$$\eta = 1 - \frac{T_1}{T_2} = 1 - \frac{1}{r_p^{\frac{\gamma-1}{\gamma}}}$$

Since γ is >1 , the efficiency of the Brayton cycle increases with the Pressure Ratio

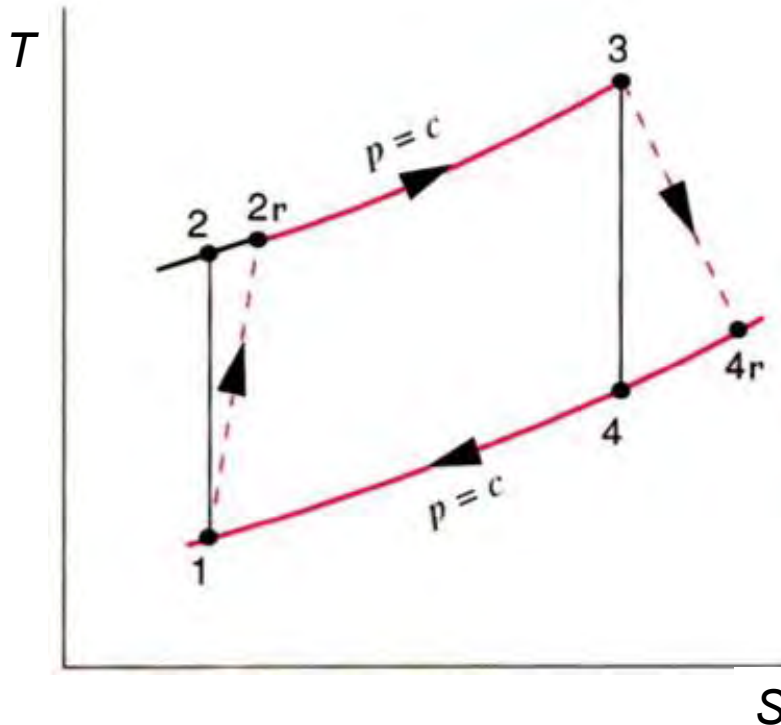
Proceso 1-2 $T_1 P_1^{\frac{1-\gamma}{\gamma}} = T_2 P_2^{\frac{1-\gamma}{\gamma}} \rightarrow \frac{T_1}{T_2} = \left(\frac{P_2}{P_1}\right)^{\frac{1-\gamma}{\gamma}} = \frac{1}{\left(\frac{P_2}{P_1}\right)^{\frac{\gamma-1}{\gamma}}} = \frac{1}{r_p^{\frac{\gamma-1}{\gamma}}}$

$r_p = P_2/P_1$ Pressure Ratio



The real Brayton Cycle (Irreversibilities)

- Due to irreversibilities in the compressor and turbine, neither the compression nor the expansion are isentropic processes
- Usual values of the compressor and turbine efficiencies are 80-90%,



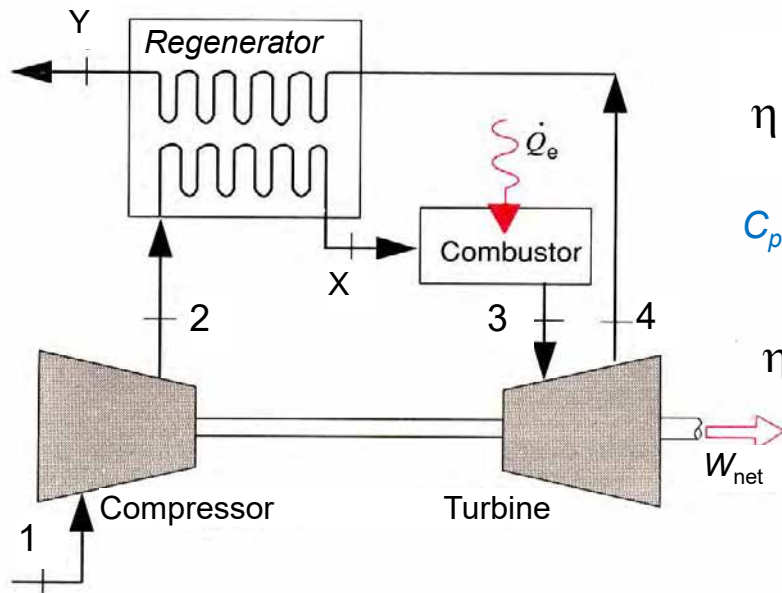
$$\mu_C = \frac{W_{IC}}{W_{RC}} = \frac{h_2 - h_1}{h_{2R} - h_1}$$

$$\mu_T = \frac{W_{RT}}{W_{IT}} = \frac{h_3 - h_{4R}}{h_3 - h_4}$$

Improvements of the basic Brayton Cycle

The Regenerative Brayton Cycle

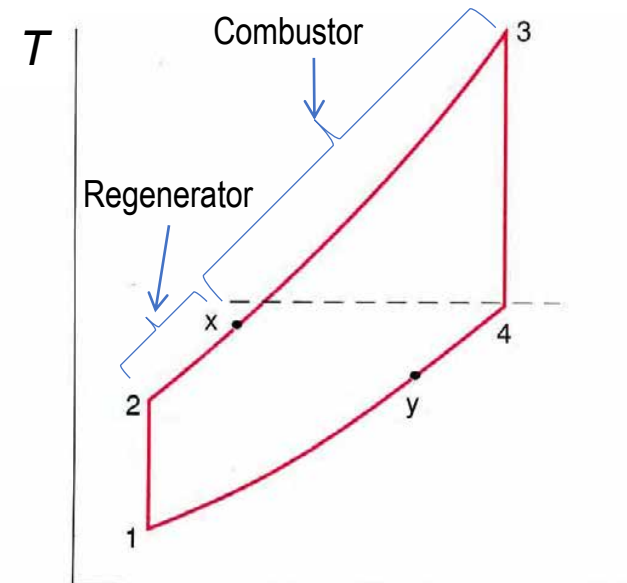
In a Regenerative Brayton Cycle the thermal energy of the air at the outlet of the turbine is used to preheat the compressed air before entering into the combustor, thus reducing the amount of thermal energy consumed by the cycle and increasing its thermal efficiency of the cycle.



$$\eta = 1 - \frac{(h_y - h_1)}{h_3 - h_x}$$

$C_p = \text{constant}$

$$\eta = 1 - \frac{(T_y - T_1)}{T_3 - T_x}$$



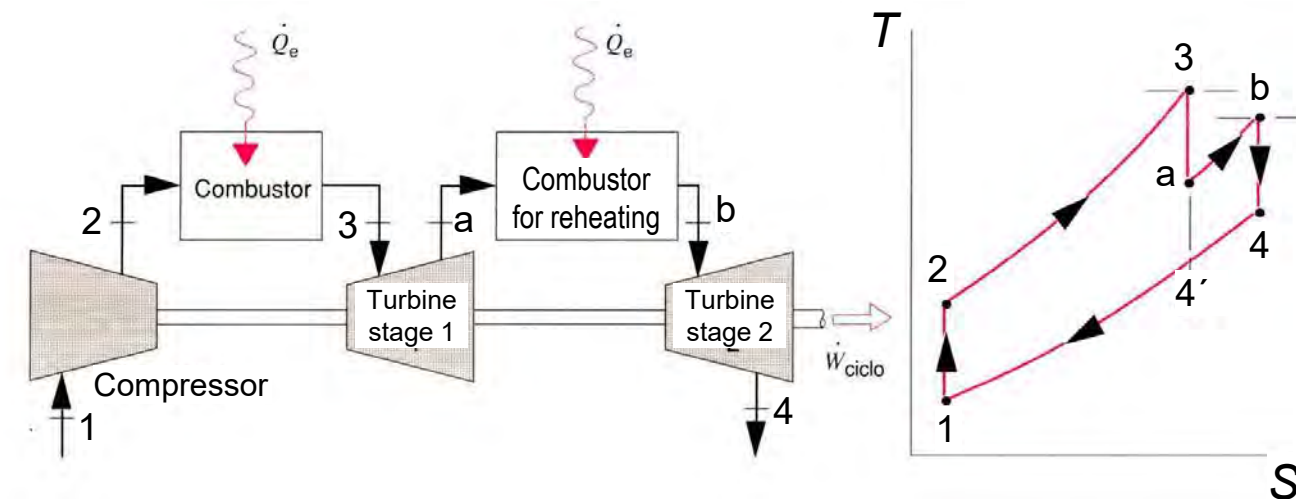
S

egeneración, producen incrementos sustanciales en el rendimiento térmico, con

Improvements of the basic Brayton Cycle

2.1 Turbina de gas con recalentamiento Brayton Cycle with Reheating

- The expansion process has two stages (segments 3-a and b-4), so that the air is reheated at constant pressure (segment a-b) between the first and second expansion (segment a-b)



$$= 1 - \frac{h_4 - h_1}{(h_3 - h_2) + (h_b - h_a)}$$

Figura 14: Turbina de gas ideal con recalentamiento

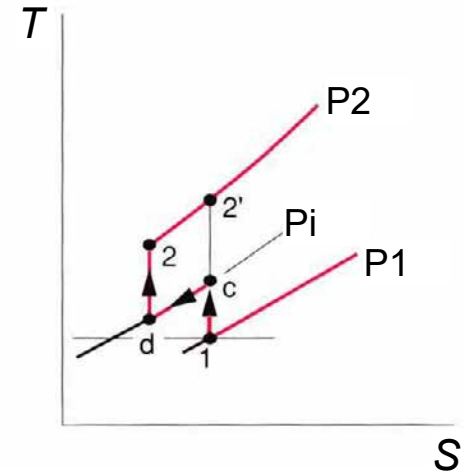
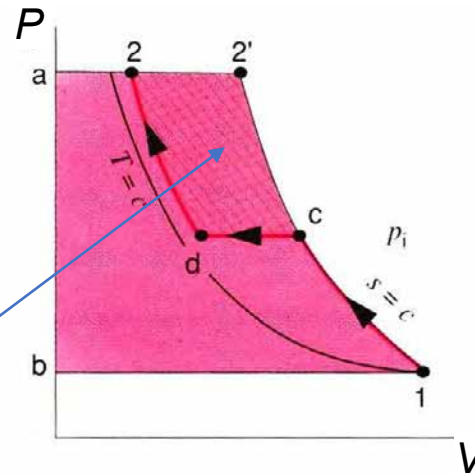
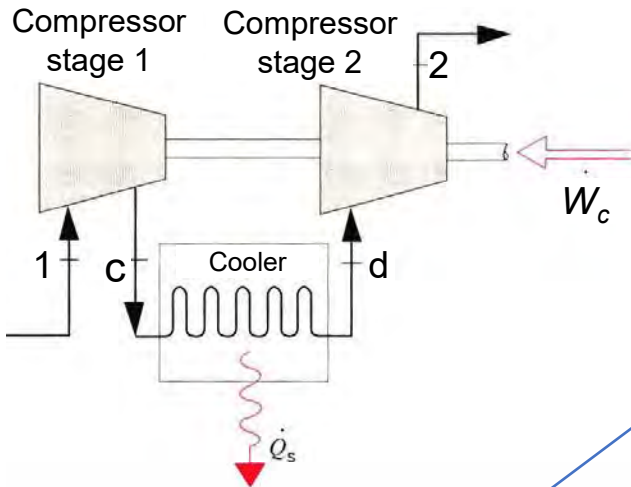
- Although the net mechanical work is higher the thermal energy consumption is higher too → the efficiency is not necessarily higher than that of a basic Brayton cycle! The efficiency will be higher than the basic cycle only if $T_b - T_a > T_4 - T_{4'}$

Después de la expansión del estado 3 hasta el a en la primera etapa de la turbina, el gas se calienta a presión constante desde el estado a al estado b. La expansión se completa en la segunda etapa de la turbina desde el estado b hasta el estado 4.

Improvements of the basic Brayton Cycle

Compression with intercooling

- Air compression is performed in two stages (segments 1-c and d-2) with a cooling between the two stages (segment c-d). **This cooling reduces the mechanical work required for the overall compression**, thus increasing the net output mechanical work

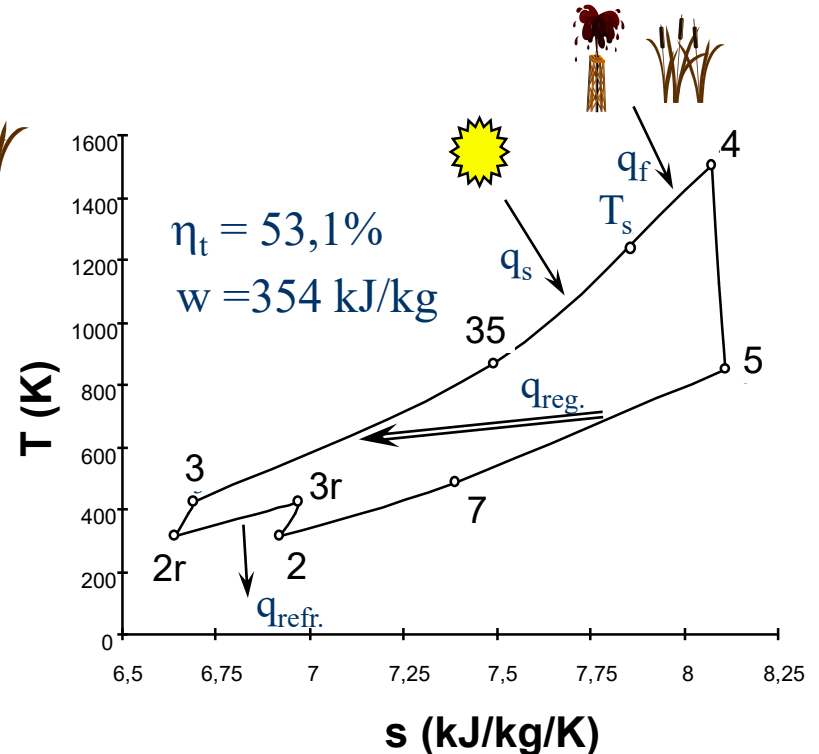
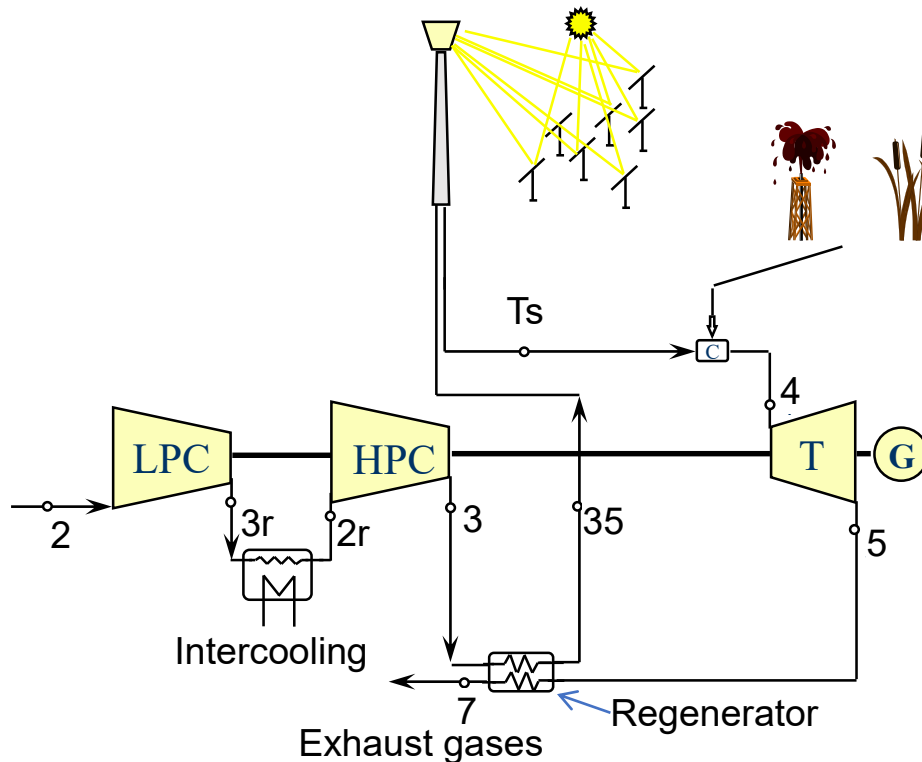


- The marked area in the P-V diagram represents the reduction of mechanical work for the compression process when we have an intermediate cooling (intercooling)
- The mechanical work saving depends on the outlet temperature T_d at the cooler **and** the intermediate pressure P_i

Integration of a Brayton Cycle in STE Plants

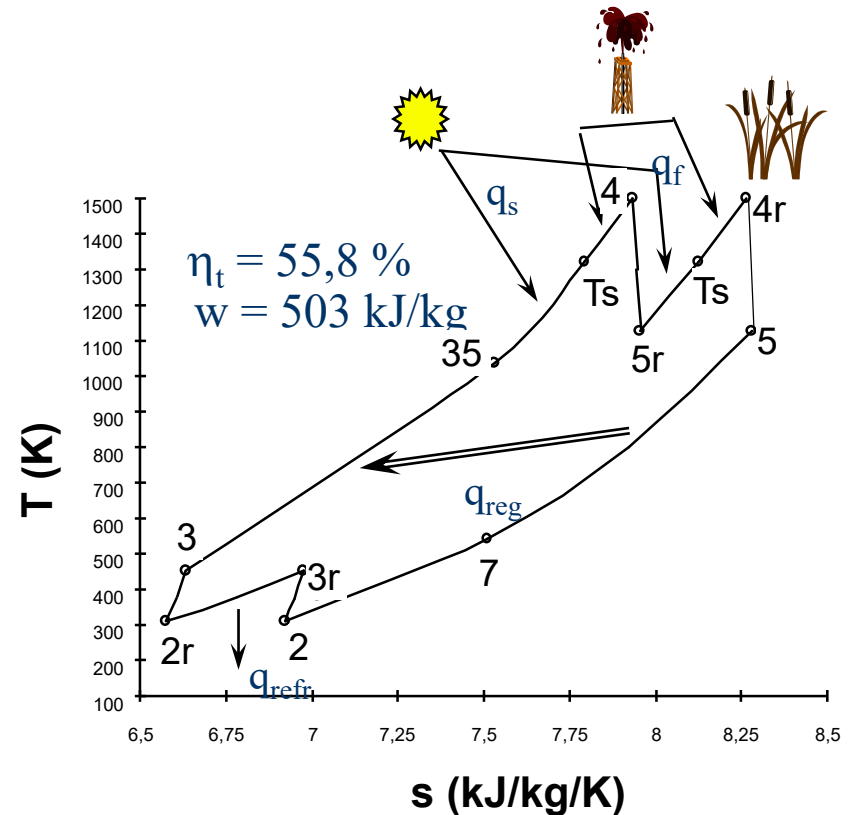
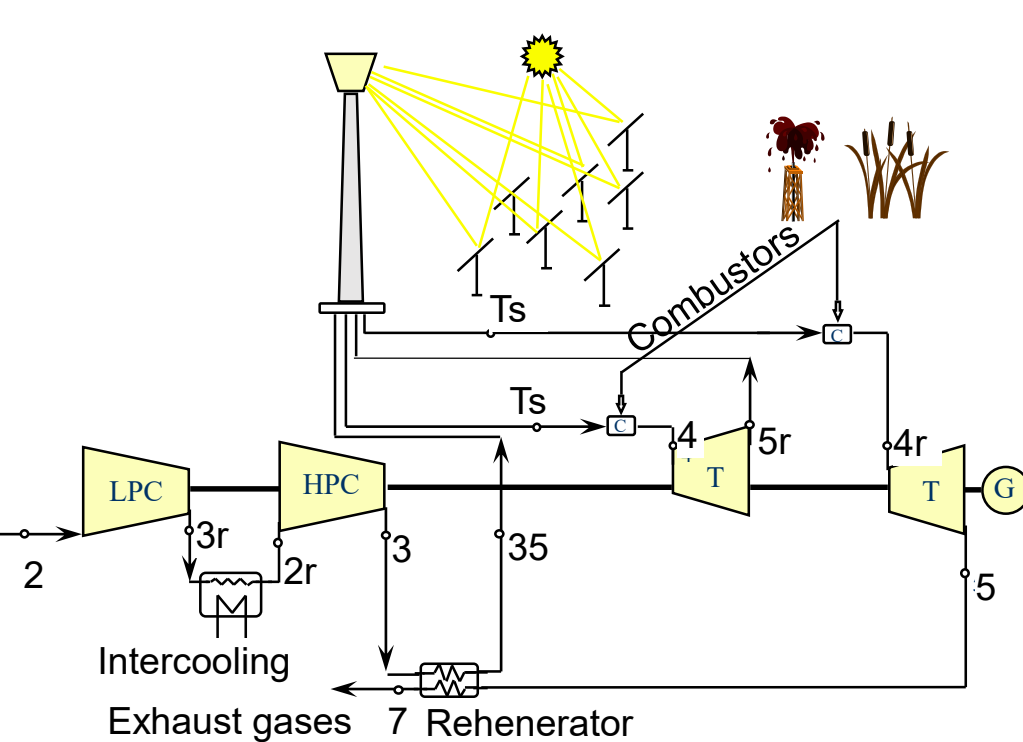
Regenerative Brayton Cycle with Intercooling

Because of the high temperatures required to achieve a good cycle efficiency, the Brayton cycles are usually integrated in solar tower plants:



Integration of a Brayton Cycle in STE Plants

Regenerative Brayton Cycle with intercooling and reheating



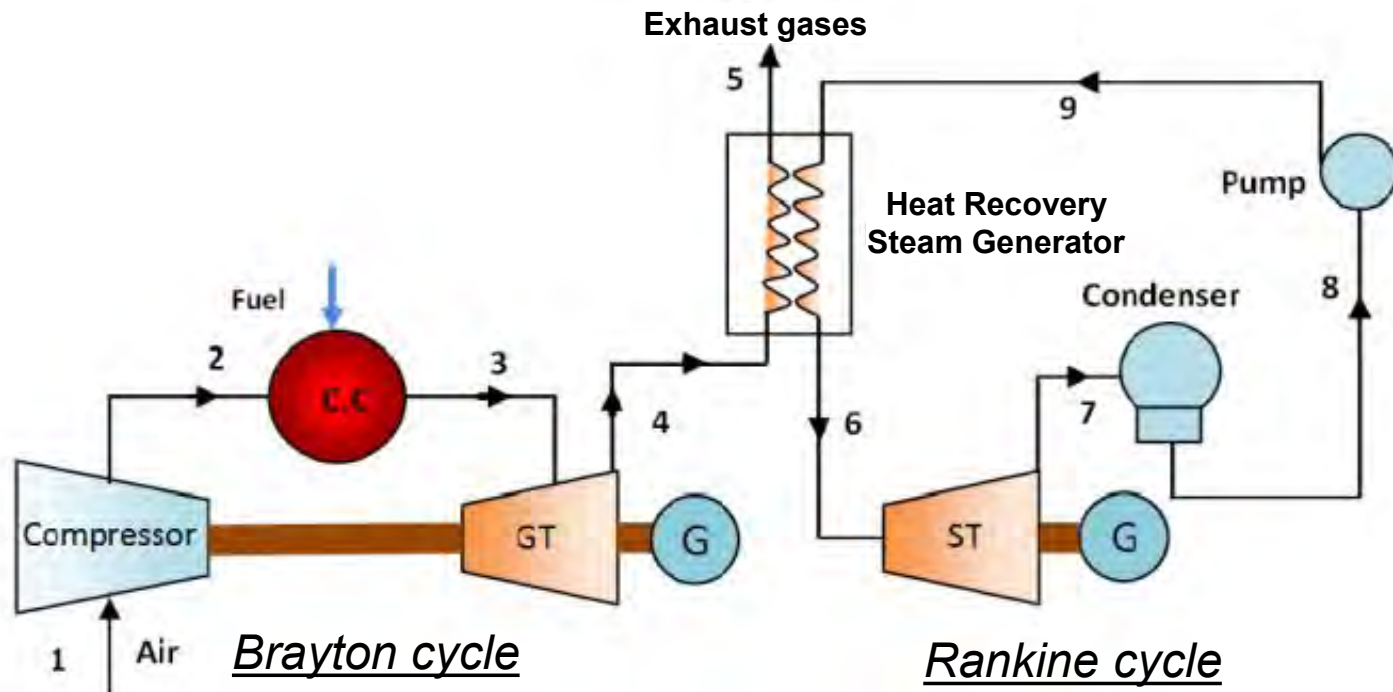
Power Cycles for STE Plants

Content

- Introduction to Thermodynamic Cycles
-  Power Cycles used in STE Plants
 - Rankine Cycle
 - Organic Rankine Cycle
 - Brayton Cycle
 -  Combined Cycle
 - Supercritical Cycles
 - Stirling Cycle

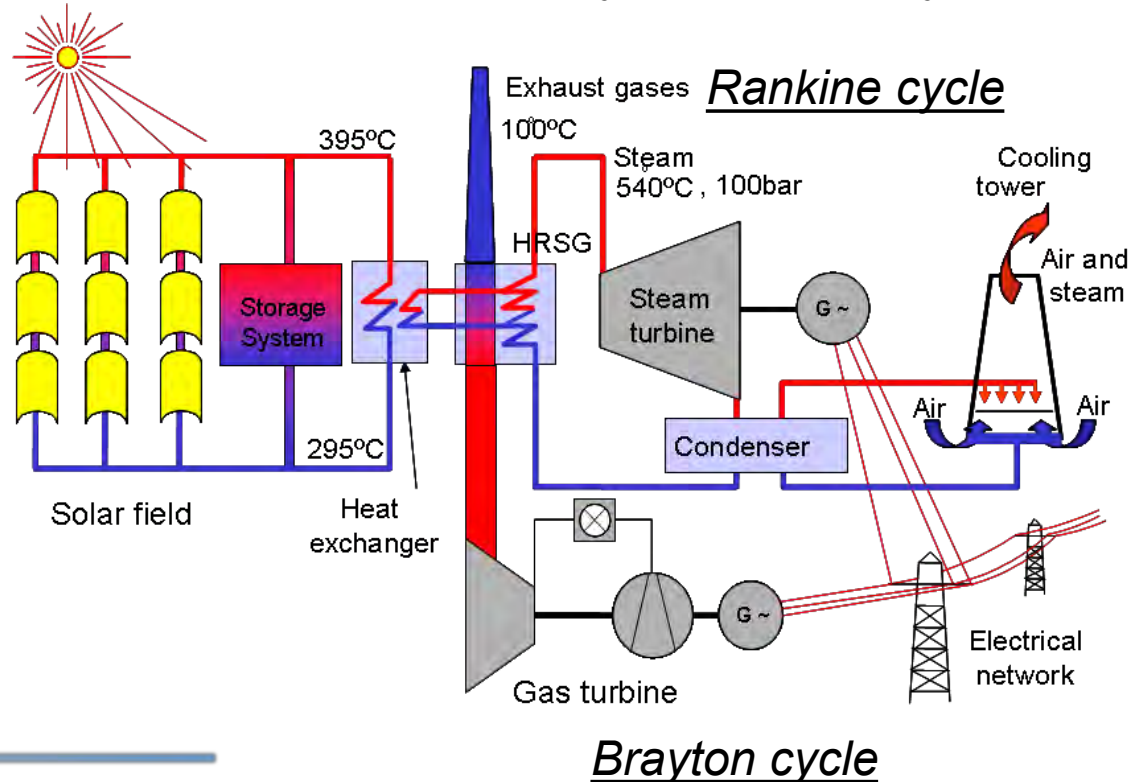
Combined cycle

- A combined cycle is composed of a Brayton cycle coupled to a Rankine cycle in a way that the heat of the gas turbine exhaust gases are used to evaporate the water of a Rankine cycle
- The heat recovery from the exhaust gases increases the overall efficiency up to about 50%, which is higher than the efficiency of any of the basic cycles separately.



Integrated Solar Combined Cycle (ISCC) Plant

- A ISCC plant is composed of a combined cycle with a solar field connected to the Rankine cycle to increase the electricity production of the steam turbine.
- The yearly solar fraction is small (~10%). However, this type of solar plant is an excellent option for countries willing to learn about solar thermal plants without taking a significant risk, because an ISCC plant is basically a combined cycle plant
- There are three ISCC plants in operation at Morocco, Algeria and Egypt



Power Cycles for STE Plants

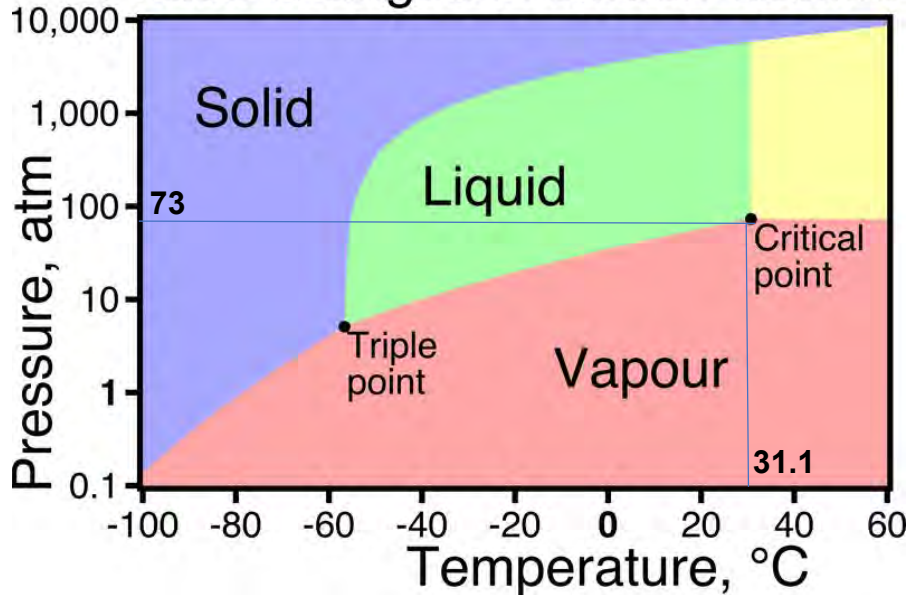
Content

- Introduction to Thermodynamic Cycles
-  Power Cycles used in STE Plants
 - Rankine Cycle
 - Organic Rankine Cycle
 - Brayton Cycle
 - Combined Cycle
 -  Supercritical Cycles
 - Stirling Cycle

Supercritical Fluids

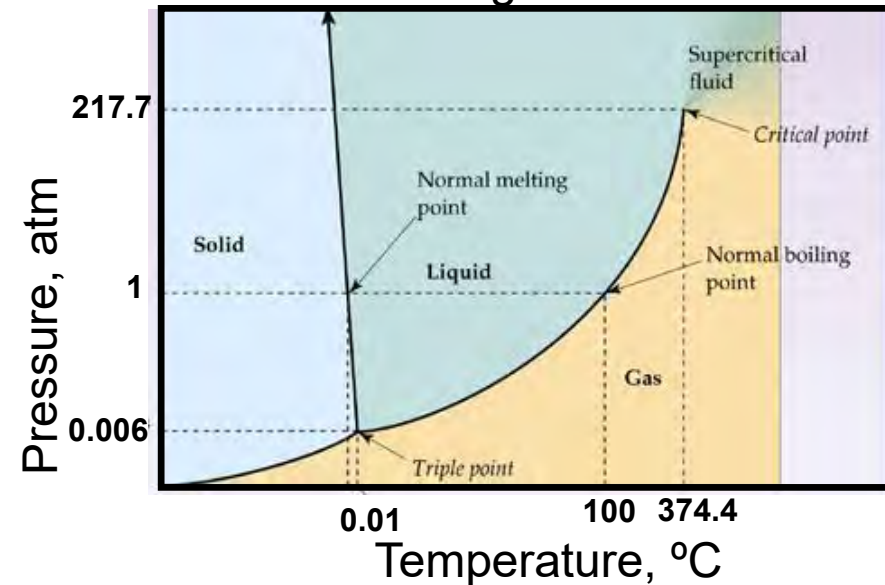
- When the fluid is at a pressure/temperature higher than those of its “*Critical Point*” is named “**Supercritical Fluid**”
- A *Supercritical Fluid* has both gas-and liquid-like properties. It is gas-like in that it is compressible, and liquid-like in density

Phase changes in carbon dioxide



$$\underline{\text{CO}_2}: P_c = 73 \text{ atm}, T_c = 31,1^\circ\text{C}$$

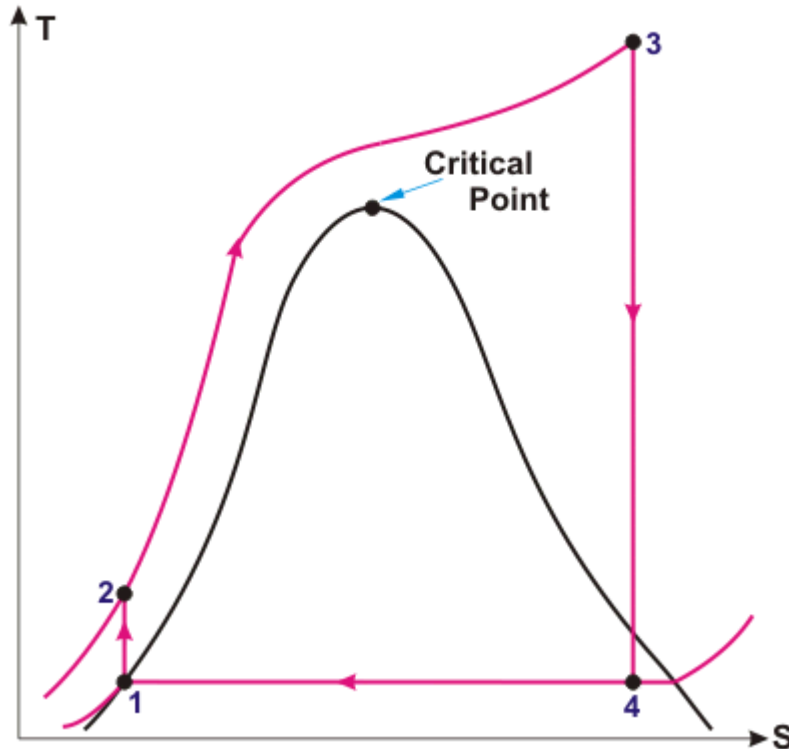
Phase changes in water



$$\underline{\text{H}_2\text{O}}: P_c = 217.7 \text{ atm}, T_c = 373.4^\circ\text{C}$$

Supercritical Rankine Cycle (SBC)

➤ In a Supercritical Rankine Cycle (SBC) the water is in the boiler at a pressure higher than > 218 bar, so that the water does not change from liquid to steam in the boiler, but expands as it increases its temperature. Typical water pressure/temperature in commercial SRCs are 300 bar/600°C



- The main benefit of a SBC is a higher efficiency than a superheated Rankine cycle (43% \rightarrow 46%)
- The main drawback is the high pressure that the boiler and the steam turbine must withstand
- The water entering the boiler has to be of extremely high levels of purity to avoid deposits on the turbine blades

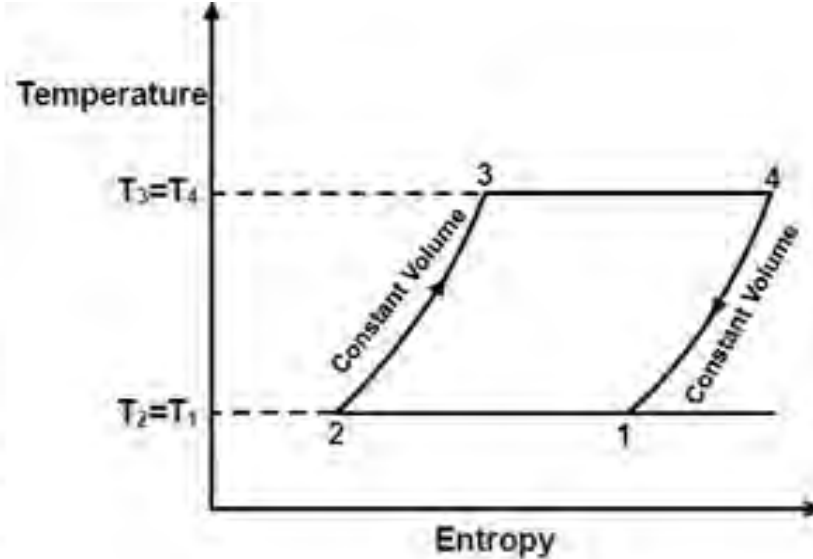
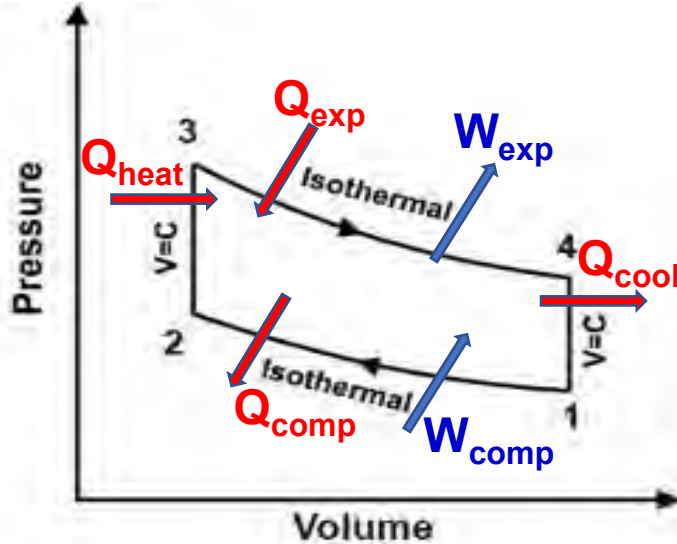
Power Cycles for STE Plants

Content

- Introduction to Thermodynamic Cycles
-  Power Cycles used in STE Plants
 - Rankine Cycle
 - Organic Rankine Cycle
 - Brayton Cycle
 - Combined Cycle
 - Supercritical Cycles
 -  Stirling Cycle

The Stirling cycle

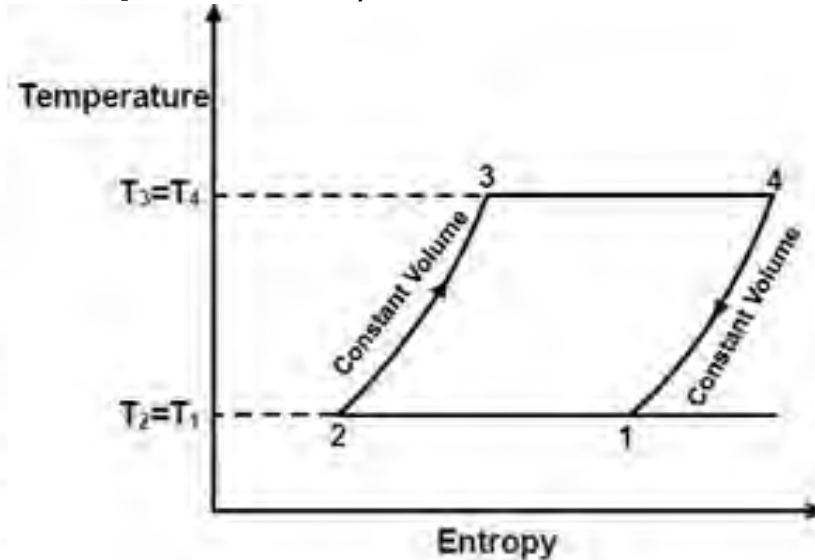
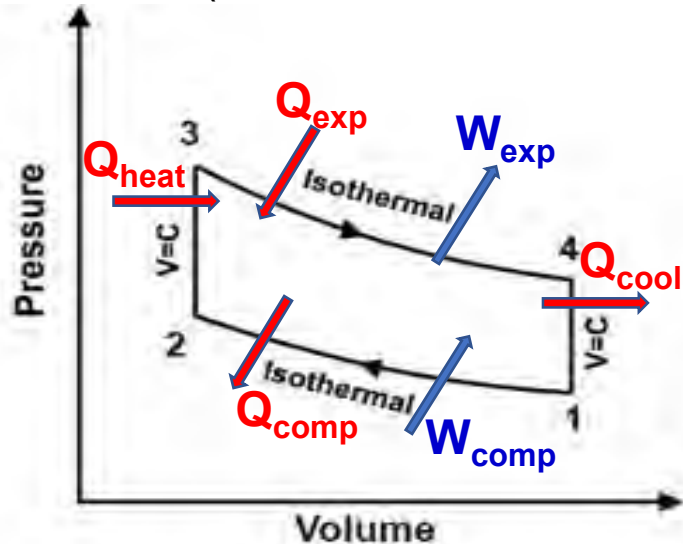
- This cycle was patented by Robert Stirling in 1860 and it is composed of four processes (2 isothermal + 2 isochoric processes):



- Process 1-2: Isothermal compression extracting heat at constant temperature and adding mechanical work
- Process 2-3: Isochoric compression absorbing heat at constant volume
- Process 3-4: Isothermal expansion adding heat at constant temperature and extracting mechanical work
- Process 4-1: Isochoric expansion extracting heat at constant volume

The Stirling cycle

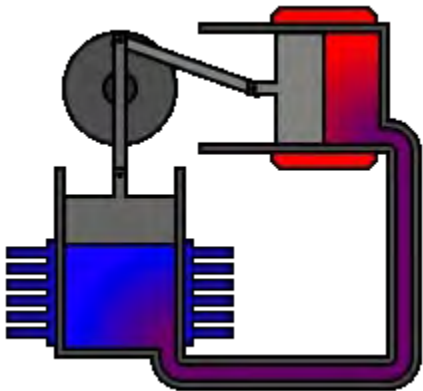
- This cycle was patented by Robert Stirling in 1860 and it is composed of four processes (2 isothermal + 2 isochoric processes):



- Since the amount of heat added in 2-3 and extracted in 4-1 are quite similar, an **internal regenerator** is used in Stirling engines to temporarily store Q_{cool}
- Since $W_{exp} > W_{comp}$ there is a net positive mechanical work

Integration of the Stirling cycle in STE plants

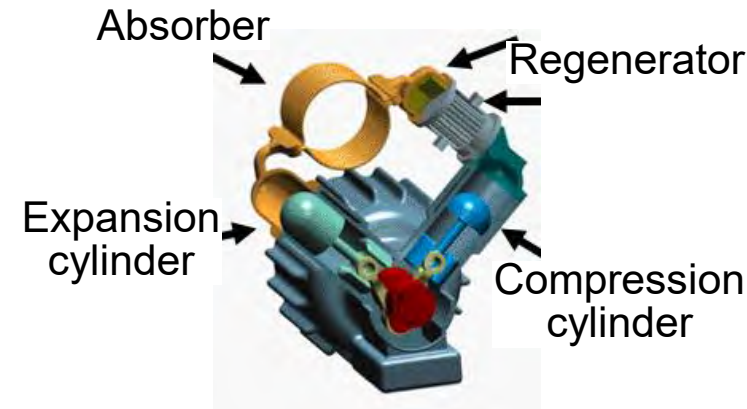
- Stirling cycle is commercially implemented using the so-called **Stirling engines**, which are **closed-cycle regenerative heat engines with a permanently gaseous working fluid (He or H₂)**.
- Due to the technical features of Stirling engines, they are very suitable to be used with parabolic dish concentrators (600°C-800°C / 150-200 bar)



Simple sketch of a Stirling engine



A solar Stirling dish



A solar Stirling engine

- The two main benefits of Stirling engines are their high thermal efficiency (>30%) and the absence of pollutant combustion gases



SFERA-III



1st Summer School

September, 9th- 10th, 2019

CNRS- PROMES, Odeillo, France

Power Cycles for CSP/STE Plants

End of Slide Show

Questions ?

SFERA-III

Solar Facilities for the European Research Area

1st Summer School “Thermal energy storage systems, solar fields and new cycles for future CSP plants”
WPI Capacity building and training activities
Odeillo, France, September 9th-11th 2019



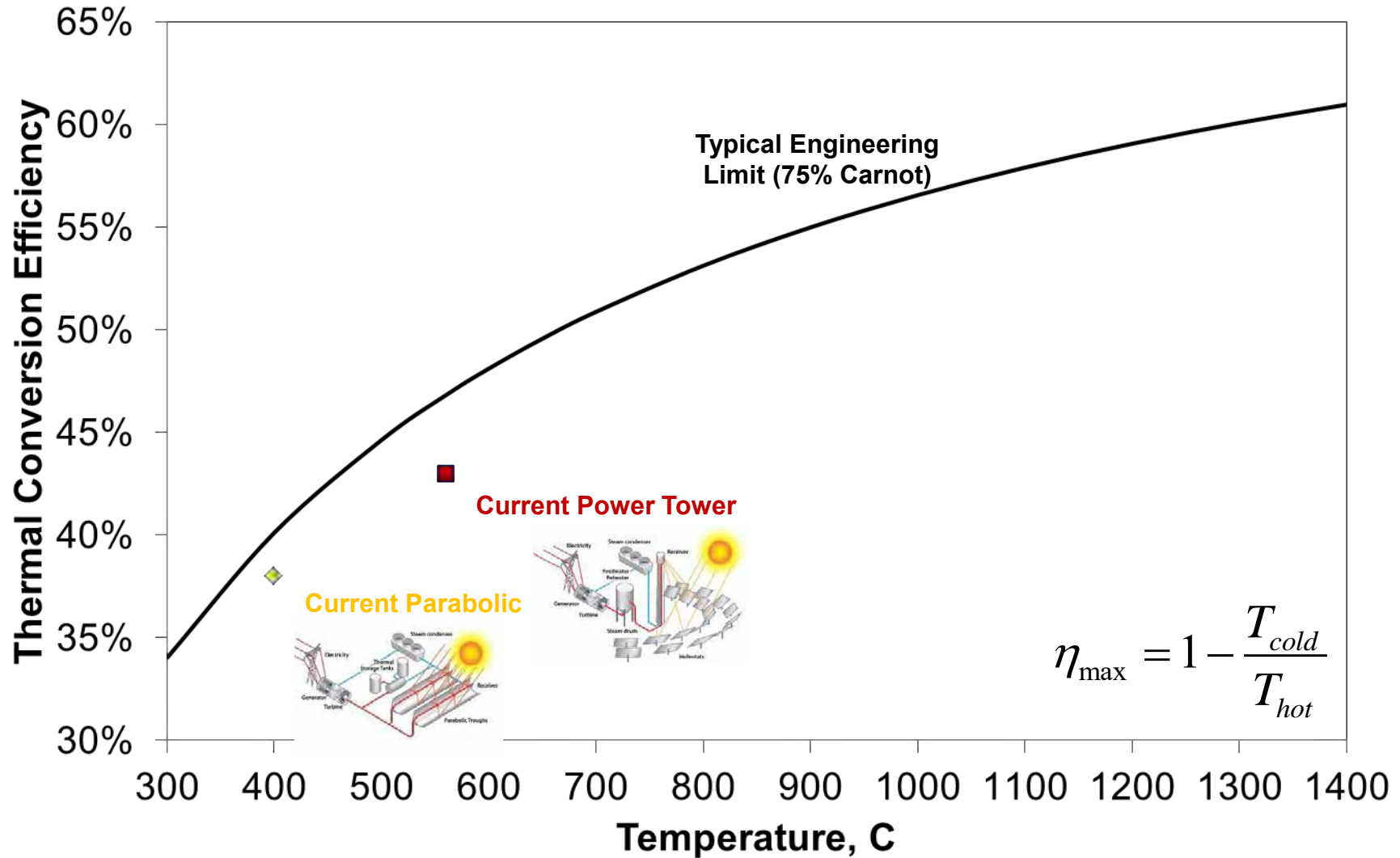
sCO₂ cycles for CSP plants: challenges and issues
Manuel Romero, IMDEA Energy, Spain



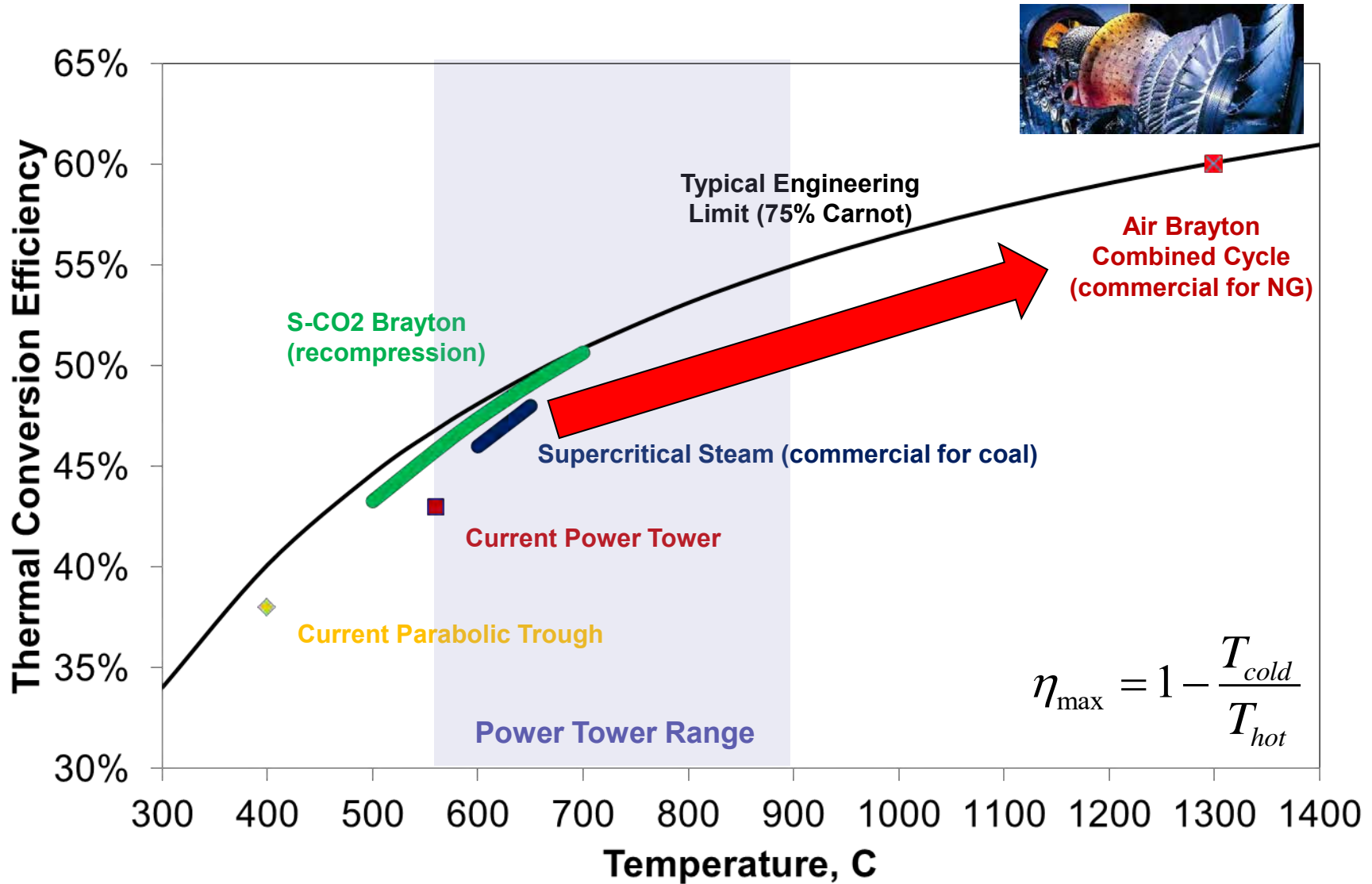
NETWORKING



Thermodynamics cycles application

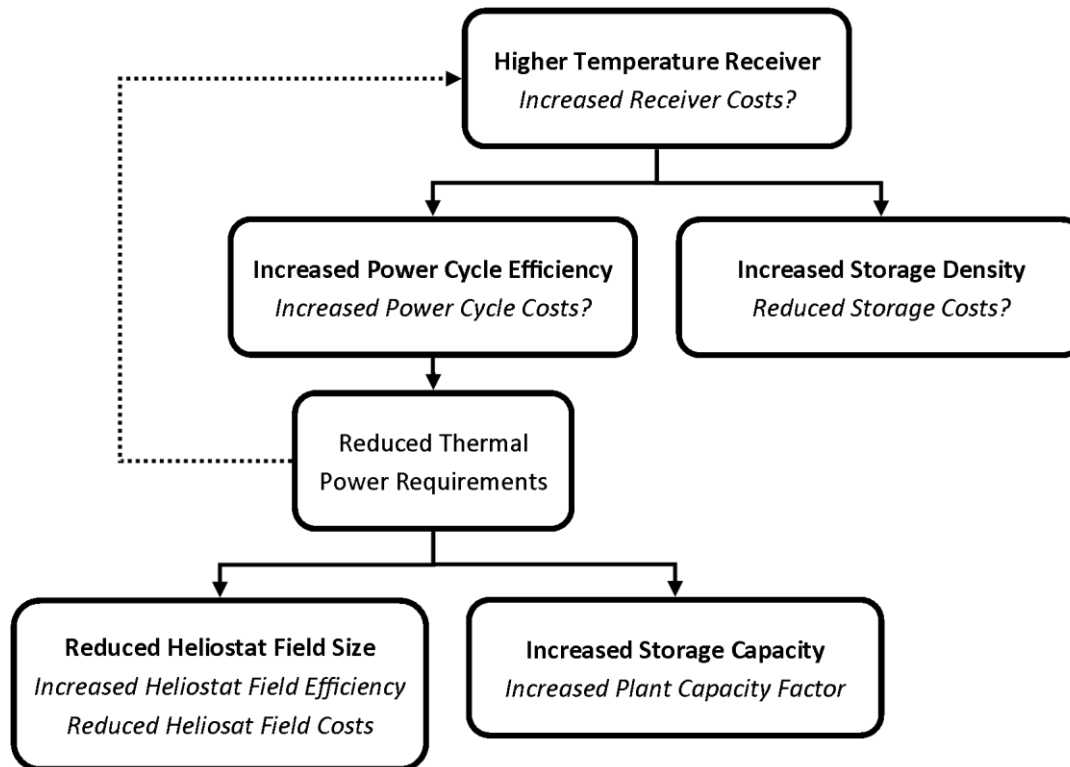


Thermodynamics cycles application



The Effects of Higher Temperatures

Increasing the operating temperature of the receiver has a cascade of effects throughout the entire power plant



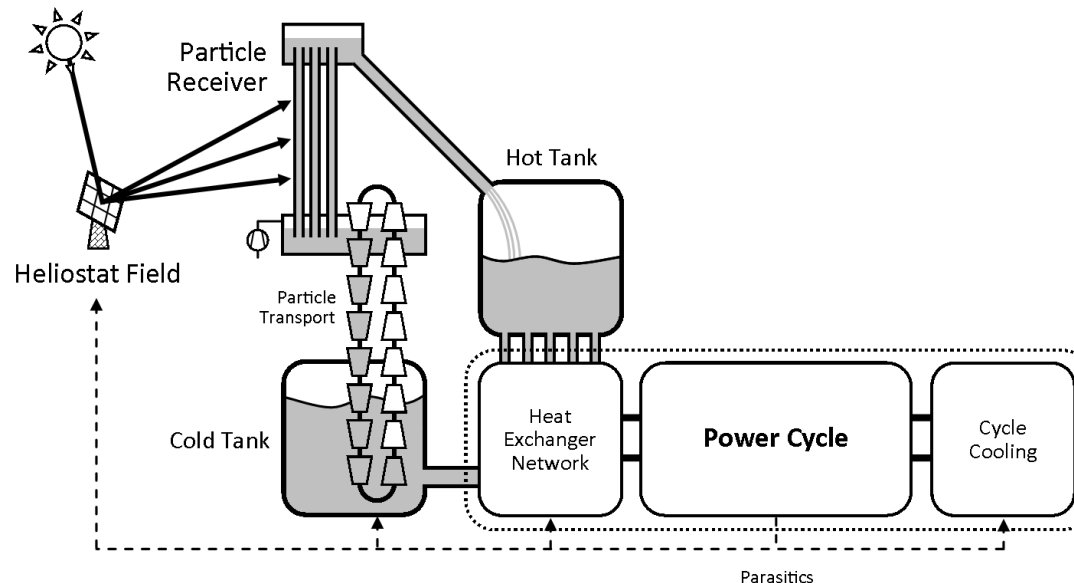
➤ Integrated **techno-economic analysis** is needed

NEXT-CSP Project



Main objective of Next-CSP project is:

- To improve the reliability and performance of Concentrated Solar Power (CSP) plants through the development and integration of a new technology based on the use of high temperature (650-800 °C) particles as heat transfer fluid and storage medium.

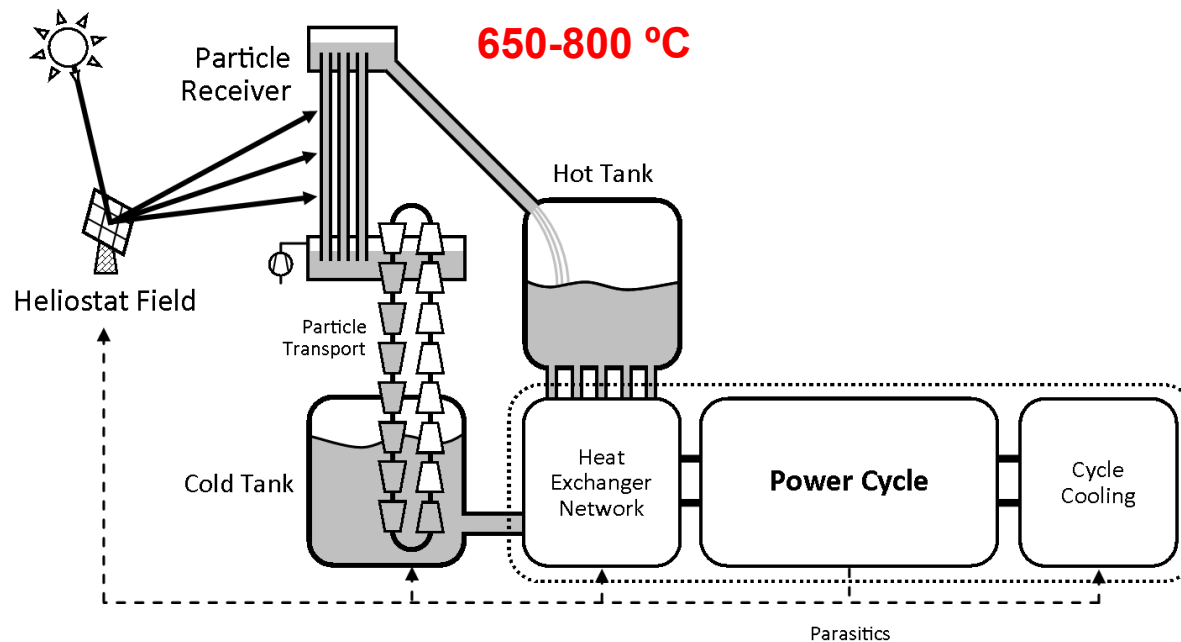


IMDEA Energy (in collaboration with EDF) role on NEXT-CSP project:

- Assessment of the highly efficient thermodynamic cycles that can be combined with the high temperature solar loop (WP6)
- Scale-up to a 150 MW solar power plant – Preliminary design, risk analysis, cost and value assessment (WP7)

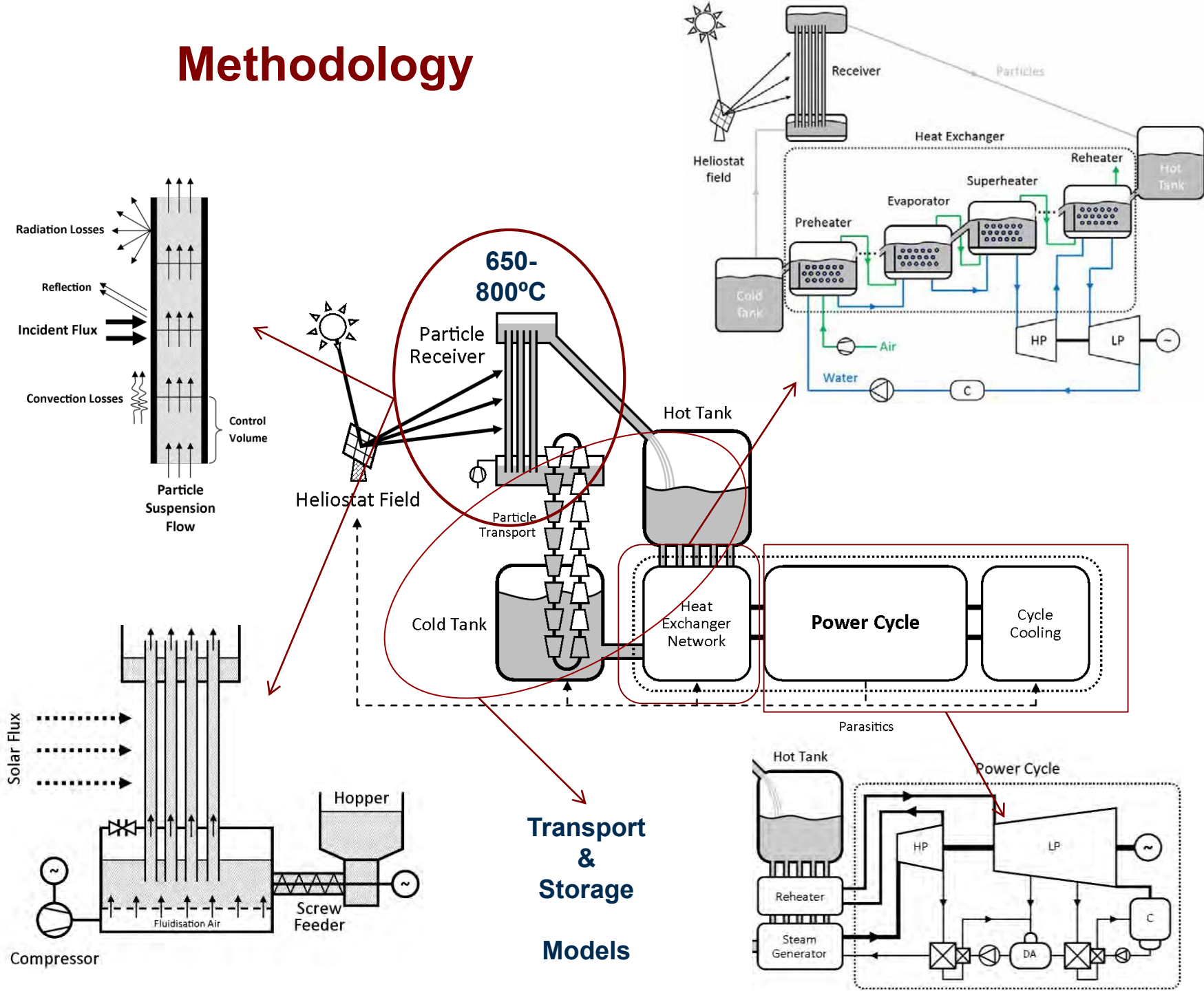
NEXT-CSP Project Objective

- ❑ To improve the reliability and performance of Concentrated Solar Power (CSP)
- ❑ Commercial state-of-the-art technology for CSP < 565 °C ----- $\eta \approx 42\%$
- ❑ Higher temperature solar receiver (up to 800 °C) allows for highly efficient cycles (Carnot's Theorem)



- ❑ Cycles screened: supercritical steam, supercritical CO₂, Combined Cycle
- ❑ Target: Cycle efficiency > 45 % (up to 50 %)

Methodology



Comparison of thermodynamic cycles

- ❖ Investigating novel work transfer fluids for the power block (supercrit. CO₂)
 - ✓ *Excellent thermal properties (& compact turbomachinery). Excellent theoretical thermodynamic power cycle efficiency*

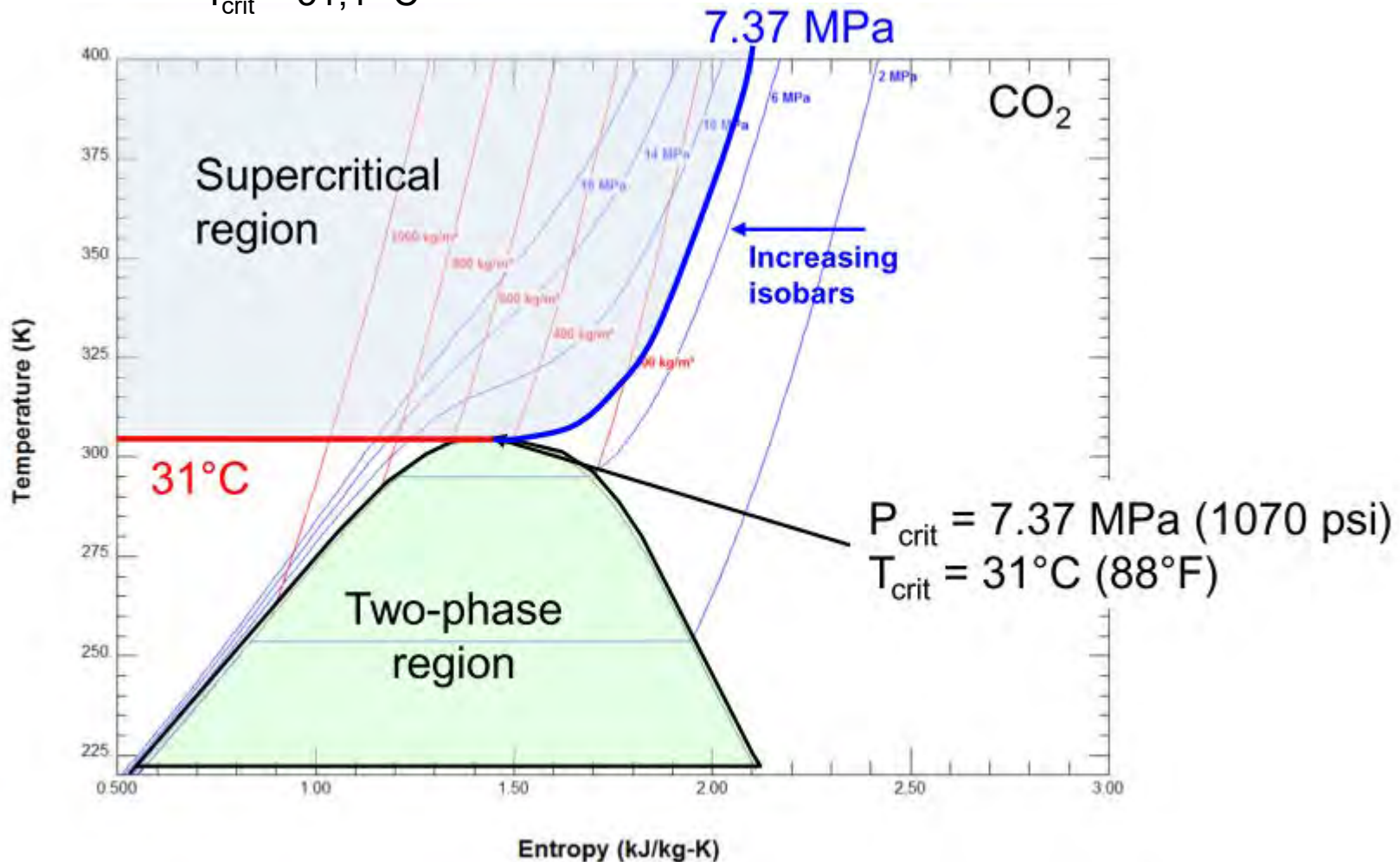
| Plant Nominal Performance | Units | Std. Rankine | Brayton 650 °C | Brayton 750 °C | Brayton 1,000 °C | Combined Cycle | Brayton He | Brayton sCO ₂ | Reference M. Salts |
|--|-------|--------------|----------------|----------------|------------------|----------------|------------|--------------------------|--------------------|
| Heliostats efficiency | [%] | 72.1 | 72.1 | 72.1 | 67.8 | 72.1 | 72.1 | 72.1 | 72.1 |
| Receiver efficiency | [%] | 82.3 | 80.7 | 77.3 | 72.2 | 83.1 | 81.0 | 79.7 | 87.5 |
| Thermal power to storage / power block | [MW] | 23.4 | 23.0 | 21.7 | 20.6 | 23.7 | 23.1 | 22.7 | 25.7 |
| HTX efficiency | [%] | 95.0 | 95.0 | 95.0 | 95.0 | 95.0 | 95.0 | 95.0 | 99.0 |
| Net Electrical power | [MW] | 9.1 | 6.8 | 7.6 | 9.4 | 21.5 | 7.4 | 10.4 | 10.0 |
| Net Power cycle efficiency | [%] | 40.8 | 31.26 | 37.1 | 47.9 | 42.6 | 33.9 | 48.2 | 40.0 |
| Sun-to-electricity efficiency | [%] | 22.9 | 17.3 | 19.4 | 22.3 | 24.2 | 18.8 | 26.4 | 24.9 |

DPS plant conditions:

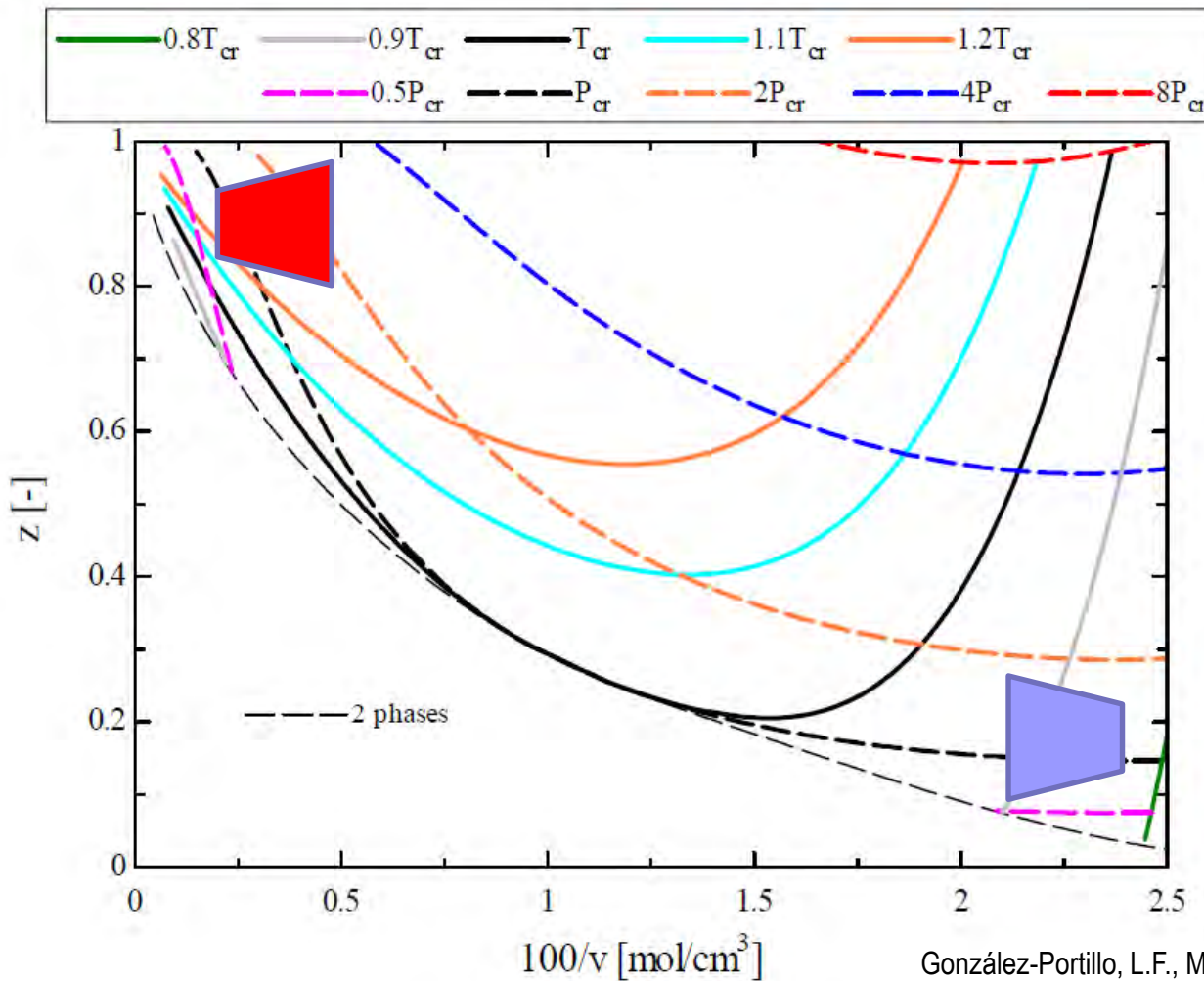
- ✓ 57 MW_{th} (receiver)
- ✓ Very high net power cycle efficiency (at moderate temperature range). Much more room of improvement at higher temperatures
- ✓ Very sensitive cycle depending on working operative conditions. Detailed optimization process required for power cycle working operative conditions selection

What is supercritical CO₂

- sCO₂ is a fluid state above critical temperature and critical pressure
 - $p_{\text{crit}} = 73,9 \text{ bar}$
 - $T_{\text{crit}} = 31,1 \text{ °C}$

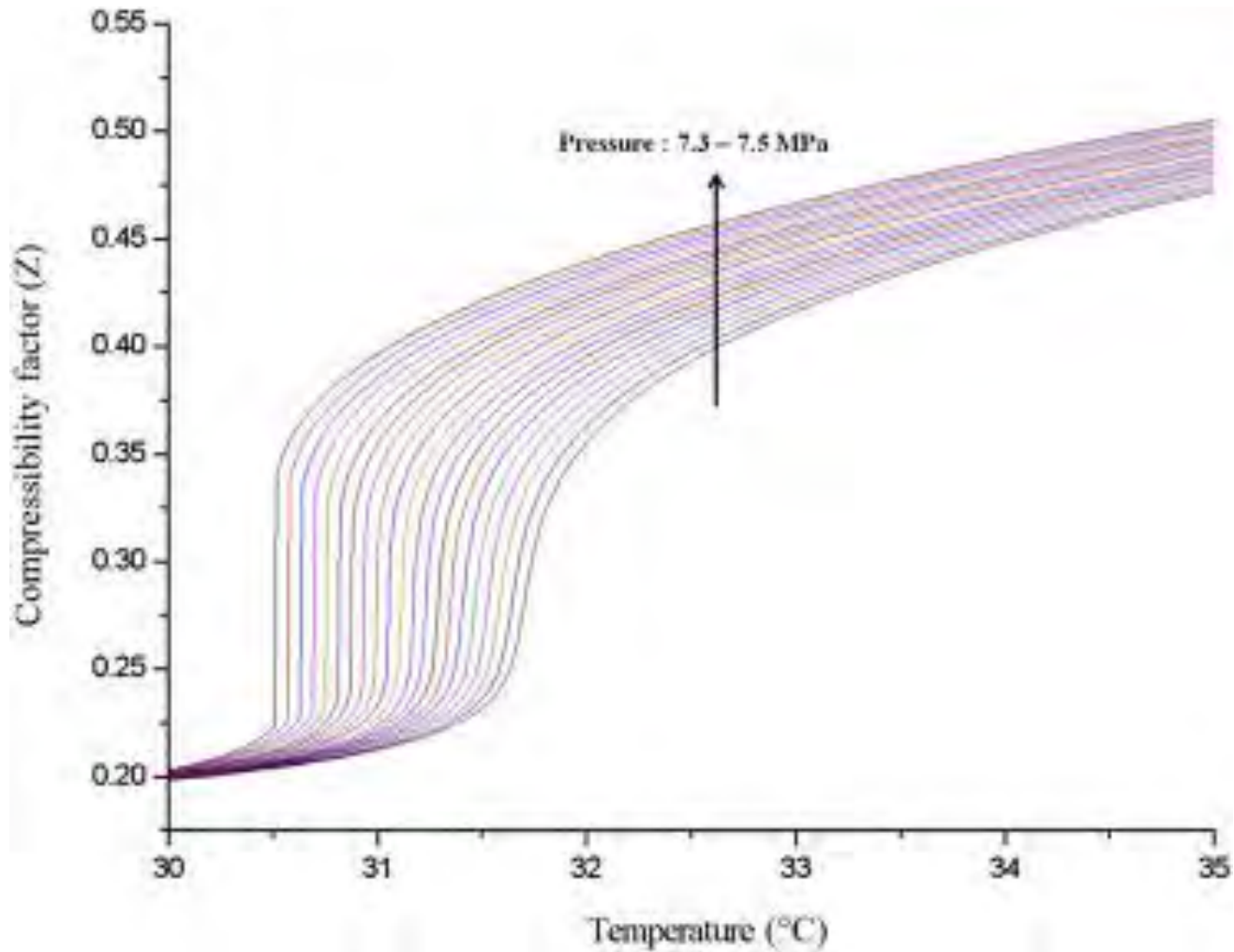


Compressibility factor, z , of CO₂ versus density, $100/v$, for different values of pressure and temperature (expressed as a function of the critical pressure, P_{cr} , and critical temperature, T_{cr} , respectively).

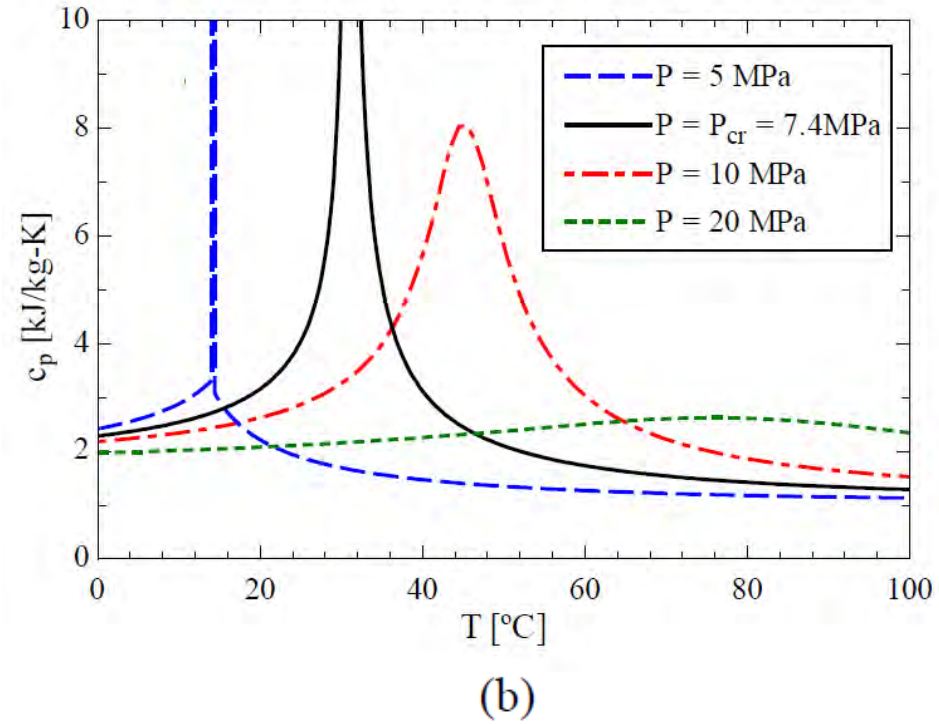
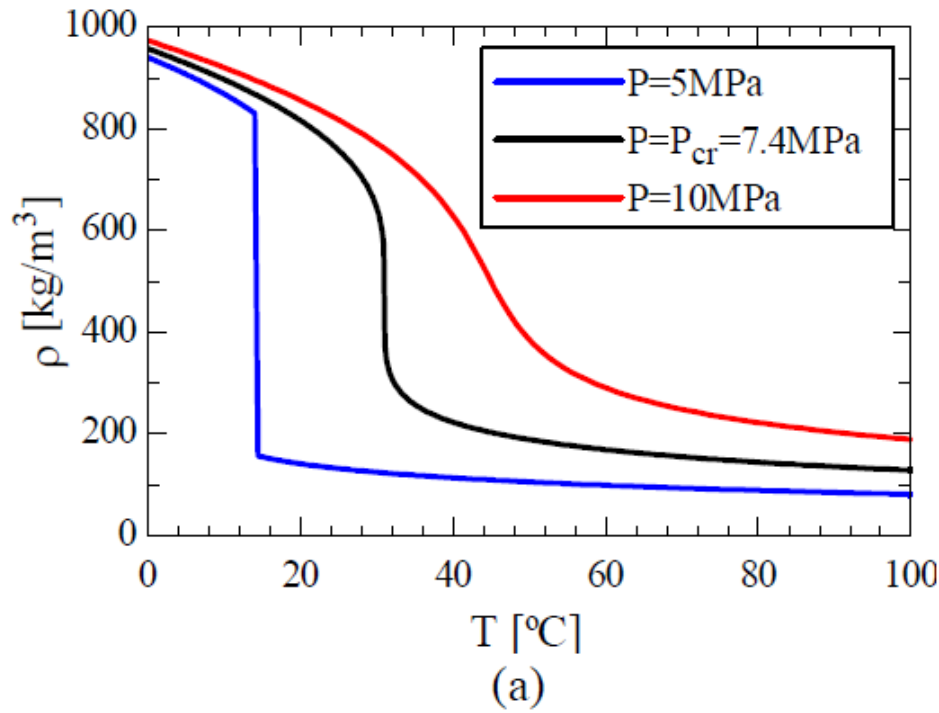


The compressibility factor, Z , is defined as the molecular volumetric ratio of a fluid compared with ideal gas.

$$Z = \frac{Pv}{RT}$$



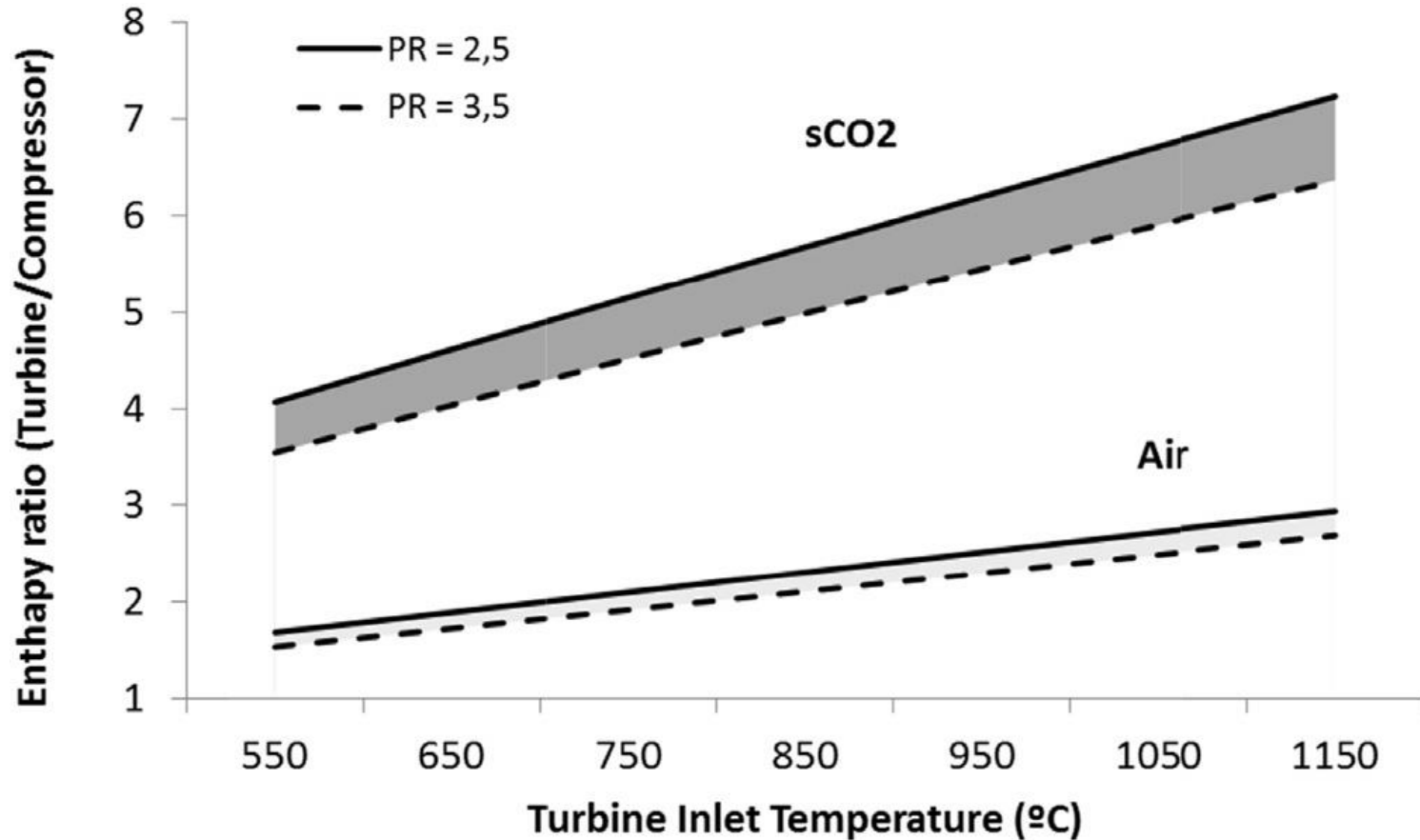
For CO₂ near the critical point, the compressibility factor decreases to 0.2–0.5 and the compression work can be substantially decreased.



(a) Density, ρ , and (b) isobaric specific heat capacity, c_p , of CO₂ at subcritical, critical and supercritical pressures as a function of temperature, T

$$dh = c_p dT \quad \text{isobaric}$$

Enthalpy ratio between turbine and compressor for sCO₂ (solid lines and dark grey shaded area) and air (slashed line and light grey shaded area). For two pressure ratio cases (PR).



M.A. Reyes-Belmonte, A. Sebastian, M. Romero, J. Gonzalez-Aguilar. Energy 112 (2016) 17-27

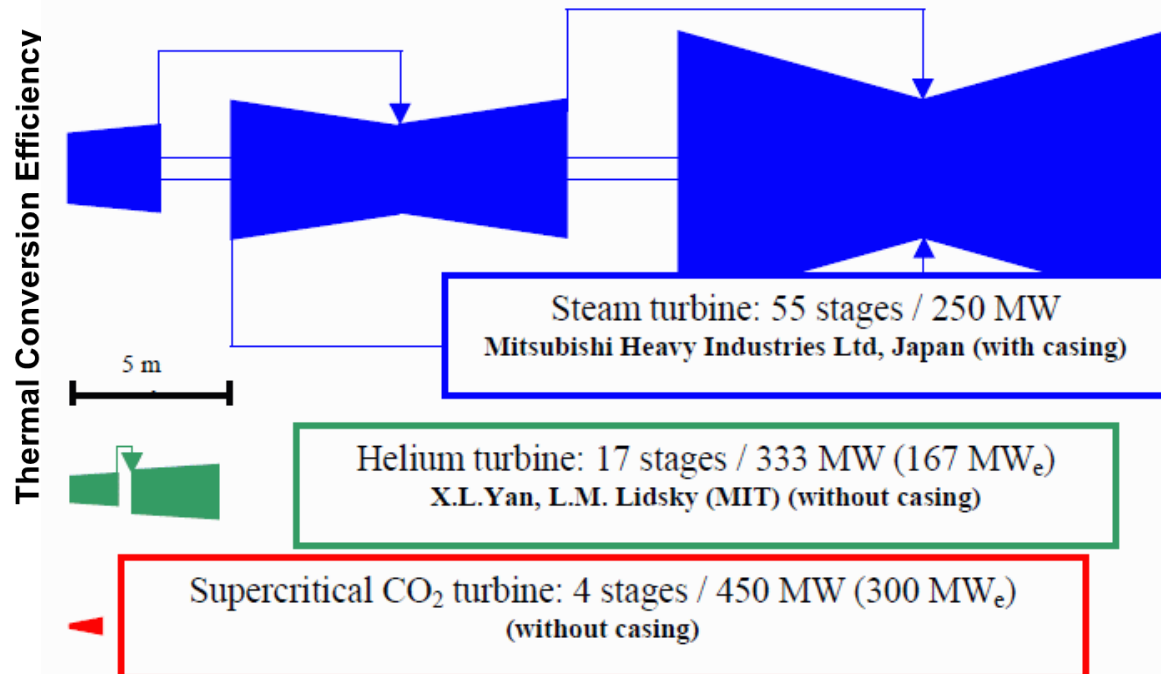
Attractive features of sCO₂ Brayton Cycle

- Higher efficiency than steam Rankine
- High density working fluid (compact turbomachinery)
- Low-cost, low toxicity
- Thermally stable fluid at temperatures of interest to CSP (550 °C to 750 °C)
- Single phase reduces operational complexity; integrates well with sensible heat storage in CSP systems

▪ Industry interest

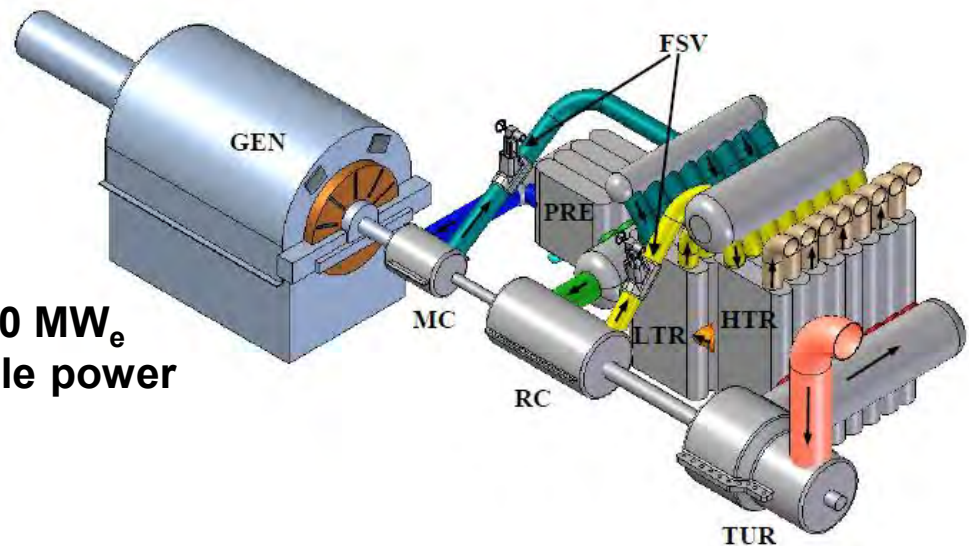
- Nuclear
- Fossil
- CSP
- Heat recovery
- Marine powering

Fig. 51 Comparison of turbine sizes for steam, helium and CO₂

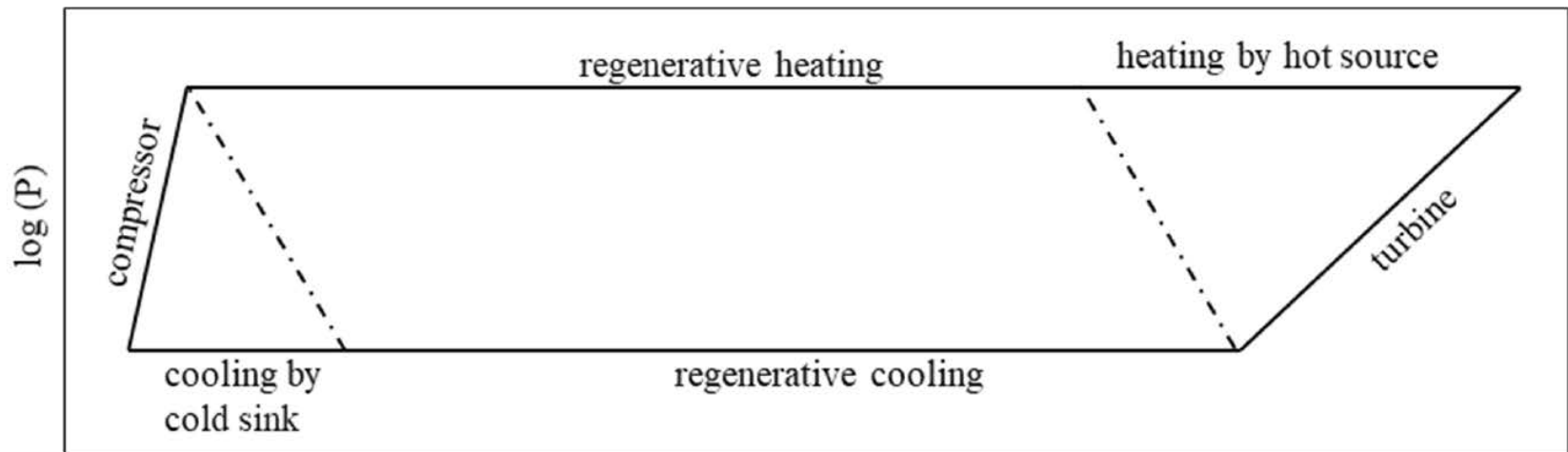
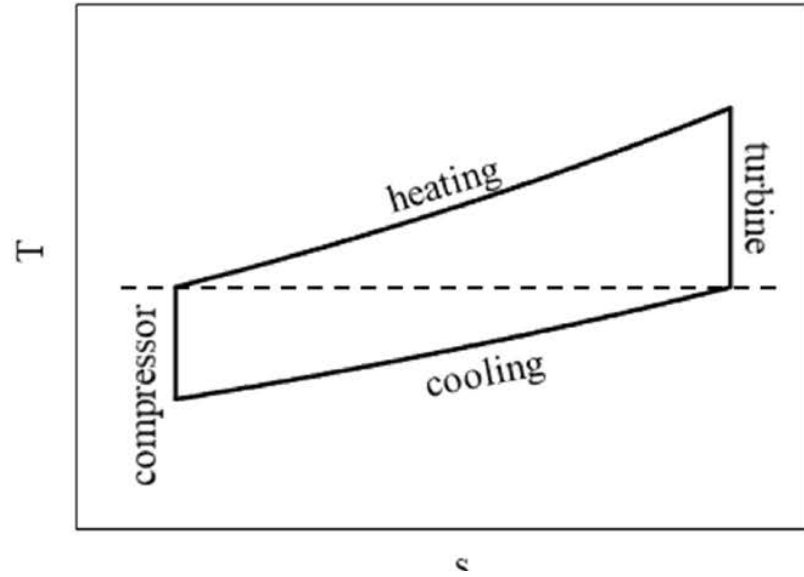
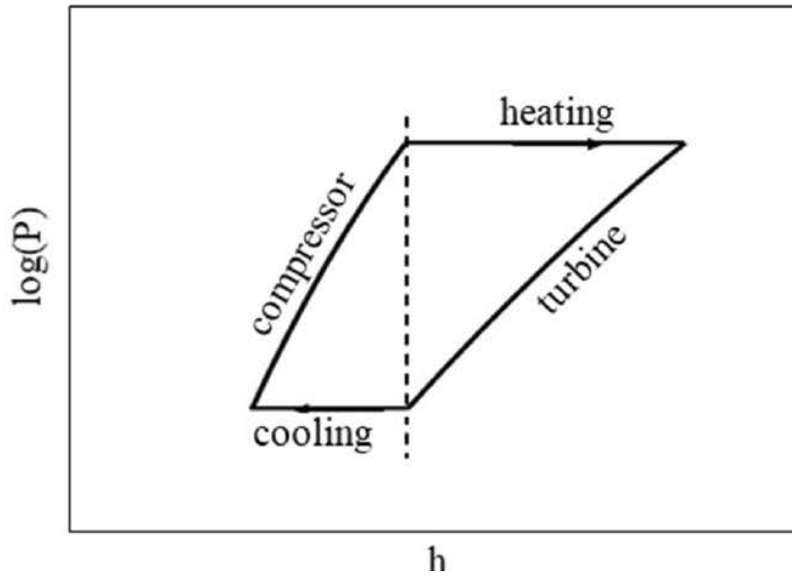


However, the cycle pressure ratio of the S-CO₂ Brayton cycle is much smaller compared with the steam Rankine cycle and the turbine outlet temperature is relatively high. Therefore, a large amount of heat must be recuperated to increase the thermal efficiency. In other words, the recuperation process in the S-CO₂ Brayton cycle greatly influences the thermal efficiency.

**MIT depiction of 150 MW_e
recompression-cycle power
system (2006)**

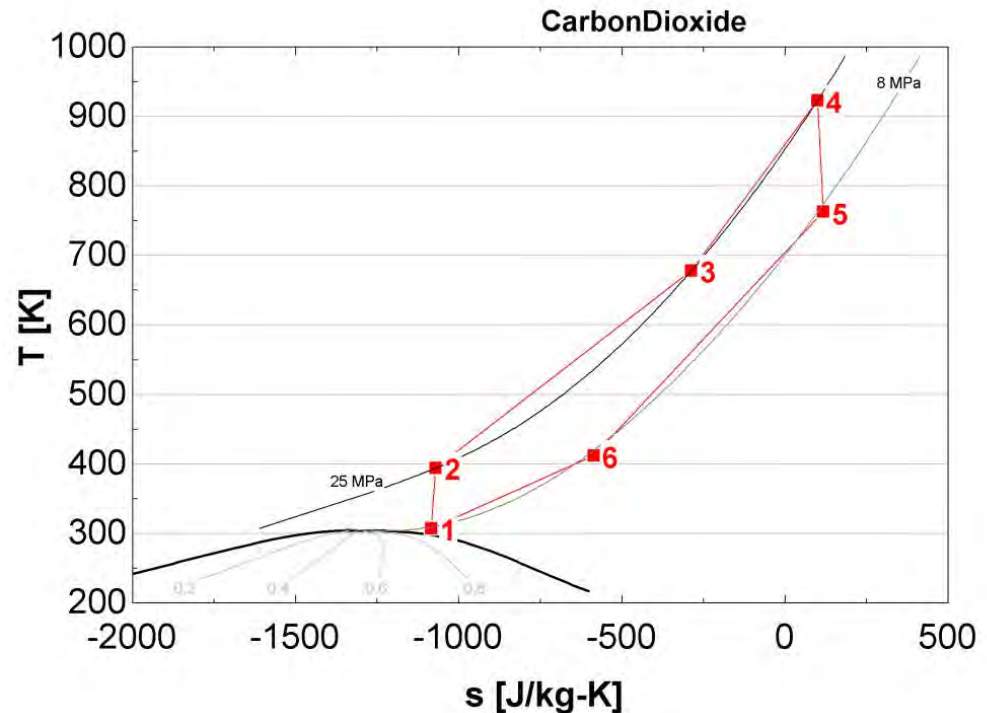
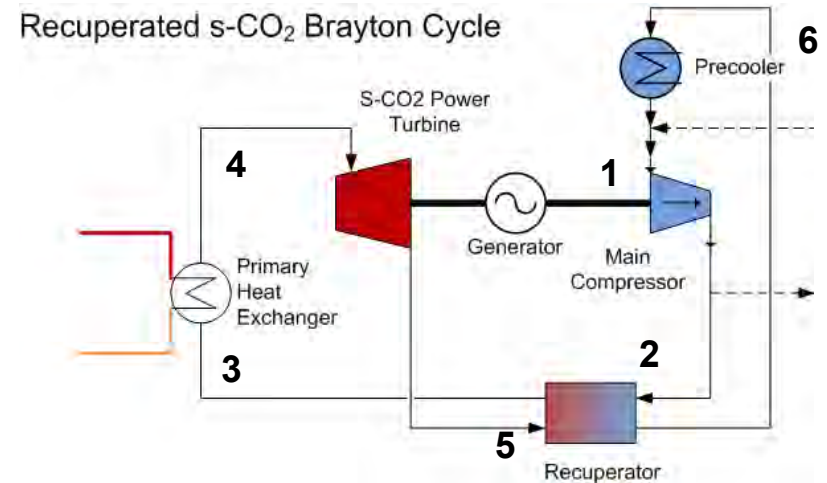
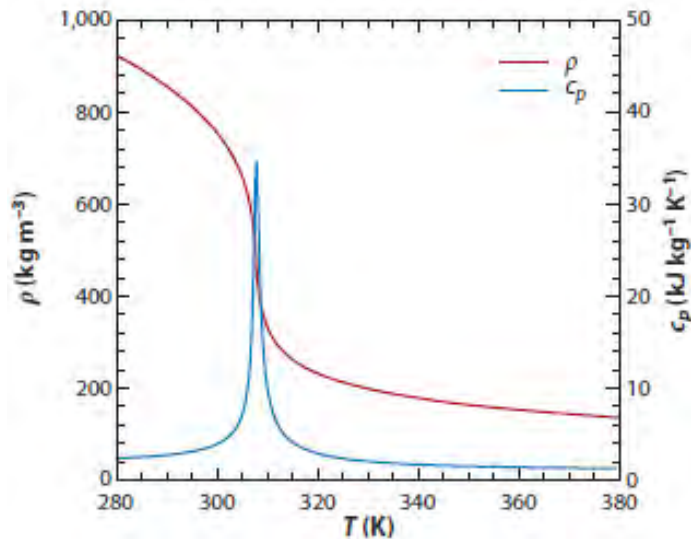


$$dh = Tds + vdP$$

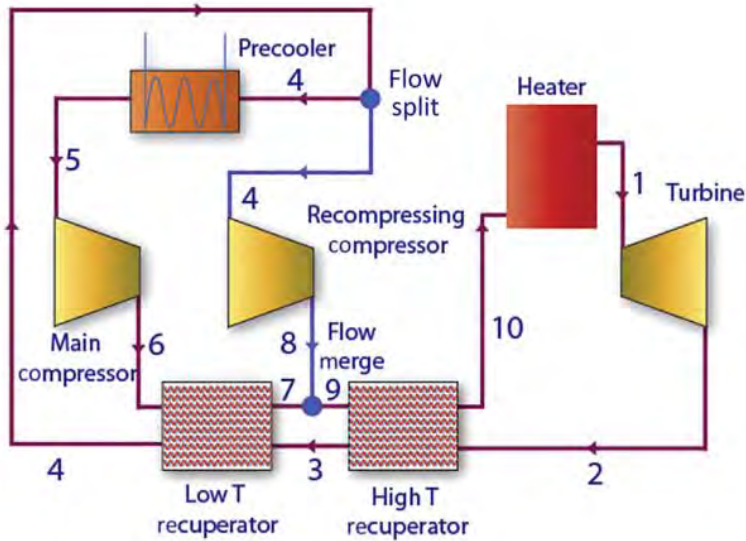


What is supercritical CO₂

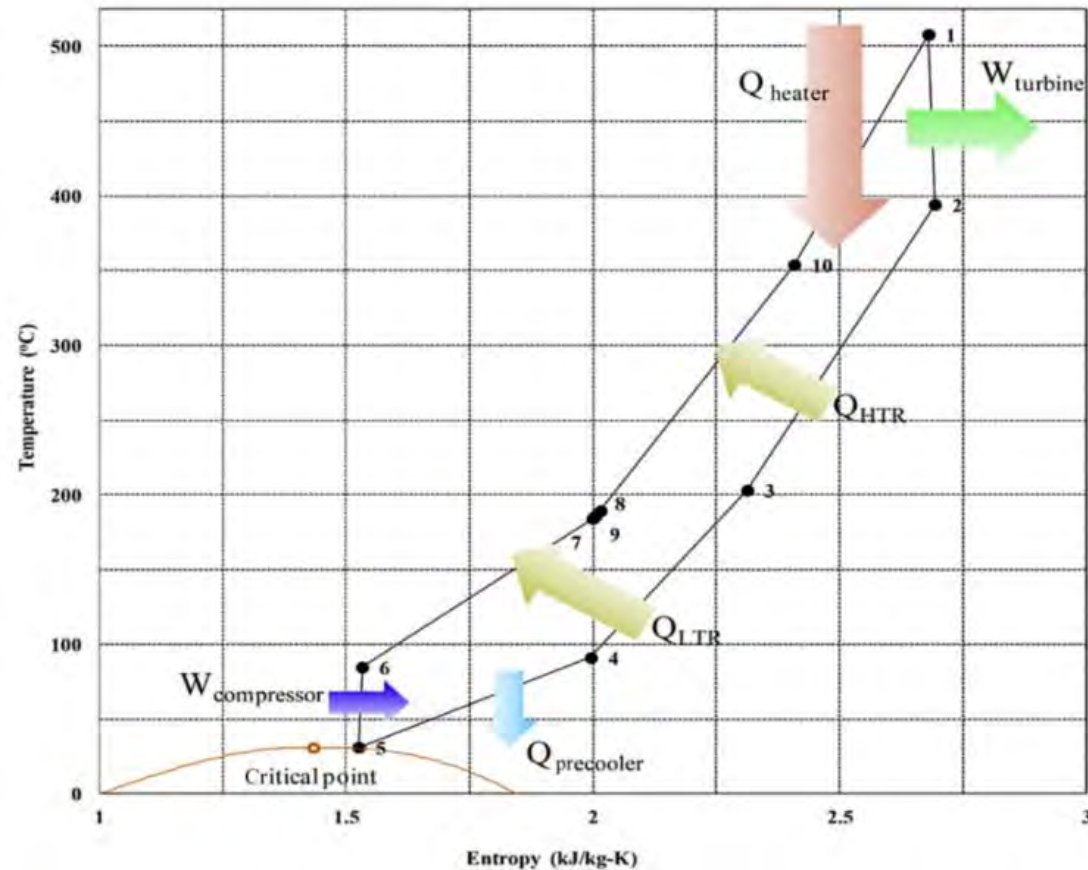
- sCO₂ is a fluid state above critical temperature and critical pressure
 - $p_{\text{crit}} = 73,9 \text{ bar}$
 - $T_{\text{crit}} = 31,1 \text{ °C}$
- Peculiar properties midway between a gas and a liquid (drastic changes near critical temperature)



Supercritical CO₂ Power Recompression Cycle



- Large amounts of heat must be recuperated
- Need of compact heat exchangers
- specific heat of the cold side flow is two to three times higher than that of the hot side flow in recuperators.
- CO₂ flow is split to compensate for the specific heat difference.
- Recompression improves
- Air cooling strong penalty

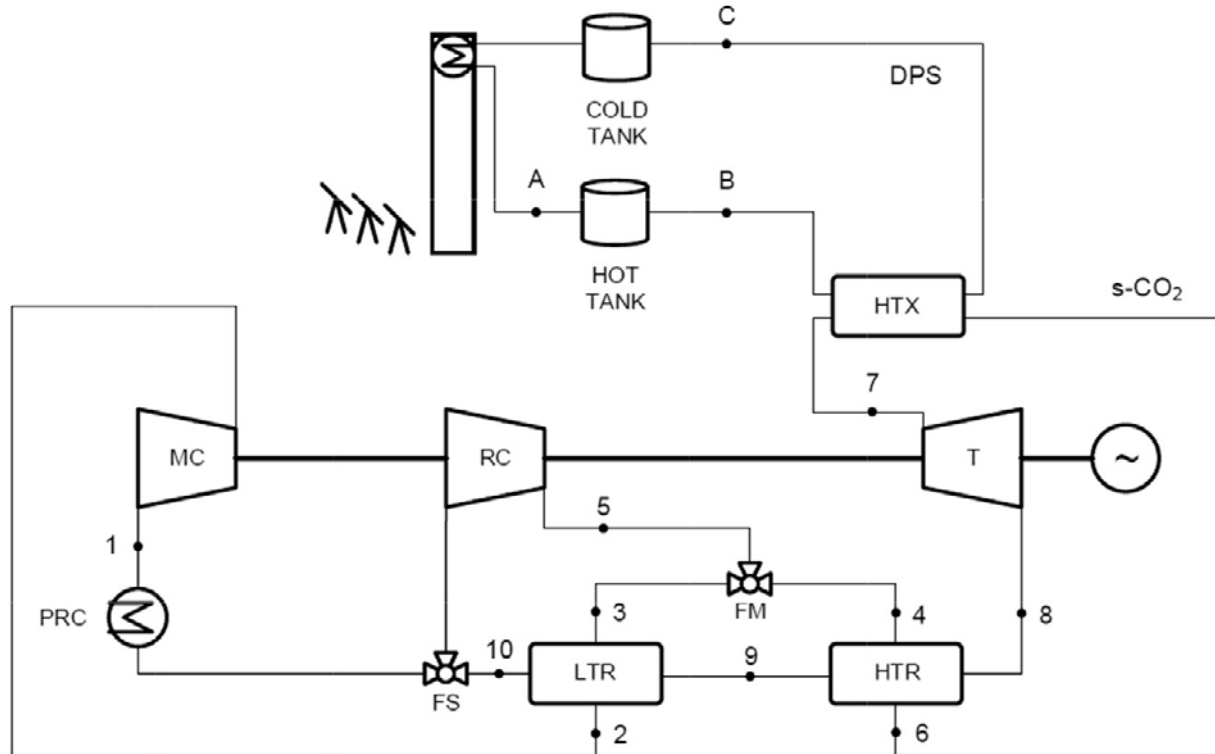


Ahn, Y. et al. (2015) *Nuclear Engineering and Technology*, 47(6), 647–661.

Supercritical CO2 Power Cycle Design: Boundary conditions

| | | SANDIA | NREL | Tokyo Institute of Technology | CEA Cadarache | MIT | Indian Institute of Science | IMDEA Energy |
|--|-------|-----------|------|-------------------------------------|------------------|------------|-----------------------------------|-----------------|
| Main Compressor Inlet Temperature | (°C) | 32-40 | 50 | 35 | 35 | 32-50 | 35-50 | 40 |
| Main Compressor Inlet Pressure | (bar) | 77-80 | - | 68-82.6 | 81-85 | - | 75-85 | 78 |
| Upper Pressure | (bar) | 200-300 | 250 | 120-260 | 253 | 150-300 | 200-300 | 248 |
| Turbine Inlet Temperature | (°C) | 400-750 | 650 | 650 | 497-515 | 550-700 | 550-750 | 650-730 |
| HT Recuperator Effectiveness | (-) | - | 0.97 | 0.91 | <0.925 | 0.93-0.98 | - | 0.88 |
| LT Recuperator Effectiveness | (-) | - | 0.97 | 0.91 | <0.925 | 0.88-0.94 | - | 0.85 |
| Minimum ΔT | (°C) | - | 5 | - | 10 | - | 10 | 10 |
| HP Turbine Efficiency | (-) | 0.90-0.93 | 0.93 | 0.92 | 0.93 | 0.90-0.93 | 0.75 | 0.92 |
| Compressor Efficiency | (-) | 0.85-0.87 | 0.88 | 0.88 | 0.87-0.88 | 0.89-0.95 | 0.8 | 0.88 |
| Relative Pressure Losses | (-) | 0.01 | - | 0.008-0.02 | 0 | 0.005-0.02 | 0.035 | 0.01 |
| Recompression Mass Fraction | (-) | 0.4 | - | 0.4 | 0.31-0.44 | 0.2-0.4 | 0.1-0.33 | 0.25 |
| Cycle Thermal Efficiency | (%) | 45.5-48.3 | 49.7 | 46.5-49.9 | 42.6-43.9 | 45.3-53.0 | 36.7-49.8 | 49.3 |

II. Supercritical SO₂ power cycle

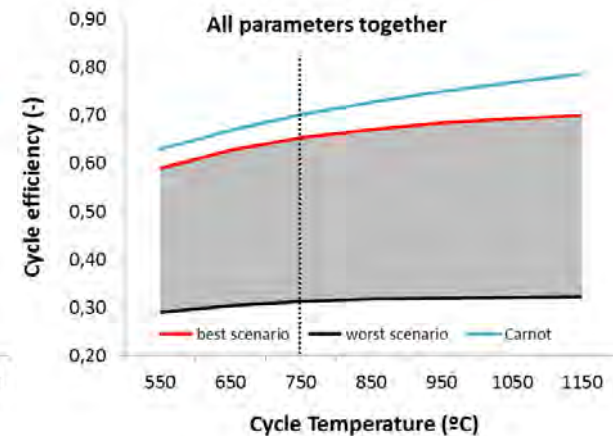
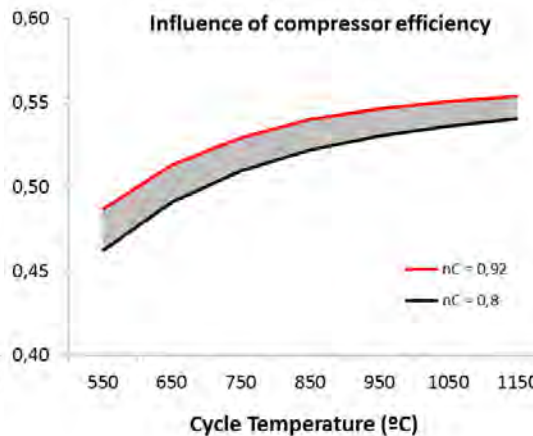
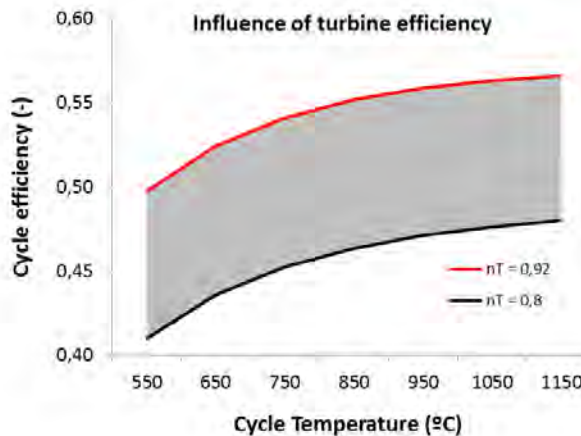
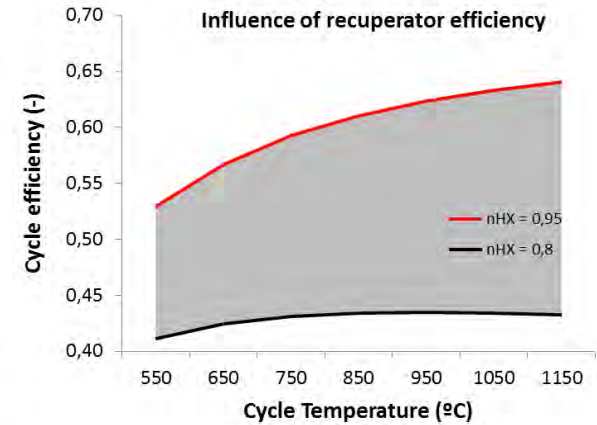
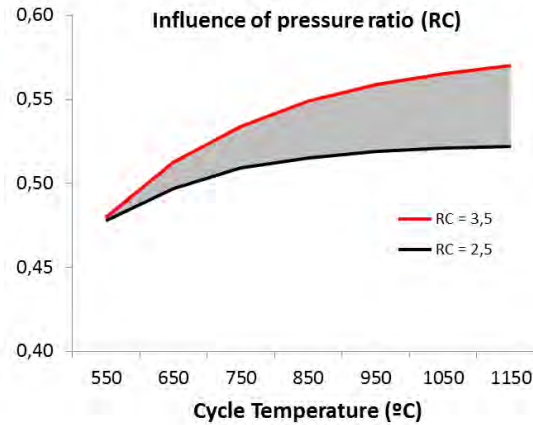
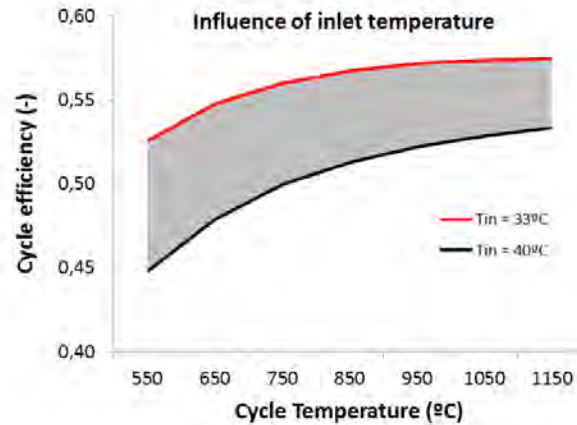


| Parameter | Unit | Value | Parameter | Unit | Value |
|-----------------------------------|------|-----------|----------------------------------|------|---------|
| Main compressor inlet temperature | °C | 33 - 40 | HT Recuperator effectiveness | % | 90 - 95 |
| Main compressor inlet pressure | bar | 78 | LT Recuperator effectiveness | % | 90 - 95 |
| Turbine inlet temperature | °C | 650 - 730 | Turbine isentropic efficiency | % | 92 |
| Upper pressure | bar | 248 | Compressor isentropic efficiency | % | 88 |

II. Supercritical SO_2 power cycle

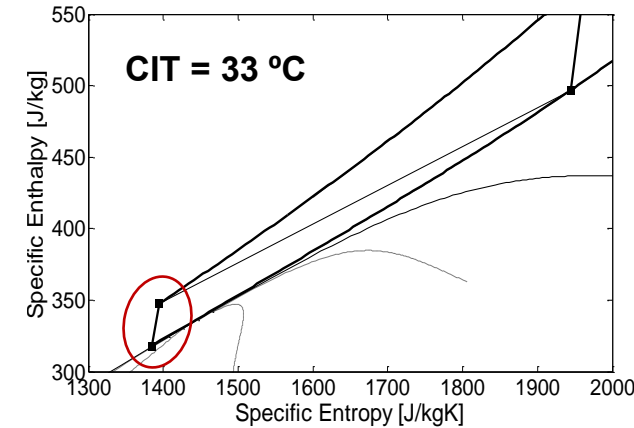
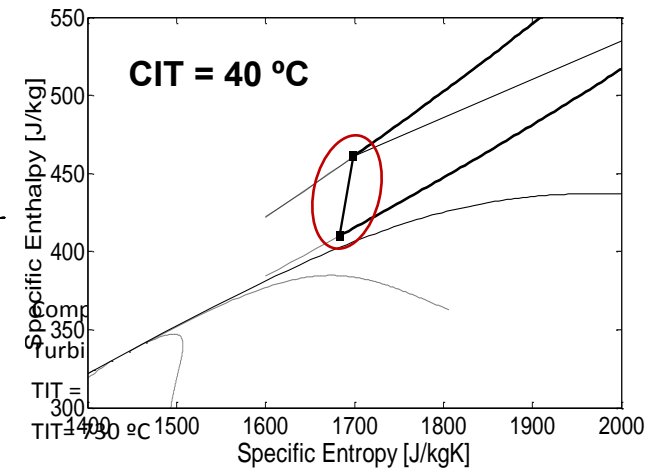
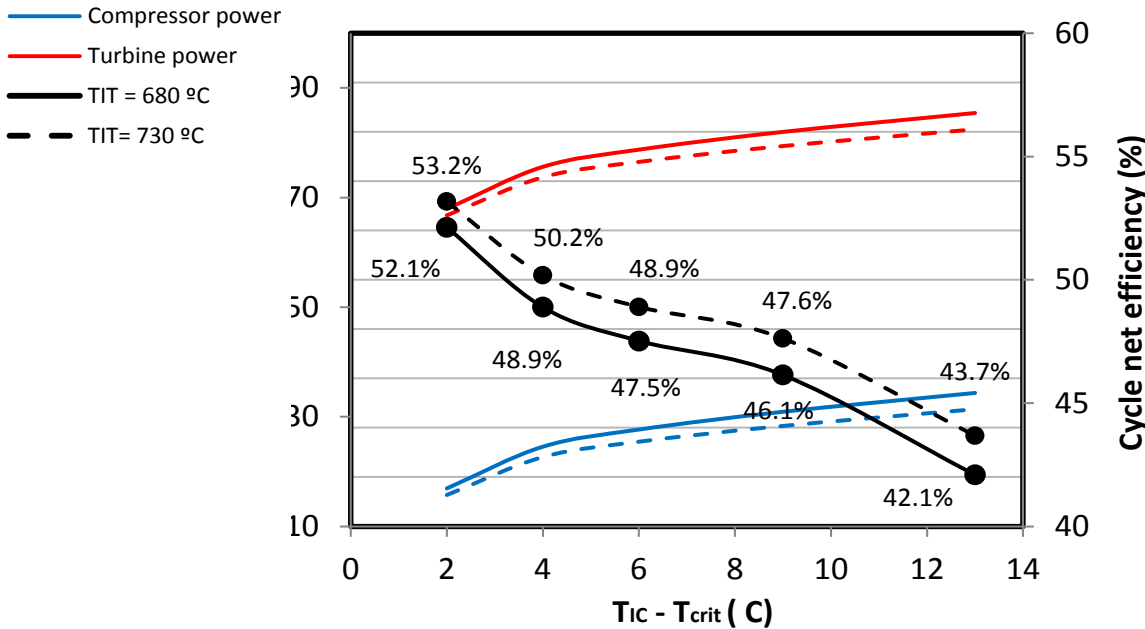
➤ Sensitivity study

| Cycle- efficiency (reference case) | | | 51% |
|------------------------------------|--------|------------------------|-----|
| Inlet temperature | 35 °C | Compressor efficiency | 0.9 |
| Maximum temperature | 650 °C | Turbine efficiency | 0.9 |
| Pressure ratio | 3 | Recuperator efficiency | 0.9 |



II. Supercritical SO_2 power cycle

(Effect of hot and cold temperatures)



$T_{crit} = 31,1 \text{ } ^\circ\text{C}$

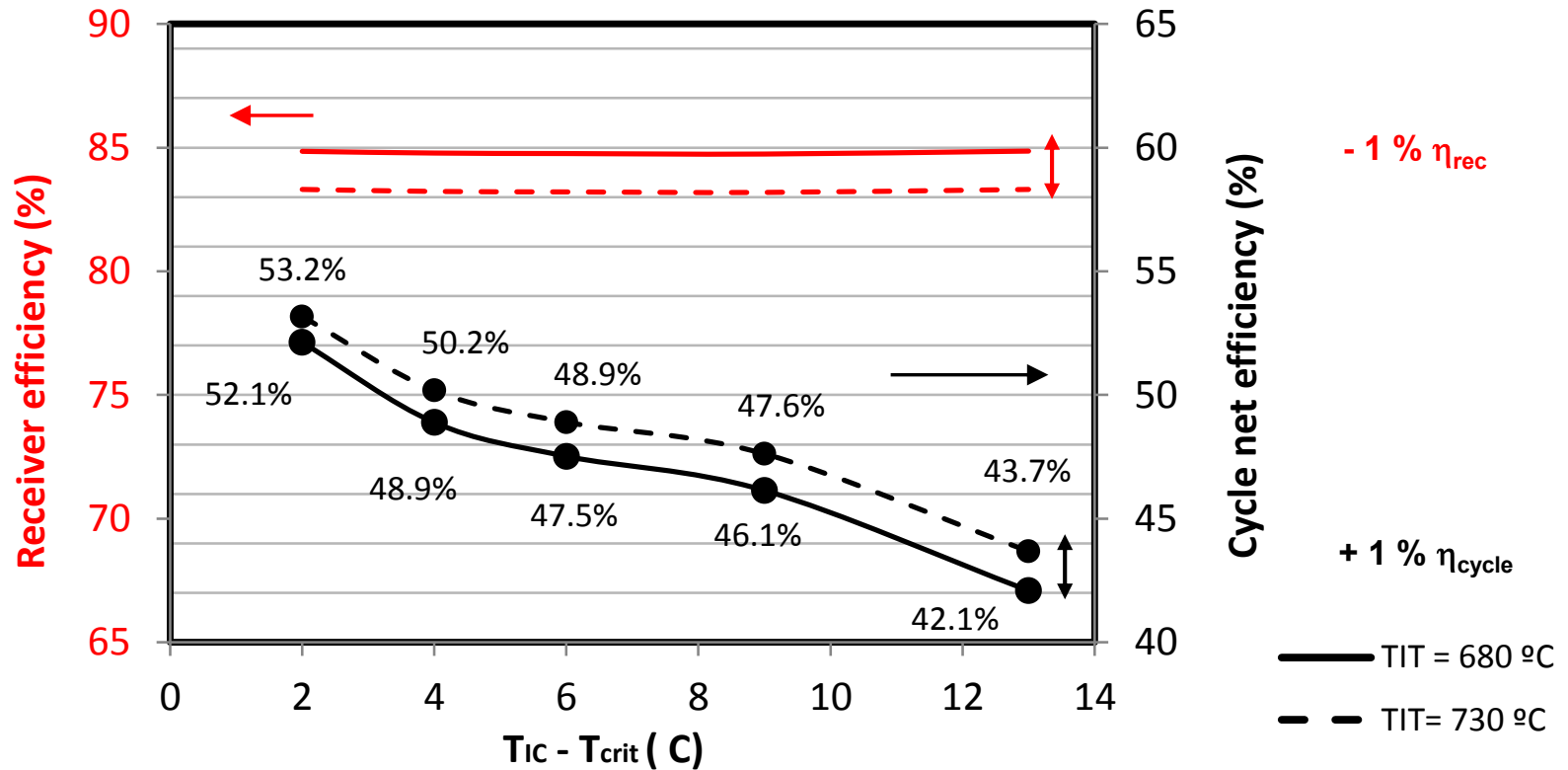
| Parameter | Unit | Case 1 | Case 2 | Case 3 | Case 4 |
|----------------------------------|------------------|--------|--------|--------|--------|
| Compressor inlet temperature | $^\circ\text{C}$ | 33 | 40 | 33 | 40 |
| Turbine inlet temperature | $^\circ\text{C}$ | 680 | 680 | 730 | 730 |
| LP Compressor inlet pressure | bar | 78 | 78 | 78 | 78 |
| HP Compressor outlet pressure | bar | 248 | 248 | 248 | 248 |
| LP Compressor power consumption | MW | 9.02 | 18.65 | 8.38 | 17.09 |
| HP Compressor power consumption | MW | 7.91 | 12.26 | 7.35 | 11.24 |
| Turbine power production | MW | 67.94 | 81.98 | 66.76 | 79.40 |
| Power cycle net power production | MW | 50 | 50 | 50 | 50 |
| sCO_2 mass flow | kg/s | 401.14 | 484.02 | 373.02 | 443.67 |
| Cycle thermal efficiency | % | 53.20 | 47.13 | 54.25 | 48.64 |
| Net cycle efficiency | % | 52.13 | 46.14 | 53.17 | 47.62 |

Conclusions:

- CIT severe effect on η_{net}
- TIT small effect on η_{net}

II. Supercritical SO₂ power cycle

(Effect of hot temperatures and receiver)

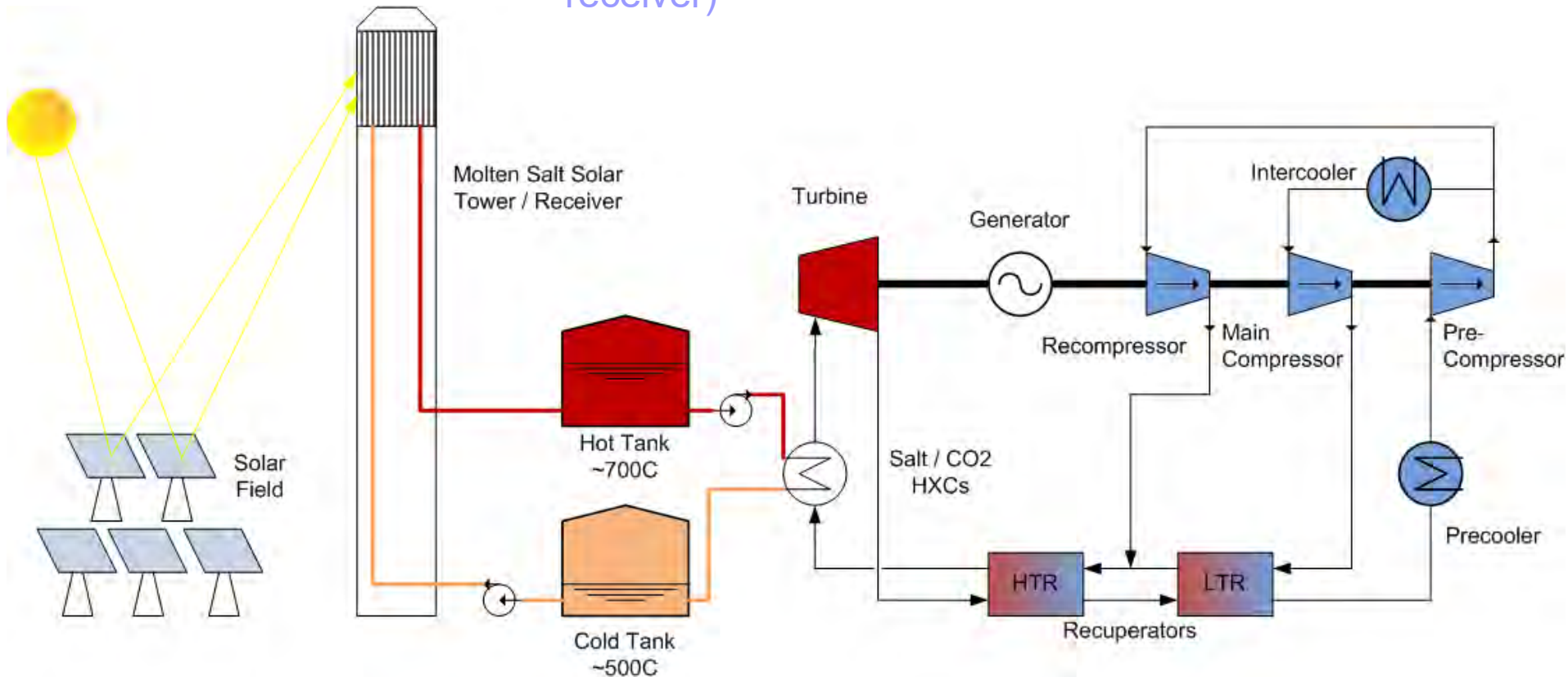


Conclusions:

➤ Increasing 50 °C TIT → + 1 % η_{cycle} but - 1 % η_{rec}

CSP with sCO₂ Conceptual Design – example

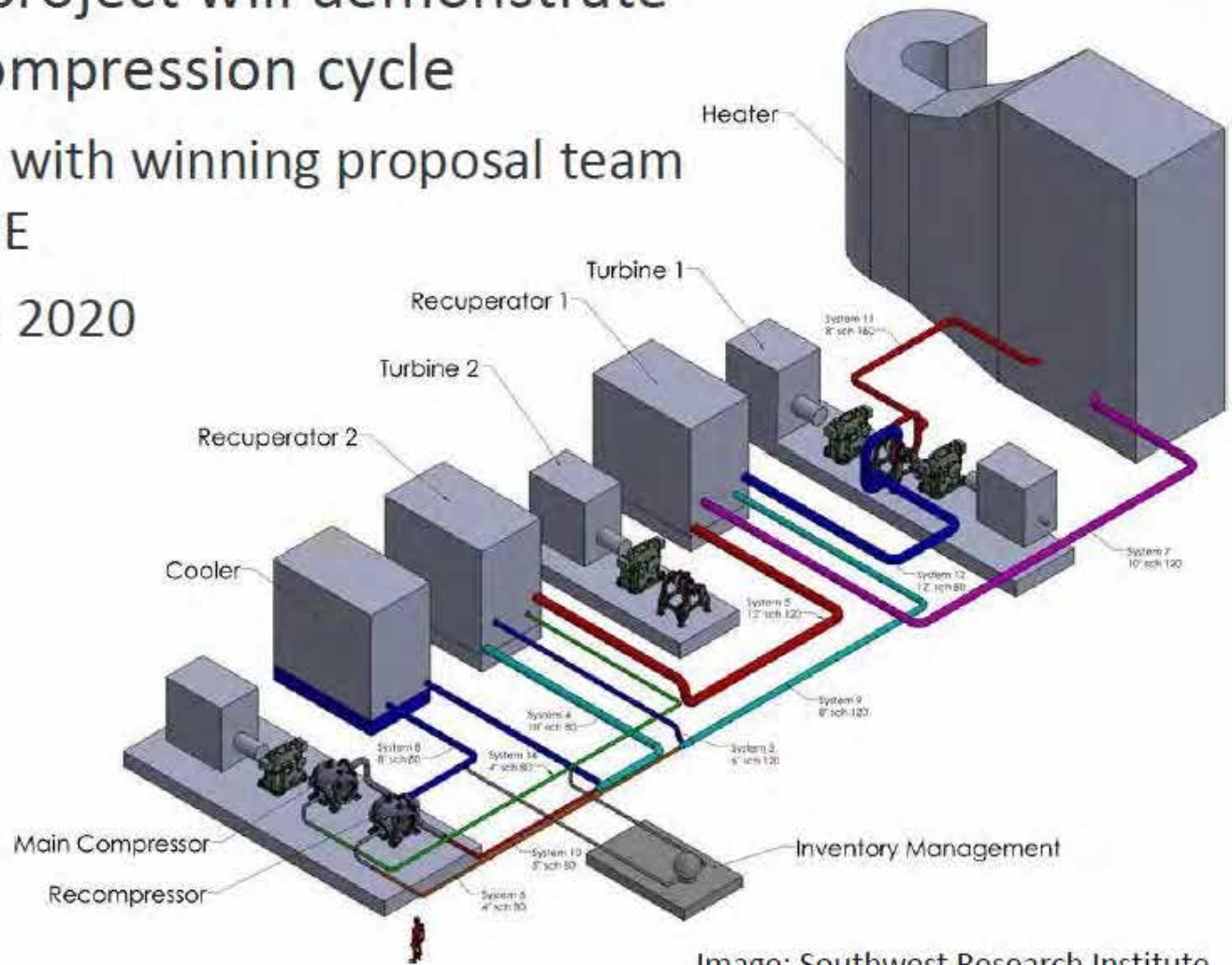
Dry-cooled, “partial-cooling” cycle coupled to high-temperature molten salt power tower (or particle receiver)



sCO₂ Cycle Development under STEP

DOE's "STEP" project will demonstrate a 10 MW_e recompression cycle

- In negotiation with winning proposal team of GTI/SwRI/GE
- Operational in 2020



Supercritical
Transformational
Electric
Power

Image: Southwest Research Institute

Supercritical Transformational Electric Power (STEP)

Cross-program DOE initiative to demonstrate the sCO₂ power cycle at commercial scale.

Up to \$80M federal contribution, 20% industry cost share, and 6-year duration (see DE-FOA-0001457, released March 2016)

10 MW_e Pilot Plant Test Facility:

sCO₂ Recompression Brayton Cycle at turbine inlet operating temperatures of 700°C,

Reconfigurable facility to support testing a variety of components or subsystems, and

Capability to monitor and characterize primary components or subsystems (turbomachinery, heat exchangers, recuperators, bearings, seals, etc.)

Map pathway towards an overall power cycle efficiency of 50% or greater

Demonstrate steady-state, dynamic, transient load following, and limited endurance operations

sCO₂ Brayton Cycle Research Activities

- Corrosion and materials compatibility data at high T, P
 - Cost-effective and durable recuperators
 - Design and validation of primary heat exchangers; understanding of sCO₂/HTF interactions
 - Validation of power turbine bearings, seals, stop-valves
 - Modeling start/stop, off-design and other transient operations
 - Cycle operating methodology for dry-cooled systems
 - Demonstration of cycle operations and equipment durability at commercially relevant scale (10 MW_e)
-
- Major research institutions and power companies from around the world are engaged in its development
 - E.g., GE, Dresser-Rand, Toshiba, Samsung

SCO₂-Flex: design a 25MWe coal-fired SCO₂ cycle



SCO2-Flex Objective

Developing and validating (at simulation level the global cycle and at relevant environment) a scalable/modular design of a **25MWe Brayton cycle using supercritical CO₂**, able to increase the operational **flexibility** and the **efficiency** of existing and future coal and lignite power plants

Budget

- 5.6 million Euros (~42 million RMB)

EDF's role in this project

- Project management
- Thermodynamic and process engineering
- SCO₂ Brayton cycle specification

Partners

- | | |
|--|--|
| <ul style="list-style-type: none"> • BAKER HUGHES, GE • UJV REZ • CENTRO SVILUPPO MATERIALI • CENTRUM VYZKUMU REZ • FIVES | <ul style="list-style-type: none"> • ZABALA • POLITECNICO DI MILANO, • UNIVERSITAET DUISBURG-ESSEN, • UNIVERSITAET STUTTART. |
|--|--|



Offen im Denken



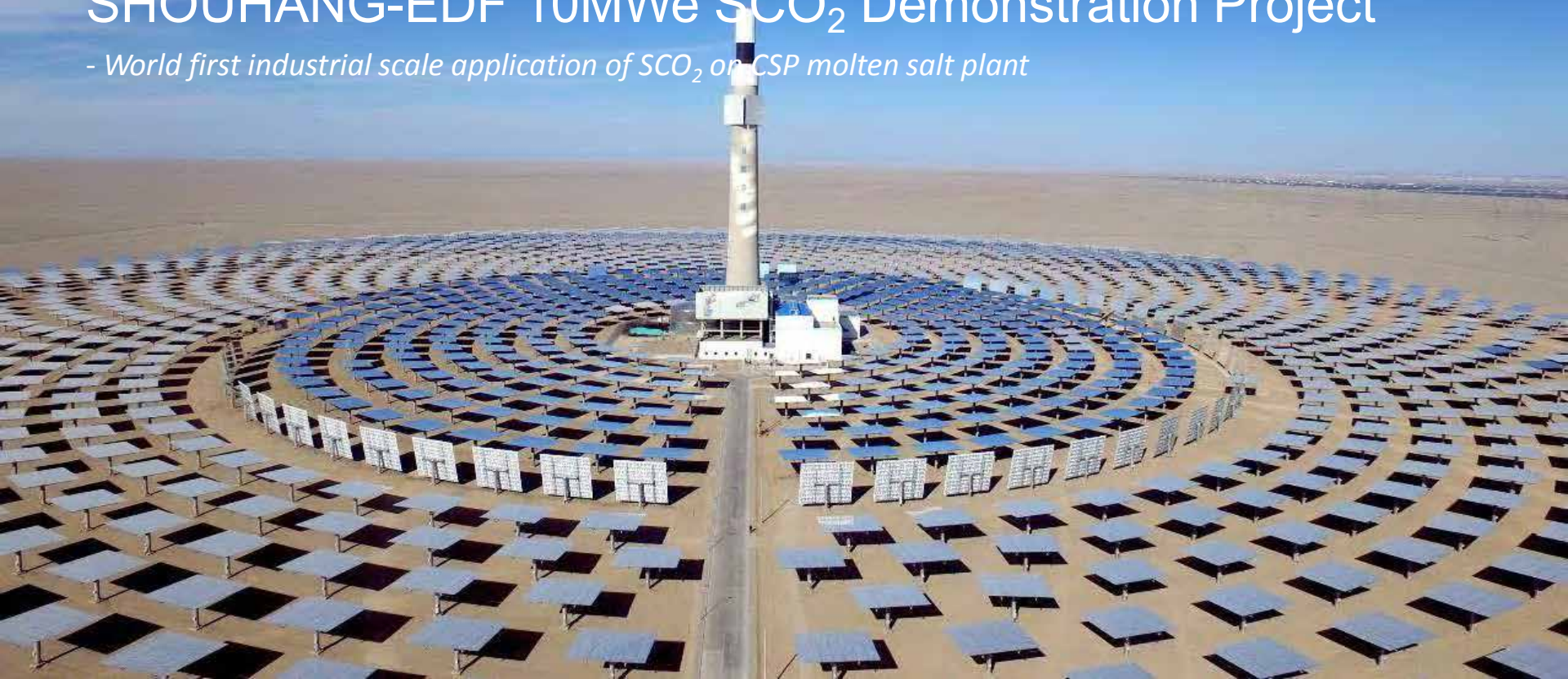
Universität Stuttgart



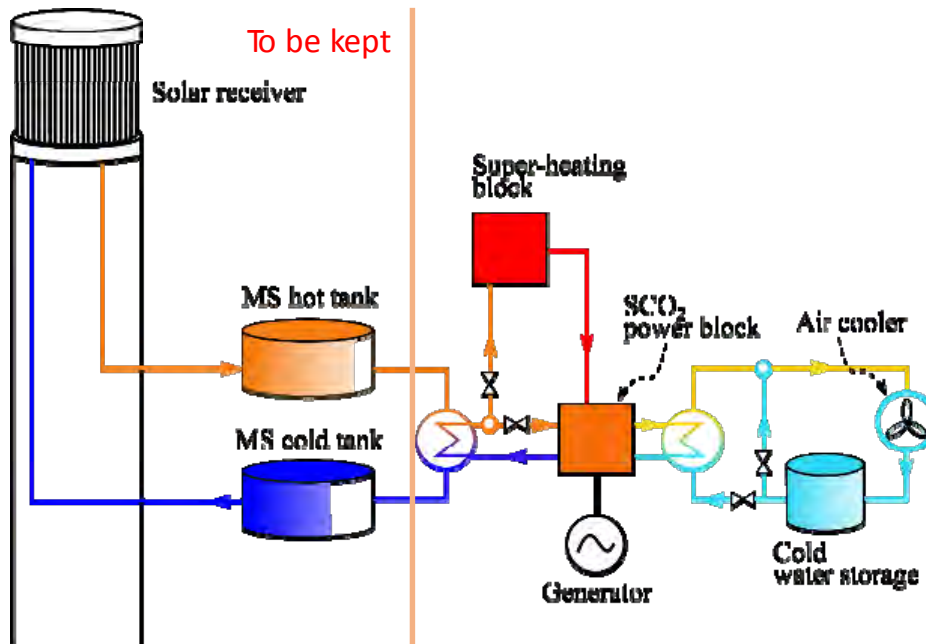


SHOUHANG-EDF 10MWe SCO_2 Demonstration Project

- World first industrial scale application of SCO_2 on CSP molten salt plant



Shouhang-EDF 10MWe SCO_2 demo project: system concept



System design concept

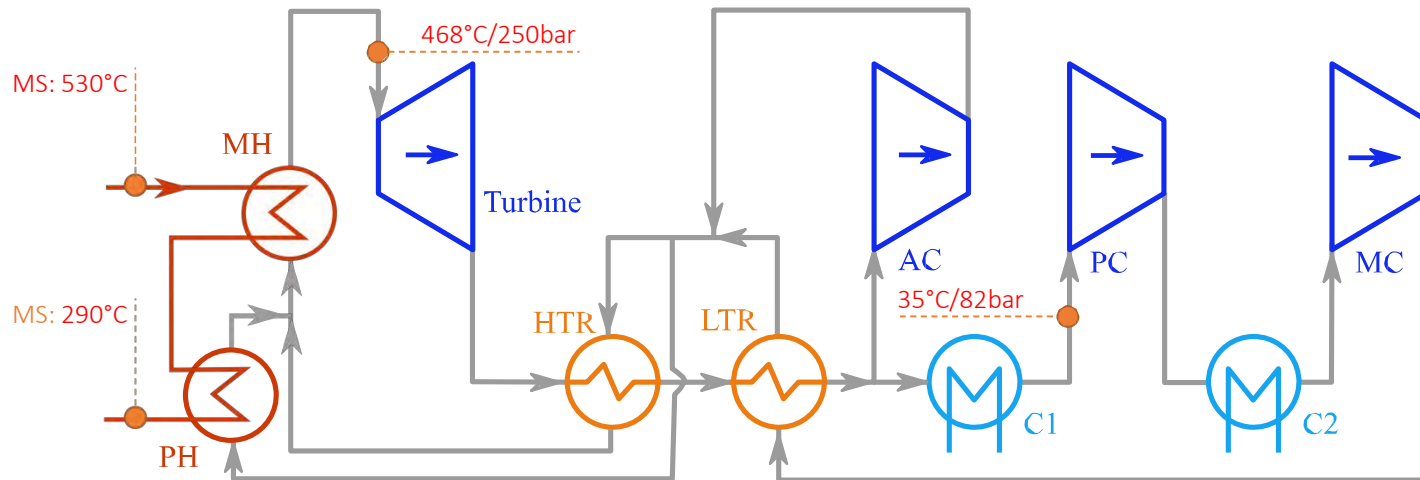
- Keep the current solar field
- Keep the current thermal storage system
- Install a 10MWe SCO_2 power block in parallel with the current 10MWe water steam Rankine cycle
- Use dry cooling
- Optimized cycle for CSP application
- Super-heating to further increase CO_2 temperature to a $>600\text{ }^\circ\text{C}$

Cycle design for Shouhang-EDF SCO₂ project: recompression cycle with intercooling and preheating

Key cycle features:

- Recompression to increase the recuperation effectiveness
- Intercooling to reduce compressor consumption and to increase thermal storage utilization
- Pre-heating to better utilize the low-temperature molten salt

Cycle net efficiency: 35.6%
Thermal storage utilization: 100%
Design power output: 10.3MWe

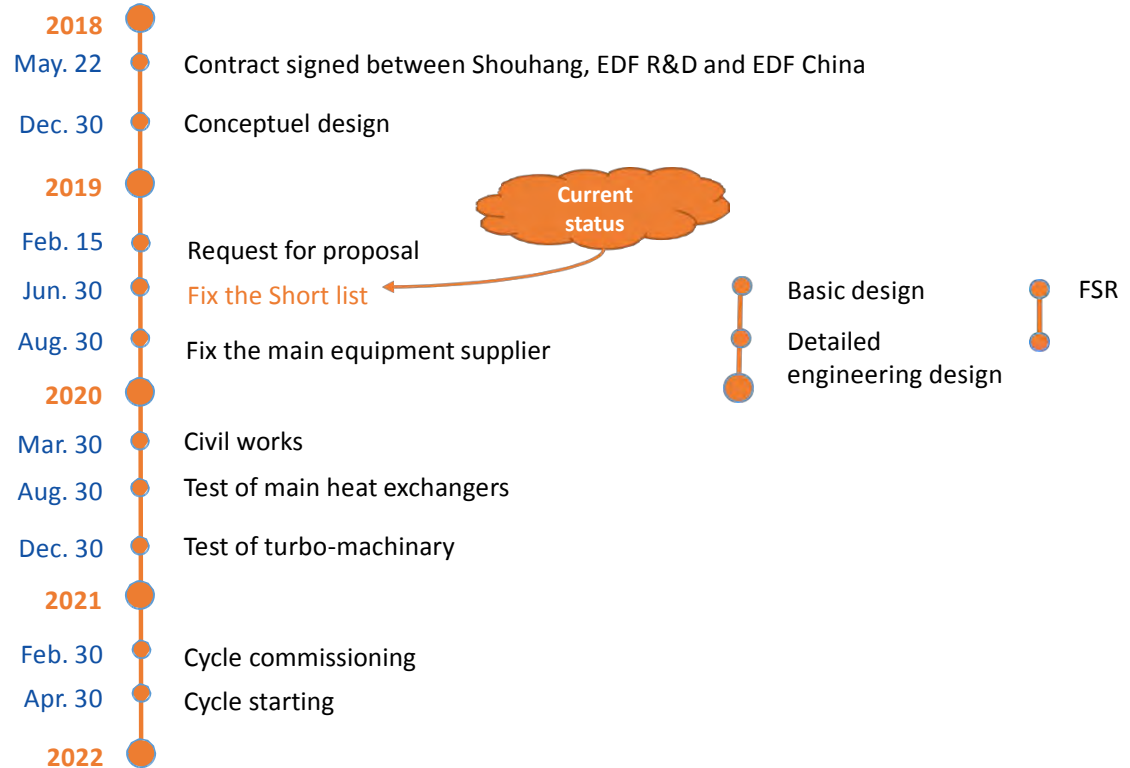


Commercial interest for SCO_2 cycle: Even with a not so- complex cycle, it could achieve higher efficiency

For a recompression cycle with intercooling and pre-heating



Shouhang-EDF 10MWe SCO₂ demo project: Brief planning



Conclusions

- The thermal efficiency can be increased up to 5% point compared with the steam Rankine cycle.
- The turbomachinery can be much smaller and the overall system size can be reduced up to four times compared with the conventional steam Rankine cycle.
- Efficiency very sensitive to CIT.
- The competitiveness of the dry air cooled S-CO₂ cycle has been investigated by multiple researchers without consensus
- Recuperation becomes critical and recuperators require very compact designs
- Early demonstrations foreseen in couple of years with CSP

References

- *Optimization of a recompression supercritical carbon dioxide cycle for an innovative central receiver solar power plant*, M.A. Reyes-Belmonte, A. Sebastián, M. Romero, J. González-Aguilar, Energy 2016)– Vol. 112 – pp: 17-27
- *Annual performance of subcritical Rankine cycle coupled to an innovative particle receiver solar power plant*, M.A. Reyes-Belmonte, A. Sebastián, J. Spelling, M. Romero, J. González-Aguilar Renewable Energy 130 (2019) 786-795
- *Flexible electricity dispatch for CSP plant using un-fired closed air Brayton cycle with particles based thermal energy storage system*. F. Rovense, M.A. Reyes-Belmonte, J. Gonzalez-Aguilar, M. Amelio S. Bova, M. Romero. Energy 173 (2019) 971-984
- *Particles-based Thermal Energy Storage Systems for Concentrated Solar Power Applications*, M.A. Reyes-Belmonte, E. Diaz, J. González-Aguilar, M. Romero, SolarPACES 2017
- *Heat Exchanger Modelling in Central Receiver Solar Power Plant Using Dense Particle Suspension*, M.A. Reyes-Belmonte, F. Gómez-García, J. González-Aguilar, M. Romero, H. Benoit, G. Flamant, AIP Conference Proceedings 1850 (1), 030042
- *Performance Comparison of Different Thermodynamic Cycles for an Innovative Central Receiver Solar Power Plant*, M.A. Reyes-Belmonte, A. Sebastián, J. González-Aguilar, M. Romero, AIP Conference Proceedings 1850 (1), 160024
- *Preliminary design and performance analysis of a multi-megawatt scale dense particle suspension receiver*, A. Gallo, J. Spelling, M. Romero, J. González-Aguilar, SolarPACES 2014
- *Plant layout proposal: A high-efficiency solar thermal power plant using a dense particle suspension as the heat transfer fluid*, J. Spelling, A. Gallo, M. Romero, J. González-Aguilar. SolarPACES 2014

Thank you for your attention



SFERA-III

Solar Facilities for the European Research Area



1st Summer School “Thermal energy storage systems, solar fields and new cycles for future CSP plants”

WP1 Capacity building and training activities

Odeillo, France, September 9th-11th 2019

Hybrid CSP – PV Plants

Examples and simulations using **greenius**

Daniel Benitez, DLR

NETWORKING



THIS PROJECT HAS RECEIVED FUNDING FROM THE EUROPEAN UNION'S HORIZON 2020 RESEARCH AND INNOVATION PROGRAMME UNDER GRANT AGREEMENT NO **823802**

Content

| | |
|---------------|---|
| 16:30 – 16:40 | Concepts and examples about hybrid CSP-PV plants |
| 16:40 – 16:50 | General introduction on the greenius software |
| 16:50 – 17:20 | Setting up a simulation of a hybrid power plant with solar tower, fossil back-up and PV |
| 17:20 – 17:30 | Questions and discussions |

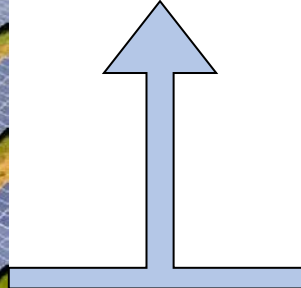
What are hybrid CSP – PV plants?

Decoupled non-compact (or co-located) PV-CSP hybrid: independent CSP and PV plants integrated together by the electric power dispatching and management system

Energy coupled PV-CSP hybrid: Via PV-topping technology, spectral beam splitting (SBS) technology or their combination. *New Trend: PV power in CSP plant's thermal energy storage?*



PV plant. Source: www.zdnet.com



Bokpoort CSP Plant (Sener). Source: www.solarpaces.org

Why hybrid CSP – PV plants?

For solar systems, **PV offers the lowest Levelized Cost of Electricity (LCOE) of around 3 cent€/kWh**

Storage system (batteries) for commercial PV plants are too expensive (400 – 600 €/kWh_e)

CSP integrates low cost energy storage for a total LCOE of around 7 cent€/kWh (about 20 - 35 €/kWh_{th} for the storage)

➡ **The hybridization of both technologies combines their main advantages:**

Low investment cost of PV

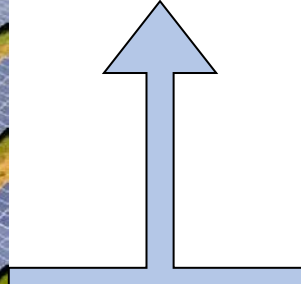
+

cheap storage capability of CSP

= 24/7 power at an “average” LCOE around 5 cent€/kWh



PV plant. Source: www.zdnet.com



Bokpoort CSP Plant (Sener). Source: www.solarpaces.org

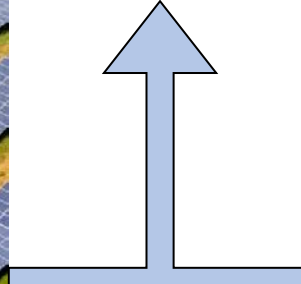
Why hybrid CSP – PV plants?

Key Features of PV plants:

- Low investment costs
- Low site preparation required
- Low Operation & Maintenance efforts
- Very low water consumption
- Expensive energy storage = unstable electricity generation



PV plant. Source: www.zdnet.com



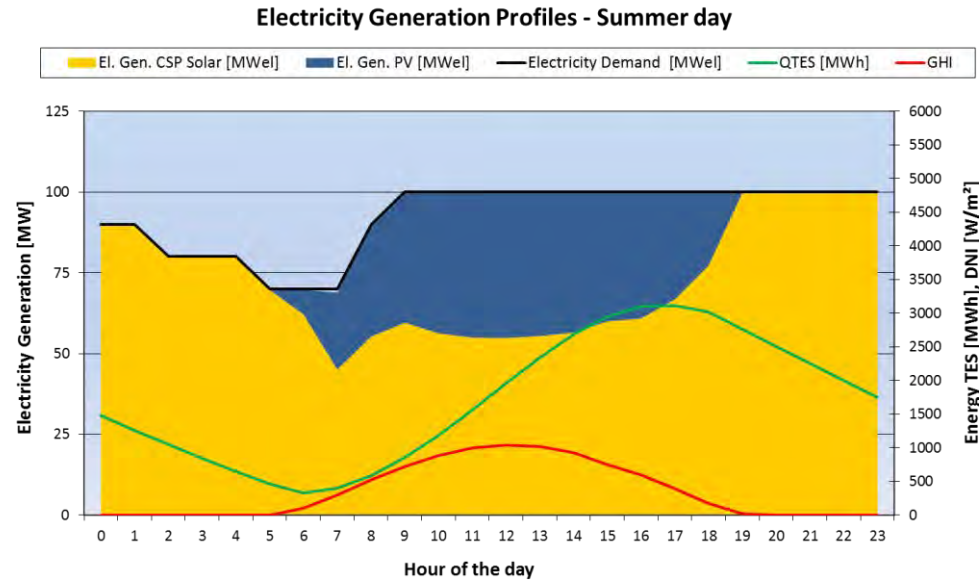
Key Features of CSP plants:

- More difficult site selection & preparation
- Use of Direct Normal Irradiance (DNI)
- Operation & Maintenance efforts similar to a conventional power plant
- Medium to high water consumption
- Cheap energy storage = base load electricity generation



Bokpoort CSP Plant (Sener). Source: www.solarpaces.org

Why hybrid CSP – PV plants?



PV plant. Source: www.zdnet.com



Bokpoort CSP Plant (Sener). Source: www.solarpaces.org

Examples of Hybrid CSP – PV plants



SFERA-III

Solar Facilities for the European Research Area

Plant name: Cerro Dominador (previously Atacama-1)

Location: Calama, Chile

CSP capacity: 110 MW (net)

Storage capacity: 17,5 hours (2-tanks molten salt)

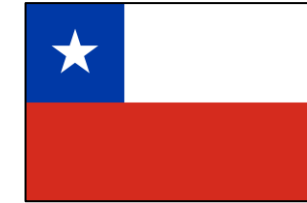
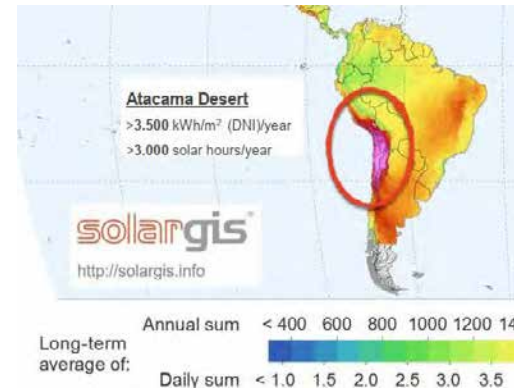
Number of heliostats: 10.600

Tower height: 250 m

PV capacity: 100 MW

Total electrical power capacity: 210 MW

Current status: under construction
(~80% completion by July 2019)



SFERA-III

Solar Facilities for the European Research Area

Plant name: NOOR Middelt

Location: Middelt, Morocco

CSP capacity: 2 x 150 to 190 MW

Storage capacity: TBD, minimum 5 hours

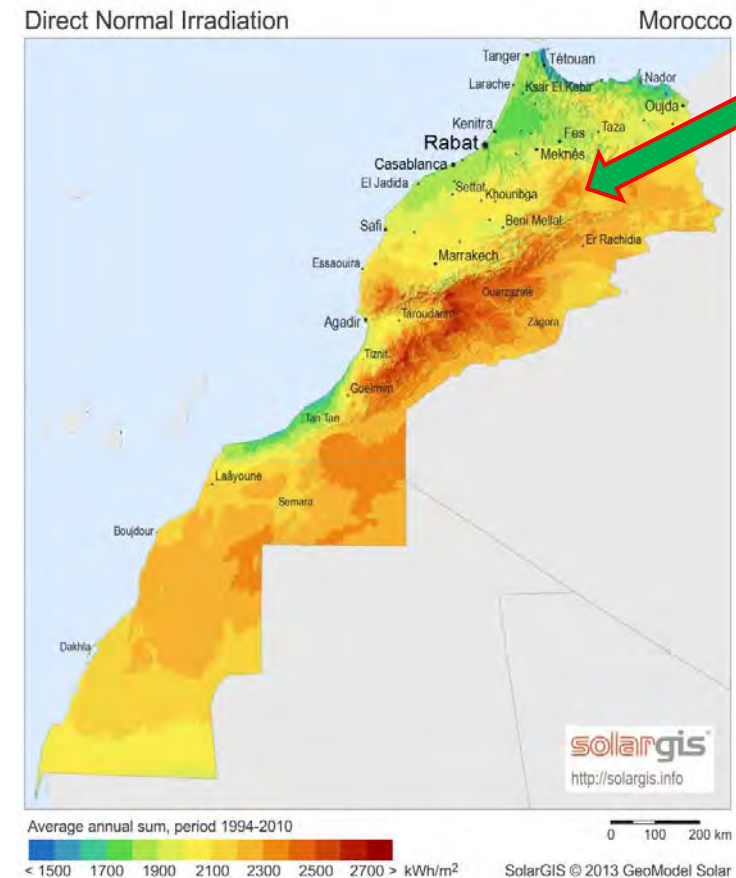
CSP technology: TBD, probably parabolic troughs

PV capacity: 2 x 210 to 250 MW

Total electrical power capacity: 2 x 400 = 800 MW

Record lowest LCOE: 7 \$cent / kWh

Current status: Consortium selected (EDF EN 35%, Masdar 30%, Green of Africa 10%, and 25% by MASEN), next financial steps ongoing.



SFERA-III

Solar Facilities for the European Research Area

Plant name: Noor Energy 1

Location: Dubai

CSP capacity: 700 MW

Storage capacity: 15 hours

CSP technology: parabolic trough 3 x 200 MW
tower system 1 x 100 Mwe

Tower height: 260 m

PV capacity: 250 MW

Total park power capacity: 950 MW

PPA of 7,3 cent\$/kWh (35 years)

Current status: under construction
(completion expected end 2022)



SFERA-III

Solar Facilities for the European Research Area

Plant name: Distrito Tecnológico Solar Diego de Almagro

Location: Diego de Almagro, Chile

CSP capacity: 6 x 110 MW (net)

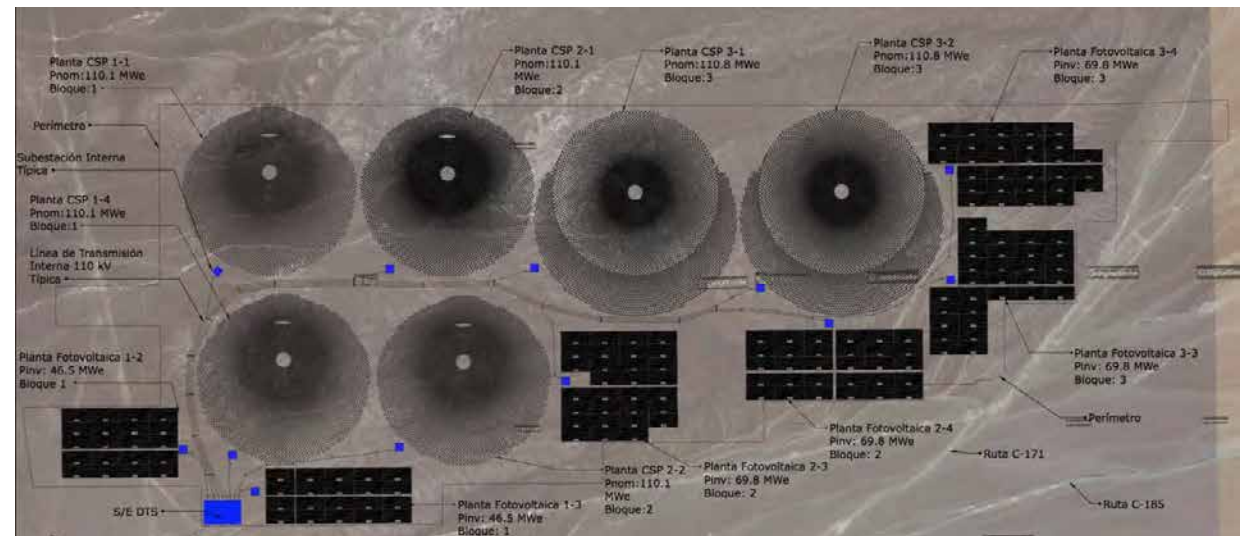
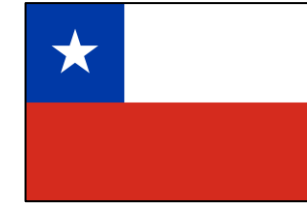
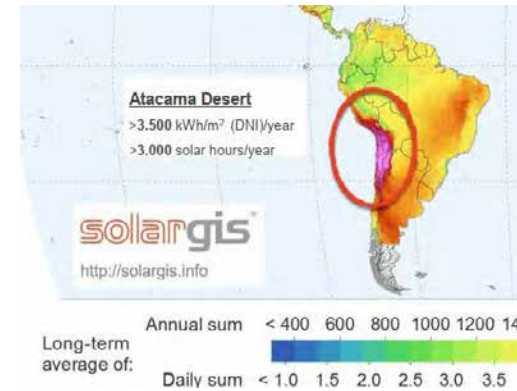
Storage capacity: about 12 hours

Tower height: about 220 m

PV capacity: 6 x 50 MW

Total electrical power capacity: about 900 MW

Current status: under project development

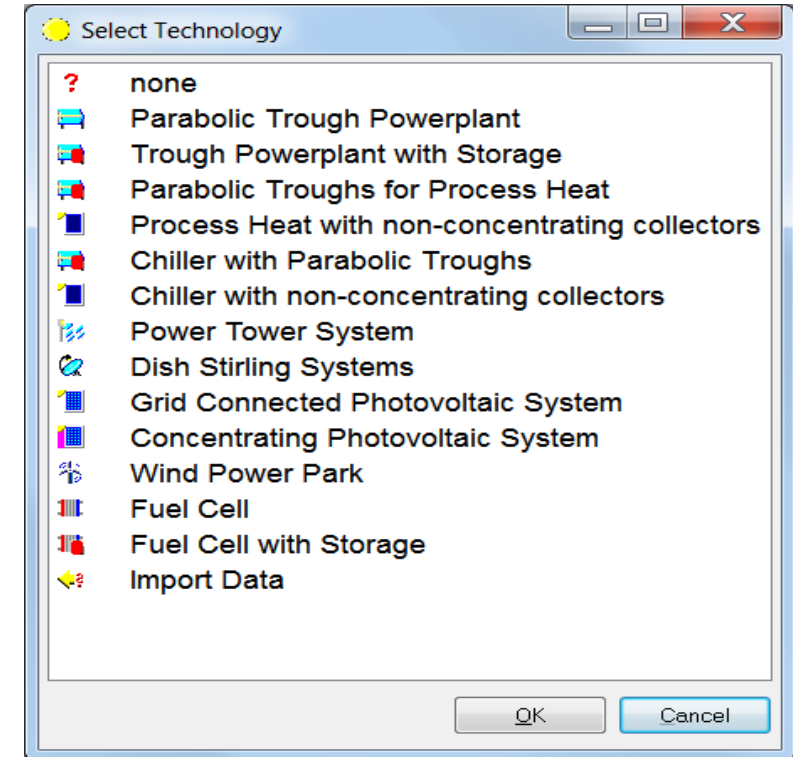


Simulation of Hybrid CSP – PV plants



The software tool **greenius**

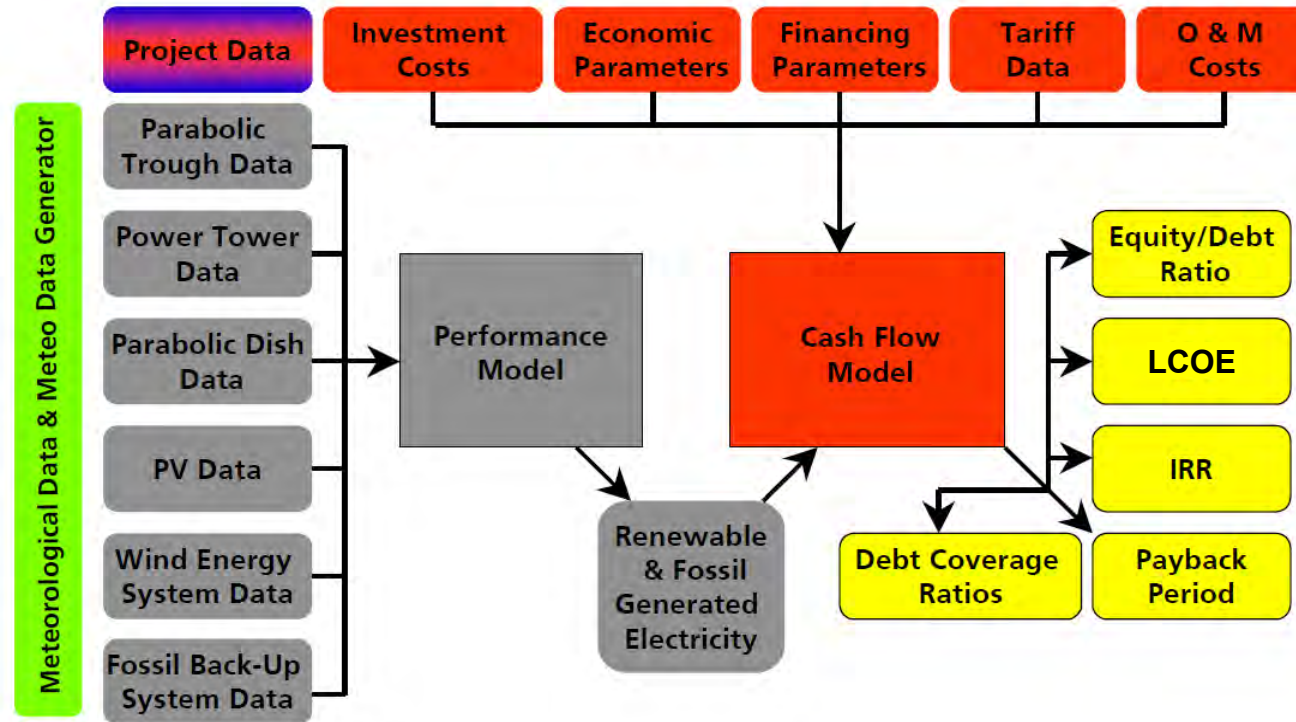
- Free of charge & easy to install
- Simulation of different renewable energy systems for heat or electricity generation
- Main focus on concentrating solar technology
- Customized for fast and simple calculations
- Based on hourly performance simulation of a typical year (min. time step length 10min)
- Utilization for feasibility studies, technology comparisons, etc.
- User support by DLR



Homepage of **greenius**:

<http://freegreenius.dlr.de/>

General purpose of **greenius**

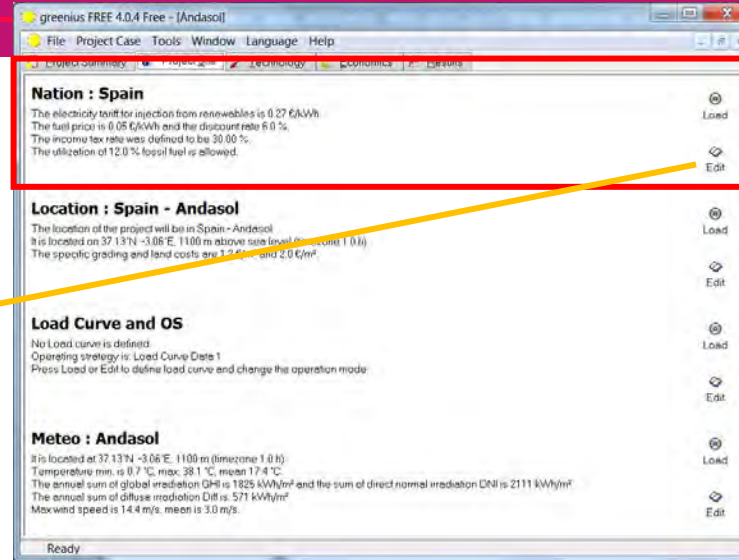


Independent simulation of power plants

SFERA-III

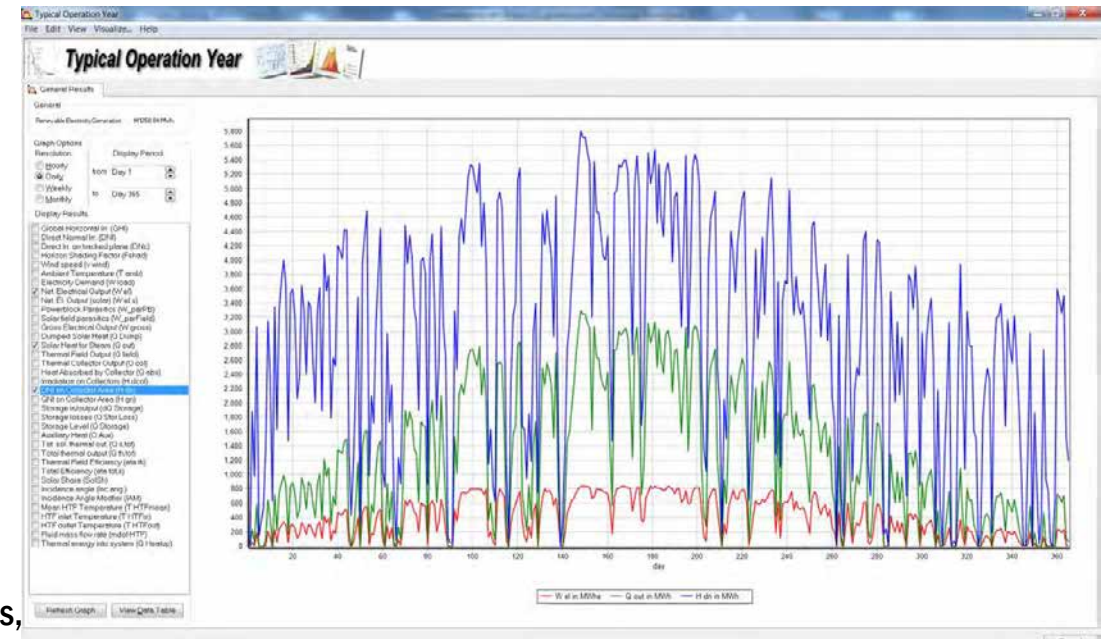
Solar Facilities for the European Research Area

greenius graphical user interface



Inputs

Outputs:



Structure of the greenius directory

Several installations of greenius may exist on local drive

The greenius root directory contains the executable and required DLLs

The data directory contains all datasets, those installed with greenius as well as those generated and saved by you

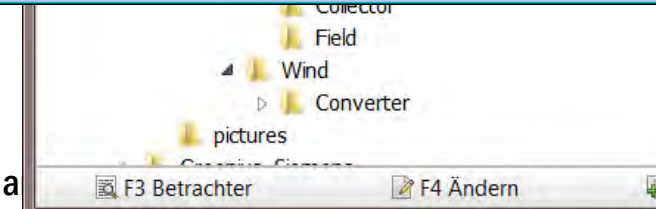
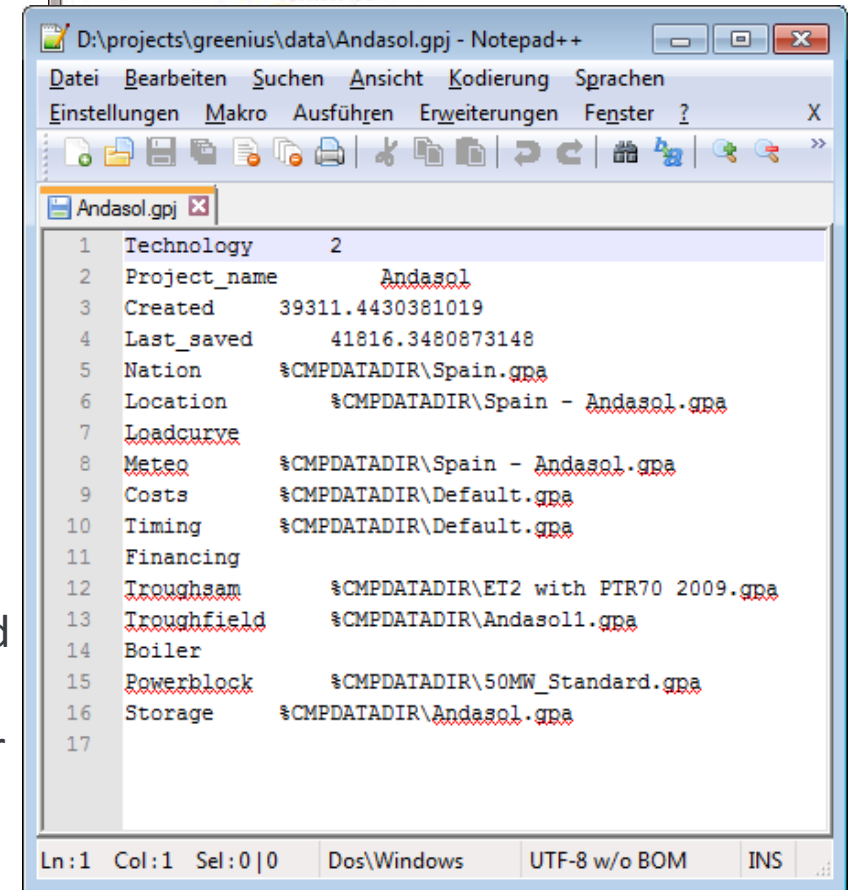
Sub-directories under „data“ are named according to the equivalent component/form

greenius projects are saved as *.gpj files, default directory is the „data“ directory

These *.gpj files contain only names of *.gpa- files which have to be used for the project

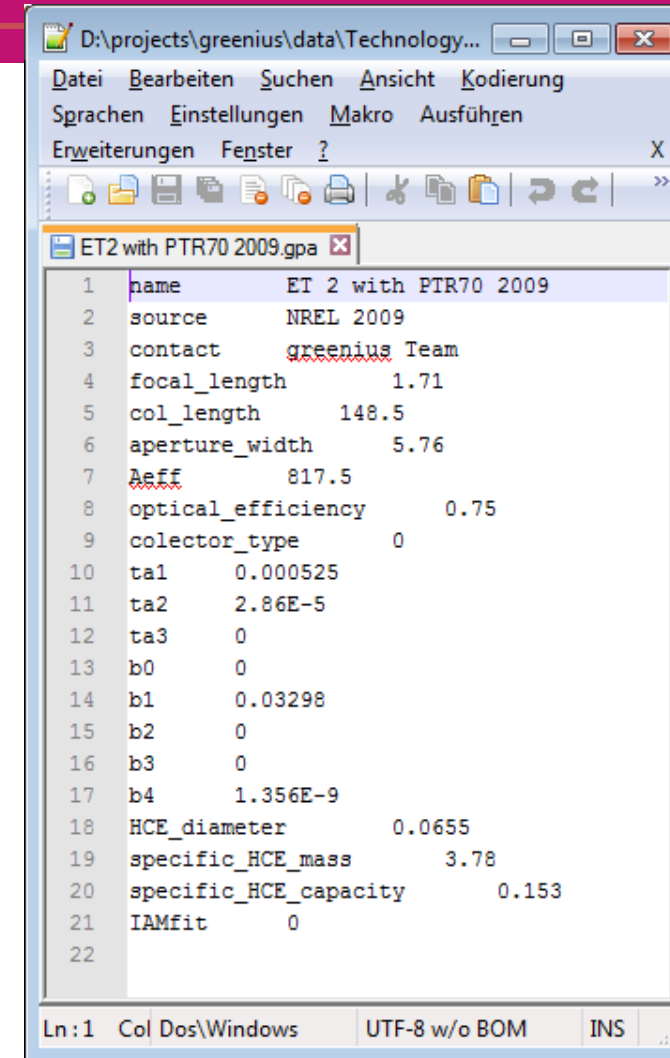
All *.gpa and *.gpj files are ASCII files and may be viewed by a text editor

For exchange of whole projects, greenius offers the „export“ and „import“ functions



Component file structure in greenius

- All component files are found under
... \Greenius-Directory\data\...
- Each Component type has its own subdirectory
- Content in form:
Parameter <TAB> Value
- Commas and points are both interpreted as decimal markers
- NO separators for thousands allowed



```
D:\projects\greenius\data\Technology...
Datei Bearbeiten Suchen Ansicht Kodierung
Sprachen Einstellungen Makro Ausführen
Erweiterungen Fenster ?
ET2 with PTR70 2009.gpa
1 name ET 2 with PTR70 2009
2 source NREL 2009
3 contact greenius Team
4 focal_length 1.71
5 col_length 148.5
6 aperture_width 5.76
7 Aeff 817.5
8 optical_efficiency 0.75
9 collector_type 0
10 ta1 0.000525
11 ta2 2.86E-5
12 ta3 0
13 b0 0
14 b1 0.03298
15 b2 0
16 b3 0
17 b4 1.356E-9
18 HCE_diameter 0.0655
19 specific_HCE_mass 3.78
20 specific_HCE_capacity 0.153
21 IAMfit 0
22
Ln: 1 Col: Dos\Windows UTF-8 w/o BOM INS
```

Example project in **greenius**:

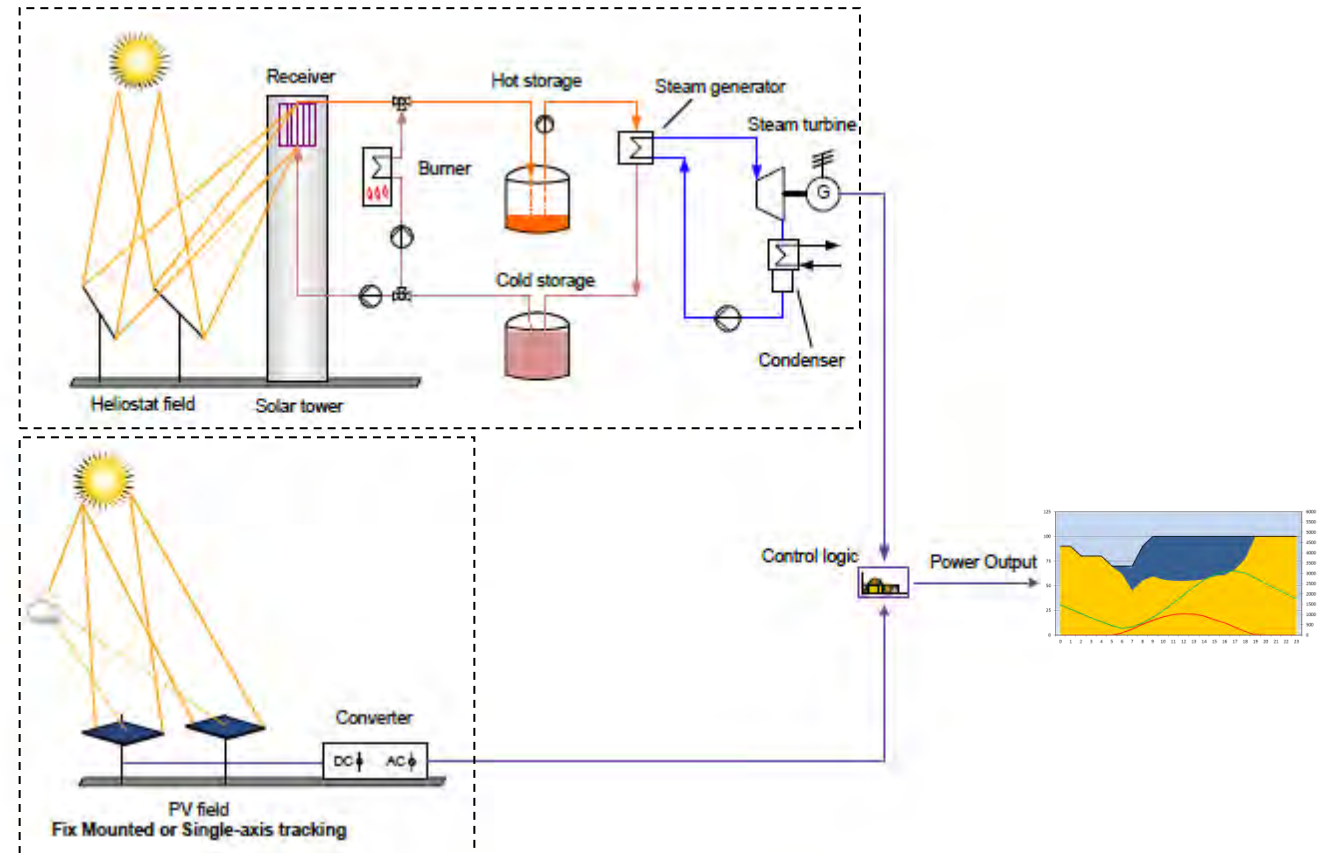
Simulation of a Hybrid
Solar Tower CSP + PV plant



Technology Configuration



Source:
Crescent Dunes power plant: www.solarreserve.com
<https://www.nextracker.com/product-services/solar-storage/truecapture/>



Main Steps

1. Select **plant configuration**: overall plant nominal net electrical power, technology types, PV capacity, CSP solar multiple, thermal storage size, back-up thermal power, etc.

| Design Parameters | | |
|--|------|-------|
| Overall Plant Net Output | MWeI | 100.0 |
| CSP: Solar Tower with Molten Salt and TES | | |
| Nominal Capacity | MWeI | 112.0 |
| Solar Multiple | - | 2.4 |
| Thermal Storage Capacity | h | 12.0 |
| Auxiliary HTF Heater | MWt | 254.0 |
| PV: Polycrystalline 1-axis tracked | | |
| Nominal Capacity (DC) | MWp | 142.2 |
| Inverter Capacity | MWp | 123.1 |
| Battery Capacity | h | 0.0 |

Main Steps

2. Create a data book with the required input parameters and performance characterization: component types (module & inverter, CSP collector, turbine, back-up heater, etc.), efficiency curves, auxiliary consumptions, heat losses, etc.

→ greenius has examples, but it is not a component-design software!

| Parameters PV & Inverter fixed | | | ALL COUNTRIES |
|--------------------------------|--|------|---------------------------|
| No. | Item | Unit | 2015 |
| parameter 1 | PV Manufacturer | - | JA Solar |
| parameter 2 | PV Module Type | - | JAP6 72-320/3BB |
| parameter 3 | Tracking y/n | - | y |
| parameter 4 | Nominal Module Power | W | 380 |
| parameter 5 | Nominal Module Efficiency | % | 19.6 |
| parameter 6 | Number of serial modules | - | 20 |
| parameter 7 | Number of parallel module strings | - | 220 |
| parameter 8 | Number of Systems | - | 100 |
| parameter 9 | Collector distance (shadowing) | m | 9.50 |
| parameter 10 | Inverter Manufacturer | - | SMA |
| parameter 11 | Inverter Type | - | SunnyCentral CP1000-XT ** |
| parameter 12 | Nominal Inverter Power | kW | 1,190 |
| parameter 13 | Nominal Inverter DC Voltage | V | 688 |
| parameter 14 | Inverter design efficiency | % | 98.7 |
| parameter 15 | Wiring losses at full power (STC), AC+DC | % | 1.44 |
| parameter 16 | Module quality + module array losses | % | 1.1 |
| parameter 17 | Other losses (soiling?) | % | 2 |
| parameter 18 | PV / Battery config (AC or DC) | - | AC |
| parameter 19 | Availability | % | 98 |
| parameter 20 | Degradation | %/y | 0.5 |

| No. | Item | unit | Value |
|---------------------|-----------------------------------|--------------------|--|
| a. Heliostat | | | |
| 1. | Heliostat type/name | [-] | Multi-facetted glass metal heliostat with 2-axes drive, pedestal mounted |
| | Net reflective area per heliostat | [m²] | 121 |
| | Aperture width | [m] | 12.93 |
| | Aperture height | [m] | 9.57 |
| | Number of facets | [-] | 28 (4x7) |
| | Annual mean reflectivity | [%] | 95 x 97 x 99 = 91.23 |
| | Beam error | [mrad] | 3.50 |
| | Canting | [-] | On-axis |
| | Parasitic consumption | [kW _e] | - |

| b. Solar field – system definition | | | |
|---|--|------|-----------|
| | Field layout | [-] | Surround |
| | Solar Multiple | [-] | 2.4 |
| | Number of heliostats | [-] | 8860 |
| | Net field reflective area | [m²] | 1,072,060 |
| | Optical efficiency of solar field @ DP | [%] | 68.5 |
| | Total land area | [m²] | 5,407,294 |

| f. Power block general | | | |
|-------------------------------|--------------------------------|--------------------|----------|
| | Design net electrical Power | [MW _e] | 100 |
| | Design gross electrical Power | [MW _e] | 112.1 |
| | Design gross efficiency | [%] | 42.82 |
| | Design net efficiency | [%] | 38.20 |
| | Cooling type | [-] | ACC |
| | Design condenser conditions | [mbar / °C] | 155 / 54 |
| | Minimum / maximum thermal load | [%] | 20 / 100 |

Main Steps

3. Local data preparation – Meteofile

- a) Obtain the measured meteorological data: ground based or satellite derived
- b) Open an existing meteofile from greenius in excel
- c) Change the information according to the new file: name, location, coordinates, timezone, resolution and meteo data (keep the header labels!)
- d) Save as text-file (*.txt) in your software folder, e.g. D:\greenius\Greenius\data\Site\Meteo
- e) Rename the file extension to *.gpa

The screenshot shows a Microsoft Excel spreadsheet titled 'Jordan_Meteofile.gpa'. The spreadsheet is organized into two main sections: metadata and meteorological data.

Metadata (Rows 1-7):

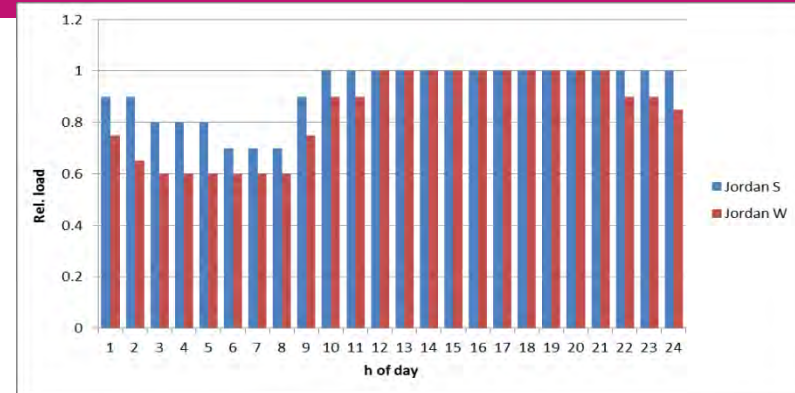
- 1 Name: Jordan Maan Hymenso
- 2 Source: EnerMENA
- 3 Contact: greenius Team
- 4 Coords: 35.8183°N 30.172°E 1012mNN
- 5 Timezone: 2
- 6 Res: 365x24

MeteoData (Rows 8-31):

| 9 | GHI | DNI | Diff | Tamb | Hum | p | Wind | Winddir |
|----|-------|-------|-------|------|------|-------|------|---------|
| 10 | 0 | 0 | 0 | 11.7 | 28 | 902.3 | 1.4 | 251.2 |
| 11 | 0 | 0 | 0 | 11.7 | 27.5 | 901.9 | 2.1 | 271 |
| 12 | 0 | 0 | 0 | 11.8 | 26.9 | 901.4 | 2.8 | 290.8 |
| 13 | 0 | 0 | 0 | 11.9 | 26.6 | 900.9 | 3 | 267.1 |
| 14 | 0 | 0 | 0 | 11 | 28 | 900.7 | 2.9 | 288.4 |
| 15 | 0 | 0 | 0 | 9.9 | 28.7 | 900.9 | 1.3 | 223.3 |
| 16 | 0 | 0 | 0 | 9.6 | 26.8 | 901.2 | 0.7 | 162.3 |
| 17 | 8.3 | 32.7 | 7.6 | 10 | 24.4 | 901.5 | 4 | 261.9 |
| 18 | 71.7 | 126 | 49.1 | 11.2 | 20.5 | 902.2 | 2.9 | 290.7 |
| 19 | 243.2 | 312.2 | 133.1 | 13.1 | 20.4 | 902.9 | 1.2 | 148.5 |
| 20 | 298.4 | 138.9 | 230.7 | 14.6 | 19.1 | 903.5 | 2.4 | 143.1 |
| 21 | 324.2 | 45.9 | 293.6 | 15.8 | 15.5 | 903.3 | 3.2 | 65 |
| 22 | 467.4 | 230.3 | 324.4 | 17 | 14.1 | 902.6 | 3.1 | 51.7 |
| 23 | 468.6 | 300.3 | 288.5 | 18.1 | 13.2 | 902.3 | 2.2 | 93.9 |
| 24 | 240.6 | 16.3 | 229.4 | 16.9 | 18.7 | 902.3 | 4.5 | 21.9 |
| 25 | 156 | 9.7 | 150.3 | 16.2 | 23.9 | 902.5 | 4.4 | 27.7 |
| 26 | 93.6 | 7.5 | 91.8 | 15.5 | 26.2 | 902.6 | 3.7 | 35.1 |
| 27 | 30.9 | 83.2 | 23.1 | 14.4 | 31.4 | 903 | 2.9 | 22.5 |
| 28 | 0 | 0 | 0 | 12.1 | 40.6 | 903.6 | 3.4 | 172.3 |
| 29 | 0 | 0 | 0 | 10.4 | 54.4 | 904.4 | 3.5 | 227.3 |
| 30 | 0 | 0 | 0 | 9.8 | 55.4 | 904.9 | 2.5 | 241.6 |
| 31 | 0 | 0 | 0 | 9.4 | 46.5 | 904.9 | 2.5 | 307.9 |

Main Steps

3. Local data preparation – Load Curve (total)
 - a) Obtain the load curve data: electrical demand for the complete power plant
 - b) Open an existing load file from greenius in excel
 - c) Change the information according to the new file: name, resolution and scaling factor (nominal output in W) and load relative to maximum load
 - d) Save as text-file (*.txt) in your software folder, e.g. D:\greenius\Greenius\data\Site\Loadcurve
 - e) Rename the file extension to *.gpa

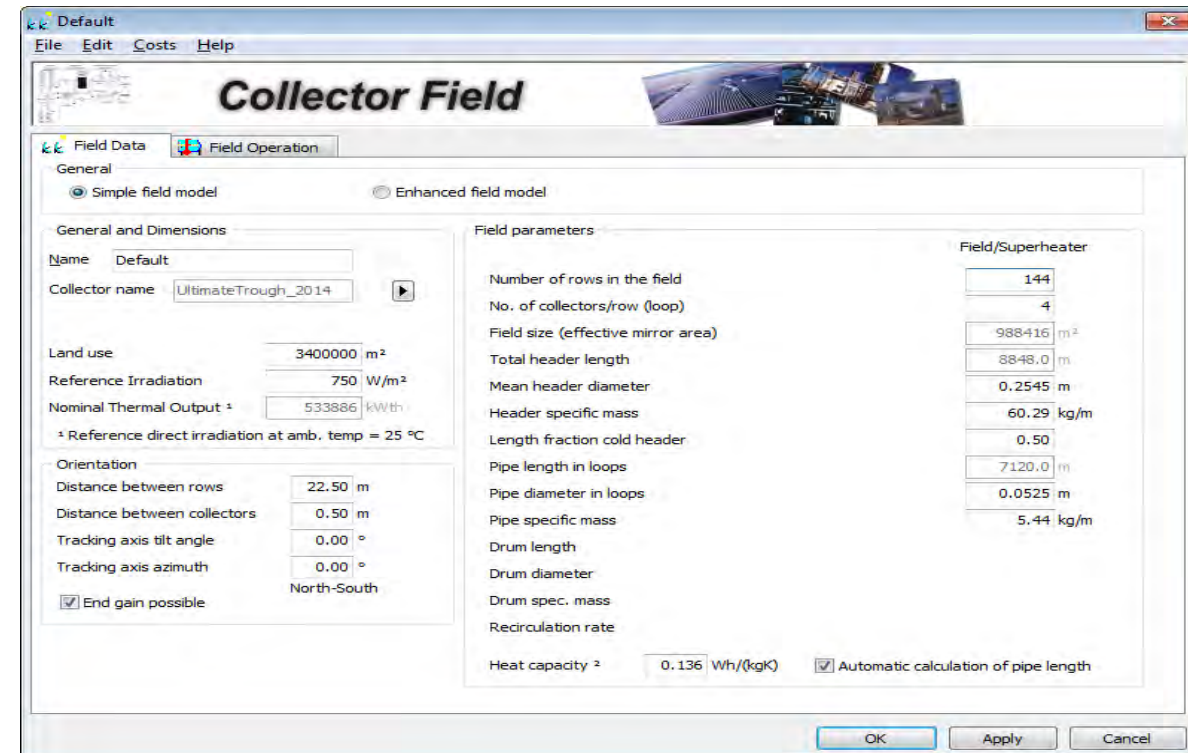
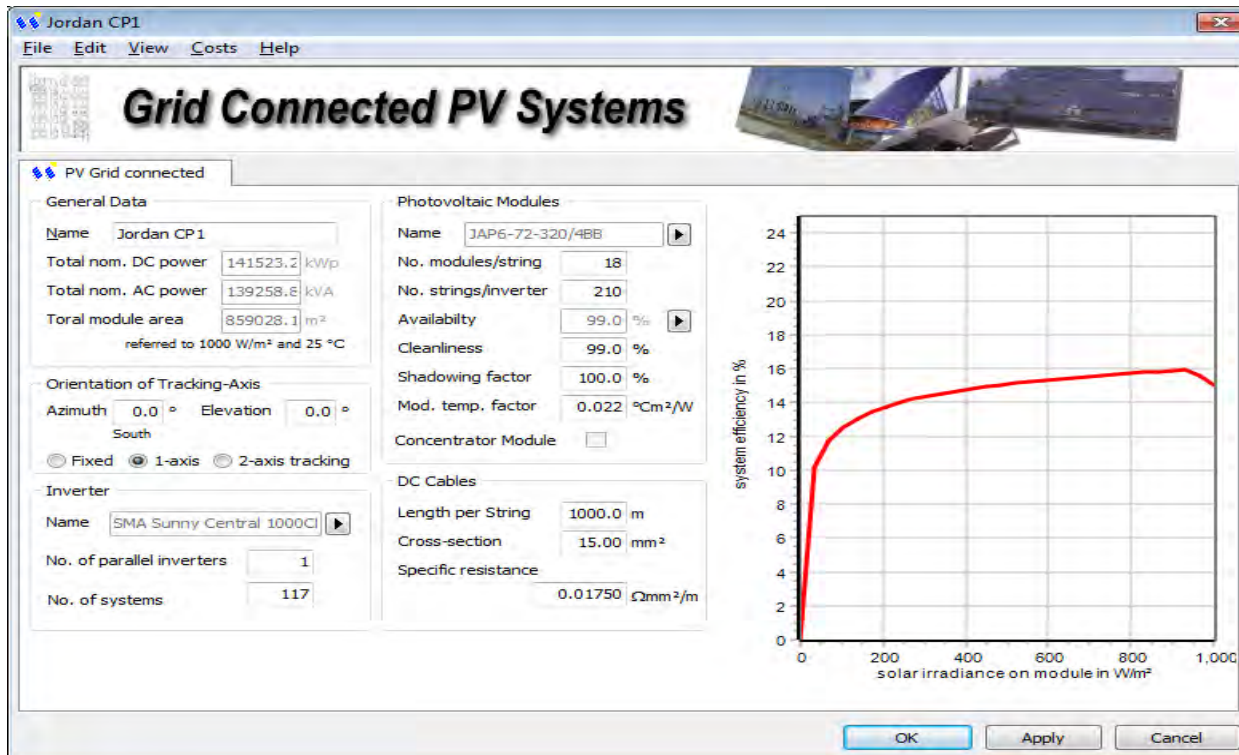


| LoadData | PeriodData |
|----------|------------|
| 0.75 | 1 |
| 0.65 | 1 |
| 0.6 | 1 |
| 0.6 | 1 |
| 0.6 | 1 |
| 0.6 | 1 |
| 0.6 | 1 |
| 0.6 | 1 |
| 0.6 | 1 |
| 0.75 | 1 |
| 0.9 | 1 |
| 0.9 | 1 |
| 1 | 1 |
| 1 | 1 |
| 1 | 1 |
| 1 | 1 |



Main Steps

4. Determine **cost factors**: fuel cost, land cost, equipment CAPEX & OPEX, financing parameters, etc.
5. Create a **new project** in greenius and **adjust the parameters**.



Main Steps

6. For the case of hybrid CSP-PV plant:
 - a) First simulate the **PV plant** with the **total load curve**
 - b) Determine the **rest load** not covered with the PV plant
 - c) Then simulate the CSP plant with **new load curve** based on rest load
 - d) Combine “manually” the results of PV and CSP to obtain the **total yield** and **overall LCOE**.

See now example in **greenius** and MS Excel

Steps for combining PV and CSP results

Rest load not covered with the PV plant:

1. Copy all the hourly results of PV into excel sheet
2. Determine residual load in MW: difference $W_{load} - W_{ToGrid}$

New load curve for CSP:

1. Set values of residual load > 0 and $<$ minimum load to minimum load
2. Calculate relative load (0 to 1) as residual load / nominal load
3. Generate gpa-file as shown on slide 19 above

Calculate CSP plant with new load curve (if allowed, use fossil fuel under “Load Curve / Operation Strategy / “Gas support up to” = 1)

Steps for combining PV and CSP results

Merge CSP and PV results (total net electrical output):

1. Sum net electrical output of both plants (“W_{net}” PV + “W_{el}” CSP)
2. Calculate corrected PV to grid. Demand cannot be exceeded although CSP is forced to run at minimum load, therefore PV output must be reduced.
3. Calculate final sum of net electrical output

Determine if part of the **offline auxiliary consumption of CSP plant** can be covered with **excess generation from PV**:

1. Calculate generation above demand
2. Determine original offline auxiliary consumption of CSP
3. Calculate adjusted offline auxiliary consumption of CSP after using excess energy from PV. Energy to be taken from electrical grid.
4. Calculate new reduced PV curtailment (for information only)

Steps for combining PV and CSP results

Calculate combined LCOE for hybrid plant

1. Write down the LCOE and net electrical output of PV calculated by greenius
2. Calculate new LCOE of PV adjusted with reduced electricity production (due to minimum load limitation of CSP):

$$LCOE_{PV\ new} = \frac{E_{net\ PV\ original}}{E_{net\ PV\ new}} * LCOE_{PV\ original}$$

3. Write down the LCOE and net electrical output of CSP calculated by greenius
4. Calculate the average of the LCOE of PV and CSP weighted with the electricity generation:

$$LCOE_{hybrid} = \frac{LCOE_{PV\ new} * E_{net\ PV\ new} + LCOE_{CPS} * E_{net\ CSP}}{E_{net\ PV\ new} + E_{net\ CSP}}$$

THANK YOU
for your attention!

THANKS to my colleagues
for their work and input